AD-A116 733 ARMY MATERIALS AND MECHANICS RESEARCH CENTER WATERTOWN MA F/G 11/4
PROCEEDINGS OF THE CRITICAL REVIEW: TECHNIQUES FOR THE CHARACTE--ETC(U)
MAY 82

UNCLASSIFIED AMMRC-MS-82-3 NL

1 OF 6
AD A116733

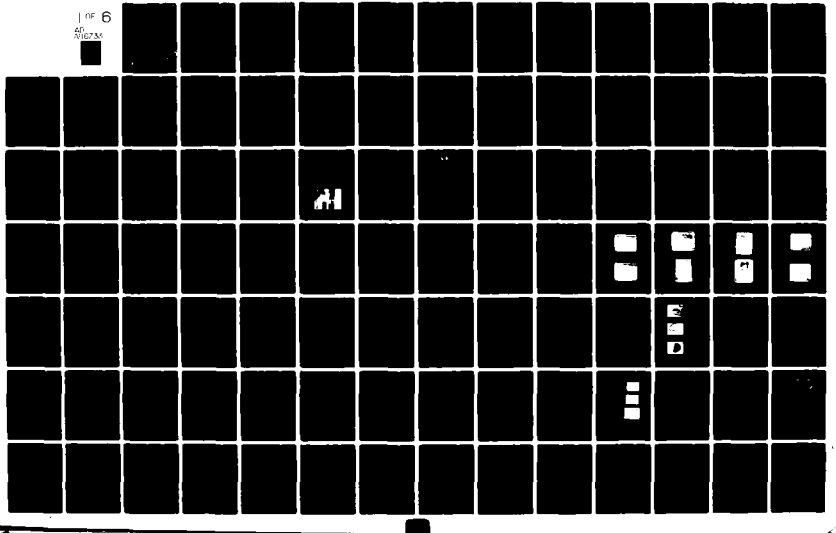

AMMRC MS 82-3

AD

PROCEEDINGS OF THE CRITICAL REVIEW: TECHNIQUES FOR THE CHARACTERIZATION OF COMPOSITE MATERIALS

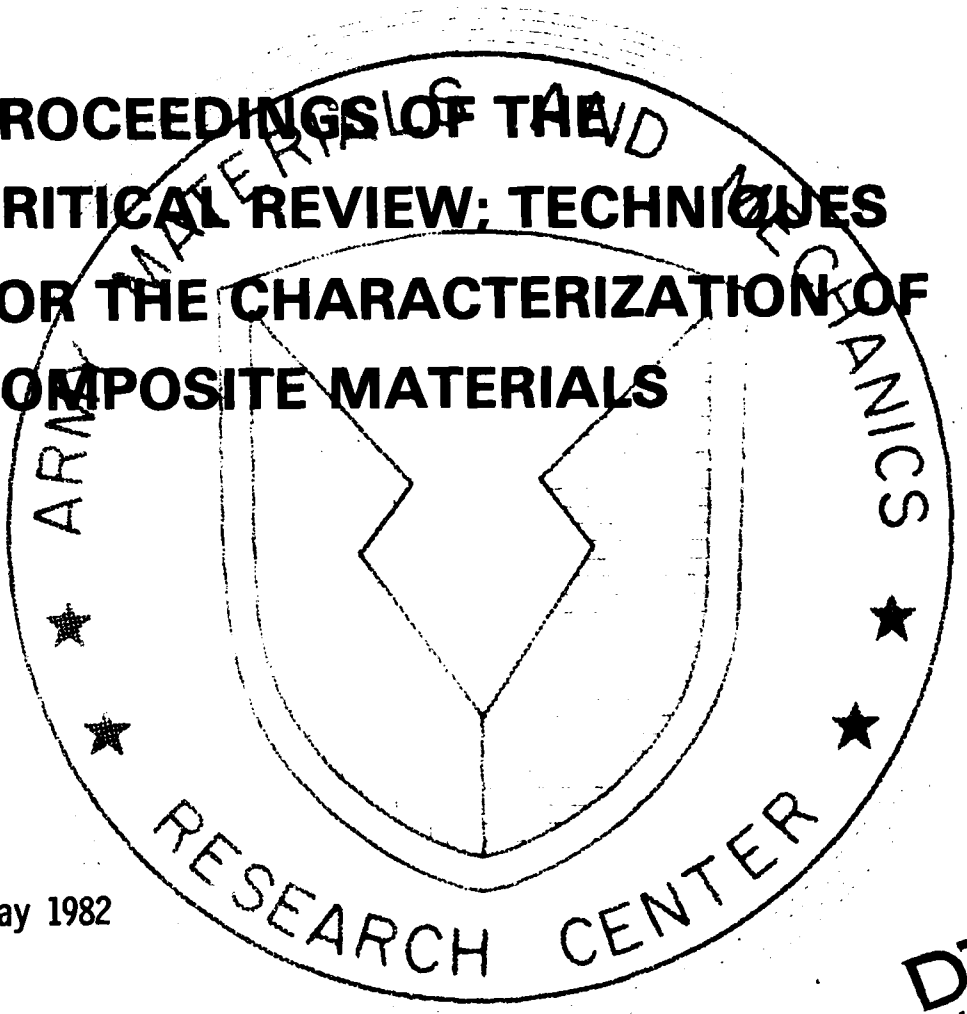

May 1982

Approved for public release; distribution unlimited.

ARMY MATERIALS AND MECHANICS RESEARCH CENTER
Watertown, Massachusetts 02172

ORGANIZING COMMITTEE

Mr. R. L. Dempsey	**NAVAIR**
Dr. R. W. Lewis	**AMMRC**
Dr. L. H. Peebles, Jr.	**ONR East**
Dr. R. J. Shuford	**AMMRC**
Dr. G. R. Thomas	**AMMRC**

Arrangements

Dr. L. H. Peebles, Jr.	**ONR East**
Mrs. G. Fitzgerald	**MIT**
Ms. C. Taylor	**MIT**

UNCLASSIFIED

SECURITY CLASSIFICATION OF THIS PAGE (When Data Entered)

REPORT DOCUMENTATION PAGE		READ INSTRUCTIONS BEFORE COMPLETING FORM
1. REPORT NUMBER AMMRC MS 82-3	2. GOVT ACCESSION NO.	3. RECIPIENT'S CATALOG NUMBER
4. TITLE (and Subtitle) PROCEEDINGS OF THE CRITICAL REVIEW; TECHNIQUES FOR THE CHARACTERIZATION OF COMPOSITE MATERIALS		5. TYPE OF REPORT & PERIOD COVERED Final Report 6. PERFORMING ORG. REPORT NUMBER
7. AUTHOR(s)		8. CONTRACT OR GRANT NUMBER(s)
9. PERFORMING ORGANIZATION NAME AND ADDRESS Army Materials and Mechanics Research Center Watertown, Massachusetts 02172 DRXMR-OC		10. PROGRAM ELEMENT, PROJECT, TASK AREA & WORK UNIT NUMBERS
11. CONTROLLING OFFICE NAME AND ADDRESS U. S. Army Materiel Development and Readiness Command, Alexandria, Virginia 22333		12. REPORT DATE May 1982 13. NUMBER OF PAGES 506
14. MONITORING AGENCY NAME & ADDRESS(if different from Controlling Office)		15. SECURITY CLASS. (of this report) Unclassified 15a. DECLASSIFICATION/DOWNGRADING SCHEDULE

16. DISTRIBUTION STATEMENT (of this Report)

Approved for public release; distribution unlimited.

17. DISTRIBUTION STATEMENT (of the abstract entered in Block 20, if different from Report)

18. SUPPLEMENTARY NOTES

Sponsored by Office of Naval Research
Eastern/Central Regional Office
Boston, MA 02210

19. KEY WORDS (Continue on reverse side if necessary and identify by block number)

Polymers	Nondestructive evaluation	Dielectric properties
Composite materials	Moisture	Characterization
Spectroscopy	Cure monitoring	Process control

20. ABSTRACT (Continue on reverse side if necessary and identify by block number)

(SEE REVERSE SIDE)

DD FORM 1 JAN 73 1473 EDITION OF 1 NOV 65 IS OBSOLETE

UNCLASSIFIED

SECURITY CLASSIFICATION OF THIS PAGE (When Data Entered)

Block No. 20

ABSTRACT

Proceedings of "A Critical Review: Techniques for the Characterization of Composite Materials" sponsored by Office of Naval Research, Eastern/Central Regional Office, Boston, MA.; held at Massachusetts Institute of Technology, Cambridge, Massachusetts, 8-10 June 1981.

The objective of this Review was to evaluate the potential of new and/or improved techniques for predicting the performance of composite materials. A total of thirty-five technical papers were presented at the Review. The topics covered by session were:

I. Cure Monitoring.
II. Moisture,
III. Predictive Composite Characterization,
IV. Advances of Significance to Composites,
V. Recapitulation.

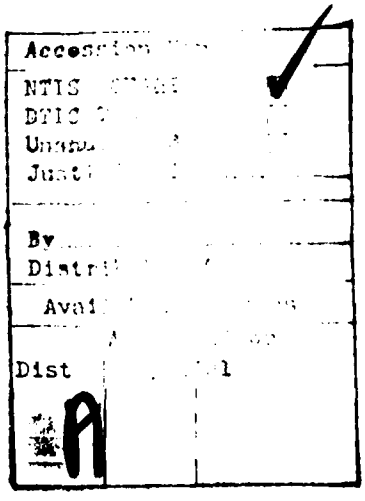

CONTENTS

Opening Remarks

DR. G. R. THOMAS

Army Materials and Mechanics Research Center
Watertown, Massachusetts 02172

I would like to discuss where we have been and where we are going. From the U.S. Army point of view, we have a considerable number of applications for composite materials. Approximately 75 discrete combinations of fibers, polymers, and resins are either in use or are planned for use in Army systems. This does not include materials used by the U.S. Navy or Air Force, Canada, United Kingdom, or Australia. In 1968 when we started out in this venture looking at composite materials, there was very little environmental/mechanical data available on composites. Composites evaluated after long term environmental exposure were losing strength after five years, on the order of 20%-30%, even up to 50% in tropic areas. This was not satisfactory because the loss of strength would diminish the weight advantage in using composites.

Helicopter rotor blades represent one of the main applications of composites for the Army. Early on we looked at a variety of resins and fibers that were being proposed by aircraft manufacturers for use in composite blades. Differences in mechanical properties were observed by various manufacturing groups for "identical" materials with "comparable" cure histories. What caused these differences? What analytical techniques can be used to monitor/assure quality control? These were some of the questions that needed to be addressed. What happened was that The Technical Cooperation Program (TTCP) elected to approach the problem from a fundamental point of view. What we said was that if we could characterize the fiber, resin, and cure process, we would then be able to predict the performance of the composite. This international characterization program has been going on since 1977. As a result of this work we came out with two systems: Fourier transform-infrared spectroscopy (FTIR) and high performance liquid chromatography (HPLC). These systems can be used to distinguish differences in chemistry between resins, but the significance of the differences was unknown. This brings us to the point of this conference. We feel we have enough techniques for characterizing the starting materials, now what we are looking for is understanding of what goes on in the fabrication process and what properties should we measure in order to predict the performance of a particular composite, not one or two but 20 years from now. Another goal of TTCP is to develop an adequate materials data base (for present and future military systems) containing minimum-risk design factor requirements and appropriate materials property data. If an adequate data base is developed and proper quality control/processing procedures followed, we should ideally be able to fabricate composites with improved performance and durability.

Session I: CURE MONITORING

Chairperson: DR. G. R. THOMAS

Army Materials and Mechanics Research Center

APPLICATION OF NEW TECHNIQUES FOR CURE MONITORING OF EPOXIES

Gary L. Hagnauer

Polymer Research Division
Army Materials and Mechanics Research Center
Watertown, Massachusetts 02172 U.S.A.

ABSTRACT

A variety of new techniques have been developed for monitoring the cure of epoxy resins and are being considered for process control of composite materials. Generally, the techniques involve the measurement of changes in the thermal, rheological, electrical, or mechanical properties as a function of cure time and temperature. Unfortunately, because of the complex nature of the properties being monitored, and since relative rather than absolute parameters are often measured, extents of cure determined by different techniques are seldom in good agreement. Also, for most techniques there is a problem of defining the state of full or ultimate cure. This paper describes the problems and limitations of some of the new techniques.

In considering the application of new monitoring techniques, it is desirable to understand how the measured parameters correlate with intrinsic chemical and structural changes in the epoxy resin matrix and at the fiber-resin matrix interface as the resin reacts and crosslinking develops. This paper will present the results of a study in which advanced chromatographic and spectroscopic techniques were applied to analyze chemical changes taking place during the initial stages of cure and to elucidate the structure of the resin matrix at the onset of gelation. The chemical and structural changes are compared with differential scanning calorimetry, torsional braid analysis, and DC resistance cure monitoring techniques.

DISCUSSION

A variety of new techniques have been applied to study the curing behavior of the glass fiber-epoxy resin prepreg SP250. The chemical composition of the SP250 resin has been evaluated using liquid chromatography and Fourier transform infrared spectroscopy; and special high performance liquid chromatography (HPLC) procedures have been developed to quantitatively analyze the principal resin components - ECN 1273, Epon 828, dicyandiamide (dicy) and the accelerator (Monuron).[1,2] (Figure 1)

HPLC techniques are particularly useful in monitoring changes in the concentrations of resin components as the prepreg ages or cures. (Figure 2)

33% RESIN 67% GLASS FIBER

45.8% ECN 1273

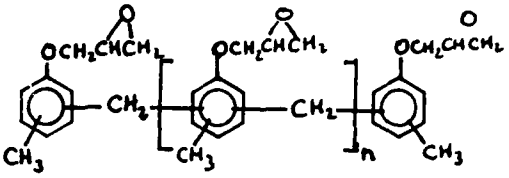

38.2% Epon 828

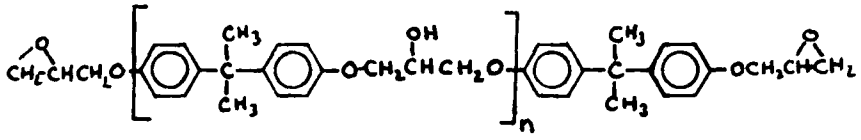

7.1% dicy

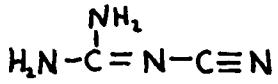

3.9% Monuron

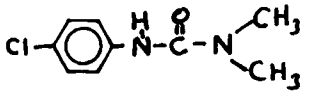

5% epoxy resin #3

Figure 1. Chemical composition of SP250 epoxy resin. SP250-S2 glass prepreg = 33 wt% resin + 67 wt% glass.

The solution concentration and gel content (wt % insoluble resin) are determined by extracting the weighed prepreg specimen with tetrahydrofuran and weighing the fibers after they are heat-treated at 800°C to remove insoluable organic material. Component concentrations (wt %) are determined from peak areas using a solution of the standard resin formulation for calibration.

The isothermal curing behavior of an SP250 S2-glass prepreg has been investigated in considerable detail using HPLC. Changes in component concentrations and gel content were analyzed as a function of reaction time over the temperature range 40°-120°C. (Figure 3) In the early stages of reaction up tc 60% gelation, the rate of reaction of each component follows first-order kinetics:

$$-\frac{dC}{dt} = kC \qquad \text{or} \qquad \ln(C_o/C) = kt$$

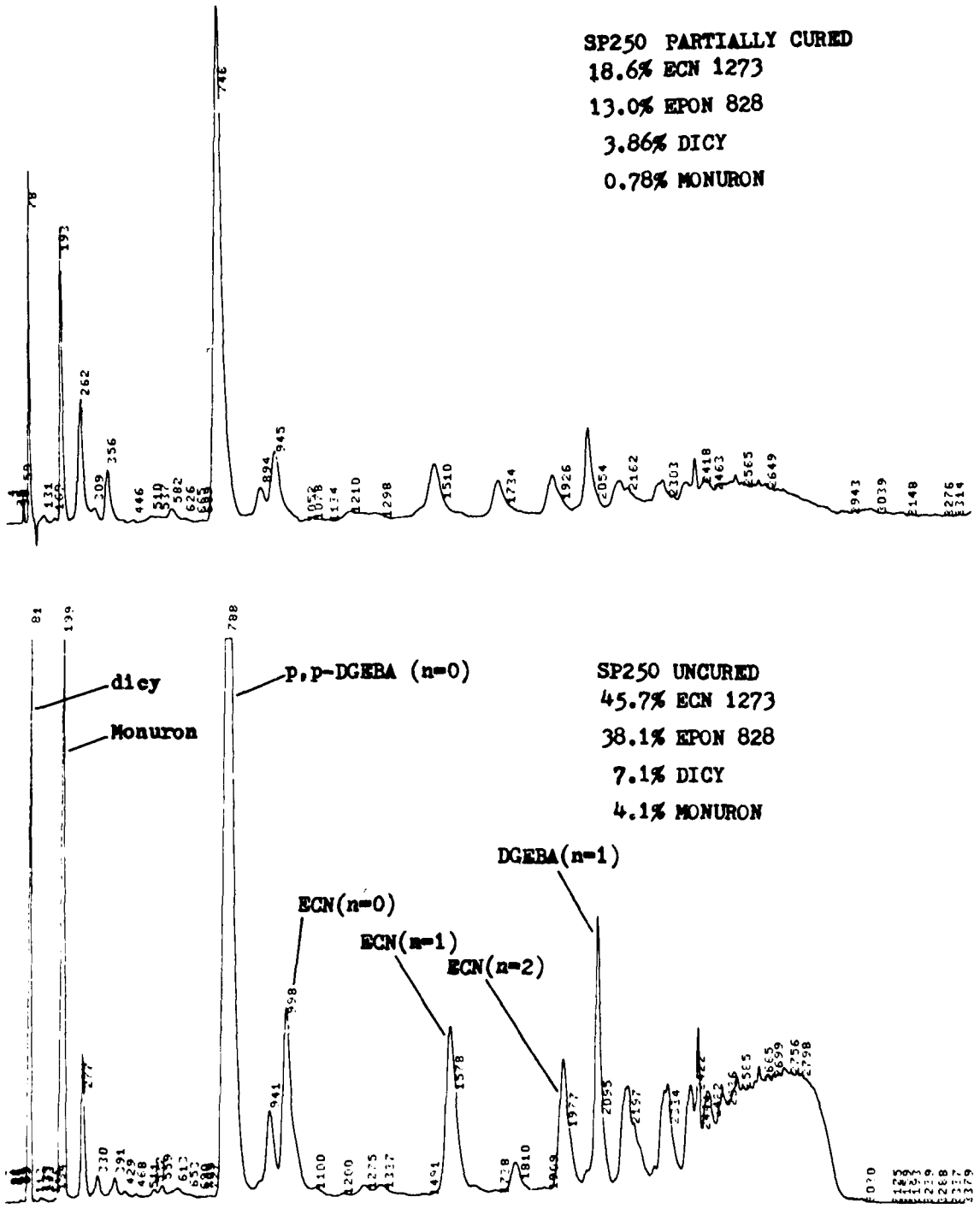

Figure 2. HPLC analysis of uncured and partially cured SP250 resin.

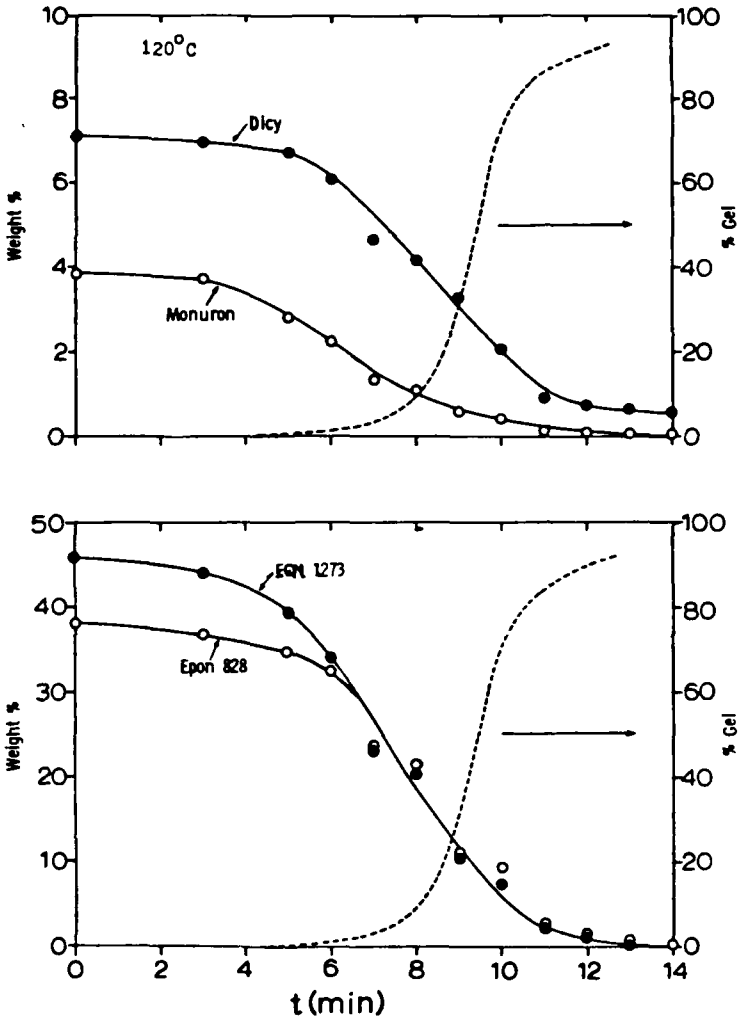

Figure 3. Isothermal curing behavior of SP250-S2 prepreg resin at 120°C - HPLC analysis of composition.

where C_o is the initial concentration of the component, C is the concentration at time t (minutes) and k is the first-order rate constant (min^{-1}). Activation energies E_o were determined from the temperature dependence of the time to the onset of gelation

$$t_{gel} = A_o e^{E_o/RT}.$$

The time/temperature dependence of gelation is described by the expression

$$\% \text{ gel} = A_1 e^{-E_1/RT}(t - t_{gel}) \qquad \text{(Figures 4 and 5)}$$

It is noted that the slope of the Arrhenius plot and hence the activation energy is different above and below ca 70°C. The temperature dependence of the rate constants of dicy, Monuron, and the epoxy components also changes at approximately the same temperature which suggests a possible change in

$$\% \text{ gel} = A_1 e^{-E_1/RT}(t - t_{gel})$$

$$t_{gel} = A_0 e^{E_0/RT}$$

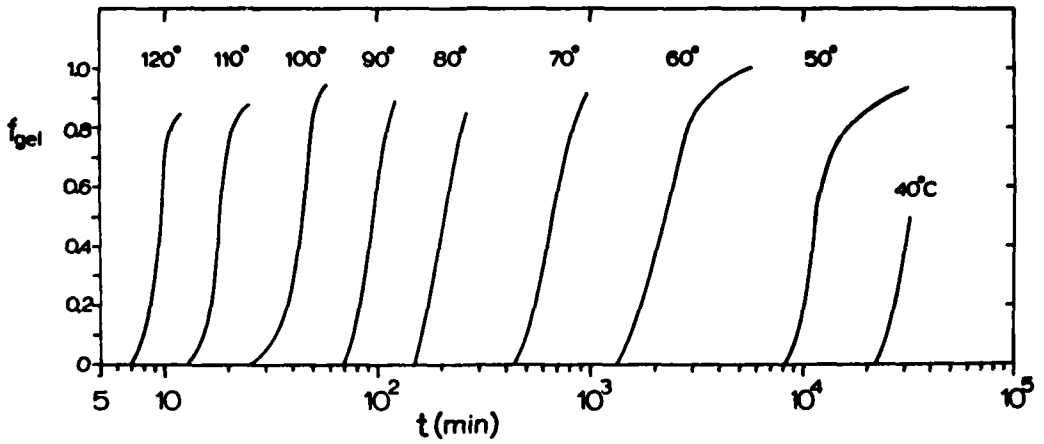

Figure 4. Time/temperature dependence of SP250-S2 prepreg resin gelation - gel fraction f_{gel} determined by Gravimetric Analysis.

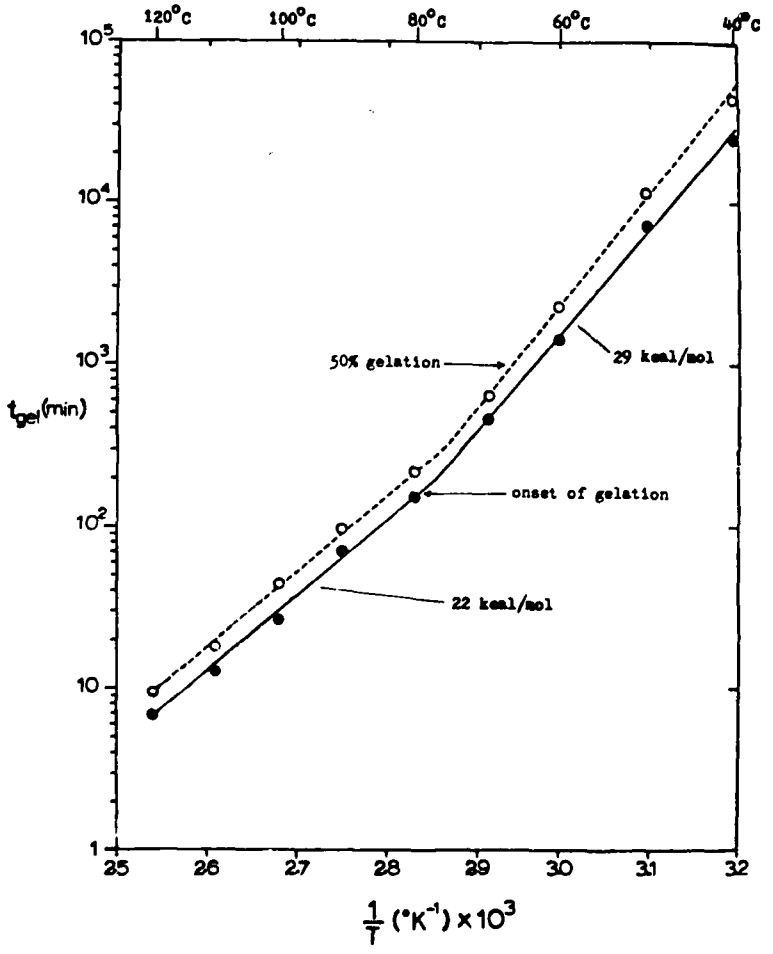

Figure 5. Arrhenius plots of time to onset of gelation (o) and time to 50% gelation (o) versus 1/T (°K^{-1}).

reaction mechanism. (Figure 6) Between 100°and 110°C, a sharp increase in the temperature dependence of the rate constant of Monuron occurs and results in an unusually large apparent activation energy E* = 44.3 kcal/mol. (Figures 7 and 8) Activation energies determined by torsional braid analysis (TBA)[3], differential scanning calorimetry (DSC)[4,5], dynamic spring analysis (DSA)[6], DC resistance[7], and charge-flow transistor (CFT)[8] measurements are in good agreement with the value calculated from the onset of gelation data. (Figure 9)

Additional information about the chemistry of the cure process is obtained when the % gelation is plotted against the % reaction of each component. For example, the onset of gelation occurs when 33-40% of the epoxy components have reacted regardless of temperature. (Figure 10) However the percentage of dicy and Monuron reacted at the onset of gelation is quite dependent upon temperature. At curing temperatures below 90°C, significant amounts of dicy and Monuron remain unreacted in the insoluble resin (100% gelation). Figures 11 and 12) Plots of the moles of reacted dicy and epoxy components per 100 grams of resin versus reaction time show that nearly equivalent amounts of the amine and epoxy functional groups react at 120°C but that considerably smaller amounts of dicy are incorporated into the resin matrix as the reaction temperature is lowered. (Figures 13 and 14)

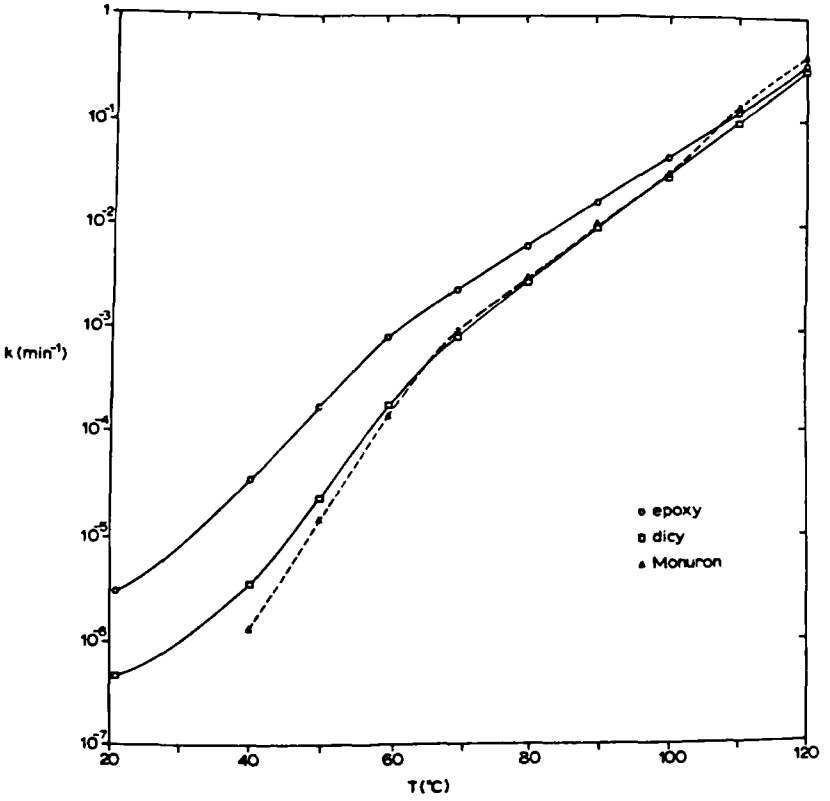

Figure 6. Temperature dependence of first-order rate constants (k^{-1}) for reaction of epoxy (o), Dicy (□), and Monuron (Δ) molecules.

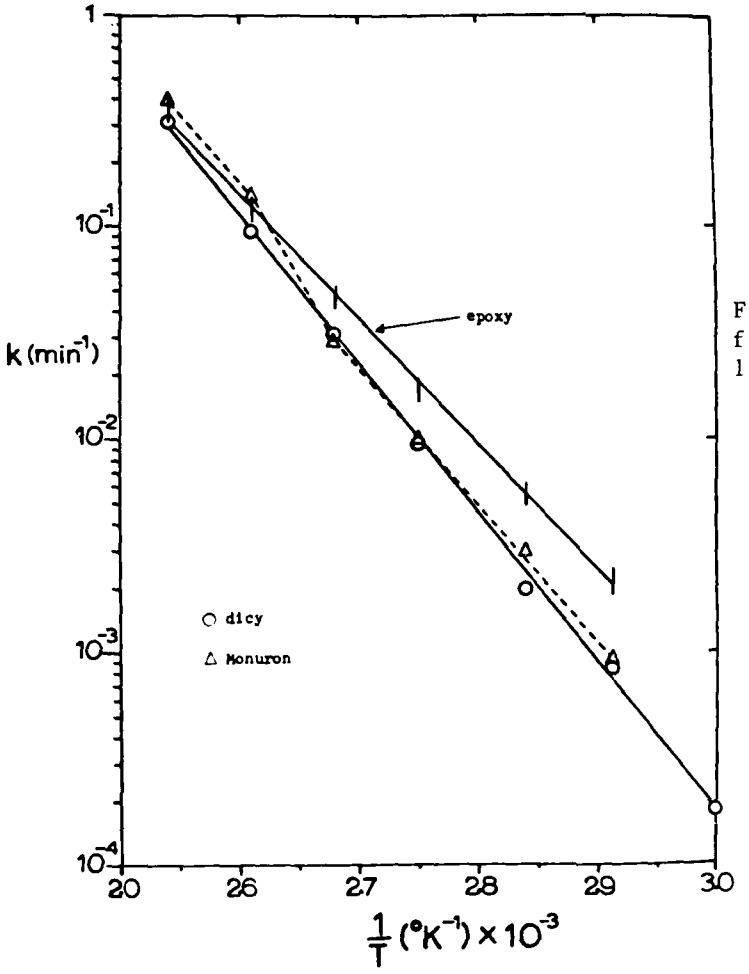

Figure 7. Arrhenius plots of first-order rate constants versus 1/T (°K^{-1}).

MEASUREMENT	TEMP RANGE	E* (kcal/mol)
ONSET OF GELATION	40-70°C	28.9
	70-120	22.7
	80-120	22.0
DGEBA (n=0)	70-120	26.3
(n=1)	"	26.4
ECN (n=0)	"	26.9
(n=1)	"	27.5
(n=2)	"	27.4
EPOXY OLIGOMERS	"	26.9
MONURON	70-100	29.1
	100-110	44.3
	110-120	29.1
DICY	60-120	31.6

Figure 8. Tabulation of activation energies.

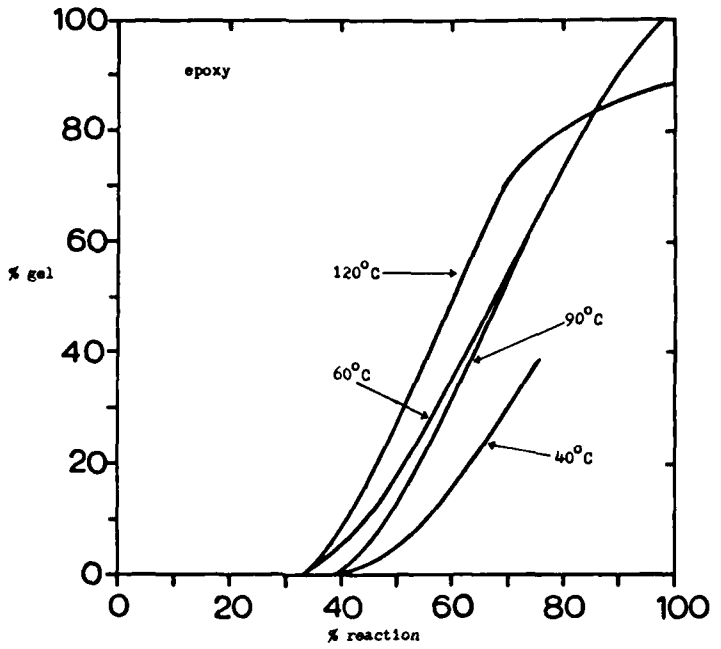

Figure 9. Comparison of activation energies determined by different cure monitoring techniques.

MEASUREMENT		E_a (kcal/mol)	
isothermal			
TIME TO GELATION (TBA)	82-112°C	19.7	Schneider et al
"	63-103°C	24.4	Schneider and Gillham
TIME TO 30% CONVERSION (DSC)	100-162°C	20.3	Schneider et al
DYNAMIC SPRING ANALYSIS (DSA)	80-110°C	21.0-21.6	MacKnight et al
TIME TO GELATION (DC RESISTANCE)	50-120°C	22.7	Shuford
CHARGE-FLOW TRANSISTOR (CFT)	90-120°C	17.8	Senturia et al
dynamic			
DSC 0.5 - 20°C/min	110-180°C	21.8	LaLiberte

Figure 10. Plot of % reaction epoxy components versus % gel at different temperatures.

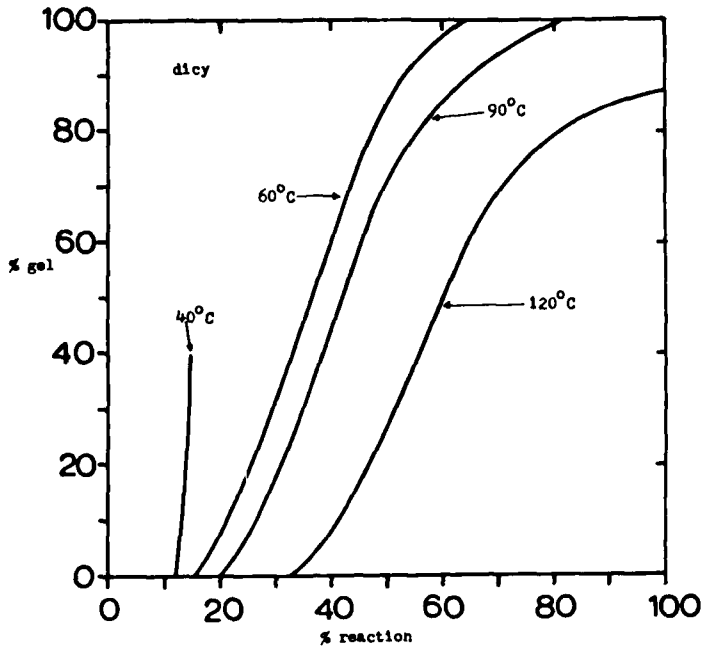

Figure 11. Plot of % reaction dicy components versus % gel at different temperatures.

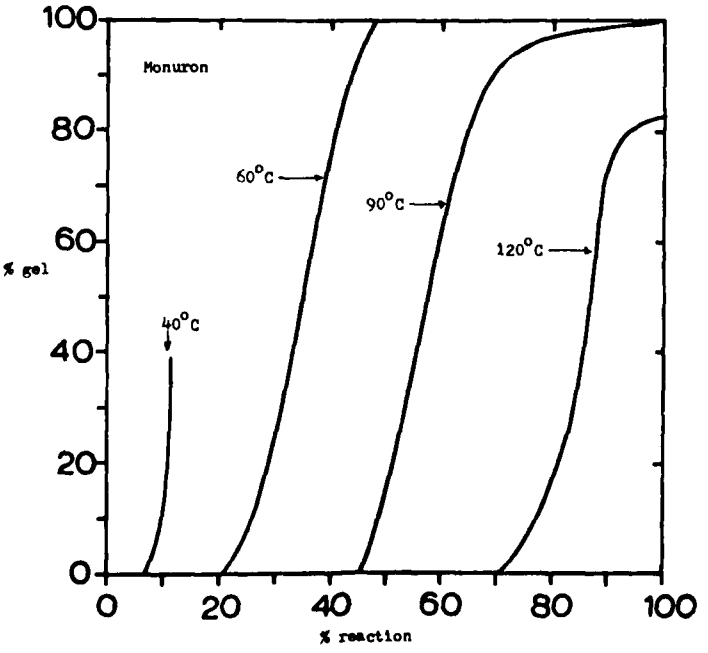

Figure 12. Plot of % reaction Monuron vs % gel at different temperatures.

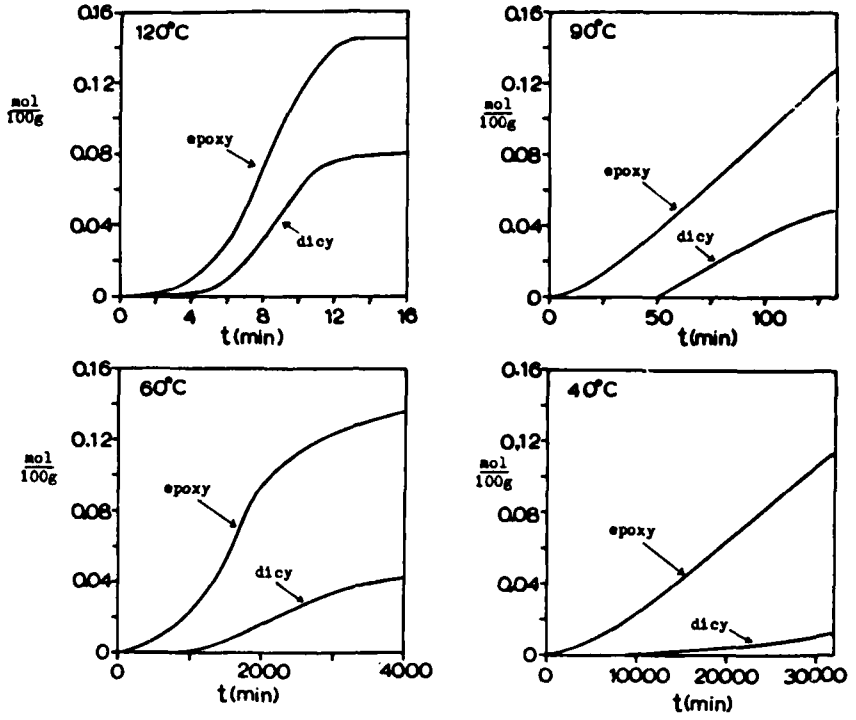

Figure 13. Plots of moles dicy and epoxy components per 100 g resin versus reaction time at different temperatures.

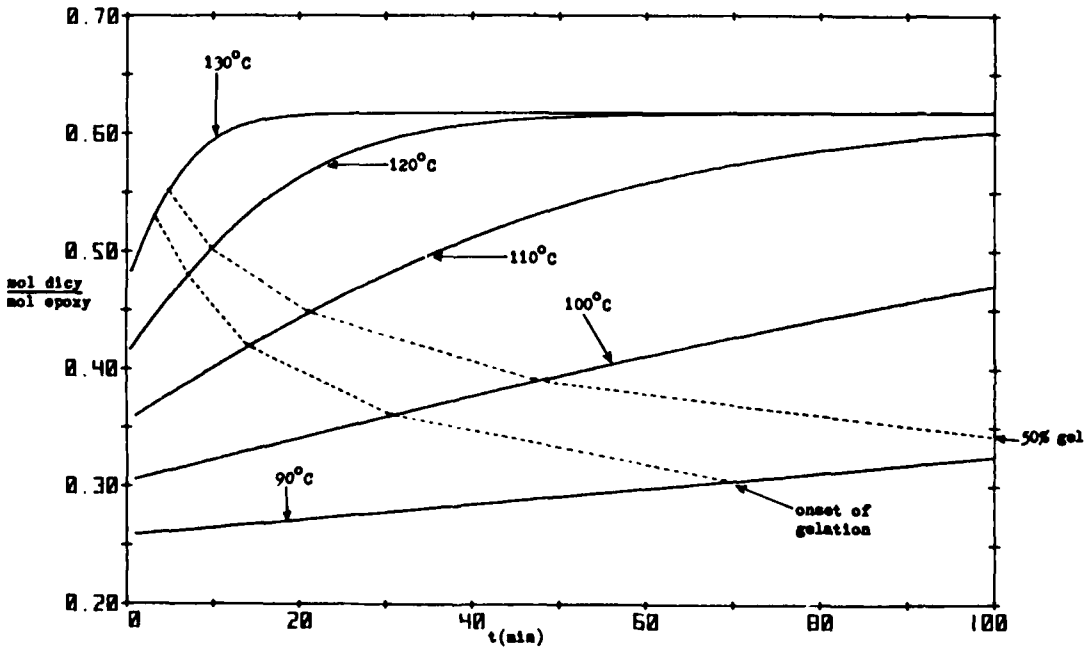

Figure 14. Plot of mole ratio of dicy/epoxy components reacted versus reaction time at different temperatures.

A special computer program was written which uses rate equations derived from the isothermal curing study to calculate changes in the composition of the SP250 resin with programmed changes in temperature. Predicted concentrations were comparable to experimental values (e.g., within 2-3 wt % for the epoxy components) up to about 60% gelation. The effects of different temperature programming rates on the curing behavior of SP250 were calculated. (Figure 15) The program was used to simulate cure cycles and to correlate changes in prepreg compositon with parameters measured by other cure monitoring techniques. Upon comparing calculated compositional changes with DC resistance measurements over the standard SP250 cure cycle, a sharp upturn in DC resistance is observed to occur at the same time (ca. 65 minutes) when most of the accelerator undergoes reaction. (Figure 16) For isothermal cure curves, the predicted times for the onset of gelation were in exact agreement with the "times to gelation" determined by TBA but did not correlate with the usually designated "gel-point" determined by the DC resistance method. (Figures 17 and 18) Correlations were also made with the DSC cure monitoring technique. (Figure 19)

In summary, chemical changes taking place during the initial stages of cure may be described in considerable detail using HPLC techniques. Correlations between changes in prepreg compositon and parameters measured by other cure monitoring techniques are essential in establishing cure monitoring criteria. Currently, advanced chromatographic and spectroscopic techniques are being applied to elucidate the structure of the SP250 resin matrix during the early stages of gelation. (Figures 20 and 21) Since the structure of the resin matrix is quite dependent upon curing conditions, it should be possible to control the matrix structure during curing and then relate structure to changes in the properties of the cure composite.

REFERENCES

1. G. L. Hagnauer and I. Setton, "compositional Analysis of Epoxy Resin Formulations," J. Liq. Chromatogr., 1, 55 (1978).

2. G. L. Hagnauer and D. A. Dunn, "Quality Assurance of an Epoxy Resin Prepreg Using HPLC," Materials 1980, SAMPE 12th National Technical Conference, Seattle, WA (1980).p. 648-655.

3. N. S. Schneider and J. K. Gillham, "TBA Studies of Prepreg Curing Behavior," Polymer Composites, 1, 97 (1980).

4. N. S. Schneider and J. F. Sprouse, G. L. Hagnauer, and J. K. Gillham, "DSC and TBA Studies of the Curing Behavior of Two Dicy-Containing Epoxy Resins," Polymer Eng. & Sci., 19, 304 (1979).

5. G. L. Hagnauer, B. R. LaLiberte, and D. A. Dunn, "Isothermal Cure Kinetics of an Epoxy Resin Prepreg," Org. Coat. & Appl. Polym. Sci. Proc., Am. Chem. Soc., 46, 646-650 (1982).

6. G. A. Senich, W. J. MacKnight, and N. S. Schneider, "A Dynamic Mechanical Study of the Curing Reaction of Two Epoxy Resins," Polymer Eng. & Sci., 19, 313 (1979).

7. R. J. Shuford, unpublished results.

8. S. D. Senturia, N. F. Sheppard, S. Y. Poh, and H. R. Appelman, "The Feasibility of Electrical Monitoring of Resin Cure with Charge-Flow Transistors," Polymer Eng. & Sci., 21, 113 (1981).

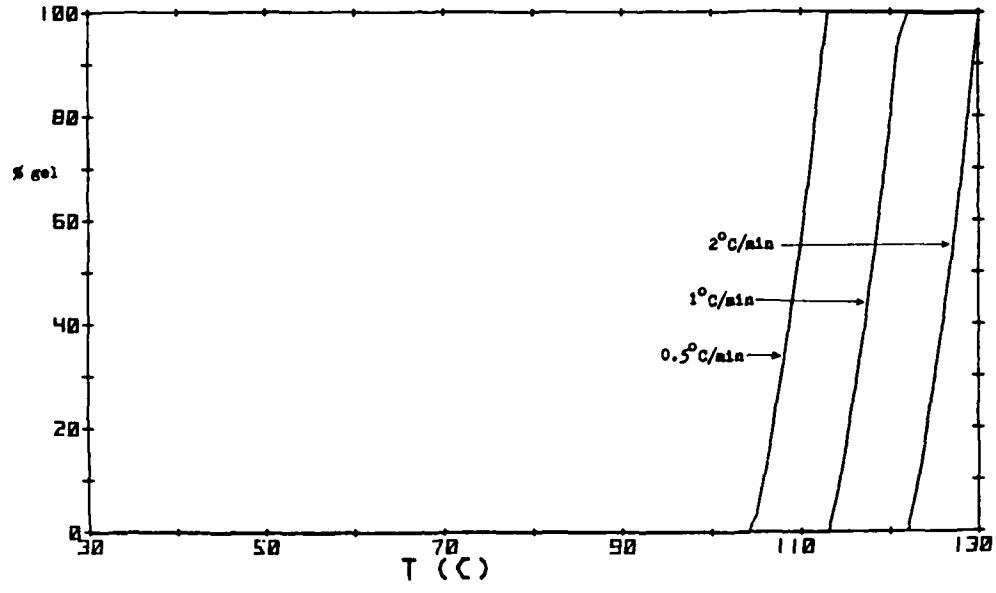

(a)

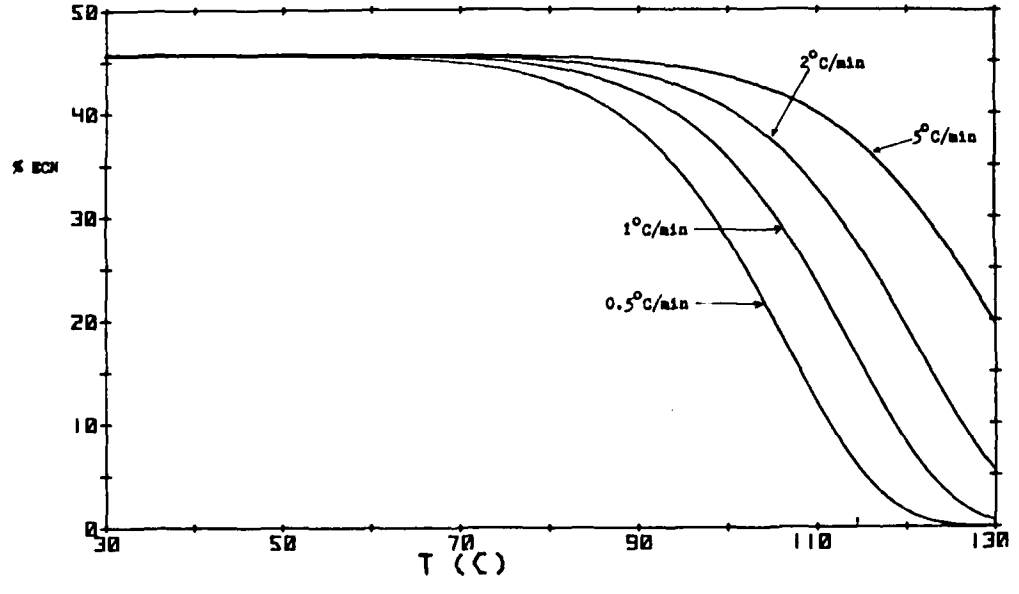

(b)

Figure 15. Effects of heating rate on curing behavior of SP250-S2 prepreg.

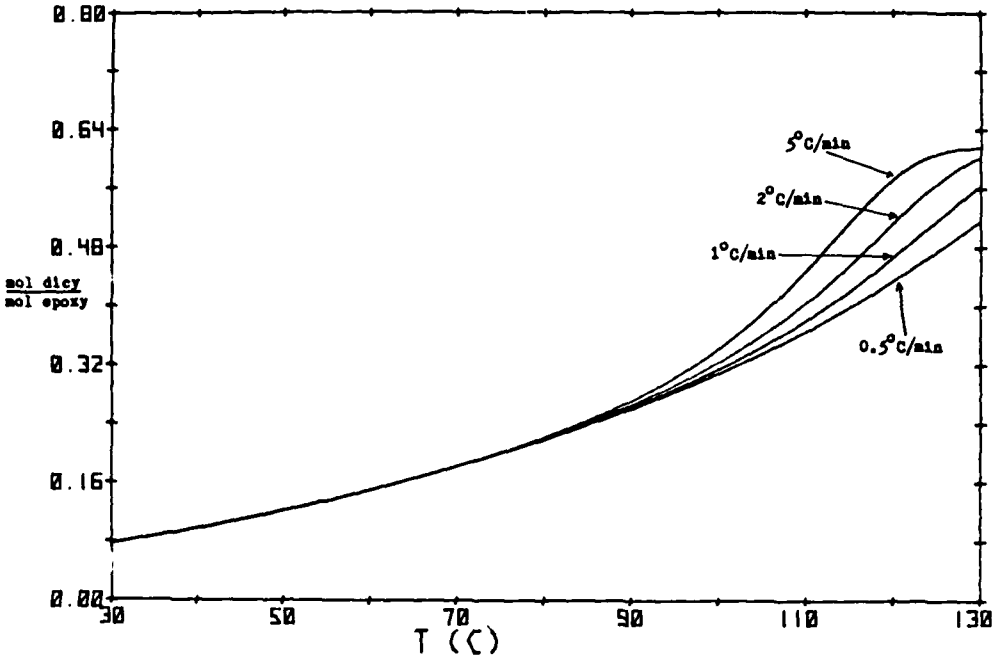

(c)

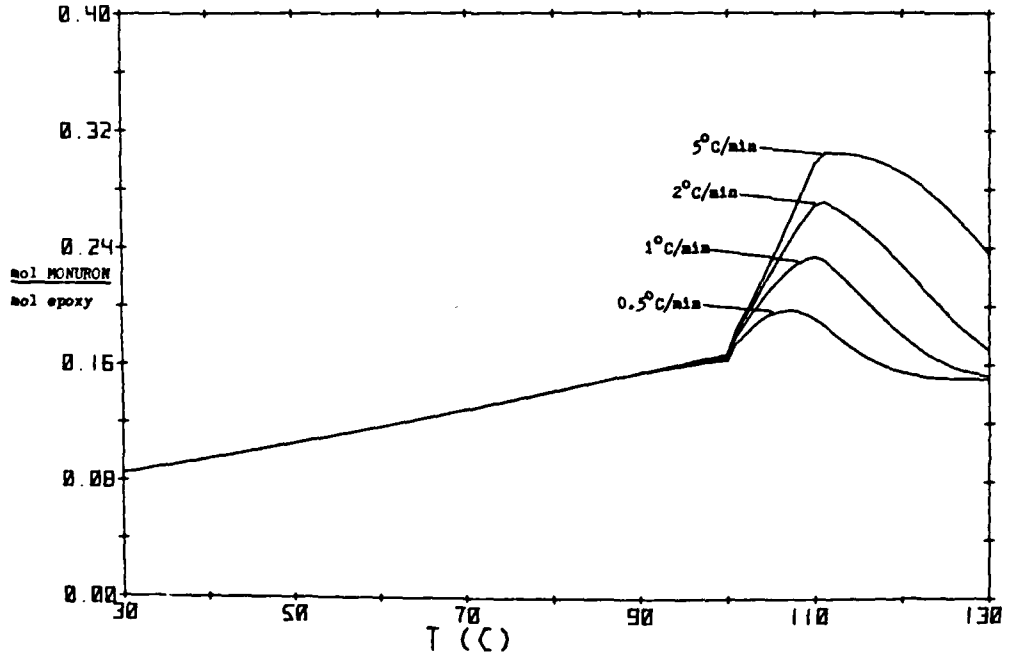

(d)

Figure 15 (cont). *Effects of heating rate on curing behavior of SP250-S2 prepreg.*

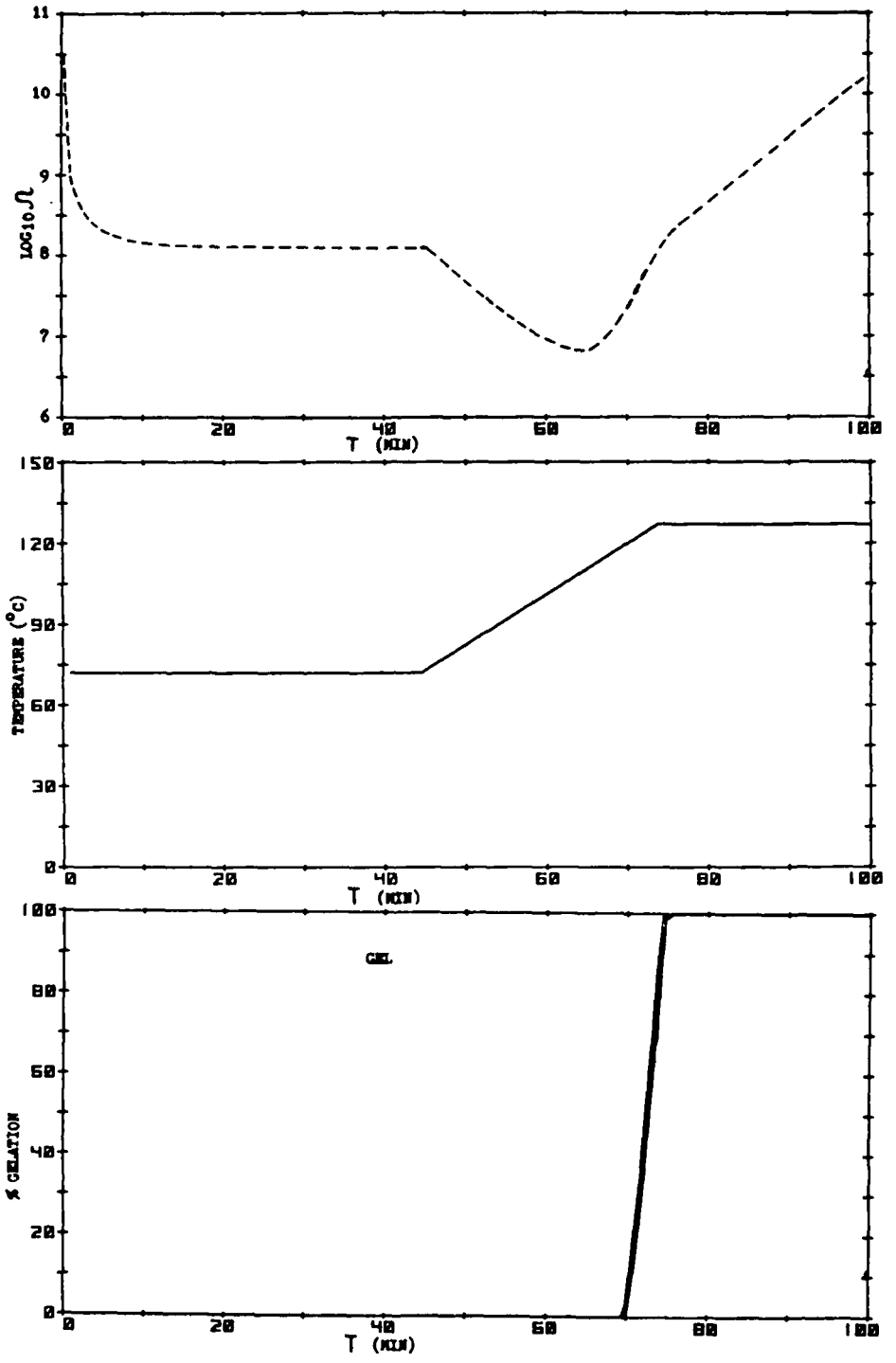

(a)

(b)

(c)

Figure 16. Effect of SP250-S2 prepreg cure cycle (plot b) on dc-resistance measurement Ω (plot a), gel formation (plot c), % resin components unreacted (plot d), mole ratio dicy/epoxy components reacted (plot e), and mole ratio Monuron/epoxy components reacted (plot f).

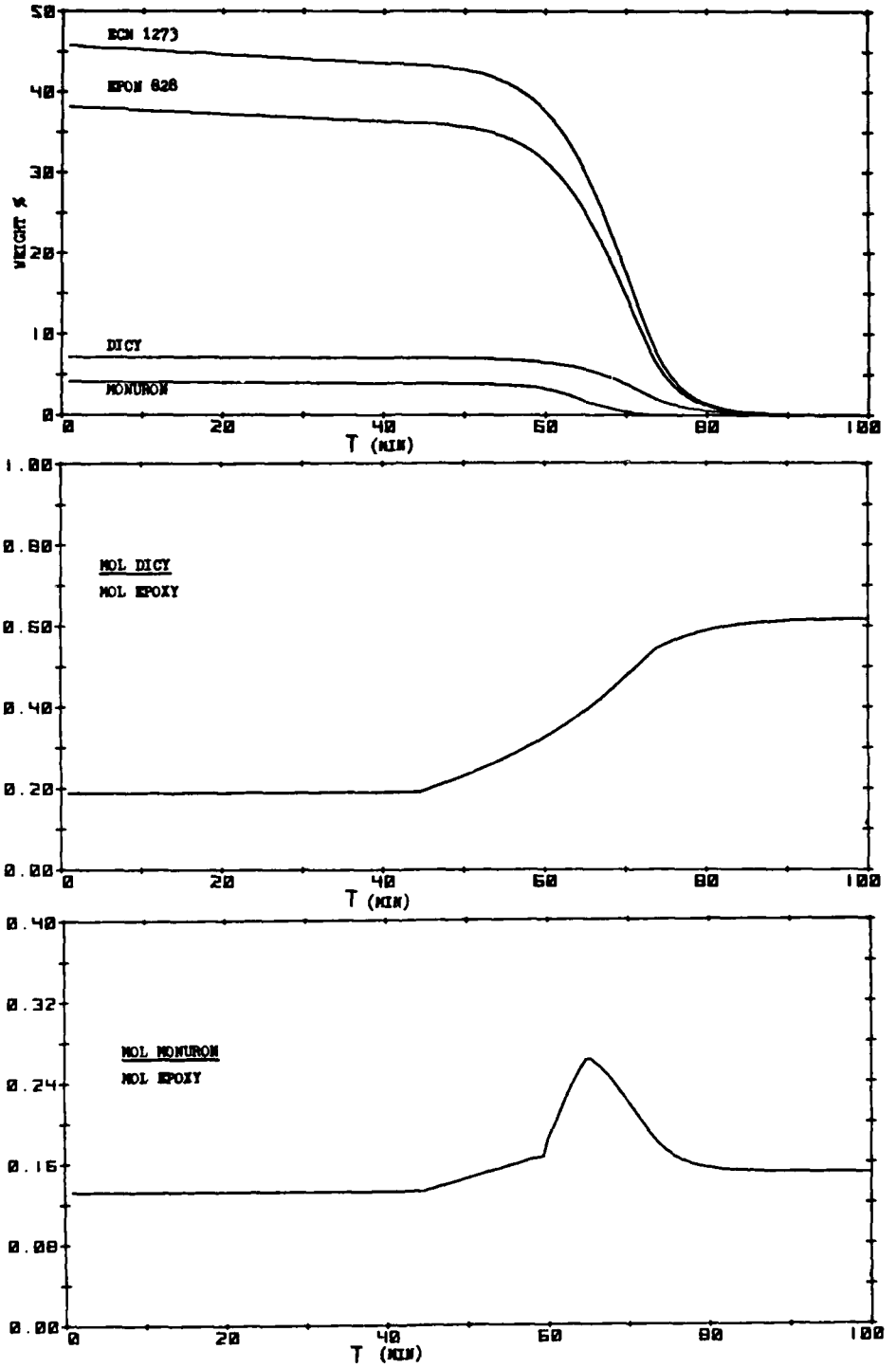

(d)

(e)

(f)

Figure 16 (cont). Effect of SP250-S2 prepreg cure cycle (plot b) on dc-resistance measurement Ω (plot a), gel formation (plot c), % resin components unreacted (plot d), mole ratio dicy/epoxy components reacted (plot e), and mole ratio Monuron/epoxy components reacted (plot f).

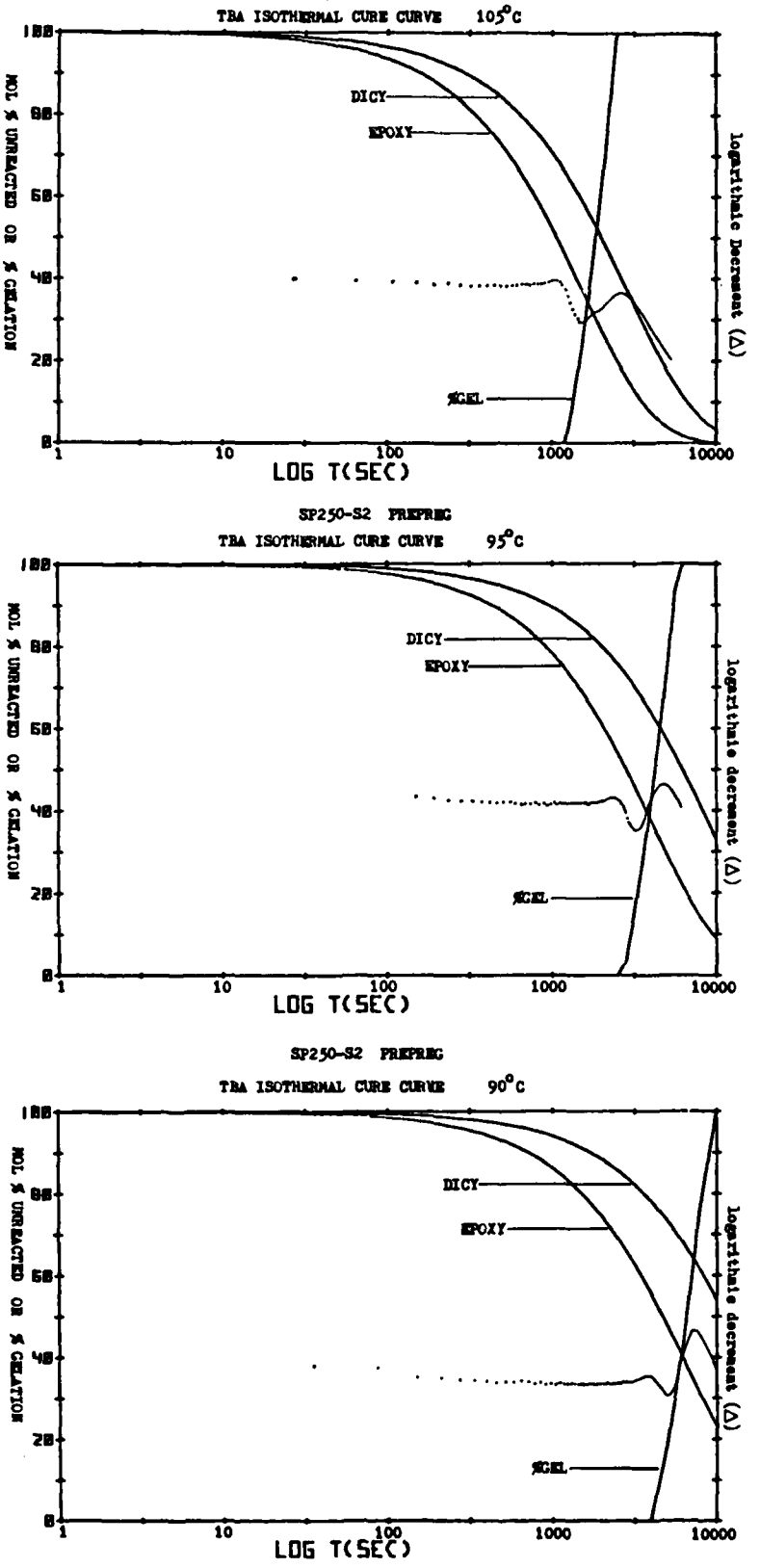

Figure 17. Isothermal cure monitoring using torsional braid analysis (TBA) - correlation with compositional changes.

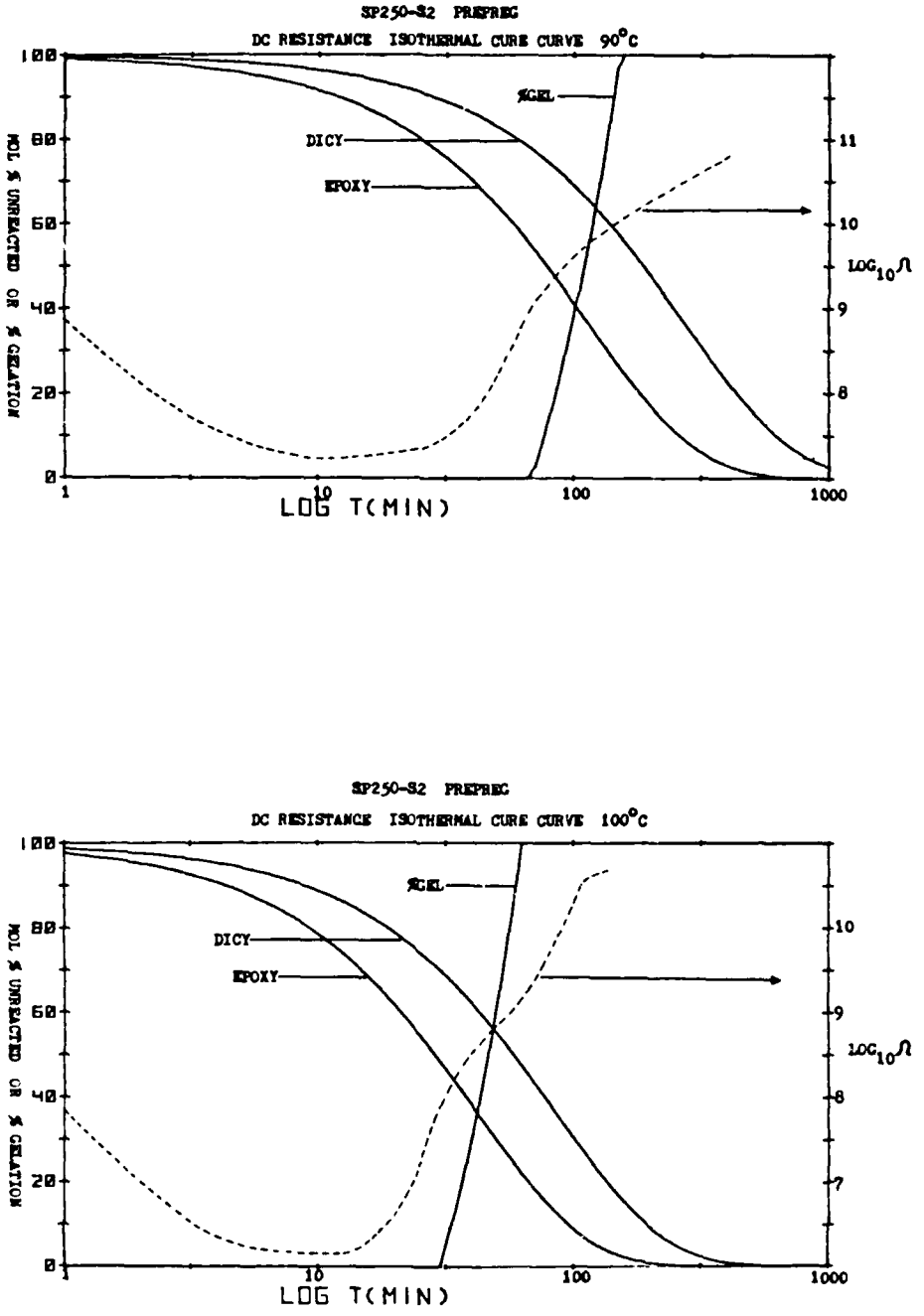

Figure 18. Isothermal cure monitoring using dc-resistance measurements - correlation with compositional changes.

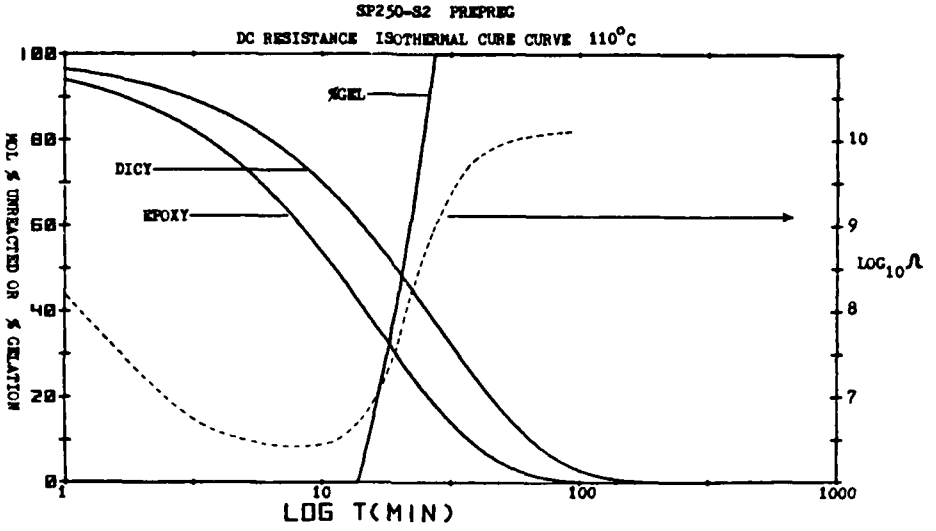

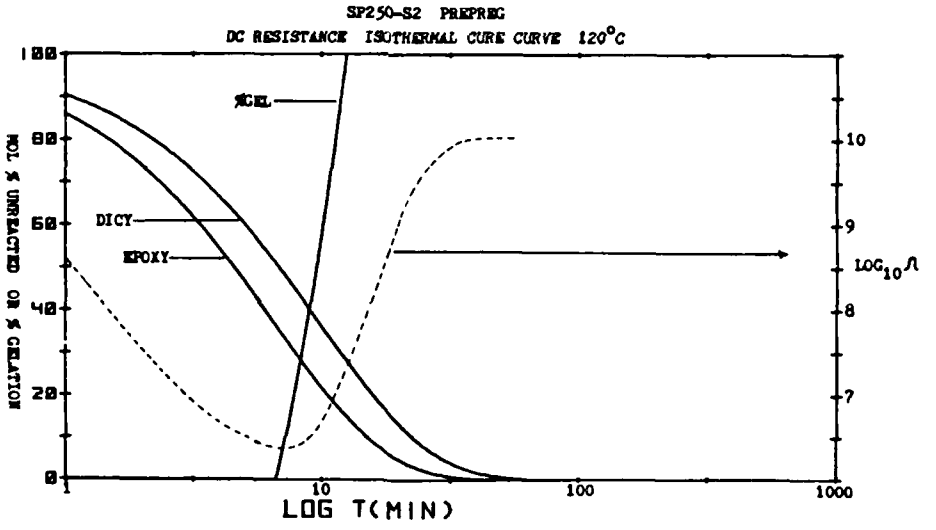

Figure 18 (cont). Isothermal cure monitoring using dc-resistance measurements - correlation with compositional changes.

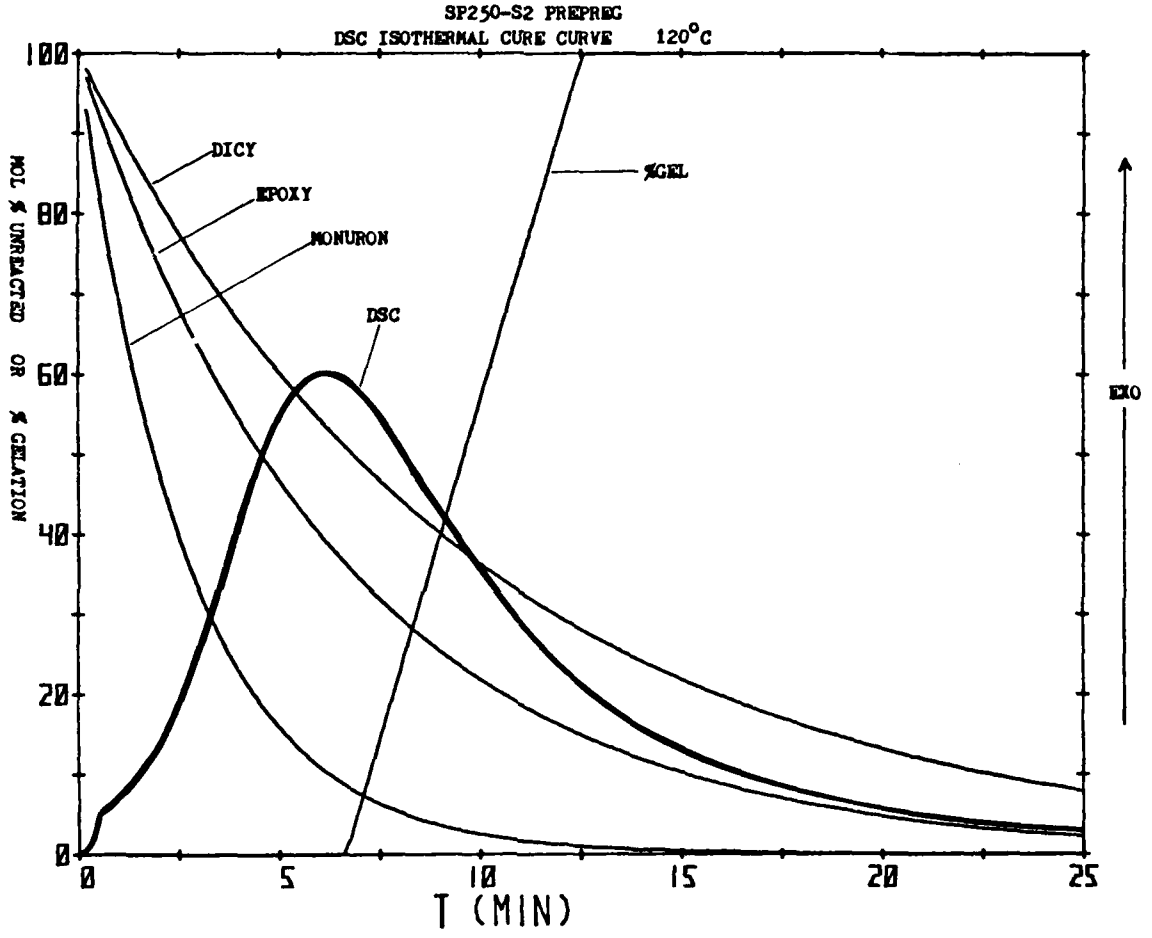

Figure 19. Isothermal cure monitoring using differential scanning calorimetry (DSC) - correlation with compositional changes.

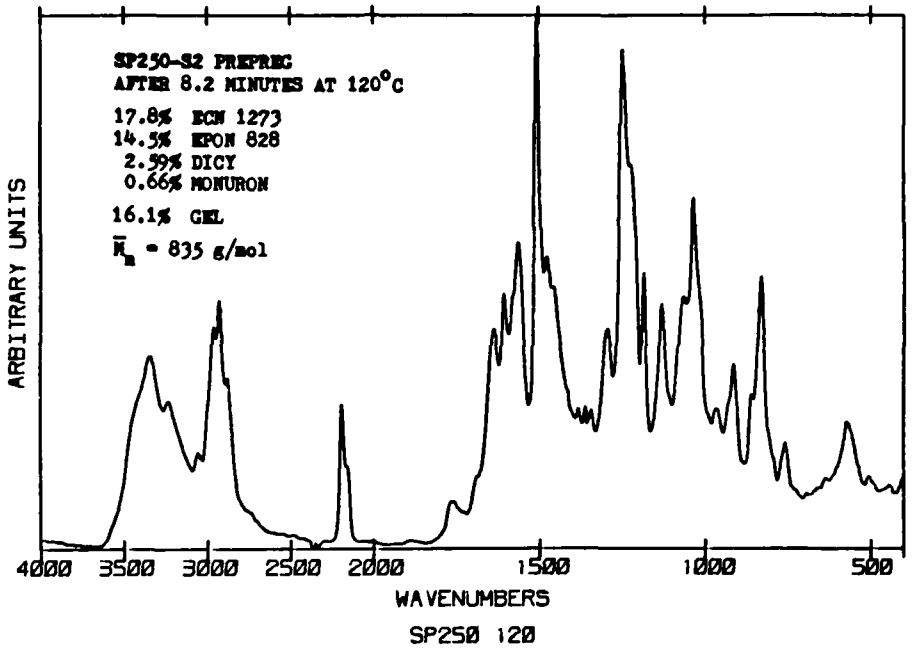

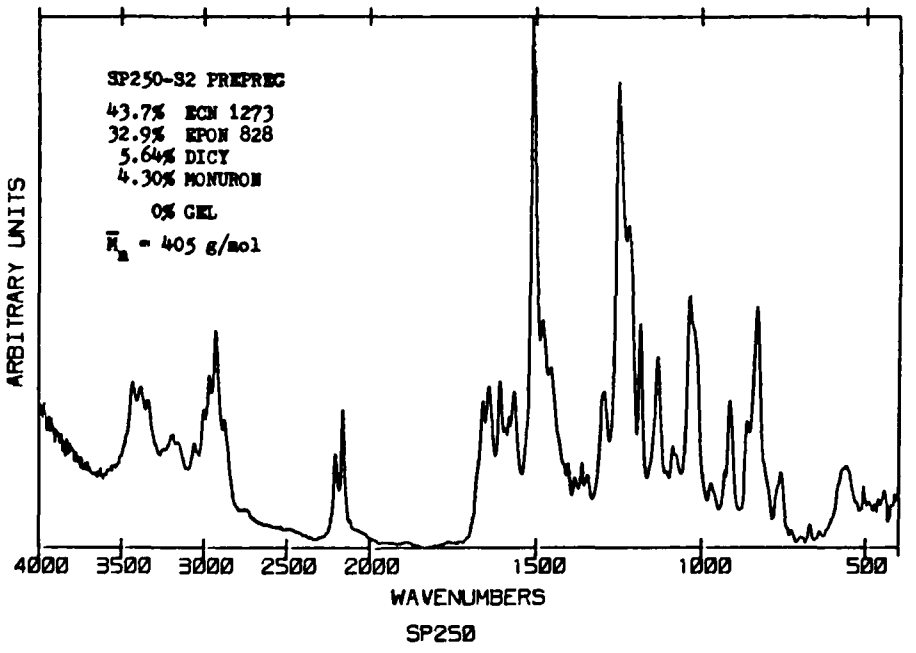

Figure 20. FTIR fingerprints of uncured and partially cured SP250-S2 prepreg. % reaction of components determined by HPLC analysis. Number-average molecular weights (Mn) determined by vapor phase osmometry.

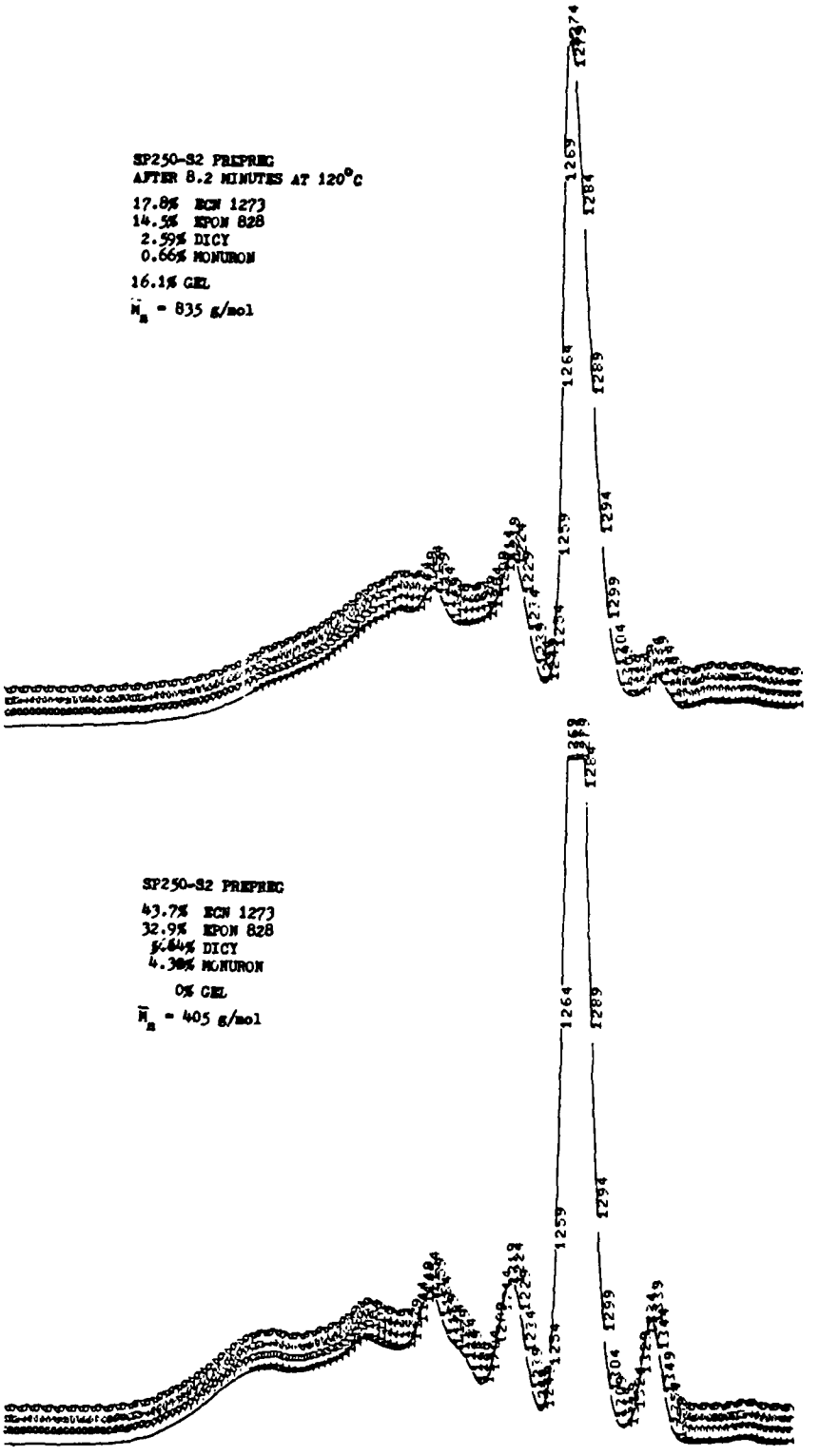

Figure 21. Liquid size exclusion fingerprints of uncured and partially cured SP250-S2 prepreg.

ACOUSTIC EMISSION DURING CURE OF FIBER REINFORCED COMPOSITES

Y. L. Hinton, R. J. Shuford, and W. W. Houghton

Composites Development Division
Army Materials and Mechanics Research Center
Watertown, MA 02172

ABSTRACT

Acoustic emission shows promise as an in-process quality control technique for monitoring the cure of fiber-reinforced laminates. Acoustic emission (AE) data (including events, counts, count rate, rms, and amplitude distribution) and dc-resistance data were collected during the cure (heating) and cool-down of 6-ply SP250/S glass and Fiberite 934/kevlar 49 prepreg laminates. Acoustic emission appears to be very sensitive to microstructural changes in laminate occurring during the cure. The AE observed during the heating phase is thought to be due to outgassing of the resin and cure shrinkage (caused by polymerization/cross-linking), whereas the AE during cool-down is due to residual stresses created in the laminate because of the mismatch in coefficients of thermal expansion between the fiber and the resin. Under identical experimental conditions, kevlar/epoxy laminates produced significantly more counts with higher amplitudes than the glass/epoxy laminates. Correlations were found between the acoustic emission activity, the dc-resistance and the resultant residual stresses.

INTRODUCTION

Acoustic emission as a nondestructive testing technique is becoming widely used for proof testing, defect detection and damage assessment in pipes, tanks, and structural components. Houghton, et al, (1) have investigated the use of acoustic emission during the cure of glass/epoxy systems to predict damage to and subsequent performance of fiber-reinforced composites as a result of the manufacturing process. This paper reviews that work, extends the study to Kevlar/epoxy systems, and investigates pulse/attenuation monitoring during cure.

EXPERIMENTAL

Two composite systems were used in this study: SP250/E-glass and Fiberite 934/Kevlar 49. The SP250 resin is a diglycidyl ether of bisphenol A (DGEBA)/Epoxy Cresol Novolac (ECN) cured with dicyandiamide and Monuron. It has a cure temperature of 122°C. Fiberite 934 is a tetraglycidyl methylene dianiline (TGMDA) cured with diaminodiphenyl sulfone (DDS) and BF_3MEA. Its temperature is 177°C. Six-ply unidirectional laminates were hand layed up and faced with 4" x 1" aluminum coated Kaptan (polyimide) electrodes. The laminates were placed between layers of 1 mil Tedlar (polyvinyl fluoride) film, and between 1/4" aluminum caul plates. A thermocouple was inserted between the top caul plate and the Tedlar film. This assembly was placed in a nylon vacuum bag, and then inserted in a Tetrahedron Pneuma Press with a layer of 5-mil Teflon film between the vacuum bag and the platens of the press (see Figure 1).

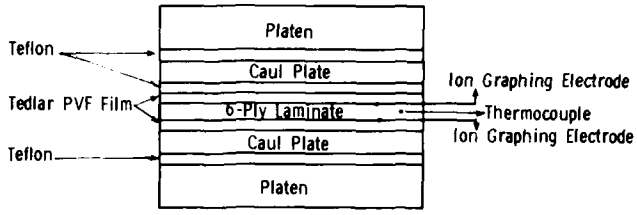

Figure 1. LAYUP CONFIGURATION FOR PRESS CURE

A 6-volt battery was connected in series with the aluminum coated Kaptan electrodes, and the dc-amplifier of the strip-chart recorder (see Figure 2). This allows measurement of current through the 1-MΩ internal resistance of the amplifier, an indication of dc-resistance of the laminate. This signal is used to determine the correct time to apply pressure to the laminate.

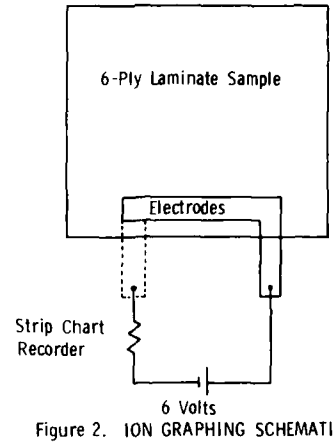

Figure 2. ION GRAPHING SCHEMATIC

The cure cycles are:

1. Apply vacuum and 20 psig.
2. Raise temperature to 77°C for SP250/E-glass, 122°C for Fiberite 934/Kevlar; hold for 30 minutes.
3. Raise temperature to 122°C for SP250/E-glass, 177°C for Fiberite 934/Kevlar; hold for two hours.
4. Increase pressure to 50 psig when ion graphing signal decreases.
5. Cool.

The press is water cooled at 1-2°C per minute for two hours.

Figures 3 and 4 show a photograph and a block diagram of the Dunegan Endevco Series 3000 Acoustic Emission system used in this study. A high temperature DE Model D9205M2 transducer mounted in the bottom caul plate was used to detect AE signals. A silicone vacuum grease was used as the couplant. The transducer response is 100-300 kHz with a peak at 180kHz. The signal is then routed to a DE1801 preamplifier

(40 dB gain) with a 170B filter (118-236 kHz at -3 dB points). A 302 dual signal conditioner amplifies the filtered signal (50 dB during cure, 40 dB during cooling) and routes it to a counter, amplitude detector and RMS/TMS module.

A model 303 dual counter counts pulses above an internally set 1V (120 dB) threshold, and measures count rate with a 0.2-second time base set by the 402 reset clock. The model 921 amplitude detector detects events above a 30 dB (+ system gain) threshold, and routes them to a model 920 distribution analyzer, which outputs counts vs amplitude to a Textronix monitor. An AET (Acoustic Emission Technology) model 404 RMS/TMS module monitors TMS of the AE signal, which is directly proportional to energy. The TMS, counts and/or count rate are recorded on a Gould 4-channel strip chart recorder, as are temperature and ion graphing voltage.

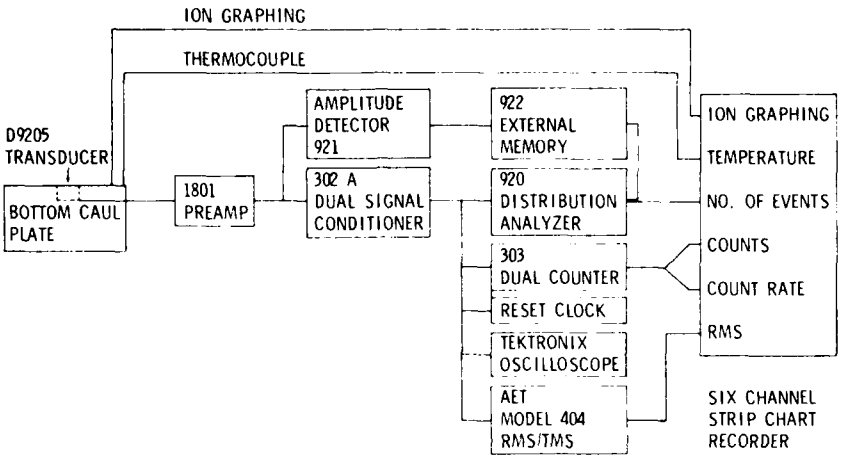

Figure 3. BLOCK DIAGRAM OF ACOUSTIC EMISSION/CURE MONITORING SYSTEM

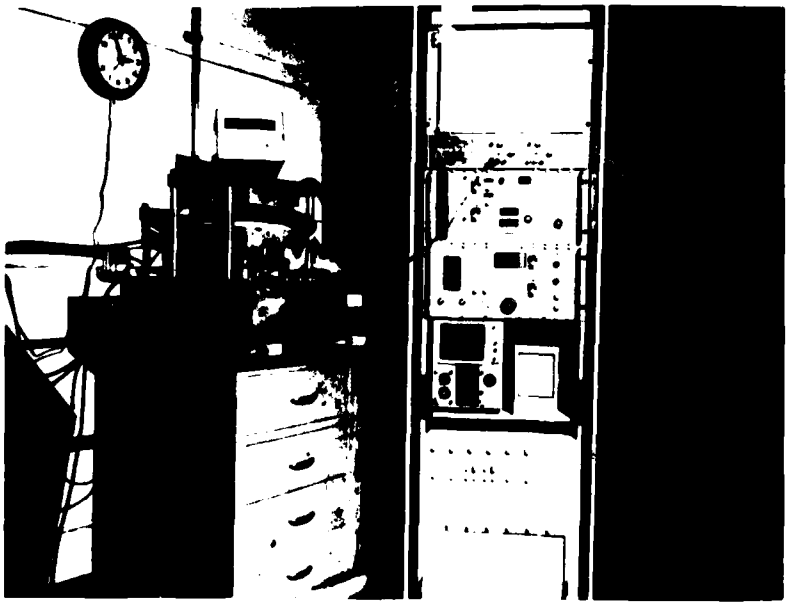

Figure 4. ACOUSTIC EMISSION INSTRUMENTATION

PULSE ATTENUATION STUDIES

Figure 5 shows a block diagram of the system used to monitor attenuation of simulated AE events. A DE S140B/HS transducer mounted in the top caul plate, and connected to a model 908 pulser with 3.5 Vdc power supply, pulsed the laminate 100 times per minute. The amplitude of the signal received by the transducer in the bottom caul plate was monitored during the entire cure cycle. Amplitude distribution (counts vs amplitude) was displayed on the Tektronix monitor and a hard copy taken on a Hewlett-Packard X-Y recorder at 2000-event intervals. Because of the lower temperature capability of the S140B/HS transducer, both the Kevlar and glass/epoxy laminates were cured at 122°C.

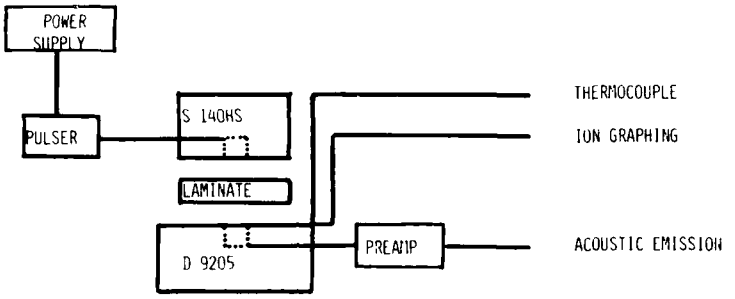

Figure 5. BLOCK DIAGRAM OF ACOUSTIC EMISSION/CURE MONITORING SYSTEM

RESULTS

AE Produced During Cure Cycle

Houghton found an increase in AE activity with an increase in temperature during the early part of the cure of SP250/E glass laminates (see Figure 6). There was a more significant increase in AE activity with the second temperature increase, from 77°C to 122°C. AE activity then quieted down until pressure was increased, and dropped off as temperature was held constant. The early activity is likely caused by outgassing of the resin, and the latter activity by cure shrinkage of the resin relative to the fiber. E-glass has a thermal coefficient of expansion an order of magnitude less than that of the epoxy; Kevlar 49 has a negative coefficient of thermal expansion (see Table 1).

Table 1. COEFFICIENTS OF THERMAL EXPANSION ($°C^{-1}$)

Temperature (°C)	Fiber			Epoxy	
		Kevlar 49			
	E Glass	(Axial)	(Radial)	SP 250	934
0 - 100	3.1×10^{-6}	-2×10^{-6}	60×10^{-6}	42×10^{-6}	50×10^{-6}
100 - 200	9.4×10^{-6}	-4×10^{-6}	-	52×10^{-6}	60×10^{-6}

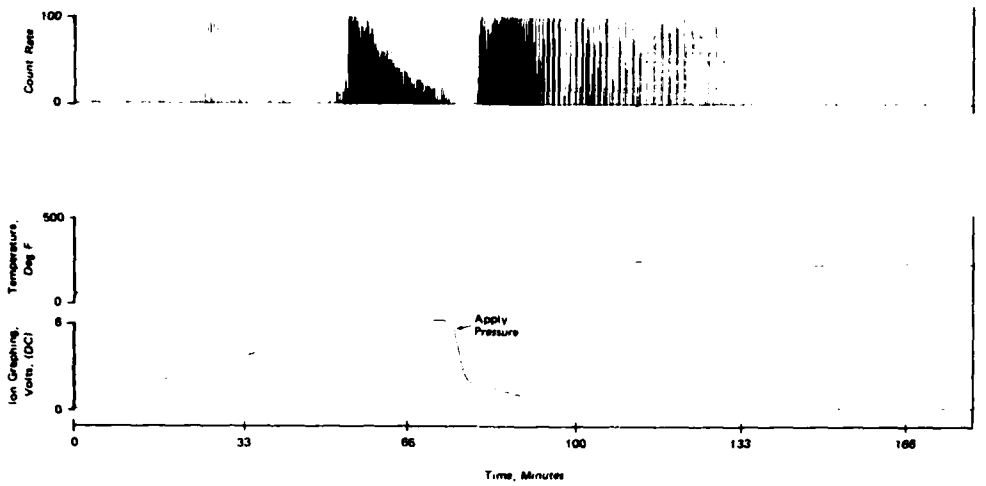

Figure 6. TYPICAL ACOUSTIC EMISSION/ION GRAPHING RESULTS FOR CURE OF SP250/E GLASS LAMINATE

Typical amplitude distributions obtained at the end of cure (prior to cooling) for both unidirectional glass and Kevlar laminates are shown in Figures 7 and 8. Most of the counts observed with the glass laminate are below 50 dB, with very few at higher amplitudes. The Kevlar laminate also showed most of the counts at less than 50 dB, but there are a greater number of low amplitude events, and a significant number of high amplitude counts around 100 dB.

Houghton also found that a faster cooling rate, 2°F/min vs. 0.5°F/min, produced greater AE counts (see Figure 9) with only slight changes in mechanical properties (see Table 2). The greatest change was in radius of curvature of a fully cured laminate, artificially unbalanced by pulling off two 90° plies, and allowed to bend under the differential contractive strain of the remaining 0° and 90° lamina. The greater radius of curvature in the fast cooled specimens indicates lower residual stresses. Microcracking and plastic deformation of the matrix have probably relieved much of the stress and caused the increase in AE activity. During cooling, no AE activity was detected until the temperature had decreased to ~90°C. Until this point, the material is apparently viscoelastic enough that any induced stresses may be relieved before damage to the material can occur. Subsequent AE activity is relatively infrequent. Figure 10 shows typical AE data obtained during the cool down of glass/epoxy laminate; Figure 11 shows typical results obtained during the cooling of Fiberite 934/Kevlar 49 laminate. AE activity was not observed until the temperature had decreased to approximately 150°C. It is apparent from Figures 12-14 that Kevlar laminates gave significantly more AE than the glass/epoxy laminates. Amplitude distributions (plotted near the end of the cool cycle) show that Kevlar laminates produced significantly more higher amplitude events (50-85 dB) than did the glass laminates. Visual examination of the Kevlar laminates after cooling revealed large longitudinal cracks. The negative coefficient of thermal expansion for Kevlar induces sufficient internal stresses to cause Fiber/matrix debonding and even fiber breakage.

Table 2. EFFECT OF COOLING RATE ON MECHANICAL PROPERTIES OF SP250/E GLASS COMPOSITE (90/90/0)S

	Fast 2 F/min	Slow 0.5 F/min
Initial Modulus $X10^6$ psi	3.49	3.34
Tensile Strength $X10^4$ psi	5.13	4.72
Radius of Curvature (in.)	9.81	9.23
Volume Percent Fiber	54.53	55.31
Void Volume %	0.36	0.38

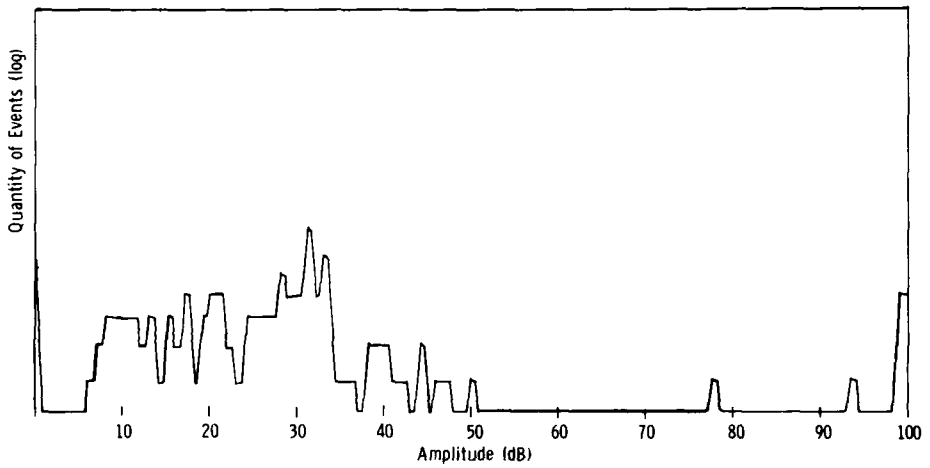

Figure 7. TYPICAL AMPLITUDE DISTRIBUTION FOR CURE OF SP250/E GLASS LAMINATE AFTER CURE AT 250°F FOR 2 HOURS, 118 EVENTS, 2530 COUNTS

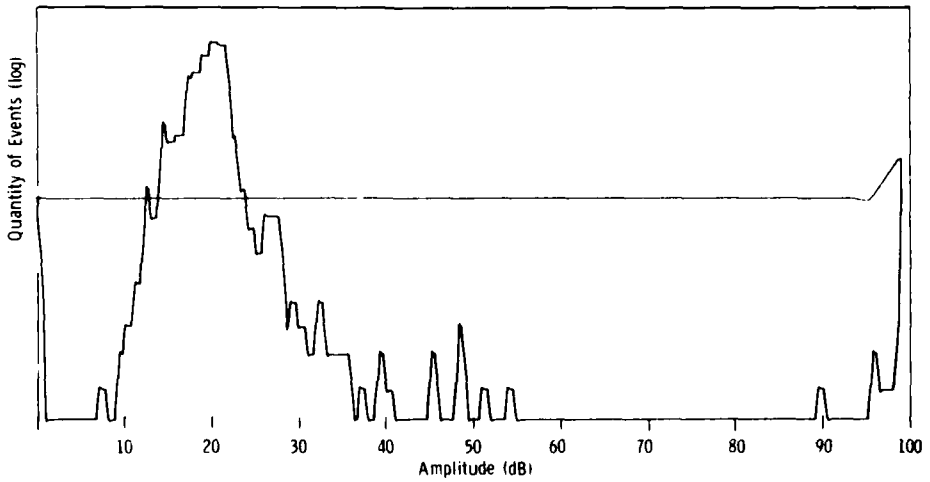

Figure 8. TYPICAL AMPLITUDE DISTRIBUTION FOR CURE OF FIBERITE 934/KEVLAR 49 LAMINATE AFTER CURE AT 350°F FOR 2 HOURS, 595 EVENTS, 2160 COUNTS

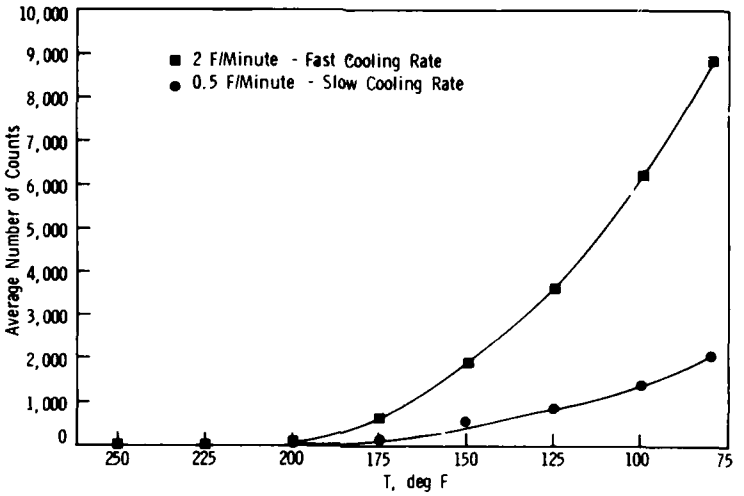

Figure 9. ACOUSTIC EMISSION DURING COOL DOWN OF SP250/E GLASS LAMINATE

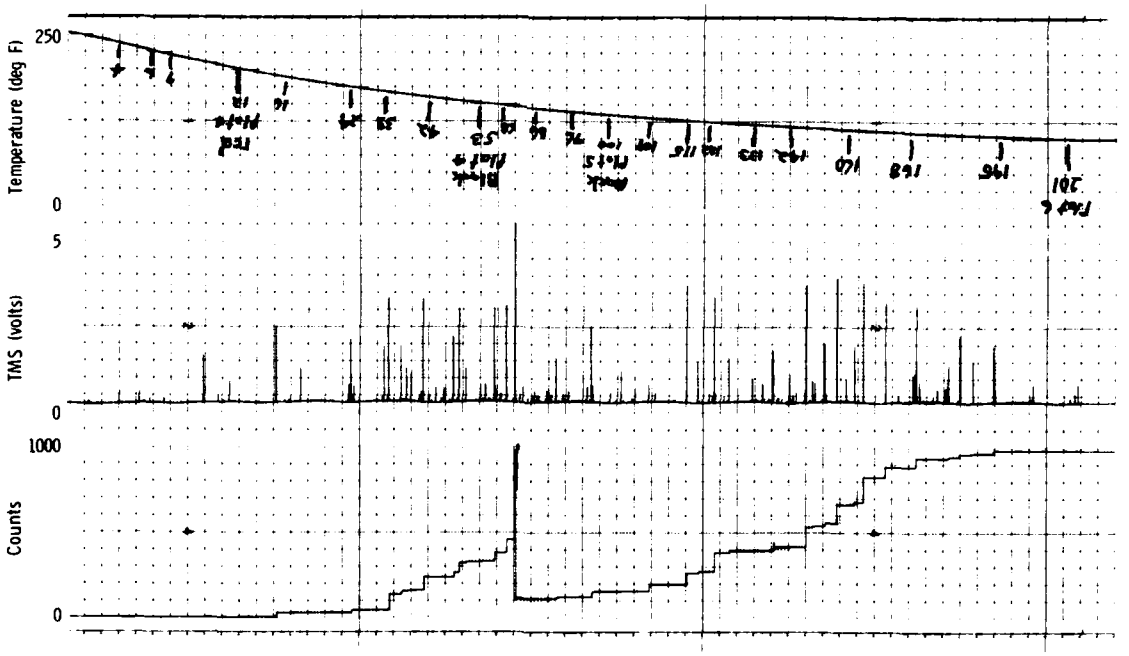

Figure 10. TYPICAL ACOUSTIC EMISSION DATA OBTAINED DURING COOL DOWN OF SP250/E GLASS LAMINATE

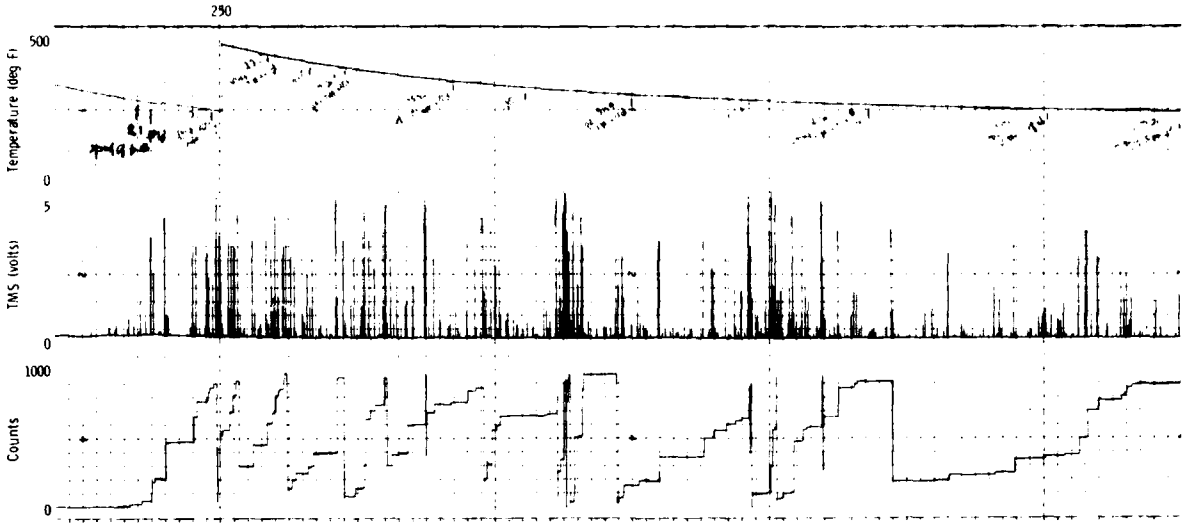

Figure 11. TYPICAL ACOUSTIC EMISSION DATA OBTAINED DURING COOL DOWN OF FIBERITE 934/KEVLAR 49 LAMINATE

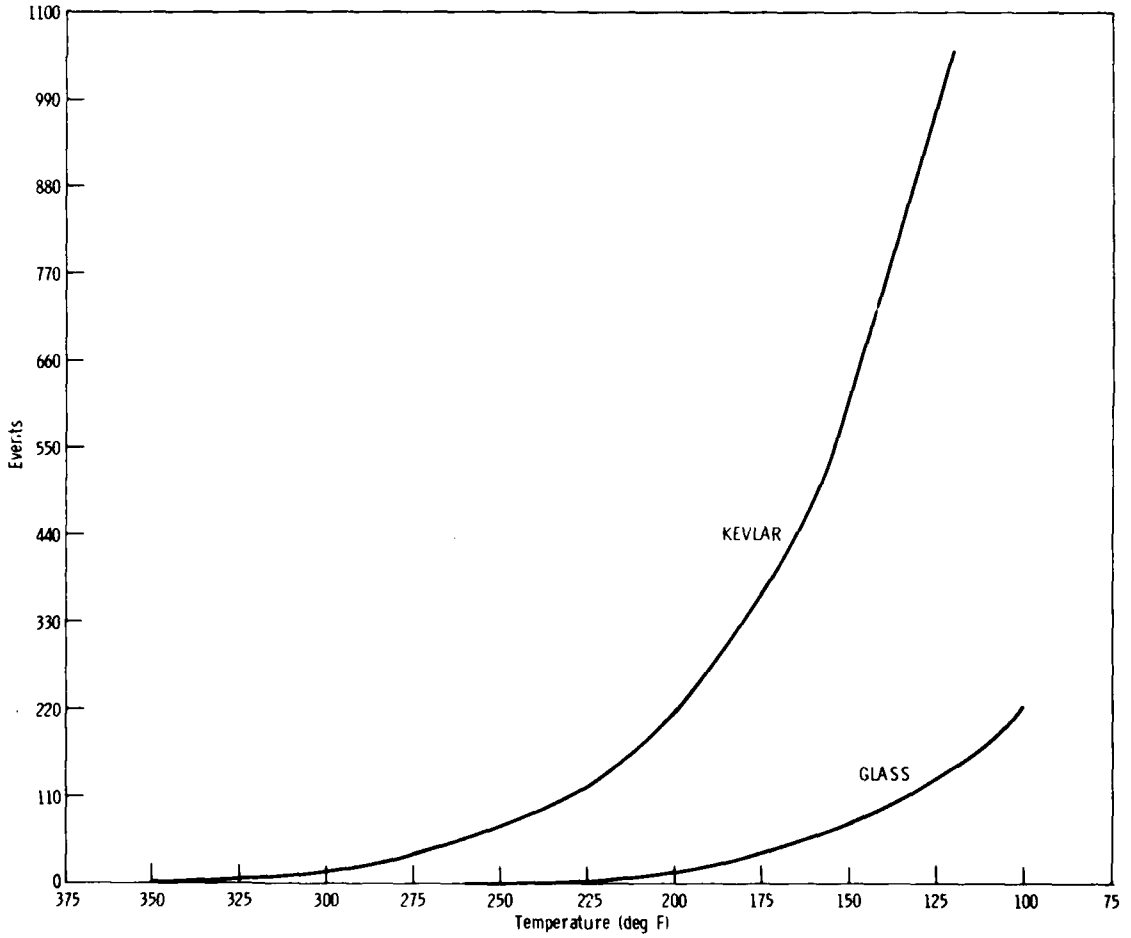

Figure 12. ACOUSTIC EMISSION DURING COOL DOWN OF SP250/E GLASS AND FIBERITE 934/KEVLAR 49 LAMINATE

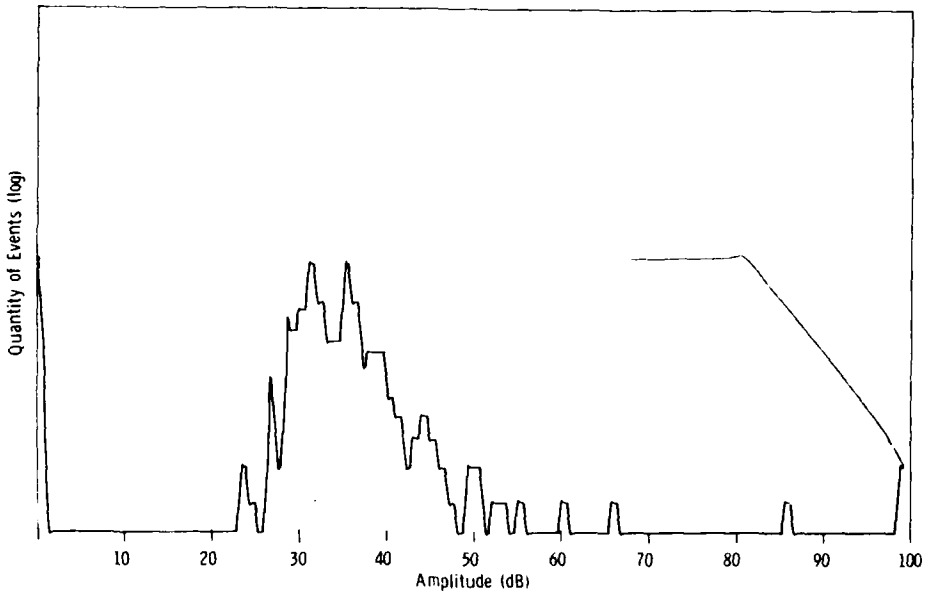

Figure 13. TYPICAL AMPLITUDE DISTRIBUTION FOR CURE OF SP250/E GLASS AFTER COOL DOWN (2-3°F/min) TO 100°F, 201 EVENTS, 1992 COUNTS

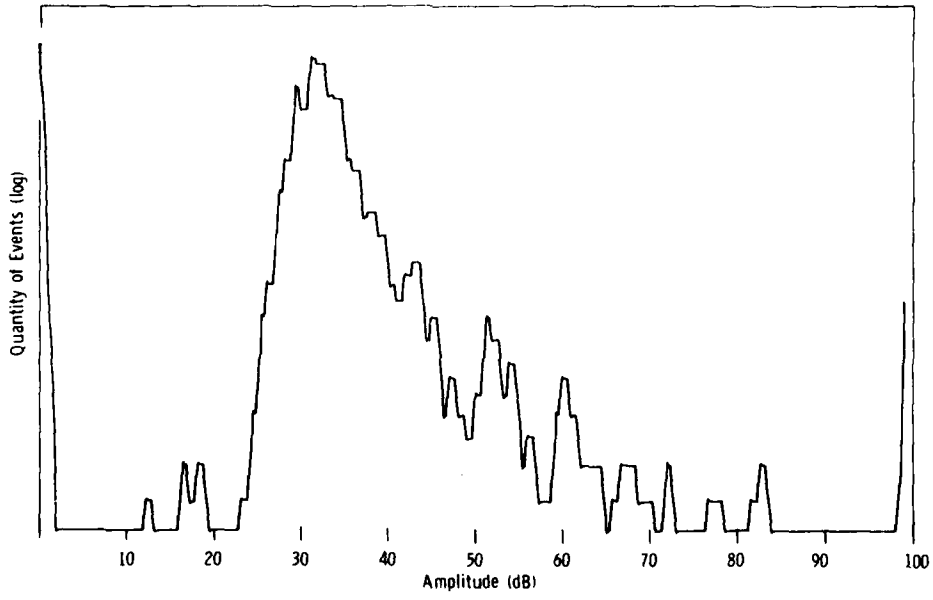

Figure 14. TYPICAL AMPLITUDE DISTRIBUTION FOR CURE OF FIBERITE 934/KEVLAR 49 LAMINATE AFTER COOL DOWN (2-3°F/min) TO 120°F, 1067 EVENTS, 21910 COUNTS

Pulse Attenuation Studies

Typical pulse attenuation and ion graphing results for cure of SP250/E-glass laminates are shown in Figure 15. The amplitude of the received pulse decreases during the early part of the cure cycle as temperature is raised, held and raised again. At the point where the ion graphing signal decreases, the pulse amplitude increases. This is at or near the resin gel points where the chemical reactions accelerate. The pulse amplitude increases to nearly its original value and levels off during the remainder of the cure cycle. It begins to fall again as the temperature decreases during the cooling stage. Pulse amplitude data for the cure of 934/Kevlar 49 laminates, Figure 16, show the same general trends. These laminates were never heated to the recommended cure temperature of 177°C because the pulser transducer has a maximum working temperature of only 122°C. The laminate, therefore, never fully cures, and the pulse amplitude continues to rise throughout the 122°C hold stage of the cure cycle. Pulse amplitude does again decrease slightly as the laminate is cooled.

An amplitude distribution plot taken for 2000 events during heat-up of a glass/epoxy laminate, Figure 17, shows the shift in pulse amplitude from 52 dB to 40 dB. The amplitude distribution plot for 2000 events during cool down, Figure 18, shows the laminate AE at 30-40 dB, as well as the pulser amplitude at 62-63 dB.

CONCLUSIONS

The present work further substantiates Houghton's conclusions that AE during cure is likely caused by outgassing of the resin and cure shrinkage, while AE during cooling is largely a result of mismatched thermal coefficients of expansion leading to microcracking of the matrix. Especially in the cure of Kevlar/epoxy composites where thermal coefficients are opposite in sign, precautions must be taken to prevent longitudinal cracking of the composites.

The pulse attenuation studies indicate that the method, like ion graphing, may be useful in monitoring the cure cycle, particularly in determining the point where pressure should be applied and the point where the laminate is fully cured. The technique used allows monitoring of AE produced during cure, as well as the attenuation changes. The former indicates the viscosity of the resin, and the degree of cure, while the latter indicates damage caused by internal and residual stresses. When used in conjunction with other techniques such as ion graphing, and results of chemical, FTIR spectroscopy and other studies, we now have the tools to fully monitor the cure cycle of fiber-resin systems.

ACKNOWLEDGEMENTS

The authors gratefully acknowledge the assistance of Michael Gostanian and Steven Schultz in preparation and monitoring of the laminates, Technical Reports Office for preparation of figures and tables, and Cheryl Pokornicki for typing of this manuscript.

REFERENCES

1. HOUGHTON, W. W., Shuford, R. J., and Sprouse, J. F., "Acoustic Emission as an Aid for Investigating Composite Manufacturing Processes," New Horizons - Materials and Processes for the Eighties, Volume 11, National SAMPE Technical Conferences Series, 1979.

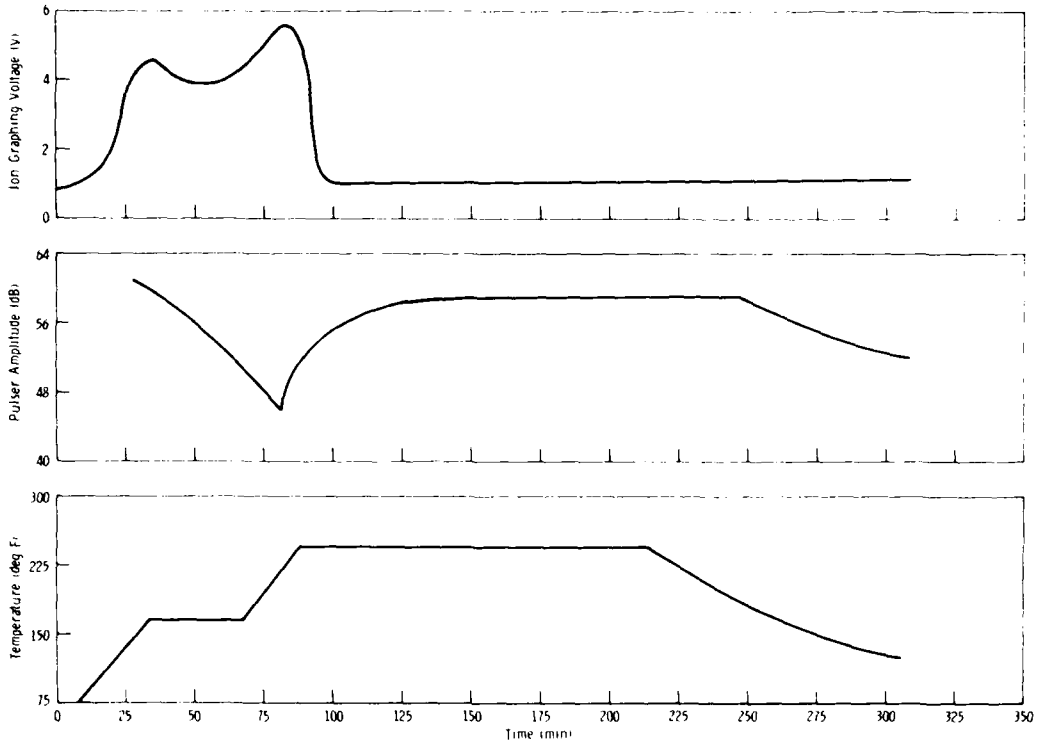

Figure 15. TYPICAL ACOUSTIC EMISSION/ION GRAPHING RESULTS FOR CURE OF SP250/E GLASS LAMINATE

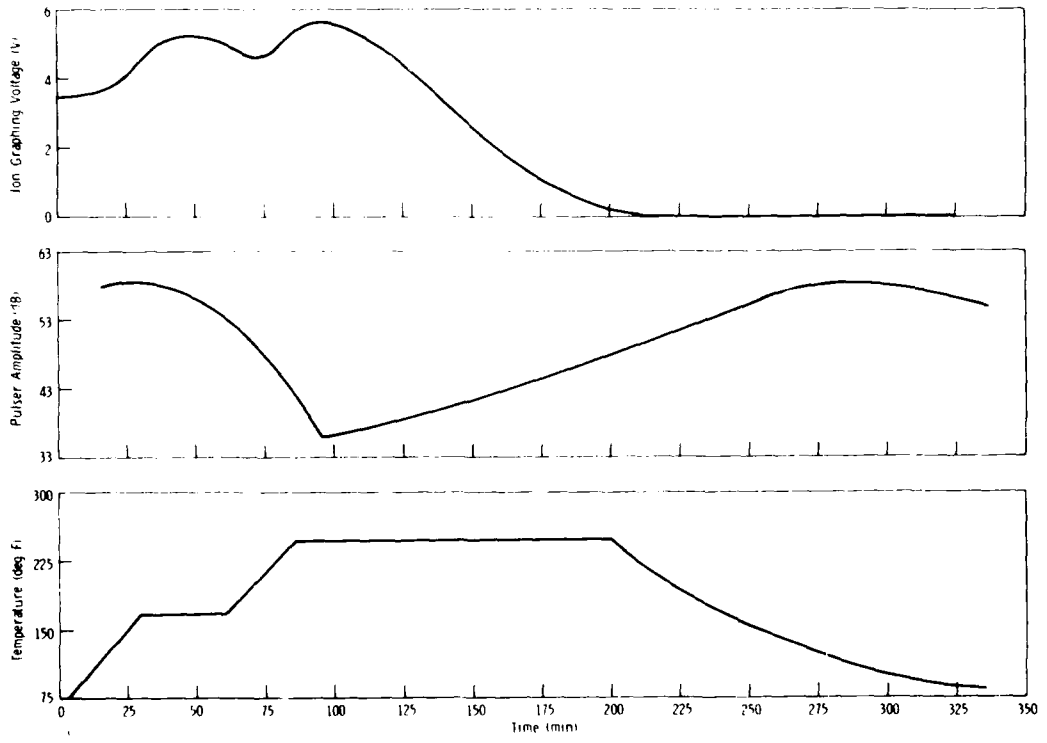

Figure 16. TYPICAL ACOUSTIC EMISSION/ION GRAPHING RESULTS FOR CURE OF FIBERITE 934/KEVLAR 49 LAMINATE

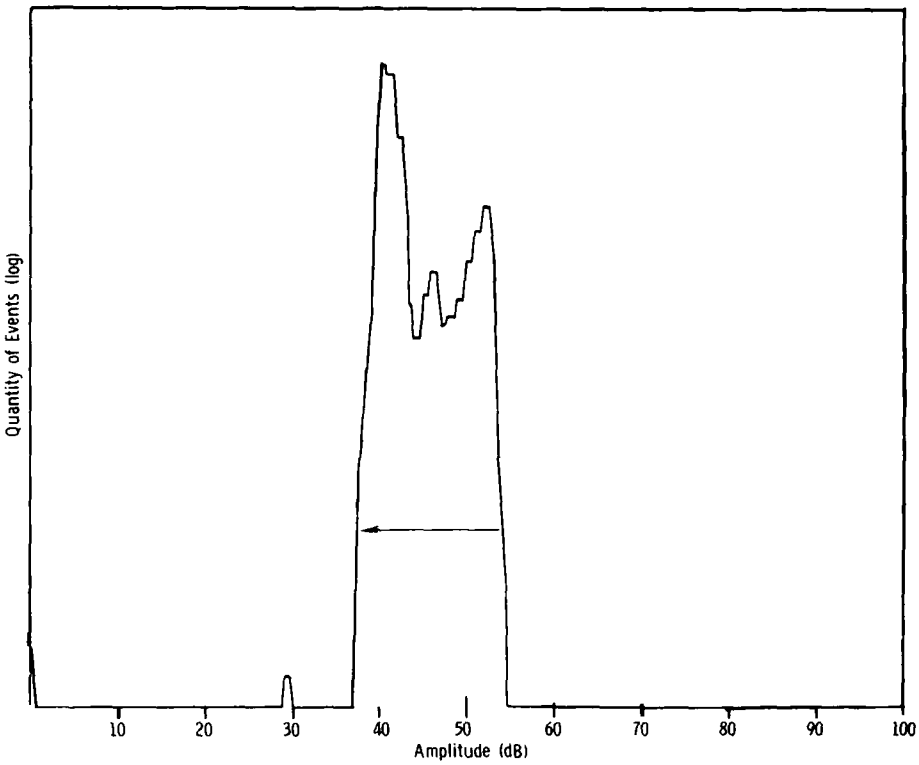

Figure 17. TYPICAL AMPLITUDE DISTRIBUTION/PULSER DATA OBTAINED DURING CURE OF SP250/E GLASS LAMINATE FOR 2000 EVENTS, TEMPERATURE INCREASING FROM 165°F TO 220°F

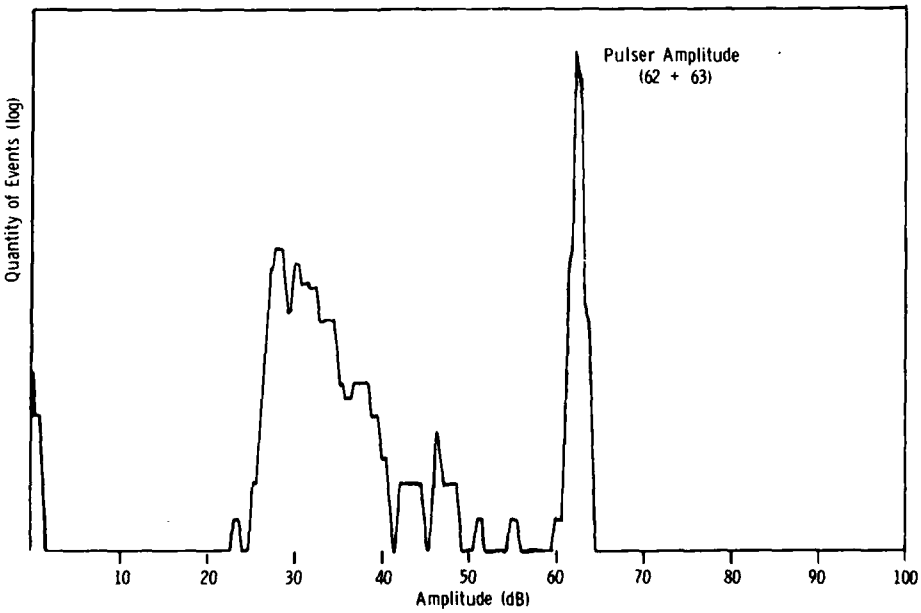

Figure 18. TYPICAL AMPLITUDE DISTRIBUTION/PULSER DATA FOR SP250/E GLASS LAMINATE DURING COOL DOWN (2-3°F/min) FROM 115°F TO 95°F, 2000 EVENTS

AN INTERFEROMETRIC STUDY OF EPOXY RESIN GELATION*

K. R. Hirschbuehler
Sandia National Laboratories**
Albuquerque, New Mexico 87185

Abstract

The transition of epoxy resins from a mobile liquid to a rubbery gel is a complex process depending on chemical reaction kinetics and both heat and mass transfer. The purpose of this study is to determine the locus of initial gelation in an epoxy resin, and the course of gelation through both neat resins and glass fiber/epoxy resin composites. This was accomplished by monitoring the local changes in refractive index in transparent epoxy castings using laser interferometry, supplemented by temperature profiles obtained from thermocouple arrays. These experiments were carried out on pure DGEBA epoxy (DOW DER-332) cured with a variety of primary amine, secondary amine, and anhydride curing agents.

The gelation behavior of DGEBA epoxy was found to depend on the active group of the curing agent. Primary amine curing agents resulted in gelation initiating at the top of the resin sample and then propagating uniformly downward through the resin. Anhydride curing agents caused gelation to initiate at the sample edges and propagate towards the center, while secondary amine curing agents in DGEBA resin showed no abrupt gel transition, only a steady increase in viscosity. For primary amines the time required for the gel front to nucleate was highly variable, having a coefficient of variation of 19.2% between identical experiments. However, the time required for the gel front to pass through the sample was far less variable, with a coefficient of variation of 6.6%. Each of the curing agents evaluated showed one or more pre-gelation transitions. Comparison with the temperature profiles shows that the heat transfer mechanism deviates considerably from pure conduction theory and that convection must be considered. Introduction of glass fibers into the resin affected both the nucleation site for gelation and the gelation path.

*This work was supported by the U.S. Department of Energy (DOE), under contract DE-AC04-76-DP00789.
**A U.S. DOE facility.

I. Introduction

As epoxy resins have come to be used more frequently for thick reinforced structural composites and large encapsulating masses, it has become important to know the course of gelation through the material and the resulting temperature distribution. The purpose of this study is to use laser interferometry to observe the locus of gel initiation and its progress through a sample of clear epoxy. This data is supplemented by temperature profiles of the curing epoxy. Parts of the process have been modeled using conventional heat and mass transfer and reaction formulations.

Much work has already been published on the cure behavior of epoxy resins. The system of primary interest in this study, diglycidylether of bisphenol A (DGEBA) cured with primary amines, has been studied using torsional braid analysis (1), differential scanning calorimetry (2,3,4,5), infrared transmission (6), and by electrical conductivity in conjunction with calorimetry and infrared transmission (7). All these studies employed samples sufficiently small that uniform isothermal conditions could be assumed. The experiments in this study deliberately employ large cubical samples, weighing from 200 g to 800 g, to observe the effects of internal heat generation and convection on the cure behavior. The effect of internal heat generation on the cure of large masses of thermoset resins has been studied (8,9), but only for cases where free convection in the resin could be neglected.

The work presented in this paper deals mainly with experiments on neat epoxy resins. If results are promising, the program will later be expanded to include filled resins.

II. Experimental

A. Materials

The resin employed in all experiments was diglycidylether of bisphenol A (DGEBA), supplied by Dow Chemical Company as DER-332.* Unlike many commercial

formulations, it consists of a single chemical constituent. The resin and all the curing agents were used as received from the manufacturer, and all samples were mixed from the same batch of chemicals.

Three primary amine curing agents were employed: triethylene tetramine (TETA), supplied as Hysol HB 3404; metaphenylenediamine (MPDA), supplied as a 99+% reagent by Aldrich Chemical Co.; and Jeffamine T-403, an aliphatic triamine supplied by the Jefferson Chemical Co. A secondary amine, diethanolamine (DEA), supplied by Dow Chemical Company and an acid anhydride curing agent, NADIC® Methylanhydride (NMA), supplied by MCB Manufacturing Chemists were also used. All curing agents were reacted in stoichiometric proportion to the DGEBA resin. Curing agent amounts and cure temperatures are listed in Table 1.

Prior to reaction, the resin and curing agent were equilibrated at the desired cure temperature. The two components were then mixed in a high speed blender for 30 seconds, evacuated for 5 minutes to remove entrapped air, then weighed into the mold and placed in the oven for curing.

B. Laser Interferometry Setup

The interferometry technique used was a Schlieren imaging technique, and described in detail by Greer and Cross (10). Briefly, this technique involves a coherent light source, e.g., a laser, whose beam is focused to infinity with a collimating lens. This light beam is projected through the transparent epoxy, then focused on a blocking dot. In this way, only light rays that are bent by the sample are picked up by the camera beyond the blocking dot. Thus a sample of epoxy having a uniform index of refraction will appear dark. Because of the refractive index change which occurs as liquid epoxies react to a solid, the locus of gelation and its subsequent path within a block of epoxy can be determined.

The light source was a 15 milliwatt Helium-Neon laser (Jodon HN-1576). The air temperature outside of the epoxy samples was maintained at desired levels

*Mention of specific brand names or suppliers does not imply endorsement by DOE.

Table 1. Mass of Curing Agents Employed and Nominal Cure Temperature

Curing Agent	g used per 100 g DGEBA	Starting Cure Temperature (°C)
TETA	10.0	32
MPDA	15.5	71
T-403	43.0	60
DEA	11.9	82
NMA	85.1 (+1.85 g DMP-30)	82

with a Statham Temperature Test Chamber, Model SD 606. The epoxy samples were cured in cubical or rectangular molds constructed of plexiglas sheets. For most experiments the Schlieren images were recorded with a video camera (GBC Mini-Max Model CTC 3010) and Sony Videocassette Recorder (Model VO-2600).

C. Temperature Measurements

The temperature profiles of the epoxy resin systems were measured using arrays of thermocouples. Type J thermocouples were secured to a planar wooden framework and placed vertically across the mid-plane or diagonal of cubic epoxy samples. Temperatures were monitored at 1.5 second intervals for the thermocouple array using a Fluke model 2200B Datalogger, and recorded onto magnetic tape with a Memodyne Digital Cassette Recorder model M-80. The temperatures were printed at a later time to allow data acquisition at the maximum rate. Between 15 and 25 thermocouples were used for each experiment.

III. Mathematical Model

To help understand the observed reaction of epoxy, work has been carried out on a numerical model of the cure process. Initial work was based on a model which neglected fluid convection. However, when initial temperature data showed that the epoxy did not have the spherically-symmetric temperature distribution such a model would predict, a more complex model which included convection was formulated. For this model, the internal heat generation is calculated from the kinetic equation and the heat of reaction. For the initial modeling effort, the reaction of DGEBA with MPDA was chosen as the subject. The kinetics of this reaction have been studied by numerous authors (2,3,4,5,6), and the kinetic equation derived by Kamal, et al. (4) is used here:

$$\text{heat generation} = Q_R \cdot (k_1 + k_2\alpha)(1 - \alpha) \tag{1}$$

where:

$$k_1 = 4.033 \times 10^4 \exp \frac{-7458.6}{T} \text{ sec-1} \tag{2}$$

$$k_2 = 8.833 \times 10^3 \exp \frac{-5795.5}{T} \text{ sec-1} \tag{3}$$

$$Q_R = -301.7 + 2.528T - 1.278 \times 10^{-3}T^2 \text{ (joules/cm}^3\text{)} \tag{4}$$

In the above equations, α = conversion (dimensionless) and T is temperature in °K. In order to include the internal heat generation described above, the model must include the continuity, energy, and momentum balance equations, as well as the mass balance for unreacted epoxy. To simplify the computations, the Boussinesq approximation is made in which the fluid density, ρ, depends on temperature according to:

$$\rho - \bar{\rho} = -\bar{\beta}\,\bar{\rho}(T - T_o) \tag{5}$$

Here $\bar{\rho}$ is the density of the fluid at a reference temperature T_o, and $\bar{\beta}$ is the volume coefficient of expansion of the fluid. This density dependence is used in

the buoyancy force term of the momentum equation. The epoxy density is assumed constant in all other terms. With the above data, the governing differential equations become:

Continuity:
$$\frac{\partial v_x}{\partial x} + \frac{\partial v_y}{\partial y} = 0 \tag{6}$$

Energy:
$$\rho C_p \left(\frac{\partial T}{\partial t} + v_x \frac{\partial T}{\partial x} + v_y \frac{\partial T}{\partial y} \right) =$$

$$k \left(\frac{\partial^2 T}{\partial x^2} + \frac{\partial^2 T}{\partial y^2} \right) + Q_R \, (k_1 + k_2 \alpha)(1 - \alpha) \tag{7}$$

Momentum (x-component):
$$\bar{\rho} \left(\frac{\partial v_x}{\partial t} + v_x \frac{\partial v_x}{\partial x} + v_y \frac{\partial v_x}{\partial y} \right) = \mu \left(\frac{\partial^2 v_x}{\partial x^2} + \frac{\partial^2 v_x}{\partial y^2} \right)$$

$$+ \frac{\partial \mu}{\partial x} \frac{\partial v_x}{\partial x} + \frac{\partial \mu}{\partial y} \frac{\partial v_x}{\partial y} \tag{8}$$

(y-component):
$$\bar{\rho} \left(\frac{\partial v_y}{\partial t} + v_y \frac{\partial v_y}{\partial y} + v_x \frac{\partial v_y}{\partial y} \right) = \mu \left(\frac{\partial^2 v_y}{\partial x^2} + \frac{\partial^2 v_y}{\partial y^2} \right)$$

$$+ \frac{\partial \mu}{\partial x} \frac{\partial v_y}{\partial x} + \frac{\partial \mu}{\partial y} \frac{\partial v_y}{\partial y} - \bar{\rho} \, \bar{\beta} (T - T_o) g \tag{9}$$

Mass:
$$\frac{\partial \alpha}{\partial t} = (k_1 + k_2 \alpha)(1 - \alpha) \tag{10}$$

In the above equations, C_p is the heat capacity of the epoxy, t is time in seconds, v_x is the x-component of the fluid velocity, k is the thermal conductivity of the epoxy, μ is the viscosity of the epoxy, and g is the acceleration due to gravity. In the above equations, the origin is at the geometric center of the sample, and the y-axis is oriented vertically as shown in the schematic following.

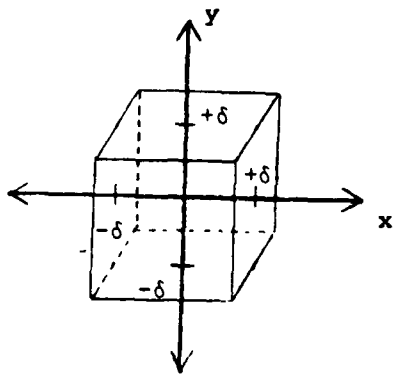

The epoxy viscosity is modeled using experimental viscosity versus temperature data for pure DGEBA taken from Kamal, et al. (4). The effect of conversion (α) on viscosity is approximated by using the pure DGEBA data for $\alpha < 0.55$, then increasing viscosity to infinity exponentially for $0.55 < \alpha < 0.60$. The boundary conditions are:

$$\text{at time} = 0: \quad \alpha = 0,\ v_x = v_y = 0,\ T = T_o \tag{11}$$

$$\text{at } x = \pm\delta \text{ (the vertical walls):} \quad v_x = 0,\ \frac{\partial T}{\partial x} = h(T - T_o) \tag{12}$$

$$\text{at } y = \pm\delta \text{ (the horizontal walls):} \quad v_y = 0,\ \frac{\partial T}{\partial y} = h(T - T_o) \tag{13}$$

$$\text{at } x = y = 0 \text{ (the center of the sample):} \quad T,\ v_x, \text{ and } v_y \text{ are finite} \tag{14}$$

In these boundary conditions, the h is a heat transfer coefficient, and T_o is the initial epoxy temperature and the temperature maintained in the oven outside the sample during the experiment. The heat transfer coefficient h is modeled as a constant over all surfaces. Since the top surface of the mold is open, while the other five surfaces are covered with lucite sheets, the modeling of h is an approximation. The above set of equations and boundary conditions is very similar to the model formulated by Jones (11) to describe the explosion of reacting gases

in a cylinder. The most significant difference is the variation in viscosity (and resulting phase change) incorporated in this model.

The solution of this model is being carried out using a finite element method on a CDC-7600 digital computer. The program is a modification of one written by D. K. Gartling (12). The program solves the Navier-Stokes and energy equations for a fluid in laminar flow. The program has now been modified to calculate and retain chemical conversion values for the epoxy, and use these to calculate the heat generated at each time step using the kinetic equation. Because of the exponential heat generation, a variable time step must be employed in the solution.

At present, a solution for the DGEBA/MPDA epoxy system has been obtained up to the time at which gelation initiates. Temperature profiles calculated from this model will be presented in the Results and Discussion section along with experimental data. After gelation has initiated, the computer program must solve the equations for a two-phase system. Calculations have proceeded for some gel front propagation, but have not been successful in following front propagation to completion. Modifications to the program will be required to complete the solution.

IV. Results and Discussion

A. Interferometry Results

When this study was begun, my presumption was that the epoxy resin systems would cure with negligible convection. In this case, the temperature distribution would be symmetric in all directions about the sample center, which would also be the locus of maximum temperature. Because the cure reaction would proceed most quickly at the highest temperature, the center of the sample would reach the Flory gel point first, and gelation would initiate there and proceed radially outward. The experimental data for the several curing agents showed a number of gelation patterns, none of them resembling the above scenario.

Figures 1-8 are Schlieren photographs of the gelation behavior for three curing agents. Figures 1-3 show the cure behavior of DGEBA cured with TETA. Figs. 4-6 show the case of MPDA curing agent, and Figures 7 and 8 show NMA curing agent. Figure 1 shows the image of curing DGEBA/TETA 2140 s after they are mixed at 32°C in a sample of dimensions 75 x 75 x 62 mm (grid marks on the mold are 2.5 mm spacing). This photograph shows a pre-gelation transition which appears as nodules which form at the top center surface of the resin and move slowly downward. Qualitatively, these modules are considerably more viscous than the surrounding liquid resin, but are definitely not a cross-linked solid. Figure 2 shows the same sample 2230 s after mixing. Here the nodules have moved further down into the sample, and more have appeared closer to the sides of the resin. Figure 3 shows the sample 2410 s after mixing. The light area on top is the gelled epoxy and the lower dark area is the ungelled material with nodules still suspended in it. This horizontal gel front initiated at the top surface and is moving vertically downward through the resin, taking approximately 500 seconds to traverse a sample of this size.

Figure 4 shows the image of curing DGEBA/MPDA 3360 s after they are mixed at 71°C in a sample of dimensions 50 x 50 x 68 mm. As in the TETA experiments, a pre-gelation transition is observed in the form of nodules. In these MPDA runs, the nodules form at both the top and bottom surfaces of the sample and move vertically toward the center. Qualitatively, the nodules in the MPDA cured sample appear less viscous than those in the TETA cured sample, and do not move purely vertically. Figure 5 shows the same sample 5175 seconds after mixing. Here the nodules have filled the sample and left a vertical ripple pattern of refractive index gradients. Figure 6 shows the sample 5705 s after mixing, with the gelation front about halfway through the sample. As in the TETA cured samples, this gel front starts at the top surface and moves downward as a plane, although traversing the sample takes only about 300 s.

The gel behavior of the TETA and MPDA curing agents is qualitatively very

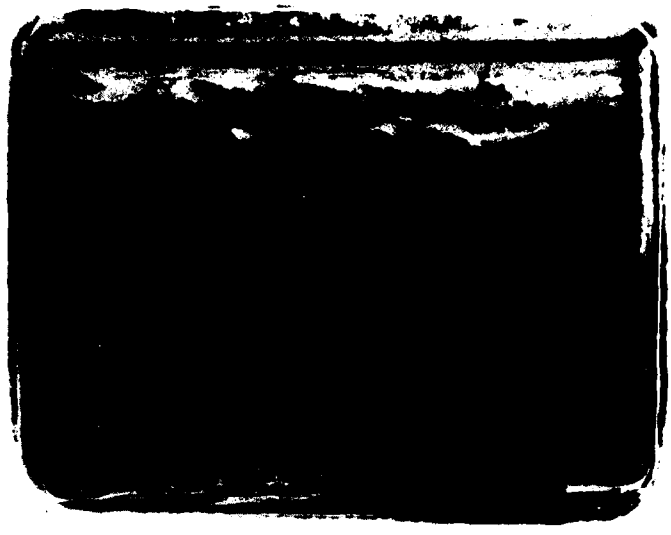

Figure 1. DGEBA/TETA cure 2140 s after mixing at 32°C. Nodules are forming at the top center of the sample and descending.

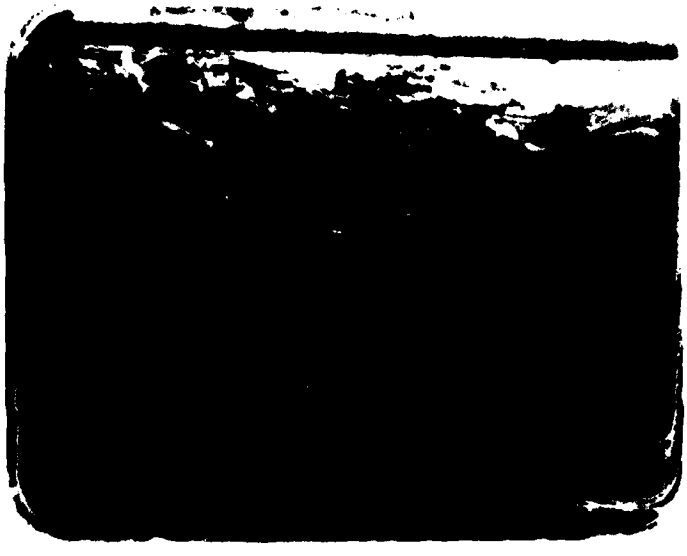

Figure 2. DGEBA/TETA cure 2230 s after mixing. Nodules have moved further down into the sample.

Figure 3. DGEBA/TETA cure 2410 s after mixing. Light area on the top is the gelled epoxy, and the lower dark area is the ungelled material with nodules still suspended in it.

Figure 4. DGEBA/MPDA 3360 s after mixing at 71°C.

Figure 5. DGEBA/MPDA 5175 s after mixing.

Figure 6. DGEBA/MPDA 5705 s after mixing; gelation front about halfway through sample.

Figure 7. DGEBA/NMA 5670 s after mixing at 82°C. Nodules initiate at both top and bottom surfaces, then move together in a vertical ripple pattern.

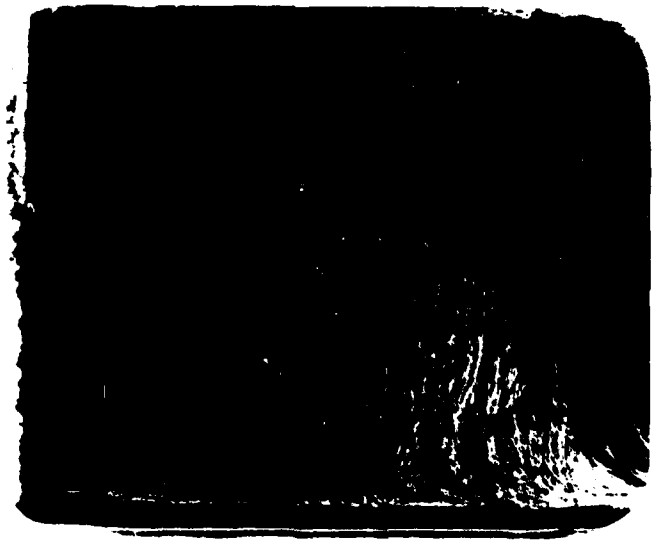

Figure 8. DGEBA/NMA 8332 s after resin and curing agent were mixed. Gel front moving down the edges of the sample.

similar, both having a pre-gelation transition and a planar gel front. These two curing agents are both primary amines, TETA being an aliphatic tetramine, and MPDA an aromatic diamine. A third primary amine was studied, T-403. This is an aliphatic triamine, and its cure behavior as seen in the interferometry setup was virtually identical to that seen with MPDA, although proceeding more slowly.

To date, one acid anhydride curing agent, NMA, has been studied. Figure 7 shows a sample of this system 5670 s after mixing at 82°C in a 75 x 75 x 61 mm mold. This photo is very similar to Figure 4 for the MPDA sample. Initially the NMA cured resin behaves very much like the MPDA, with nodules initiating at both top and bottom surfaces, then moving together to leave a vertical ripple pattern. However, the gelation transition for NMA is quite different, as shown in Figure 8. This picture, taken 8332 s after the resin and curing agent were mixed, shows the gel front moving down the edges of the sample. The gelled region initiated at the upper corners of the sample, and then spread along the edges both vertically and horizontally. Once all the sample edges are gelled, the liquid region in the center is gradually reduced in size until the entire cube is gelled. This process takes about 2000 seconds from the time the first gelled region formed.

One secondary amine curing agent, DEA, has been studied. The initial stages of cure with DEA in DGEBA appear similar to those for MPDA (Figures 4 and 5). However, the DEA system then shows no abrupt gel transition, only a very gradual increase in viscosity over the entire sample.

Although limited, the above data seem to imply that a family relationship may exist with regard to cure behavior. The three primary amine curing agents studied (TETA, MPDA, T-403) all showed very similar behavior with the top-initiating gel front and similar pre-gel transitions. The two nonprimary amine curing agents studied (NMA and DEA) each showed a unique gelation behavior. Additional curing agents will be tested to see if anhydrides and secondary amines show similar cure behavior among themselves.

One of the more striking aspects of the data is the sample to sample variability in time required to initiate gelation. Figure 9 shows the gel front position versus time curves for two identical TETA cured experiments. The gelation initiation time, the elapsed time since the resin was mixed until the gel front forms, shows a large amount of scatter. The gel initiation time for run 14 was 2180 s, and 2755 s for run 15. In contrast, the gel propagation time, the time required for the gel front to traverse the sample after gel initiation, is quite consistent. Gel propagation times are 506 s for run 14 and 525 s for run 15. One consequence of the variability in gel initiation is its potential effect on processing. If runs 14 and 15 were being cured using a fixed schedule which called for pressure application 2700 s after mixing, the sample in run 14 would have completely gelled, while run 15 would still be a liquid.

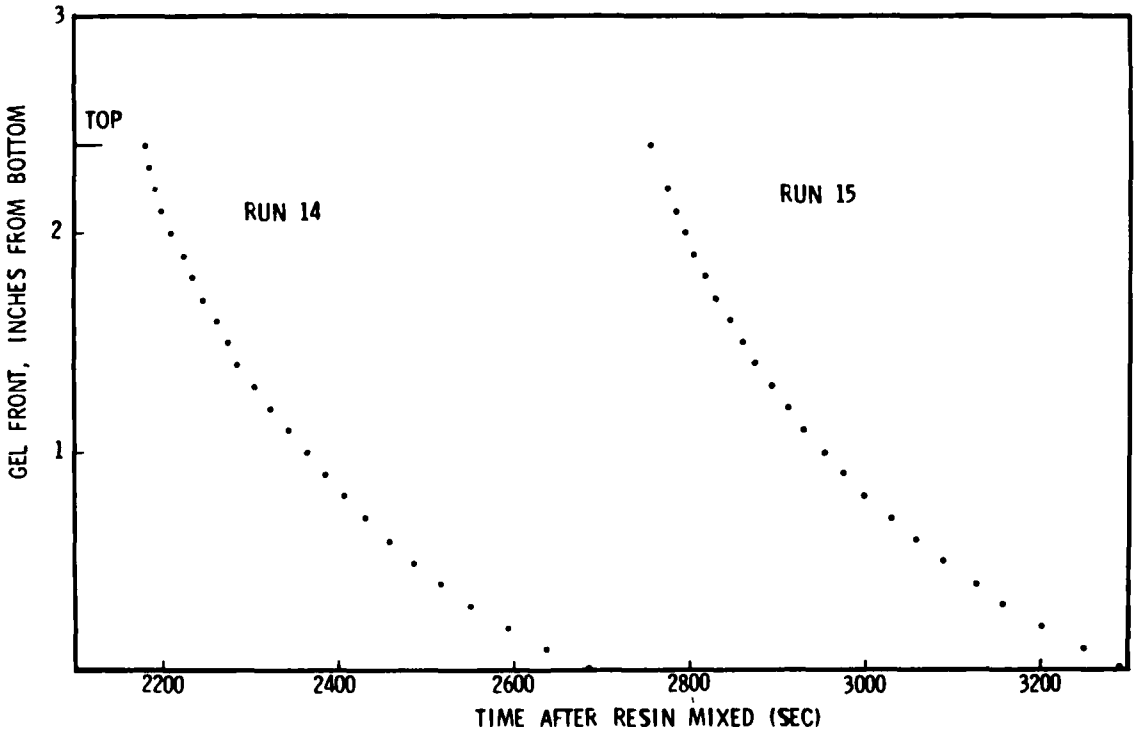

Figure 9. Experimental gel front position vs time, DGEBA/TETA epoxy.

Figure 10 shows a summary of gel initiation and gel propagation times for all TETA cured experiments. All data are reported as the sample mean ± one standard deviation. This plot confirms the trend suggested by Figure 9. The time required for the gel front to initiate has a coefficient of variation of 20 to 30%, depending on sample size. On the other hand, the time required for gel propagation after the front has initiated shows a coefficient of variation of about 6% for all samples. As the time required for gel propagation (540 to 780 s for all sample sizes) is much smaller than one standard deviation for gel initiation (1100 to 2100 s), the processing difficulty mentioned for Figure 9 is quite possible.

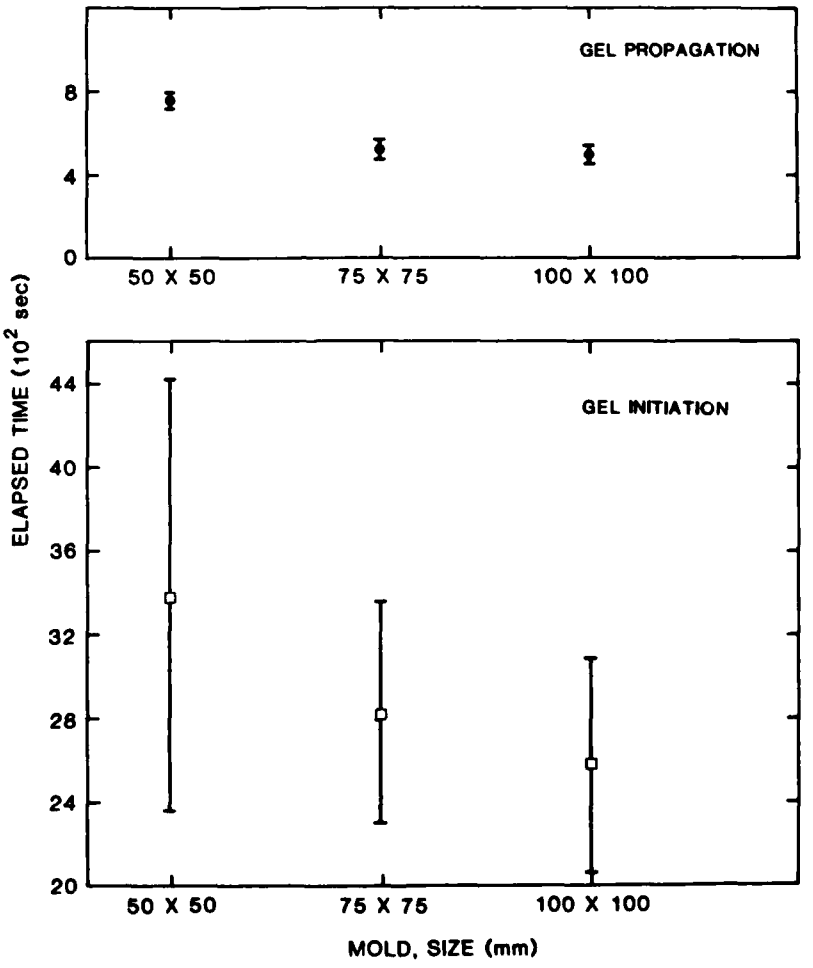

Figure 10. Gel initiation and gel propagation times for DGEBA/TETA epoxies.

Two experiments have been run with layers of glass fabric in the resin. Five horizontal layers of glass fabric at 13 mm intervals were placed in a TETA-cured material. The effect of these glass layers was to break up the cure process into 5 separate cells with a gel front initiating at the bottom of each glass layer, then moving downward. This behavior confirms that the gelation seen in primary amine cured DGEBA is caused by convection, and the relatively impermeable glass fabric broke up the convection cells into smaller compartments. This would also indicate that a composite with a high fiber loading could break up the convection cells to such a small scale that convective flow would be inhibited, causing the gel process to approach the conduction case discussed earlier.

B. Temperature Profiles

Temperature profiles have been measured for TETA and MPDA cured DGEBA, and the results correlate with the interferometry data. Figure 11 shows the time versus temperature curves for five points on the centerline of a 100 x 100 x 65 mm TETA cured sample. The peak temperature at any point occurs as the gel front passes, and the five curves peak in sequence starting with the top thermocouple and ending with the bottom, requiring about 500 s between first and last peaks. The absolute maximum temperature achieved is at the center point of the sample, as a conduction model would predict, but this occurred after the sample had gelled. Prior to the gel front passage, the highest temperature occurs midway between the center and top surface. This is the type of behavior predicted by Jones (11) in his model of enclosed exothermically reacting gases. These data established the need for the complex mathematical model presented in Section III.

For the initial solution, the model was set up for the DGEBA/MPDA system, as there is a large body of existing kinetic data for it (2,3,4,5,6). The qualitative behavior of the model has been good, predicting the very rapid heat up at the top of the sample just prior to gelation, with gelation initiating at the top surface. With the proper time step size in the computer model (1/2 sec),

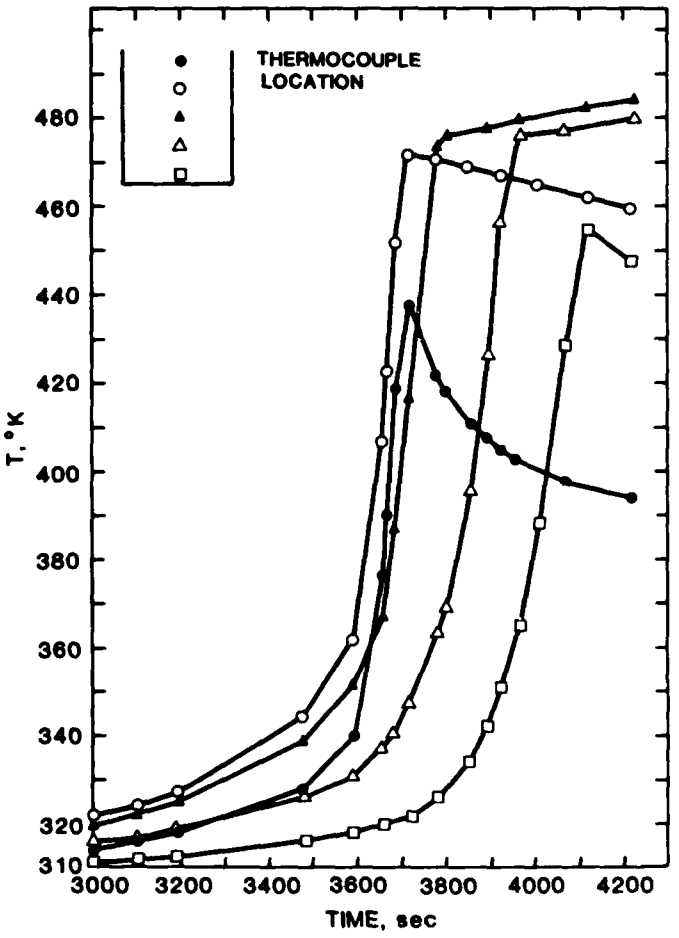

Figure 11. Experimental time vs temperature profiles, DGEBA/TETA epoxy.

good quantitative agreement has been achieved. Figures 12 and 13 show the agreement between the model and three MPDA experiments. Time zero on both figures is the time at which both the experiments and the model achieved 346°K, 2°K above the initial temperature. This was done to reduce the large scatter in the experimental data resulting from the variations in gel initiation times. Figure 12 compares data for a point in the sample midway between the center and edge, and 4 mm below the surface. There is still some variation in the time required for the experiments to achieve maximum temperature, as well as a 100°K variation in the maximum temperature achieved. The predicted curve from the model agrees quite well with the experiments, although it does lag behind the slowest experimental data by about 70 s. The model curve ends at 538°K. This would be the maximum

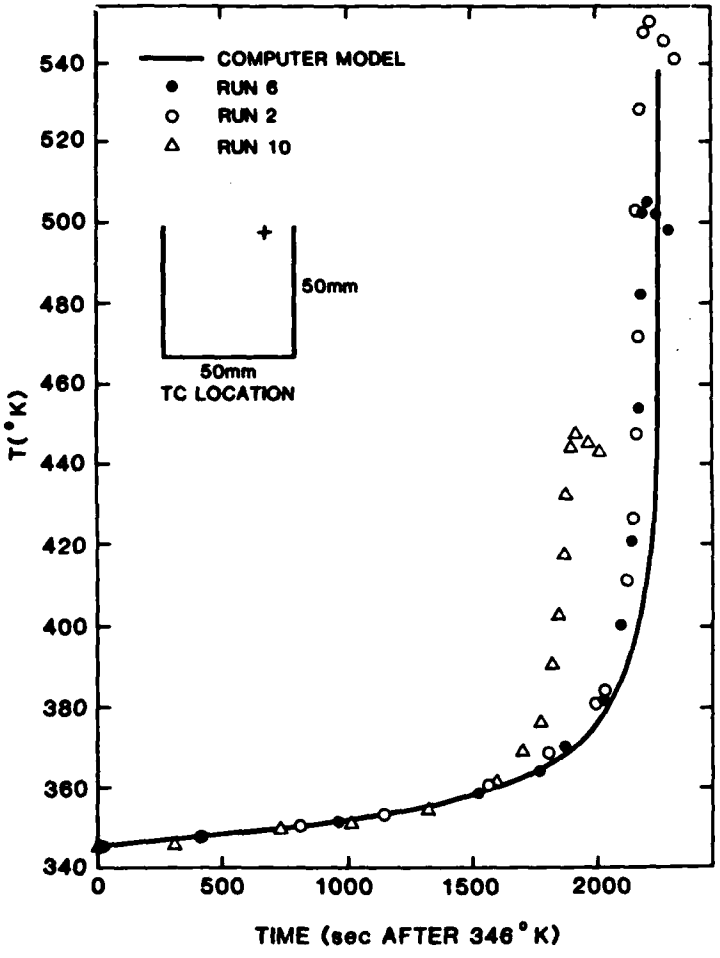

Figure 12. Comparison of predicted vs experimental temperature data, DGEBA/MPDA epoxy.

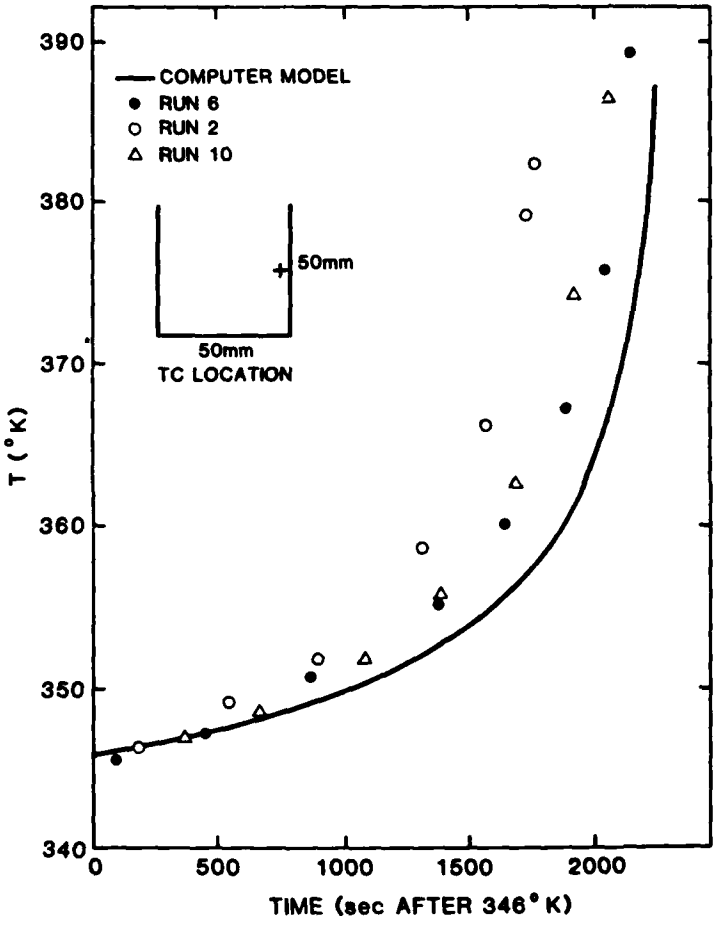

Figure 13. Comparison of predicted vs experimental temperature data, DGEBA/MPDA epoxy.

predicted temperature for that point, as the model had exceeded the Flory gel criterion, which indicates the resin had gelled. Figure 13 shows a similar trend for a sample point 4 mm in from the side wall of the sample, and midway between the top and bottom surfaces. Agreement is quite good, although the model curve lags behind the data by at least 130 seconds.

The two model curves stop before reaching the end of gelation. This occurs because of difficulties in treating the two phase system which results when gelation commences. The most recent simulations have employed a finer finite element grid, and a modified viscosity versus conversion curve in which viscosity goes to infinity more gradually at the gel point. These changes have allowed the simulation gel front to proceed about 1/2 of the distance down the sample, which shows promise that the simulation can be carried through to completion.

V. Concluding Remarks

This study has shown that the cure behavior of DGEBA epoxies is a complex phenomenon which deviates considerably from a priori expectations. A model has been proposed which partially explains the cure behavior of primary amine curing agents as a function of their kinetics, heat transfer coefficients, and convection. Work is underway to experimentally observe the convective flow in these resins using glass microballoons as tracers. This will allow assessment of the accuracy of the convection patterns this model predicts, as well as the temperature profiles. If the model correlates the experimental convective flow data as well as the temperature data, it could be a useful tool in examining the effect of cure conditions on the gelation of DGEBA epoxies.

While the proposed model provides a good qualitative match to the overall cure behavior of primary amine cured epoxies, it can not explain some fine details. It does not predict the pre-gelation transitions observed, as well as the large scatter in the time required to reach gel initiation. Finally, while such a

model could probably be extended to cover lightly filled epoxies, the gelation of heavily filled epoxies is probably far less influenced by convection.

VI. Acknowledgements

I would like to thank Bruce Hansche and Philip Walkington for their help in setting up the optical bench to run the interferometry experiments. I would also like to thank David Gartling and Charles Hickox for their help with the computer model. Finally, I would like to thank Eli Perea for running the temperature profile experiments.

VII. References

1. P. G. Babayevsky and J. K. Gillham, Journal of Applied Polymer Science, 17, 2067-2088 (1973).
2. J. M. Barton, Thermochimica Acta, 30, 153-161, (1979).
3. R. C. Progelhof and J. L. Throne, Polymer Engineering and Science, 15, No. 9, 690-695, (1975).
4. M. R. Kamal, S. Sourour, and M. Ryan, paper presented at 31st SPE ANTEC, Montreal, 1973; Technical Papers, 19, 187-190, (1973).
5. A. Dutta and M. E. Ryan, Journal of Applied Polymer Science, 24, 635-649, (1979).
6. R. Jenkins and L. Karre, Journal of Applied Polymer Science, 10, 303-313 (1966).
7. M. A. Acitelli, R. B. Prime, and E. Sacher, Polymer, 12, 335-343, (1970).
8. H. E. Adabbo, A. J. Rojas, and R. J. Williams, Polymer Engineering and Science, 19, #12, 835-840 (1979).
9. E. Broyer and C. W. Macosko, AICHE Journal, 22, #2, 268-276, (1976).
10. A. S. Greer and B. T. Cross, Non-Destructive Testing, June 1970, pp. 169-172.
11. D. R. Jones, International Journal of Heat and Mass Transfer, 17, 11-21 (1974).
12. D. K. Gartling, "NACHOS - A Finite Element Computer Program for Incompressible Flow Problems," Sandia Laboratories Report, SAND 77-1334, Nov. 1977.

MONITORING CURE OF LARGE AUTOCLAVE MOLDED PARTS BY DIELECTRIC ANALYSIS

J. Chottiner, Z. N. Sanjana
Westinghouse Electric Corporation
R&D Center
Pittsburgh, PA 15235
M. R. Kodani, K. W. Lengel, G. B. Rosenblatt
Westinghouse Electric Corporation
Marine Division
Sunnyvale, CA 94088

Abstract

A study was undertaken to determine the feasibility of using dielectric analysis as a means of monitoring and controlling cure of large closures during autoclave molding. In dielectric analysis the dissipation factor and capacitance of the sample is continuously monitored as a function of time and frequency. Dissipation factor profiles were established for the suppliers' recommended cure cycle and for modified cure cycles. Good reproducibility was obtained in dissipation factor profiles on subsequent scaling up to production size (7 ft x 20 ft) autoclaves. Good correlation was also observed during production runs of full-scale closures. The effects of cure variables on the dissipation factor profiles and on the mechanical properties of the prepared laminates were analyzed for extent of correlation. Results of this study show: (1) dielectric analysis can be used to monitor autoclave cure of composites, and (2) within limits, process control may be feasible.

"Keywords": dielectric analysis; autoclave molding; epoxy; glass; dissipation factor; capacitance

1. INTRODUCTION

The launch tube closure assembly for the Fleet Ballistic Missile (FBM) Launch System is currently autoclave molded from a phenolic/asbestos prepreg material. Because of the recognized carcenogenicity of asbestos, there has been an active program aimed at finding a suitable replacement material. The most promising of these materials are epoxy/high silica glass cloth prepregs.[1]

These launch tube closures are domed-shaped structures approximately 6 ft in diameter at the base and slightly over 2 ft high at the apex. The lay-up procedure, autoclave and post bake cycle, finish-

ing operations and qualification testing combine to form a costly and lengthly process. Improved quality control during processing is an ongoing objective. The work described in this paper is an effort to incorporate dielectric analysis as a quality control tool in production.

A useful cure monitoring technique should be capable of: (1) interrogating the material within the autoclave or press, (2) giving a response which is sensitive to changes in the incoming material and to changes that accompany cure, and (3) giving the information continuously and immediately so that, if necessary, process changes can be made based on the response. Most of the published work in cure monitoring indicates that some form of electrical measurement is the most feasible way to meet the requirements. May[2], Hudson[3], and Martin[4] have discussed the use of an automatic dielectrometer to continuously monitor the dissipation factor and the capacitance of the sample during cure. Yokota[5] has discussed the relative advantages of using ac voltage and phase angle measurements. Crabtree[6] has discussed dc resistance and voltage measurements during autoclave cure of a composite.

The technique discussed here is an ac technique in which an automatic dielectrometer is used to continuously monitor the dissipation factor (DF or tan δ) and capacitance (C) of a sample as a function of time, temperature and frequency of the sample. Both observed parameters are sensitive to dipolar motion within the matrix of the composite which is sensitive to the degree of advancement or cure of the resin. The use of dielectric analysis to follow the degree of polymerization and cure kinetics has been discussed by one of the authors[7] and in the papers referenced earlier[2-4].

2. EXPERIMENTAL

The closure application requires an unusual combination of properties including the ability to withstand substantial stresses from either side. It must, however, be readily sheared by a linear shaped charge just prior to launch of the missile. A family of epoxy/high silica glass cloth prepreg materials appear to possess the desired combination of properties.[1] Four materials from this family were selected for prototype closure evaluation and cure monitoring. These materials are Fiberite 934/Siltemp 82, Fiberite 934/Refrasil C100-48, Fiberite 30854/Refrasil C100-48 and Ferro CE321/Refrasil C100-48.

While dissipation factor (DF) and capacitance (C) can be measured by any ac bridge, continuous measurements are most conveniently done using an automatic dielectrometer. The dielectrometer is a self-balancing bridge with a frequency range of from 0.1 to 1.0 kHz and is often referred to by its acronym -

Audrey. It is manufactured by Tetrahedron Associates.

The measured sample consisted of one (for Refrasil C100-48) or two (for Siltemp 82) plies of prepreg in the middle of the stack. Each electrode consisted of copper foil to which leads had been soldered and the effective area was one square inch. One of the electrodes was "blocked", i.e., separated from the sample by one layer of 0.001" thick polyimide film. The use of the "blocking" film permits the D.F. response to exhibit frequency dependent relaxation peaks associated with the melt and flow of the resin, and with the gelation and cure process.[7] Figure 1 shows the layup of the test panel. Total number of plies in the stack was selected to provide a shell thickness of 0.220" $\pm$ .02". Figure 2 shows the panel placed in an autoclave. To reduce noise it was found beneficial, in some experiments, to ground the dielectrometer to the autoclave wall. For these preliminary experiments we selected a frequency of 1 kHz to reduce noise to a minimum.

When experimenting with a full-scale shell, it was decided to incorporate the electrodes on the flange of the shell where some machining was necessary that would subsequently remove the encapsulated electrode assembly. Figure 3 shows the molded shell with the electrodes on the flange.

The standard autoclave cure cycles for Ferro CE321 and Fiberite 934 and 30854 resin systems are shown in Tables I and II. Dielectric analyses were run with the standard cure cycles and a number of modified cure cycles, including applying the pressure at points based on the dissipation factor or capacitance profiles. The specific modifications employed are shown in Tables III through V. The effect of cycle modification was determined by testing autoclave molded panels (which were monitored using dielectrometry) for properties pertinent to the closure application. These properties are shown in Tables III through V. Standard ASTM test specimens and procedures were employed.

A minimum of three full-scale closures were molded from each of the four candidate materials. The molding cycle employed was selected on the basis of the results obtained in molding flat panels. A flat panel was also molded in the autoclave while the closure itself was being molded. Both the closure and the flat panel were equipped with electrodes and connected to the dielectric analysis equipment.

3. RESULTS AND DISCUSSION

Figure 4 shows the profiles for DF and C for the cure of Ferro CE321 resin on Refrasil C100/48 high silica glass using the manufacturer's recommended cure cycle (Table I). The figure also indi-

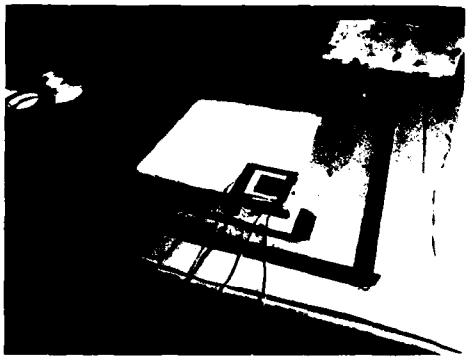

Fig. 1 - Lay-up of panel showing top electrode and thermocouple.

Fig. 2 - Vacuum bagged panel assembly in autoclave.

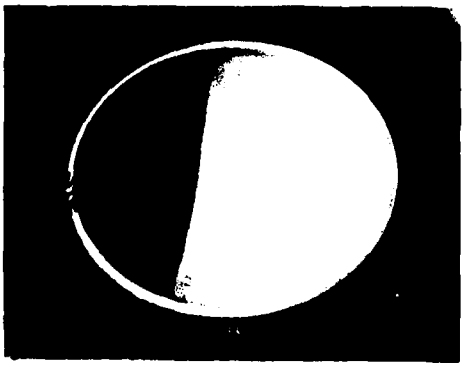

Fig. 3 - Full-scale shell showing electrodes placed on flange.

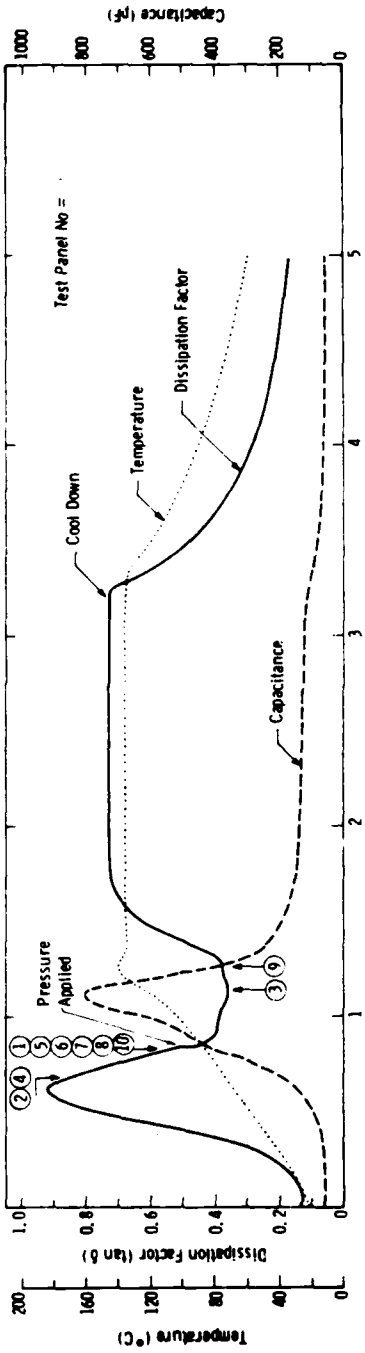

Fig. 4 – Dielectrometer profiles for Ferro CE 321 using manufacturer's recommended cure cycle. Frequency = 1 kHz

TABLE I - STANDARD AUTOCLAVE CURE FOR FERRO CE321 EPOXY RESIN SYSTEM

1. Apply full vacuum and raise temperature to 200°F at 2°-5°F per minute.
2. Apply 100 psi pressure at 200°F, vent bag and continue raising temperature to 275°F (± 5°F) at 2°-5°F per minute.
3. Hold at 275°F (± 5°F) for two hours.
4. Cool under pressure to below 175°F.

TABLE II - STANDARD AUTOCLAVE CURE CYCLE FOR FIBERITE 934 AND 30854 EPOXY RESIN SYSTEMS

1. Apply full vacuum and hold at room temperature for 30 minutes.
2. Maintain full vacuum throughout entire cure cycle.
3. Raise temperature to 250°F (+5, -10°F) at 2°-5°F per minute.
4. Hold at 250°F for 15 ± 5 minutes.
5. Apply 100 psi pressure.
6. Hold at 250°F and 100 psi for 45 ± 5 minutes.
7. Raise temperature to 350°F (+10°, -0°F) at 2°-5°F per minute.
8. Hold at 350°F for two hours ± 15 minutes.
9. Cool under pressure to below 175°F.

TABLE III - PROPERTIES OF FERRO CE321/REFRASIL C100-48 PANELS MOLDED DURING DIELECTRIC ANALYSIS EXPERIMENTS

Panel No.	Cure Cycle Modification	Flexural Str. (ksi)	Flexural Mod. (Msi)	Tensile Str. (ksi)	Tensile Mod. (Msi)	Compressive Str. (ksi)	Compressive Mod. (Msi)	Thick. (mils)	Sp. Gr.	Resin Content (%)	Void Content (%)
1	Standard	31.1	2.6	20.3	2.9	48.8	3.4	232	1.66	35.5	3.0
2	Apply Pressure at "Melt" Peak	40.2	2.9	24.8	3.2	57.1	3.6	221	1.68	33.2	3.0
3	Apply Pressure at C Peak	36.0	2.8	23.4	3.1	51.0	3.2	228	1.67	34.5	2.9
4	Apply Pressure at "Melt" Peak	36.3	3.0	23.1	3.0	55.6	3.5	223	1.68	32.9	3.1
5	Cure at 325°F	33.8	2.9	23.3	3.0	53.2	3.7	212	1.69	31.5	3.3
6	Cure at 200 psi	40.8	3.1	24.5	3.4	56.8	3.6	216	1.69	31.0	3.5
7	Standard	34.4	3.0	19.9	3.3	55.0	3.5	220	1.71	31.7	2.0
8	Standard	33.4	3.1	21.8	2.9	55.6	3.4	220	1.68	32.3	--
9	Apply Pressure Past C Peak	29.9	2.7	21.2	2.6	--	--	233	1.68	33.6	2.8
10	Standard	39.2	3.3	25.0	3.3	--	--	218	1.70	31.0	3.0

TABLE IV - PROPERTIES OF FIBERITE 934/SILTEMP 82 PANELS MOLDED DURING DIELECTRIC ANALYSIS EXPERIMENTS

Panel No.	Cure Cycle Modification	Flexural Str. (ksi)	Flexural Mod. (Msi)	Tensile Str. (ksi)	Tensile Mod. (Msi)	Compressive Str. (ksi)	Compressive Mod. (Msi)	Sp. Gr.	Resin Content (%)
1	Standard	34.0	3.5	22.1	4.6	51.1	3.8	1.68	28.1
2	Apply Pressure at "Gel" Peak	35.6	3.4	22.1	3.9	57.1	3.7	1.66	29.5
3	Apply Pressure at D.F. Minimum	38.1	3.4	21.6	4.1	59.5	3.6	1.67	29.5
4	Apply Pressure 10 Min. Past "Gel" Peak	27.5	2.7	17.4	3.4	38.9	3.0	1.48	29.7
5	30 psi Pressure	27.1	2.9	20.6	3.7	53.0	3.6	1.58	29.7
6	Standard	33.9	3.3	23.8	3.7	62.2	3.5	1.67	--
7	Apply Pressure at End of 250°F Hold	32.3	3.3	22.1	3.9	63.3	3.6	1.67	29.8
8	Apply Pressure at D.F. Minimum	35.0	3.2	23.2	3.5	59.8	3.6	1.67	29.5
9	Apply Pressure at End of 250°F Hold	33.8	3.3	24.0	4.1	62.2	3.8	1.67	30.1
10	35 psi Pressure	33.1	3.2	22.1	4.0	55.2	3.6	1.61	29.0
11	Slow Heat-up (1.5°F/Min.)	31.6	3.2	23.8	4.0	60.5	3.8	1.66	29.2
12	Standard	36.0	3.3	24.7	4.2	61.0	3.5	1.68	29.3

TABLE V - PROPERTIES OF FIBERITE 30856/REFRASIL C100-48 PANELS MOLDED DURING DIELECTRIC ANALYSIS EXPERIMENTS

Panel No.	Cure Cycle Modification	Flexural Str. (ksi)	Flexural Mod. (Msi)	Tensile Str. (ksi)	Tensile Mod. (Msi)	Compressive Str. (ksi)	Compressive Mod. (Msi)	Thick. (mils)	Sp. Gr.	Resin Content (%)	Void Content (%)
1	Standard	27.7	2.6	15.5	2.8	41.1	2.7	227	1.65	33.4	4.6
2	Apply Pressure at "Melt" Peak	28.9	2.8	19.0	3.3	41.6	2.8	224	1.67	32.0	4.7
3	Apply Pressure at Capacitance Peak	31.3	2.8	18.9	3.3	42.1	2.8	223	1.67	31.5	4.4
4	Apply Pressure at "Gel" Peak	31.4	2.5	16.9	3.2	31.6	2.3	246	1.51	31.3	13.7
5	Standard	32.5	2.9	19.3	3.6	37.6	2.6	231	1.63	31.3	6.8
6	Apply Pressure at "Melt" Peak	26.7	2.7	17.4	3.2	40.8	2.6	230	1.64	33.0	5.4
7	Apply Pressure at Capacitance Peak	27.8	2.7	18.3	3.4	43.3	3.1	227	1.66	32.7	4.4
8	Apply 150 psi at Capacitance Peak	31.7	2.9	20.6	4.1	45.9	3.3	220	1.68	30.8	5.0
9	Apply 150 psi at "Melt" Peak	27.0	2.8	17.5	3.6	39.1	3.2	225	1.67	32.2	4.0
10	Apply 150 psi at Capacitance Peak	32.8	2.9	20.8	3.6	44.6	3.4	214	1.68	29.3	4.2

cates the ten experiments performed and the points at which pressure was applied (by means of circled numbers). The numbers also refer to the panel numbers in Table III which gives mechanical test data for each panel.

As the panel was heated up at some temperature, DF went through a maximum and then declined to a minimum. The temperature of this maximum (for convenience called the "melt" peak) is a function of the frequency of observation and the degree of advancement of the prepreg.[8] The maximum in C indicates the point in time beyond which the reaction begins to reduce the mobility of the polar groups. After this point the reaction (cure) proceeds rapidly resulting in a sharp and continuous decrease in C. Simultaneously the DF rises rapidly and becomes invariant with time as the rate of reaction ceases.

Several experiments repeating the standard cycle were performed in a laboratory autoclave and showed the results to be quite repeatable. Thus we were able to perform the ten modifications shown in Table III on panels cured in a production autoclave. One modification consisted of using a higher cure temperature which is shown in Fig. 5. An interesting departure from Fig. 4 occurs when the final cure temperature is reached. The DF and C profiles continued to show a significant rate of change until cool down.

The sensitivity of dielectric measurements to frequency is also shown in Fig. 5. During the cool down, a series of peaks were obtained. The frequency dependencies of the dielectric response of polymers during cure has been previously discussed.[7] It should also be noted that in this paper whenever we mention "melt" or "gel" peak it is only for convenience. The peaks result from relaxation phenomena associated with softening and flow of the resin and gelation of the resin. The occurrence of the peaks does not define the point in time when softening or gelation occurs because the occurrence of a peak is also frequency dependent.

The data in Table III show a rather large scatter in mechanical properties but it does appear that pressure application at the "melt" peak (Panels 2 and 4) resulted in higher mechanical properties. Pressure application past the capacitance peak (Panels 3 and 9) appears to result in poorer properties. Unfortunately, the autoclaves were manually controlled and the temperature rate of rise could not be controlled as well as desired, thus contributing to the inconsistencies in the data. Improved properties were noted for Panel 6 where a higher pressure was used. Panels 7 and 8 were cured simultaneously to evaluate the effect of different bleeder systems.

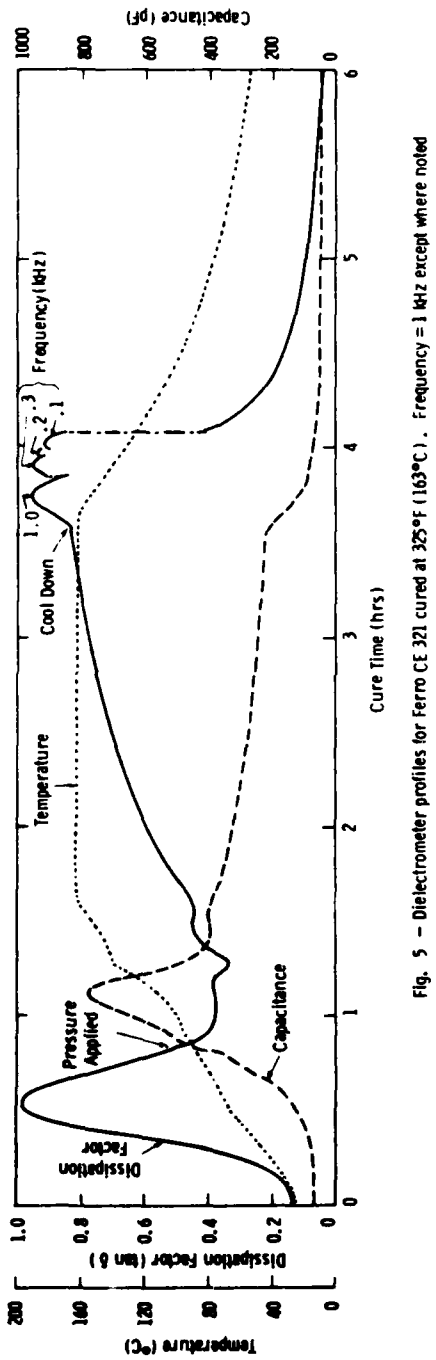

Fig. 5 – Dielectrometer profiles for Ferro CE 321 cured at 325°F (163°C). Frequency = 1 kHz except where noted

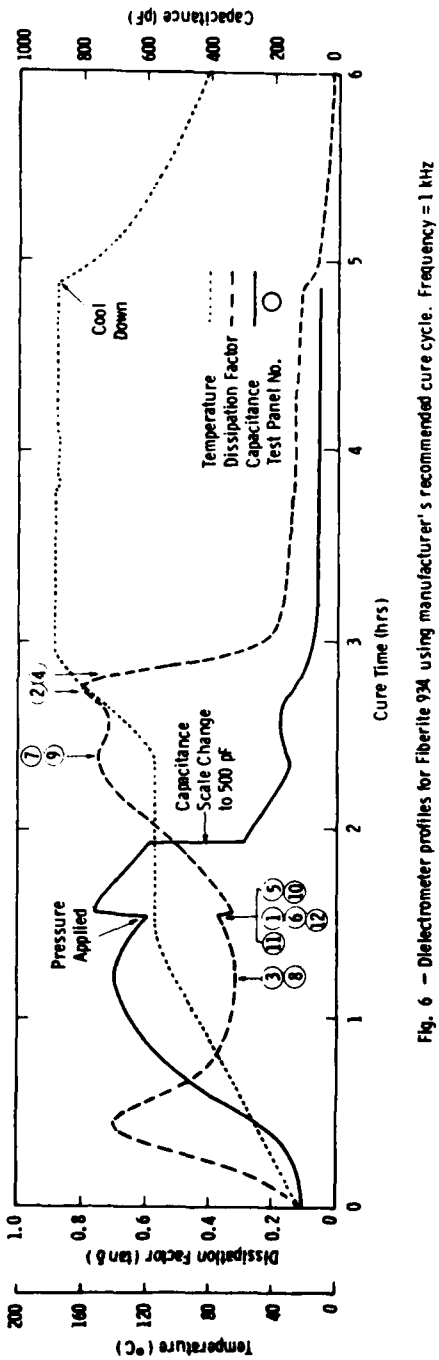

Fig. 6 – Dielectrometer profiles for Fiberite 934 using manufacturer's recommended cure cycle. Frequency = 1 kHz

Fiberite 934 is a 350°F curing resin containing a tetrafunctional epoxy resin cured with an aromatic amine. Figure 6 shows the "standard" cure profile for the resin on Siltemp 82 high silica glass. The standard cure is defined in Table II. Pressure application points for the 12 experiments with this material are shown in Fig. 6 and the modifications are shown in Table IV.

As the material is heated, a "melt" peak in DF is noted as with the Ferro CE321 material. Temperature at which this peak occurs can be used to define the advancement of the prepreg. As the heat-up continues, DF drops to a minimum which coincides with a maximum in the C response. This should be in the region of minimum viscosity and Panels 3 and 8 had pressure applied at this point. Towards the end of the hold, DF went through a maximum and then as the temperature was increased to 350°F it increased again and went through a final maximum. For convenience we define the latter as "gel" peak. After this maximum, the reaction proceeds rapidly as noted by the large drop in DF. At 350°F, the reaction continues although at a much slower rate. In Fig. 7 we see the changes in the profile resulting from the slowest heat-up rate used (1.5°F/min compared to 2.0°F/min in Fig. 6). The principal difference is the increase in breadth of the peaks. Due to increased staging, the first peak associated with gelation was much larger and more completely defined.

The data of Table IV shows considerable scatter but four observations can be made: (a) Applying pressure past the "gel" peak as in Panel 4 lowers the mechanical properties. (b) As expected, lower pressure resulted in poorer mechanicals. (c) Applying the pressure at the DF minimum which is earlier than recommended appears to improve mechanical properties, and (d) The slow heat-up rate of Panel 11 did not adversely affect mechanicals.

Prepregs of both Fiberite 30854 and 934 resin systems on Refrasil C100-48 high silica glass were obtained and cured in pairs in an autoclave at the same time. Dielectrometer readings were obtained from both materials concurrently by switching between the two, and a typical result for a standard cure cycle is shown in Fig. 8. The standard cure is identical for both materials and is shown in Table II. The numbers in Fig. 8 correspond to various modifications as noted in Table V. The 30854 resin is basically similar to 934 except it is modified to increase flexibility. The essential similarity in chemistry of the two is exhibited by the close resemblance of the two profiles in Fig. 8. Only one important difference is noted and that is at the end of cure the flexibilized 30854 displays a higher DF than does the more rigid

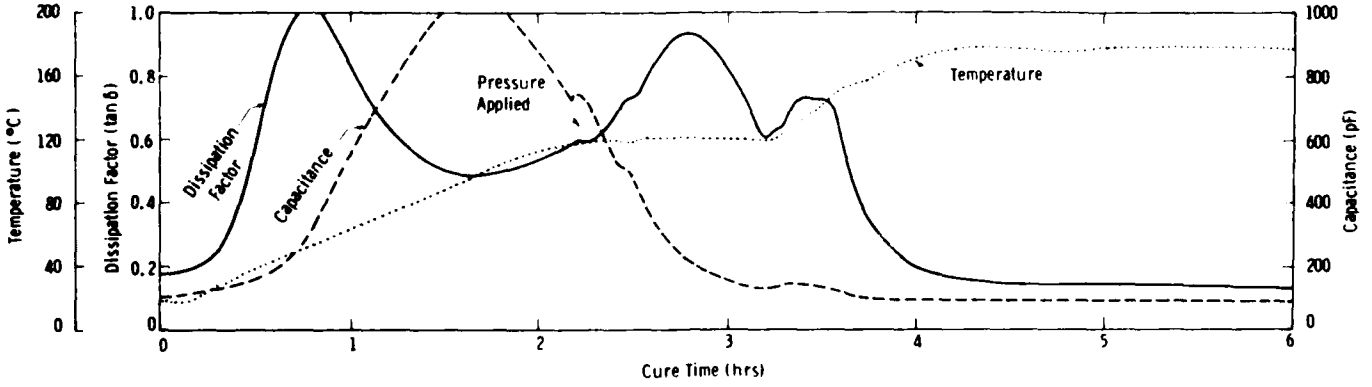

Fig. 7 – Dielectrometer profiles for Fiberite 934 using very slow (1.5°F/min) heat-up rate in cure cycle. Frequency = 1 kHz

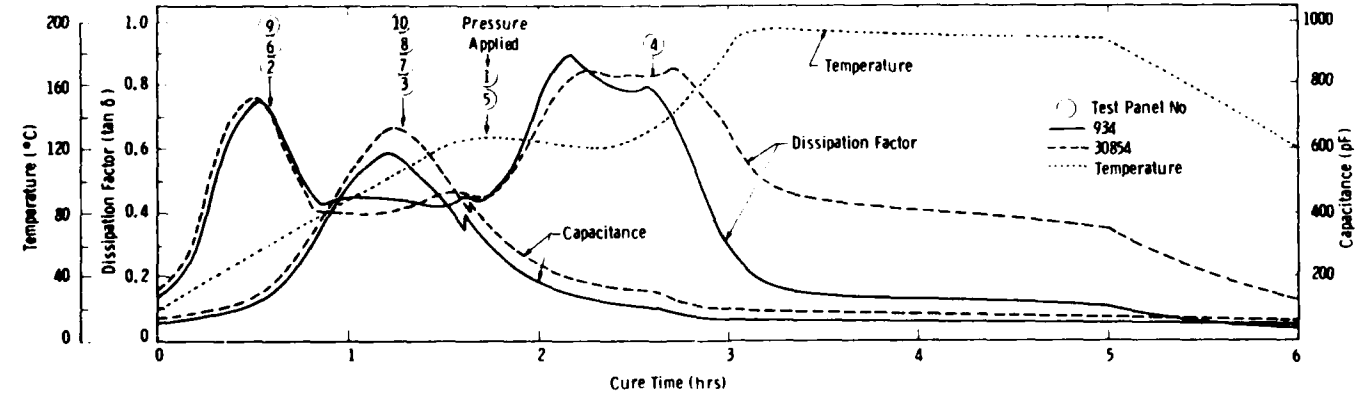

Fig. 8 – Dielectrometer profiles for Fiberite 934 and 30854 using manufacturer's recommended cure cycle. Frquency = 1 kHz

934. The enhanced flexibility allows greater dipolar mobility at any temperature and therefore a higher DF.

The results of mechanical tests are given in Table V for the 30854 system. It is seen that late pressure application at the "gel" peak is disadvantageous as shown in Panel 4. Note particularly the high void content. Applying pressure very early at the "melt" peak as for example Panel 6 appears to be disadvantageous.

Full-scale shells and test panels were simultaneously molded, in the same autoclave. Both shells and panels were monitored by switching the dielectrometer between the two. Figure 9 shows this for the Fiberite 934 material. It is interesting to note the similarity between the profiles for the panel and the shell and the similarity to Figs. 6 and 7. This program is continuing and all production shells are being monitored. The shells are being evaluated but testing is not yet complete. This evaluation includes the ability of the shells to withstand internal and external pressures and to be cleanly cut-through by the explosive charge.

4. CONCLUSIONS

1. Dielectric analysis can be used to monitor autoclave cure of composites.
2. The dissipation factor and capacitance responses of the polymer composites are quite reproducible when materials and processes are not changed, thus making process control feasible.
3. The responses that we have chosen to study are very sensitive to the temperature and the rate of change of temperature at the moment of observation, particularly in the pre-gelation period of the cure. This adds to the difficulty of instituting process control unless temperatures can be very accurately programmed.
4. The dissipation factor profile obtained during cure can be used to define a range of time in which pressure must be applied, and also may be used to define an optimum pressure application point.

5. ACKNOWLEDGMENT

The authors wish to express their appreciation to HITCO and especially to Mr. Jack Novak of that Company for their assistance in providing facilities and consultation during the course of this investigation. The assistance of J. H. Testa and R. L. Selby of Westinghouse R&D is also deeply appreciated.

6. REFERENCES

1. J. Chottiner, G. B. Rosenblatt and K. W. Lengel, "Substitute Composites for FBM Launch System Closures", Technical Proceedings, 35th Annual Conference, The Society of Plastics Industries, Feb. 1980.
2. C. A. May, Pro. SAMPE Symp., V. 20, p. 108 (1975).
3. D. Hudson, Composites, p. 247 (Nov. 1974).

3. D. Hudson, Composites, p. 247 (Nov. 1974).

4. B. G. Martin, Mater. Eval., V. 34, p. 49 (March 1976).

5. M. J. Yokota, Proc. SAMPE Symp., V. 22, p. 416 (1977).

6. D. J. Crabtree, Proc. SAMPE Symp., V. 22, p. 636 (1977).

7. Z. N. Sanjana, "Science and Technology of Polymer Processing", ed. N. P. Suh and N. Sung, p. 827, MIT Press (1979).

8. Z. N. Sanjana, SAMPE Jnl., V. 16, p. 5, (Jan. 1980).

7. BIOGRAPHIES

J. Chottiner and Z. N. Sanjana are senior engineers at the Westinghouse R&D Center, Pittsburgh, PA. Both are active in the evaluation and application of high performance composites.

M. R. Kodani, K. W. Lengel and G. B. Rosenblatt are with the Westinghouse Marine Division in Sunnyvale, CA and have all been active in the design, manufacturing and testing of FBM closures.

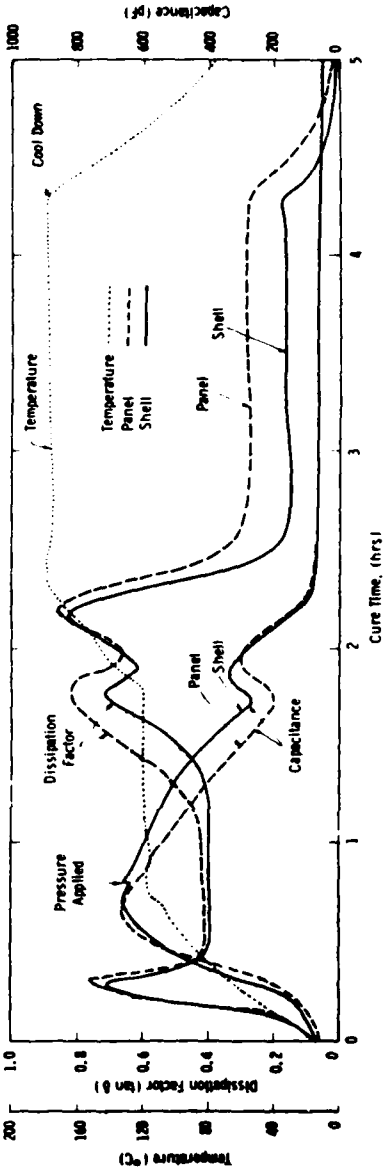

Fig. 9 – Dissipation factor and capacitance profiles for full scale shell and test panel molded in production autoclave using standard cure cycle (Fiberite 934). Frequency = 1 kHz

MICRODIELECTROMETRY

Stephen D. Senturia, Norman F. Sheppard, Steven L. Garverick,
Huan L. Lee, and David R. Day

Department of Electrical Engineering and Computer Science, and
Center for Materials Science and Engineering
Massachusetts Institute of Technology
Cambridge MA 02139

ABSTRACT

The low-frequency dielectric properties of resins provide a useful tool for characterization both of the curing process and of fully cured material. We have used integrated circuit technology to develop a miniaturized dielectric probe that combines small size with built-in amplification to achieve sensitivity at frequencies as low as 1 Hz. The device combines a planar interdigitated electrode structure with a pair of matched field-effect transistors. The microdielectrometer "chip" can be implanted in a specimen, or a small sample of material (a few milligrams) can be placed on the active area of the device. When combined with an off-chip electronic feedback system, the device can be used to measure the complex dielectric constant of the sample material either as it cures, or after cure. The device is capable of operating at temperatures up to 200°C, making it useful for a wide variety of curing and post-cure studies. Device calibration is based on a two dimensional computer model which has been experimentally confirmed for a variety of control samples. Several typical applications are illustrated by experiments, and the use of the data to follow changes in the dominant low-frequency dielectric relaxation during the cure of a model epoxy resin system are presented.

I. INTRODUCTION

This paper presents a new microelectronic technique for the measurement of low-frequency dielectric properties of materials, with particular emphasis on application to the in-situ monitoring of resin cure (1). Measurements of dielectric properties of polymers and other materials are used in a variety of applications (2). In the case of resin cure, the technique has proved sufficiently useful to prompt the development of commercial instrumentation dedicated to this application (3). This commercial "dielectrometer" instrument uses a conventional parallel plate capacitor geometry, either in fixed plate form or in the form of thin foils to which leads can be attached, and operates in the nominal frequency range 100 Hz to 100 kHz.

The technique that we call "microdielectrometry" differs from the conventional measurement in several ways. First, it uses as sense electrodes a pair of very small planar interdigitated electrodes fabricated as part of a silicon integrated circuit (the "microdielectrometer" chip). This electrode geometry, while much less efficient than the parallel plate geometry in terms of electric field coupling between the electrodes, can be manufactured with great precision using microelectronic techniques, and therefore can yield an electrode pattern with known and highly reproducible calibration. Second, the

technique incorporates high impedance amplifiers in the form of depletion-mode MOSFET's built into the microdielectrometer chip, achieving a sensitivity improvement that more than compensates for the relatively inefficient electrode structure, and permits succesful operation of the device down to 1 Hz and below, an advantage for studying slow relaxations in materials. Finally, with the use of a specially designed electronic feedback circuit, such potential sources of problems as FET temperature and pressure dependences can be cancelled out, permitting the microdielectrometer chip to be used over a wide temperature range (up to 250°C), even when implanted in a bulk specimen of curing material.

Section II of this paper contains a description of the microdielectrometer device and accompanying measurement system. Section III presents examples of the raw data, in the form of gain-phase plots, obtained during the cure of a two-component epoxy-amine system (DGEBA/MPDA). Section IV illustrates how this raw data can be converted into the conventional real and imaginary parts of the dielectric constant by the use of calibration curves developed from two-dimensional computer simulations of the device. Finally, Section V demonstrates how the resulting dielectric constant data can be interpreted to obtain a dynamical relaxation time which is shown to be strongly correlated with the behavior of the viscosity during cure.

II. THE MICRODIELECTROMETER CHIP AND MEASUREMENT SYSTEM

The microdielectrometer chip contains a planar interdigitated electrode and two depletion-mode metal-oxide-semiconductor field-effect transistors (MOSFET's). A top view of a portion of the device is shown in Fig. 1. The outer electrode is called the driven gate, and is connected to a normal bonding pad. The inner electrode is called the floating gate, and extends

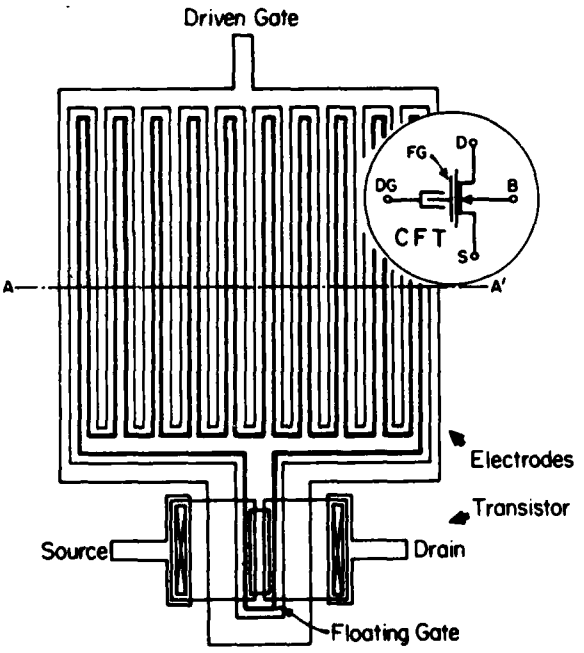

Fig. 1 Top view of sensor portion of microdielectrometer chip

over the channel region of one of the FET's as shown. The silicon dioxide layer between the floating gate and the silicon substrate effectively isolates the floating gate, with the result that there is no electrical connection between the driven and floating gate except through the sample material under study, which is placed over the electrodes as in the schematic cross section in Fig. 2. A sinusoidal voltage applied to the driven gate causes time-varying current (both conduction and displacement current) to flow through the sample toward the floating gate. The capacitance between the floating gate and the substrate collects the charge from this current, this time-varying charge on the floating gate serving to modulate the conductance of the FET channel. Thus, the primary measurement consists of determining the magnitude and phase of the charge on the floating gate produced by a sinusoidal waveform applied to the driven gate. Clearly, this will depend on the dielectric properties of the sample.

In order that the measurement not depend on the electrical characteristics of the FET's (which are subject to manufacture-related variations as well as temperature and pressure dependences), two identical FET's are fabricated on the microdielectrometer chip. The second "reference" FET is connected in a specially designed feedback "interface circuit" which permits measurement of the floating gate voltage by applying to the gate of the reference FET exactly that voltage required to make the two FET currents identical. The details of this circuit are described elsewhere (4).

The microdielectrometer chip as presently designed is 75 mils square, and has a total of eight contacts. The device is mounted onto a standard TO-8 transistor header, and wire bonded. Other, more compact mounting and packaging methods could also be used. The device can be used either by placing a small sample of material over the electrodes or by implanting the entire device into a bulk specimen. In either case, the device can readily be placed in an oven for isothermal or ramped temperature studies. Because of the feedback circuit, no temperature compensation of the measurement is required.

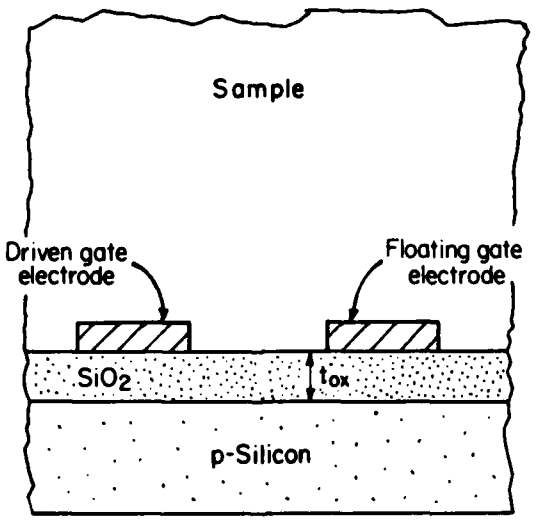

Fig. 2 Cross section of electrode portion of microdielectrometer

A block diagram of the instrumentation system is shown in Fig. 3. The device and interface circuit are connected to a computer-controlled function generator, and the magnitude and phase of the floating gate voltage are measured with a gain-phase meter, also linked to the computer. As will be explained in more detail below, the transfer function between the driven gate and the floating gate depends only on the real and imaginary parts of the dielectric constant (ε' and ε''), and not explicitly on the frequency of the sinusoid. Therefore, there is a unique mapping between measured gain and phase, on the one hand, and ε' and ε'' on the other hand. At present, the graphics display on the HP-85 computer used to run the system is set up for real-time display of the gain-phase characteristic. Typical data for a cure cycle will be presented in the following section. Other components of the system include a link to a larger computer (HP-1000), and access to line printers, cassette storage, and a graphics plotter. All data is stored in files on cassette, permitting very flexible data analysis procedures and with no transcription or re-formatting required.

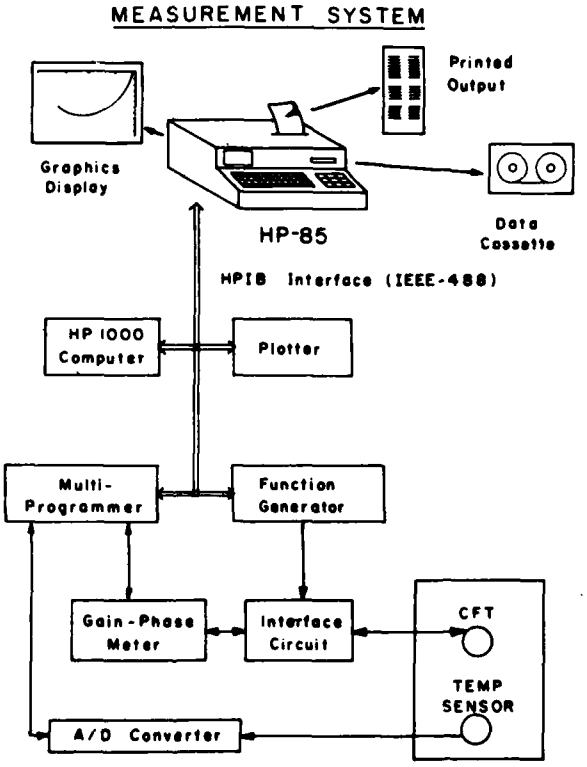

Fig. 3. Block diagram of the measurement system.

III. GAIN-PHASE DATA

The typical experimental sequence is established by a program residing in the HP-85. The operator selects a set of frequencies to be used, and establishes how often measurements are desired. Following initiation of a run, the computer automatically sequences the frequency of the function generator, waits a prescribed settling time, and then records the magnitude and phase of the floating gate voltage from the gain-phase meter.

Figure 4 illustrates a typical run as seen from the graphics display of the HP-85. The sample consists of a stoichimetric mix of DGEBA and MPDA, cured at 80°C, on a device with an oxide thickness of 10,000 Å. For each measurement, a point is plotted in gain-phase space. In the first photograph, two sets of readings at each of seven frequencies have been completed. The pair of points farthest from the origin correspond to 1000 Hz, the next pair to 300 Hz. The remaining points are still clustered at the origin, an expected result given the relatively high conductance of the resin early in cure.

The second photograph shows the display ten minutes later. Two more measurement sequences have been completed. One can easily visualize the "trajectories" followed by the data for each frequency in gain-phase space as the resin cures. As will be explained in Section IV, the trajectory for a particular frequency is due to the variation of the dielectric properties (at that frequency) during cure.

This particular resin system shows a remarkably simple behavior of the various trajectories: they all overlap. The data for 300 Hz follow the same path through gain-phase space as the data for 1000 Hz. Indeed, throughout the frequency range 1-1000 Hz, the data follow a single trajectory with only minor variations, as shown in the third photograph in Fig. 4, taken at the end of cure. Two major trajectories are seen, a primary large trajectory, and a second small trajectory late in cure. The only important difference between the data for the different frequencies is how fast the point moves around the path of the trajectory. The highest frequency goes first, and the lowest frequency last. The strong structure inherent in the data suggests that the behavior of this resin can be modeled with simple relaxation times. This subject is discussed further in Section V.

That the cure trajectory is a well behaved property of the resin system is illustrated by a comparison of the plots in Fig. 5. Figs. 5a and 5b show data from cures at two different temperatures. The path followed is virtually identical in the two cases, but because of the lower temperature, the 60°C data requires a longer time to move across the gain-phase trajectory.

The importance of the device dimensions is illustrated by a comparison of Figs. 5b and 5c. The data in each case are for a cure at 100 C, but the device in Fig. 5c has a thinner oxide layer, resulting in a different apparent gain-phase trajectory. However, since the device dimensions are different, one would expect that the mapping between gain-phase and ε', ε'' might differ. Indeed, it will be shown below that the dielectric data obtained from these two devices using the appropriate calibration curves are the same.

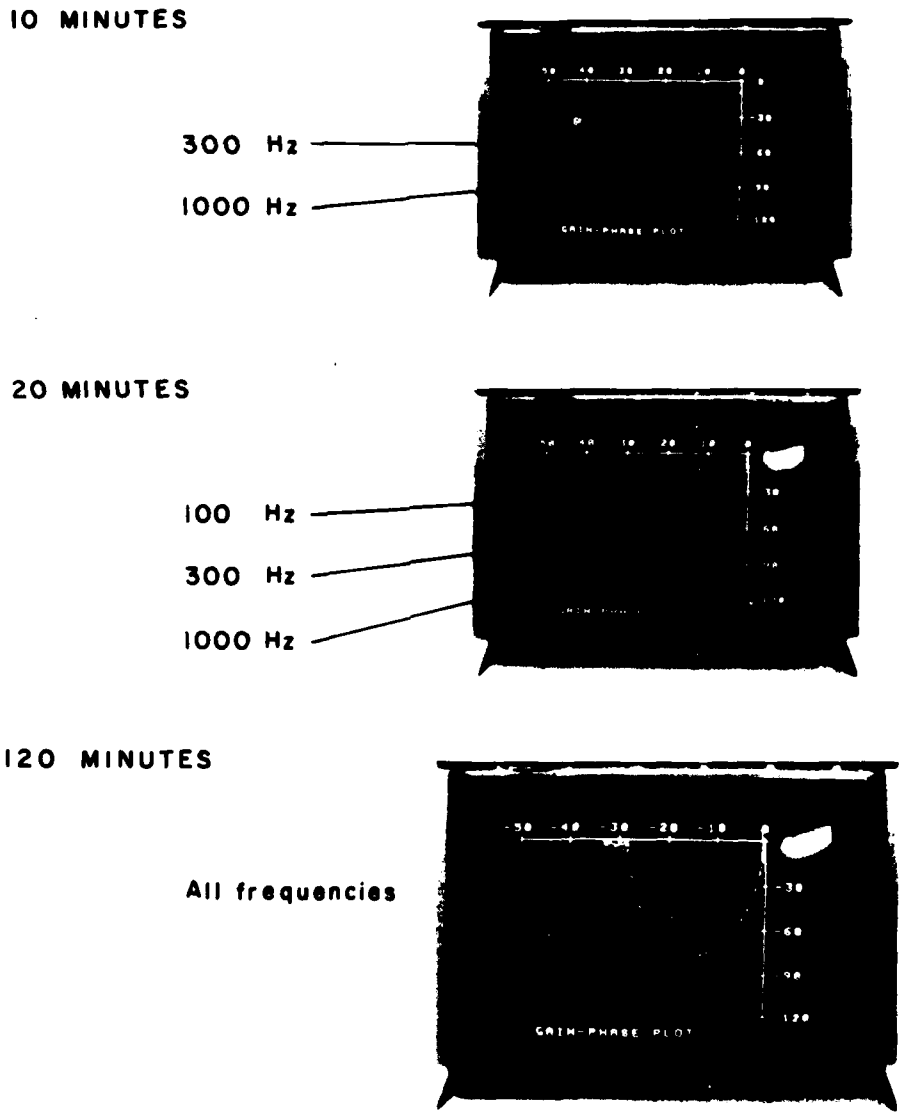

Fig. 4. Typical cure data.

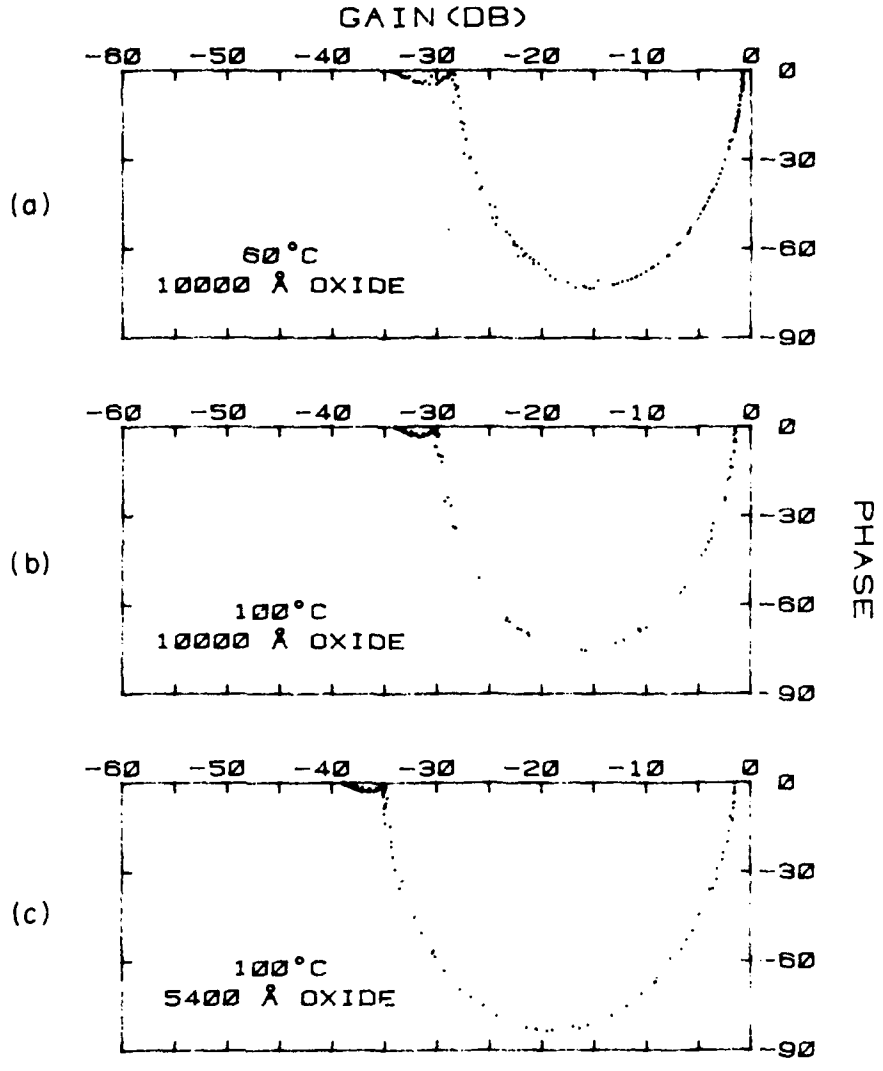

Fig. 5 Gain-phase data for DGEBA/MPDA a) 60°C cure, 10000 Å oxide, b) 100°C cure, 10000 Å oxide, c) 100°C cure, 5400 Å oxide

It is important to note that the present system configuration, in which the raw data is displayed in gain-phase format, can be replaced by a display in which ε' and ε'' are the primary variables. This modification is planned for the near future.

IV. EXTRACTION OF DIELECTRIC DATA FROM GAIN-PHASE DATA

There is a unique correspondance or mapping between the gain-phase data and the real and imaginary parts of the sample dielectric constant (ε' and ε''). Calibration of the microdielectrometer device consists of determining this mapping. The first device models were based on a very approximate distributed RC transmission line (1). This paper uses a much more accurate calibration procedure in which a two-dimensional numerical solution to Laplace's equation is obtained using a complex amplitude for the potential, thereby permitting the effects of both the dielectric constant ε' and the dielectric loss ε'' to be included on an equal footing. This is important since early in the cure, the conductance, or loss term can dominate, whereas toward the end of cure, the dielectric term always dominates. Details of the calibration calculation are available elsewhere (5).

Figure 6 shows a typical set of calibration curves obtained for the device with the 10,000 Å oxide. Several features can be noted. For a perfect dielectric ($\varepsilon'' = 0$), the gain-phase points lie on the gain axis (zero phase shift). This permits a check of the calculated calibration by measuring the high-frequency transfer function of the device in air ($\varepsilon' = 1.0$). The accuracy of the in-air calibration is found to be better than 1 dB for both oxide thicknesses used in these experiments. Examination of the calibration curves shows that near the origin (corresponding to early in cure), the various curves crowd together. This means that the measurement is most prone to error when the data are near the origin, and that small gain offsets or spurious sources of either magnitude or phase errors might produce problems early in cure. Indeed, we have had problems with the calibration for gains above -3 dB, due to a spurious conduction path in the chip design which creates magnitude and phase errors when the resin is highly conductive, and due to a small gain offset (of order 1 dB) between the floating gate FET and reference FET. The details of the origins of these errors, their implications for the interpretation of measurements early in cure, and ways to remove the errors in future designs will be discussed elsewhere (6). For the present discussion, we have elected to ignore all data closer to the origin than -3 dB, and have compensated for the gain offset by a small correction for each device which makes the final high-frequency dielectric constant agree with the result of a parallel plate capacitor measurement on fully cured material. In no case is the gain correction more than 1.2 dB.

The time dependence of ε' and ε'' at three different frequencies for each of the runs illustrated in Figs. 5a, 5b, and 5c are plotted in Figs. 7, 8, and 9. Times to gelation t_g for this resin system are also shown for reference (7). Figs. 8 and 9, which correspond to different device geometries but the same cure temperature, show excellent agreement with one another. This demonstrates that the calibration procedure is basically correct. Comparison between Figs. 7 and 8, corresponding to the same device geometry but differ-

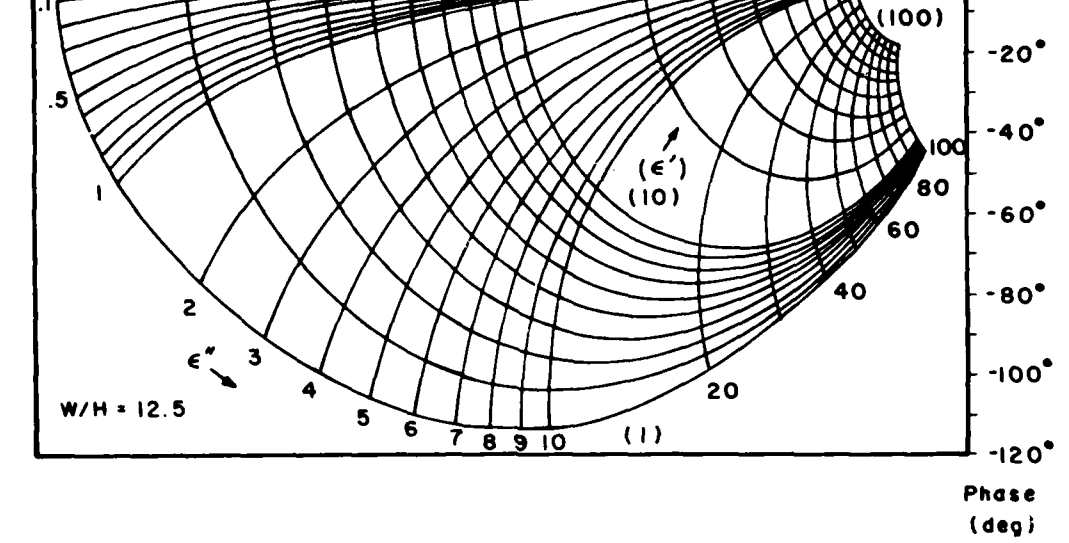

Fig. 6 Calibration plot showing contours of constant permittivity (ε') and loss factor (ε")

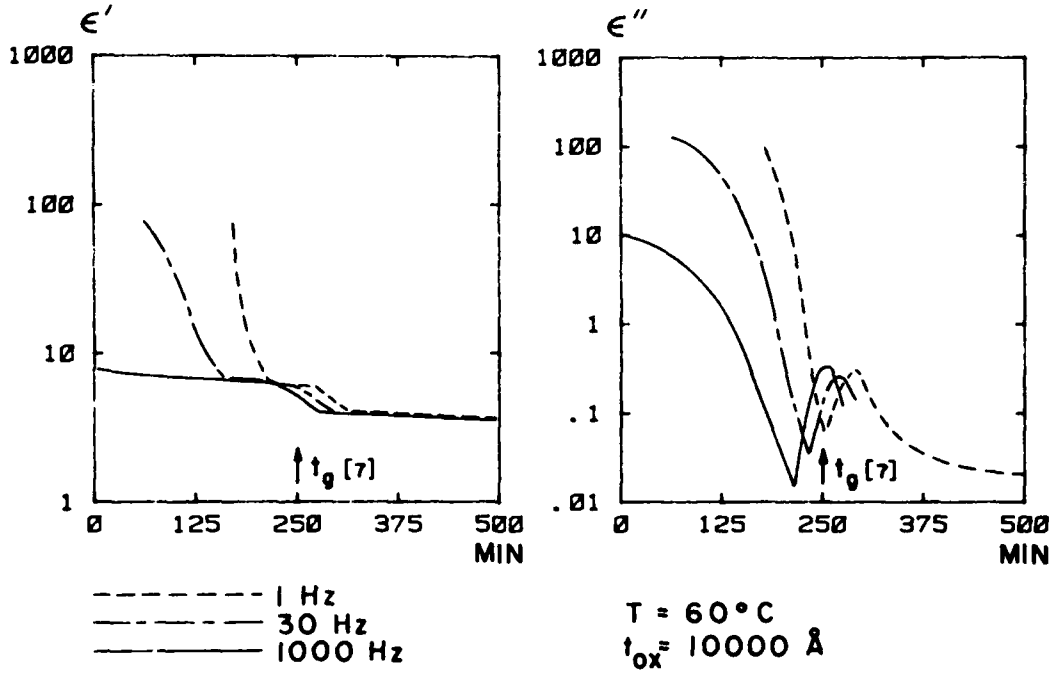

Fig. 7 Time dependence of ε' and ε" for data of Fig. 5a

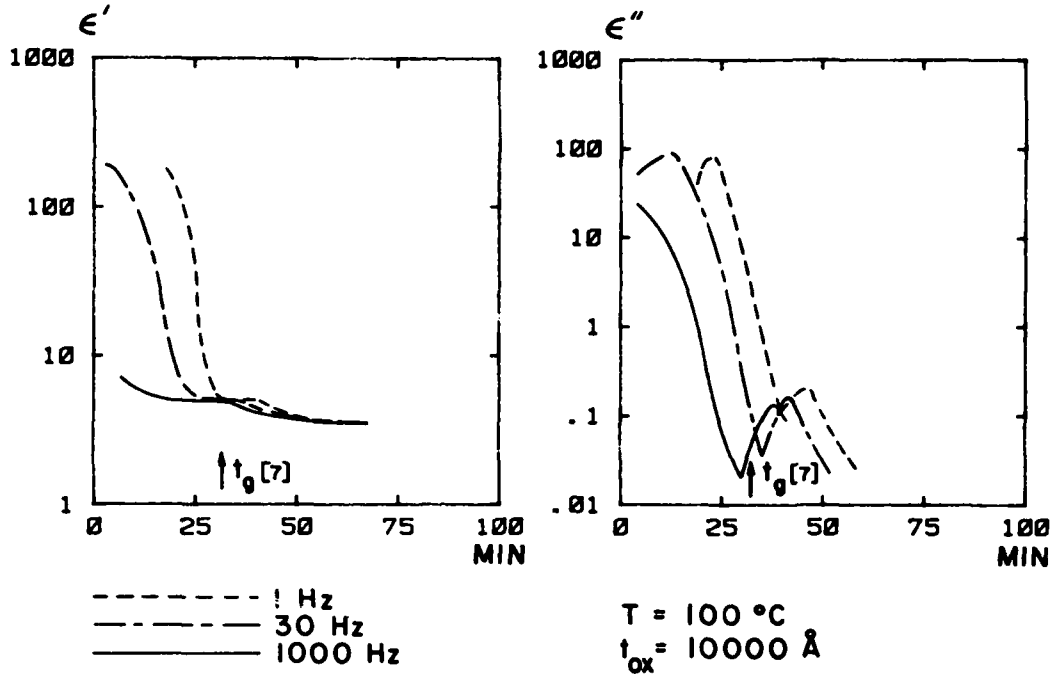

Fig. 8 Time dependence of ε' and ε" for data of Fig. 5b

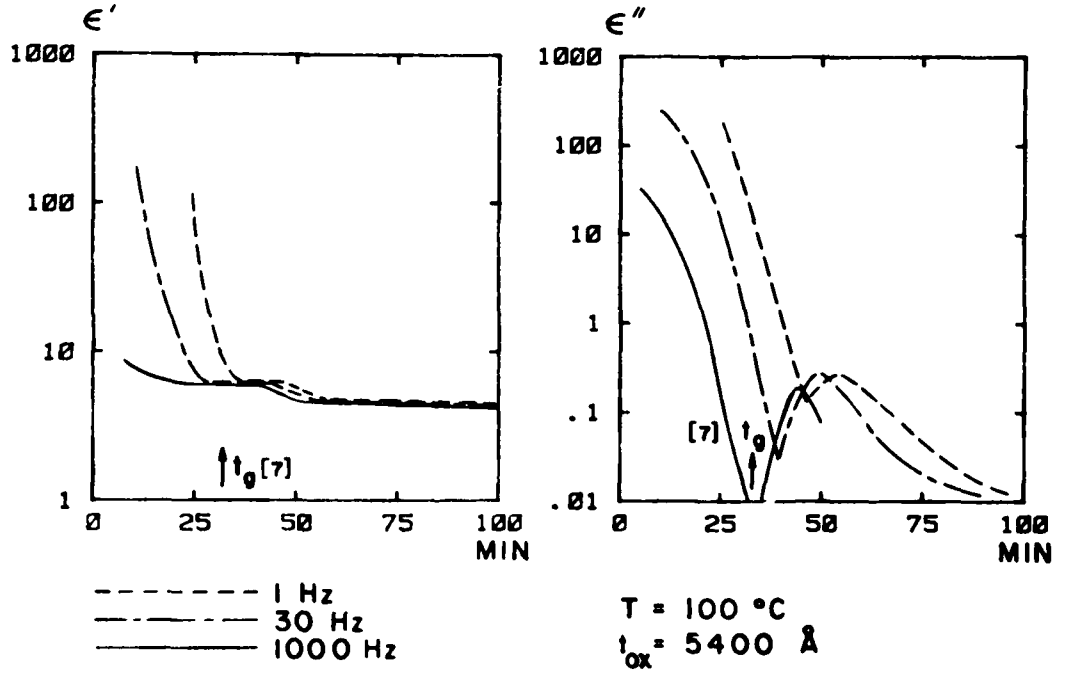

Fig. 9 Time dependence of ε' and ε" for data of Fig 5c

ent cure temperatures, shows that the changing features of the dielectric constant are the same, but occur over a longer time scale as the temperature is decreased, due to the activation of the curing reaction.

The results in Figs. 7 and 8 show that two relaxations are occuring: a large one prior to gelation, and a smaller one after gelation. The frequency dependence demonstrates that the 1 Hz measurement is more sensitive to these relaxations than higher frequencies, which is consistent with a model of dipole orientation. Increased frequency or extent of cure makes it more difficult for the dipoles to respond to the alternating electric field. This leads us to attribute the first relaxation to the increasing viscosity of the liquid phase as the epoxy polymerizes and approaches gelation, and the second to further crosslinking in the gel phase. The principal conclusion is that reliable low frequency dielectric data can be obtained with this device, and with the improved low-frequency sensitivity, direct comparison with other measurement techniques, such as torsional braid analysis, becomes possible.

V. INTERPRETATION WITH A RELAXATION TIME MODEL

The dielectric data presented in the previous section show a great deal of structure. In particular, prior to the classical gelation time, there is a strong dielectric relaxation evident. It can be easily shown that if the dielectric properties of a material obey a simple Debye model (that is, a model for the dielectric constant in which the frequency dependence is described by a single relaxation time), and if only the relaxation time changes with cure conditions, then one would expect all the trajectories in gain-phase space to overlap, as they do in our experiments. This prompted us to attempt to fit the data with a relaxation time model, and to determine how this relaxation time varies with cure.

A good way to examine relaxation time models is to plot ε'' versus ε' (the so-called Cole-Cole plot (8)), using frequency as the plotting parameter. If the Debye model holds, the data lie on a semicircle. The position of a point on the semicircle is determined by the product of the angular frequency and the relaxation time, so knowledge of the frequency permits determination of the relaxation time.

Fig. 10 shows a Cole-Cole plot for the data of Fig. 8 prior to gelation. The points correspond to the values of ε' and ε'', and the dashed curve represents the case for an ideal Debye model having a limiting low frequency dielectric constant of 450 and a limiting high frequency dielectric constant of 6. Agreement with the Debye model is seen to be very good. It should be emphasized that although it appears that only a small portion of the semicircle is covered by the data, the fit to the ideal Debye model is justified by the fact that the approach of the data to the ε' axis is fully perpendicular (8).

The relaxation time was determined at each point in cure prior to gelation, and the results are plotted in Fig. 11 for each of the six devices tested (two oxide thicknesses at each of three temperatures). For any one device, the agreement between the relaxation times determined from different

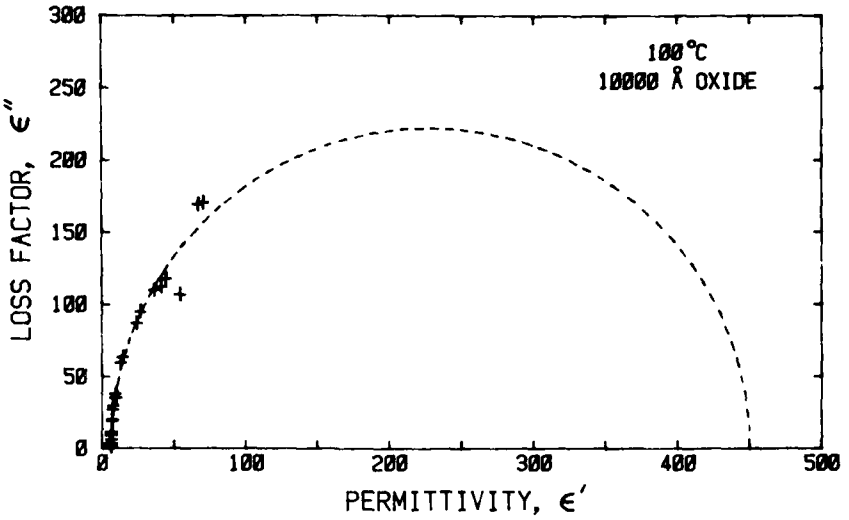

Fig. 10 Cole-Cole plot for data of Fig. 8 before gelation. Dashed line represents Debye model fit.

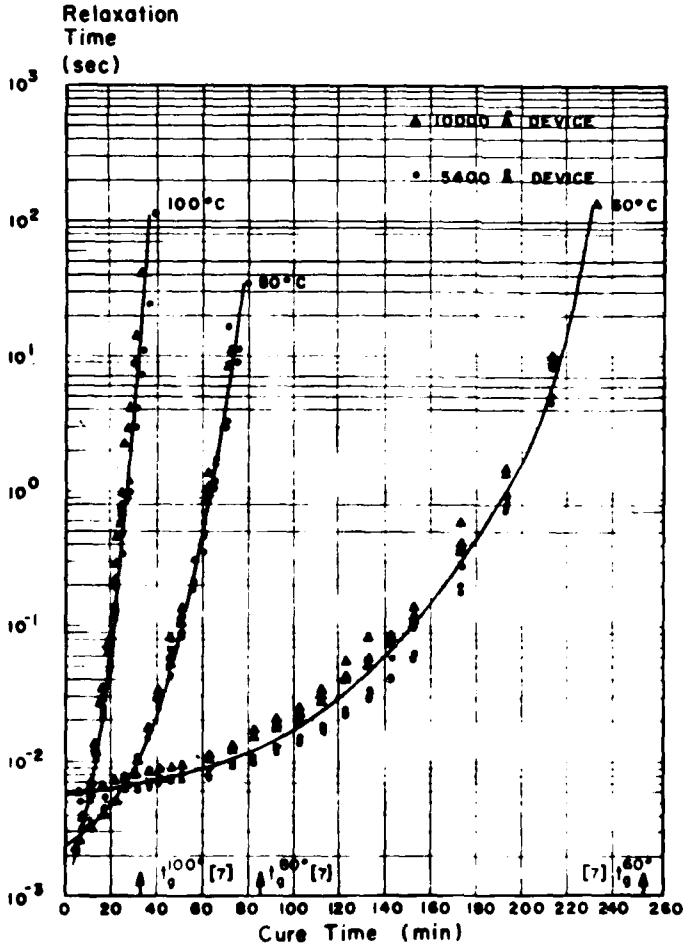

Fig. 11 Relaxation time versus cure time for all experiments.

frequencies at the same elapsed cure time was within 20%. The agreement between the relaxation times determined from the devices with different oxide thicknesses at the same cure temperature was within 50%.

The time dependence of the relaxation time resembles the time dependence of the viscosity of thermosetting systems. The slope of a plot of log viscosity versus time breaks to a much steeper slope as cure proceeds, and is attributed to chain entanglement among the branched polymers formed early in cure (9). Another important similarity to viscosity is that the relaxation time at the start of cure increases as the temperature decreases. In fact, we have found an excellent correspondence between the time dependence of the relaxation time, as determined in our experiments, and the viscosity data reported by Kamal (10), by simply scaling the relaxation time axis appropriately (see Fig. 12). (A similar scaling of dielectric relaxation time and viscosity has been reported by Denney in a very different chemical system (11).) The viscosity data and relaxation time data for various temperatures form a smooth progression. As confirmation of the correspondence between the two, we have plotted in Fig. 13 an Arrhenius plot for the time to reach 400 poise or 8 seconds relaxation time. The points fall on one straight line characterized by an activation energy of 11.5 kCal/mole, indicating that the same process is responsible for the behavior of both the viscosity and the dielectric relaxation time.

VI. DISCUSSION

The results of this paper have been presented in fairly condensed form, and have been organized to emphasize the measurement technique, and the kinds of data that can be obtained with it. Clearly, there is more work to be done on device design, device packaging, and device calibration, particularly near the gain-phase origin. Nevertheless, we have found that it is possible to extract from low frequency dielectric data a quantity (the low-frequency dielectric relaxation time) which appears to carry the same information as bulk viscosity. This relaxation time can be measured entirely electrically, and the data-processing needed to convert gain-phase data to relaxation time is modest enough to be performable on a real-time basis. Thus, one can anticipate being able to monitor the viscosity of a curing system, in situ, and in real time. Given the role played by the viscosity in the determination and control of cure cycles for composites, the microdielectrometer should prove an advantageous addition to the family of cure monitoring methods.

VII. ACKNOWLEDGEMENTS

This work was supported in part by the Office of Naval Research. Particular thanks is due Dr. Leighton H. Peebles, Jr., of ONR, who originally suggested that our work on MOS sensing devices might be usefully applied to cure monitoring problems. Device fabrication was carried out in the M.I.T. Microelectronic Laboratory, a Central Facility of the Center for Materials Science and Engineering which is sponsored in part by the National Science Foundation under contract DMR-78-24185. Some of the instrumentation used in

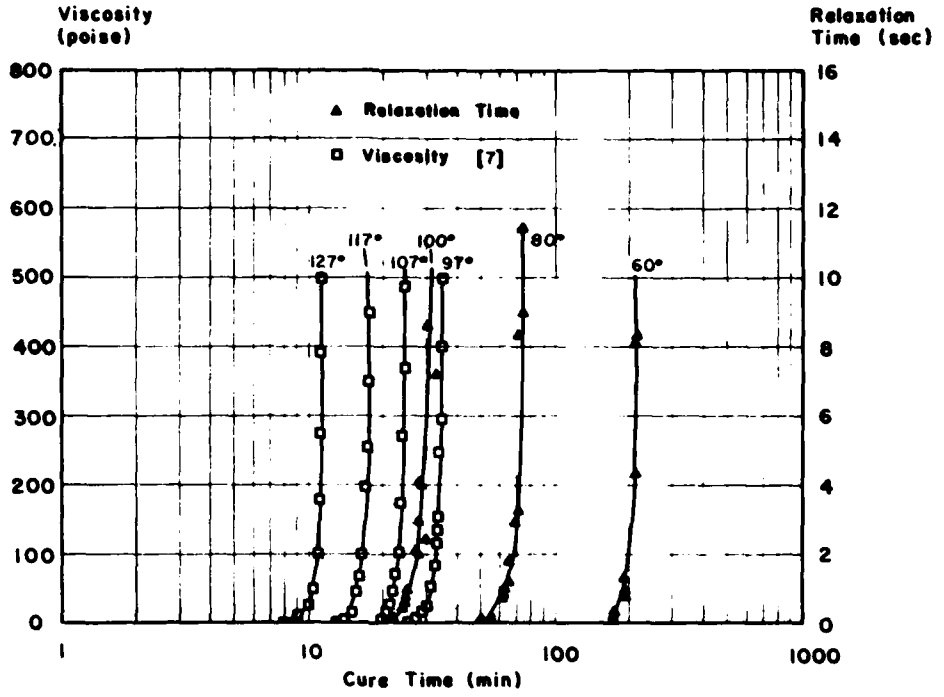

Fig. 12 Comparison between time dependences of relaxation time and viscosity.

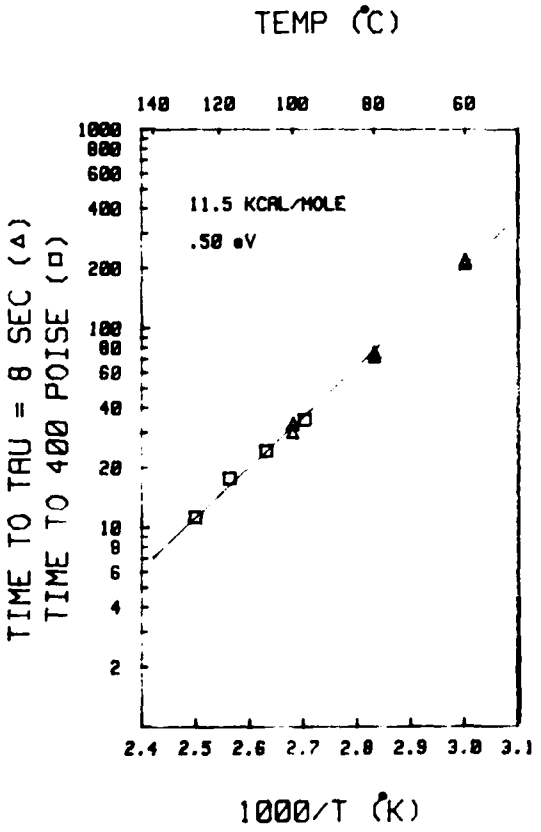

Fig. 13. Arrhenius plot of time in minutes to reach either a fixed relaxation time or a fixed viscosity.

the microdielectrometry system was purchased under NSF contract ENG-7717219. Resin samples used in these experiments were obtained from Dr. N. Schneider of the Army Materials and Mechanics Research Center.

REFERENCES

1. Norman F. Sheppard, Steven L. Garverick, David R. Day, and Stephen D. Senturia, "Microdielectrometry: A New Method for In Situ Cure Monitoring", Proc. 26th SAMPE Symposium, Los Angeles, April, 1981.

2. P. Hedvig, Dielectric Spectroscopy of Polymers, Wiley, New York, 1977.

3. S. Yalof, "Probing Structure with Dielectric Spectroscopy", Chemtech, March 1975, pp. 165-71.

4. Steven L. Garverick and Stephen D. Senturia, "An MOS Device for Surface Impedance Measurement and Moisture Monitoring", IEDM Technical Digest, pp. 685-8 (1980).

5. Huan L. Lee, S.M. Thesis, Massachusetts Institute of Technology, 1981.

6. Norman F. Sheppard, S.M. Thesis, Massachusetts Institute of Technology, 1981.

7. S. Sourour and M. R. Kamal, "Differential Scanning Calorimetry of Epoxy Cure: Isothermal Cure Kinetics", Thermochimica Acta 14, 41 (1976).

8. K. S. Cole and R. H. Cole, "Dispersion and Absorption in Dielectics", J. Chem. Phys. 9, 341 (1941).

9. F.G. Musatti and C. W. Macosko, "Rheology of Network Forming Systems", Polymer Eng. Sci. 13, 236 (1973).

10. M. R. Kamal, S. Sourour, and M. Ryan, "Integrated Thermo-rheological Analysis of the Cure of Thermosets", Technical Papers, 31st Annual Technical Conference, Society of Plastics Engineers, Montreal, May 1973, p. 187.

11. D. J. Denney, "Viscosities of Some Undercooled Liquid Alkyl Halides", J. Chem. Phys. 30, 159 (1959); "Dielectric Properties of Some Liquid Alkyl Halides", J. Chem. Phys. 27, 259 (1957).

INTERACTIVE COMPUTER PROCESS SYSTEM FOR COMPOSITE AUTOCLAVE FABRICATION

Richard J. Hinricks

Applied Polymer Technology
Costa Mesa, CA 92627

ABSTRACT

A computerized system was developed to monitor and control autoclave cure process. Feedback sensors were used to follow rheological state of the composite material during cure and actually drive the autoclave controller.

Session II: MOISTURE

Chairperson: D. M. PINKERTON

Materials Research Laboratories, Australia

EFFECTS OF MOISTURE ON THE MECHANICAL PROPERTIES OF GLASS/EPOXY COMPOSITES

C. D. Douglas and E. R. Pettie
Army Materials and Mechanics Research Center
Composites Development Division
Watertown, Massachusetts

ABSTRACT

Two glass/epoxy systems differing only in coupling agents have been analyzed. The effects of moisture on the mechanical properties have been found as a function of immersion time. The specimens were all six-ply unidirectional laminates cut at five different fiber angles. Temperatures of the immersion baths range from 25°C to 80°C.

It was found that there was up to a 60 percent decrease in ultimate strengths after three months of immersion in the 80°C bath. Stiffnesses have been found to decrease also but to a lesser extent than that of ultimate strengths.

Changes in specimen weight were monitored and observed to increase as much as 3.5 percent by weight.

After extended immersion time at elevated temperatures, specimen weights began to drop, possibly as a result of some leaching phenomena. It was also noticed that moisture content did vary as a function of fiber angle for one of the composite systems.

INTRODUCTION

Advanced composites are being used more and more as structural materials in military and commercial applications. The mechanical properties of these composites undergo a variety of changes during their service life due to specific loading conditions and environment.

The scope of this paper is to present data showing the effects of moisture on the mechanical properties of a specific glass/epoxy composite system. The reason for choosing this composite is that the SP250 prepreg (3M Company, St. Paul, MN) is a candidate material for the fabrication of Army composite helicopter rotor blades.

There have been a number of researchers who have looked into the change in properties of these composites as a function of temperature and moisture content (1-10). At lower temperatures, the degradation process is usually quite slow, but at elevated temperatures, this process affects the material very rapidly. There are three possible areas where the material may be attacked:

1. degradation of the matrix material
2. degradation of the fiber
3. degradation of the matrix/fiber interface

It has also been shown that the loss of mechanical properties levels out after the material has come to equilibrium with its surroundings (8). Degradation of the composite has been found to be reversible provided that the matrix, glass, or interface is not chemically attacked. In this work, there is evidence that the matrix was indeed altered during immersion at elevated temperatures. As a result it is expected that those specimens when dried, will not return to their original strengths. Moisture content, modulus and strength retention were measured for two glass/epoxy systems differing only in coupling agents, and there was no attempt to measure the strength of the specimens once dried after immersion. We are currently in the process of performing these experiments. The test results reported in this paper used laminates fabricated with materials as received from the supplier. Five fiber angles and four immersion bath temperatures were examined.

The data presented here is intended to be used as a tool for the designer who uses glass/epoxy composites that might be subjected to a similar environment.

EXPERIMENTAL

The material used for this study was Scotch Ply reinforced plastic. Specifically, two systems were used, differing only in the coupling agent that was applied to the glass.

The matrix material for this composite is an epoxy (SP250). The complete formulation for this resin has been established (11) and is presented in Table I.

Table I

Component	Wt %
ECN 1273, epoxy cresol novalac	45.8
EPON 828, diglycidyl ether of bisphenol A resin	38.1
Cardolite 513, epoxy resin flexibilizer and reactive diluent	4.7
Dicyandiamide, curing agent	7.5
Monuron, accelerator	3.8
TOTAL	99.9

The glass used for the prepreg was S2 and is supplied by Owens Corning Fiberglas (OCF). Two silane-based coupling agents were used in preparation of the

composite systems analyzed. These agents are proprietary to OCF and designated as 463 and 449, where the 449 coupling agent is the newer of the two developed to enhance composite performance when subjected to a hygrothermal environment.

The materials were used as received to fabricate 6-ply unidirectional laminates having dimensions of 76.2 cm x 137.2 cm.

Unidirectional prepreg tape, 15.24 cm in width, was used to fabricate the laminates by standard hand layup procedures. The laminates were then cured in an autoclave according to the manufacturer's recommended cure cycle. Once cured, tension specimens were cut from the laminates at five different fiber angles. These angles are 0°, 10°, 30°, 45° and 90° off-axis. After cutting, all specimens were preconditioned at 50°C and under full vacuum in a Univar vacuum oven. The changes in weight were monitored and found to decrease by less than one percent. All specimens stabilized within 275 hours.

After preconditioning, approximately 20 specimens for each system were sacrificed for matrix burnout experiments to determine fiber volume.

Because of variations in processing conditions a range of specimen thicknesses was observed. Figures 1 and 2 show fiber volume versus average specimen thickness curves for the two systems used.

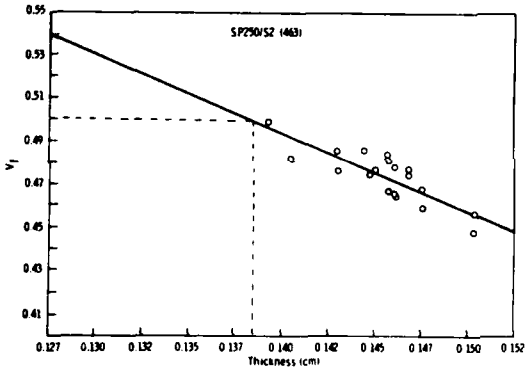

Figure 1. Volume fiber percent versus specimen thickness for the system with the 463 coupling agent. Dotted lines indicate V_f = 0.5 at a thickness of .138 cm.

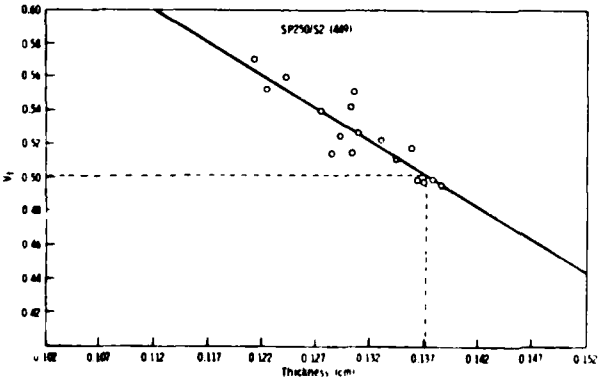

Figure 2. Volume percent versus specimen thickness for the system with the 449 coupling agent. Dotted lines indicate V_f = 0.5 at a thickness of .137 cm.

From these curves, the thickness was found which correlated to a fifty percent fiber volume. This data was used to normalize the strength values found for each specimen. It is interesting to note that although the specimens using the 463 coupling agent were generally thicker, the 50 percent fiber volume thicknesses for each system were very close.

Next, five specimens for each angle from the two systems were tested in the dry state, and used as controls. The remaining specimens were immersed in distilled water baths at four different temperatures. These temperatures were 25°C, 40°C, 60°C, and 80°C. Temperature fluctuations were not greater than $\pm$1°C.

Seven data points for strength and stiffness were obtained over a period of one year. The testing times from the date of immersion were: one week, one month, two months, three months, six months, nine months, and one year. At each temperature, five specimens from each system and fiber angle were immersed to obtain one data point, giving a total of 1600 specimens used for the program. During the early stages of immersion, specimen weights were monitored more frequently to obtain the necessary data used for calculating diffusion coefficients.

The specimens required for a given data point were removed from the bath on their due date and their time of removal was recorded. The specimens were weighed after being wiped gently to remove any excess water droplets on the surface. The final weight percent was then calculated. Next the specimens were left on a bench for one half hour before testing. This was done in order to equilibrate the sample temperature. Tension testing was performed in a temperature- and humidity-controlled laboratory. Laboratory conditions were maintained at 25°C and 50 percent relative humidity.

All tension testing was done on an Instron floor-model machine at a constant crosshead speed of 0.127 cm per minute. A clip-type extensometer was used to determine tangent modulus.

RESULTS

Because of the size of the test matrix used for this study, more data was acquired than could be fully analyzed at the time of this writing.

It was evident at early stages that the SP250/S2 composite system with the newer 449 coupling agent behaved differently than that of the system which used the original 463 coupling agent. Weight percent change was followed throughout the complete testing program by periodic weighing on a Mettler balance. At no time during each weighing was any specimen out of the water for more than 20 minutes. For this reason no significant amount of moisture could have diffused out of the specimen.

Figure 3 shows the weight percent change as a function of root time at an immersion temperature of 25°C.

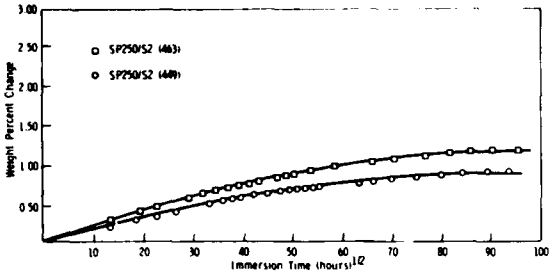

Figure 3. Percent weight change as a function of root time at an immersion temperature of 25°C.

It can be seen that the system with the 449 coupling agent did not absorb as much water as that of the system using the 463 coupling agent. The difference after one year of immersion was approximately 0.3 percent, where the total weight change was 1.2 percent.

Figure 4 shows how the dimensionless strength was affected during the experiment, where the dimensionless strength is that strength at testing time divided by the dry strength. Table II gives values of dry strength for all angles for the two systems.

Table II

Angle of Axis	σ_o (463)	σ_o (440)
0°	1430	1400
10°	320	290
30°	115	110
45°	76	76
90°	50	--

Note. Value of dry strength (σ_o) in MPa

At this point it should be mentioned that there were no 90° off axis specimens for the SP250/S2(449) system. Due to a loss of coolant during cutting the specimens were burned and had to be discarded.

Figure 4 shows the change in dimensionless strength during the immersion time.

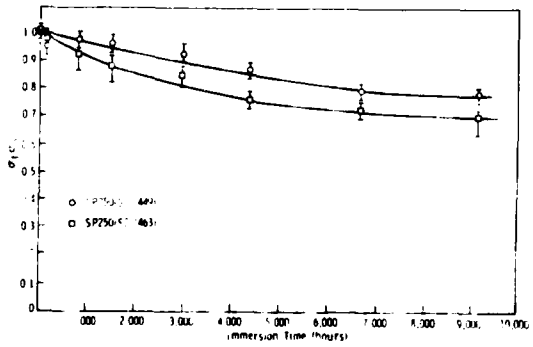

Figure 4. Change in dimensionless strength versus immersion time at 25°C.

From this plot it is apparent that the strengths are affected by diffusion of water into the specimens. At the time of the last test, the system using the 449 coupling agent fell to approximately 80 percent of its initial strength while the system using the 463 coupling agent fell to 70 percent of its original strength. At this immersion temperature [25°C] it was not possible to notice any difference in the dimensionless strengths for the various angles tested, although as shown in Table II they differ greatly as a function of angle.

Figure 5 shows how the modulus of each system was affected by immersion at 25°C. It can be seen that for each angle there was little or no change, and both systems behaved the same although there was a significant amount of scatter in the data.

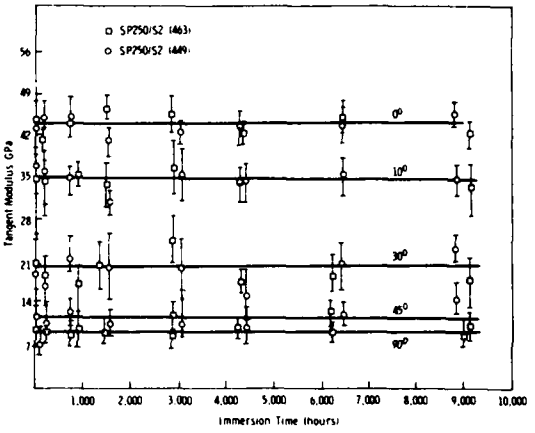

Figure 5. Plot of modulus versus immersion time at 25°C for all angles.

At higher immersion temperatures the differences in the behavior of the two systems became more noticeable.

Figure 6 shows the weight percent change versus root time for the two systems immersed in 40°C water.

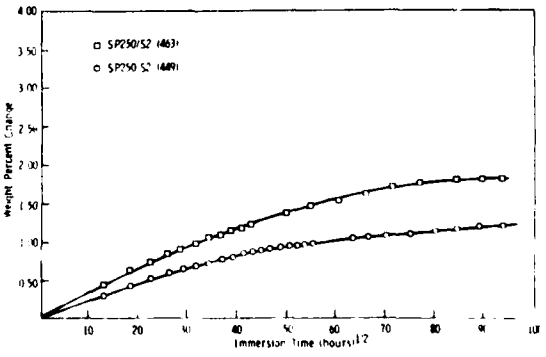

Figure 6. Percent weight change as a function of root time at an immersion temperature of 40°C.

At the last testing time, the 463 system appears to have gained approximately 1.75 percent weight while the 449 system had increased in weight by only 1.2 percent. As compared to the 25°C immersion tests, there is a noticeable difference in total weight gain between the two systems. At this temperature [40°C] it was not possible to notice any difference in absorptive behavior for the five different angles used in each system. It was also difficult to notice any angle dependence on the dimensionless strength as a function of time. Figure 7 present this data.

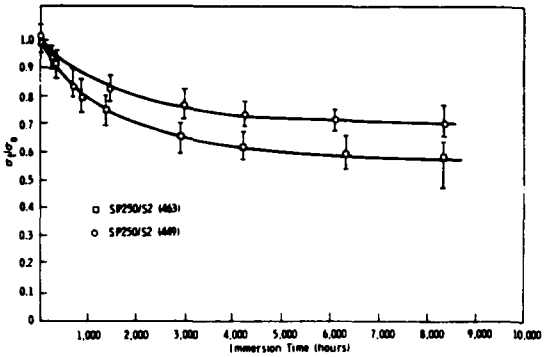

Figure 7. Change in dimensionless strength versus immersion time at 40°C.

It is apparent from Figure 7 that the composite using the 463 coupling agent fell to approximately 60 percent of its original strength during the test program, while the composite using the 449 coupling agent fell to roughly 75 percent of its dry strength. It should be noted that both curves appear to level out at an immersion time of 2800 hours.

The change in moduli of the two systems as a function of immersion time is shown in Figure 8.

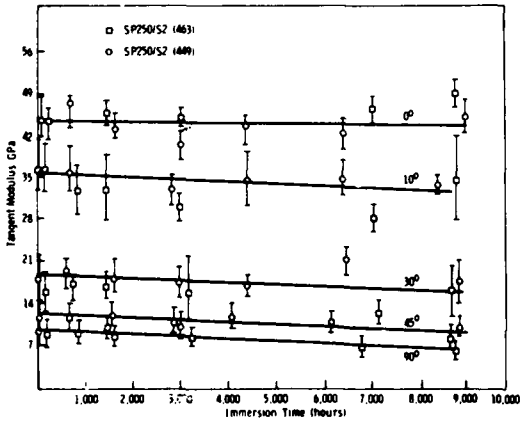

Figure 8. Change in Modulus versus immersion time at 40°C for all angles.

At a 40°C immersion temperature there is no change in modulus for the specimens with zero degree orientation, although at angles off-axis there is a slight effect. We are also unable to see a difference between the two systems as far as a modulus change is concerned.

As specimens were tested at higher temperatures, 60°C and 80°C, the effects of moisture on the mechanical properties became more noticeable.

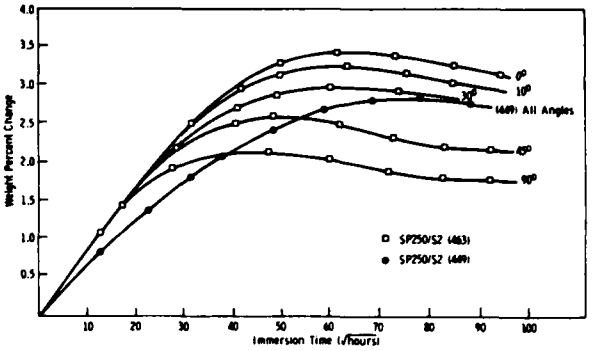

Figure 9. Percent weight change as a function of root time at an immersion temperature of 60°C.

Absorption rates and decreases in strengths changed dramatically. Figure 9 presents the change in weight percent as a function of root immersion. At this immersion temperature there were noticeable effects of fiber orientation on the moisture content for the specimens using the 463 coupling agent. The specimens that had the 90° off axis fibers in them exhibited the least amount of moisture pickup, and as the fiber angle decreased with respect to the axis, the specimen picked up more moisture. It was also noticed that at this temperature the specimens began to lose weight at a time of approximately 2500 hours. The system that used the 449 coupling agent, however, did not exhibit this angle-dependent moisture absorption, nor did it show as great an effect in loss of weight as the 463 system.

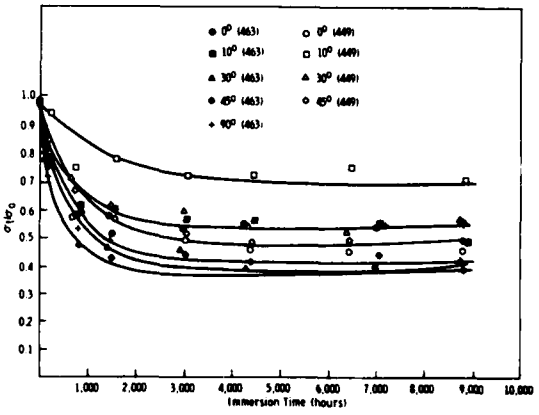

Figure 10. Change in dimensionless strength versus immersion time at 60°C.

The change in dimensionless strength as a function of immersion time is presented in Figure 10. At a temperature of 60°C, the absorption of water into the composite had a severe effect on the ultimate strength. Strengths have decreased by up to 60 percent. The change in dimensionless strength were not independent of fiber angle as was previously observed at 25°C and 40°C immersion temperatures. Nor were the strengths of the specimens using the 449 coupling agent consistently higher than those of specimens using the 463 coupling agent.

It was observed that the system using the 449 coupling agent was slightly higher in strength for the 30° and 45° off axis specimens while the 10° off axis specimens were considerably higher. The only angle where the system using the 463 coupling agent was stronger was that of the 0° off-axis specimens.

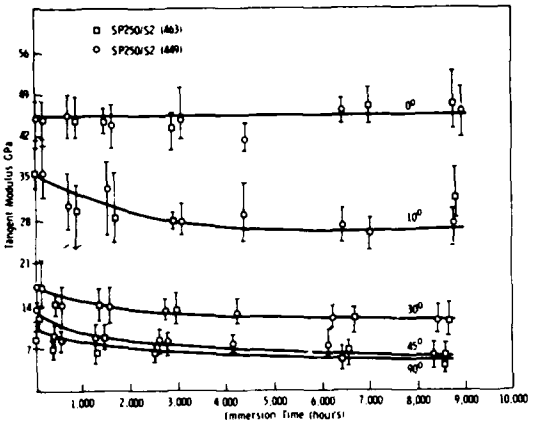

Figure 11. Change in modulus versus immersion time at 60°C for all angles.

The moduli of the specimens immersed at this temperature were also significantly affected. Figure 11 presents this data. Again the specimens with 0° orientation showed little or no effect of moisture on the modulus whereas the off-axis specimens were definitely affected. The 10° off-axis specimens lost roughly 20 percent of their stiffness as did the 30° off-axis specimens, while the 45° and 90° off-axis specimens lost up to 50 percent of their original stiffness after one-year immersion at 60°C.

The final temperature that specimens were immersed at was 80°C. As expected, immersion at this temperature had the greatest effect on moisture absorption, strength, and stiffness change.

Figure 12 shows how the weight changed for both systems when exposed to this environment.

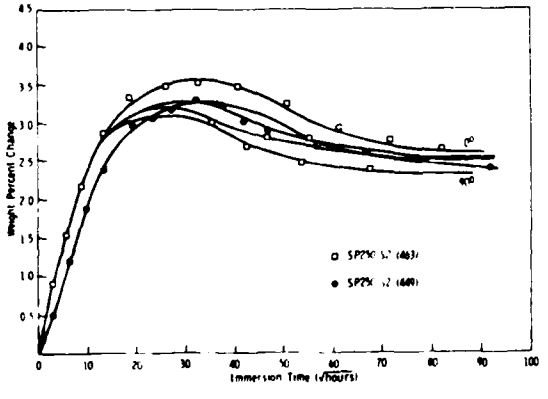

Figure 12. Percent weight change as a function of root immersion time at temperature of 80°C.

At this temperature, 80°C, again some angle dependence is apparent, but to a lesser degree than that exhibited at 60°C immersion. The system using the 463 coupling agent is less banded than before, but the zero degree specimens still show more moisture uptake than do the 90° specimens. It is apparent that the system using the 449 coupling agent does not exhibit angle dependence. It can also be seen that after 8000 hours there is a weight loss of up to 1.5 percent.

The strengths of the 80°C immersion specimens were affected drastically. Figure 13 shows the drop in strength retention at this temperature. Within 100 hours, the strengths of some specimens fell to within 50 percent of their original value. Again, all but the 0 degree off-axis specimens of the 449 system exhibited better strength retention characteristics that the 463 system. As in the 60°C immersion tests, the 10 degree off-axis specimens showed the greatest amount of strength retention.

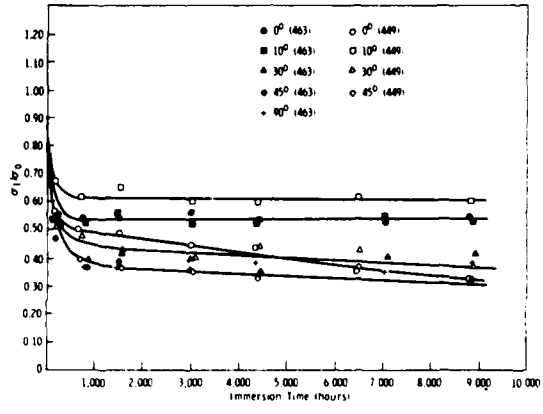

Figure 13. Change in dimensionless strength versus immersion time at 80°C.

Finally in Figure 14, modulus change as a function of immersion time is shown. It can be seen that the 0 degree off-axis specimens are affected very little if at all, whereas the 10-, 30-, 45-, and 90-degree off-axis specimens show a significant reduction in modulus, with decreases of up to 50 percent after 2000 hours. After this initial reduction, the modulus remains constant throughout the remainder of the experiment.

DISCUSSION

It has been shown that the mechanical properties of glass/epoxy laminates are greatly affected by the presence of moisture within the composite. The strengths of the specimens have decreased by 60 percent in cases where the immersion temperature of the water bath was 80°C, and to a lesser extent at lower immersion temperatures. The moduli of the specimens tested were also affected by this hygrothermal environment. At 80°C the modulus dropped to approximately 50 percent of its original value for the 90 degree off-axis specimens while the 45-, 30-, and 10-degree off-axis specimens were not affected quite as much. The 0 degree off-axis specimens showed no change in modulus as would be expected. It was not possible to notice any difference in moduli between the two systems using the 449 and 463 coupling agents.

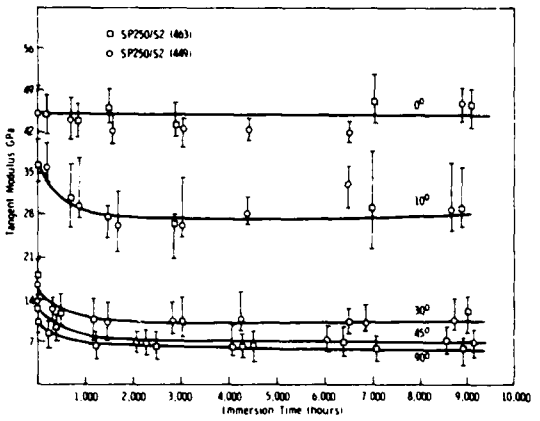

Figure 14. Change in modulus versus immersion time at 80°C for all angles.

Generally, as was shown in Figures 1 and 2, the specimens from the system using the 449 coupling agent were thinner, therefore having a higher fiber volume and lower resin content. This fact could explain the reason that the 449 system picked up less weight during the immersion time, but does not explain why the slopes of the curves were different. One possible explanation for the different rates of absorption could be that the 449 system did not allow moisture to be transported along the matrix-fiber interface as readily. If this were the case, an angle dependence would be noticed during the uptake portion of the curve. At elevated temperatures, (60°C and 80°C) the amount of moisture absorbed was dependent on the fiber angle of the specimen. This was noticed only in the system using the 463 coupling agent. The specimens using the 449 coupling agent showed some separation but it was not defined well enough to determine which angle was affected most. At 80°C the specimens using the 463 coupling agent showed an angle dependence, but at longer immersion times both systems exhibited a loss in weight. The weight losses were quite severe, with some specimens losing up to 15 percent by weight. Upon noticing this, a number of specimens were extracted from the water baths and placed in a vacuum oven at 50°C to dry. It was found that when dry, the specimen weight was less than the original dry weight before immersion. This weight difference was equal to the weight loss during immersion, indicating that there was some material loss from the specimens.

To determine what was lost, the water in the immersion baths was analyzed. Water was extracted from individual baths and drawn off by evaporation. The residue remaining was then put into a pellet form with a KBr salt. This was analyzed using Fourier transform infrared spectroscopy. From the infrared curves, it is suspected that the residue contained dicyandiamide, the curing agent, and a small amount of hydrolized epoxy groups. Further chemical analyses have yet to be performed to determine whether any material was carried away during the evaporation process.

The time at which the change in dimensionless strength approaches zero is roughly 2000 hours for the 60°C immersion baths and 500 hours for 80°C. It can be seen from the absorption curves that this is well before the time at which the maximum moisture content is reached and also before any loss of weight in the specimens is noticed. This implies that once the strength has initially dropped, it is unaffected at high moisture contents and even after material has been lost from the specimen when tested in the wet condition. The strengths of the 0-degree specimens were affected more than was expected. Because the number of specimens used in this program exceeded 16000 it was not feasible to tab them all. It is thought that the 0-degree specimens did not fail in pure tension, but shear at the grip surfaces.

It should also be noted that because these were all unidirectional laminates, there was coupling between extension and shear on the 10-, 30-, and 45-degree off-axis specimens. Little microscopic information has been obtained on the material tested. There is evidence that cracking of the specimens has taken place. Photomicrographs of the specimens show many damaged areas, especially near the specimen surface. Also, on the surface of the specimens it was noticed that a significant amount of blistering had occurred. If the specimens were tested shortly after immersion, the strengths tended to increase slightly. This has been observed by other investigators. It is believed that this is due to a relaxation, possible because of resin plasticization, of the residual stresses caused by the curing cycle.

CONCLUSION

At this point, we are just beginning to analyze the data that was obtained. Much more work needs to be done. The next step would be to perform an in-depth chemical analysis of the water used in the immersion baths to determine quantitatively what is lost from the material. Further work should be devoted to microscopic examination of the failed specimens to determine what type of failure mechanism is most dominant, and whether this will change as a function of moisture content in the material. It is also suggested that strengths be found for the specimens that have been dried after losing weight.

Finally, it should be mentioned that water immersion at temperatures higher that 50°C is an extremely severe environment for glass/epoxy composites. Under normal outdoor exposure, this amount of deterioration is virtually not existent.

REFERENCES

1. Browning, C. E. and Hartness, J. T., "Effect of Moisture on the Properties of High-Performance Structural Resins and Composites," ASTM, STP, pp 284-302, 1973.

2. Ishai, O. and Mazor, A., Journal of Composite Materials, Vol. 9, 1975, p 370.

3. Herz, J., "Investigation into the High Temperature Strength Degradation of Fiber-Reinforced Resin Composites during Ambient Ageing," No 1-1-50-13649, National Aeronautics and Space Administration, 1973.

4. Augl, J. M. and Berger, A. E., "The Effect of Moisture on Carbon Fiber Reinforced Composites. III Prediction of Moisture Sorption in a Real Outdoor Environment," NSWC/WOL TR 77-13, June 1977, Naval Surface Weapons Center, Dahlgren, Virginia.

5. Augl, J. M. "Prediction and Verification of Moisture Effects on Carbon Fiber-Epoxy Composites," NSWC/TR 79-43 March 1979, Naval Surface Weapons Center, Dahlgren, Virginia.

6. Renton, W. J. and Ho, T., "The Effect of Environment on the Mechanical Behavior of AS/3501-6 Graphite/Epoxy Materials," Final Phase 1 Report, NASC No. N00019-77-C-0309, June 1978. Vought Corporation, Dallas, Texas.

7. Whitney, J. M. and Browning, C. E. in Advanced Composite Materials - Environmental Effects, ASTM STP 658, J. R. Vinson, Ed , American Society for Testing and Materials 1978, p43.

8. Ishai, O. "The Effect of Environmental-Loading History on the Transverse Strength of GRP Laminates," Journal of Composite Materials, Vol. 9, October 1975, p 370.

9. Allred, R. E. and Roylance, D. K. "The Influence of Moisture on the Transverse Mechanical Behavior of Kevlar 49/Epoxy Composites at 25°C," to be published in the Proceedings of a Critical Review: Characterization of Composites, held at MIT, June 1981.

10. Ho, T. and Schapry, T. A., "The Effect of Environment on the Mechanical Behavior of AS/3501-6 Graphite/Epoxy Material, Phase III" ATC Report No. R-92100/1CR-5, January 1981, Vought Corporation, Dallas, Texas.

11. Sprouse, J., Personal Communication, Army Materials and Mechanics Research Center, Watertown, Massachusetts..

AD-A116 733 ARMY MATERIALS AND MECHANICS RESEARCH CENTER WATERTOWN MA F/G 11/4
PROCEEDINGS OF THE CRITICAL REVIEW: TECHNIQUES FOR THE CHARACTE--ETC(U)
MAY 82
UNCLASSIFIED AMMRC-MS-82-3 NL

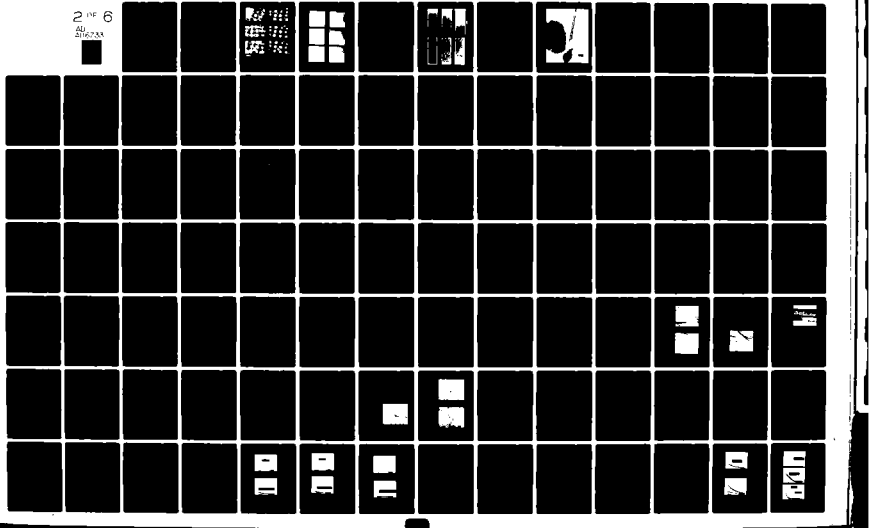

"ACCOMMODATION AND RELAXATION OF STRAIN DURING MOISTURE SORPTION".

K H G Ashbee, J P Sargent and Elizabeth Walter

University of Bristol, H H Wills Physics Laboratory,
Royal Fort, Tyndall Avenue, Bristol BS8 1TL, England.

Data from three different experiments will be presented. In one experiment, the radial and tangential components of the stress field present around an individual glass fibre after cooling from the resin cure temperature have been measured. In order to reduce the problem to one of two-dimensional elasticity, thin transverse sections are cut from a long unidirectional composite. Accommodation of shrinkage by way of rigid body displacements in the transverse plane are prevented by casting the composite inside a thick walled glass tube to the inside wall of which, the resin remains firmly adhered. The unrelaxed radial and hoop principal stresses within any slice subsequently removed from the specimen are then measured using the oblique incidence photoelastic method described by Durelli and Riley. The radial principal stress for the square fibre array adopted in the Adams finite element model is compressive and more or less constant with distance from the fibre, at 6 MPa. The hoop principal stress is of the order of 100 MPa tensile at the fibre/resin interface, falling to approximately 20 MPa tensile at a distance of one fibre diameter from the interface.

In a second experiment, designed to investigate swelling anisotropy during water uptake, a microscope cover slip is bonded to the composite or laminate specimen and its deflection is observed during exposure to an aqueous environment. The gap between the free surface of the deformed cover slip and an optical flat is used to generate optical interference and, by creating Moiré images from photographs of the pattern of interference fringes, it is possible to monitor and measure the displacement field as it develops during resin swelling.

By applying thin plate elasticity theory to the deformation of the cover slip, measured displacements have been converted into stresses in the plate. For a unidirectional S2 glass fibre reinforced epoxy specimen, the maximum compressive stress is 1 bar where diffusion has occurred transverse to the fibres and 2 bars where it has occurred parallel to the fibres. These numbers are presumably relevant to the phenomenon of interlaminar swelling.

Anisotropy of swelling in a laminate can be further investigated by bonding a rectangular cover slip to a surface cut and polished transverse to the plane of lamination. Measurements on a 57-ply carbon fibre/epoxy laminate indicate swelling stresses large enough to fracture the cover slip. The rate of swelling and the level of swelling at saturation are both significantly lessened by dissolving inorganic salts in the aqueous environment to which the composite is exposed.

Differential thermal contraction between fibre and matrix materials during cooling to room temperature from the highest temperature reached during curing amounts to net shrinkage of the resin and introduces stress into both materials. The principal stresses in the fibre include an axial compressive stress, which arises by way of a shear stress transferred at the interface that builds up with distance from each fibre end plus, in short fibre composites, a normal compressive stress transferred across the fibre ends. When the composite is viewed between crossed polars, birefringence associated with this stress causes glass fibres to appear bright. Analysis of the stress field shows that, for light travelling through a fibre diameter in the x-direction, the fast and slow axes of polarisation are parallel and perpendicular to the fibre axis. The relative retardation is of the form:

$$R = \frac{d}{\lambda} [\, \mu_1 (x) - \mu_2 (x) \,]$$

where μ_1 and μ_2 are the refractive indices in the directions of the fast and slow axes.

Some of the contrast is, of course, due to birefringence in the resin above and below each fibre. In addition to birefringence arising from elastic strain in the resin, there is the possibility of birefringence due to molecular orientation. The highly polar fibre surface attracts specific groups in the resin, such as double carbon bonds, polar end groups and polar ester linkages. Also, part of the stress arising from resin shrinkage is relieved by flow in resin adjacent to fibres and some of this flow takes the form of molecular orientation rather than viscoelastic flow. Birefringence arising from molecular orientation mimics the symmetry of the elastic field, i.e. the directions of fast and slow axes are as predicted for the elastic field.

Following Poritsky (1934), if we consider a single fibre surrounded by a concentric cylinder of resin, it can be shown that the retardation of light transmitted adjacent to the inner cylinder (fibre) and through the outer cylinder (resin) arises solely from the axial stress in the resin. This conclusion is true only where conditions of plane strain prevail. It offers a means of measuring the retardation due to axial stress in the resin (which can then be subtracted from measurements of the retardation of light passing through resin and through the fibre. Ashbee and Wyatt (1969) have confirmed that the order of magnitude of measured retardations agree with those expected and have defined as load transfer index the difference between the retardation measured through a diameter at the centre of the fibre and that measured through a diameter near the fibre end, both measurements being corrected for the resin contribution. Any deterioration in the ability to transfer shear stress across the interface reduces the build-up of axial stress towards the fibre centre and this is reflected by a decrease in the magnitude of the index. When the interfacial bond is destroyed, all of the resin shrinkage has to be borne by the fibre ends. This increase in compression transmitted across the ends is readily detected by its associated increase in optical retardation measured in the adjacent resin. Since this measurement is made through neat resin, it offers a means for detecting loss of load transfer when the fibre material is opaque.

Many of the formulations developed for use as commercial coupling agents in GRP attempt to exploit the ability of amines to form chemical bonds with both silica glass and epoxy resin. An alternative approach to achieving the same end, namely deposition of amines onto the surface of glassfibre during drawing, has recently been attempted in Professor Martin's laboratory at Ames. Martin has drawn OCF E and S2 glassfibres in atmospheres of methane, and destruction of load transfer by diffused water in composites made from samples of these fibres in epoxy resin has been compared by Vaudin with that in identical composites manufactured with OCF commercial grades of E and S2 glassfibre. Exposure of these composites to deionised water at 80°C demonstrates that load transfer to the S2 glassfibre drawn in ammonia deteriorates prematurely after 8 hours.

A similar comparison of the incidence of loss of load transfer during uptake of hot water has been made for epoxy composites reinforced with two commercial grades of carbon fibre, one of which contains a surface sodium ion concentration of 4 at %. It was anticipated that the certain production of interfacial caustic soda solution would accelerate the deterioration of chemical and/or mechanical linkages between matrix and fibre materials and photoelastic evidence has been found to support this prediction.

This research has been supported partly by the US Army (grant no. DA-ERO-78-G-117 and partly by the Science Research Council (Grant No.80303111). The matrix materials used were supplied by Ciba-Geigy Ltd. Some of the glass fibres were supplied by Owens Corning Fiberglass Corp, some were drawn in our own laboratory from gobs supplied by Pilkington Bros Ltd, some were drawn in Professor Martin's laboratory from marbles supplied by OCF and others were specially prepared by OCF for the US Army Materials and Mechanics Research Center (Dr B Halpin). The carbon fibres were obtained from the US Air Force Materials Laboratory (Dr L Drzal).

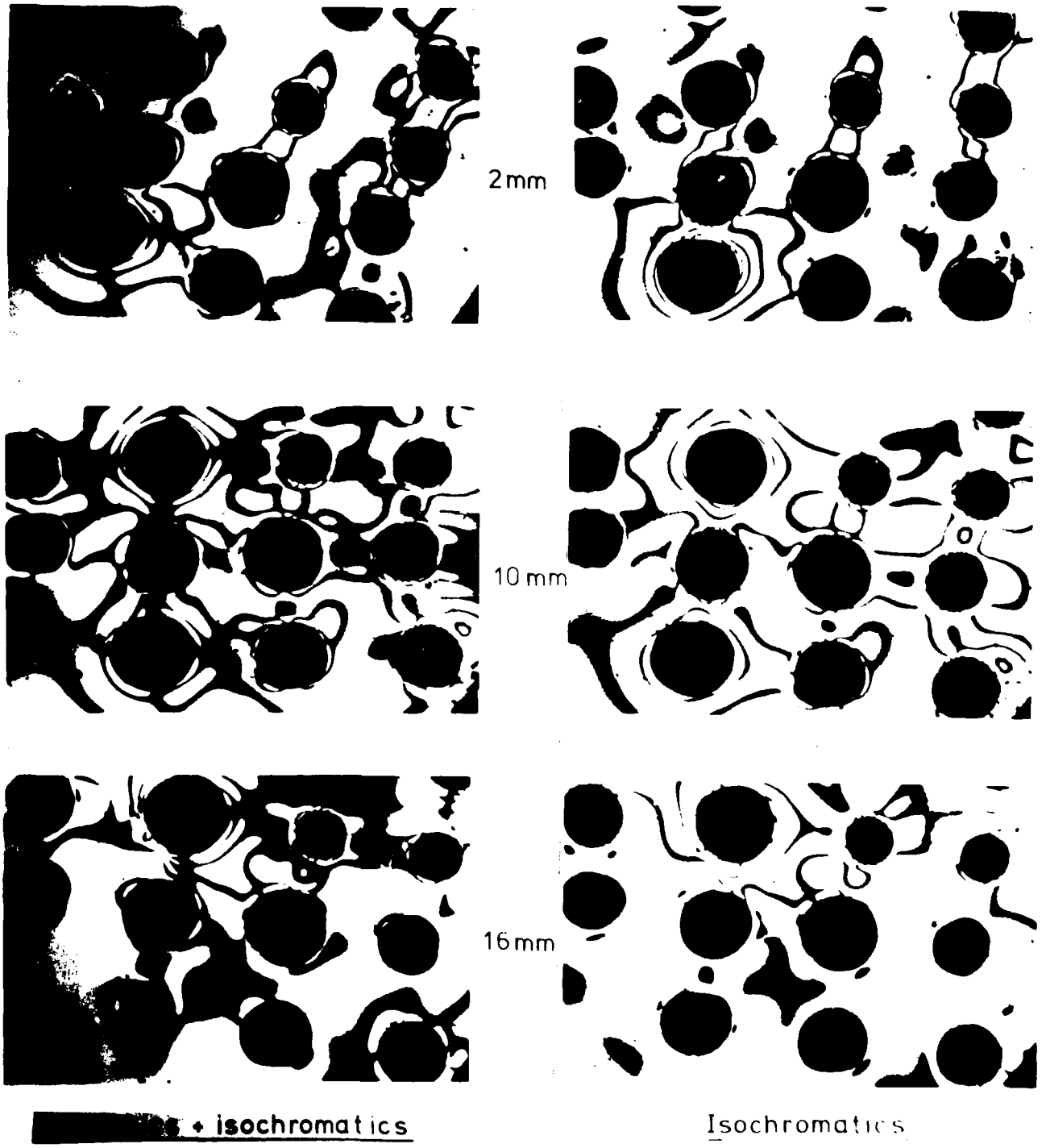

1. Photograph of a transverse section of a model unidirectional composite examined with both plane and circularly polarised light.

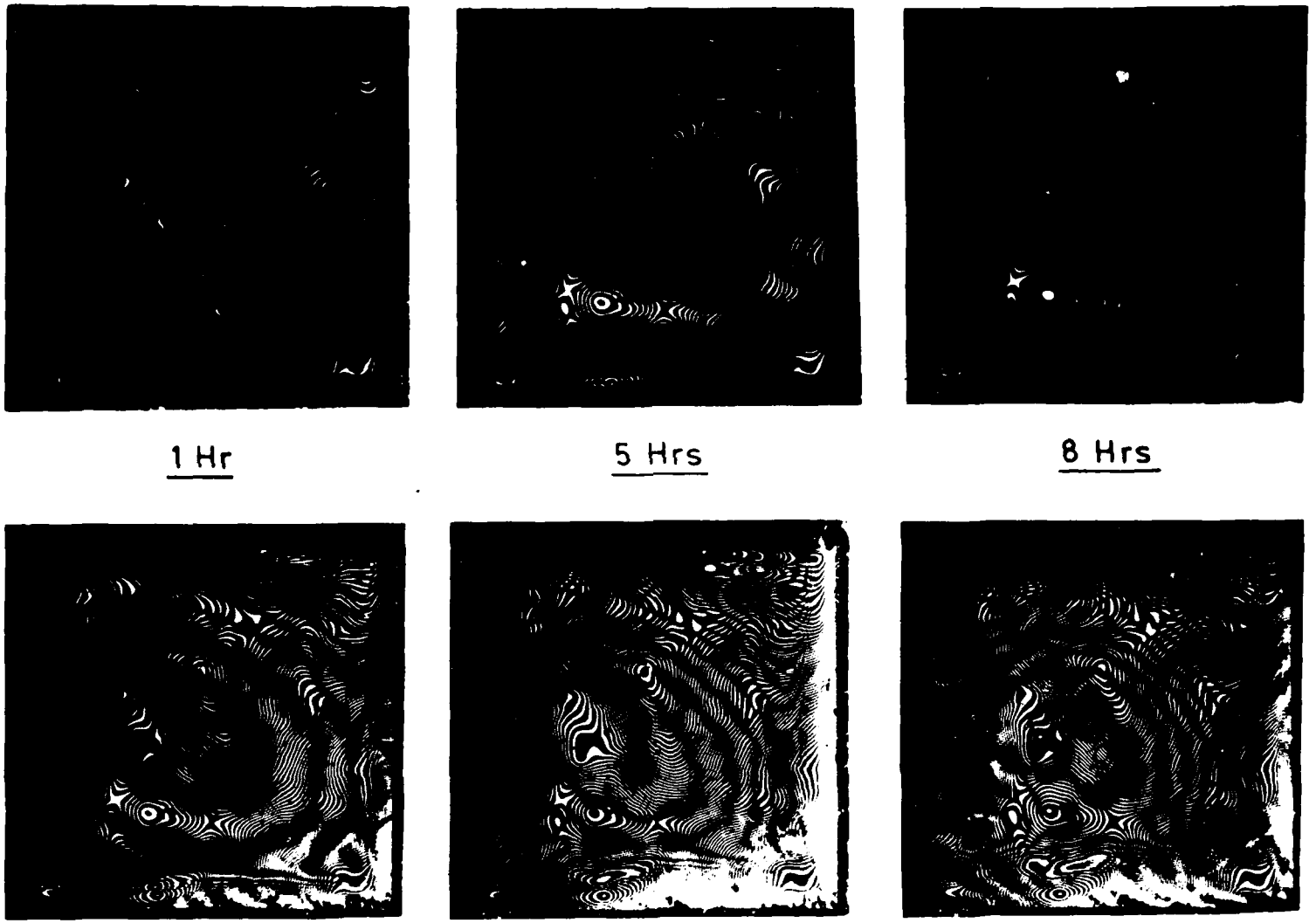

2. Development of the Moire pattern (around the circumference of the cover slip) for a unidirectional glass fibre reinforced composite immersed in distilled water at 60°C.

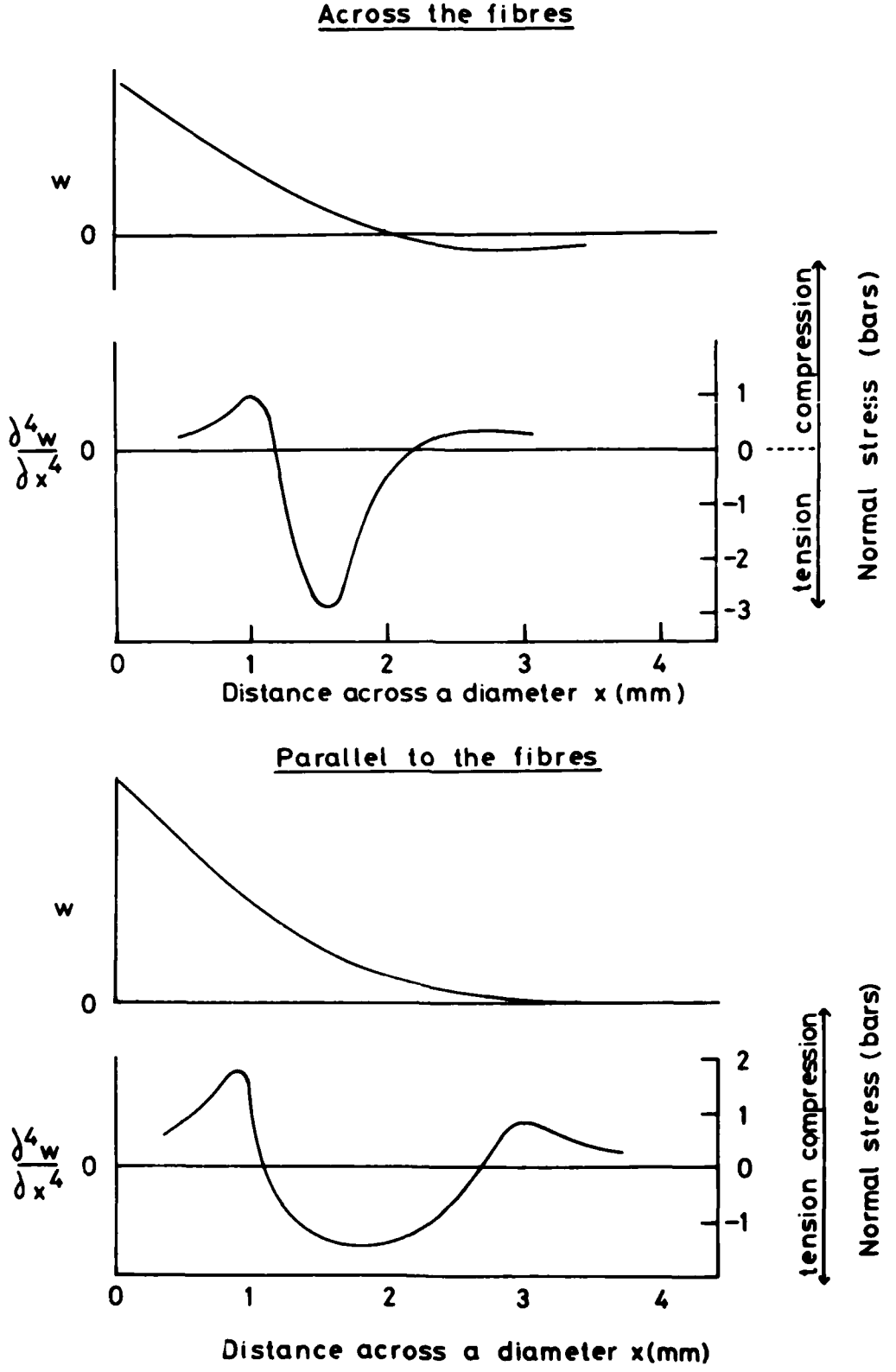

3. The normal displacement (w) and its fourth derivative, obtained from Figure 2.

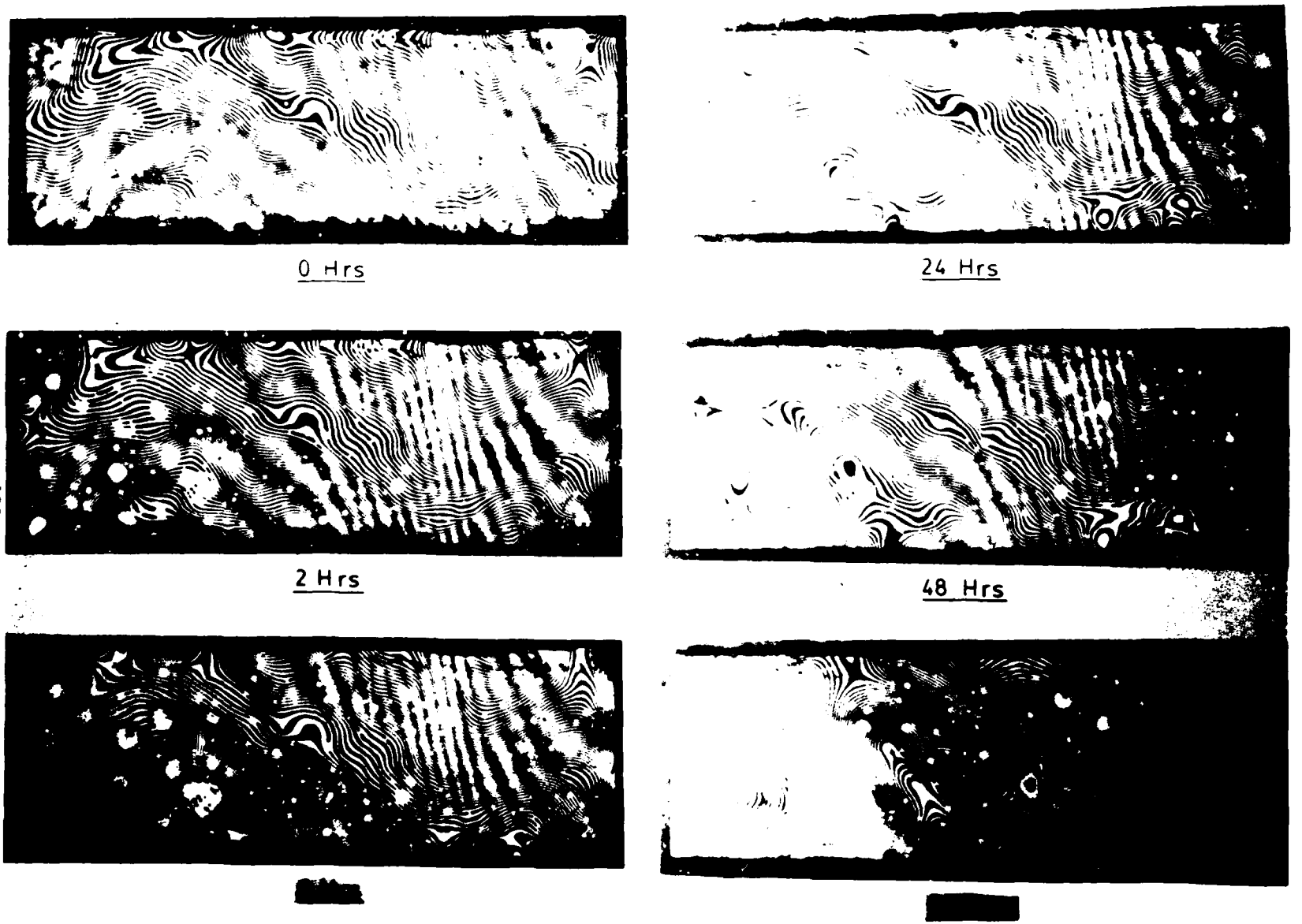

4. Interference pattern for a "57-ply carbon fibre epoxy laminate/cover slip" joint immersed in water at 60°C.

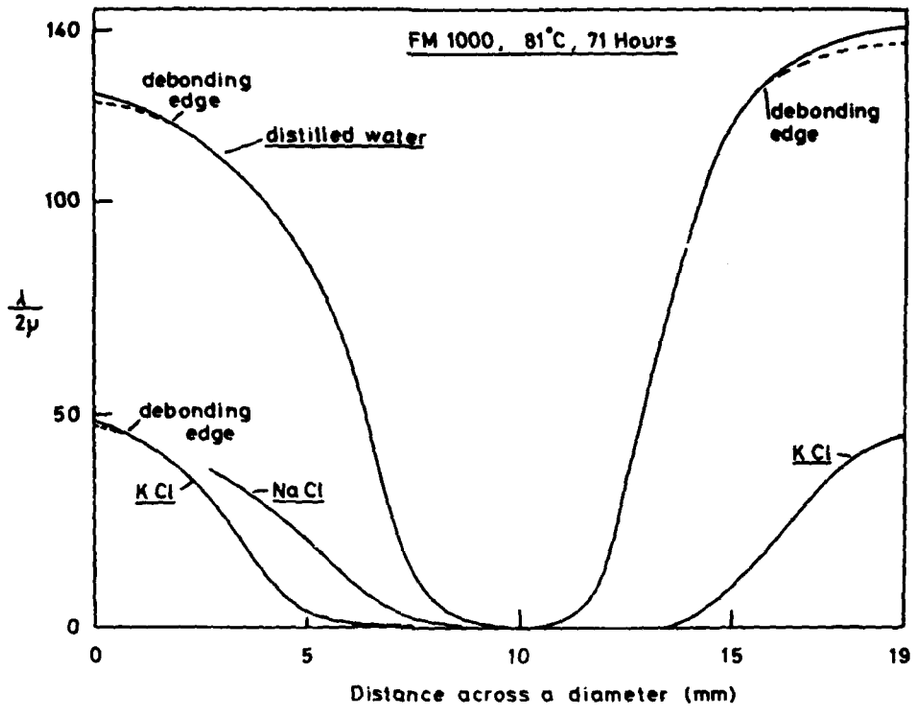

5. Effects on normal swelling $\left(\frac{\lambda}{2\mu}\right)$ of inorganic salts dissolved in the immersion water.

References

1. Durelli A J and Riley W F, "Introduction to Photomechanics" Prentice-Hall Inc, Englewood Cliffs NJ (1965)

2. Ashbee K H G and Wyatt R C, "Water Damage in Glass Fibre/Resin Composites" Proc Roy Soc A 312, 553 (1969)

3. Poritsky H, Physics 5, 406 (1934)

6. "HMU" Carbon fibre in epoxy, 83 hours immersion in distilled water, 80°C

ENVIORNMENTAL FAILURE OF ADHESIVE BONDING IN COMPOSITES

E.H. Andrews, Ho Ping Sheng, H.A. Majid
and C. Vlachos

Department of Materiels
Queen Mary College, London

ABSTRACT*

A recently developed fracture mechanics test (the A-S test), which involves pressurization of an enclosed circular flaw, has been used to investigate the adhesion of two epoxy resins (Shell Epikote 828 and 3 M's SP 250) to glass. Specimens were tested after various times of immersion in water at 80°C and the adhesive failure energy determined. The effects of adding silane coupling agents to the epoxy resin, and the influence of water pH were particularly studied.

The theory of generalized fracture mechanics is used to derive, from θ, an intrinsic failure energy θ_o which is the energy to break unit area of interatomic bonds across the interface. The decrease of θ_o with time follows first order reaction kinetics, with a rate constant controlled by the type and concentration of coupling agent as well as by the pH of the aqueous environment. The results are interpreted in terms of the chemical hydrolysis of interfacial bonds.

---

* Paper presented by Margaret E. Roylance, AMMRC. Full paper to be published as final report for European Research Office, Grant No. DAERO 78-G-118.

Spatial Distribution of Volatile Compounds in Epoxy Resins for Composites*

M. A. Grayson and C. J. Wolf
McDonnell Douglas Research Laboratories
St. Louis, MO 63166

Abstract

Precision abrasion mass spectrometry (PAMS) was used to determine the quantitative distribution profile of water in three epoxy resin systems: tetraglycidyl diaminodiphenyl methane (TGDDM) cured with dicyandiamide (DICY), diglycidyl ether of bisphenol A (DGEBA) cured with DICY, and TGDDM cured with diaminodiphenyl sulfone (DDS). The first two resin systems also contain an epoxy cresol novolac. Specimens of the three resins were exposed to a humid environment for 4 to 2000 h. The water distribution was determined immediately following environmental exposure. Distribution profiles of oxygen, carbon dioxide, and dichloromethane were also measured in the specimens. A brief description of the PAMS apparatus and a discussion of the distribution profiles of the sorbed gases in the three epoxy resin systems as a function of exposure time will be given.

*This research was conducted in part under Army Materials and Mechanics Research Center Contract DAAG46-80-M-1371 and in part under the McDonnell Douglas Independent Research and Development program.

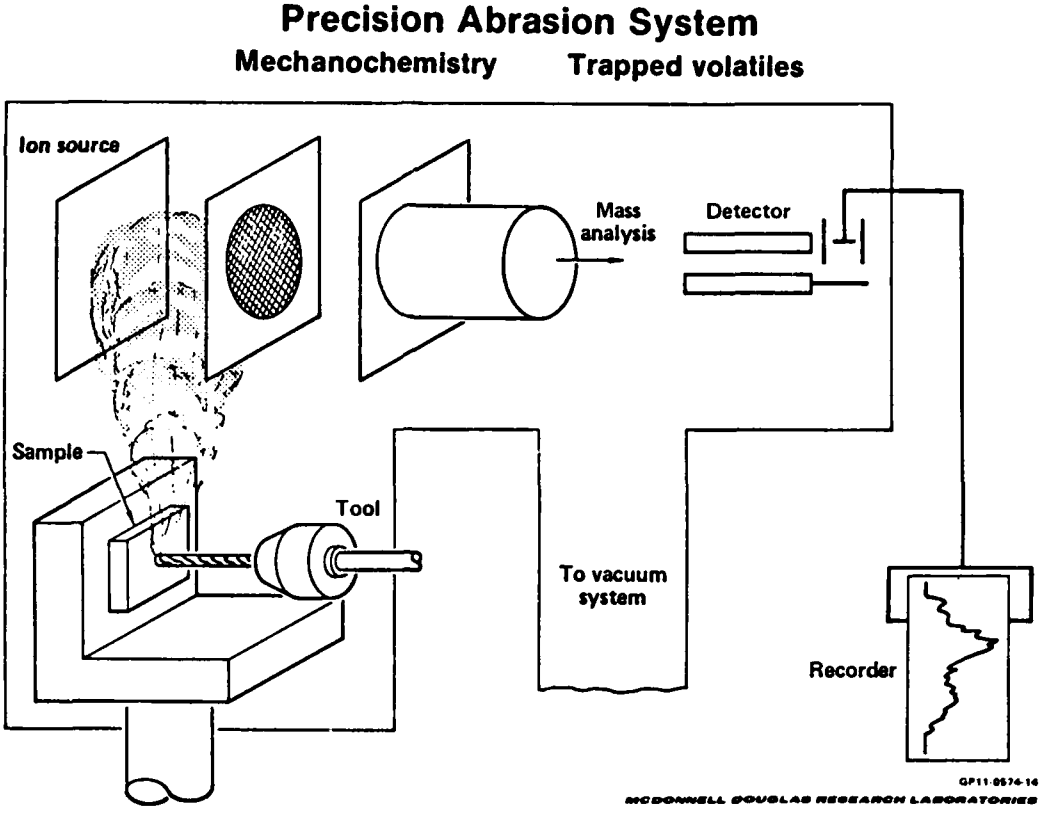

PRECISION ABRASION MASS SPECTROMETRY (PAMS)

(Figure 1)

The sample is mounted inside the ion source housing on a sample stage whose position is controlled in each of the three principal axes by stepping motor/lead screw drives. Upon abrasion of the sample by the cutting tool, the indigenous volatile compounds trapped in the sample bulk are desorbed. These gases expand in the vacuum of the mass spectrometer into the ion source region where they are ionized. Subsequently, mass analysis of the compounds occurs with the time-of-flight mass spectrometer (TOFMS). The detector output is set to record the ion current for up to nine different mass-to-charge ratios on a continuous basis. Thus, one or more ions characteristic of the desorbed volatile compounds can be followed during the abrasion process, thereby revealing the distribution profile of that volatile compound in the bulk sample.

Quantitation of PAMS Data

$$W_d\% = \frac{I_d \cdot S_d}{\pi \rho r^2 v} \times 100$$

Where
- $W_d\%$ = weight percent of diffusant
- I_d = ion current at a mass characteristic of the diffusant (μA)
- S_d = sensitivity of the mass spectrometer to the diffusant (g/s·μA)
- ρ = bulk density of the abraded sample (g/cm^3)
- r = radius of the cutting tool (cm)
- v = stage velocity (cm/s)

GP11-0574-4

MCDONNELL DOUGLAS RESEARCH LABORATORIES

QUANTITATION SCHEME FOR PAMS

(Figure 2)

Weight percent data can be calculated from the definition:

$$W_d\% = \frac{\dot{Q}_d}{\dot{M}} \times 100,$$

where $\dot{Q}_d$ is the mass flow rate of the desorbed volatile compound (g/s); and $\dot{M}$ is the rate of mass abrasion by the cutting tool (g/s).

$\dot{Q}_d$ is determined by multiplying the measured ion current signal, I_d, by the sensitivity factor, S_d, correlating the response of the mass spectrometer to the mass flow rate.

$\dot{M}$ is determined by computing the mass of material abraded per second from the radius of the tool, the density of the sample and the velocity of the sample stage.

Data System for PAMS

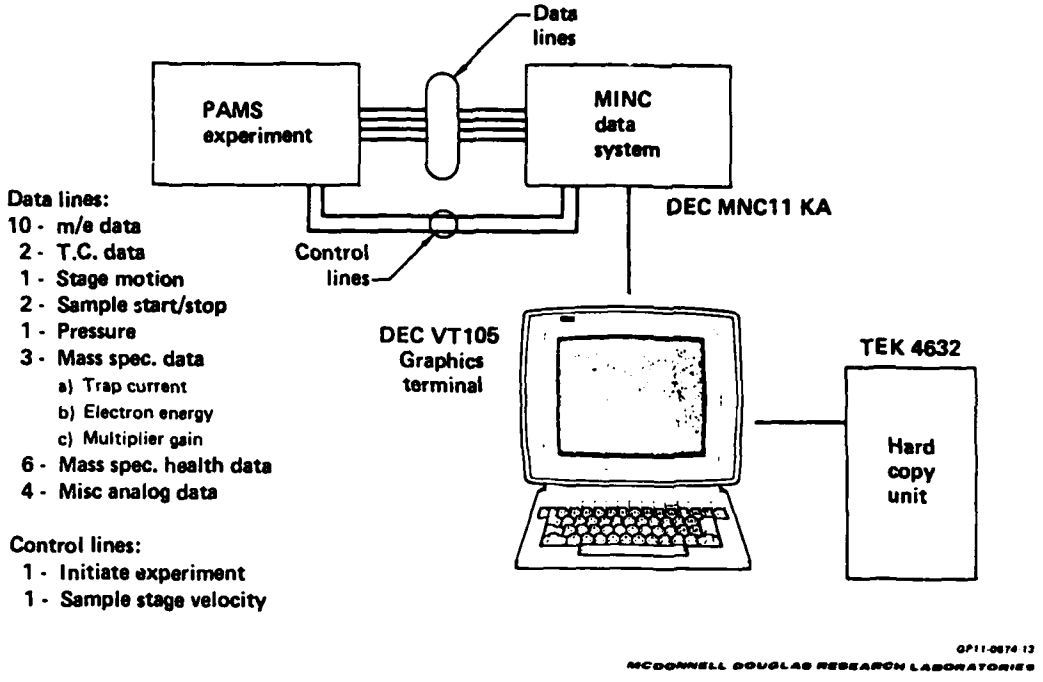

DATA SYSTEM FOR PAMS

(Figure 3)

The data for PAMS experiments are acquired and processed by a microprocessor-based computer system. A variety of analog data is digitized by an analog-to-digital converter (ADC) and multiplexor. The instrument pressure is read in digital form from a VEECO digital ionization gauge controller. The control lines are used to set the stage velocity and initiate stage movement. Interactive programs for the acquisition, processing, and display of data from PAMS experiments are executed from the graphics terminal.

SP Resin System

(Figure 4)

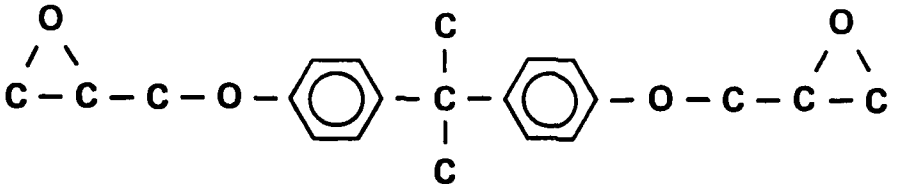

DGEBA and epoxy cresol novolac cured with DICY

GP11-0574-2

MCDONNELL DOUGLAS RESEARCH LABORATORIES

RAC Resin System

(Figure 5)

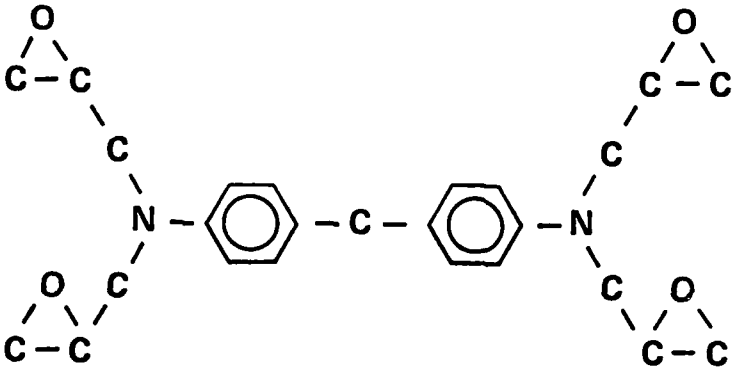

TGMDA and epoxy cresol novolac cured with DICY

GP11-0574-3

MCDONNELL DOUGLAS RESEARCH LABORATORIES

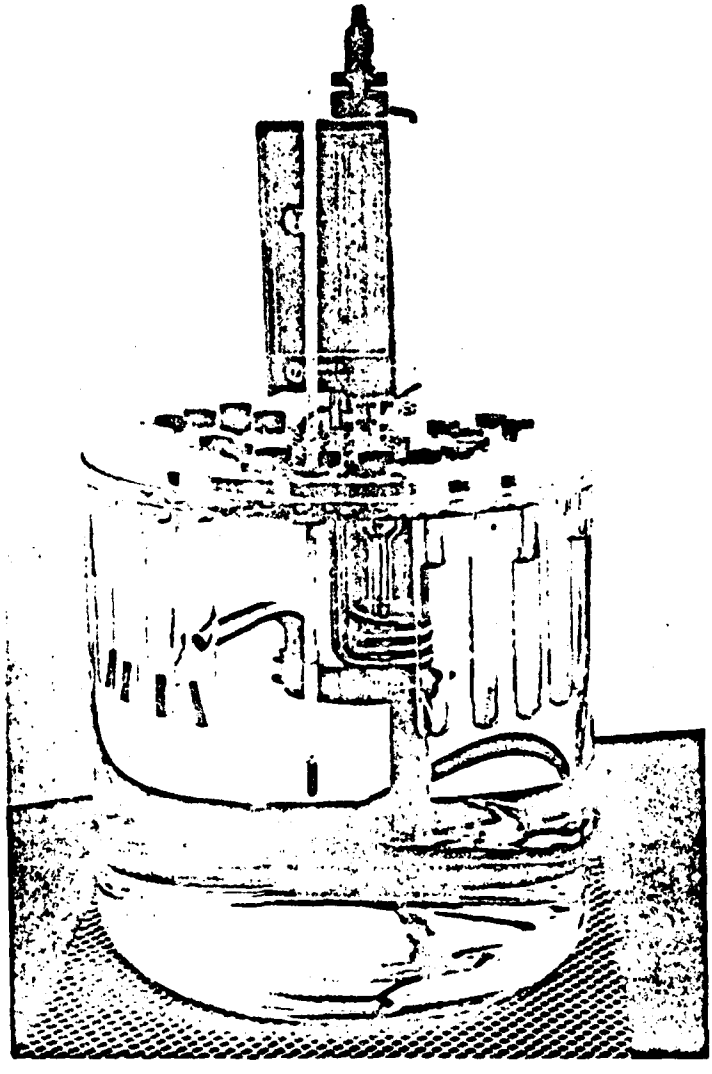

IMMERSION BATH FOR ENVIRONMENTAL EXPOSURE OF THE EPOXY RESINS

(Figure 6)

Samples were immersed in distilled water contained in the test tubes suspended from the plexiglass bath cover. Only one sample (25 x 6 x 1 mm) was placed in each tube, thereby ensuring even exposure on all sides. The test tubes were covered with Parafilm to prevent water loss. Samples were dried for one week at 50°C in a vacuum oven prior to immersion in the water bath. The immersion circulator maintains the water bath temperature at 60° $\pm$ 1°C. Vacuum dried samples were exposed for the following time periods prior to measurement of the water distribution profiles by PAMS: 4, 8, 16, 26.5, 64, 128, 256, 512, 1024, and 2048 hours.

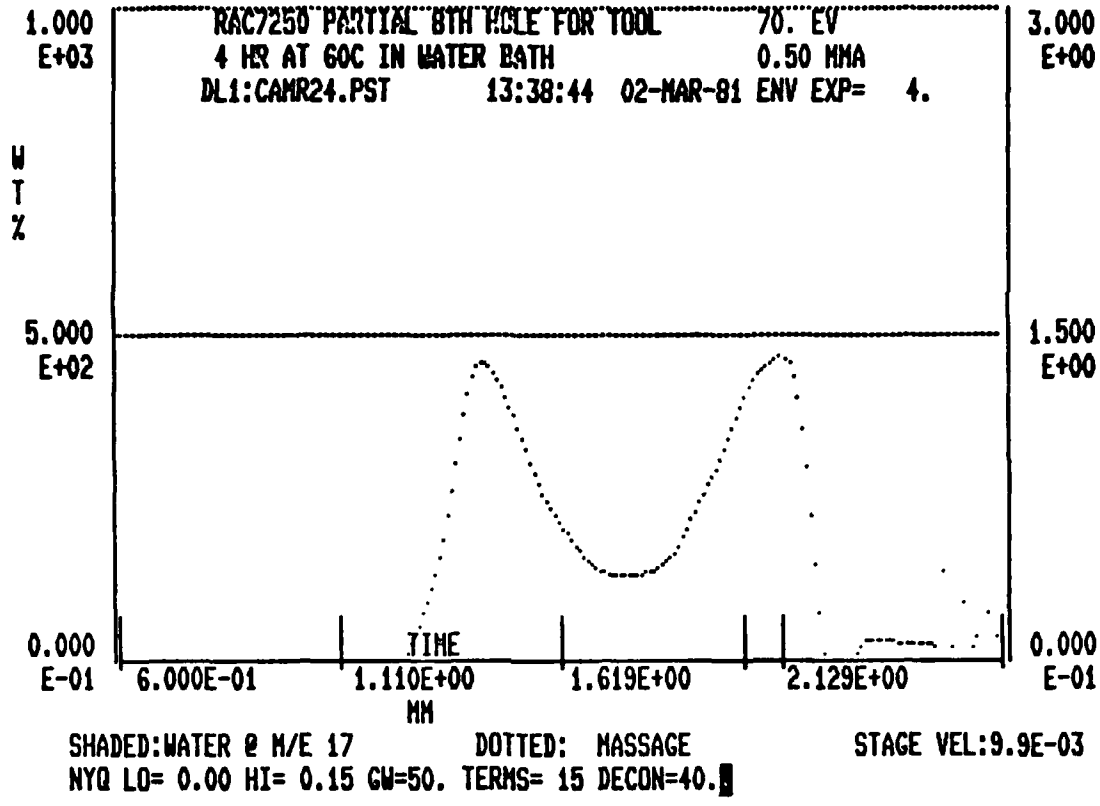

TYPICAL MOISTURE PROFILE

(Figure 7)

The labeling information at the top of the graph describes the sample, whether the hole is full or partial, and the number of holes cut with the tool. Roman numerals, where present, refer to the sample so labeled for the purposes of gravimetric water uptake measurements.

The environmental exposure data are given in the next line of descriptive information. The file name for data in this series of experiments is given by CAMRnn.PST or CAMnnn.PST, where nn is the serial number of the experiment and PST is a three letter descriptor of the type of data and its stage of processing. Time and date of the experiment are shown along with the ionization potential and trap current settings for the mass spectrometer.

The abscissa is the stage position in millimeters, and the ordinate is water content in weight percent. Prior to and following abrasion of the sample, the tool is abrading a piece of vacuum-baked scrap material. The stage velocity, or rate of feed of sample to the tool, is shown at the bottom right of the moisture distribution profile.

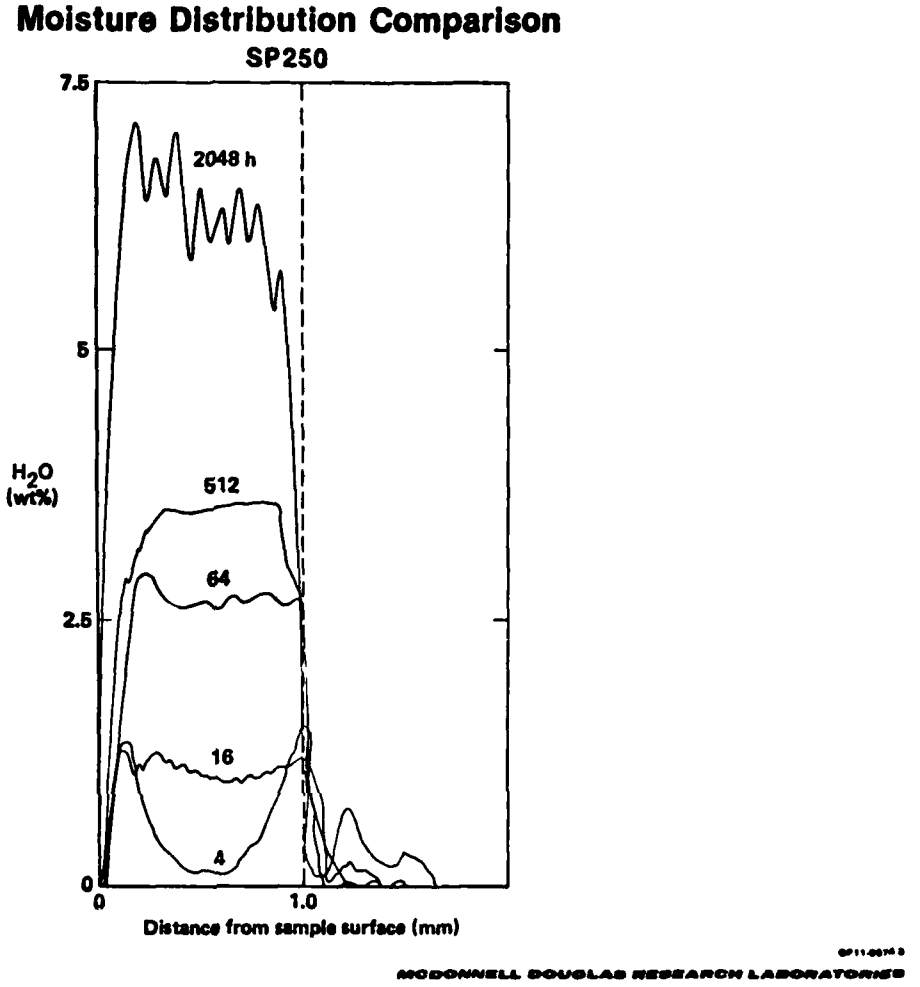

A COMPARISON OF THE MOISTURE PROFILES IN THE SP250 RESIN AT SELECTED ENVIRONMENTAL EXPOSURE TIMES

(Figure 8)

Up until 16 hours immersion, the moisture distribution profiles measured by PAMS suggest that water transport in the epoxy resin sample is governed by Fick's law. Thus, the equilibrium water content of the resin is established at the sample surface upon immersion and the transport process as described by Fick accounts for subsequent water uptake. However, after 16 hours exposure, the equilibrium moisture content starts to increase with increasing immersion time until at 2048 hours, it is almost four times that measured during the early exposure of the sample. These data suggest that after initial saturation of the sample with water, a second, non-Fickian water transport mechanism accounts for continued moisture sorption.

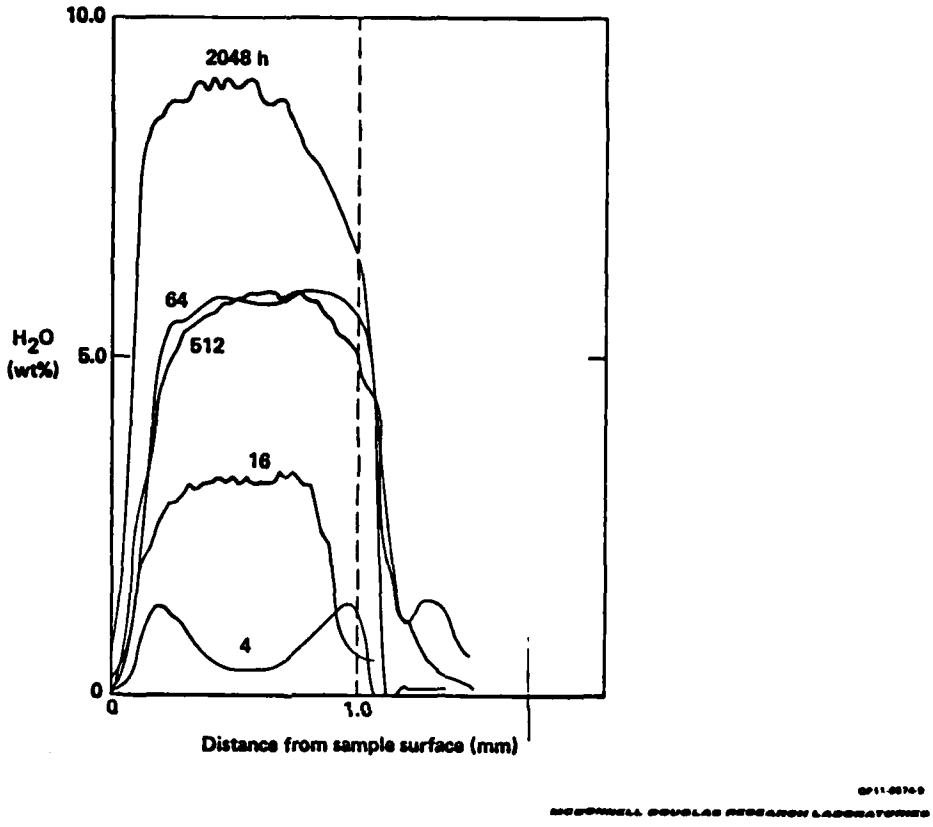

A COMPARISON OF THE MOISTURE PROFILES IN THE RAC7250 RESIN AT SELECTED ENVIRONMENTAL EXPOSURE TIMES

(Figure 9)

As in the SP250 resin, water transport appears to be governed by two different mechanisms: Fickian diffusion prior to 16 hours to saturate the sample with water at about 3% by weight followed by a non-Fickian diffusion in which the equilibrium moisture content of the sample increases with increasing exposure to about 10% by weight.

The water sorbed by the RAC sample is greater than that sorbed by the SP sample for the same exposure time. Also, a comparison of the moisture profiles for the two samples at the same exposure time indicates that the RAC has a higher diffusion coefficient than the SP sample.

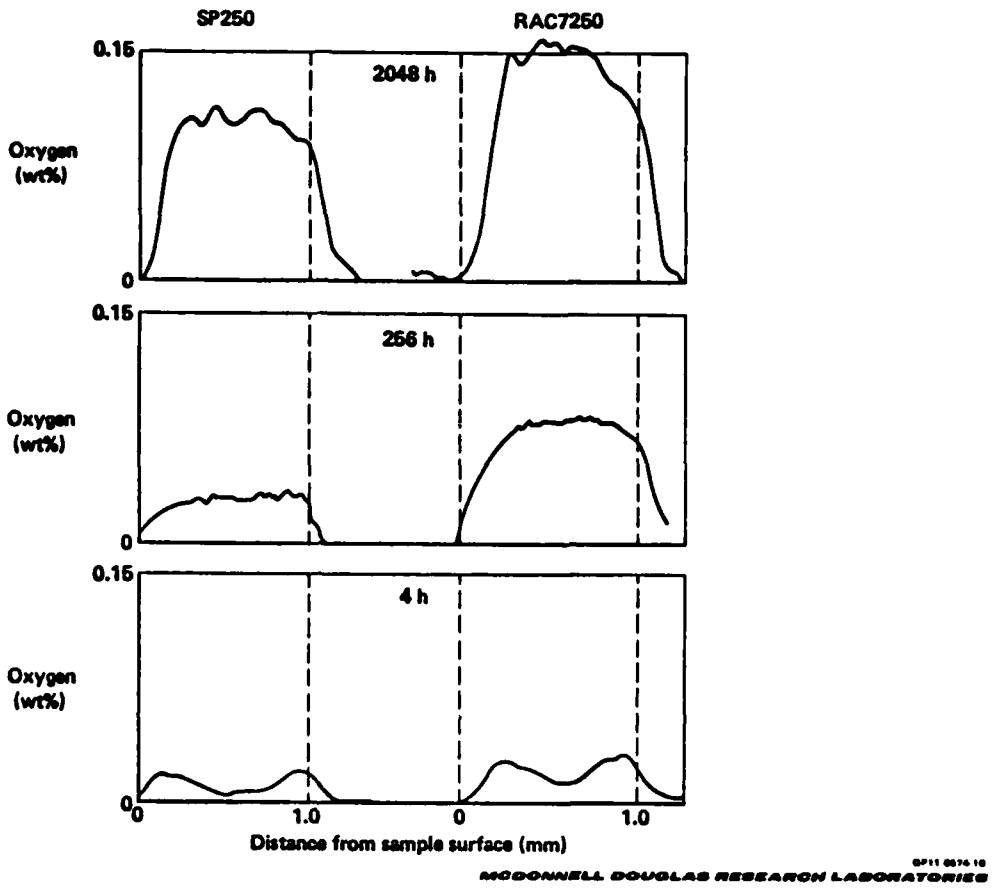

A COMPARISON OF THE OXYGEN CONTENT OF BOTH THE SP250 AND RAC7250 RESINS AS A FUNCTION OF IMMERSION TIME IN A DISTILLED WATER BATH AT 60°C

(Figure 10)

From these comparative distribution profiles for oxygen in the epoxy resin, it is apparent that the total oxygen content in the RAC sample for a given exposure time is greater than in the SP sample and that the diffusion coefficient of oxygen for the RAC resin is greater than that for the SP resin. It is interesting to note that the oxygen content of the distilled water bath at 60°C from the oxygen in the air is on the order of 5 parts per million by weight. Yet after 2048 hours exposure, the oxygen content of the epoxy resin samples is on the order of 0.15% by weight or nearly 300 times that of the surrounding water bath.

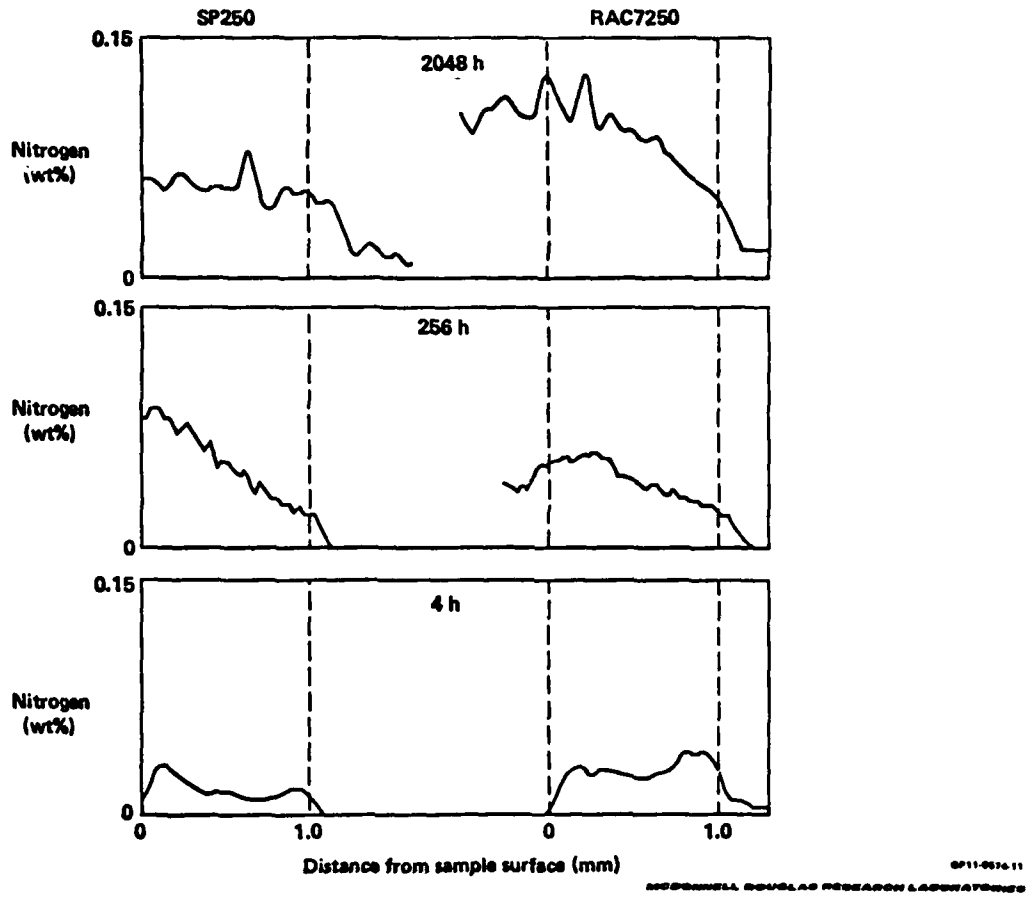

A COMPARISON OF THE NITROGEN CONTENT OF BOTH THE SP250 AND RAC7250 RESINS
AS A FUNCTION OF IMMERSION TIME IN A DISTILLED WATER BATH AT 60°C
(Figure 11)

These distribution profiles are provided to serve as a comparison with the oxygen profiles in Figure 10. Not only is there less nitrogen than oxygen distributed through the samples, the nitrogen distribution is random after four hours exposure to the water bath.

Exposure Comparison of Dichloromethane in RAC7250

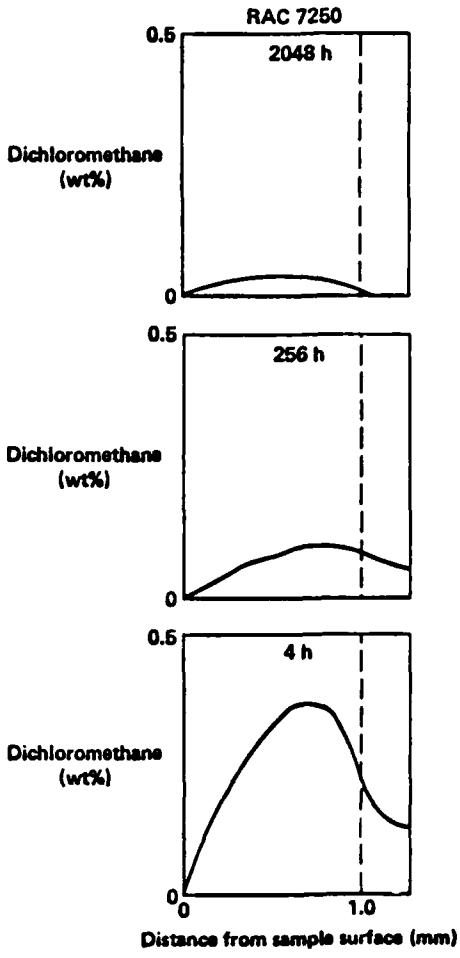

A COMPARISON OF THE DICHLOROMETHANE DISTRIBUTION PROFILES IN RAC7250 AS A FUNCTION OF IMMERSION TIME IN A WATER BATH AT 60°C

(Figure 12)

Of the two resins, the RAC7250 has considerably more indigenous compounds. Dichloromethane is the major volatile compound trapped in the "as-received" RAC sample. These distribution profiles show how the dichloromethane is leached from the sample as it is immersed in the water bath for longer time periods. From the shape of the distribution profiles, it is apparent that the diffusion coefficient for dichloromethane is much smaller than that of water in the same sample.

MECHANISTIC AND PHENOMENOLOGICAL THEORIES FOR PREDICTING COMPOSITE BEHAVIOR AND ENVIRONMENTAL EFFECTS

Joseph M. Augl

Naval Surface Weapons Center
White Oak
Silver Springs, MD 20910

ABSTRACT

To describe the response of a structure to various loading conditions (such as static, dynamic and hygro-thermal), it is necessary to know quite a number of elastic strength and and hygro-thermal parameters (such as E_x, E_y, ν_x, ν_y, ν_z, (G_{xy}, G_{xz}, G_{yz}) α_x, α_y, α_z, β_x, β_y, β_z, X, X', Y, Y', S) and all of these as a function of temperature, moisture concentration (possibly moisture distribution) and time (if viscoelastic behavior-creep and relaxation-play a role). And all these properties would be valid for only a specific composite, and would have to be remeasured for any changes in ply ratios, ply angles, stacking sequence, symmetry, fiber volume fraction, nature in matrix or fiber or curing conditions.

However, many composite (laminate) properties and their changes in the environment (temperature, moisture) can be predicted from the changes in the (unidirectional) ply properties. For instance, the elastic, the viscoelastic, the elastic-plastic, the thermal expansion coefficients, the hygro-thermal swelling, the internal (residual stresses due to cool-down from cure temperature or due to moisture absorption) and failure surface (in terms of first ply failure FPF, using the quadratic interaction criterion for instance by Tsai and Wu) can be predicted reasonably well by analysis from the corresponding ply properties.

Some of the ply properties (such as elastic, viscoelastic and elastic-plastic behavior) can, in turn, be quite well predicted if the changes in matrix and fiber properties are known for the respective environments. Thus, the number of tests to be performed for predicting composite and structural behavior can be substantially reduced.

This does not mean that design allowables can be directly derived from matrix and fiber properties, but optimization to a well tailored composite should be done, in a first approximation, by analysis before a composite is actually made and tested. Testing for design allowables is still expensive enough.

The primary objective of this work is to predict as many laminate properties as possible from known matrix-fiber prepare and test composites where the matrix properties dominate the composite properties and investigate discrepancies between theory and experiment only when they become evident.

Since moisture, absorbed in the matrix, has quite often a pronounced effect on the matrix properties (as does temperature), it is quite an obvious extension of micromechanical and lamination theories to predict the effect of moisture on composites.

Analyses of the mechanical state of stress and strain can be carried out at various levels; on a macromechanical level, dealing with average stress distributions in a laminate structure, on a semimicromechanical level, which looks into various ply and interply stress-strain fields (such as interlaminar stresses, edge effects or stresses around holes), and finally, micromechanics, which tries to describe the stress-strain fields on a microscopic scale inside the fiber, and the resin between the fibers, and the stresses at the interface. Micro and macromechanics are not really different; the question is only whether the models that are used are sufficient to describe the real composite behavior. From the standpoint of macromechanics most advanced composites appear to follow quite well linear elasticity almost up to fracture. However, micromechanics suggests that on a scale of smaller than fiber diameter highly nonlinear deformations may occur.

While the methods of linear elasticity, viscoelasticity and even nonlinear elasticity become well established via finite element analyses, there is still a lot to be done in the field of predicting fracture and fatigue in general composites as a function of the environment. Fortunately, it appears from recent investigations (Ref. 1) that a conservative static design of composite structures is reasonably insensitive to fatigue damage at least they do better than a corresponding metal design.

Over the past 10 or 15 years, engineers have gained enough confidence in composites that even primary aircraft structures are being built. Now it is time to look into the finer details of composite behavior and failure, and to sharpen the tools for a "second approximation."

Ref. 1. R. S. Whitehead (Northrop Co.), "A Review of the Rational for Durability Validation of Composite Structures." Paper at the 5th DOD/NASA Conference on Composites in Structural Design, New Orleans, January 1981.

INTRODUCTION

Composite materials are considerably more complex than metals in both their physical-mechanical properties and in their application as structural materials. No longer is it sufficient for structural design purposes to determine a few material constants such as Young's modulus, Poisson's ratio, thermal expansion coefficient, yield and tensile strength, and perhaps fracture toughness K_{1c}. Obviously, one does not expect a composite, made even from the same fiber and resin and with the same fiber volume fraction, to have unique properties because angular variation in fiber directions, number of plies in each direction, stacking sequence of the various ply groups, temperature and moisture distributions in the composite, and a few other parameters have a pronounced effect on the material response to external loading conditions. It is therefore necessary that the design engineer understand the material properties. He also has to understand how changes in the composite structure can benefit his structural design effort. On the other hand, the materials engineer has to become more sympathetic to the needs of the structural designer and should be able to make recommendations on how to optimize the material for the specific purpose. It is not surprising that the use of composites for structural applications has met a lot of skepticism and has been slow in its acceptance. Yet the potential pay-off in the use of composites was incentive enough for the Navy to use carbon fiber composites in advanced aircraft such as the F18 and the AV8B. Other important applications of composites used by the Navy are the motorcases of the Poseidon and Trident missiles. The increase in pay-load of such structures together with savings in fabrication (manhours) have become strong driving forces for composite applications even with less than optimal design. An optimal design, though, is possible only, after a full understanding of composites, their response

under multiaxial loading conditions, and their behavior under longterm services, and, environmental exposure has been gained. Such a task, however, is not simple and should not be expected to be complete in the immediate future.

The intent of this paper is to consider some of the problems we face in predicting composite behavior and changes of it due to environmental and service conditions. That such an attempt can hardly be more than superficial is obvious from (1) the time available to discuss this subject (2) the limited understanding we have thus far about composites.

The class of composites that we shall consider here are those that are composed of layers of unidirectional plies with different fiber orientations, thus forming more or less anisotropic plates or shells.

Theories of Composite Behavior

Most predictive scientific theories are either mechanistic or phenomenological. Although we will use these terms somewhat loosely we think it will be heplful to explain what we mean by them. The mechanistic theory uses generally a physical model, simple enough to be understood in all its complexities and amenable to quantitative mathematical analysis. Thus the mathematical model is an image of the underlying mechanism to predict the response. In situations where the underlying mechanisms are either not sufficiently understood, or too complex, a phenomenological approach is better suited. A phenomenological theory is essentially a fictitious, mathematical model that relates measurable loading conditions to the resulting responses, at least as good as the experimental uncertainties. Here the mathematical model is not an image to an underlying mechanism but a sort of interpolation

function or as Wu (Ref. 1) has called it the transfer function relating excitation to response.

Of course, one might call Hook's law a phenomenological theory since the modulus (in this case the transfer function) relates the applied load to deformation. The requirements of the physical model in this case are those of continuums mechanics where matter is continuous (not necessarily isotropic) and endowed with certain stiffness and strength properties without reguard to an atomistic model of matter. Yet, this model permits to establish a mathematical image, in form of certain partial differential equations, that can predict a great variety of mechanical responses of structural members to external loading conditions once the geometry of the member and the required boundary conditions are established. Therefore, in this respect we consider the physical model of continuums mechanics and its well established methods of analysis a mechanistic theory. (We shall ignore that it is possible, at least for some simple solids, to predict also the stiffness from atomistic or molecular models since the complexity of everyday engineering materials is far too great to be of practical value.)

The strength of composites, on the other hand, is presently best described by phenomenological theories where a certain minimum number of experiments have to be made that will describe a failure surface. Experimental observations suggest that at least tension, compression, and shear tests be made in the principal axes of anisotropy together with certain biaxial stresses that are material dependent. Phenomenological models are not unique. Many different models are possible some may be only special cases of others. The choice is sometimes a question of taste yet, at least in engineering applications, they must be adaptable to the established

engineering methods of analysis. Although, in principle, it is possible to derive mechanistic models for predicting the failure surface of lamina, the local rather than the global response of the material together with the random nonhomogeneous nature of fiber and matrix in a lamina prevent sufficient accuracy in prediciron to be useful for structural design.

Although, we strongly believe that detailed microscopic investigations of failure phenomona is of great value for the understanding of the underlying processes, we will pay less attention to them here since, at least at the present time, they can not be used for quantitative predictions.

Engineering Parameters for Structural Materials

Since we think of composites to be used primarily as structural materials it is obvious that we would like to predict those material responses that are important in a structure and their temporal changes, i.e., in addition to the structural integrity we would like to estimate the lifetime in a given environment and under given loading conditions.

Among the material parameters the engineer wants to know, are the elastic, the viscoelastic, the hygrothermal, the elastic plastic responses; he also wants to know the failure surface, the fracture behavior, the fatigue life and the response to impact (shockloading). As we go down the list of these properties (see Table 1) our understanding of the governing mechanisms becomes either less and less or the various mechanisms interact and overlapp which make a detailed analysis exceedingly difficult so that the choice between a mechanistic and a phenomenological approach becomes a question of practicality and attainable accuracy rather than of principle. In some cases the mechanistic and phenomenological theories are not exclusive and a hybrid

approach is useful as demonstrated in the laminated plate theory by Reisner and Stavsky (Ref. 2), where the lamina is treated on a phenomenological, and the laminate on a mechanistic basis. Either approach, however, should be amenable to structural analysis, i.e., there should be a unique conversion between stress and strain space and the components of the stiffness (compliance) tensor have to be obtained, derived or measured).

Table 1 Prediction of Composite Behavior

Approach	Behavior	Predict Behavior	Environmental Effects
Mechanistic (Continuum Mechan. Analysis of physical Model; governed average, global)	Elastic	Theory, Experiments	Theory, Experiments
	Viscoelastic	Theory, Experiments	Theory, Experiments
	Hygrothermal	Theory, Experiments	Theory, Experiments
	Elastic-Plastic	Theory	Theory
Phenomenological (Mathematical Model correlates events; governed local or global)	Strength	Theory, (Experiments)	(Theory?) (Experiments)
	Fracture	Theory, (Experiments)	(Theory?) (Experiments)
	Fatigue	(Theory), (Experiments)	(?), (Experiments)
	Impact Damage	-- (Experiments)	--- ----

Mechanistic Approach

Our desire to predict composite behavior from a mechanistic standpoint via the properties of resins and fibers will become apparent when we take the following consideration into account.

For the prediction of the elastic response of a general (multi angle-multiply) composite plate with respect to inplane stresses and bending a 6x6 compliance or stiffness matrix is required (i.e., 21 of its stiffness components are independent). Further reduction of independent matrix components is obtained if the composite has one symmetry plane (13), if it is orthotropic (9), and if it is transversely isotropic (5). From experimental as well as mechanistic considerations we also know that these stiffness components are temperature dependent. So we have to know them as a function of temperature, (say five (5) different temperatures within the range of

interest). We also know that these components change with moisture content, (say five (5) different moisture levels), and five (5) tests for each point. Thus over 2000 sample tests for a single composite plate may be required to predict only its elastic response. This still would not tell us what we should expect if the temperature and moisture distribution is not uniform in the interior of the composite, or, how the response would change if we change the distribution of ply angles, the number of ply groups, the stacking sequences of the plies, the fiber volume fraction, or the curing conditions.

However, if we can predict the composite behavior from the properties of the resin and the fiber, the number of required tests would be drastically reduced, and, tailoring and optimization of composite properties to specific needs can be attained with a realtively minor effort, i.e., testing can be limited to those properties that are sensitive to the predicted changes. We can also estimate environmental effects (aging) if we determine these effects on the resin itself.

Such a mechanistic approach is possible as we have stated in a previous TTCP meeting (Ref. 3) and, as we have shown in the meantime (Ref. 4), the predicted and experimentally found properties are in excellent agreement. Generally, we expect to see good agreement between predicted and experimental properties with respect to the global elastic, viscoelastic and hygrothermal composite behavior. The reason why we think that the above predictions will be reasonably successful, while mechanistic failure prediction will be less, if at all, is, that the elastic effects are governed by average global responses while failure is a discontinuous, local effect strongly dependent on local stress concentrations, weak spots, defects etc. which are essentially

unknown. Though we do not discard the possibility of a mechanistic-phenomenological hybrid approach where failure is treated in terms of statistical distribution functions.

Elastic Behavior

For the prediction of the elastic behavior of composite laminates it is not necessary that both the fiber and the matrix behave linerarly elastic. Nonlinear elasticity (characterized by a unique one to one relationship of stress and strain without hysteresis) requires only more computational effort. Finite element analysis is usually best suited for calculating nonlinear elastic behavior (using incremental methods (Ref. 5-9)).

The general assumptions in calculating the lamina compliance (or stiffness) components is that the fiber properties (E_{11f}, E_{22f}, ν_{12f}, G_{12f}) and the matrix bulk properties (E_m, ν_m) are known over the temperature range and moisture content of interest (E = Young's moduli, ν = Poisson's ratio, G = shear modulus, the subscripts 1, 2 stand for the longitudinal and transverse direction to the fiber and m and f stand for matrix and fiber). Since the fiber stiffness properties (such as in carbon, glass and boron) remain constant over the temperature range (dictated by the matrix properties) these can be determined once and for all, so that one has only to measure the temperature and moisture dependence of E_m and ν_m. Further, is is assumed that a regular arrangement of fibers will, in the average, be a good approximation to a random array (at least with respect to the global stiffness). Thus, the geometry of the analytical model is very simple (Fig. 1) i.e., a quarter of a repating unit cell. The engineering constants for this plain strain problem can be readily obtained by finite

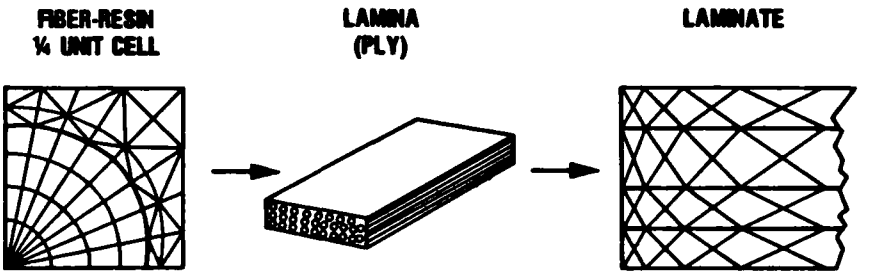

FIGURE 1 FINITE ELEMENT APPROACH FOR OBTAINING LINEAR AND NONLINEAR ELASTIC PROPERTIES

element analysis (Ref. 5-9) though other analytical methods lead to the same results (Ref. 10-17). Halpin and Tsai (Ref. 18) have judiciously simplified certain analytic expressions (see Appendix A) which agree quite well with finite element calculations (Ref. 6).

The finite element method is particularly useful because it can readily model the effect of an interface layer of finite thickness between resin and matrix thus estimating the effect of fiber surface sizing or debounding. Changes in fiber radius on the finite element grid shows the effect of the changes in fiber volume fraction. The effect of the environment (temperature and moisture) on the ply properties is readily obtained when the corresponding changes in the matrix properties are made. Typical resin data for the calculation of lamina elastic properties are obtained from stress-strain measurements on the resin equilibrated at different relative humidities and tested at different temperatures (see Figures 2-8). Not only are thus the average (global) stiffness parameters obtained but also the varying stress strain fields inside and between matrix and fiber. If it were not for the local dominance and the discontinuous nature of failure, one would also expect to be able to calculate the failure surface of a ply from the known matrix failure surface by using a maximum stress-strain or energy failure criterion. The next step, the prediction of composite laminate behavior, is accomplished

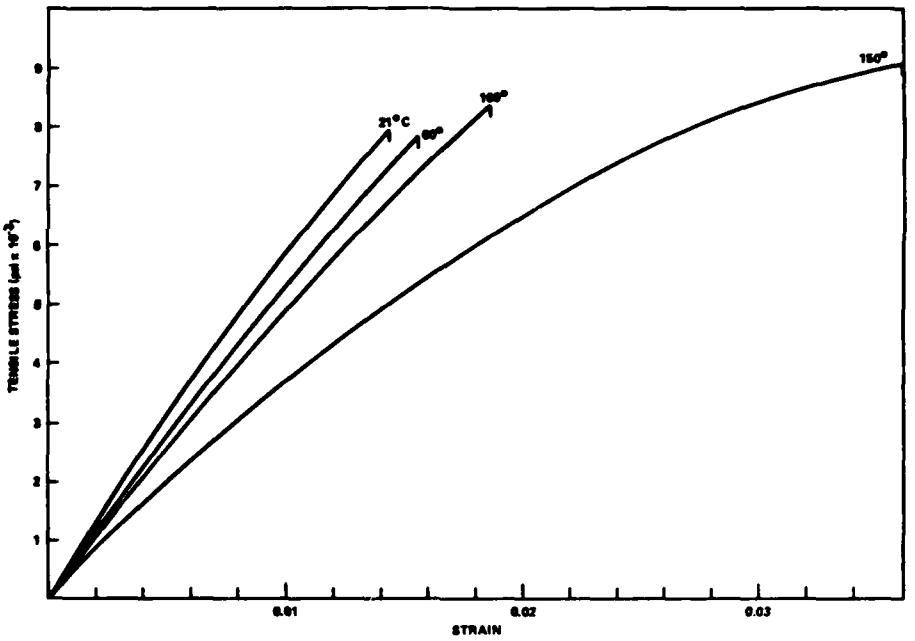

FIGURE 2 TYPICAL STRESS STRAIN CURVES OF HERCULES 3501–6 RESIN (DRY) AT DIFFERENT TEMPERATURES

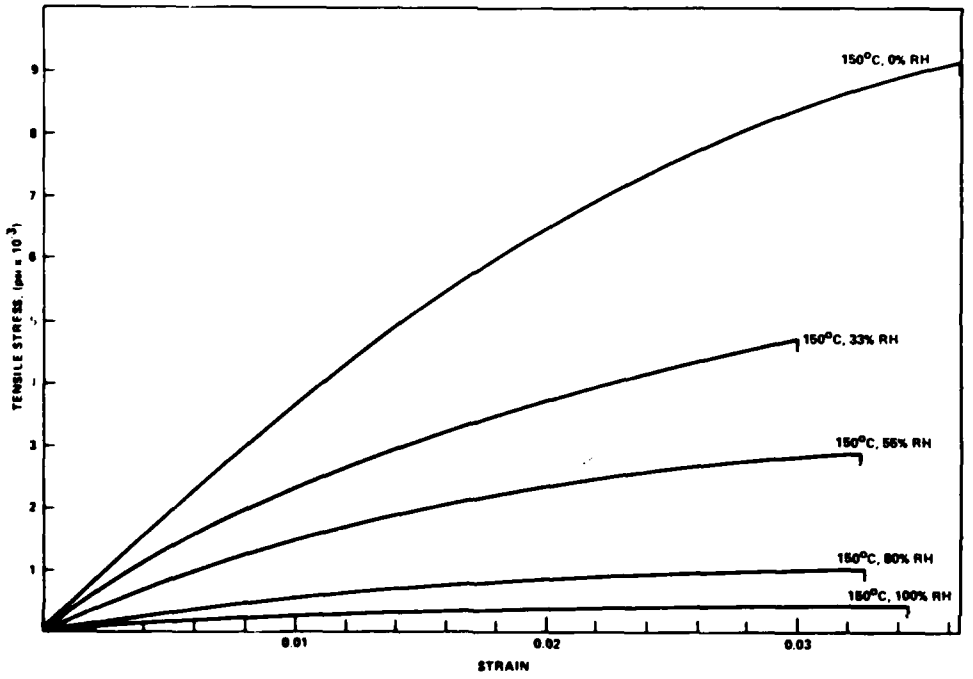

FIGURE 3 TYPICAL STRESS STRAIN CURVES OF HERCULES 3501-6 EPOXY RESIN (AT 150°C) EQUILIBRATED AT DIFFERENT RELATIVE HUMIDITIES

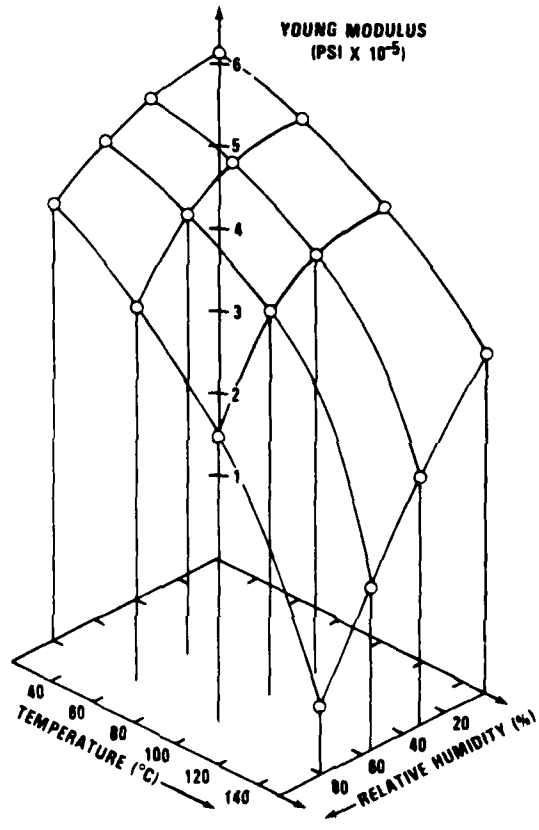

FIGURE 4 YOUNGS MODULUS OF HERCULES 3501 6 AS A FUNCTION OF TEMPERATURE AND MOISTURE (CORRESPONDING TO THE EQUILIBRIUM CONCENTRATION OF INDICATED RELATIVE HUMIDITIES)

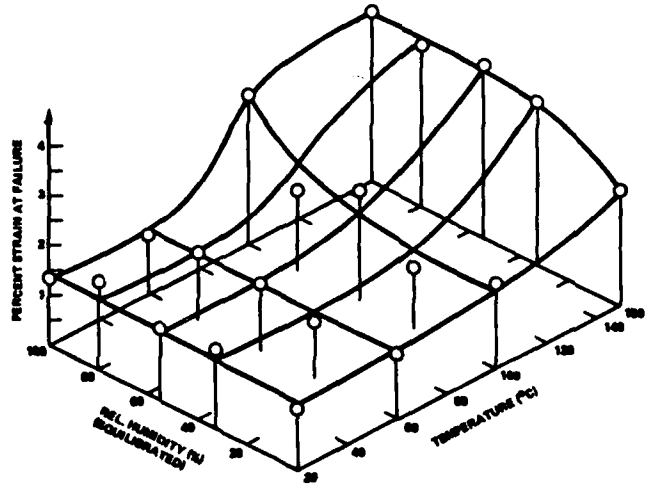

FIGURE 5 FAILURE STRAIN OF HERCULES 3501-6 (EQUILIBRATED AT DIFFERENT REL. HUMIDITIES) AS A FUNCTION OF TEMPERATURE

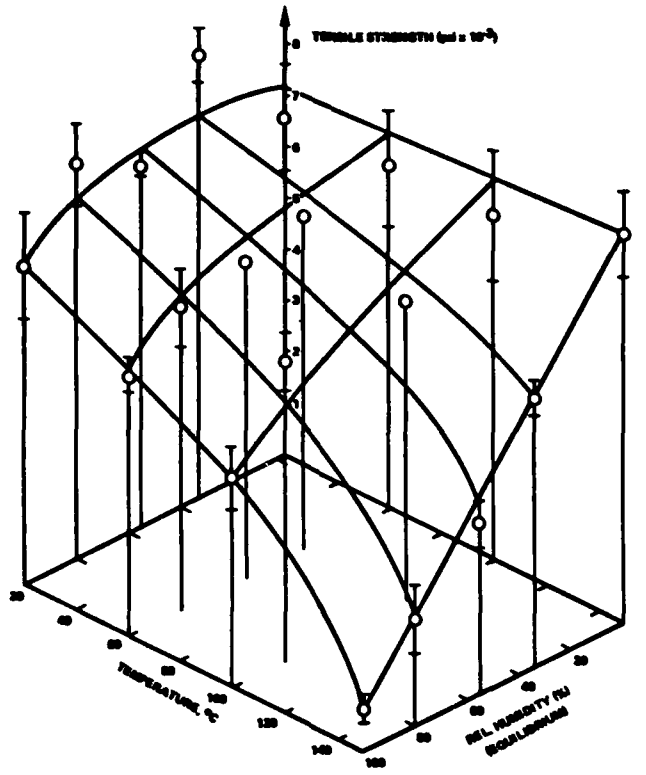

FIGURE 6 SMOOTHED OUT TENSILE STRENGTH PROFILE OF HERCULES 3501-6 EPOXY RESIN AS A FUNCTION OF TEMPERATURE AND EQUILIBRIUM MOISTURE CONCENTRATION (CORRESPONDING TO THE INDICATED REL. HUMIDITIES)

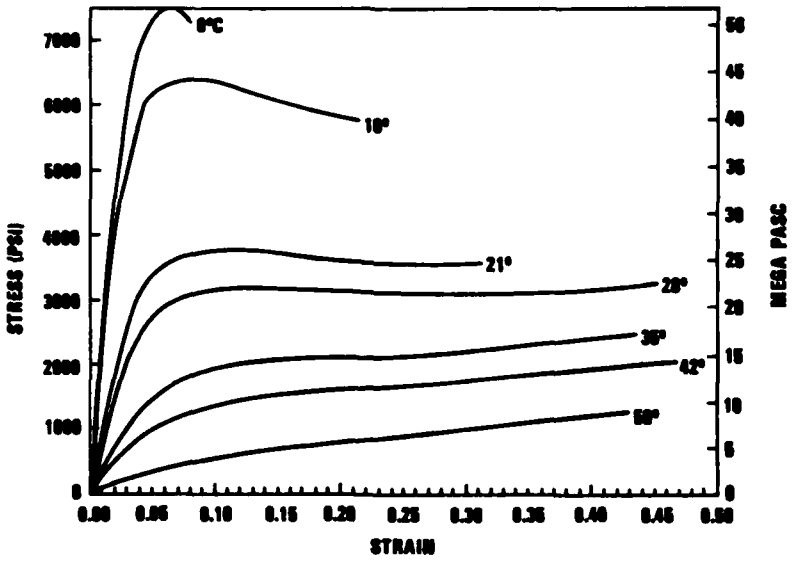

FIGURE 7 STRESS STRAIN BEHAVIOR OF HBRF 241 RESIN (DRY) TESTED AT DIFFERENT TEMPERATURES

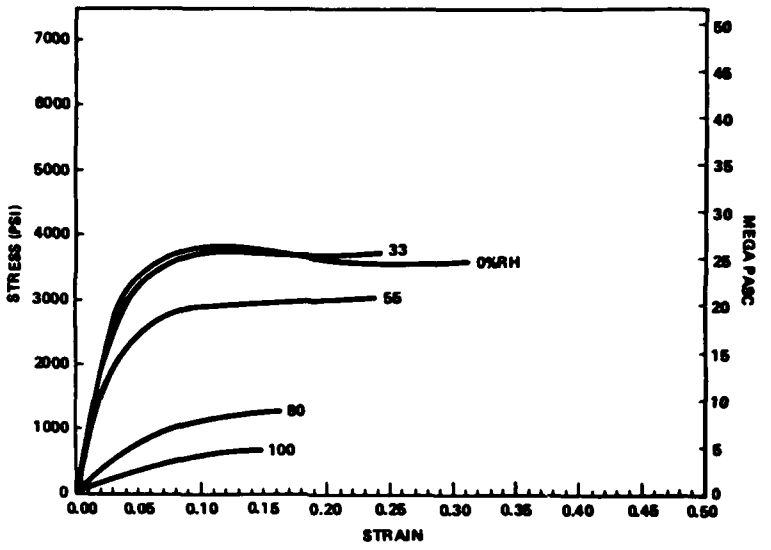

FIGURE 8 STRESS STRAIN BEHAVIOR OF HBRF 241 RESIN EQUILIBRATED AT DIFFERENT RELATIVE HUMIDITIES, TESTED AT 21°C.

by applying the well established laminated plate theory where the angular dependence of the stiffness is obtained by matrix multiplication of the stiffness matrix with a transformation matrix. An intergration over all the plies results in a global stiffness matrix (see Appendix A) which allows one to predict the stretching and bending behavior of composites (Ref. 17-20). From the measured resin data the change in composite properties was calculated and compared with the actually measured composite properties (see Fig. 9). The full three dimensional analysis (instead of the simpler two dimensional plain stress model is discussed in Reference 17).

Viscoelastic Behavior

Here we want to show that there is a well established theory that allows us to draw conclusions of how a composite laminate will behave viscoelastically and how it will change with changing environment if only the corresponding resin data are available. For the moment we shall disregard that the theory is exact only under the following assumptions: (1) the resin in the composite has the same properties as the bulk resin, (2) the composite

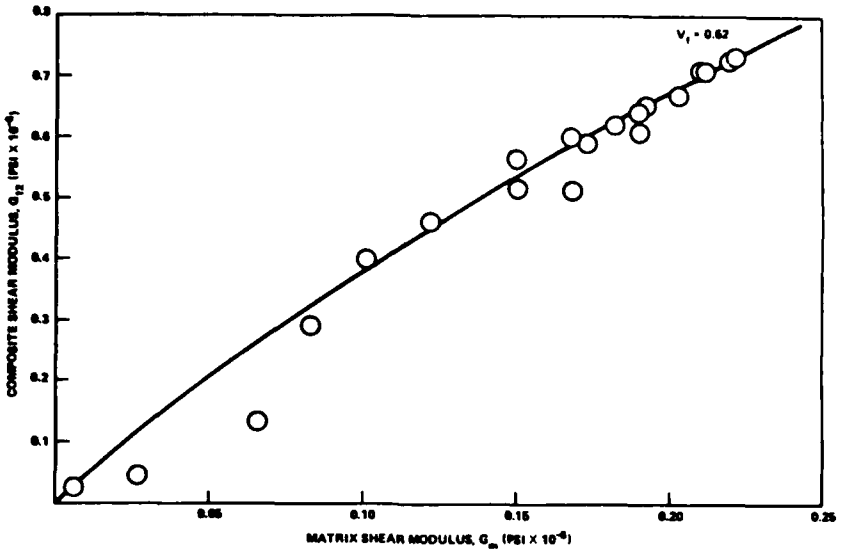

FIGURE 9 PREDICTED CHANGE IN THE COMPOSITE SHEAR MODULUS (SOLID LINE, FOR V_f = 0.62) THE DATA POINTS ARE THE OBSERVED VALUES FOR A 3501-6/AS COMPOSITE AT DIFFERENT TEMPERATURES AFTER EQUILIBRATION AT 0, 33, 55, 80, AND 100% RH

has no voids (Although (2) is not a restriction of the theory, it only makes the quantitative prediction more difficult).

To establish the theoretical basis we have to show only the validity of two suppositions: (1) that there exist a static solution for the boundary value problem of the micromechanical model of the composite laminate considered, and (2) that the so-called elastic-viscoelastic correspondence principle is a valid physical principle. The correspondence principle of viscoelasticity states that, if a static solution of a structure is known, it is possible to obtain the viscoelastic solution of the same structure if the material stress relaxation moduli (creep compliances) are known. (This also applies to steady state harmonic vibrational solutions).

First, we shall explain what is meant under the so-called elastic-viscoelastic correspondence principle. (It was first applied by Biot (Ref. 21) to anisotropic media. Further discussions may be found in Reference 17 and 22). It has been found that the Laplace transformed viscoelastic stress strain relations are of the same form as the corresponding elastic

results if we identify $s\bar{C}(s)$ with the elastic modulus C (where $\bar{C}$ stands for the Laplace transform). Thus, if all governing relations for an elastic boundary value problem are Laplace (or Fourier) transformed they are indentical with those of the transformed viscoelastic problem. It follows that solutions of static elastic problems can be converted to transformed solutions of the corresponding viscoelastic problems simply by replacing the elastic moduli by $s\bar{C}(s)$ and reinterpreting the elastic field variables in the solution as transformed viscoelastic variables. All that is required now is a transform inversion. (The same is true for the complex moduli of dynamic mechanical problems.)

We have already shown in the previous section that analytical and numerical solutions are available for the static, micromechanical lamina properties and those for laminated plates, therefore, solutions can be found for the corresponding viscoelastic problems from known resin behavior. An example of the effect of moisture on the relaxation modulus or creep compliance of the resin is shown in Fig. 10-12. Obviously, a composite with voids will have an increased static compliance and so it will have an increase in creep rate. Also, if the fiber does not creep, the composite creep will be governed by the matrix under transverse and shear loading. Generally, with carbon, glass or boron fibers, one only has to know the resin relaxation or creep behavior as a function of temperature and moisture content to predict composite creep behavior. Relaxation modulus and creep compliance are related through the convolution integral equation

$$t = \int_0^t \phi(t-\tau)\psi(\tau)d\tau$$

for which a numerical solution is given in Reference 23.

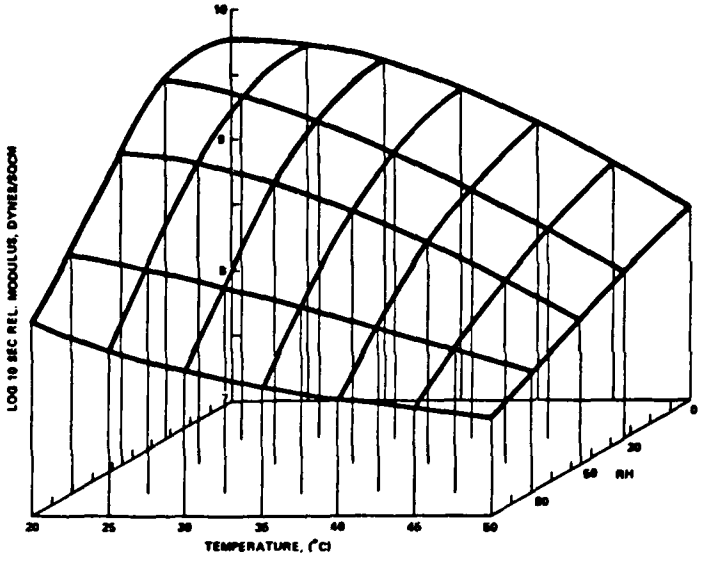

FIGURE 10 TEN SECOND STRESS RELAXATION MODULUS OF HBRF 241 AS A FUNCTION OF TEMPERATURE AND EQUILIBRIUM CONCENTRATION CORRESPONDING TO DIFFERENT RELATIVE HUMIDITIES

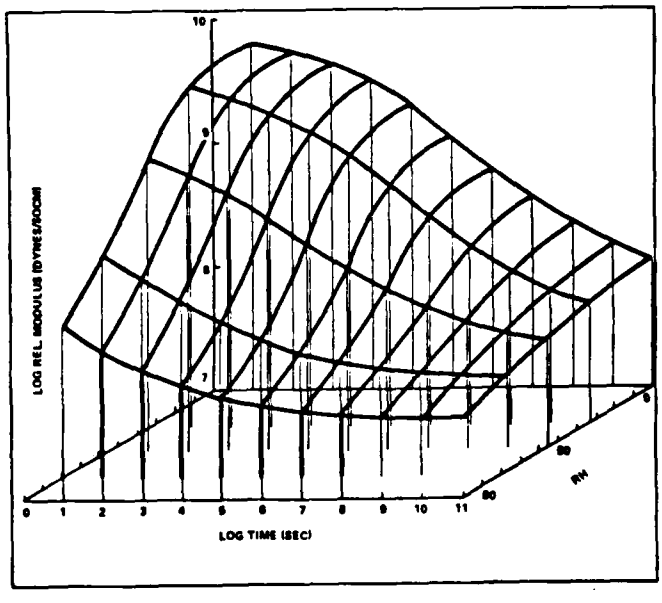

FIGURE 11 MASTER SURFACE OF THE STRESS RELAXATION MODULUS OF HBRF 241(REFERENCE TEMPERATURE 21°C).

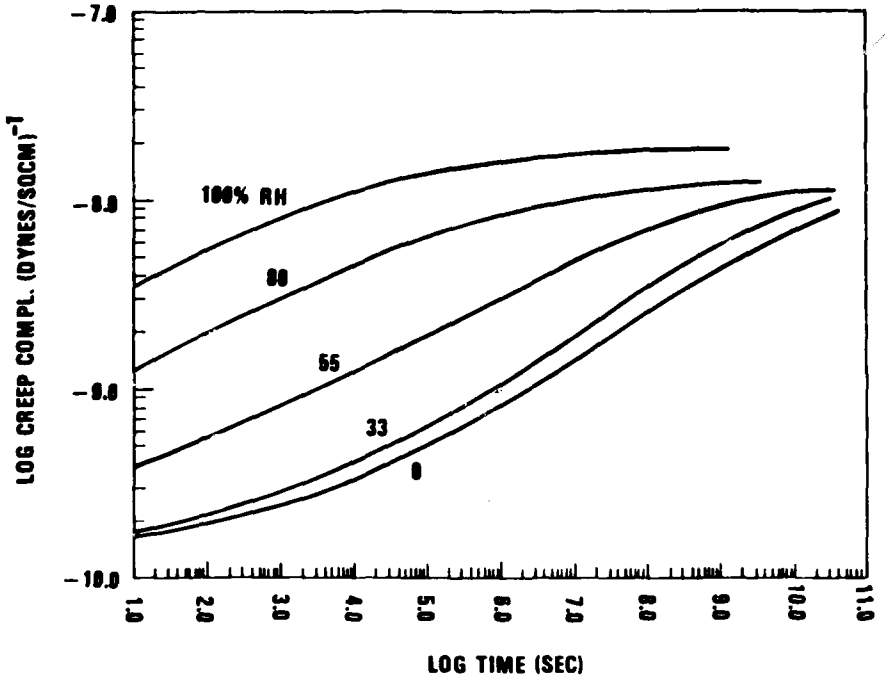

FIGURE 12 CREEP COMPLIANCE OF HBRF 241

Crossman et al (Ref. 24) have demonstrated that, by using their special finite element viscoelastic laminate code, they can predict the change in warping of unsymmetric laminates due to changes in temperature and moisture (using the viscoelastic lamina properties). Schwartz et al. have shown that even a somewhat simplified quasi-elastic treatment of a laminate gives reasonable viscoelastic predictions of laminates if only resin and fiber properties are used (Ref. 25).

Hygrothermal Behavior

Although most hygrothermal effects fall under either of the sections elastic, viscoelastic or failure we shall mention here some special cases because they are sufficiently important in composite behavior. These are: thermal expansion, cooldown stresses from cure temperature (residual stresses), hygroscopic swelling stresses (and the hygro-thermal combination),

temperature and moisture diffusivities with the resulting non-uniform distributions, and the expected climatic effects. If the moisture uptake is only a physical sorption without chemical hydrolysis, the moisture effects on the composite mechanical properties appear to be reversible i.e., virgin properties can be regained when the moisture is removed. Obviously, this would not be the case if the matrix is hydrolyzed.

With the exception of failure these effects can again be treated by a mechanistic theory.

Thermal Stresses and Expansion Coefficients

Since during cure of an epoxy composite the glass transition temperature of the resin hardly exceeds the cure temperature (and may not even reach it if Tg_∞ is lower than the cure temperature) one may consider the cure temperature or Tg_∞ (whatever is lower) as the stress free temperature. Cooldown below the stress free temperature will cause a buildup of internal stresses (due to the mismatch in thermal expansion coefficients). Part of these stresses may be reduced if the cooldown is sufficiently slow (within about $30^{o}C$ below Tg) to allow for a viscoelastic relaxation. Below this temperature range the relaxation is probably too slow to be of practical value. As long as the internal stress build-up is within the linear elastic range of the constituent materials it does not affect the modified rule of mixture calculation for the elastic constants. However, one will expect a difference in strength calculation for first ply failure theory of laminates because some of the plies are under positive and some are under negative stress. The prestress will contribute (positively or negatively) to the first ply-failure stress upon loading of the laminate. (For this reason one has to be careful in using

laminated plate theory in conjunction with unidirectional ply failure-strains by using "unrestrained" uniaxial ply strength data (X, $X^{'}$, Y, $Y^{'}$S and $S^{'}$). (Where X, Y, S stand for positive longitudinal, transverse and shear strengths and the primed values for the corresponding negative strengths). Of course, the corresponding correction can be made analytically.

Thermal and Hygroscopic Expansion

Strains caused by temperature and moisture changes are called nonmechanical strains which may be analytically expressed by

$$e_x = \frac{V_f E_f e_f + V_m E_m e_m}{V_f E_f + V_m E_n}$$

$$e_y = V_f e_f + V_m e_m + V_f \nu_f e_f + V_m \nu_m e_m - (V_f \nu_f + V_m \nu_m) e_x$$

(e = nonmechanical strain, V = volume fraction, ν = Poisson's ratio, subscript x, y, f, m stand for longitudinal transverse, fiber and matrix). By introducing $\alpha_i = e_i/T\text{-}T_o$, the average thermal expansion coefficient, and $\beta_i = e_i/C$, the moisture swelling coefficient for the resin and fiber, gives readily the corresponding α_{ic} and β_{ic} of the composite (Ref. 19, 26, 27) (see Appendix). For determining the laminate thermal expansion coefficients one uses again the laminated plate theory. The angular dependence of these coefficients is obtained, as usual, by multiplying the coefficient matrix with the corresponding transformation matrix. Thus it can be easily seen that the average internal stresses will depend on the combined effect of temperature and moisture concentration. The simultaneous interaction of temperature and moisture can either tend to reinforce or to cancel each other with respect to internal, nonmechanical stresses.

Microscopic details of intra and inter resin and fiber stresses can be obtained by finite element analysis as was demonstrated by Adams et al (Ref. 8). The agreement of theoretical predictions and experimental measurements is probably as good as one might expect within the limits of experimental errors (Ref. 28,29).

Cooldown Stresses from Cure Temperature

For a rapid cooldown from cure temperature the internal stresses can be easily estimated (using static analysis), keeping in mind that the equations for the thermal strains at the respective temperatures should be replaced by integrals since the moduli and the Poisson's ratio are not linear around glass transition temperature. A slow cooldown, however, requires to replace the static elastic treatment by a viscoelastic formulation (as indicated in the section viscoelastic behavior) since there will be a partial relaxation when the viscoelastic relaxation rates are still high enough. These rates, however, decrease exponentially with decreasing temperature and are quickly frozen in for all practical purposes. An excellent experimental verification of the predicted values was furnished by Crossman et al (Ref. 24) who measured the change of internal stresses from the change in radius of curvature of warped unsymmetric laminates. (Again they used a finite element approach in their work with a hereditary integral formulation of viscoelasticity). From these considerations it becomes obvious, that the composite elastic, viscoelastic and strength properties will change with time as moisture slowly diffuses through the matrix and changes it properties.

It is fairly straight forward to predict the elastic changes of laminate properties with time by combining the solutions of the respective moisture

diffusion problem with micromechanics lamination theory and modelling of the environment (Ref. 30,31). For temperature sufficiently below Tg the static elastic solution will suffice. If the environmental temperature approaches Tg it is advisable to use a viscoelastic formulation. Internal moisture gradients which are stronger at the beginning of environmental exposure are simply treated as if the composite were made of a finite number of layers with different stiffness coefficients (corresponding to the average local moisture concentration). If moisture only plastisizes the resin then the deteroration of the laminate properties reaches a limiting value when the absorbed moisture is in equilibrium with the environment. The original mechanical properties may be regained after the moisture is removed (Ref. 32), (reversible moisture effect). Some matrix materials, however, have hydrolyzable groups, in which case an irreversible property degradation may result without a limiting value of deterioration.

While the elastic and viscoelastic behavior is readily predicted there is no such simple scheme for predicting changes in strength properties.

Elastic-Plastic Behavior

Since the stress-strain curves of organic matrix materials look sometimes very similar in shape to stress-strain curves of metals one is tempted to use a nonlinear elastic-plastic formulation in solving the composite boundary value problem (which seems to work reasonably well with metal matrix composites).

However, the elastic-plastic formulation is a time independent formulation (where the assumption is made that below a certain

(Yield strain) the matrix behaves elastic, and above, more or less plastic). The plastic deformation mechanism is caused by long range slippage, (shear) of crystallographic planes which generates no memory and restoring forces (although the stress strain behavior may be history dependent as seen from the effect of "workhardening.") A viscoelastic, crosslinked polymer, however, generates restoring forces upon deformation (memory) and the relaxation modulus (or creep compliance) is a function of time, temperature, moisture-content and stress. Thus we believe that an elastic-plastic formulation is not a good physical model for organic epoxy composites, although it may, in some special application, be sufficient to describe experimental results. The nonlinearity of the elastoplasticity is solved by an incremental finite element method (see Ref. 8).

Phenomenological Approach

Strength

Although, a great number of papers have been published on strength fracture, fatigue, (and less so on impact damage) of composite materials, there is, at present, no mechanistic theory that would predict with sufficient accuracy failure surfaces of composites under general loading conditions and even less so for environmental effects.

Of course, one hopes to be able to define what constitutes a failure and if the definition is simple, clear enough, and not too difficult to observe, one may agree on what may be called a failure. Some of these criteria have been adapted from metallurgy and from the strength of anisotropic materials. Yet the approaches are essentially phenomenological i.e., one looks for a

transfer function that correlates experimentally observed strength values to the applied forces. Such a function must give a closed surface (because a material is assumed to have only a finite strength) and the solution must be single valued for a given stress vector, also, most theories assume a path independent strength at a given point on the failure surface. The maximum stress and maximum strain criteria (which state that certain maximum values of stresses or strains must not be exceeded if failure is to be prevented) are simple but have significance only for one-dimensional states. More generalized failure criteria have been presented by Hill (Ref. 33), Norris (Ref. 34), Marin (Ref. 35), Hoffman (Ref. 36), Chamis (Ref. 37), Azzi and Tsai (Ref. 38), and Sandhu (Ref. 39). Wu (Ref. 1) showed that they are all restricted special cases of the "tensor polynomial failure criterion" that Tsai and Wu (Ref. 40) suggested. Since the tensor polynomial criterion is perhaps the most general with all the required features necessary for design analysis (coordinate transformation, adaptable to real composite behavior without redundancy and nonphysical behavior by a judicial elimination of certian coefficients) we will briefly discuss only this criterion which is stated as:

$$F_i \sigma_i + F_{ij} \sigma_i \sigma_j + F_{ijk} \sigma_i \sigma_j \sigma_j + ... = 1$$

where i,j,k, = 1,2,.....,6. For the special case of plain stress i,j,k, = 1,2,6. If in addition the polymonial is truncated after the cubic terms and if there is orthotropic symmetry in a composite, which allow further simplification and if redundant and nonphysical (non single valued) terms are eliminated the expression becomes relatively simple:

$$F_1\sigma_1 + F_2\sigma_2 + F_{11}\sigma_1^2 + F_{22}\sigma_2^2 + F_{66}\sigma_6^2 + 2F_{12}\sigma_1\sigma_2$$
$$+ 3F_{112}\sigma_1^2\sigma_2 + 3F_{122}\sigma_1\sigma_2^2 + 3F_{166}\sigma_1\sigma_6^2 + 3F_{266}\sigma_2^2\sigma_6 = 1$$

From tensile, compression and shear measurements along the 1,2 and 6 axes the F_i and F_{ii} can be obtained. The F_{ij} and F_{ijj} must be obtained from biaxial measurements as described in (Ref. 41).

As was pointed out by Wu (Ref.1) the various failure polynomials represent certain characteristics of the failure envelope, for instance:

F_i determines the center of failure envelope along the σ_i axis

F_{ii} determines the failure envelop intercept of the σ_i axis (or the size of the ellipsoid)

F_{ij} determines the inclination of the ellipsoid in the $\sigma_i\sigma_j$ plane and characterizes the strength coupling between σ_i and σ_j

F_{ijj} distorts the failure surface from an ellipsoid

If we want to see how temperature or moisture will affect the various polynomial coefficients then we have to know how the strength behavior will change. If we consider for instance a symmetric 0/90 laminate with only tensile and compression loadings ($X_1 = X_1'$, $Y_1 = Y_1'$,) then we expect little change in tensile strength in σ_1 and σ_2 axes, however, we expect a change in compression strength. The center of the envelope moves towards the first quadrant and F_1 and F_2 will decrease and F_{11} and F_{22} will increase. There will be some rotation if F_{12} was $\neq 0$. Since the F_{ijj} are functions of the other F_i, F_{ij}, F_{ijj}, their changes are less obvious, however, their trends can be estimated by small perturbations of corresponding strengths.

What becomes obvious from this qualitative consideration is, that a definite trend in the change of F_i, F_{ij}, F_{ijk} is expected and that experimental work, determining their derivatives $\partial F_i/\partial T$ or $\partial F_i/\partial M$ may give functions, simple enough, to be of practical value. It should also be investigated (experimentally) how the lamina transverse and shear strengths relate to moisture and temperature conditions i.e.,

$$\partial X_m/\partial T = \lambda_T \, \partial X_c/\partial T \text{ or } \partial X_m/\partial M = \lambda_M \, \partial X_c/\partial_M$$

(where λ_T may be temperature and λ_M moisture dependent).

Fracture

We have seen that strength of a composite material is a very complex problem to analyze. The question of fracture and fracture toughness is even more so. Mulville and Wolock have recently discussed this subject in a review of over 130 papers (Ref. 42). We are not trying even to attempt a summary on this subject since very little is known about environmental effects.

One could try to approach the problem of environmental effect with a sort of a naive mechanistic model by using the Griffith-Irwin equation. The effective maximum static flaw size which can exist just prior to fracture of an unnotched unidirectional transverse tensile specimen is given by

$$a_c = \frac{E_t \, G_c}{\pi \, \sigma_{TS}^2}$$

where σ_{TS} is the transverse tensile strength, E_T the transverse modulus and G_c the critical strain energy release rate measured.

It seems however that the ratio of a_c to G_c does not remain constant during moisture absorption. Observations made by Springer et al (Ref. 43) show that the room temperature transverse tensile strength in T300/5208 and AS/3501 is reduced 40-50 percent upon absorption of 1.5 - 2.0% water, while the transverse modulus is reduced only 10-15%. If these data are representative then one has to assume that G_c or a_c or both are also moisture dependent. Thus a simple mechanistic model for even the simple case of the transverse fracture of a lamina is not apparent.

Again a phenonenological fracture criteria was described by Wu (Ref. 44) where he separates the stress distribution around the crack tip in symmetric and skew symmetric parts. The stress distribution in the neighborhood of the crack is given by:

$$\sigma_i = \frac{k_1}{r^{1/2}} g_i (S_{k,e,\theta}) + \frac{k_2}{r^{1/2}} (S_{k,e,\theta}) + 0 \left(\frac{r}{a}\right)^{1/2}$$

where the k_1 and k_2 are stress intensity factors characterizing the intensity of the singularity of $1/r^{1/2}$. Again, the same failure tensor polynomial as described under strength is employed. Wu and Reuter obtained (Ref. 44) an exceptional fit of the data in the first quardrant. They concluded that fracture initiates from the failure of a constant volume r_c under complex states of stress characterized by the tensor polynomial failure criterion. The critical volume which is characteristic of a given composite can be determined from a simple test such as fracture under pure tension. Under any other simple or complex loading fracture can be characterized through stress analysis of the crack tip and the phenomenological failure criterion. The incorporation of this criterion into fracture provides the necessary and sufficient conditions for fracture under combined loading.

A very interesting experimental approach to failure is taken by Mast et al (Ref. 45) with their "inplane loader". The sample is exposed to in plane tension, rotation and shear loading. Their failure criterion is defined as the point at which there is a significant increase in the non-recoverable strain energy in the specimen. This increase in the dissipated energy is attributed to the initiation of fracture. The advantage of the method is, that being computer controlled, it permits a rapid test of many samples (2x2 inches) and there is no reason why it should not be used with some mathematical (phenomenological) criterion equivalent to the tensor polynomial criterion. This method does not require composite cylinders for biaxial testing.

Fatigue

Fatigue in metals is fairly well understood. This is not the case in composites. Cracks in composites do not have the same implications as those in metals. Data in the form of S-N diagrams are available for various types of loadings: axial, tension, compression; in-plane, interlaminar and torsional shear; and failure. A recent review by Hahn (Ref. 46) discusses the various failure mechanisms in light of the observed failure modes. An attempt is made to describe fatigue behavior in terms of uniaxial fatigue strength with a failure criterion of the form:

$$\max_{\alpha} \{ f_{\alpha}(\sigma_i, S_{\beta}) \} = 1$$

(σ_i = applied stresses in the material symmetry axes. S_β = parameters such as uniaxial fatigue strengths). These parameters depend on the fatigue cycles, but the functions f_α do not. The S_β-N relations are to be obtained

under similar loading conditions. Hahn compared several static failure models (Ref. 47-50). His major conclusions were that the fatigue limit is dominated by the matrix. A strong matrix coupled with a strong interface may render the composite more fatigue sensitive because of increased crack growth rate resulting from brittle fracture of fibers. However, it seems that very little difference is observed microscopically between the static and the fatigue failure modes. The important point is that composite laminates exhibit very low fatigue notch sensitivity. A review by Lauraitis (Ref. 51) pointed out that there are inconsistencies in the conlusions by different authors. Some researchers observed increases in residual strengths others observed no such changes. Some authors maintain that the failure modes are the same as those of static loading, others claim differences. In a later review by Mulville and Wolock (Ref. 42) the authors point out that there is generally a lack of adequate details of the test conditions and in many cases there are alarmingly few specimens tested and examined which make many reports doubtful.

In a recent, rather extensive study by Whithead (Ref. 52) the author made at least some reassuring observations. His major conclusion was that static design criteria and current composite design allowables causes fighter aircraft composite structures to be fatigue insenstitive. He also noted the excellent fatigue properties of composite materials under the projected flight loading spectrum and environments.

Impact Behavior

If fracture and fatigue is a difficult problem with composite materials, then impact is even more so. Although it is an important practical problem to get a feeling for the kind of damage that may be encountered from accidentally dropping a tool on a composite airwing skin, the problem is very difficult to

solve since the dynamic load distribution, stress-strain propagation, composite geometry and fastening, location of impact, geometry of impacting body, velocity, etc., play all an important role. A falling ball test or similar impact test will be, at best, a very crude and qualitiative test. At this time there is no general theory available to solve this problem with a reasonable degree of certainty and even less so if one wants to include the effect of the environment.

Conclusions

At present, it appears that certain composite properties and their changes in the environment can be predicted by using mechanistic theories. Such properties are average, global in nature, such as elasticity, viscoelastic, and hygrothermal behavior. They can be predicted from the corresponding resin and fiber properties.

Strength and fatigue, which is governed by local, discontinuous phenomena are best described with phenomenological theories.

For impact damage there is at present no useful theory.

References

1. Wu, E. M., Phenomenological Anisotropic Failure Criterion," Composite Materials, Vol. 2, Academic Press (1974).
2. Reisner, E. and Stavsky, Y., Journal Applied Mechanics, Vol. 28, 402 (1961).

3. Augl, J. M. and Berger, A. E., "Moisture Effects on Carbon Fiber Epoxy Composites; II Prediction of Elastic Property Degradation," TTCP Critical Subject Review, London, 4 July 1977.

4. Augl, J. M., "Prediction and Verification of Moisture Effects on Carbon Fiber-Epoxy composites," NSWC TR 79-43, (March 1979).

5. Adams, D. F. and Donner, D. R., "Transverse, Normal Loading of a Unidirectional Composite," J. Composite Materials, Vol. 1, 152, (1967).

6. Karlak, R. F. and Crossman, F. W , LSMC-D457462, 1975, Lockheed Missile and Space Corp., Palo Alto, CA.

7. Lin, T. H., Salina, D., and Ito, Y. M., "Elasto-Plastic Analysis of Unidirectional Composites," J. Composite Materials, Vol 6, 48, (1972).

8. Adams, F. D. and Miller, A. K., "Hygrothermal Micorstresses in a Unidirectional Composite Exhibiting Inelastic Material Behavior," J. Composite Materials, Vol. 11, 285, (1977).

9. Reniere, G. D. and Herakovick, C. T., "Nonlinear-Analysis of Laminated Fibrous Composites," Doctoral Thesis, VA Polytech. Inst. 1976.

10. Hashin, E. and Rosen, B. W., "The elastic moduli of fiber reinforced materials," J. Applied Mechanics, Vol. 31, 223, (1964).

11. Muki, R. and Stanberg, E., "On the diffusion of an axial load from an infinite cylindrical bar embedded in an elastic medium," Int. J. Solids Structures, Vol. 5, 587, (1969).

12. Sternberg, E. and Muki, R., "Load absorption by a filament in a fiber-reinforced material," Z. Augen. Math. Physik, Vol. 21, 552, (1970).

13. Carne, T. G., "Load absorption and interaction of two adjacent filaments in a fiber-reinforced material," J. Elasticity, Vol. 6, 1, (1976).

14. Ekvall, J. C., ASME paper 61 AV-56, Aviation Conf., Los Angeles (Cal.) March 1961.

15. Behrens, E., "Elastic constants of fiber reinforced composites with transversely iotropic constituents," J. Applied Mechanics, Vol. 38, 1062, (1971).

16. Chen, C. H. and Cheng, S., "Mechanical properties of anisotropic fiber-reinforced composites," J. Applied Mechanics, Vol. 37, 186, (1970).

17. Christensen, R. M., "Mechanics of Composite Materials," John Wiley & Sons, (1979).

18. Halpin, J. C. and Tsai, S. W., "Environmental Factors in Composite Materials Design," AFML TR 67-423.

19. Ashton, J. E., Halpin, J. C., and Petit, P. H., "Primer on Composite Materials: Analysis," Technomic Publishing Co., (1969).

20. Vinson, J. R. and Chou, T. W., "Composite Materials and their use in Structures," John Wiley & Sons, (1975).

21. Biot, M. A., in Proceeding US Nat. Congr., Applied Mechanics ASME 3rd 1 (1958).

22. Schapery, R. A., "Viscoelastic Behavior and Analysis of Composite Materials," John Wiley & Sons, (1979).

23. Hopkins, I. L. and Hamming, R. W., "On Creep and Relaxation," J. Applied Physics, Vol. 28, 906, (1957).

24. Crossman, F. W. and Flaggs, D. L., "Dimensional Stability of Composite Laminates during Environmental Exposure," SAMPE Vol. 24, (1979).

25. Schwartz, E. B. and McQuillen, E. J., "Viscoelastic Creep and Relaxation in Laminated Composites," NADC Report No. 74196-30 (1974).

26. Tsai, S. W., "Introduction to Composite Materials," Technomic Publ. Co. Inc., pp. 402, (1980).

27. Shapery, R. A., "Thermal Expansion Coefficient of Composite Material Based on Energy Principles," J. Composite Materials, Vol. 2, 380, (1968).

28. Ishikawa, T., "Thermal Expansion Coefficient of Unidirectional Composites," J. Composite Materials, Vol. 12, 153, (1978).

29. Strife, J. R. and Prewo, K. M., "The Thermal Expansion Behavior of Unidirectional and Bidirectional Kevlar/Epoxy Composites," J. Composite Materials, Vol. 13, 264, (1979).

30. Augl, J. M. and Berger, A. E., "The Effect of Moisture on Carbon Fiber Reinforced Composites. III Prediction of Moisture Sorption in a Real Outdoor Environment," NSWC TR 77-13, (1977).

31. Augl, J. M. and Berger, A. E., "The Effect of Moisture on Carbon Fiber Reinforced Epoxy Composites. IV Prediction of Changes in the Elastic Behavior," NSWC TR 77-61, (1977).

32. Augl, J. M., "The Effect of Moisture on Carbon Fiber Reinforced Epoxy Composites. II Mechanical Property Changes, NSWC TR 76-149, (1977).

33. Hill, R., "A Theory of the Yielding and Plastic Flow of Anistropic Metals," Proc. Royal Soc. Vol. A193, 281, (1948).

34. Norris, C. B., "Strength of Orthortropic Materials Subjected to Combined Stresses," Forest Products Laboratory Report No. 1816, (1950).

35. Marin, J., "Theories of Strength of Combined Stresses and Nonisotropic Materials," J. of the Aeronautical Sciences, Vol. 24, No. 4, (1957).

36. Hoffman, O., "The Brittle Strength of Orthotropic Materials," J. Composite Materials, Vol. 1, 200, (1967).

37. Chamis, C. C., "Failure Criteria for Filamentary Composites," NASA TN D-5367

38. Azzi, V. D. and Tsai, S. W., "Anisotropic Strength of Composites," Experimental Mechanics, Vol. 5, 283, (1965).

39. Sandhu, R. S., "Ultimate Strength Analysis of Symmetric Laminates," AFFDL-TR-73-137, (1974).

40. Tsai, S. W. and Wu, E. M., "A General Theory of Strength for Anisotropic Materials," J. Composite Materials, Vol. 5, 58, (1971).

41. Wu, E. M., "Optimal Experimental Measurements of Anisotropic Failure Sensors," J. Composite Materials, Vol. 6, 472, (1972).

42. Mulville, D. R. and Wolock, I., "Failure of Polymer Composites," in Developments in Polymer Fracture - 1. Ed. E. H. Andrews, Applied Science Publishers.

43. Shen, C. H. and Springer, G. S., "Effect of Moisture and Temperature on the Tensile Strength of Composite Materials," J. Composite Materials, Vol. 11, 2, (1977).

44. Wu, E. M. and Rueter, R. C., "Crack Extension in Fiberglass Reinforced Plastics," TAM Rep. No. 275, University of IL, Urbana, IL.

45. Mast, P. W., Mulville, D. R., Beaubien, L. A., Sulton, S. A., Thomas, R. W., Tirosh, J., and Wolock, I., "Failure Criteria for Composite Structures," in NRL Memorandum Report 4005, p. 111, (1979).

46. Hahn T. H., "Fatigue Behavior and Life Prediction of Composite Laminates," AFML-TR-78-43, (1978).

47. Tsai, S. W. and Hahn, H. T., "Composite Materials Workbook," AFML-TR-77-33, (1977).

48. Sims, D. F. and Brogden, V. H., "Fatigue of Filamentary Composite Materials," ASTM STP 636, pp. 185, (1977).

49. Haskin, Z. and Rotem, A., J. Composite Materials, Vol. 7, 448, (1973).

50. Rotem, A. and Hashin, Z., AIAA Journal, Vol. 14, 868,(1976).

51. Lauraitis, K. N., "Fatigue of Filamentary Composites," ASTM-STP 636, Ed. Reifsnider, K. L. and Lauratitis, K. N.

52. Whitehead, R. S., "A Review of the Rational for Durability Voliolation of Composite Structures," Paper presented at the 5th DOD/NASA Conference on Fibrous Composites, New Orleans, (Jan 1981).

APPENDIX

Halpin-Tsai Equations (Modified Rule of Mixture)

The following engineering constants E_x, ν_x, E_s, K_y, G_y, and E_y can be calculated from

$$P = (V_f P_f + \eta V_m P_m)/(V_f + \eta V_m)$$

where P stands for E_x, ν_x, $1/E_s$, $1/K_y$, $1/G_y$, and $1/E_y$ respectively. The corresponding P_f, P_m and in the right hand side of the equation stand for the corresponding fiber and matrix values. The η values have the forms

$$\eta_s = (1 + G_m/G_f)/2$$
$$\eta_k = (1 + G_m/k_{fy})/[2\ (1 - \nu_m)]$$
$$\eta_G = (3 + 4\nu_m + G_m/G_{fy})/[4(1 - \nu_m)]$$

for the calculations of the longitudinal shear modulus, the plane strain bulk modulus and the transverse shear modulus.

(E_x = longitudinal Young's modulus x

ν_x = longitudinal Poisson's ratio x

E_s = longitudinal Shear modulus s

K_y = planestrain bulk modulus

G_y = transverse shear sodulus

E_y = transverse Young's modulus) y

Equations of Laminated Plates

The extension and bending behavior of laminated plates is given by the following matrix equation

$$\left[\begin{array}{c} N \\ \hline M \end{array}\right] = \left[\begin{array}{c|c} A & B \\ \hline B & D \end{array}\right] \left[\begin{array}{c} \varepsilon^o \\ \hline \kappa \end{array}\right]$$

where N and M are the stress resultants and bending moments, A, B and D are the extensional stiffness, coupling stiffness, and bending matrices respectively. ε and κ are the extension strains and curvatures.

The A, B and D components are given by

$$A_{ij} = \sum_{k=1}^{n} (\bar{Q}_{ij})_k \, (h_k - h_{k-1})$$

$$B_{ij} = \frac{1}{2} \sum_{k=1}^{n} (\bar{Q}_{ij})_k \, (h_k^2 - h_{k-1}^2)$$

$$D_{ij} = \frac{1}{3} \sum_{k=1}^{n} (\bar{Q}_{ij})_k \, (h_k^3 - h_{k-1}^3)$$

Hereditary Integral Formulation of Viscoelasticity

(used in finite element analysis).

$$\sigma_i(T,M,\tau) = \int_{0^+}^{t} C_{ij}\,(T,M,t-\tau) \frac{d\tau}{d} \left[\varepsilon_j(\tau) - \alpha_j \Delta T(\tau) - \beta_j \Delta M(\tau)\right] d\tau$$

where

$$C_{ij}(T,M,t) = A_v(T,M)\, Q_{ij}(T_o, M_o, \xi)$$

$$\xi \int_{0^+}^{t} \frac{d}{A_{TM}(T,M)}$$

where $\sigma_i(T,M,\tau)$ are the stresses as functions of temperature, moisture and time, the Q_{ij} are the stiffnesses; the expression in brackets are the applied, thermal and hygroscopic strains and $A_v(T, M)$ and $A_{TM}(T, M)$ are vertical and horizontal shift factors with respect to a standard moisture and temperature condition).

Lamina Thermal Expansion Coefficient (Ref. 26)

$$\alpha_x = \frac{V_f E_f(t)\alpha_f + V_m E_m(t)\alpha_m}{V_f E_f(t) + V_m E_m(t)}$$

$$\alpha_y = V_f\alpha_f + V_m\alpha_m + V_f\nu_f\alpha_f + V_m\nu_m\alpha_m - (V_f\nu_f + V_m\nu_m)\alpha_x$$

Lamina Hygroscopic Swelling Coefficients (Ref. 26)

$$\beta_x = \frac{V_f E_f c_{fm}\beta_f + V_m E_m \beta_m}{(V_f E_f + V_m E_m)(V_m s_m + V_f s_f c_{fm})}\, s$$

$$\beta_y = \frac{V_f(1+\nu_f)c_{fm}\beta_f + V_m(1+\nu_m)\beta_m}{V_m s_m + V_f s_f c_{fm}}\, s - (V_f\nu_f + V_m\nu_m)\beta_x$$

THE INFLUENCE OF MOISTURE ON THE TRANSVERSE MECHANICAL BEHAVIOR OF KEVLAR 49/EPOXY COMPOSITES AT 25°C

Ronald E. Allred and David K. Roylance

Department of Materials Science and Engineering
Massachusetts Institute of Technology
Cambridge, Massachusetts 02139

Abstract

Previous studies have shown that moisture can substantially affect the tensile and flexural properties of Kevlar/epoxy laminates. Coupled with moisture diffusion results, these data suggest that moisture may preferentially alter interface dominated properties. This study was undertaken to examine the magnitude of moisture effects on the transverse tensile properties of Kevlar 49/Fiberite 934 epoxy composites. The transverse tensile test was selected so that failure modes could be determined by scanning electron microscopy. Results indicate that saturation moisture concentrations (>5^{w}/o) cause substantial reductions in transverse properties at 25°C compared to dry control values. Ultimate strength and elongation are observed to decrease respectively by 35 and 27 percent. Composite transverse stiffness is less sensitive to moisture, but is degraded by 14 percent. Microscopy of the fracture surfaces reveals that property reductions are accompanied by a change in failure mode from an interface dominated mechanism in the dry condition to one of filament splitting at saturation moisture contents. Increased filament compliance and the splitting failure mode may be a consequence of moisture interrupting the interchain hydrogen bonding of the Kevlar 49 filaments.

INTRODUCTION

High performance filament-reinforced composites are finding extensive use in the areas of aerospace, defense, transportation

and sporting goods. The high specific mechanical properties which result from these materials are largely responsible for their rapid penetration into the marketplace. As composites have been employed in critical structural applications such as primary aircraft structures, environmental interactions which could reduce their performance have become a basic concern. Moisture, especially in parts which see transient elevated temperatures, has been shown to substantially degrade the mechanical response of polymer matrix composites [1,2]. Matrix plasticization by absorbed moisture has been identified as the primary degradation mechanism in the majority of cases [3,4].

Studies of moisture effects on the Kevlar/epoxy system are particularly interesting in that the fiber, being organic, also absorbs moisture which is in contrast to most high performance composite systems. Recent studies on the Kevlar/epoxy system have shown that moisture effects in bending can be substantial [5]. Flexural strength losses appear to be due to increasing ease of filament buckling as moisture is absorbed [5]. Substantial strength losses in tension with moisture have also been observed in quasi-isotropic Kevlar fabric/epoxy laminates [6]; whereas, the tensile properties of filament dominated ply orientations (0°, 0/90) are less affected by moisture [6,7] at 21°C. It has also been observed that moisture diffuses preferentially in the fiber direction of Kevlar 49/epoxy laminates [8,9].

Such strength and diffusion data seem to indicate that moisture diffuses and consequently is present preferentially at the filament-matrix interface. Such an hypothesis is further

strengthened by the well known lack of bonding at the Kevlar/epoxy interface [10-13] which would create a disordered region as well as allowing the easy intrusion of moisture. If moisture does preferentially absorb at the interface, the interface controlled properties such as transverse tension and interlaminar shear would be affected to a greater degree than filament controlled properties. Such a mechanism appears to operate in the graphite/epoxy system [14,15] which has initial transverse strengths more than twice those of Kevlar/epoxy.

The purpose of this study is to examine the effect of moisture on the transverse tensile strength of unidirectional Kevlar/epoxy composites. One of two plausible effects would be expected. Either the moisture should plasticize the matrix, which would be evidenced by an increase in composite compliance and elongation, or the interface may be degraded in which case the strength and elongation would be reduced. The later mode may be likened to grain boundary embrittlement in metals.

Experiment

Specimens for this study were taken from 0.40 inch thick unidirectional plates of Kevlar 49/Fiberite 934 epoxy supplied by the Army Mechanics and Materials Research Center. The plates were autoclave molded to a final cure temperature of 150°C and stored in a controlled 50 percent relative humidity environment. Filament volume fraction was nominally 64 percent with less than 0.5 percent voids [7]. Details of the prepreg resin

characterization and composite fabrication procedure are given in Ref. 7.

Machining was performed by diamond grinding with sacrificial aluminum plates on both sides of the composite. Final specimen dimensions were 1.0 inch wide by 5.0 inches long by the as-molded thickness. Despite the sacrifical aluminum plates, a lip of deformed material formed on the edges of the composite specimens during the grinding operation. To investigate the effect of further machining on specimen properties, half of the specimens were sanded to remove the lip at the edges and the other half were tested as-ground.

Prior to testing, the specimens were conditioned to one of four environmental exposures - dry, 50 and 75 percent relative humidity, or immersion in 80°C distilled water. Those conditions resulted respectively in 0, 2.2, 3.75, and > 5.0 weight percent absorbed moisture in the Kevlar/epoxy specimens. After environmental exposure, aluminum end tabs were bonded to the specimens with a room temperature cured epoxy adhesive to reduce stress concentration effects in the test machine grips.

Testing was performed on a universal Instron testing machine at a crosshead speed of 0.05 inch/minute. Elongation was monitored with a one inch, one percent strain gage extensometer. All tests were run at 25°C and 50 percent relative humidity. Exposure time to the laboratory atmosphere was approximately 10 minutes prior to failure. Seventeen specimens were tested in the dry condition. Ten specimens were tested at each of the various moisture exposure levels.

Results and Discussion

It was determined that sanding of the ground specimen edges did not effect measured properties and for purposes of discussion the sanded and as-ground specimens were averaged. Stress-strain behavior of all specimens was virtually linear elastic. A slight offset in strain was noted at about two-thirds of the ultimate specimen strength regardless of environmental exposure; however, the resultant increase in strain was slight. Young's moduli varied from 7.5×10^5 psi ($\pm 0.3 \times 10^5$ psi std. dev.) in the dry condition to 6.4×10^5 psi ($\pm 0.4 \times 10^5$ std. dev.) with 5 weight percent moisture. Ultimate strengths ranged from 2850 ± 330 psi dry to 1850 ± 200 psi with 5 weight percent moisture. Elongation correspondingly dropped 27 percent from 0.41 to 0.30 percent. Retained strength and stiffness as a function of moisture content is plotted for the Kevlar 49/Fiberite 934 composite system in Figure 1.

The 14 percent reduction in transverse stiffness seen in Kevlar 49/epoxy is roughly twice that observed in graphite/epoxy with similar resin matrices [16,17], or that which would be estimated by micromechanics analysis such as the Halpin-Tsai equations [18]. The larger change in transverse stiffness of Kevlar 49/epoxy with introduction of moisture than that from matrix plasticization alone indicates that a component of the system is changing in addition to the epoxy matrix. The interface or the Kevlar filaments themselves (radially) may be becoming more compliant in the presence of moisture. Kevlar/epoxy laminates

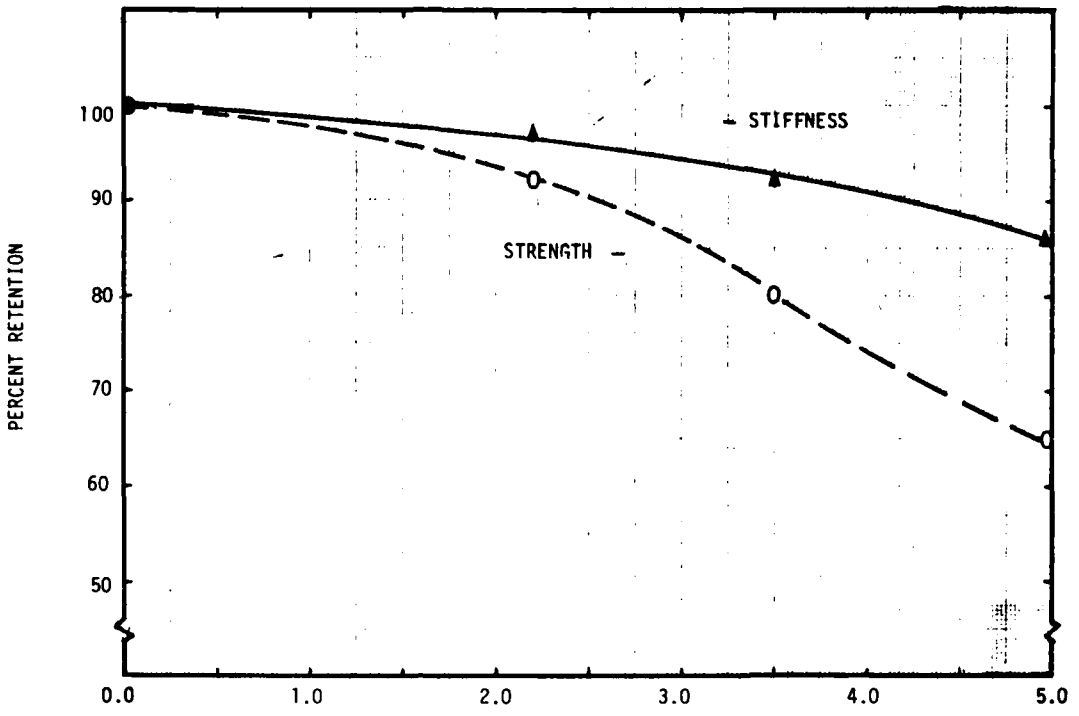

FIGURE 1. TRANSVERSE STRENGTH AND STIFFNESS RETENTION OF KEVLAR 49/934 AS A FUNCTION OF EQUILIBRIUM MOISTURE CONTENT AT 25°C.

[6] swell approximately four times that of graphite/epoxy composites [19] with equivalent resin systems and equivalent matrix moisture content. Those data indicate that the Kevlar filaments themselves undergo significant radial swelling strains in the presence of moisture. By interrupting the interchain hydrogen bonded structure, moisture may increase the filament radial compliance.

A 35 percent loss in transverse strength at 5 weight percent moisture is also seen in Figure 1. To aid in the identification of the failure modes responsible for such substantial losses at 25°C, the fracture surfaces were examined by scanning

electron microscopy. Because of the considerable filament pullout which is typical of transverse Kevlar/epoxy fracture [11, 13], it is difficult to make observations near the failure plane. As was noted in Ref. 13, it appears that failure of dry specimens initiates in the interface and that the brittle epoxy resin shatters for some distance around the crack plane which releases the filaments from the composite. Less filament pullout is visually apparent in specimens with high moisture contents.

SEM observation of the Kevlar 49/934 specimens in this study indicated that failure in the dry condition did initiate in the interface region, but that some resin could still be found adhering to the filaments. Some filament splitting could also be found; however, the dominant feature of the dry fracture surfaces is bare, intact filaments. A representative dry fracture area is given in Figure 2.

At 2.2 weight percent moisture (50 percent relative humidity exposure), the failure surface is still described by bare filaments, but with a much increased area of resin noted. It may be speculated that moisture toughens the epoxy which reduces the amount shattered from the surface. Some filaments with torn skins were also noted at 2.2 weight percent moisture.

With 3.75 percent moisture (75 percent relative humidity), even more resin could be seen in the fracture zone and large internal splits were appearing as seen in the upper portion of Figure 3. Torn filament skins over extensive distances were also evident, one of which may be seen in the central portion of Figure 3. At saturation moisture contents (above 5 weight

FIGURE 2. TRANSVERSE FRACTURE APPEARANCE OF KEVLAR 49/934 COMPOSITE IN DRY CONDITION. 450X.

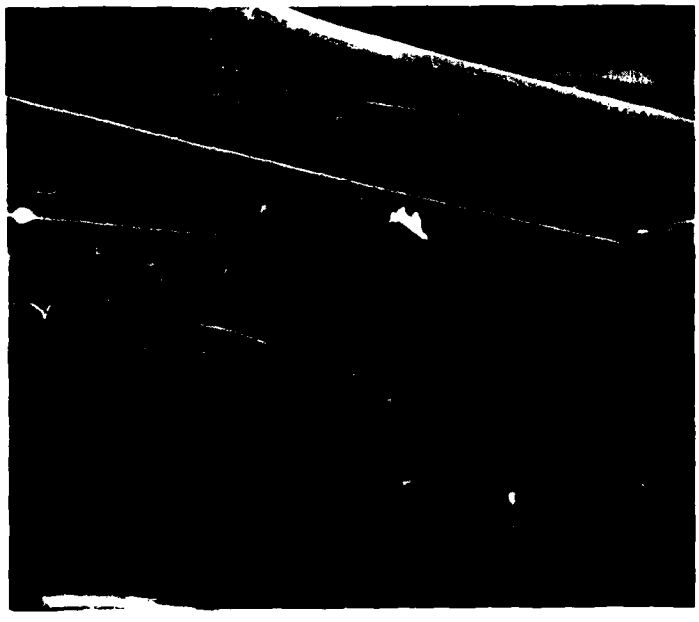

FIGURE 3. TRANSVERSE FRACTURE SURFACE OF KEVLAR 49/934 WITH 3.75% MOISTURE SHOWING BEGINNING OF FILAMENT SPLITTING. 450X.

percent) filaments split longitudinally may be seen on the fracture surface (Figure 4), although bare filaments and resin are also common. A higher magnification view of the texture of a split filament is shown in Figure 5. The area in Figure 5 is a closeup of Figure 4 where some of the outer skin of the filament is still evident.

The failure surfaces with increasing moisture content shown in Figures 2-5 indicate that transverse failure of Kevlar 49/epoxy composites is a complex process involving all the phases of the composite. To arrive at a probable failure mode, features which predominate the surface were identified as well as the appearance of previously unseen features. Failure seems to be controlled by the filament-matrix interface strength

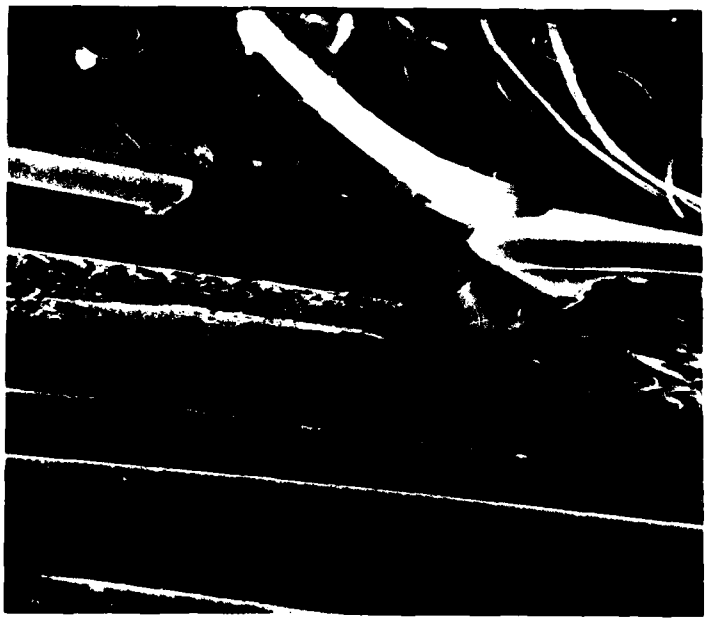

FIGURE 4. TRANSVERSE FRACTURE WITH 5% MOISTURE SHOWING LONGITUDINAL SPLIT IN KEVLAR FILAMENT. 900X.

FIGURE 5. TEXTURE OF LONGITUDINALLY SPLIT FILAMENT SEEN IN FIGURE 4. 4500X.

at low moisture contents, become a mixed interface-matrix mode at medium moisture levels, and progress to a filament splitting mode at higher moisture contents.

Conclusions

This study examined the effect of moisture on the transverse properties of unidirectional Kevlar 49/epoxy composites. Results indicate that moisture effects are substantial at a test temperature of 25°C. Losses of 14 percent in stiffness, 35 percent in strength and 27 percent in elongation were observed compared to the dry condition. The stiffness reduction seems to indicate that the Kevlar 49 filaments become more compliant radially with the introduction of moisture.

Microscopy of the failure surfaces indicates that strength and elongation losses are accompanied by a failure mode change from the interface (dry) to filament splitting at saturation moisture contents. Such effects may be explained by a mechanism of moisture interrupting the interchain hydrogen bonds in the Kevlar filaments.

Acknowledgements

The authors would like to thank Dr. Margaret Roylance and the Army Mechanics and Materials Research Center for their generous support in providing the materials, machining and testing equipment necessary to conduct this study. The insight of Abram King in conducting the electron microscopy is also gratefully acknowledged. This work was also supported by the U.S. Department of Energy through Sandia National Laboratories.

REFERENCES

[1] Environmental Effects on Advanced Composite Materials, ASTM STP 602, American Society for Testing and Materials, 1976.

[2] Advanced Composite Materials - Environmental Effects, ASTM STP 658, American Society for Testing and Materials, 1978.

[3] C.W. Browning, "The Mechanisms of Elevated Temperature Property Losses in High Performance Structural Epoxy

Resin Matrix Materials After Exposures to High Humidity Environments," Poly. Engr. and Sci. 18, 1, January 1978, pp. 16-24.

[4] R.J. Morgan and J.E. O'Neal, "The Durability of Epoxies," Polym.-Plast. Tech. and Engr., 10, 1, 1978, pp. 49-116.

[5] R.E. Allred, "The Effect of Temperature and Moisture Content on the Flexural Response of Kevlar/Epoxy Laminates: Part I. [0/90] Filament Orientation," J. Comp. Mat'ls, 15, March 1981, pp. 100-116; "Part II. [± 45,0/90] Filament Orientation," pp. 117-132.

[6] R.E. Allred, unpublished data.

[7] M.E. Roylance, "The Effect of Moisture on the Properties of an Aramid-Epoxy Composite," Ph.D. Thesis, M.I.T., Cambridge, MA, September, 1980.

[8] R.E. Allred and A.M. Lindrose, "The Room Temperature Moisture Kinetics of Kevlar 49 Fabric/Epoxy Laminates," Composite Materials: Testing and Design, ASTM STP 674, American Society for Testing and Materials, 1979, pp. 313-323.

[9] R.E. Allred, L. Orear and K.D. Boultinghouse, "Void Enhanced Moisture Diffusion in Kevlar/Epoxy Laminates," to be submitted to J. Comp. Mat'ls.

[10] "Kevlar 49 Data Manual," E.I. DuPont de Nemours, Wilmington, De. 1974.

[11] R.E. Allred and F.P. Gerstle, "Effect of Resin Properties on the Transverse Mechanical Behavior of High-Performance Composites," Proc. 30th Rein. Plas. Tech. Conf., Society

Plastics Industry, Washington D.C., February 1975, paper 9-B.

[12] L.L. Clements and R.L. Moore, "Composite Properties of an Aramid Fiber in a Room-Temperature-Curable Epoxy Matrix," SAMPE Quarterly, 9, 1, October 1977, pp. 6-12.

[13] R.E. Allred, H.K. Street and R.J. Martinez, "Improvement of Transverse Composite Strengths: Test Specimen and Materials Development," Proc. 24th Nat'l SAMPE Symp., San Francisco, CA, May 1979, pp. 31-50.

[14] C. Shen and G.S. Springer, "Effects of Moisture and Temperature on the Tensile Strength of Composite Materials," J. Comp. Matl's., 11, January 1977, pp. 2-16.

[15] F.W. Crossman, "Hygrothermal Damage Mechanisms in Graphite Epoxy Composites," Lockheed Missiles and Space Co. Report NASA CR 3189, December 1979.

[16] K.E. Hofer, Jr., D. Larsen and V. Humphreys, "Development of Engineering Data on the Mechanical and Physical Properties of Advanced Composite Materials," Air Force Materials Laboratory Report AFML-TR-74-266, February 1975.

[17] C. Shen and G.S. Springer, "Environmental Effects on the Elastic Moduli of Composite Materials," J. Comp. Mat'ls., 11, July 1977, pp. 250-264.

[18] J.C. Halpin and S. Tsai, "Environmental Factors in Composite Materials Design", Air Force Materials Laboratory Report AFML-TR-67-423, 1969.

[19] H.T. Hahn and R.Y. Kim, "Swelling of Composite Laminates," in Ref. 2, pp. 98-120.

INFLUENCE OF MOISTURE ON COMPRESSIVE FATIGUE OF GRAPHITE/EPOXY COMPOSITES

Donald F. Adams
Composite Materials Research Group
University of Wyoming

Abstract

A joint program with Northrop Corporation was conducted for the Naval Air Systems Command, to determine the combined influence of temperature and moisture on the static compression and compressive fatigue properties of graphite/epoxy laminates. Specimen fabrication and testing was performed by Northrop. Scanning electron microscopy of fracture surfaces, application of micromechanics and laminate analyses, and a detailed correlation of theory and experiment was performed by the University of Wyoming.

Unidirectional, $[\pm 45]$, and $[0_{16}/(\pm 45)_5/90_4]$ laminates of Hercules AS/3501-6 graphite/epoxy were included. The latter laminate, a typical F-18 aircraft configuration, was also modified by dropping off either two 0° plies or two (±45) sets in the test section, to study the influence of these typical types of discontinuities. These composites were analyzed and tested with and without one weight percent moisture absorption, at temperatures ranging from -65°F to 218°F.

The scanning electron microscopy study disclosed the presence of extensive fiber-matrix debonding, longitudinal cracking, ply delaminations, and fiber microbuckling. Relatively few differences were observed between static compression failure modes and compression fatigue failure modes. Typical failure modes were identified and catalogued, and related to analytical predictions of internal stress distributions at the experimentally measured failure levels. The influences of temperature and moisture on both stiffness and strength properties were predicted, and correlated with test results. Several new analytical tools and correlation techniques were developed during this study. The correlations with experimental data indicate that they represent a significant advance in the ability to predict the nonlinear response and strength of actual composites.

INTRODUCTION

A joint study is being conducted by the Composite Materials Research Group at the University of Wyoming and Northrop Corporation, sponsored by the U.S. Naval Air Systems Command. Complete reports of the work of the first two years of this ongoing joint program are contained in References [1,2]. All specimen fabrication and mechanical testing is being performed by Northrop. The test data and failed specimens are then forwarded to the University of Wyoming for detailed analysis. Particular emphasis to

date has been on deriving an adequate understanding of static test results, as a necessary initial step toward the ultimate goal of being able to analyze and predict compression fatigue response. A thorough survey of the literature was conducted initially, primarily to catalogue the fatigue damage and failure modes observed in prior studies.

Although there is a significant amount of fatigue data for composite materials in the literature, most of the data represent tension-tension loadings; and much of the remainder are for tension-compression loadings. The present study represents an attempt to define failure initiation in graphite/epoxy due to compression-compression fatigue. Early works were for glass/epoxy composites rather than graphite/epoxy; Reference [3] represents one such study, and contains a literature survey of compression fatigue up to 1972. Most of this early work was directed toward generating experimental data rather than attempting to develop a fatigue theory, or to study failure mechanisms. Even more recently, the tendency has been to take this same approach. For example, Ryder and Walker [4], in an extensive study sponsored by the Air Force Materials Laboratory through late 1976 to determine the effect of compressive loading on the fatigue lifetime of graphite/epoxy laminates, stated that primary emphasis of the program was on the accumulation of a statistically significant data base; a general model with capability to account for compressive loading was not attempted. Correspondingly, while Reference [4] lists almost 70 references, few are related to compressive fatigue.

Physical rather than phenomenological approaches to understanding compression fatigue appear to have the greatest promise. That is, by observing what is actually physically happening to the composite during the fatigue loading, or by studying the details of the fracture surfaces subsequent to failure, it is anticipated that the causes and mechanisms of failure can be identified. A number of investigators have taken this approach. A good review of work in this area up to 1973 has been presented by Dew-Hughes and Way [5]. While not addressing compression fatigue specifically, they do make a number of interesting observations, and list many references to related studies. They concluded that fatigue damage in composites generally occurs in the following sequence: local debonding of the fiber/matrix interface (crack initiation), the joining up of locally debonded regions (crack propagation along the interface), crack propagation through the matrix, fracture of fibers and final failure. They, of course, recognized occasional variations to this sequence, depending upon type of laminate and loading. Salkind [6], reviewing essentially the same time period as Reference [5], but from a different perspective, nevertheless came to a similar conclusion, viz, the limiting factor in fatigue is the interface. Over 80 references are listed to support his discussion.

Kunz and Beaumont [7] did look specifically at the physical aspects of compression fatigue, for both unidirectional and cross-plied graphite/epoxy composites. Scanning electron microscopy (SEM) of fatigue failures led to their conclusion that axial cracking is the primary fracture mechanism in unidirectional composites, and splitting within and between transverse plies is instrumental in promoting crack extension in cross-plied composites. They stated that prevention of these microfracture processes could be achieved by a high interfacial shear strength. Kunz

and Beaumont also discuss microbuckling of fibers in 0° plies as a failure mode. Local fiber buckling has been observed by many investigators, for both static and fatigue loadings in compression; fiber buckling has been prominent in the present study also, as will be discussed later.

Since relatively little has been achieved to date in identifying the physical mechanisms responsible for compression-compression fatigue, it is logical to look to the corresponding literature for static compression of composites. Orringer [8] presents a good survey of the literature to 1971, as well as an excellent discussion of the mechanisms of compressive failure, both from an analytical and an experimental viewpoint. Such models permit ready visualization of the failure sequence and have been used by a number of investigators. Greszczuk [9], in addition to presenting a good survey of the literature, also references most of his extensive prior work in this area. Greszczuk states that compression failure can occur by transverse tensile failure or fiber-matrix debonding prior to microbuckling, this failure mode resulting from transverse tensile stresses (normal to the direction of the fibers) which are induced in a composite subjected to compression loading in the fiber direction as a result of the differences between the Poisson's ratio of the fibers and the matrix. That is, while the ultimate failure is fiber microbuckling, it is governed by the fiber-matrix bond strength. Note that this is essentially the same conclusion reached in References [5-7] for fatigue loadings, as previously discussed. Greszczuk also states that another factor influencing the load level at which microbuckling failure occurs in a static compression test is the inelastic and nonlinear behavior of the matrix.

For these reasons, viz, the importance of the interface stresses and the influence of matrix nonlinear stress-strain response, the University of Wyoming's Micromechanics analysis [9,10] was ideally suited for use in the present study, and was used extensively.

In addition to the experimental study of macro models, several investigators have sectioned and examined actual composites after static compressive loadings. Of particular significance is the work of Hancox in this area. In Reference [11] he presents a good literature survey, as well as photomicrographs indicating local fiber failures in graphite/epoxy composites, including evidences of fiber microbuckling. It is, in fact, to explore in detail the physical failure phenomena associated with compression-compression fatigue that extensive SEM work is being done in the present study.

SCANNING ELECTRON MICROSCOPY

The scanning electron microscope (SEM) is an excellent tool for use with composite materials because of its good depth of field, wide range of magnification, and built-in photography capability. Specimens are being mounted and examined to provide a thorough representation of the failure modes associated with the various laminates, loading modes, and environmental conditions. Wherever possible, the actual fracture surface is examined directly. If reasonably intact, and not excessively shattered, these yield very useful information. For fracture surfaces perpendicular to the axis of loading, the surface is sometimes too irregular, or too crushed, for satisfactory observation. In these cases, a very light cut is made parallel to the fracture surface, to expose the structure, or a cut is made perpendicular to the fracture surface (parallel to the loading axis), to expose any damage below the surface.

The failures observed to date are of several types, with three general modes predominating. The first is debonding of the fibers from the matrix material within a given ply, as indicated in Figure 1. The second mode is debonding at the ply interfaces, Figure 2. This is especially pronounced in [±45] laminates, because of the high interlaminar shear stresses developed at these interfaces. The third mode of failure represents a type of column instability problem. When the fibers buckle (bend), being relatively brittle materials they break, often shattering into several segments, as seen in Figure 3.

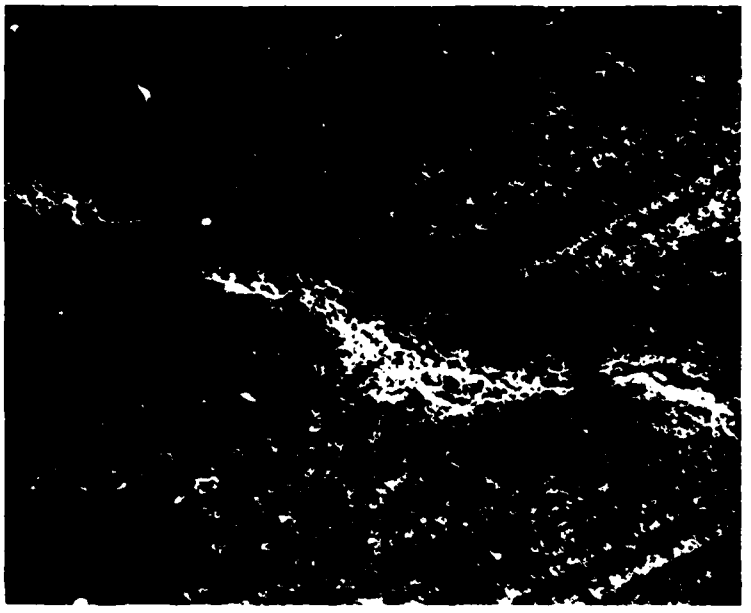

Figure 1
Static Longitudinal Compression of a Unidirectional Composite in a Room Temperature, Wet Condition. Transverse Saw-Cut Plane Close to Fracture Surface. (50X)

It is difficult to determine from the SEM observations which of the several failure modes occur first in any given test. In particular, it is not clear if the graphite

fibers buckled locally causing them to pull away from the matrix, or if the interface debonding occurred first. At this point, however, the latter appears more likely. This is evidenced in the unidirectional specimen tests where large numbers of longitudinal splits occur even when buckling is not observed.

Some general trends can be noted. In the unidirectional longitudinal static compression specimens, extensive microbuckling is observed. This appears to be coupled in many cases to longitudinal splits. In the unidirectional longitudinal compression fatigue specimens, many more longitudinal splits are observed, but microbuckling is far less pronounced. Buckling on a macro scale is observed frequently. However, this is suspected to have been caused by the prior occurrence of the longitudinal splits, which cause a loss of overall stability of the composite.

The [±45] static and fatigue specimens exhibit

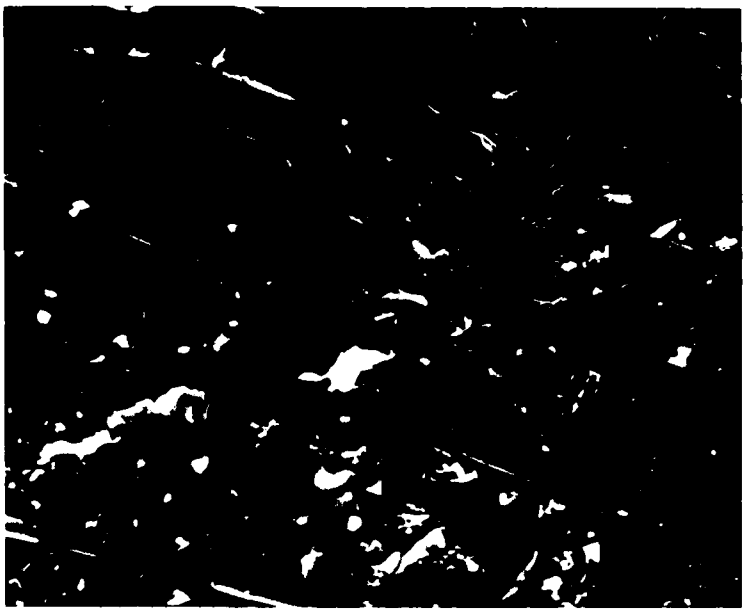

Figure 2
Longitudinal Compressive Fatigue of a $[\pm 45]_{6s}$ Laminate in a Room Temperature, Dry Condition. Stress Applied Along Vertical Axis; Fracture Surface Parallel to Laminate Plane. (300X)

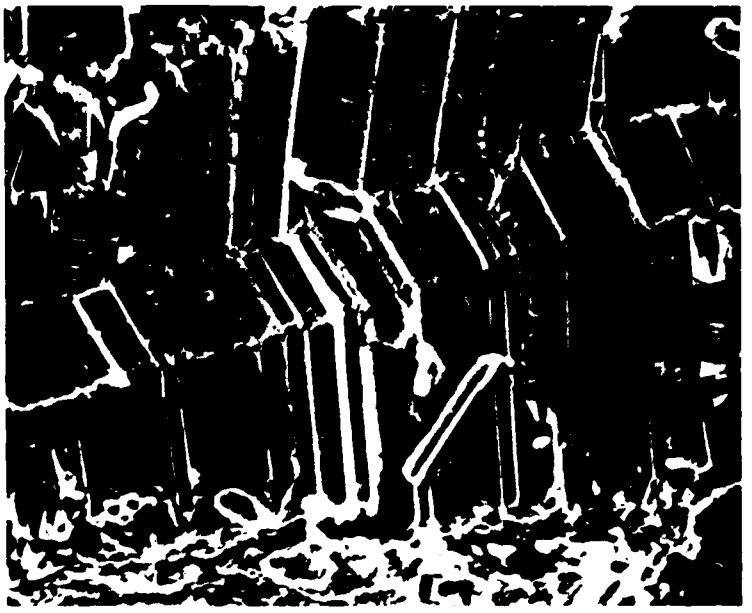

Figure 3
Static Longitudinal Compression of a $[0_{16}/\pm(45)_5/90_4]_c$ Laminate in a Room Temperature, Wet Condition. Load Applied Along Vertical Axis; Delamination Fracture Surface Parallel to a 0° Ply. (200X)

mutually similar modes of failure. This may be due to the dominance of the interlaminar failures induced by the very high interlaminar shear stress in these [±45] laminates. Axial splits within individual plies are infrequent.

The complex laminate, as might be expected, exhibits most of the observed modes of failure. However, delaminations between plies are observed more frequently than any other failure mode, and axial splits within individual plies are non-existent. The presence of the 90° plies, not present in any of the other laminates, may influence this response.

MICROMECHANICS ANALYSIS

Both the literature survey and the subsequent SEM observations indicated that the state of stress in the matrix material surrounding individual fibers, and in particular the normal and shear stresses at the fiber-matrix interface, may have a dominant influence on the response of even a complex laminate when subjected to compression. As the literature survey clearly indicated, static compression of composite materials is not yet adequately understood, and much less is known about compressive fatigue. Thus, the first step is to understand static compression. The University of Wyoming's Micromechanics analysis provides an excellent tool for this purpose since it contains many advanced features not available in most other analyses. These are described in detail in References [9,10].

Since the Micromechanics analysis predicts the complete composite response of a unidirectional ply, and the local stress state around an individual fiber in any laminate, it is most informative to analyze the response of the unidirectional laminate. This is because although the local stresses are not measured experimentally, the composite stiffness and strength properties are. Thus, direct comparisons can be made with the unidirectional composite data, and the strength of these composites can be related to the predicted internal stress states. In the present study, where compressive loadings are of primary concern, the fiber-matrix interface stresses are of particular interest. As noted in the literature survey and in the discussion of SEM observations, debonding appears to be a possible cause of compressive failure.

The unidirectional composite specimens subjected to static loadings were in one of two preconditioning states, viz, dry or wet, and tested at either room temperature or 103°C (218°F), resulting in four different sets of conditions. Both longitudinal and transverse tests were conducted in compression in all cases. In addition, static tensile tests were also conducted under room temperature dry conditions. All ten cases were modeled using the Micromechanics computer program. These results are summarized in Tables 1 and 2. As can be seen, the predicted stiffness values, i.e., modulus and Poisson's ratio, are in reasonable agreement with the experimental averages.

An important contribution of the Micromechanics analysis is the prediction of the variations of the internal stresses with various environmental and loading conditions. The ultimate success of analytical

methods of predicting composite failure will depend upon the development of physical models of the failure process, as discussed previously.

Table 1: Axial Loading - Summary of Micromechanics Predictions Versus Experimental Data

Test Series	Specimen Condition	Axial Elastic Modulus E_{11}, GPa		Major Poisson's Ratio ν_{12}	
		Theory	Experiment	Theory	Experiment
Tension					
Quality Control	RTD	140	130	0.248	0.281
Compression					
Celanese	RTD	140	110	0.248	0.344
Preliminary Celanese	RTD		113		--
Quality Control	RTD		119		--
Celanese	RTW	140	111	0.247	0.335
Celanese	ETD	140	116	0.247	0.354
Celanese	ETW	139	114	0.247	0.327

Table 2: Transverse Loading - Summary of Micromechanics Predictions Versus Experimental Data

Test Series	Specimen Condition	Transverse Elastic Modulus E_{22}, GPa		Minor Poisson's Ratio ν_{21}	
		Theory	Experiment	Theory	Experiment
Tension					
Quality Control	RTD	9.3	10.1	0.016	
Material Acceptance	RTD		9.5		--
Compression					
Celanese	RTD	9.3	11.7	0.024	--
Quality Control	RTD		10.0		--
Celanese	RTW	9.2	8.8	0.016	0.013
Celanese	ETD	8.6	11.1	0.015	0.031
Celanese	ETW	8.1	14.7	0.014	0.076

The present Micromechanics analysis is such an approach. The ultimate goal is to be able to predict fatigue life. As previously stated, it is first necessary to be able to predict the static strength of a composite material adequately. Studies such as the present one are contributing much to the achievement of this first goal. The detailed presentations of References [1,2] indicate the extent to which this has been attained to date.

CONCLUSIONS

The present study represents a very thorough and rigorous test of the University of Wyoming's Micromechanics analysis. The analytical predictions of stiffness properties have been found to be quite accurate. Considerable insight is also being provided as to why certain failure modes observed in the SEM investigation occur. Although more work needs to be done in incorporating an improved failure criterion, the predicted composite ultimate stresses do indicate general agreement with what is observed experimentally. In those cases where there is a large discrepancy, the reasons are explainable.

In certain isolated cases, the predicted trends in stiffness properties with increasingly severe environmental conditions do not correspond to what is measured experimentally. For example, the transverse elastic modulus of the unidirectional laminate is predicted to decrease slightly (Table 2), as would be expected since this is a matrix-dominated property and the modulus of the matrix is shown experimentally to decrease. However, the experimentally measured composite modulus increased with temperature. A possible conclusion is that this points to the difficulty in experimentally determining this particular property accurately under hygrothermal conditions using present techniques. No conclusions can be made in terms of the minor Poisson's ratio (Table 2). This obviously is a difficult property to measure because of its small magnitude for these composites.

The presence of normal scatter in the experimental data is suggested in the axial elastic modulus results of Table 2. Micromechanics theory predicts a very slight decrease in this property with increasingly severe environmental conditions, this being a fiber-dominated property. The experimental data indicate no clear trend, the scatter in data being greater than the actual range of the expected variation.

These types of comparisons form the basis for the conclusion that an analytical prediction technique which is based upon fundamental physical principles, as the present Micromechanics analysis is, can be very useful in establishing trends in properties which are difficult to measure accurately.

One further conclusion which is being demonstrated in this study is that an analysis, once it has been demonstrated to be of acceptable accuracy, can be used to predict properties under other conditions as well, with only spot experimental checks being made to maintain confidence. Correspondingly, the analysis predicts all of the properties directly, while a significant number of different tests need to be performed to do the same experimentally. For example, the composite coefficients of thermal expansion and moisture expansion have not been measured in the present study; yet they are automatically predicted.

With continued refinement, the Micromechanics analysis is expected to become a very powerful tool in predicting unidirectional ply performance, including the occurrence of local failure mechanisms such as

matrix microcracking, fiber-matrix interface debonding, longitudinal splitting, and fiber microbuckling. Already it has been demonstrated to be a very simple and reliable way of estimating those ply properties which have not been measured for a particular composite, or of determining the influence of process variations and environmental conditions without resorting to an extensive experimental program.

ACKNOWLEDGMENTS

This study was sponsored by the U.S. Naval Air Systems Command, under the direction of Mr. Maxwell W. Stander. A parallel experimental study was led by Mr. Glenn Grimes of Northrop Corporation. The author wishes to acknowledge the considerable cooperation by both Mr. Stander and Mr. Grimes, and the valuable assistance of Mr. Doug Cairns, Graduate Student in Mechanical Engineering. Computer runs were performed by graduate students Mohamed Monib and Brent Schaffer.

REFERENCES

1. Grimes, G.C. and Adams, D.F.,"Investigation of Compression Fatigue Properties of Advanced Composites", Final Report, Naval Air Systems Command Contracts N00019-77-0518 and -0519, October 1979.

2. Grimes, G.C., Adams, D.F., and Dusablon, E.G., "The Effects of Discontinuities on Compression Fatigue Properties of Advanced Composites," Final Report, Naval Air Systems Command Contracts N00019-79-C-0275 and -0276, October 1980.

3. Sedor, G. and Watterson, R.K., "Low Cycle Compression Fatigue Failure of E Glass-Epoxy Composites," Report No. AFOSR TR 72-0322, Air Force Office of Scientific Research, Washington, D.C., March 1972.

4. Ryder, J.T. and Walker, E.K., "Ascertainment of the Effect of Compression Loading on the Fatigue Lifetime of Graphite Epoxy Laminates for Structural Applications," Report No. AFML-TR-76-241, Air Force Materials Laboratory, Dayton, Ohio, December 1976.

5. Dew-Hughes, D. and Way, J.L., "Fatigue of Fibre-Reinforced Plastics: a Review," Composites, Vol. 4, No. 4, July 1973, pp. 167-173.

6. Salkind, M.J., "Fatigue of Composites," Composite Materials: Testing and Design (Second Conference), ASTM STP 497, American Society for Testing and Materials, Philadelphia, Pennsylvania, 1972, pp. 143-169.

7. Kunz, S.C. and Beaumont, P.W.R., "Microcrack Growth in Graphite Fiber-Epoxy Resin Systems During Compressive Fatigue," ASTM STP 569, American Society for Testing and Materials, Philadelphia, Pennsylvania, 1975, pp. 71-91.

8. Orringer, O., "Compressive Behavior of Fiber Composites," Report No. ASRL-TR-162-1, Aeroelastic and Structures Research Laboratory, Massachusetts Institute of Technology, October 1971.

9. Miller, A.K. and Adams, D.F., "Micromechanical Aspects of the Environmental Behavior of Composite Materials," Report No. UWME-DR-70-11111, Mechanical Engineering Department, University of Wyoming, January 1977.

10. Miller, A.K. and Adams, D.F., "Inelastic Finite Element Analysis of a Homogeneous Medium Exhibiting Temperature and Moisture Dependent Material Properties," Fibre Science and Technology, 1980.

11. Hancox, N.L., "The Compression Strength of Unidirectional Carbon Fibre Reinforced Plastic," J. of Materials Science, Vol. 10, 1975, pp. 235-242.

DETERMINATION OF MOISTURE IN FIBER REINFORCED COMPOSITES USING PULSED NMR*

George A. Matzkanin
Southwest Research Institute
San Antonio, Texas

ABSTRACT

Investigations were conducted of nuclear magnetic resonance (NMR) signals from hydrogen atoms in two organic matrix composite systems subjected to environmental conditioning at 51.6°C (125°F) and 95% relative humidity. The composite systems were 8 ply, ± 45° laminates fabricated from SP 250 resin/S2 glass fiber and Reliabond 9350 resin/Kevlar 49 fiber. Free induction decay NMR signals from the composite specimens consisted of a large amplitude, fast decaying component associated with hydrogen in rigid polymer molecules and a lower amplitude, slower decaying component associated with hydrogen in the mobile absorbed moisture molecules. The absorbed moisture NMR signals consisted of distinct multiple components which were attributed to moisture in various states of molecular binding. Particularly complex free induction decay signals were observed from Kevlar composite as well as from Kevlar fiber. Good correlation was obtained between the NMR signal amplitude and the dry weight moisture percentage for both composite systems. Destructive tensile tests were performed on ten oven-dried specimens and ten moisture-conditioned specimens at levels of 4.6% and 1.3% dry weight moisture for the Kevlar and glass composites, respectively. Reductions in ultimate tensile strength due to moisture absorption were 14% for the Kevlar composite and 4.3% for the glass composite.

I. INTRODUCTION

The objective of this work was to investigate the feasibility of using pulsed nuclear magnetic resonance (NMR) to nondestructively determine the amount of moisture in organic matrix composites and the extent of moisture induced mechanical degradation. NMR is a rapid, spectroscopic approach involving the resonant absorption of electromagnet energy by nuclei with magnetic moments.[1] The NMR method is well established and has been used extensively as an analytical laboratory tool in physics and chemistry. One of the important features of NMR is that not only can the amount of moisture be determined but the method can also distinguish between water in different binding states, thus providing information on the molecular structure of the material. In the experiments performed on composites, pulsed NMR free induction decay (FID) signals were analyzed to determine the feasibility of associating certain signal characteristics with moisture absorbed in different physical states within the specimens.

* Work supported by the U.S. Army Materials and Mechanics Research Center under Contract DLA 900-79-C-1266.

II. EXPERIMENTAL PROCEDURE

A. Specimens

The composite systems investigated were eight ply, ± 45° laminates fabricated from SP-250 Resin/S2 glass fiber and Reliabond 9350 Resin/Kevlar 49 fiber. Twenty-two specimen coupons, 20.3 cm (8 in.) by 2.54 cm (1 in.), were cut from the laminate panels. Fiber volumes and densities were determined as described in ASTM D792 "Specific Gravity and Density of Plastics by Displacement", while void volume for the glass composite was determined by the method described in ASTM D2584 "Ignition and Loss of Cured Reinforced Resin". Void volume could not be determined for the Kevlar composite due to disintegration of the Kevlar fiber during the ignition process. The material parameters of the two composite systems are tabulated in Table I.

Prior to moisture conditioning, all 44 composite specimens were oven-dried at a temperature of 55°C (131°F) in a vacuum oven to constant dry weight. Upon completion of oven drying, ten each of the two types of specimens were destructively tested to determine the dry mechanical properties. Of the remaining oven-dried specimens, two each of the glass composites and Kevlar composites were placed in a dessicator to be kept in a dried condition while the other twenty specimens were placed in an environmental chamber for moisture conditioning. The specimens in the dessicator were utilized throughout the remainder of the study as baseline specimens to periodically check the calibration of the NMR instrumentation system.

Moisture conditioning was accomplished under constant-humidity conditions using a commercial controlled environmental chamber (Tenny Engineering Inc., Union, New Jersey). With this chamber, heat is supplied by resistance heating elements and moisture is supplied by injecting steam into the cabinet. During environmental exposure, humidity was measured and controlled from wet and dry bulb temperature measurements. Environmental conditioning was performed at a temperature of 51.6°C (125°F) and a relative

TABLE I

Material Parameters of Composite Specimens

	Kevlar Composite	Glass Composite
Resin Type	Reliabond 9350	SP 250
Fiber Type	Kevlar 49	S2 Glass
Resin Density	1.20 g/cm^3	1.21 g/cm^3
Fiber Density	1.45 g/cm^3	2.49 g/cm^3
Composite Density	1.33 g/cm^3	1.80 g/cm^3
Fiber Volume	47.9%	47.5%
Void Volume	---	1.26%

humidity of 95%. Moisture absorption was determined by periodically measuring the weight gain for three to six specimens of each type. A typical measurement resulted in at most a ten minute period during which the specimens were exposed to room temperature conditions. The particular specimens removed for weighing were varied so that the same specimens were not removed from the chamber each time. During the first two weeks of conditioning, specimens were weighed daily with the interval increasing to weekly after this initial period.

B. NMR Measurements

Hydrogen NMR measurements were performed on the composite specimens utilizing a 30 MHz pulsed NMR spectrometer. A schematic diagram of the experimental arrangement is shown in Figure 1. The experimental procedure involved placing a specimen into the radiofrequency (RF) coil which was located within the gap of an electromagnet. The RF coil utilized for the measurements on composites was approximately 3.2 cm (1.25 in.) long and had an inner diameter slightly greater than the width of the specimens. The coil mounting assembly was constructed of hydrogen-free materials and measurements verified that no hydrogen NMR signal was observed from the empty coil.

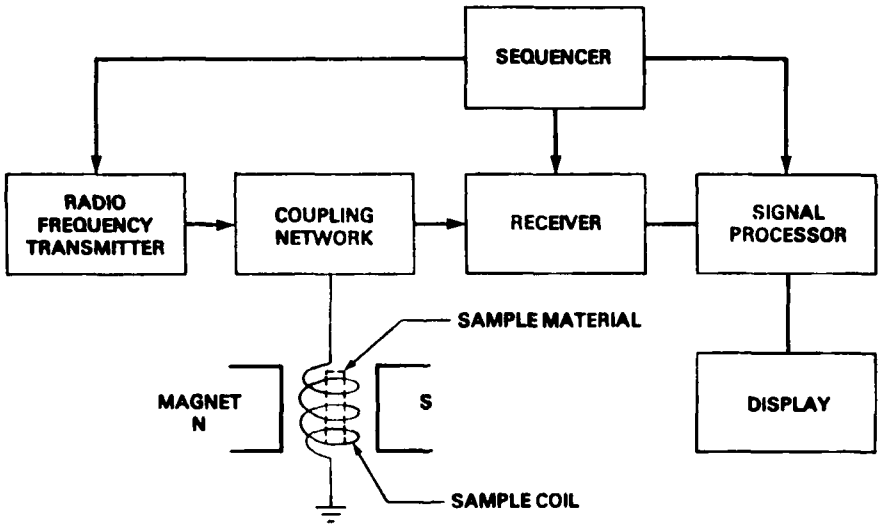

FIGURE 1. BLOCK DIAGRAM OF PULSED NMR SYSTEM

During the moisture conditioning period, NMR measurements were performed on four specimens of each type (glass and Kevlar) at several levels of moisture absorption. For these measurements, the specimens were removed from the environmental chamber and placed into the RF coil of the NMR system. The composite specimens were weighed both before and after the NMR measurements so that any change in moisture level would be noted. The average time a specimen was out of the environmental chamber during NMR measurements was approximately 30 minutes with the change in dry weight moisture percentage during this time typically being less than 0.05% for the Kevlar specimens and less than 0.01% for the glass specimens.

The principle NMR signal parameter measured was the free induction decay following a 90° RF pulse.[1] This measurement allows a determination of the nuclear spin-spin relaxation time T_2 which provides information on molecular coupling and nuclei in different chemical states. To improve the signal-to-noise ratio of the measurements, signal averaging was utilized. This involved repetitive sampling of the NMR signal and time averaging to reduce the noise level relative to the signal amplitude. The time averaged NMR signals were displayed on an XY recorder for later analysis.

Upon completion of moisture conditioning and after performing final NMR measurements, the twenty environmentally conditioned specimens were subjected to destructive mechanical testing. Mechanical testing consisted of determining tensile strength and modulus using a 222.4 kN (50 kip) hydraulic test machine with a head displacement rate of 0.13 cm (0.05 in.) per second. Strain was measured by means of a strain gage extensometer having a nominal 5.1 cm (2 in.) gage length. The stress strain curve for each specimen was recorded using an XY recorder and the modulus and ultimate strength determined from these data. These same mechanical testing procedures were used on the oven-dried specimens described earlier.

III. RESULTS

The moisture absorption curves are shown in Figures 2 and 3 for the Kevlar and glass fiber composite systems, respectively. The data are shown plotted in the usual format of dry weight moisture percentage vs time.[2] After a little over four months of environmental exposure, the Kevlar composite specimens reached a moisture level of 4.6% while the glass composite specimens reached a level of 1.3%. All of the moisture levels at which NMR measurements were made are noted on the moisture absorption curves. After three months of moisture

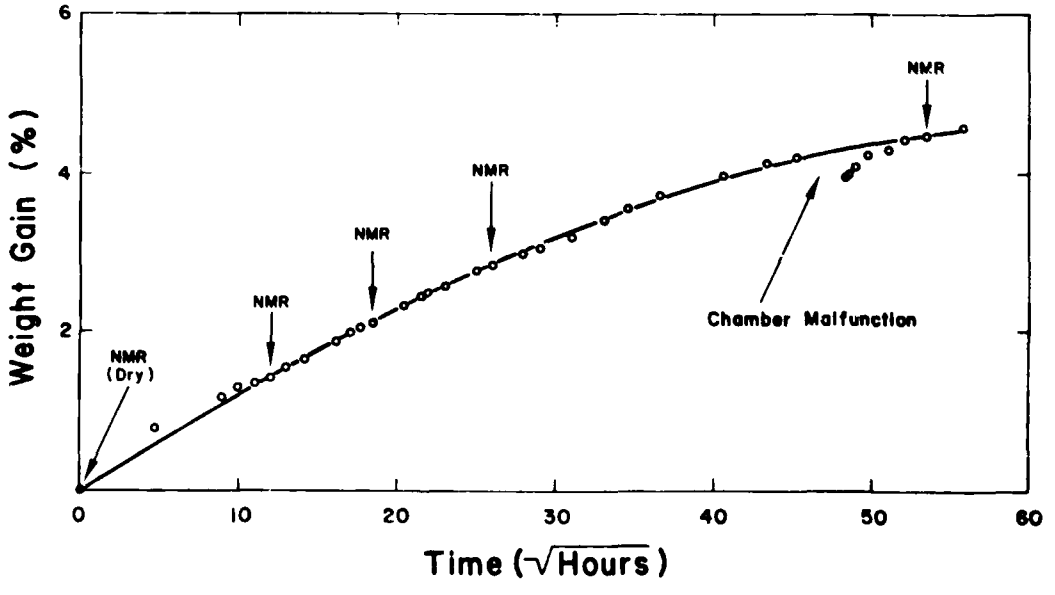

FIGURE 2. MOISTURE ABSORPTION FOR KEVLAR COMPOSITE

conditioning, the environmental chamber malfunctioned resulting in a loss of humidity for a period of approximately 24 hrs. During the time that the chamber was undergoing repair, the composite specimens were put into sealed containers and placed in an oven at a temperature of 51.6°C (125°F) in order to simulate conditions in the environmental chamber. As seen in Figures 2 and 3, the chamber malfunction resulted in a loss in moisture of approximately 0.1% dry weight moisture for both the Kevlar and glass composite specimens. After the environmental chamber was repaired, moisture reabsorption occurred quickly so that by the time final NMR and mechanical measurements were made, the moisture levels in the specimens coincided with the original moisture absorption curves.

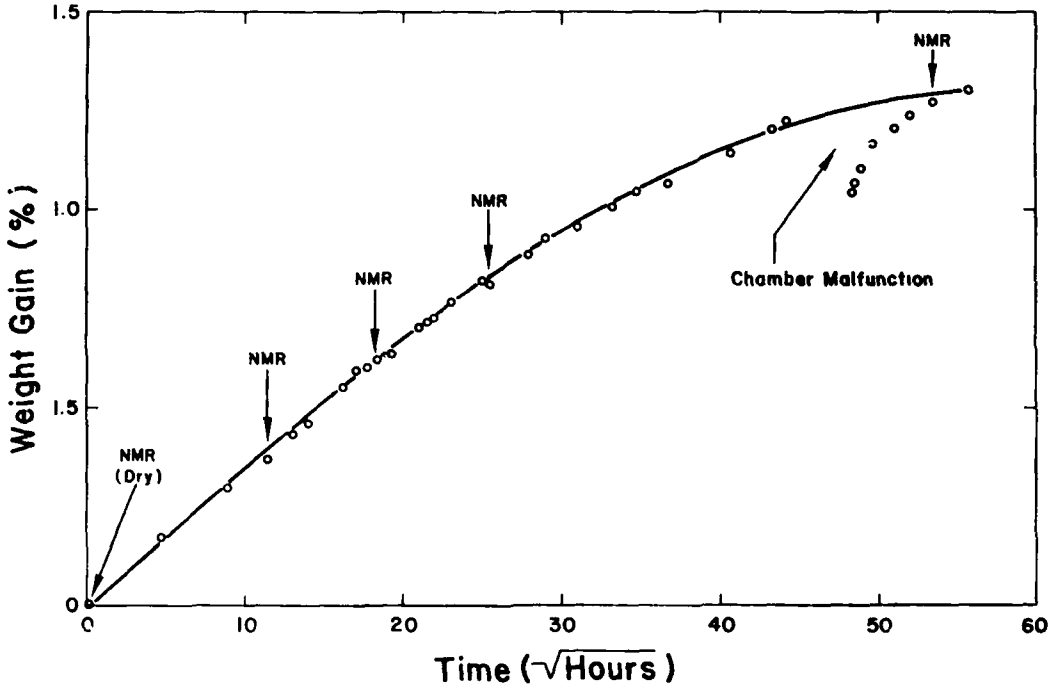

FIGURE 3. MOISTURE ABSORPTION FOR GLASS COMPOSITE

Typical NMR free induction decay signals from moisture conditioned Kevlar and glass composite specimens are shown in the oscilloscope photographs in Figures 4 and 5. The NMR free induction decay signals from the composite specimens were generally characterized by a large amplitude, fast decaying component (identified as "solid component") associated with the chemically bound structural hydrogen in the composites and a lower amplitude, slower decaying component associated with the absorbed moisture. Identification of the absorbed moisture component in the free induction decay was verified by the absence of this component for the oven-dried specimens as shown for a Kevlar specimen in Figure 6.

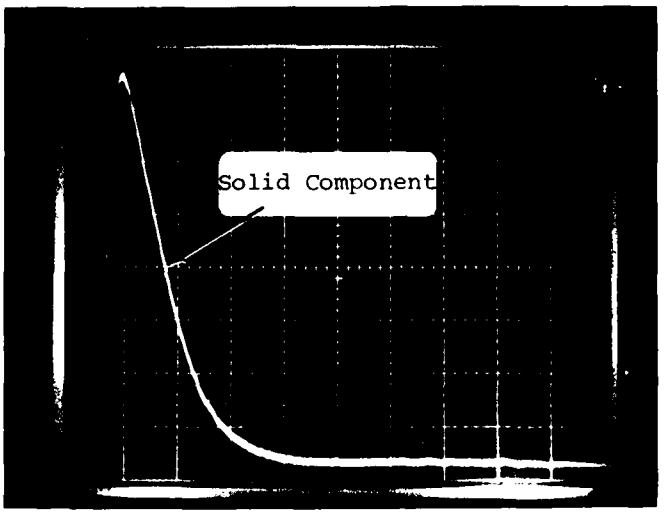

(a)

V - 0.2 V/div

H - 10 μs/div

Atten: - 28 DB

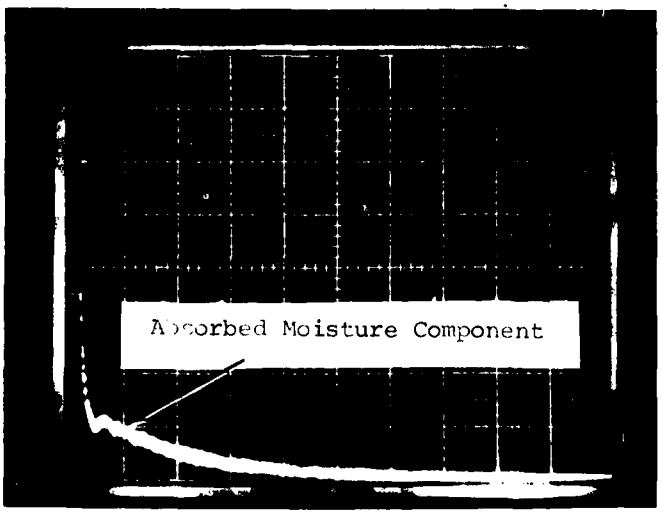

(b)

V - 0.05 V/div

H - 100 μs/div

Atten: - 28 DB

FIGURE 4. FREE INDUCTION DECAYS FROM KEVLAR FIBER COMPOSITE WITH 4.6% MOISTURE

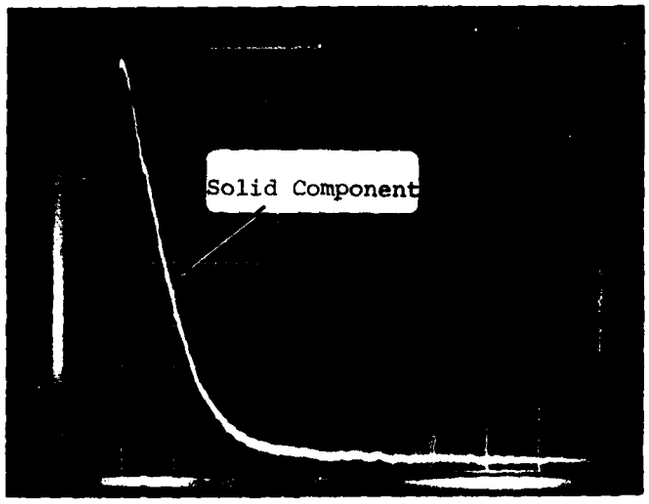

(a)

V - 0.1 V/div

H - 10 μs/div

Atten: - 28 DB

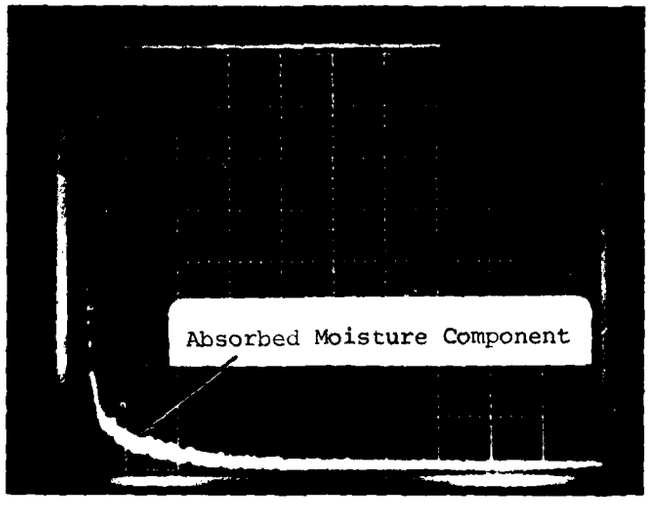

(b)

V - 0.02 V/div

H - 100 μs/div

Atten: - 28 DB

FIGURE 5. FREE INDUCTION DECAYS FROM GLASS FIBER COMPOSITE WITH 1.27% MOISTURE

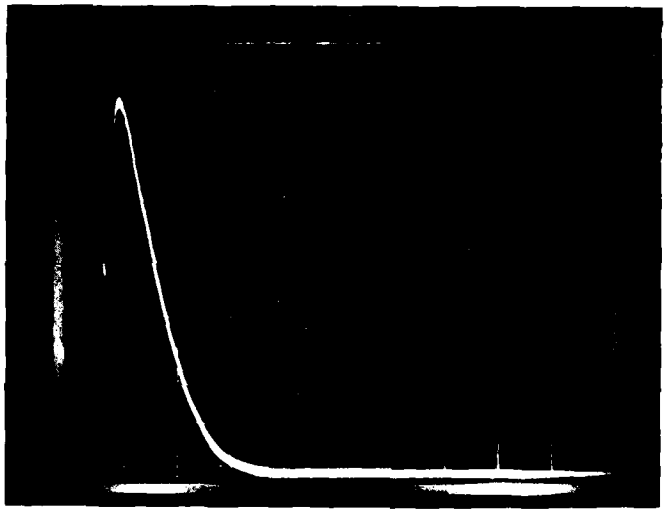

(a)

V - 0.2 V/div

H - 10 μs/div

Atten: - 28 DB

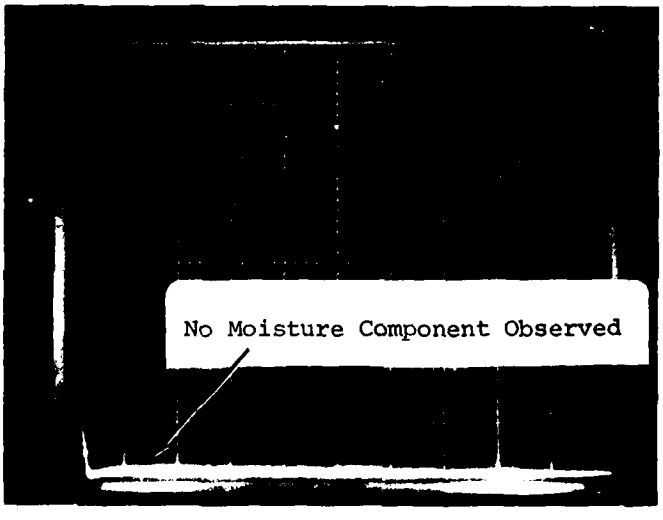

(b)

V - 0.05 V/div

H - 100 μs/div

Atten: - 28 DB

FIGURE 6. FREE INDUCTION DECAYS FROM OVEN-DRIED KEVLAR FIBER COMPOSITE

For quantitative analysis, the time averaged NMR free induction decay signals were measured from the XY recordings and plotted on semi-log graph paper. For an exponential signal decay, the semi-log plot should be linear with a slope which gives the relaxation time T_2. This result for a Kevlar composite specimen with 1.36% moisture is shown in Figure 7. The semi-log plot clearly shows a fast decaying component with a relaxation time of 6 μs and several slowly decaying components associated with the absorbed moisture; for the oven-dried specimens (both Kevlar and glass) only a single relaxation time T_2 of 6 μs was obtained. This short decay time is indicative of tight molecular coupling and is representative of the decay times observed from solid materials.[3] For the composites, this component of the free induction decay is associated with the chemically bound hydrogen atoms of the resin matrix in the case of the glass composite, and of both the matrix and organic Kevlar fiber in the case of the Kevlar composite. (Note: The relaxation time for the solid component should be obtained from a semi-log plot of t^2 since the free induction decay for solids is usually characterized by a Gaussian function. However, for this study which was primarily directed at the absorbed moisture components, a log-linear plot was used to obtain an estimate of T_2 for the solid component). As is seen in Figure 7, the absorbed moisture free induction decay component appears to be resolvable into several relaxation times which may be associated with different states of moisture absorption within the

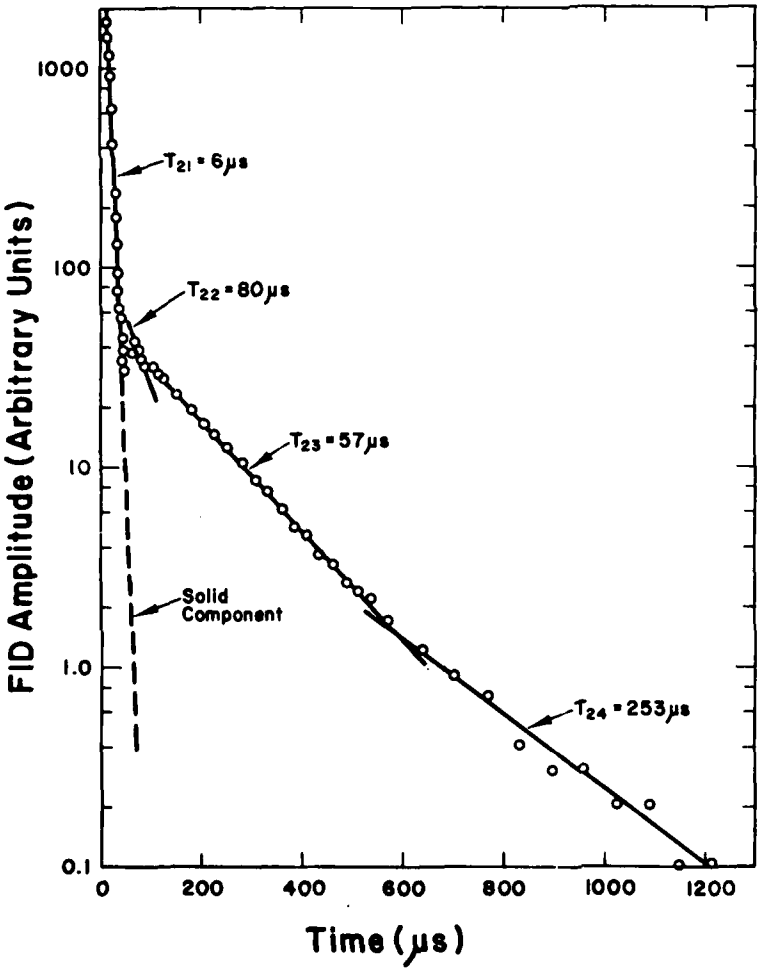

FIGURE 7. DETAILS OF FREE INDUCTION DECAY FOR KEVLAR COMPOSITE (MOISTURE = 1.36%)

composite. Although the linear segments seem to be reasonably well defined on the semi-log plot, the T_2 time constants associated with the segments only differ by approximately a factor of 3. Further work is necessary to verify the resolution of the absorbed moisture contribution to the free induction decay into distinct components. It is interesting to note that in this analysis, three components were distinguished for the absorbed moisture in the Kevlar composite whereas only two components could be distinguished for the case of the glass composite as shown in Figure 8. Since the Kevlar fiber contains hydrogen, it is not unreasonable to associate the extra component in the case of the Kevlar composite with moisture absorbed into the Kevlar fiber.

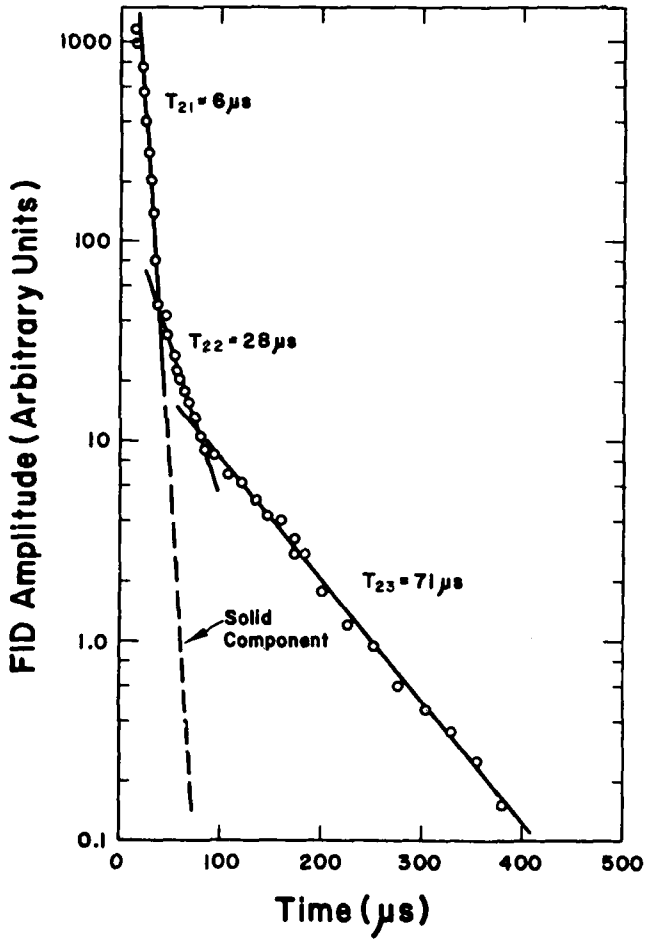

FIGURE 8. DETAILS OF FREE INDUCTION DECAY FOR GLASS COMPOSITE (MOISTURE = 0.17%)

In Figures 9 and 10 are shown the absorbed moisture components of the free induction decays for the various moisture levels investigated for both the Kevlar and glass fiber composites. These plots represent averages of the NMR data obtained from all of the specimens measured at the various moisture levels investigated. For clarity, the initial part of the free induction decay with the 6 μs time constant associated with the tightly bound hydrogen is not shown

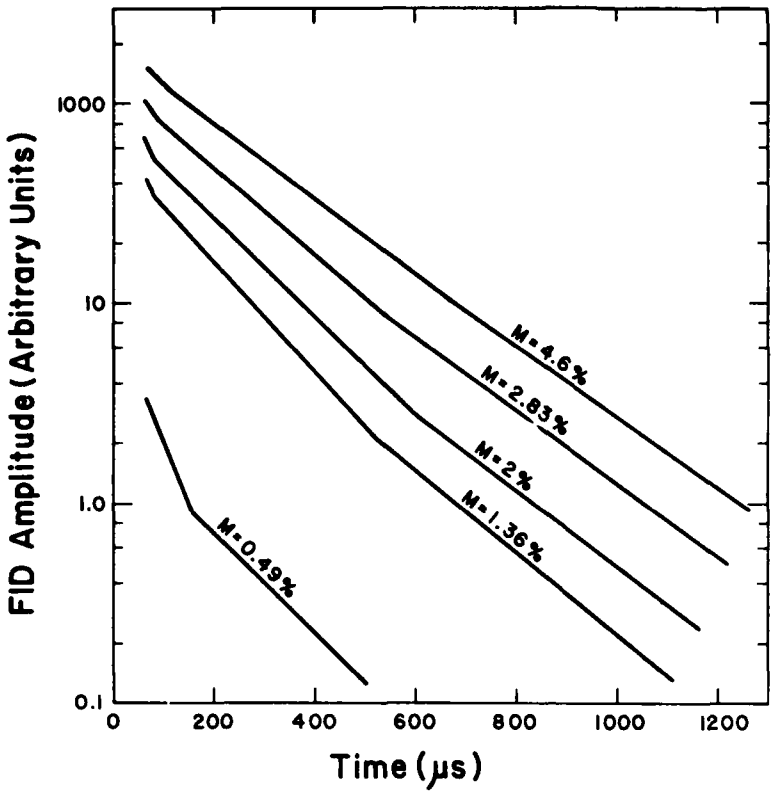

FIGURE 9. KEVLAR COMPOSITE FREE INDUCTION DECAYS FOR VARIOUS MOISTURE LEVELS

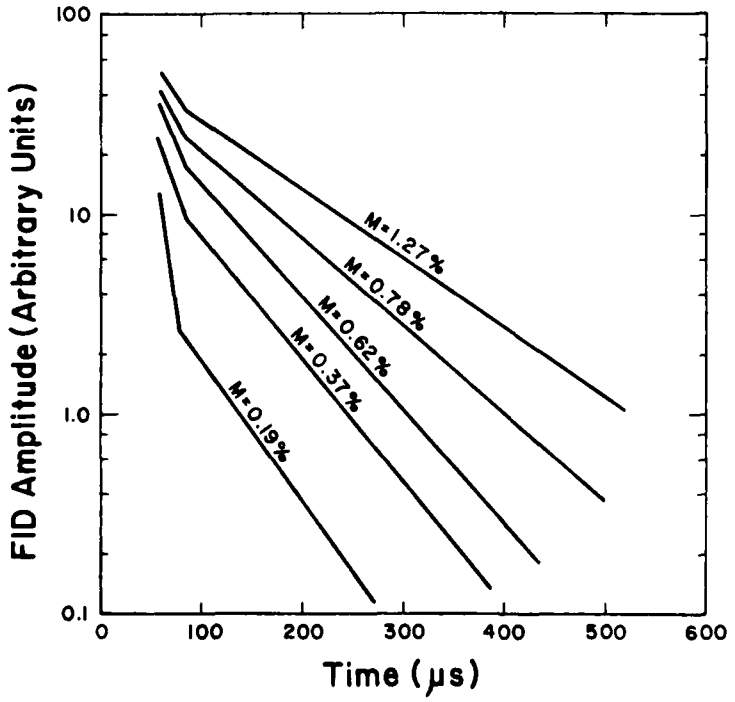

FIGURE 10. GLASS COMPOSITE FREE INDUCTION DECAYS FOR VARIOUS MOISTURE LEVELS

in these figures and the data points are omitted; only the linear segments of the free induction decays beyond approximately 50 μs are presented. The lowest moisture level data shown in these figures (0.49% for Kevlar and 0.19% for glass) were obtained from the as-fabricated composite, that is, prior to oven drying and moisture conditioning. These results illustrate the sensitivity of the NMR method since even at these low moisture levels, NMR moisture signals were easily measured. To explore the capabilities of the NMR method to provide a quantitative measure of the amount of moisture in the composites, the free induction decay signal amplitude at 200 μs was plotted vs percentage moisture. These results are shown in Figures 11 and 12. At low signal levels, this relationship is nonlinear due to nonlinearities in the NMR spectrometer diode detectors. However, above approximately 0.5% moisture, a linear relationship is observed for both the Kevlar and glass composites.

Examination of Figures 9 and 10 shows that in addition to the signal amplitude, the spin-spin relaxation times undergo a variation with moisture level. These results are tabulated in Table II. As the moisture level increases, the time constants also increase indicating that the added moisture is less restricted in motion than is the case at low moisture levels. Also, the distinction between time constants for the separate moisture components becomes less pronounced as additional moisture is absorbed into the composite systems. It should be pointed out that the spin-spin relaxation times measured for the absorbed moisture in the composites is orders of magnitude shorter than the relaxation time for pure water which is on the order of several seconds.[4]

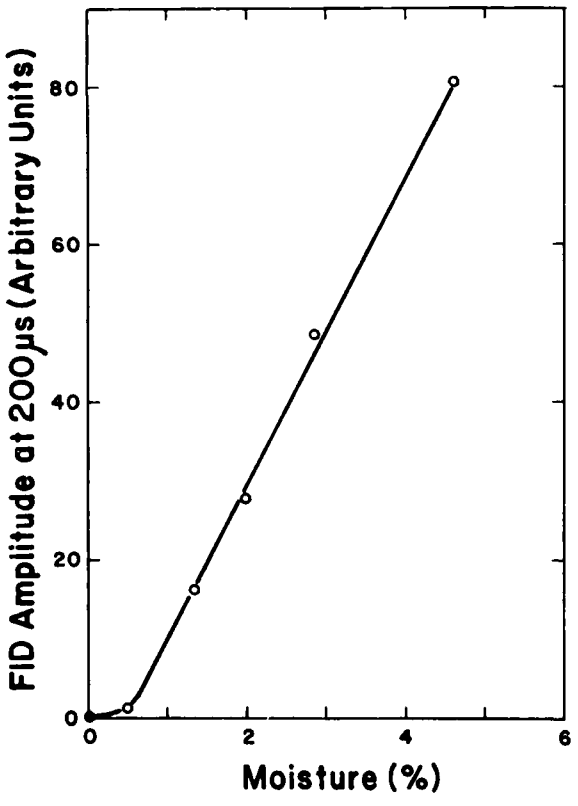

FIGURE 11. FREE INDUCTION DECAY VS MOISTURE FOR KEVLAR COMPOSITE

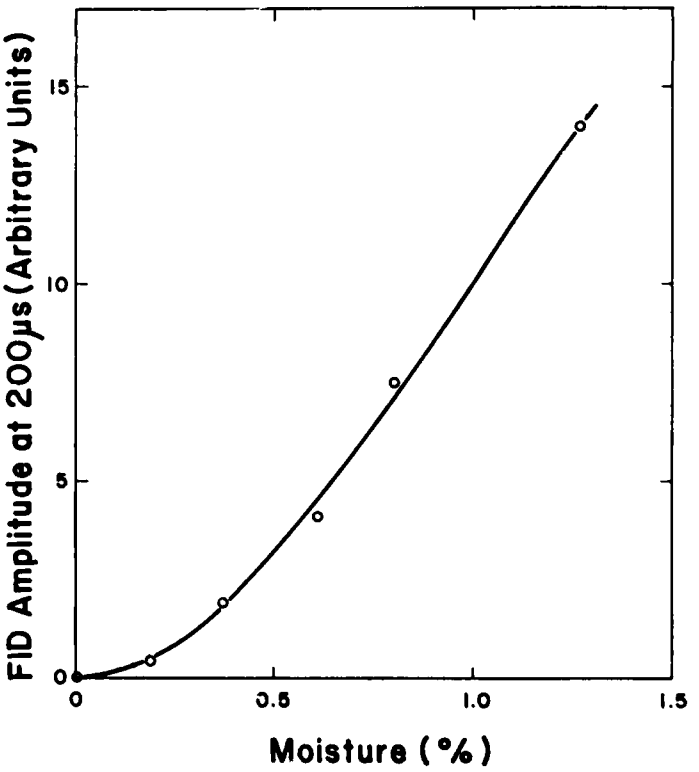

FIGURE 12. FREE INDUCTION DECAY VS MOISTURE FOR GLASS COMPOSITE

TABLE II

SPIN-SPIN RELAXATION TIMES FOR MOISTURE IN KEVLAR AND GLASS COMPOSITE

Moisture(%)	Relaxation Times (μs) T_{22}	T_{23}	T_{24}
	Kevlar Composite		
0.49	70	175	---
1.36	75	157	210
2.00	82	175	228
2.83	113	200	235
4.60	178	230	245
	Glass Composite		
0.19	13	62	---
0.37	33	70	---
0.62	35	76	---
0.78	45	99	---
1.27	54	125	---

In addition to measurements on the composite specimens, a few NMR measurements were also performed on the S2 glass and Kevlar 49 fibers. As expected, no hydrogen NMR signals were observable from the S2 glass fiber, however, a strong NMR signal was observed from the Kevlar 49 fiber which was comparable in magnitude and character to that observed from the Kevlar composite. An example of the free induction decay from less than 1 gram of Kevlar 49 fiber in the as-received condition is shown in Figure 13a. As in the case of the composite, the Kevlar free induction decay is characterized by a fast decaying initial component with a time constant of approximately 6 μs and an absorbed moisture component beginning at approximately 60 μs. Results for the Kevlar fiber after an environmental exposure of 29 hrs. at 51.6°C (125°F) and 95% relative humidity are shown in Figure 13b. The large increase in the moisture component due to the absorbed moisture is readily seen (Note the change in attenuator setting from Figure 13a).

Interesting results were obtained from one of the fractured moisture conditioned glass composite specimens after destructive testing. NMR signals obtained from the fractured specimen are shown in Figure 14. As seen in Figure 14a and 14b, a strong absorbed moisture component was observed since the

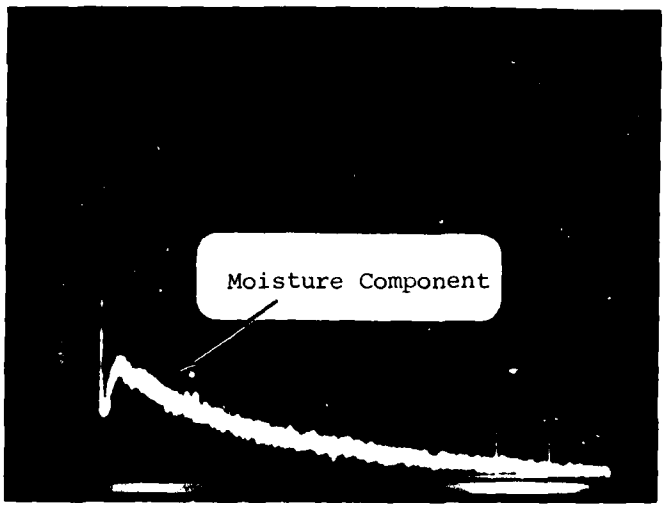

V - 0.2 V/div

H - 100 μs/div

Atten: - 16 DB

(a) Before Exposure to Environmental Chamber
(Weight = 0.088 g; moisture = 3%)

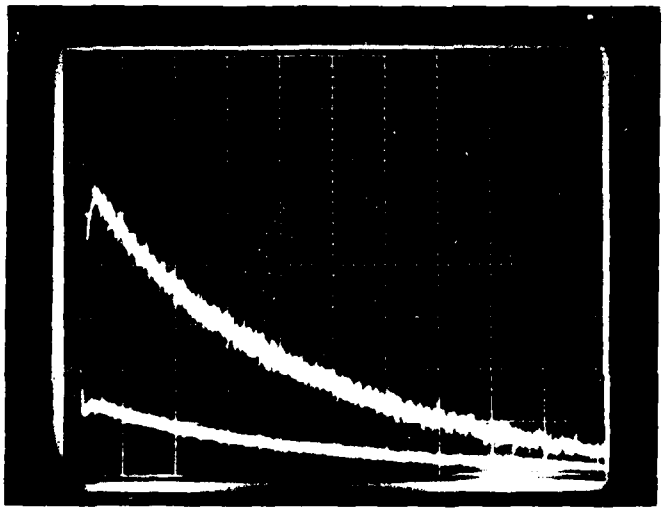

V (upper) - 0.05 V/div

V (lower) - 0.2 V/div

H - 200 μs/div

Atten: - 22 DB

(b) After Weight Gain of 0.11 g
(moisture = 14.6%)

FIGURE 13. FREE INDUCTION DECAYS FROM KEVLAR 49 FIBER

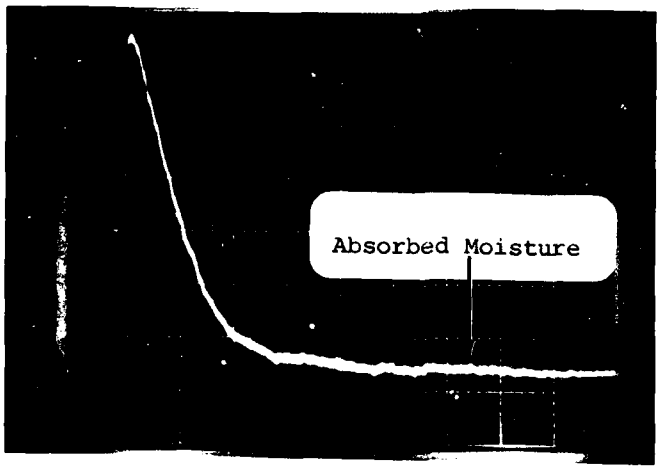

(a)

V - 0.2 V/div

H - 10 μs/div

Atten: - 23 DB

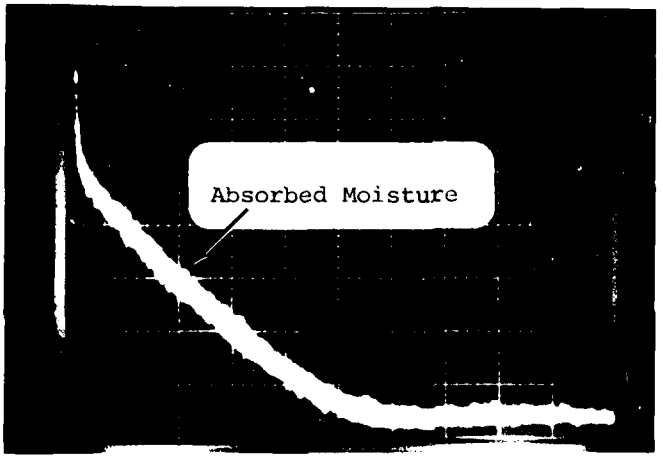

(b)

V - 0.05 V/div

H - 200 μs/div

Atten: - 23 DB

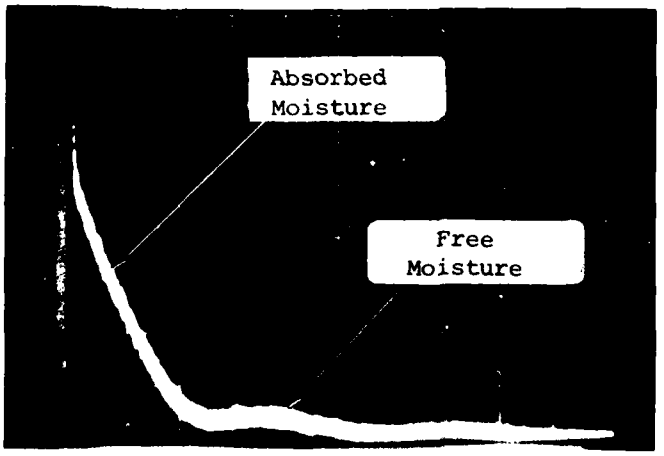

(c)

V - 0.05 V/div

H - 500 μs/div

Atten: - 23 DB

FIGURE 14. FREE-INDUCTION DECAYS FROM FRACTURED GLASS FIBER COMPOSITE

AD-A116 733 ARMY MATERIALS AND MECHANICS RESEARCH CENTER WATERTOWN MA F/G 11/4
PROCEEDINGS OF THE CRITICAL REVIEW: TECHNIQUES FOR THE CHARACTE--ETC(U)
MAY 82
UNCLASSIFIED AMMRC-MS-82-3 NL

3 OF 6
AD A116734

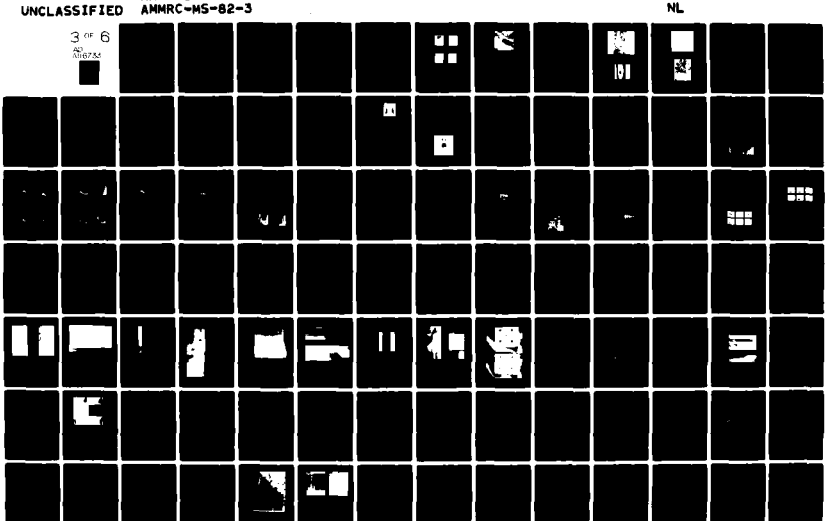

fractured specimen pieces were placed back in the environmental chamber after destructive testing. On the expanded time scale photograph shown in Figure 14c, a long time constant component having the characteristics of free moisture can be seen. Since the specimen surface was wiped dry of excess moisture the free moisture NMR signal is presumed to be associated with moisture which entered the interior of the composite through fracture surfaces.

Results of the destructive tensile testing performed on the dried and moisture conditioned specimens showed that moisture absorption caused a decrease in ultimate tensile strength of 14% and 4.3% for the Kevlar and glass composites, respectively, and an increase in the tangent modulus of approximately 11% for both types of composite.

IV. DISCUSSION

The results obtained indicate that NMR provides a useful means for nondestructively determining the moisture content in organic composites and in adddition, has the capability for providing information on different moisture absorption mechanisms. Although the ultimate sensitivity of the NMR technique for moisture detection was not determined. The results obtained show that moisture levels of 0.2% can be readily measured with NMR, and variations in moisture on the order of 0.1% can be resolved. The interpretation of the absorbed moisture free induction decay signals in terms of multiple components implies that the absorbed moisture exists in several states of molecular binding. Similar results have been obtained for various other heterogeneous materials such soil, concrete, paper and food products.[5] It is known that in composites, moisture can exist in various states including, (1) absorption in the polymer, (2) in voids, pores or cracks in the polymer system, and (3) along the fiber-matrix interface. In the case of the Kevlar composite, moisture will also be absorbed by the fiber itself; however, this moisture may be difficult to distinguish from that absorbed into the polymer matrix. Although it is possible to associate the separate components observed for the absorbed moisture free induction decays with water in these various states, Table II shows that the relaxation times for the absorbed moisture components are not very different. In a recent review of the structure of water in polymers, Hoeve has indicated that dielectric measurements and heat capacity measurements imply the existence of a single phase of water in a polymer consisting of relatively large clusters of mutually hydrogen bonded water molecules[6]. Rather than separate relaxation times, such a model would imply a distribution of relaxation times for the absorbed moisture. Clearly, more work is needed to further investigate the capability for NMR to resolve contributions from moisture in different states and to investigate the applicability of the cluster model to moisture in composites.

V. CONCLUSIONS

Results of pulsed NMR studies conducted on moisture conditioned organic matrix composites have shown that NMR can provide important information related to the nature of absorbed moisture and associated mechancial degradation. Absorbed moisture contributions to the free induction decay signals are clearly distinguishable from the signal contribution due to hydrogen in the solid

polymer matrix. The NMR results imply that water in different states of binding in the composite may be distinguished; however, further work is needed to verify the resolution capabilities of NMR. The magnitudes of the spin-spin relaxation times measured for the absorbed moisture are orders of magnitude less than for free water and indicate that the absorbed moisture water molecules are much more restricted in motion than for free water. Although further laboratory studies are needed to better understand the relationship between the components of NMR signals and moisture absorption, the results obtained indicate that NMR could be utilized for practical measurement of moisture content. Based on available technology[7], NMR instrumentation systems could be developed for moisture measurement in certain types of components such as helicopter rotor blades which can be transported through a detection cavity. For in situ measurements on larger structures, such as aircraft components, the technology exists for developing an NMR system capable of making measurements from one surface of a large specimen.[8]

REFERENCES

1. Slichter, C. P., Principles of Magnetic Resonance, Springer-Verlag, New York, 1978.

2. Shen, C., and Springer, G. S., J. of Composite Materials, 10, pp. 2-20, 1976.

3. Abragam, A., The Principles of Nuclear Magnetism, Clarendon Press, Oxford 1961.

4. Bloembergen, N., Nuclear Magnetic Resonance, W. A. Benjamin, Inc., New York, 1961.

5. Rollwitz, W. L. "Transient NMR Measurements," J. of the American Oil Chemists Soc., 48, No. 2, pp. 67-69, 1971.

6. Hoeve, C. A. J., "The Structure of Water in Polymers," ACS Symposium, Series 127, Ed by S. P. Rowland, pp. 135-146, 1980.

7. King, J. D., Rollwitz, W. L., and Matzkanin, G. A., "Magnetic Resonance Methods for NDE," Proc. 12th Symposium on NDE, San Antonio, Texas pp. 138-149, April 1979.

8. Matzkanin, G. A., King, J. D., and Rollwitz, W. L., "Nondestructive Measurement of Moisture in Concrete Bridge Decks Using Pulsed NMR," Proc. 13th Symposium on NDE, San Antonio, Texas, April 1981.

Session III: PREDICTIVE COMPOSITE CHARACTERIZATION

Chairpersons:

L. H. PEEBLES, JR., ONREast, U.S. Navy

B. I. Buck, AMTE, United Kingdom

THERMOGRAPHY AS AN OBSERVATIONAL AND PREDICTIVE METHOD FOR DYNAMIC LOADING OF COMPOSITE STRUCTURES

by

E. G. Henneke, II, S. S. Russell and K. L. Reifsnider

Virginia Polytechnic Institute and State University

ABSTRACT

In 1974, following a program of developmental research, the Materials Response Group at Virginia Tech introduced a new nondestructive evaluation technique which incorporates a video-thermography device as a sensor. They named the technique "vibrothermography," a term coined by the developers to describe a concept and related techniques whereby the internal integrity and uniformity of materials and components is interrogated by observing the heat pattern produced by the energy dissipation which occurs when a specific vibratory excitation is applied to the test piece. In particular, vibrothermography consists of the study of thermographic (heat) patterns which are recorded or observed in real time during such an excitation. Since that time, the investigators have determined that the details of the mechanisms which produce such dissipative heat are directly related to the mechanisms of material deformation and degradation in several important ways, a fact that provides the basis for the use of such a scheme as a nondestructive test and evaluation method, and for a general nondestructive investigative philosophy.

Vibrothermography is based on active heating, usually induced by small amplitude high frequency mechanical vibrations in the kilo-to megaHertz range. These vibrations do not cause material degradation or damage development. However, active heating (which is frequently greater in total amplitude) is also induced by dissipation during low frequency, high amplitude cyclic (fatigue) loading for durability studies. By observing the specimen surface during fatigue testing with such a device, using a proper technique, the initiation and growth of damage can be monitored.

Since the video-thermography device is a photon device, this technique can be used to observe large structures just as well as small specimens. The technique provides results which indicate the collective effect of all defects acting together so that, for complete damage states for individual flaw analysis is not possible, this scheme provides exactly the type of information the engineer must have, the collective effect of all the damage on the response of the component in question.

This paper describes the application of the large-amplitude active heating thermography scheme to the detection of damage in a helicopter rotor blade during full-scale testing at a resonant frequency of about 13 Hz. The effort was successful in that a region of damage was located which, later, was identified by the other nondestructive evaluation techniques, and which was the general location of eventual failure of a rotor blade. Operational and interpretational information regarding the effort are described.

BACKGROUND

Thermography is thermal imaging, or the mapping of isotherms over a surface. Video-thermography is the real-time imaging of isotherms on a cathode-ray tube. In this instance, the lines of constant temperature may be mapped either by a continuous gray scale on a black-and-white monitor or by distinct colors on a color monitor. Video-thermography is performed by detecting infrared radiation from the surface of the scanned object. The detector is usually a photon-effect device whose response depends upon the wavelength of the received infrared radiation. These detectors generally have a very rapid response time so that real-time imaging, of the order of 16 frames/sec., can be performed by electronically conditioning the output signal for proper display on the cathode-ray tube.

The infrared thermography technique is actually quite old: it dates to the discovery of infrared radiation by Sir William Herschel in 1800 and the observation of the first: "Heat-picture" by his son Sir John Herschel in 1840.[1] Major impetus was given to the development of the technique by the military during the First and Second World Wars. The devices used were limited to the near-infrared wavelengths, and the most interesting targets had to be illuminated by infrared search beams. Not until the 1960's were sufficient advances made in the technology to allow for real-time imaging over a very wide temperature range. Since then, a great deal of literature has appeared indicating a wide variety of applications of thermography, including medical diagnosis, quality control, and the examination of electronic circuits or transformers for abnormally hot parts. Our laboratories have used thermography to follow the down range motion of the exhaust cloud from a rocket,[2] the thermal effluent downstream of an electrical generating plant, and damage development in materials.

There are basically two ways a temperature gradient can be established around a region of damage (or flaw). These are classified as either passive or active. In passive generation of the thermal gradient, the test object is heated or cooled by an external source. Differences in thermal conductivity in the region of the flaw lead to gradients which are observable on the surface (if the flaw is not too deep) by thermography. Active generation of a thermal gradient refers to self-heating (or relative self-cooling) of the test object with respect to its surroundings. The work reported here deals entirely with active generation of thermal gradients around flawed or damaged regions. In particular, the thermal gradients are produced by introducing steady-state mechanical energy into the test objects.

The mechanical energy is preferentially transformed into thermal energy around the damage sites. Two methods have been applied in our laboratory to introduce mechanical energy into the specimen: high amplitude, low frequency, mechanical excitation (such as in a fatigue test) and low amplitude, high frequency vibrations (such as in a shaker) have been used.

DETECTION OF DEVELOPING DAMAGE DURING CYCLIC FATIGUE LOADING

The basic mechanisms of fatigue damage in composite materials and homogenous materials are quite different. Instead of the initiation and propagation of a self-similar fatigue crack commonly identified with homogenous materials, fatigue damage in composites consists of various combinations of matrix cracking, fiber-matrix debonding, delamination, void growth, and local fiber breaking. The mechanisms, types, and distribution of fatigue damage depend upon the material system, the stacking sequence of plies, fabrication techniques, geometry of the component, stress state, and loading history. Furthermore, the fatigue response of composites is sensitive to other parameters including hole sizes (if present), type loading, frequency of cyclic loading, temperature, and moisture.

A technique to nondestructively detect and monitor damage development in composite materials must be capable of assessing the combined effect of the numerous damage modes which form the damage state. Since a large percentage of the energy released during the damage process is converted to heat, thermographic techniques are directly applicable to detecting damage initiation and monitoring damage development. Furthermore, video-thermography enables real-time damage investigations.

Figure 1 shows the use of video-thermography to follow the development of internal damage in a graphite-epoxy laminate containing notched 0° plies constrained on both sides by un-notched ±45° plies. Here the damage which developed at moderate cyclic loads was confined to the 0° ply and the interface between it and the unflawed constraining ply.[3] As the fatigue test continues the damage worsens and enlarges as is evidenced by the increase in size and temperature of the hot region. By monitoring the position of the hot spots with video-thermography, damage growth rates can be measured in real time to determine the effect of different constraining ply orientations on fatigue damage development in composite laminates.

A K-747 rotor blade for an AH-1S helicopter was monitored during a fatigue study with video-thermography. Figure 2 is a thermogram of a region of heat production during the simulated flight fatigue test. This region was subsequently determined by use of ultrasonic techniques to be a region of large delaminations.[4]

DECTECTION OF DEVELOPED DAMAGE USING ULTRASONIC EXCITATION

In addition to using video-thermography to study developing damage in materials under fatigue loadings, it is also possible to use the technique to locate and study existing damage. In this case, it is desirable to have a method which does not add to the damage state. For this purpose, our laboratory developed vibrothermography. Vibrothermography combines low-amplitude, high frequency, steady-state mechanical vibrations with infrared detection to locate flaws.

Vibrations in the test object are introduced by any convenient source. In this case, as seen in figure 3., an ultrasonic shaker

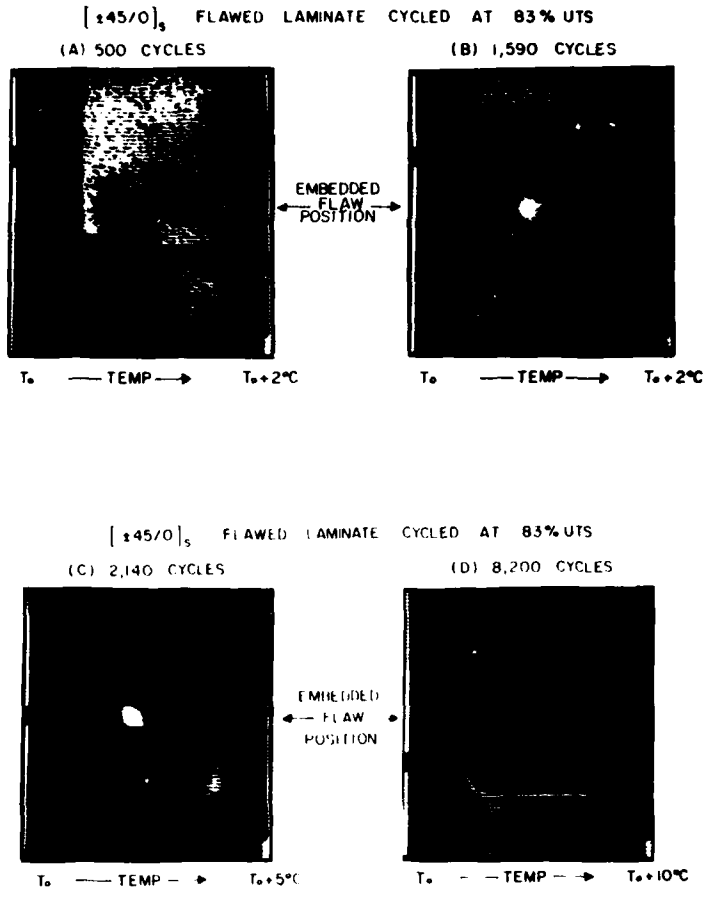

Fig. 1. Heat pattern of a Gr-EP $[\pm 45,0]_s$ flawed laminate under cyclic loading at 83% UTS. The maximum nominal axial stress in the 0 degree plies is 130% of the notched tensile strength of these specimens. (A) 500 cycles, (B) 1590 cycles, (C) 2140 cycles and (D) 8200 cycles.

Fig. 2. Heat pattern generated at root end of a K-747 main rotor helicopter blade during simulated flight service.

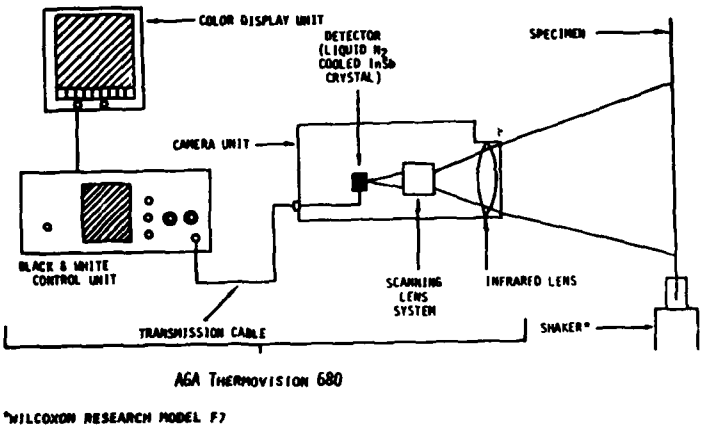

Fig. 3. Schematic of Ultrasonic Vibrothermographic Test.

was used. The frequency of vibration was varied from about 8 to 40 kHz. The speciment was attached by only one end to the vibrations source and was inertially loaded. The resulting stress field was far below the value required for initiating damage in these specimens as determined by other observations. The resulting thermal gradients established in the region of delaminations and delamination-like flaws evidence themselves to the thermographic camera within seconds. The appearance of particular flaws can, moreover, be controlled by varying the frequency of vibration by less than 10%.

For purposes of comparison of test results, a C-scan inspection and isotherms from a vibrothermogram have been superimposed in figure 4 for a 2-inch (5.12 cm) long random fiber sheet molding compound specimen with 65% fibers by weight. The C-scan in this case indicates areas of imperfections as black regions. The area indicated as an 8°C isotherm in the vibrothermogram corresponds well to the C-scan. Further investigation using optical methods showed this region to be an area of delamination. Delaminations of this type often determine the location of the final fracture in a tension test to failure for this type of material. Vibrothermography proved to be a means of locating the particular delaminations which determined the failure location for tension test coupons.

Figure 5 is a vibrothermogram of a simulated delamination in a four ply 0° E-glass laminate being excited by 16.7 KHz frequency ultra sound. The simulated delamination consisted of two strain gages between two sheets of milar which was laminated in the specimen at the midplane. Electrical leads were run out of the specimen to allow the strain gages to be powered electrically. By heating the strain gages electrically to simulate the vibrothermographic pattern, an order of magnitude estimate for the power dissipated by the simulated delamination was obtained. The electrical power needed to simulate this vibrothermogram was of the order of 0.1 watts. It should be emphasized that the measure only reflects an order of magnitude of the energy being dissipated by the simulated delamination during ultrasonic vibrothermographic inspection.

An air compressor seal for a worm type air compressor is shown in figure 6. This seal is composed of ±45° plys of E-glass epoxy to a thickness of approximately 1/4 inch (0.63 cm). This seal had been subjected to operation for one predicted life before these tests. Figure 7 is a thermogram of this seal during excitation by 13KHz sound. In the thermogram the large hole is at the bottom. Going clockwise from the tooth with the hole the following teeth appeared to have large heat generators and hence suspected imperfections;1,3,6,9,10. Particularly large hot regions were evidenced on teeth 3 and 6. Also the region between the large hole and tooth 11 generated heat. The seal was tested by other nondestructive evaluation techniques (C-scan, penetrant ehnanced x-radiography, and optical). However these NDE techniques failed to determine if there were imperfections within the seal, so no correspondence between vibrothermography and the other NDE techniques can be claimed. Work is proceeding on a similar seal which has visibly present delamination type flaws.

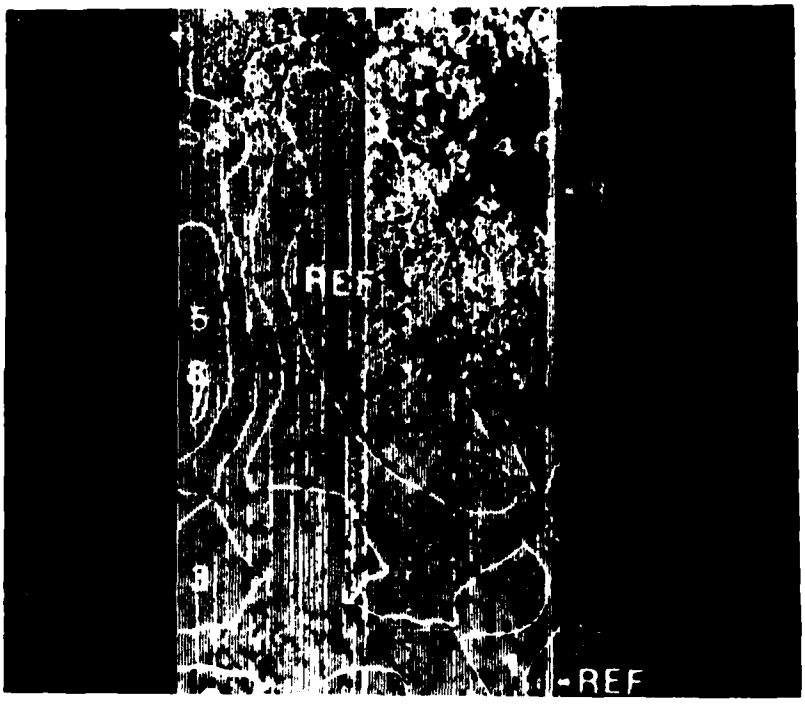

Fig. 4. Superposition of Ultrasonic C-scan inspection (grey and black) and Vibrothermographic inspection (white isotherm lines indicating °C rise over reference temperature) of a random fiber glass-epoxy sheet molding compound specimen with a region of delamination in the upper right corner.

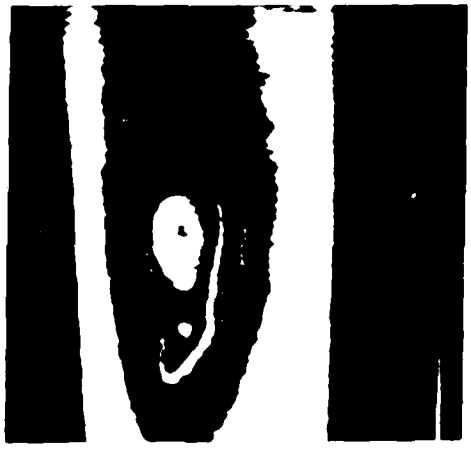

Fig. 5. Heat pattern of a simulated delamination in E-glass $[0^{\circ}_{2}]_{s}$ specimen during Ultrasonic Vibrothermographic inspection.

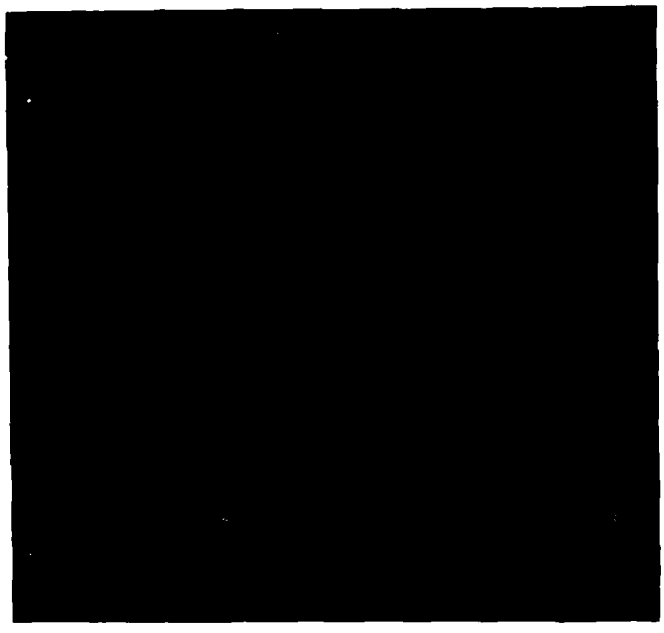

Fig. 6. Screw type air compressor seal composed of ±45° continuous glass-epoxy.

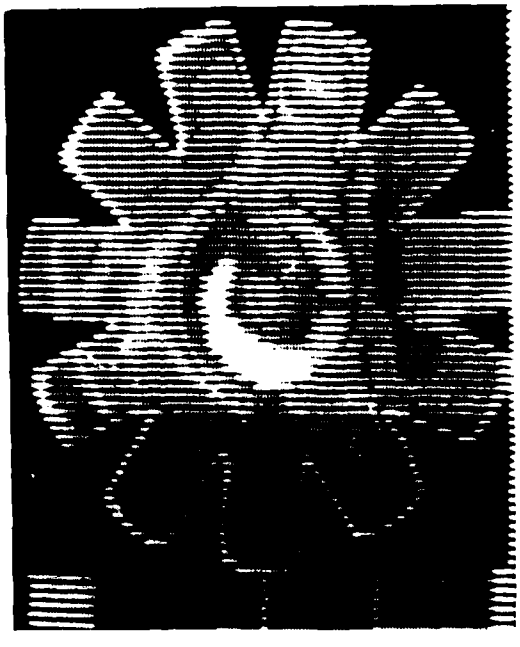

Fig. 7. Heat pattern generated during Ultrasonic Vibrothermographic inspection of air compressor seal shown in Fig. 6.

CONCLUSIONS

1. Real-time video-thermography can be used to investigate damage initiation and progression in many composite systems, both laboratory specimens and full-scale structures.
2. Vibrothermography is a nondestructive test technique since the inspection does not cause additional damage to the structure being interrogated.
3. Vibrothermography offers the potential, through control of parameters such as the excitation frequency, to quantify the size or extent of the damaged region.

ACKNOWLEDGEMENT

Portions of this research were sponsored by the Air Force Materials Laboratory, Contract No. F33615-77-C-5044, and the Army Research Office, Grant No. DAAG29-79-0037 and Contract No. DAAG29-81-K0017.

REFERENCES

1. "AGA Thermovision System 680/102B," Operating Manual, AGA Aktiebolag, Lidingo, Sweden, 1974.

2. K.L. Reifsnider and W.W. Stinchcomb, "Investigation of Dynamic Heat Emission Patterns in Mechanical and Chemical Systems,: Proceedings of 2nd Biennial Infrared Information Exchange, AGA Corp., St. Louis, MO., 1974, p. 45-58.

3. W.W. Stinchcomb, K.L. Reifsnider, P. Yeung, and T.K. O'Brien, "Investigation and Characterization of Constraint Effects on Flaw Growth During Fatigue Loading of Composite Materials,"2nd Semi-Annual Status Report, NASA Grant NSG-1364, Virginia Polytechnic Institute and State University, Jan., 1978.

4. D.G. Orlino, "Evaluation of the Effect of Voids in Composite Main Rotor Blades," American Helicopter Society Journal, to be published.

5. K.L. Reifsnider, E.G. Henneke,II, and W.W. Stinchcomb, "Defect-Property Relationships in Composite Materials," Technical Report AFML-Tr-76-81 (III), Air Force Materials Laboratory, Wright-Patterson AFB, Ohio, June 1978.

6. J.C. Duke, Jr "Nondestructive Characterization of Chopped Glass Fiber Reinforced Composite Materials," ASTM STP, Symposium on Short Fiber Reinforced Composite Materials.

7. E.G. Henneke,II, K.L. Reifsnider, and W.W. Stinchcomb, "Thermography An NDI Method for Damage Detection," Journal of Metals Vol. 31. No. 9 September 1979, pp. 11-15.

THERMOELASTIC STRESS ANALYSIS

L. R. Baker and J. M B. Webber

SIRA Institute Limited
United Kingdom

ABSTRACT

After discussions on the need to measure the distribution of stress on the surface of a structure under load, the connection between stress concentration, mechanical design and safety, a new technique for recording stress patterns, called Thermoelastic Stress Analysis (TSA) is described. For given material constants, the change in temperature on the surface of a structure, subject to dynamic loading, is directly proportional to the change in stress at that point. A specially designed high sensitivity IR camera is described which can present a colour display of the distribution of stress which could arise from temperature variations as small as 0.001 K resulting from a few units of micro strain in metals. A selection of typical results obtained by recording the stress concentration on the surface of a model pedestal structure are given to illustrate how TSA could be used as an aid to design. The likely useful areas of application of TSA can be identified with the help of a list of the principal characteristics of the method provided at the end of the paper.

1. INTRODUCTION

All materials, whether employed in aero-engines, oil rigs, high rise buildings, railway lines, golf clubs, or paper clips, will eventually fail if subjected to overload conditions. The task of the mechanical designer is to ensure that the product or structure will survive the extremes of environment, to which it is likely to be subjected, with its performance characteristics substantially unimpaired. A compromise must be struck between adequate safety margins and constraints imposed by parameters such as weight and cost, the ever-present variations in properties of the materials used and in the strength of fabrication joints. If every conceivable hazard were taken into account and each given a significant safety margin, the product could well be too heavy or too expensive. A critical study of the margins for safety is therefore an essential aspect of design and indeed of product inspection. High concentrations of stress on the surface of a product, due either to poor design or material faults, could eventually lead to structural failure and are therefore to be avoided.

The usual methods of measuring stress distribution on a product subject to loading are to measure the strain or movement of the surface by the application of a brittle coating, a photo-elastic coating, or by the use of electrical strain gauges, and then calculate the stress from the known mechanical constants of the material. The problem with all these methods is that they are time consuming to apply, they depend upon good adhesion and considerable skill in application, and they have a limited application to surfaces at an elevated temperature. The strain gauge is more appropriate for obtaining selected spot values of stress rather than providing a full area coverage of measurement as would be necessary in order to locate a point of maximum stress on the surface.

Surface strain patterns can also be recorded by the technique of holography in which the difference in the surface contours between the object in the unstressed and stressed state are seen as dark bands superimposed on the brightly illuminated surface of the structure under test. The small movements of the surface giving rise to these bands can be converted to stress information by an appropriate computation. The

limitations of this technique are that a powerful laser is required to inspect large areas of a structure and the computation to convert surface displacements to stress is often complex.

An alternative method of visualising the distribution of stress on the surface of a structure subject to dynamic loading by measuring small changes in surface temperature is showing great promise, due to the recent availability of the high sensitivity radiation detectors employed in modern thermal imaging systems. The technique, known as Thermoelastic Stress Analysis, was anticipated by Thomson (Lord Kelvin) (1) in 1853. A paper describing the basic thermodynamics was written by Biot (2) in 1956, and the idea of using an infrared radiometer for measuring the surface temperature was suggested by Belgen (3). Mountain and Webber (4) described the first laboratory instrument capable of measuring stress patterns down to a level of sensitivity likely to be of practical interest to a wide range of designers. This paper describes the design and performance achieved by the latest version of this high sensitivity IR camera capable of measuring the very small changes in surface temperature down to 0.001 K which are directly related to the stress on the surface of a structure subject to dynamic loading.

2. THEORY

A body subjected to tension or compressive stress within the elastic limit experiences a reversible conversion between mechanical and thermal forms of energy. In general, it can be said that bodies which expand on being heated become hotter when put under sudden pressure and cooler when under tension. Although the heating or cooling of a gas when suddenly subjected to compression or expansion is a familiar effect, similar changes although generally of a much smaller magnitude can also be observed in solids. Whereas the pressure change in a gas is quickly equalised throughout its volume, pressures in a solid may be concentrated in highly localised regions where heat is generated or absorbed. The technique of thermoelastic stress analysis involves recording the pattern of small temperature changes over the surface of a structure subject to dynamic loading which are directly related to stress.

An equation relating surface temperature changes to applied stress under adiabatic conditions has been developed by Biot (2) and Belgen (3) as follows:

$$\theta = - K_M TS$$

where θ is the temperature change, K_M is the thermoelastic constant of the material, T is the average temperature of the structure and S is the sum of the principal stresses.

The thermoelastic constant of the material can be expressed as:

$$K_M = \frac{\alpha}{\rho . Cp}$$

where α is the coefficient of linear thermal expansion, ρ is the density and Cp is the coefficient of specific heat at constant pressure. From this we see that the change in temperature produced by a given stress is linearly proportional to the absolute temperature so that the effect is greater and therefore in principle more easily measured at elevated temperatures.

The temperature change is linearly related to the stress for a given material and independent of loading frequency, providing adiabatic conditions are maintained. Finally, as expected, for materials with a positive α, such as metals, the temperature decreases with increasing stress.

Although the effect was first verified experimentally by Joule (5) in 1859, work still continues to examine the true limits of the parameters within which the above relation remains valid.

3. DESCRIPTION OF IR CAMERA

Typical values for the thermoelastic constant for metals are 0.28×10^{-11} m^2/N for steel and 0.86×10^{-11} m^2/N for aluminium. The temperature changes of interest for the smallest stress values of practical interest (2×10^6 Nm^{-2} in aluminium) to the ultimate strength point would be in the range 0.001 K to 0.3 K.

The instrument to be described has been designed to measure these very small changes in temperature over an area of an object under study.

A schematic representation of the IR camera is shown in Figure 1. The thermal radiation emitted from a small area of the model on the left after reflection by scanning mirrors and transmission by a dichroic beamsplitter is focused by an f/0.8 IR transmitting germanium lens on to the IR detector mounted vertically. Rotation of the scanning mirrors enables an extended area on the object to be scanned and hence the generation of a television type raster on a colour cathode-ray tube, the guns of which are fed from the output of the detector via a computer signal processing unit. In this way, one of 16 possible colours can be related to the level of absolute or bipolar stress at a particular point on the object. Typical colour prints have been reproduced in an article by Wright (6).

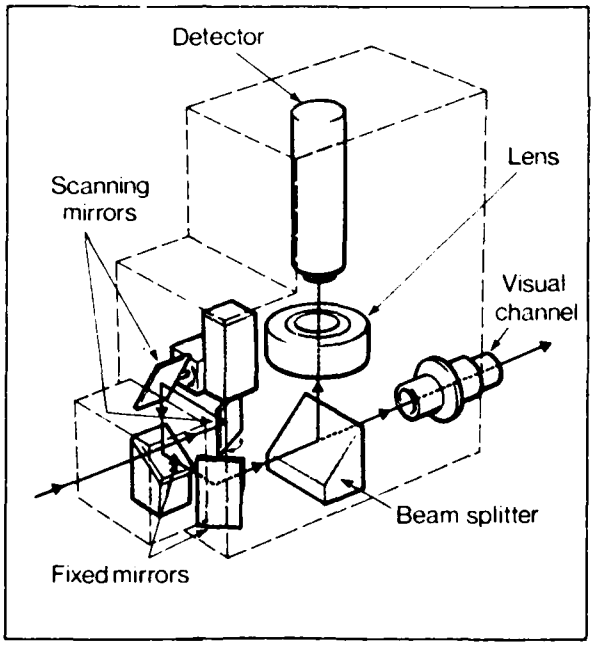

Fig 1 SCHEMATIC REPRESENTATION OF THE IR CAMERA

In addition to the optical head, which is tripod mounted, there is also a remote hand control unit for setting up the scanned area, as defined by its centre and extremities. An analogue/digital control unit for selecting the frequency and amplitude of the mirrors, a TV monitor for a real time stress display and an operator's terminal are also provided.

Fields of view set by the limits of the mirror scans can be varied from 0.1° x 0.1° to 25° x 25° and the angular resolution, defined by the focal length of the lens and the diameter of the detector, is 0.1°. The optical head can be used at a separation from the object varying from 0.5 m to 10 m and can view objects at angles up to $\pm 45^{\circ}$ from the direction of normal incidence. The area of the object to be scanned can be acquired either by using the direct vision eyepiece or by the use of a beam of light which can be projected on to the surface since the axes of these visual channels are set to be coincident with the axis of the system transmitting IR radiation.

The frequency of loading of the object may be in the range 0.5 Hz to 5 kHz depending on the particular object to be studied. If an aluminium object is used, the sensitivity of the instrument to stress changes is 2×10^{6} Nm^{-2} which is approximately equivalent to 5 μ strain units. A dynamic range of 1000 to 1 can be achieved.

Stress information, at a selected point, is provided on a 4 digit LED display, as a two dimensional colour TV display, or as an analogue plot along a chosen line over the surface of the object. The number of pixels of stress information over a chosen scan field can be selected from the following options: 256 x 256, 128 x 128, 64 x 64, 32 x 32, or 16 x 16 and up to 16 levels of stress, which can be related to 16 different colours, can be displayed at each pixel. The colour range can be expanded to fill a selected stress range which may exist either as an absolute value or, in the bipolar sense, to distinguish between compression or tensile stress. The angular separation of the pixel sampling points can be selected in the range 0.1° to 1.5°.

The time to complete a full area scan depends on the rate of loading and the number of pixels of information to be sampled over the surface area

and this in turn depends on how rapidly the stress is changing over the surface. If the stress is low, many loading cycles up to 256 may be used to obtain an adequate ratio of signal-to-noise. In most cases, however, one or two loading cycles are sufficient. If Nx and Ny are the number of sample points in the x and y directions, L is the number of loading cycles per point and f is the loading frequency, the time, t, to complete a full area scan is given by:

$$t = \frac{Nx\ Ny\ l}{f}$$

Typical values would be:

Hz	L	Pixels	t
1	2	16 x 16	8.5 mins
10	2	16 x 16	1 min
100	2	128 x 128	5.5 mins
1000	2	256 x 256	2 mins

A synchronous reference signal, required to operate the phase sensitive demodulator used to detect the output from the radiation detector, is derived from a convenient transducer, such as a strain gauge. This is attached to the object and as part of the setting up procedure its phase output is adjusted to be equal to that of the detector.

4. EXPERIMENTAL RESULTS

The first results were obtained on a model of a pedestal structure machined in aluminium from the solid. A section through this model and a monochrome CRT display where the beam intensity was arranged to be proportional to stress are shown in Figure 2. The arrow shows the direction of the periodic thrust applied at 20 Hz. The camera was about 600 mm from the model. High stress regions show up brightly in the picture taken of the area between the dotted lines at the base of the web. In the presence of colour, the brighter areas are red and the lower stressed areas blue. When more accurate results are required, an individual pixel can be addressed by a flashing cross indicator driven by the hand set and the value of the stress at that particular

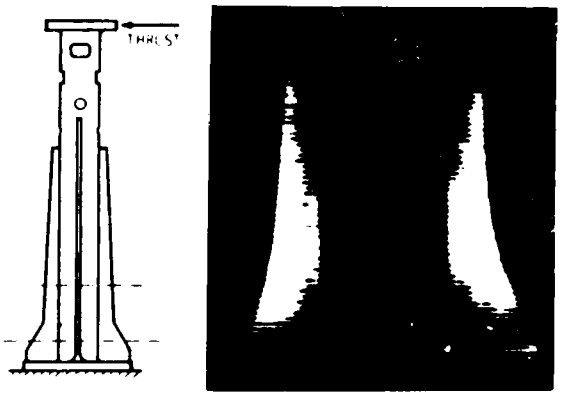

Fig 2 STRESS IS CONCENTRATED NEAR BASE OF WEBS

point can be digitally displayed. Alternatively, an analogue plot, such as that shown in Figure 3, across a chosen section can be displayed on an x y plotter. Since at any given moment, one side of the model is in compression and the other side is in tension, half the trace is above and half below the zero line. The ease with which the stress across a section can be obtained can be judged from the fact that once set up such a scan takes about 15 seconds to produce. The maximum of the curve represents a peak stress of about 2×10^{8} Nm^{-2} and a resolution of 2×10^{6} Nm^{-2} was achieved. The measurements of stress on this model using the TSA technique have been compared directly with corresponding values obtained by conventional electrical strain gauges and the results have agreed to within the limits of experimental accuracy.

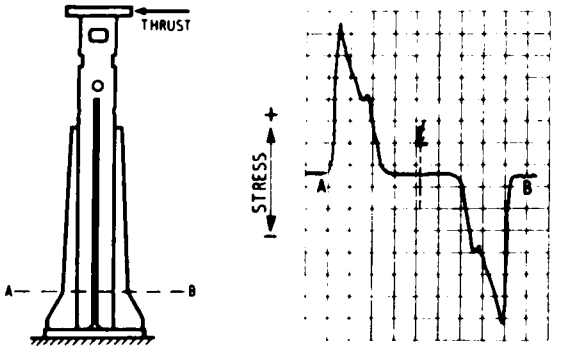

Fig 3 PLOT OF STRESS ACROSS WEAKEST SECTION

As the technique operates over a wide range of distances between the object and the camera with constant sensitivity, the object may either be small such as an individual turbine blade or as large as a complete 10 m aerial system.

Useful results have also been obtained on rolling stock axle boxes and marine engine casings. A wide variety of application studies are now under active study on objects made from materials such as rubber, composites and plastics.

5. APPLICATIONS

The value of the method as an aid to design can be appreciated from the stress concentration at the top of the strengthening web and around the small circular hole above it using the model shown in Figure 2, now loaded in a direction at right angles to the plane of the paper. Figure 4 shows these stress concentrations as bright areas and Figure 5 the drop in stress when recording a trace across the specimen immediately below the top of the web. To reduce weight in such a structure and minimise stress concentration, it would clearly be better to elongate the hole and remove the metal at the top of the web.

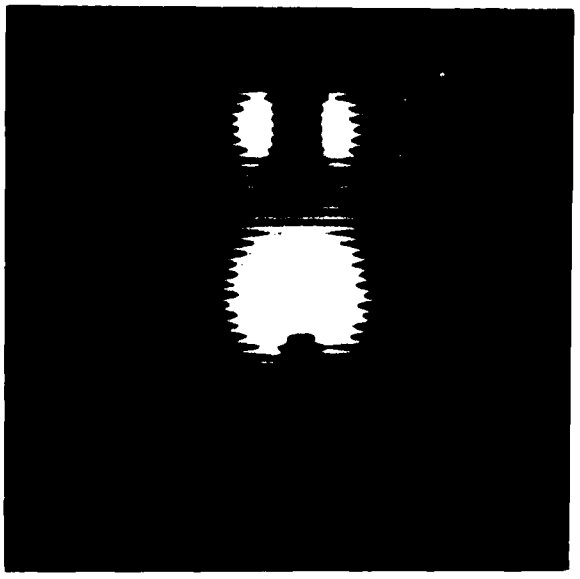

Fig 4 STRESS IS CONCENTRATED AT TOP OF WEB AND EITHER SIDE OF CIRCULAR HOLE

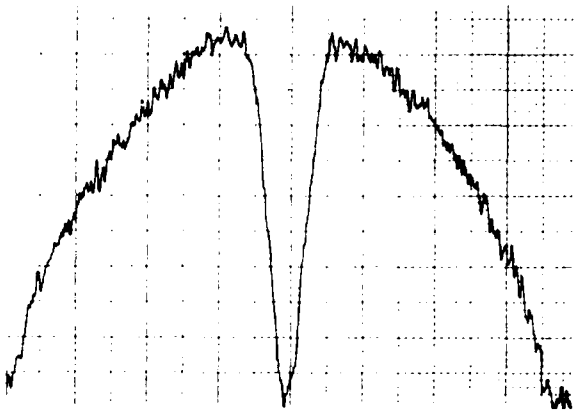

Fig 5 PLOT OF STRESS NEAR TOP OF WEB

It was soon realised that the magnitude of the stress at a particular point on the surface of an object under load was significantly influenced by the precise conditions of loading errors in the geometry of the structure, the material history, faults, and the integrity of welds and joints. This fact suggests the application of TSA to non destructive testing (NDT) and also for the study of crack propagation in fatigue testing.

The principal characteristics of TSA which are as follows will help the reader to identify useful areas of application:

* Non-contacting remote reading is possible
* Measures stress directly without the need for the computation associated with strain measurements
* A quick assessment of stress distribution at long range to locate highly stressed regions can be followed by short range high resolution measurements
* Method is quantitative knowing the material parameters
* Large or small areas can be measured with the same angular resolution and sensitivity
* Large dynamic range of measurement possible
* Tolerates oblique incidence viewing

* Quick and easy to use
* Unskilled personnel can operate
* Three dimensional objects can be examined (± 10 mm at range of 1 m)
* Instrument is portable
* Tolerant to vibration smaller than resolution limit
* Due to easy storage of pictorial information, dynamic events such as crack propagation can be studied
* Useful in NDT of materials and structures
* Measurements of stress can be undertaken at elevated temperatures as the steady component of IR radiation is rejected in the signal processing
* Environmental temperature does not need to be controlled
* Highly reflecting objects need to be sprayed with black paint to increase emissivity
* Radiation detectors with liquid nitrogen cooling are required to achieve the highest sensitivity
* If the material characteristics are unknown, the output has to be calibrated with a strain gauge at a selected point
* The object has to be periodically loaded and a reference signal created for phase-sensitive detection of the detector output
* The output records the sum of the principal stresses and so contains no direction data
* The optical head, signal processors, and displays appear more costly than some other techniques for strain measuring, which do, however, need subsequent computation
* Method does not measure static stress
* Method requires clear view of the object to be measured without an intervening medium, which could absorb radiation in the spectral range of 8 - 14 μm.

6. CONCLUSIONS

The principle of TSA has been embodied in a simple IR scanning camera to record 16 levels of stress on the surface of a structure subjected to dynamic loading in terms of different colours on a TV display. This information can be obtained easily and quickly and is readily interpreted and stored for more detailed analysis. The technique has been proved of value for producing stress pattern records on small components as well as large structures. Its application in the NDT of a wide variety of components, structures and materials has proved to be just as great as its use as an aid to mechanical design. Due to the inherent fast response of the measuring system, TSA technology has also demonstrated its value in fatigue testing and crack propagation studies.

ACKNOWLEDGMENTS

Thanks are due to Dr L J Cox for the design of the IR camera and Dr P E Holbourn for the development of the video signal processing and display system.

REFERENCES

1. Thomson W (Lord Kelvin): General theory of thermoelastic effect, Trans Roy Soc, Edinburgh (1853), No 20, p 261.

2. Biot, M A: Thermoelasticity and Irreversible Thermodynamics, J Applied Physics, 27, No 3, 240, March 1956.

3. Belgen, M H: Structural Stress Measurements with an Infrared Radiometer, ISA Transactions, Vol 6, No 1, pp 49, January 1967.

4. Mountain, D S and Webber, J M B: Stress Pattern Analysis by Thermal Emission, Fourth European Electro- [illegible]s Conference, October 1978, Utrecht, Netherlands, SPIE, Vol 164.

5. Joule, J P: Phil Trans, 149, 91 (1859).

6. Wright, J: Camera System transforms Stress Analysis, Eureka, 1, No 6, p 29, 1981.

LOCAL CHARACTERIZATION OF FIBER COMPOSITES BY ACOUSTIC EMISSION*

M. A. HAMSTAD

Lawrence Livermore National Laboratory
Livermore, California 94550

March 25, 1981

ABSTRACT

The performance of a fiber composite article is often critically dependent upon the local conditions throughout the composite. For the purposes of this discussion, the local conditions include such items as matrix crack density, fiber damage or fraying, matrix content, matrix cure, moisture content, residual stress field, matrix to fiber bonding, etc.. Without a proper characterization of those local conditions, analytical descriptions of composite performance and failure are inadequate. The local conditions of a composite article in service have been determined by two important factors. Namely, the local conditions that were originally fabricated and the modification of these conditions by the macroscopically distributed microfailure and deformation which occurred during proof testing and/or loading the composite article when it was put into service as well as the modification of these conditions during service life. Acoustic emission (AE) has demonstrated its usefulness as a tool for use in characterizing the original fabricated local conditions and in monitoring and characterizing the change in these conditions as a result of proof testing and service loading. Examples of the use of AE for these purposes will be drawn from the published literature and the authors own research.

---

*This work was performed under the auspices of the U.S. Department of energy by LLNL under contract No. W-7405-ENG-48.

EXAMPLES OF ACOUSTIC EMISSION (AE) CHARACTERIZATION OF POPULATION CHANGES DUE TO CHANGES IN FABRICATION VARIABLES

The characteristic performance of a fiber composite article in service is predictable if two conditions are met. First, a sufficient design data base must exist, and second each composite article must belong to the same material population which is represented in the data base. Acoustic emission (AE) has been used as a sensitive technique to characterize changes in material populations caused by changes in process or fabrication variables. Characteristic AE "signatures" or "fingerprints" obtained during proof or initial service loading can distinguish population changes. Figure 1 demonstrates the large change in damage accumulation when a high elongation matrix system (approx. 40% elongation) is used in place of a low elongation system (approx. 8% elongation). Figure 2 shows that AE can characterize a population change due to altering the sequence of filament winding. Similarly, Figures 3-7 demonstrate population changes due to other filament winding and process variable changes.

DURING PROOF TESTING TWO DISTINCTIVE DIFFERENCES WERE PRESENT: i) VERY HIGH AMPLITUDE AE IN STIFF MATRIX COMPOSITE; ii) EARLY PEAK OF AE IN STIFF SYSTEM VERSUS GRADUAL INCREASE AE IN FLEXIBLE SYSTEM

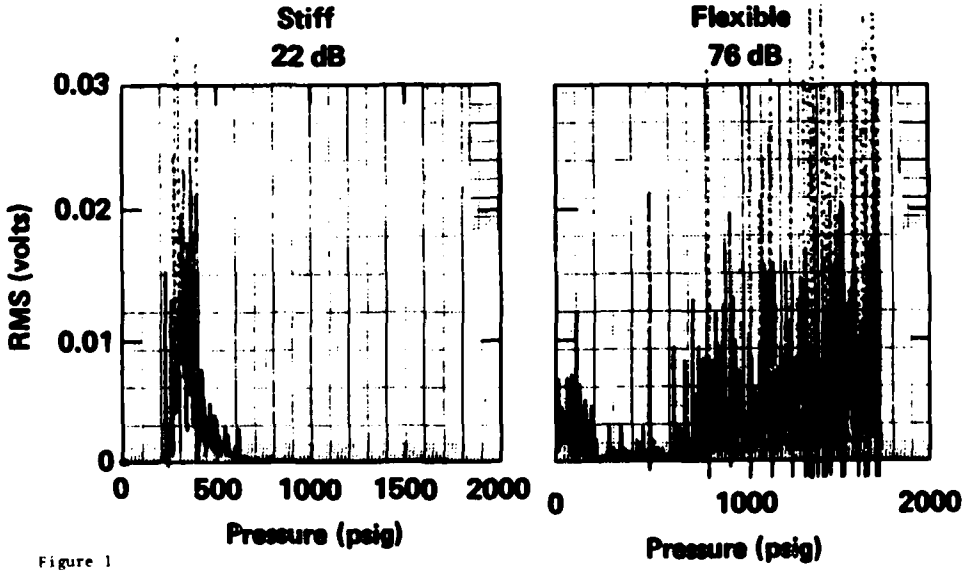

Figure 1

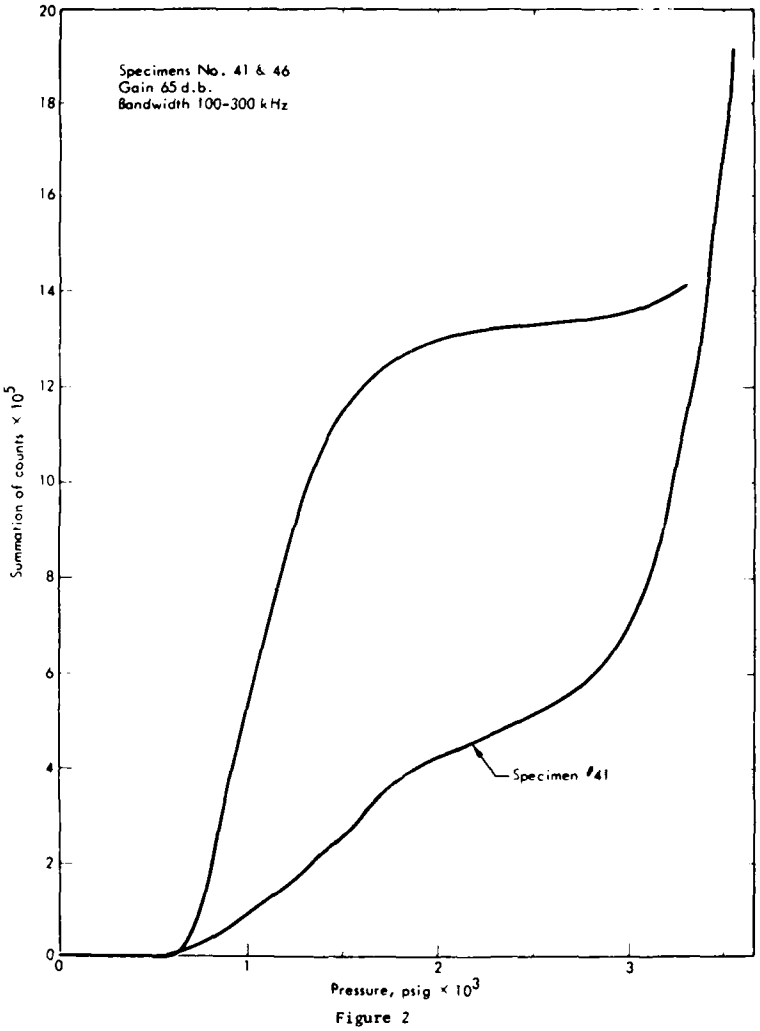
Specimens No. 41 & 46
Gain 65 d.b.
Bandwidth 100-300 k Hz
Summation of counts × 10^5
Pressure, psig × 10^3
Specimen #41
0
2
4
6
8
10
12
14
16
18
20
1
2
3

Figure 2

EXCESS EPOXY IN THE MATRIX RESULTS IN LOWER FIRST AE PEAK

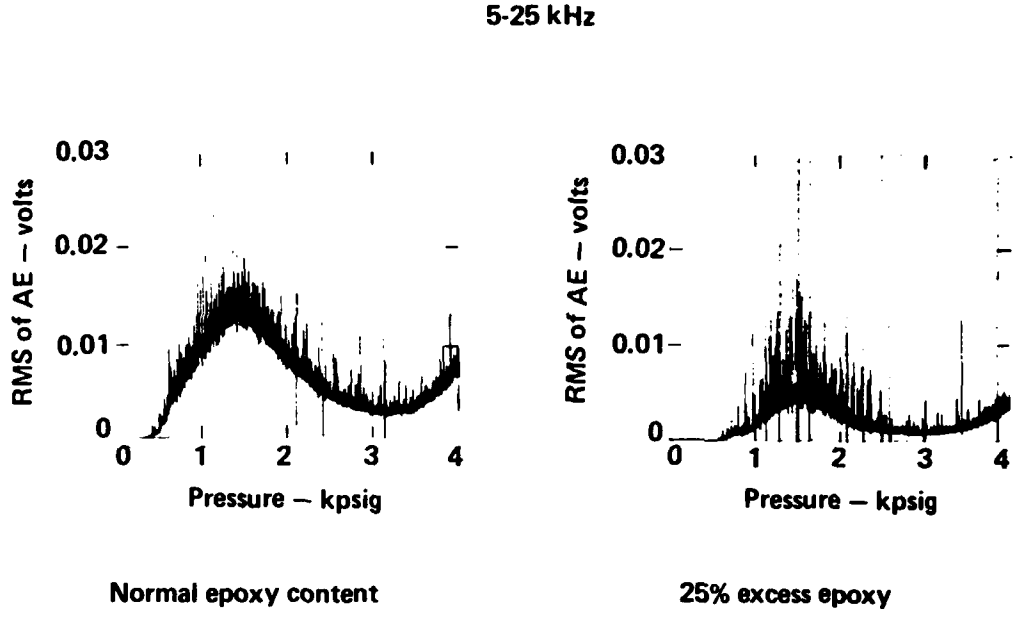

Figure 3

HIGH MATRIX CONTENT RESULTS IN: 1) DELAYED FIRST PEAK; AND 2) INDICATIONS OF TWO SEPARATE AE SOURCE MECHANISMS

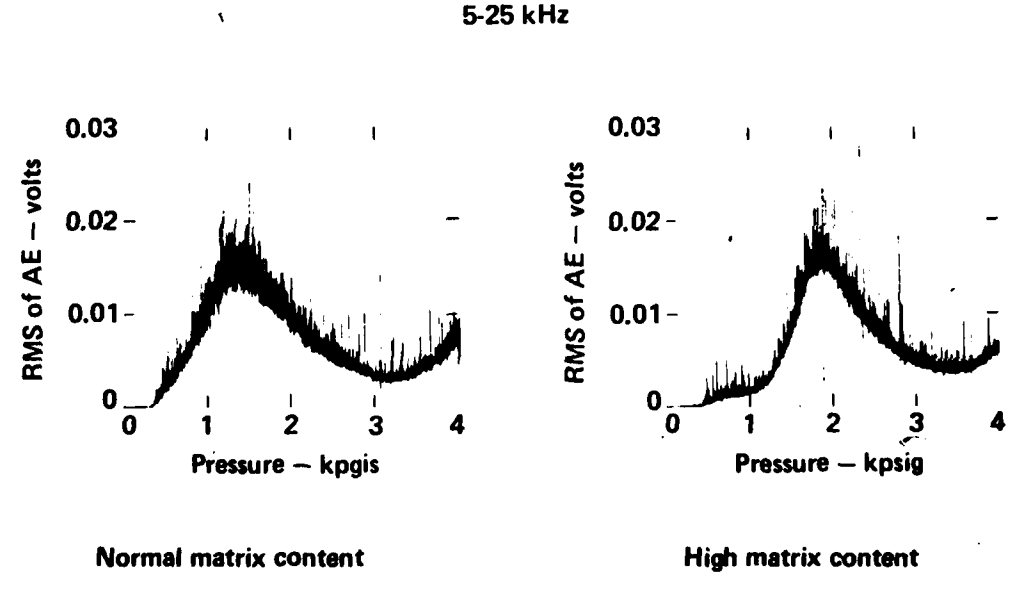

Figure 4

LOW MATRIX CONTENT SUBSTANTIALLY REDUCES AE LEVELS IN THE FIRST PEAK STRESS REGION

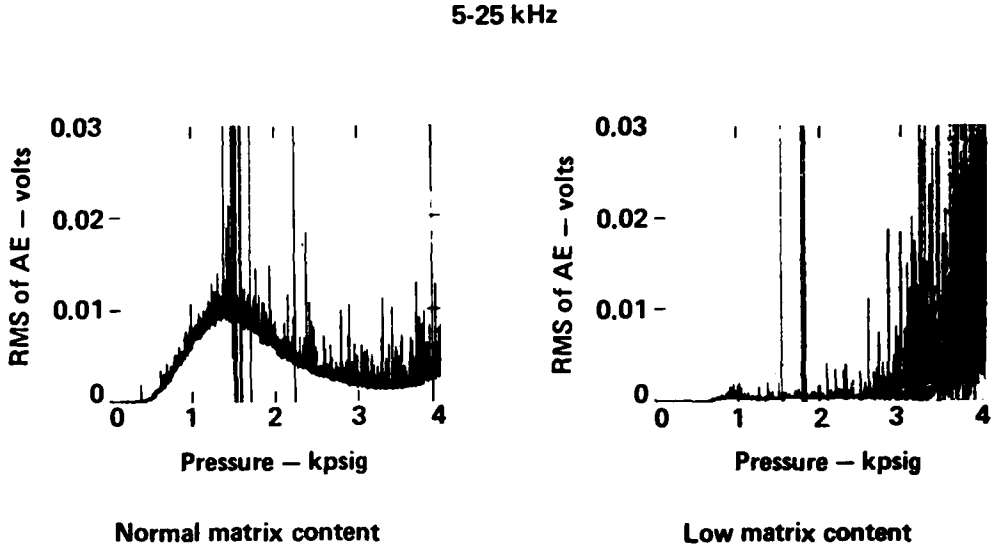

Figure 5

DAMAGING OR CHANGING THE FIBER BY REWINDING IT AND HEATING IT TO 180°C FOR ONE HOUR SUBSTANTIALLY INCREASES THE FIRST AE PEAK AND RESULTS IN MORE BURST TYPE AE AT HIGHER PRESSURES

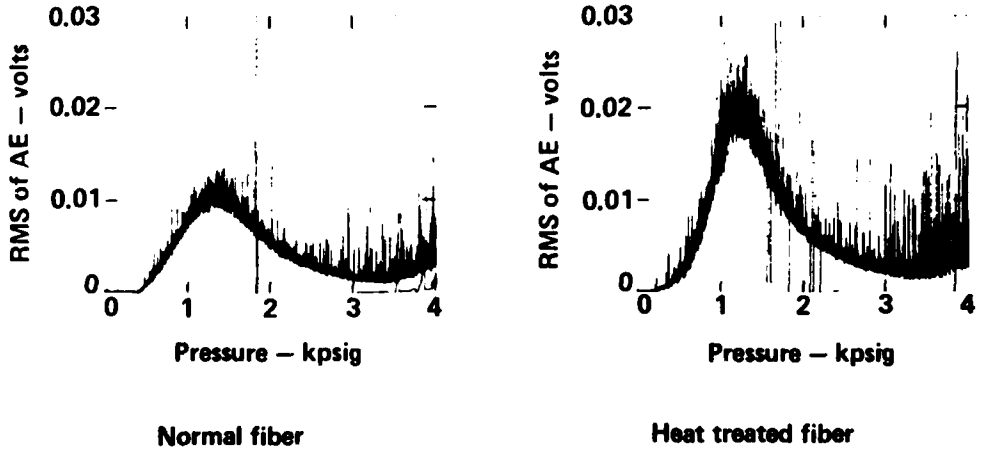

Figure 6

HIGH HUMIDITY REDUCES THE LEVEL OF THE FIRST AE PEAK

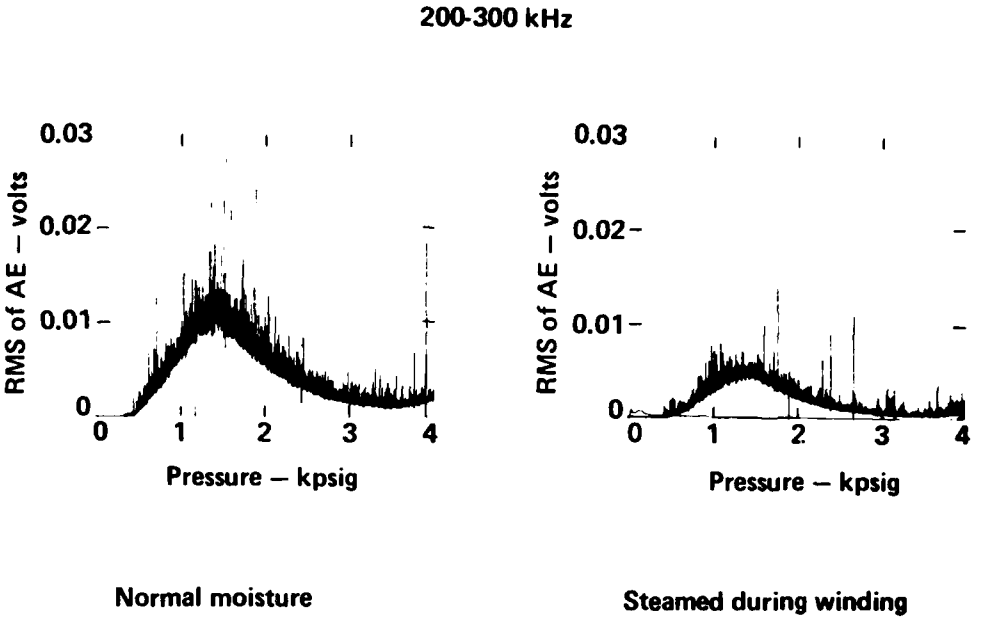

Figure 7

EXAMPLES OF ACOUSTIC EMISSION (AE) CHARACTERIZATION OF DAMAGE CONDITIONS DURING INITIAL LOADING OR UNDER SERVICE LIFE

The usefulness of analytical descriptions of performance of fiber composite articles under loading depends upon the degree to which the analytical description accounts for the real condition of the composite article. Analytical descriptions which do not account for significant changes in the condition of the composite as a function of load and/or time have limited usefulness. Acoustic emission (AE) is a convenient technique to characterize the load and/or time dependent damage accumulation. Figure 8 demonstrates that the application of a proof load induces considerable damage which changes the condition of the composite material. In Figs. 9 and 10, the accumulation of damage under stress rupture and fatigue test conditions is shown. Figure 11 shows the dramatic drop in damage which results from changing from a room temperature to an elevated temperature proof test. Figure 12 illustrates the potential of AE techniques to characterize damage according to particular damage mechanisms.

HIGH SENSITIVITY NECESSARY FOR MEASUREMENT OF UNIFORMLY DISTRIBUTED DAMAGE AND LOW SENSITIVITY FOR LOCAL DAMAGE

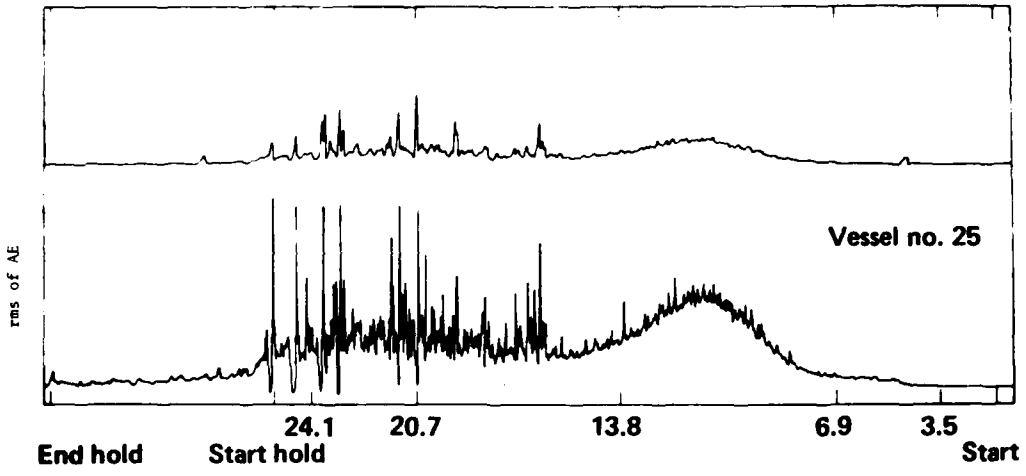

Figure 8

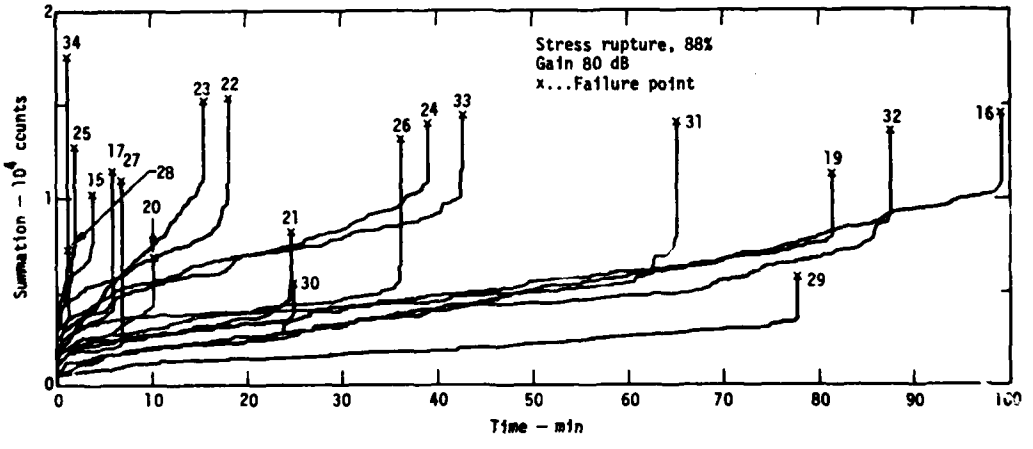

Figure 9

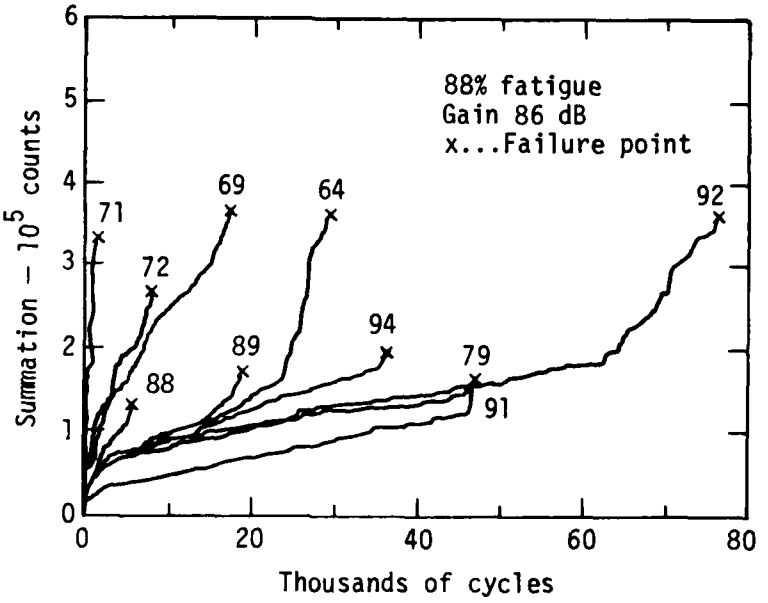

Figure 10

AE CHARACTERIZATION OF REDUCTION IN DAMAGE DUE TO ELEVATED TEMPERATURE PROOF TEST

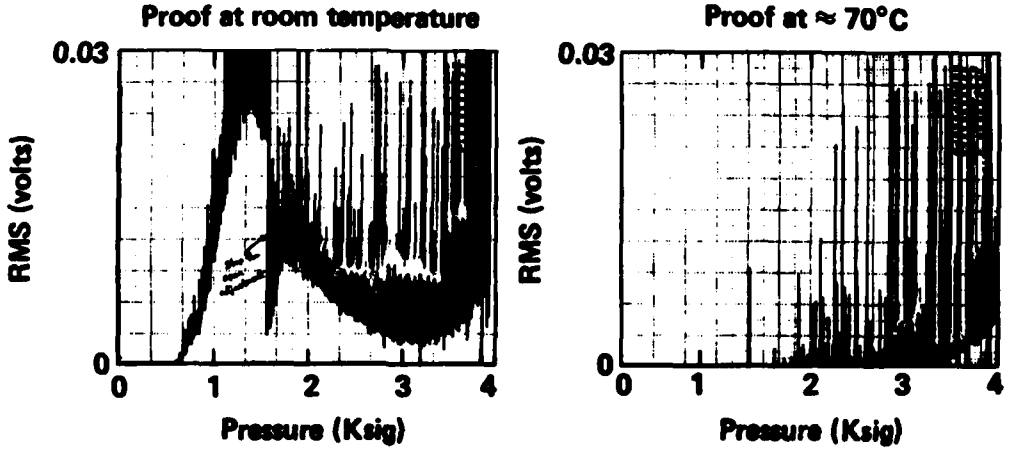

Figure 11

AE USED TO CHARACTERIZE DAMAGE BY INDIVIDUAL SOURCE MECHANISMS

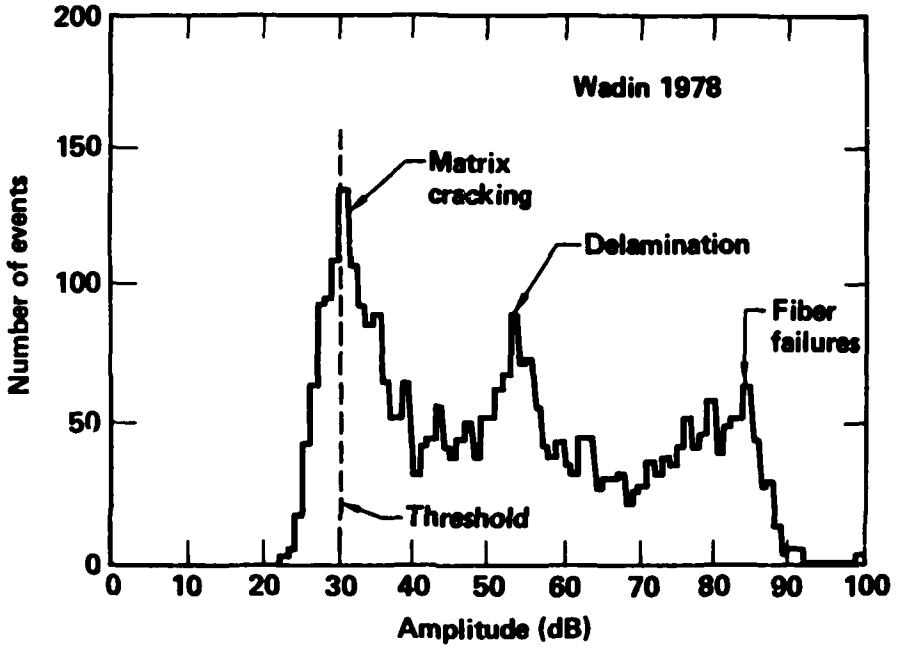

Figure 12

ACOUSTO-ULTRASONIC CHARACTERIZATION OF FIBER REINFORCED COMPOSITES

by Alex Vary

National Aeronautics and Space Administration
Lewis Research Center
Cleveland, Ohio

ABSTRACT

The acousto-ultrasonic technique combines advantageous aspects of acoustic emission and ultrasonic methodologies. Acousto-ultrasonics operates by introducing a repeating series of ultrasonic pulses into a material. The waves introduced simulate the spontaneous stress waves that would arise if the material were put under stress as in the case of acoustic emission measurements. These benign stress waves are detected by an acoustic emission sensor. The physical arrangement of the ultrasonic (input) transducer and acoustic emission (output) sensor is such that the resultant waveform carries an imprint of morphological factors that govern or contribute to material performance. The output waveform is quite complex, but it can be quantitized in terms of a "stress wave factor." The stress wave factor, which can be defined in a number of ways, is essentially a relative measure of the efficiency of energy dissipation in a material. If flaws or other material anomalies exist in the volume being examined, their combined effect will appear in the stress wave factor.

INTRODUCTION

The acousto-ultrasonic approach provides a potential alternative to widely used acoustic emission and ultrasonic techniques for verification of composite integrity and strength as well as degradation due to service conditions. Although conventional pulse-echo ultrasonics readily detects flaws, it is often difficult to correlate a detected flaw to overall performance. Additionally, evaluation of strength loss after use may depend on sensing subtle changes that are distributed throughout the material rather than isolated flaws. Acoustic emission techniques can be used to evaluate the integrity of a material as a whole. The problem with acoustic emission is that the material structure must be put under stress to produce spontaneous emissions from induced flaw growth. It is difficult to predict what such application of stress does to the life of the item being tested especially in the case of composites.

Laboratory studies have uncovered strong correlations between the acousto-ultrasonic stress wave factor and ultimate and interlaminar shear strength in composite laminates. This is in addition to the technique's ability to locate overt defects. Studies are underway to define the full application spectrum of the technique especially relative to measurements of material strength, impact damage, and degradation from thermal and chemical exposure. This report highlights salient aspects of the acousto-ultrasonic technique, the nature of the equipment used, and typical results obtained with composite laminates.

BACKGROUND

Fiber reinforced composite laminates exhibit a variety of failure modes due to their complex, anisotropic nature. The initial stage of failure can be explained in terms of three fundamental modes: tensile, shear, or compressive failure of the matrix; tensile or compressive failure of the fibers; or fiber/matrix interface failure. Subsequent to the occurence of any of these modes, ultimate failure will tend to involve complicated interactions of all three. Governing factors include variations in fiber fraction, microvoid content, matrix material condition, etc. (Ref. 1).

The most widely used nondestructive evaluation (NDE) techniques, i.e., pulse-echo ultrasonics, C-scan ultrasonics, acoustic emission, etc., do not provide a clear correlation between the presence of overt defects and their effects on the failure of fiber reinforced composites. Attempts to relate defects to fracture mechanisms have met with mixed results. When artificial defects are introduced in laboratory specimens, they may exhibit failure modes unrelated to these intentional flaws. Moreover, adverse effects of many naturally-occuring defects cannot be accurately predicted in all cases and their presence may often be ignored (Ref. 2).

Conditions that predispose composite structures to eventual failure can consist of dispersed microstructural irregularities that surround larger, discrete, and readily-detectable flaws. Even when these overt flaws are quite large, as in the case of significant delaminations, the entire integrated defect state should be considered. As illustrated in Fig. 1, a holistic approach combines nondestructive characterization of defects with characterization of material environments in which the defects reside. There is a need for NDE techniques that provide information on how defects, both maroscopic and microscopic, are likely to interact in the material as a whole (Ref. 3). Even in the absence of these types of defects appropriate NDE techniques are still needed to verify that a composite has the strength and endurance properties intended by the designer.

The acousto-ultrasonic approach described herein is aimed at characterization of composite laminates in accordance with the above-mentioned needs. The novel approach described addresses problems peculiar to highly attenuating, anisotropic materials such as fiber reinforced composites. It will be shown that this approach does yield information on the integrated defect condition in such materials. In the cases cited the integrated defect condition is associated with anomalous distributions of microvoids, global variations in fiber/resin ratio, and fiber orientation.

ACOUSTO-ULTRASONIC CONCEPT

The acousto-ultrasonic technique is predicated on the concept that during failure, spontaneously-generated stress waves interact with material morphology and contribute to microcracking and catastrophic crack extension (Refs. 3 and 4). This stress wave interaction is governed by factors such as scattering, dispersion, and reflection due to microstructure and boundary conditions. As indicated in Fig. 2, the same factors modulate ultrasonic signals used in NDE. It is natural to expect that because of their similarity to spontaneous stress waves, artificially introduced ultrasonic waves simulate the way stress waves respond to material conditions. By use of benign ultrasonic interrogation it should be possible to determine a modulation transfer function that describes the behavior of actual stress waves. This would reveal the character and magnitude of stress wave energy transfer during failure processes, at least during initial stages.

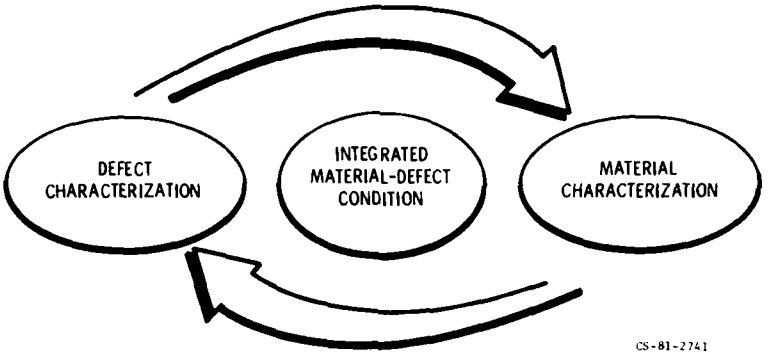

Figure 1. - Diagram illustrating the relation of defect and material characterization to defining the integrated effect of the material-defect state on stuctural integrity and life.

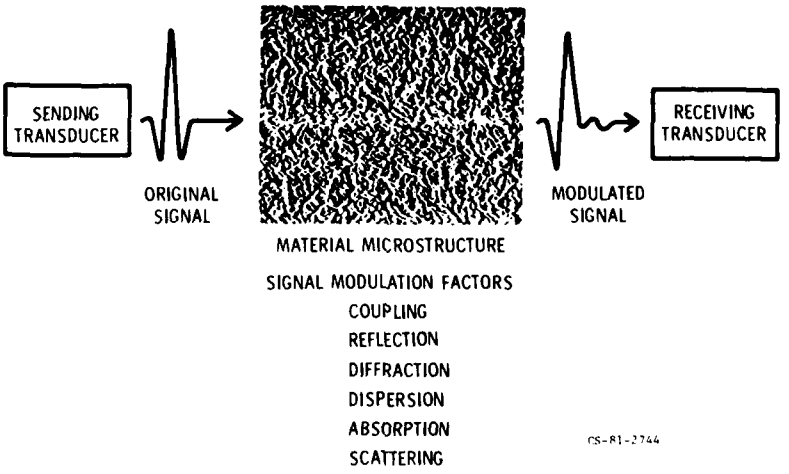

Figure 2. - Depiction of material microstructure as an ultrasonic wave filter in which a standard reference signal becomes modulated according to a definable transfer function.

The technique described herein affords an indirect but effective means for characterizing the stress wave energy propagation characteristics of composite laminates. The procedure and apparatus are designed to evoke wave interactions that mimic acoustic emission (stress) waves in a material undergoing deformation or experiencing microcracking (Refs. 5 and 6). It will be seen that measurement of these simulated acoustic emission waves correlates strongly with material microstructure and mechanical strength in the case of composite laminates.

Correlations with material properties are obtained by measurement of a "stress wave factor" (Refs. 7 and 8). The stress wave factor may be defined as a measure of the efficiency of stress wave energy transmission. The factor provides a means for rating the efficiency of dynamic strain energy transfer. In unidirectional composite laminates tested thus far (Ref. 9), the stress wave factor is greatest along the fiber direction which is also the direction of maximum strength.

Once microcracking starts in the brittle matrix or fibers, it is to be expected that prompt dissipation of stress wave energy away from crack initiation sites contributes to dynamic integrity and ultimate strength. Regions of

small values of the stress wave factor are regions of higher ultrasonic attenuation (Ref. 10). These are also observed to be weaker regions where dynamic strain energy is likely to concentrate and promote further microcracking and failure (Ref. 9).

APPARATUS AND OPERATIONAL FACTORS

Apparatus for making acousto-ultrasonic measurements is shown in Fig. 3 and a block diagram appears in Fig. 4. The acousto-ultrasonic wave is generated by means of a series of broadband ultrasonic pulses. The pulses are introduced into the material of normal incidence by means of an ultrasonic transducer directly coupled to the surface. A fixed distance away an acoustic emission receiving transducer is coupled to the surface. The simulated stress wave sensed by the receiving transducer consists of a large number of oscillations due to multiple reverberations within the material specimen.

Typical waveforms for the ultrasonic input and acousto-ultrasonic output are illustrated in Fig. 5. On the right-hand side of Fig. 5 are the echoes that rebound from the back surface of the specimen opposite the input transducer. For each pulse of the input transducer there will be a set of discrete back surface echoes. The left-hand side of Fig. 5 shows a typical signal sensed by the receiving transducer. The received signal is complex because it consists of the superposition of a large number of reflected signals as indicated by the ray traces in Fig. 6. Each ray represents a unique portion of a reflected wavefront and each has a unique arrival time, depending on the number of reflections from the boundary surfaces of the material.

The acousto-ultrasonic waveform is a "composite" waveform and its characteristics depend on a number of factors: constructive/destructive interference between individual wavefronts, angle of incidence of the individual reflections, mode conversions, etc. Because of these factors the composite waveform will be influenced by material density, tensile modulus, Poisson's ratio, and other material properties. The character of the acousto-ultrasonic waveform will also be influenced by ultrasonic velocity, attenuation, and frequency bandpass properties peculiar to the material macro- and micro-structure.

It is possible to compare different materials by analyzing the acousto-ultrasonic waveform provided other test conditions are reproduced exactly, e.g., thickness, spacing, coupling. As indicated in Fig. 5 the analysis of

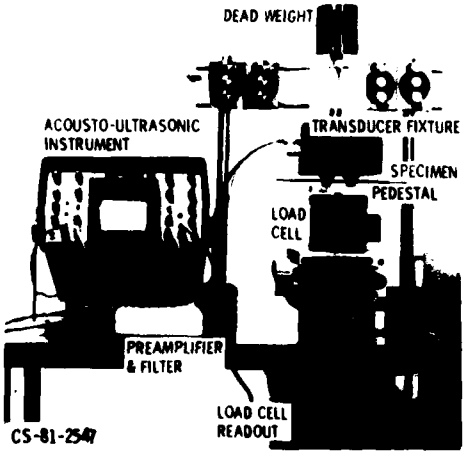

Figure 3. - Apparatus for measuring acousto-ultrasonic stress wave factor. The transducer fixture houses the sending and receiving transducers shown coupled to a composite laminate panel. The weight and load cell readout serve to assure reproducible coupling forces. The equipment shown is intended only to typify one of the numerous alternative arrangements possible, it should not be inferred that data presented herein was obtained with this particular arrangment.

the acousto-ultrasonic waveform can proceed by measuring its acoustic energy or spectral signature. Variations in acoustic energy or spectral signature will arise from variations in the material properties, macro- and micro-structure, flaws, etc.

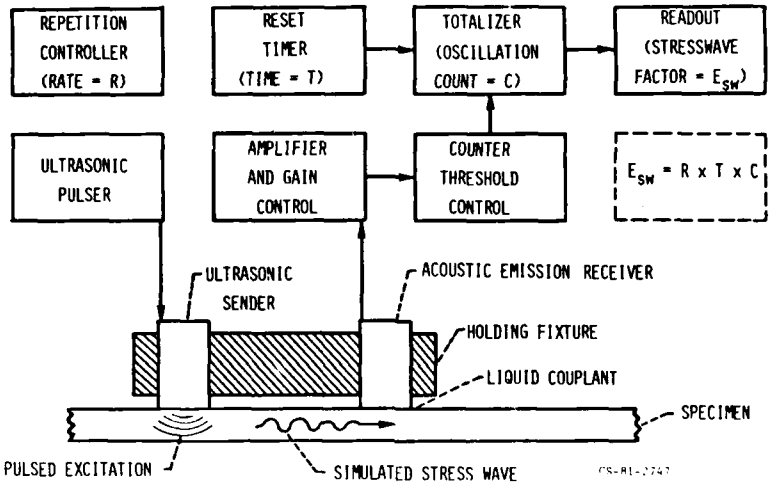

Figure 4. - Diagram of acousto-ultrasonic apparatus for measurement of the stress wave factor E_{SW} = (R)(T)(C). The quantity C is the number of "ringdown" oscillations exceeding a preset threshold voltage as in the acousto-ultrasonic waveform shown in figure 5.

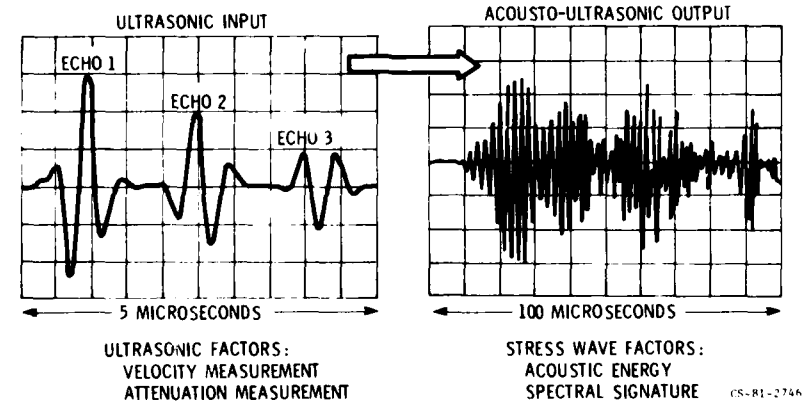

Figure 5. - An ultrasonic plused input (left) is used to excite the acousto-ultrasonic output waveform (right) from which the stress wave factor, E_{SW}, is measured. Both the ultrasonic input pulse echoes and acousto-ultrasonic output can be measured by means of the factors indicated: velocity, attenuation for through-transmission pulse echoes; acoustic energy, spectral signature for the acousto-ultrasonic stress waveform.

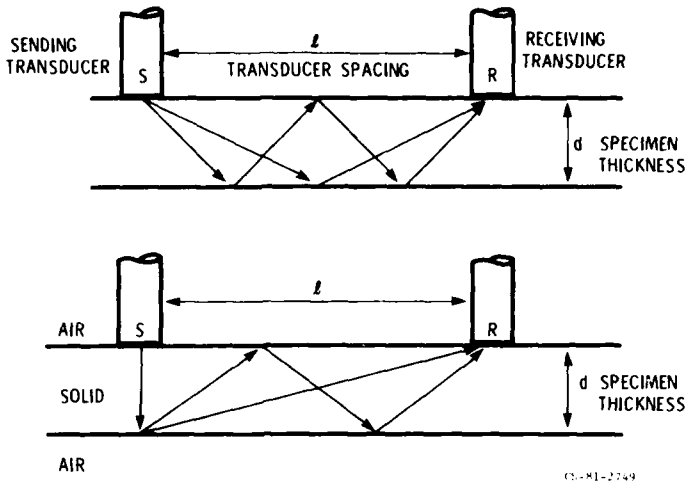

Figure 6. - Generalized ray traces of principal longitudinal wave reflections that become superimposed in the "composite" acousto-ultrasonic waveform. Each successive ray will be delayed by some multiple of the "round-trip" travel time associated with the specimen thickness. The amplitude of each successive wavefront will depend on its particular angle of incidence during reflections. These factors contribute to constructive and destructive interference effects that determine the complex character of the resultant acousto-ultrasonic waveform as in figures 5 and 7.

STRESS WAVE FACTOR

There are several ways to measure the energy content of the acousto-ultrasonic waveform: peak detection, decay or attenuation slope, root-mean-square, or a simple ring-down count. This latter method borrowed from acoustic emission technology is illustrated in Fig. 4.

After the pulse repetition rate (R) is set, a reset timer in the receiver circuit is set to a predetermined interval (T). The acousto-ultrasonic signal is fed to a counter-totalizer that counts the number (C) of oscillations that exceed a voltage threshold just above the noise level for a given amplification setting appropriate to the material and transducer spacing conditions. The product (R) (T) (C) is taken as the "stress wave factor" E_{sw} which in this case is the ring-down count for a standard number of identical waveforms.

With above-described method the stress wave factor can be used to rank a series of material specimens according to the stress wave energy intensity transmitted. Higher values for E_{sw} correspond to higher intensities (longer ring-down) which correspond, in turn, to materials that transmit acousto-ultrasonic stress wave energy more efficiently.

An alternative method for assigning a numerical value to the stress wave factor is that of first generating an energy envelope for the stress waveform and assigning the peak value to E_{sw}. A further alternative is to perform a spectrum analysis of the stress waveform and assigning the peak value of a particular spectral component to E_{sw}. It is true that each method for evaluating a stress wave factor will give a different numerical result. Each method will also highlight a particular aspect of the stress waveform and yield information on a different aspect of a material's characteristics. The idea is to choose a consistent method to rank a series of specimens. Illustrative examples of methods for analyzing acousto-ultrasonic waveforms are presented in the next section.

EXPERIMENTAL CORRELATIONS

Examples of acousto-ultrasonic waveforms their energy curves and frequency spectra appear in Figs. 7 and 8. The effect of increasing microvoid content and corresponding decrease in transmitted energy in a unidirectional fiber composite laminate is apparent in Fig. 7. In these graphite/polyimide composites strength decreases rapidly as microvoid content rises above approximately 3 percent. The effect of laminate ply orientation on spectral signature is evident in Fig. 8. The frequency spectra were made with acousto-ultrasonic waves propagating parallel to the major axis of tensile specimens (Ref. 9). For both the graphite/epoxy and glass/epoxy specimens there is an obvious decrease in spectral peak energy corresponding to the decrease in plys with fibers running in the 0-degree or axial direction. These specimens exhibited a corresponding decrease in ultimate tensile strength, Fig. 9.

Figure 10 shows the stress wave factor, E_{sw}, plotted against the cure pressures used in making a series of graphite/polyimide 12-ply unidirectional laminates. Higher cure pressure is expected to yield higher-quality, higher-strength panels. The acousto-ultrasonic measurements revealed, however, that even when a key processing variable like cure pressure is controlled, inferior material can still result. In Fig. 10 the upper bound curve shown represents optimum stress wave transmission and, hence, optimum quality for a given cure pressure. Stress wave factor data appearing below the curve are for panels that exhibited higher void content and erratic fiber/resin ratio.

Figure 11 shows that increases in the value of the stress wave factor correspond to increases in interlaminar shear strength for the graphite/polyimide laminates. The interlaminar shear strength measurements were made with short beam shear specimens cut from composite panels made with a range of cure pressures. The data in Figs. 9 through 11 were all obtained using the previously-described ring-down method for evaluating E_{sw}. In the case of Figs. 9 and 11 a normalized stress wave factor N_{sw} is plotted against material strength. The normalization is based on the observation that for each class of composite structure there is a maximum E_{sw} ($= E_{max}$) for a

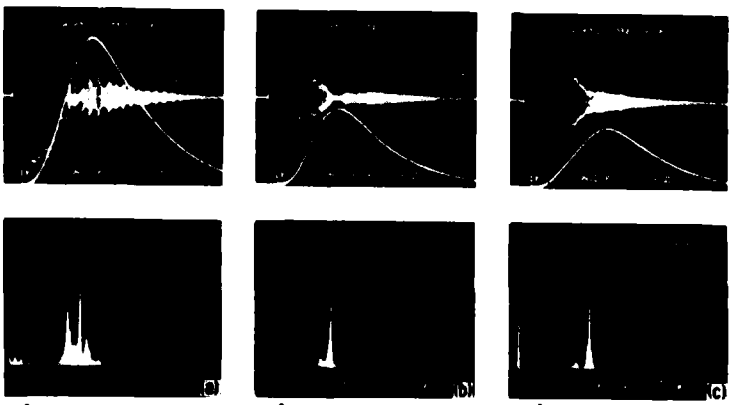

Figure 7. - Effect of microvoid content in fiber composite laminate. At the top are CRT traces of typical acousto-ultrasonic waveforms for graphite/polyimide samples with 0, 4, and 8 percent microvoid content. Superimposed are energy curves corresponding to the individual waveforms. Decreasing stress wave energy with increasing void content is also evident from the frequency spectra below the waveforms.

CS-81-2548

given set of operational conditions. This corresponds to a maximum strength that can be realized for that structure. It is convenient, therefore, to plot a normalized stress wave factor, $N_{SW}=(E_{SW}/E_{max})$ versus a normalized strength, as in Fig. 11.

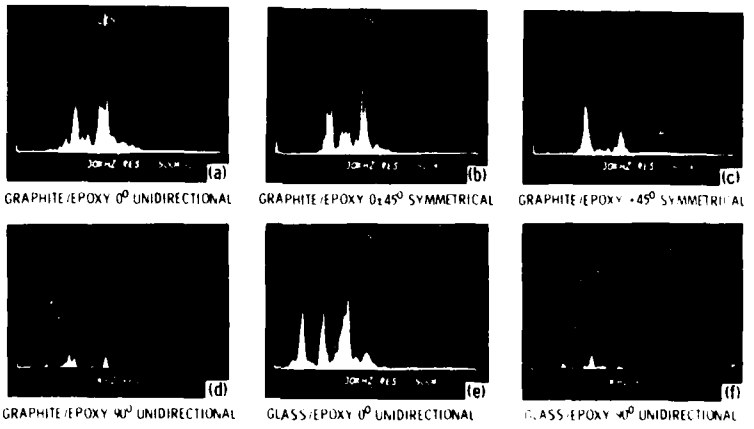

Figure 8. - Effect of various ply orientations in graphite/epoxy and glass/epoxy laminates. Results obtained with 8-ply tensile specimens. Frequency spectra shown are for typical acousto-ultrasonic waveforms obtained under standardized conditions. Spectral signatures, location of peaks, are functions of material thickness and also transducer and instrument bandpass characteristics.

CS-81-2549

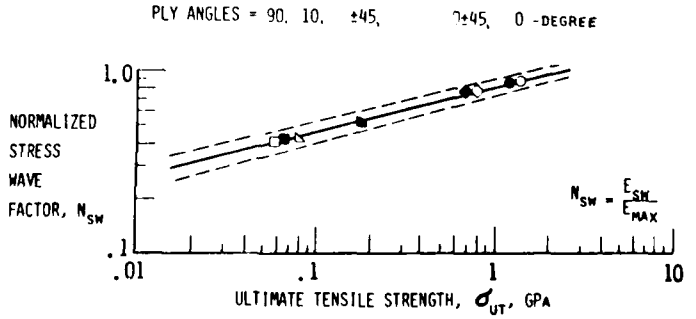

Figure 9. - Stress wave factor as a function of ultimate tensile strength for graphite/epoxy fiber composite laminates. Stress wave factor is normalized relative to its maximum value for the particular material specimens tested. The specimens were eight ply thick and the ply angles given are relative to the tensile loading axis (from ref. 9).

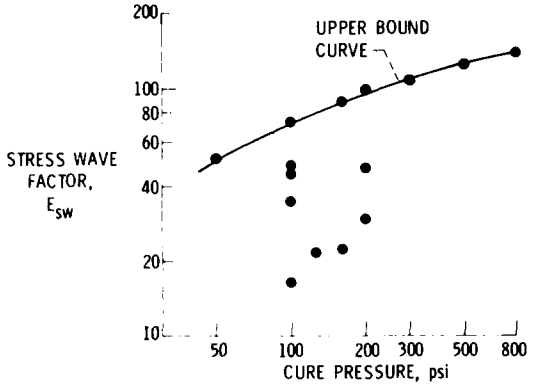

Figure 10. - Stress wave factor as a function of cure pressure applied during thermal forming of fiber composite laminates. The laminate panels were all 12-ply unidirectional. Upper bound curve represents highest quality panel for the indicated cure pressure. Data points below the curve have lower quality as indicated by stress wave factor and confirmed by other tests. Each data point represents 90 uniformly-spaced stress wave factor measurements per panel (from ref. 7).

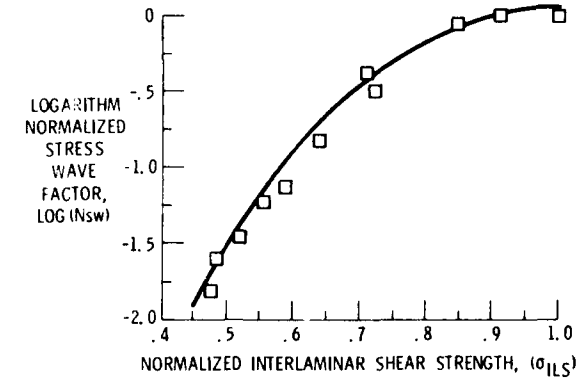

Figure 11. - Variation of acousto-ultrasonic stress wave factor with interlaminar shear strength in a 12-ply unidirectional fiber compostie laminate (ref. 10).

DISCUSSION

Acousto-ultrasonics is an unconventional approach to nondestructive evaluation of material properties. Nevertheless, it has clearly demonstrated potentials for assessing variations in mechanical strength and performance due to flaws and macro- and micro-structural anomalies in composite laminates.

In acousto-ultrasonics broadband pulses (typically 0.1 to 2 megahertz) are introduced and allowed to interact repeatedly within the material boundaries. When the resultant signal is finally extracted, it carries an imprint of numerous factors that govern or contribute to material performance. In many ways the acousto-ultrasonic waveform resembles the burst-type acoustic emission waveform that arises spontaneously in a material undergoing microcracking or crack extension. This similarity to spontaneous stress waves is the key to inferring material behavior and response to dynamic loading.

Although the acousto-ultrasonic waveform is quite complex it is susceptible to analysis by a variety of straightforward methods. It can be quantitized in terms of a "stress wave factor" which is essentially a relative

measure of the efficiency of energy dissipation in a material. If flaws or other anomalies exist in the volume being examined, their combined effect will be reflected in the stress wave factor. The stress wave factor can be readily evaluated in a number of different ways to give numerical ratings of the relative strength of a series of material specimens.

It should be noted that correlations between ultrasonic measurements and material strength have been obtained by other techniques (Ref. 11). For example, measurements of ultrasonic attenuation through the thickness of composite laminates have been correlated with interlaminar shear strength. Ultimate tensile strengths of composite specimens have been correlated with ultrasonic moduli based on combining density and velocity measurements. Although in execution these techniques are more complicated they are complementary to acousto-ultrasonics. Obviously, there will be situations in which one of these techniques is the preferred one for assessing relative variations in composite strength.

One of the advantages of the acousto-ultrasonic method described herein and depicted in Figs. 4 and 6 is that the stress wave signal propagates in a direction parallel to the bounding surfaces of laminate panels. This is significant because the signal can run parallel to a major fiber direction or the direction that actual loads assume in use. Note also that the method requires only one side access and, in principle, accomodates a range of curvatures since the laminate surfaces will act as waveguides.

Alternate send-receive transducer arrangements can, of course, be employed. Certainly, the proximity of the transducers can be modified for best effect in a given composite structure. Or the transducers can be deployed on opposite sides of an article, possibly in exact opposition. This latter transducer arrangement would resemble that used in pulse transmission ultrasonics. The principal difference between acousto-ultrasonics and conventional ultrasonics, regardless of transducer arrangement, is in the manner of sensing and handling signals.

Perhaps the most advantageous aspect of acousto-ultrasonics relative to the more conventional techniques such as those mentioned previously is in overcoming the high attenuation common to most composite structures. It is often difficult to recover a set of undistorted echoes needed for velocity or attenuation measurements. As an alternative, acousto-ultrasonics affords a method for sensing and measuring the results of introducing discrete ultrasonic pulses after pronounced attenuation and dispersion by material factors. The acoustic emission sensor and circuitry provide the necessary sensitivity and amplification. In addition, acoustic emission processing tactics such as ring-down counting provide excellent methods for analysis of the resultant signals (Ref. 6).

Studies are progressing to define the operational spectrum and to examine other potential applications of the acousto-ultrasonic and stress wave factor concepts. For example, preliminary tests show that acousto-ultrasonics is a viable inspection tool for bonded structures like composite skin bonded to honeycomb reinforcement. Other preliminary tests currently in progress demonstrate the utility of acousto-ultrasonics in monitoring degradation of composite laminates due to thermal exposure and impact damage (Ref. 8).

It is apparent from a consideration of results obtained thus far that the acousto-ultrasonic approach can operate on three levels of sophisticaton: Firstly, as a coarse, go-no-go indicator of serious flaws or discontinuities. Secondly, as a means for ranking essentially defect-free materials according to inherent strength. Thirdly, as an investigative tool for identification of factors that govern or contribute to material property variations. This

latter aspect of acousto-ultrasonics, similarly with acoustic emission, depends on improving the understanding of waveform and frequency modifications induced by stress wave propagation in various composite media (Ref. 12).

Except in the first sense mentioned above, i.e., as an indicator of flawed regions in composite structures, current versions of the acousto-ultrasonic technique are essentially laboratory oriented. Accomplishment of the more sophisticated measurements suggested and illustrated herein is currently confined to laboratory specimens. In these latter cases careful control must be maintained over transducer positioning, coupling mode, pressure, etc. to achieve reproducible results. Possible field applications of the acousto-ultrasonic technique can be realized only if the necessary accomodations between the apparatus and test article are recognized and employed.

SUMMARY AND CONCLUSION

Acousto-ultrasonics combines complementary aspects of acoustic emission and ultrasonic technology. Acousto-ultrasonics provides an alternative that overcomes problems of conventional acoustic emission and ultrasonic techniques for the nondestructive evaluation of fiber reinforced composite laminates. The inspection of this class of materials can benefit from the sensitivity and signal processing methods of acousto-ultrasonics.

Examples given herein demonstrate the acousto-ultrasonic methodology and its viability for ranking composite laminates according to their mechanical strength as influenced by local flaws and anomalies in fiber content, fiber orientation, and microvoids. Although adaptable to field use for indicating serious flaws in composite structures the more sophisticated uses demonstrated for the technique have thus far been based on experiments conducted under laboratory conditions.

REFERENCES

1. A. Vary, "A Review of Issues and Strategies in Nondestructive Evaluation of Fiber Reinforced Composites," Proceeding of the Eleventh National SAMPE Technical Conference: New Horizons - Materials and Processes for the Eighties, Vol. 11, Society for the Advancement of Material and Process Engineering, Azusa, California (1979), pp. 166-177.
2. M. A. Hamstad, "On a Philosophy for Nondestructive Testing of Fiber Composites," Lawrence Livermore Laboratory Report UCID-17454 (1977).
3. A. Vary, "Concepts and Techniques for Ultrasonic Evaluation of Material Mechanical Properties," Mechanics of Nondestructive Testing (W. W. Stinchcomb, ed.), Plenum Press, New York (1980), pp. 123-141.
4. A. Vary, "Correlations Between Ultrasonic and Fracture Toughness Factors in Metallic Materials," Fracture Mechanics (C. W. Smith, ed.), American Society for Testing and Materials, Philadelphia (1979), STP-677, pp. 563-578.
5. D. M. Egle and A. E. Brown, "A Note on Pseudo-Acoustic Emission Sources," Journal of Testing and Evaluation, Vol. 4, No. 3 (1976), pp. 196-199.
6. D. M. Egle, "A Stochastic Model for Transient Acoustic Emission Signals," Journal of the Acoustical Society of America, Vol. 65, No. 5 (1979), pp. 1198-1203.
7. A. Vary and K. J. Bowles, "An Ultrasonic-Acoustic Technique for Nondestructive Evaluation of Fiber Composite Quality," Polymer Engineering and Science, Vol. 19, No. 5 (1979), pp. 373-376.

8. J. H. Williams, Jr. and N. R. Lampert, "Ultrasonic Evaluation of Impact-Damaged Fiber Composite," Materials Evaluation, Vol. 38, No. 12 (1980), pp. 68-72.
9. A. Vary and R. F. Lark, "Correlation of Fiber Composite Tensile Strength with the Ultrasonic Stress Wave Factor," Journal of Testing and Evaluation, Vol. 7, No. 4 (1979), pp. 185-191.
10. A. Vary and K. J. Bowles, "Ultrasonic Evaluation of the Strength of Unidirectional Graphite/Polyimide Composites," Proceedings Eleventh Symposium on Nondestructive Evaluation, American Society for Nondestructive Testing, Columbus, and Southwest Research Institute, San Antonio (1977), pp. 242-258.
11. A. Vary, "Ultrasonic Measurement of Material Properties," Research Techniques in Nondestructive Testing, Volume 4 (R. S. Sharpe, ed.), Academic Press, London (1980), pp. 159-204.
12. R. E. Green, Jr., "Basic Wave Analysis of Acoustic Emission," Mechanics of Nondestructive Testing (W. W. Stinchcomb, ed.), Plenum Press, New York (1980), pp. 55-76.

APPLICATION OF FOURIER TRANSFORM INFRARED SPECTROSCOPY FOR QUALITY CONTROL ANALYSIS OF EPOXY RESIN PREPREGS USED IN HELICOPTER ROTOR BLADES

T. F. Saunders, M. Ciulla, S. Wehner, and J. Brown

Army Materials and Mechanics Research Center
Watertown, MA 02172

ABSTRACT

SP-250 epoxy resin/glass fiber prepreg (3M Co.) is one of the basic materials of prime importance to the U.S. Army. It is presently being used for helicopter rotor blades, for CH-46 and CH-47 helicopters. Present quality control methods involve complex and time-consuming HPLC procedures. However, FT-IR provides enough information from a single spectrum, with five functional group peak absorbances being measured, to allow acceptance or rejection of lots of prepreg.

FT-IR allows reproducible quantitative absorbance determinations of the 3400 cm^{-1}-OH, 2180 cm^{-1} -C≡N, 1140 cm^{-1} aliph. ether and 915 cm^{-1} epoxide. Spectra are obtained on thin films of THF/DMF extracts from the epoxy/glass prepreg cast on KBr plates. ATR spectra were not good enough for precise quantitative determination.

INTRODUCTION

The SP-250 epoxy resin/glass fiber prepreg system is one of the basic organic materials of prime importance to the U.S. Army and U.S. Navy. It is presently being used in the rotor blades for the CH-46 and CH-47 helicopters. Present quality control analytical methods involve complex and time-consuming HPLC or GPC procedures. In the present work, Fourier Transform Infrared Spectroscopy (FT-IR) spectra were interpreted quantitatively with relative absorbances being determined for five peaks - the $3400cm^{-1}$ -OH peak, $2180cm^{-1}$ -C≡N, $1140cm^{-1}$ C-O-C, $1080cm^{-1}$ aromatic Cl, and $915cm^{-1}$ epoxide peaks. These frequencies were normalized to the $1510cm^{-1}$ aromatic peak. Quantitative absorbances were determined using the baseline method. FT-IR allows reproducible quantitative absorbance determinations with statistically good reproducibility. Spectra were obtained from thin films of THF/DMF extracts from the epoxy/glass prepreg cast on KBr plates. (See Figures 1-3.) Quantitative absorbance determination from FT-IR provides enough information from a single spectrum, with five functional group peak absorbances being measured, to allow acceptance or rejection of lots of prepreg.

DISCUSSION

The current state-of-the-art technique of Fourier-Transform Infrared Spectroscopy was employed to obtain IR spectra of thin films of real and simulated SP-250 prepreg formulations from thin films cast on KBr salt plates. A statistical population of 30 spectra each, were obtained from each of the following:

1) Non-B-staged SP-250 resin system with 2% dicyandiamide.
2) Non-B-staged SP-250 resin system with 4% dicyandiamide.
3) Non-B-staged SP-250 resin system with 6% dicyandiamide.
4) Non-B-staged SP-250 resin system with 8% dicyandiamide.
5) AMMRC SP-250 prepreg #178 (3M).
6) AMMRC SP-250 prepreg #180 (3M).

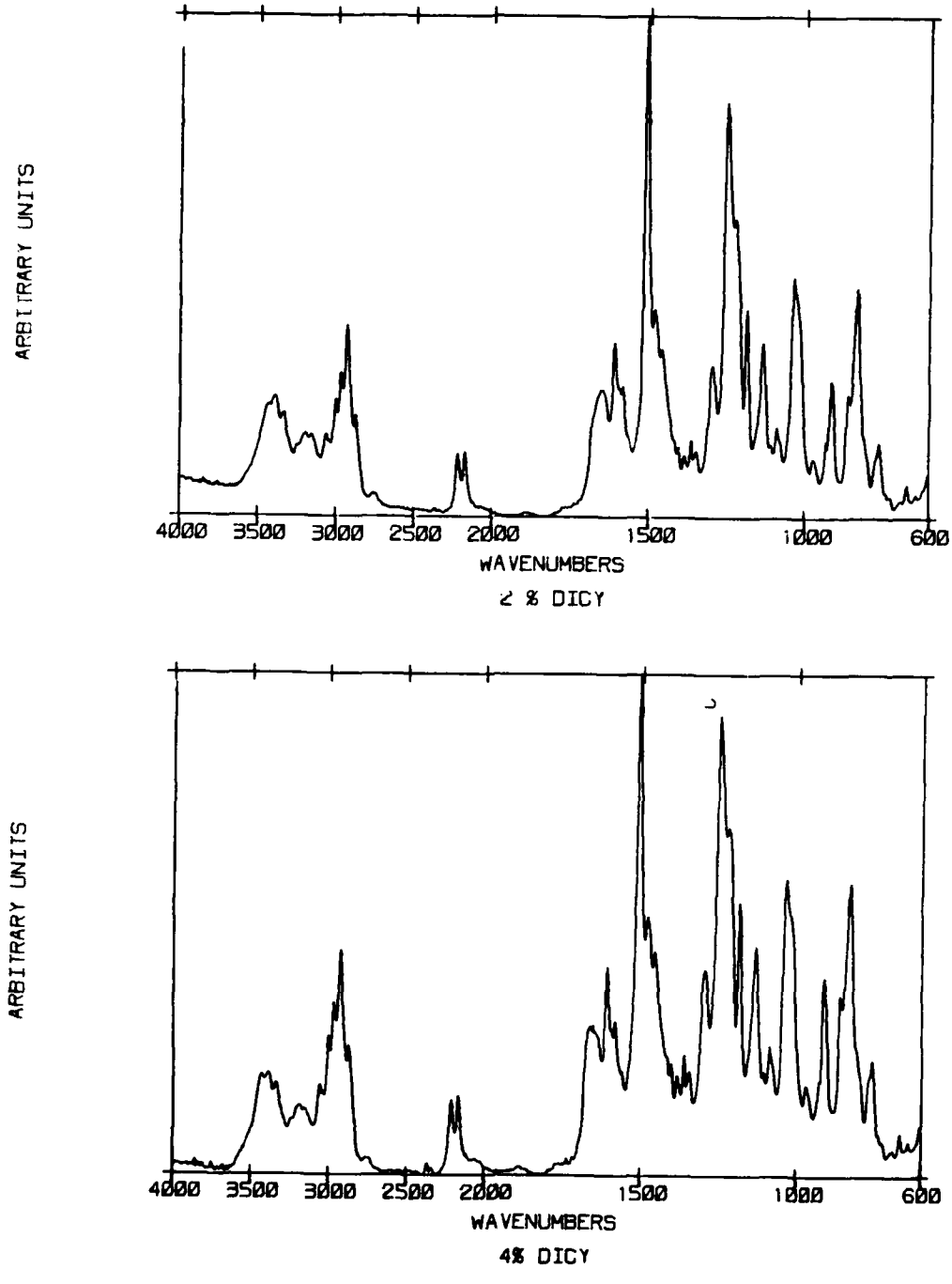

Figure 1. FT-IR spectra of SP-250 epoxy formulations.

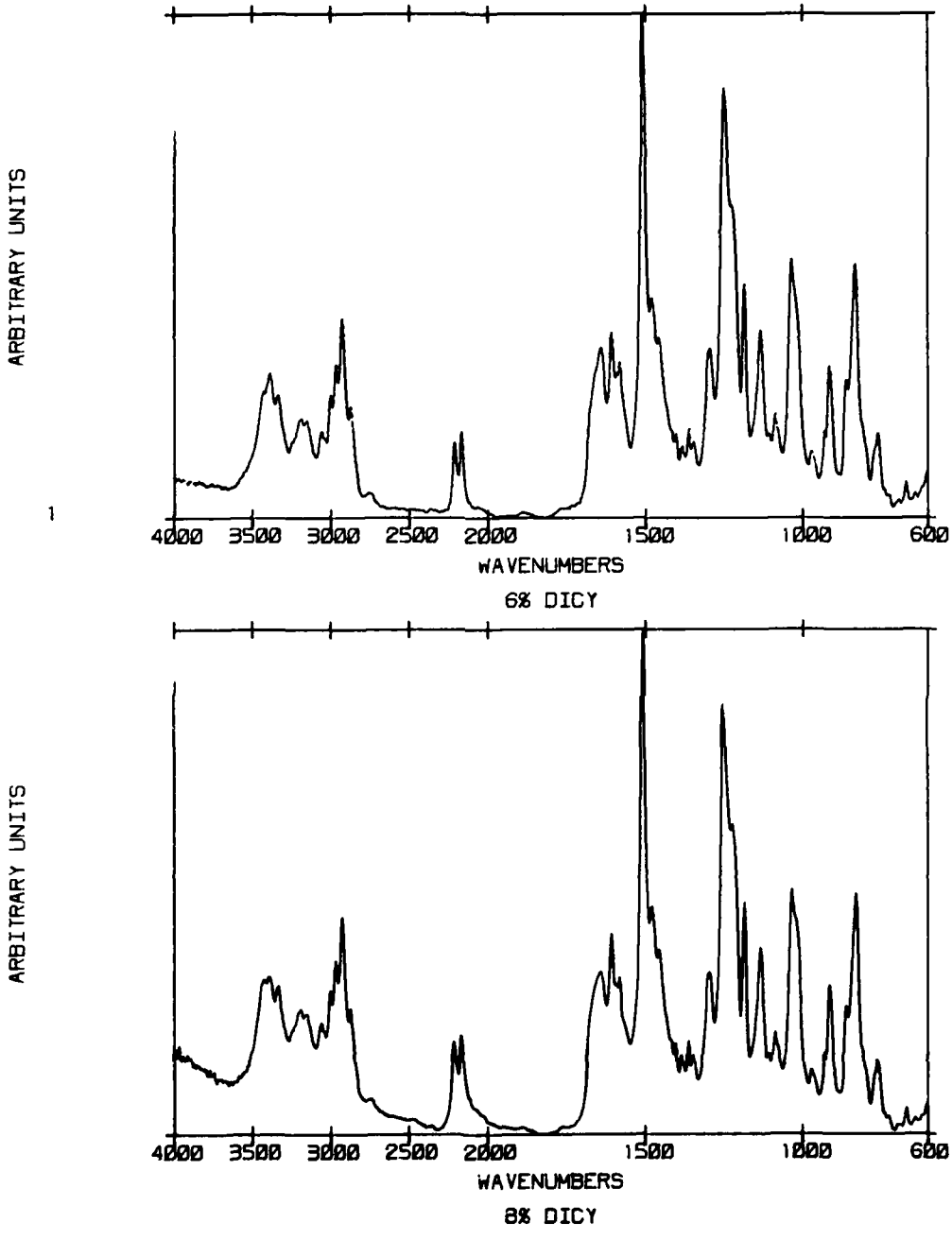

Figure 2. FT-IR spectra of SP-250 epoxy formulations.

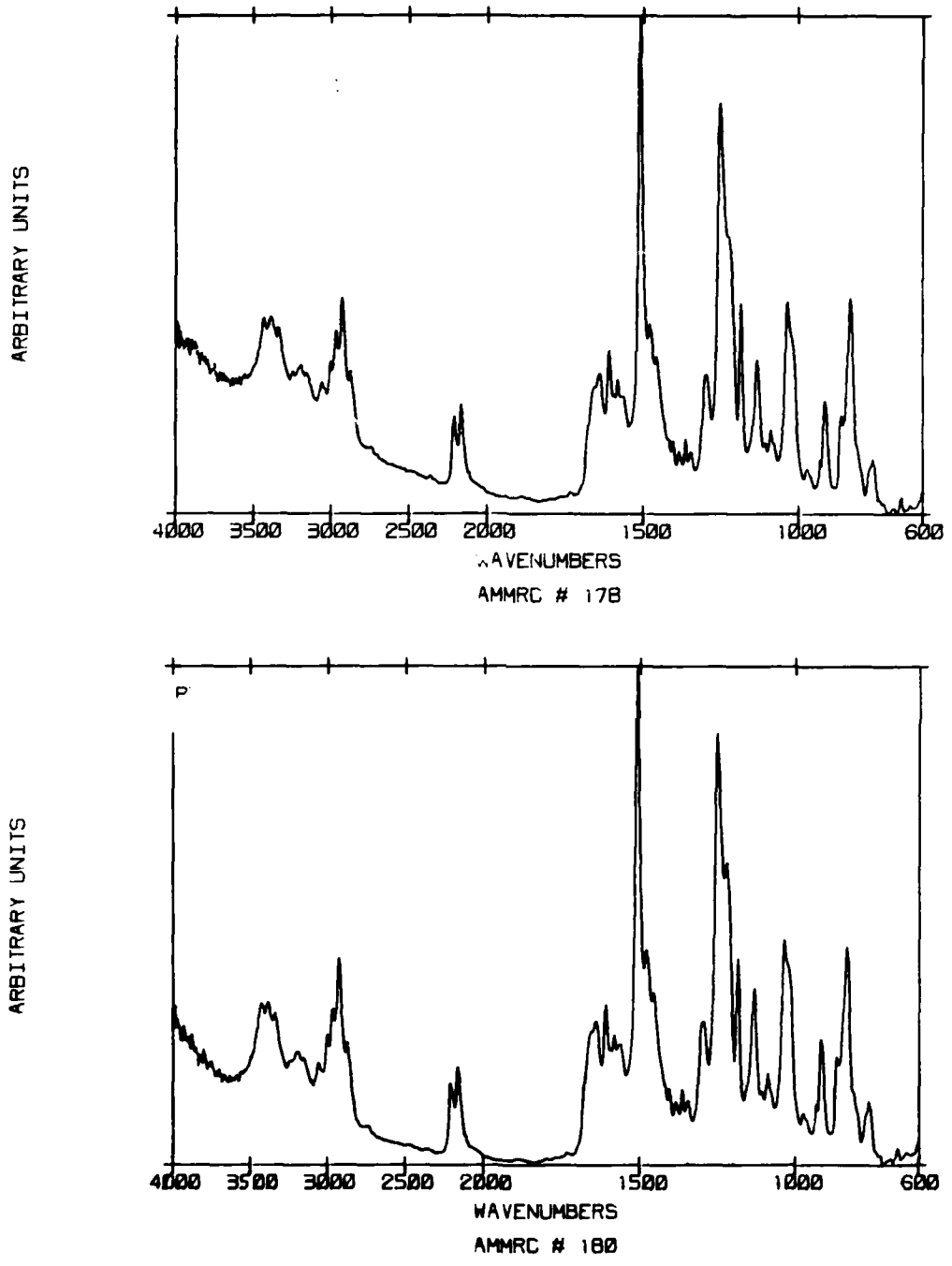

Figure 3. FT-IR spectra of SP-250 prepregs.

3M's SP-250 epoxy prepreg resin system consists of the following ingredients:

Resins

1) Epoxy Cresol Novolac (ECN)

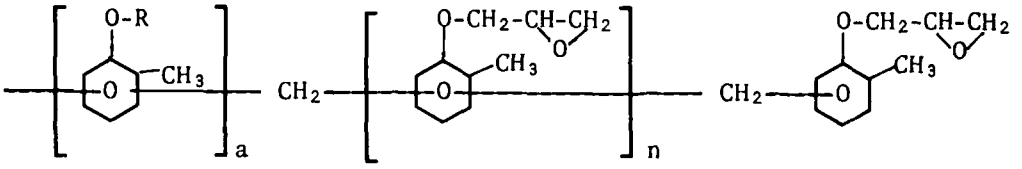

2) Diglycidyl Ether of Bisphenol A (DGEBA)

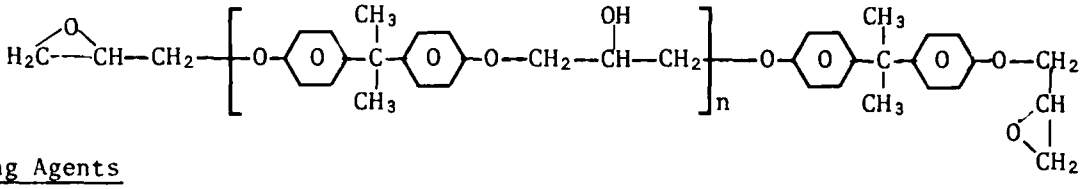

Curing Agents

1) Dicyandiamide

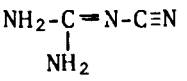

2) Monuron

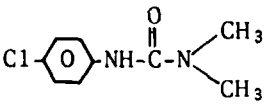

SP-250 prepregs contain approximately 30 weight percent resin formation and approximately 70 weight percent glass fiber.

The thin films for FT-IR analysis were cast on KBr plates from dilute solution in a 50/50 by volume blend of THF/DMF. This particular combination of solvents provided thin films with the best optical clarity, since there was no precipitation of dicy, as occured with other solvents. Two-inch squares of prepreg were extracted with the THF/DMF blend to provide solutions for thin films. Thin films were cast on KBr plates with just enough heat to flash off the solvent.

Thirty spectra were obtained from thirty different thin films for each of the aforementioned six groups of resin formulations and prepregs. Relative absorbances were determined using the baseline method for the purposes of this investigation,

although FT-IR computer software for doing this analysis is available. The base line method was chosen for two reasons:

1) Ready adaptability of the method to less sophisticated instruments, including dispersive types of instruments.

2) Speed and convenience of making a single determination in practice.

Statistical averages, standard deviations, and % standard deviations were computed for each group of 30 samples, for each of the quantitative absorbances of the five peaks chosen. These are listed in Table I.

TABLE I

STATISTICAL REPRODUCIBILITY OF FT-IR ABSORBANCES

	A3400/A1510	A2180/A1510	A1140/A1510	A1080//A1510	A915/A1510
8% Dicy					
average	0.233	0.259	0.244	0.076	0.234
standard dev.	0.0109	0.0177	$4.47X10^{-3}$	$3.74X10^{-3}$	$4.59X10^{-3}$
% st'd. dev.	4.68%	6.84%	1.83%	4.94%	1.96%
6% Dicy					
average	0.231	0.227	0.256	0.076	0.237
standard dev.	0.0208	$9.90X10^{-3}$	$3.33X10^{-3}$	$4.29X10^{-3}$	$2.93X10^{-3}$
% st'd. dev.	9.04%	4.36%	1.30%	5.66%	1.23%
2% Dicy					
average	0.253	0.183	0.256	0.0714	0.247
standard dev.	$8.47X10^{-3}$	0.0101	$5.71X10^{-3}$	$1.79X10^{-3}$	$6.30X10^{-3}$
% st'd. dev.	3.35%	5.50%	2.23%	2.50%	2.55%
4% Dicy					
average	0.205	0.188	0.245	0.0705	0.265
standard dev.	$8.95X10^{-3}$	$8.89X10^{-3}$	$5.89X10^{-3}$	$2.61X10^{-3}$	0.0112
% st'd. dev.	4.37%	4.72%	2.41%	3.69%	4.22%
AMMRC #178					
average	0.200	0.255	0.222	0.0649	0.219
standard dev.	0.0123	0.0144	$3.54X10^{-3}$	$1.17X10^{-3}$	$5.56X10^{-3}$
% st'd. dev.	6.17%	5.65%	1.60%	1.80%	2.53%
AMMRC #180					
average	0.160	0.189	0.260	0.0744	0.219
standard dev.	$4.57X10^{-3}$	$5.61X10^{-3}$	$4.63X10^{-3}$	$1.35X10^{-3}$	$4.16X10^{-3}$
% st'd. dev.	2.86%	2.96%	1.78%	1.82%	1.90%

Examination of Table I permits the following pertinent observations:

1) The small values of % standard deviation for all groups are indicative of the excellent reproducibility of the FT-IR method for prepreg quality control.

2) Ascending concentrations of dicy exhibit ascending absorbances, for the Non-B-staged material.

3) In spite of the low absorbance of the $1080cm^{-1}$ aromatic chlorine peak, the standard deviations were small.

4) In all cases, the quantitative absorbances of Non-B-staged resin formulations and prepregs agreed closely, with the expected significant differences in $915cm^{-1}$ epoxide absorbance.

5) AMMRC #178 prepreg has an average valve for $2180cm^{-1}$ nitrile absorbance corresponding to 7-8% dicy, whereas AMMRC #180 prepreg has a value corresponding to 4% dicy. SP-250 should have 7% dicy. Since dicy is incompletely dissolved in SP-250 resin, the dicy deficiency may or may not be sufficient grounds for rejecting this lot of prepreg. Backup physical testing of actual composites must be performed.

CONCLUSIONS

Quantitative FT-IR provides a reliable, quick method for doing quality control analysis of epoxy/glass prepreg such as 3M's SP-250. A single infrared spectrum, quantitatively interpreted, provides all the information necessary for deciding whether to accept or reject a lot of prepreg, with a total elapsed time, from delivery to decision, of less than one hour.

ACKNOWLEDGMENT

The authors are indebted to Mr. Bernard LaLiberte who prepared the model SP-250 resin formulations with varying concentrations of dicyandiamide.

RHEO-OPTICAL STUDIES OF THE PLASTIC DEFORMATION OF POLYMERS

Richard S. Stein

University of Massachusetts
Amherst, MA 01003

ABSTRACT

The plastic deformation of polymers is accompanied by molecular orientation. For an amorphous polymer, conventional ways for measurement of amorphous orientation are birefringence and infrared dichroism. These characterize the second moment of the orientation distribution $\langle\cos^2\theta\rangle$ where θ is the angle between the chain axis and the orientation direction. For rubbers and polymers above their T_g, these are related to the entropic stress. Below T_g, distortional birefringence contributions ensue. Methods have been developed for the rapid measurement of birefringence during drawing or vibration so as to characterize the time dependence of orientation. New methods involving fourier transform infrared spectroscopy are being developed for measurement of the time dependence of dichroism. Fluorescence polarization of tagged polymers may be used for characterizing the fourth moment orientation $\langle\cos^4\theta\rangle$ as well as $\langle\cos^2\theta\rangle$. A recent development is the use of small angle neutron scattering for the measure of radius of gyration of a molecule in an oriented polymer. In such cases, the anisotropy of the radius of gyration serves as a measure of the overall molecular disposition in space.

For crystalline polymers, the specification of deformation entails the description of the orientation of crystals and their superstructure as well as that of the amorphous regions. The birefringence is a sum of contributions from both crystalline and amorphous phases. The crystalline contribution may be independently measured by x-ray diffraction for which dynamic methods have also been developed. From these, the crystalline component birefringence may be calculated and subtracted from the total measured birefringence to obtain the amorphous contribution. The orientation and deformation of the lamellar structure may be followed by small angle x-ray scattering. Time-dependence of this has recently become possible using the facilities at Oak Ridge National Laboratory. Changes in larger structures such as spherulites and fibrils may be studied using small angle light scattering. Time dependence of such measurements may be now conveniently studied using a computer interfaced optical multichannel analyzer.

NEUTRON RADIOGRAPHIC NON-DESTRUCTIVE INSPECTION OF COMPOSITE AND COMPOSITE/METAL STRUCTURES

W. E. Dance
Vought Corporation
Advanced Technology Center
P. O. Box 226144
Dallas, Texas 75266

ABSTRACT

The use of neutron radiography for nondestructive inspection of a variety of composite and mixed composite/metal structures is being explored. Radiographic data are presented in this paper which illustrate the sensitivity of this method for imaging defects in laboratory specimens of complex, difficult-to-inspect structures. In some cases neutron radiography provides a direct complement to X-Ray inspection, with resin porosity being imaged by the neutrons and the fiber distribution patterns being imaged by X-Ray. In other cases involving complex adhesively bonded composite/metal structures, neutron radiography provides the only existing accurate and reliable method of imaging certain types of bondline deficiencies. Radiographic results are presented from three types of neutron sources, including californium-252, Van de Graaff accelerator, and the mobile on-off neutron radiography system engineering model fabricated by Vought Corporation for the Army Materials and Mechanics Research Center.

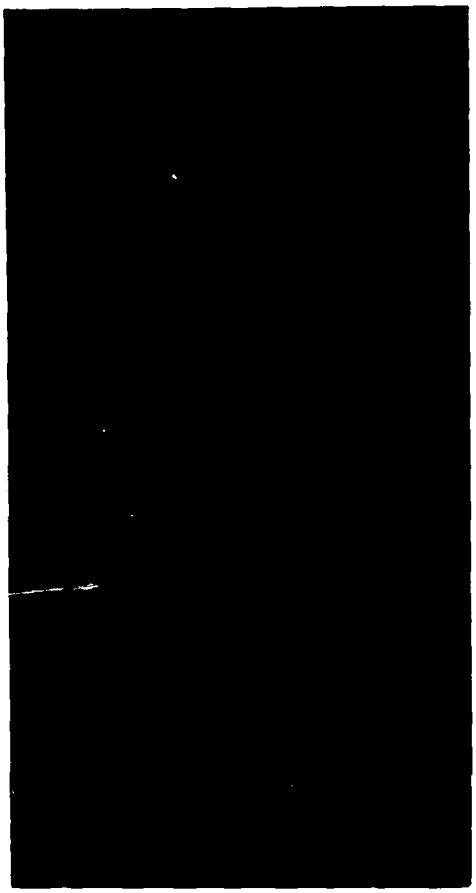

Neutron Radiography Revealing Gross Nonuniformities in Rejected Panel

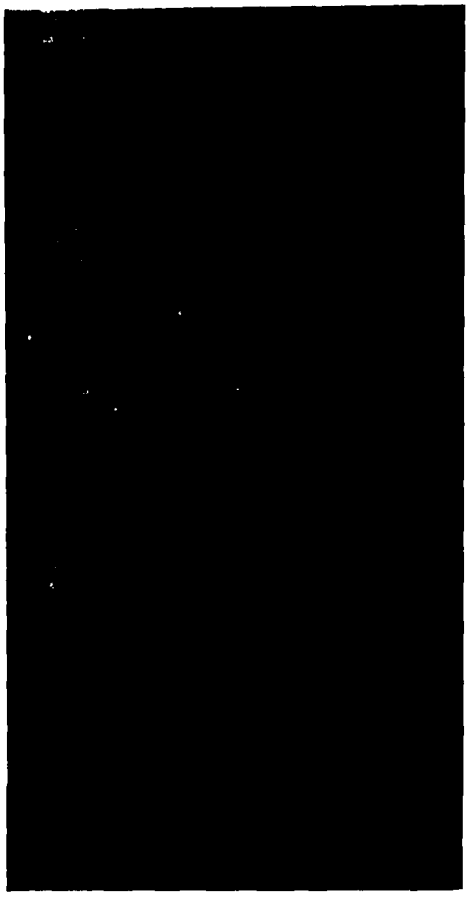

Neutron Radiopgraph of Acceptable Normal Panel

FIGURE 1. N-RAY INSPECTION OF UNIDIRECTIONAL GRAPHITE/EPOXY COMPOSITE PANELS

FIGURE 1. Anomalous voids, ply mismatch, and areas of excessive resin or fiber content are problems that are common in the manufacture of graphite/epoxy composites. Shown here are neutron radiographs of two different graphite/epoxy laminate specimens which were prepared to demonstrate the effects of bonding pressure and bleeder ply variations during manufacture on the final density of the laminates. The laminate in each case comprised 16 plies of unidirectional 5208/T-300 (Narmco) prepreg tape. The radiograph on the left shows a panel with no bleeder application and no autoclave pressure. Vacuum pressure alone [~0.013 N/m^2 (~15 psi)] was maintained during fabrication of this panel. The gross nonuniformities observed in the N-ray indicate that this composite would be unacceptable. The radiograph on the right images a panel which was fabricated by following the manufacturer's recommended procedure, and indicates a fully dense, acceptable panel. Final evaluation of each panel was based on C-scan nondestructive inspection (NDI) as well as N-ray radiography. Also used for determination of structural integrity were short-beam shear strength tests (room temperature and elevated temperature/humidity), fiber volume/resin content measurements, and photomicroscopy. The specimen on the left demonstrates the type and extent of voids that can be induced in a composite when improper layup is made or when loss of pressure in autoclaving occurs.

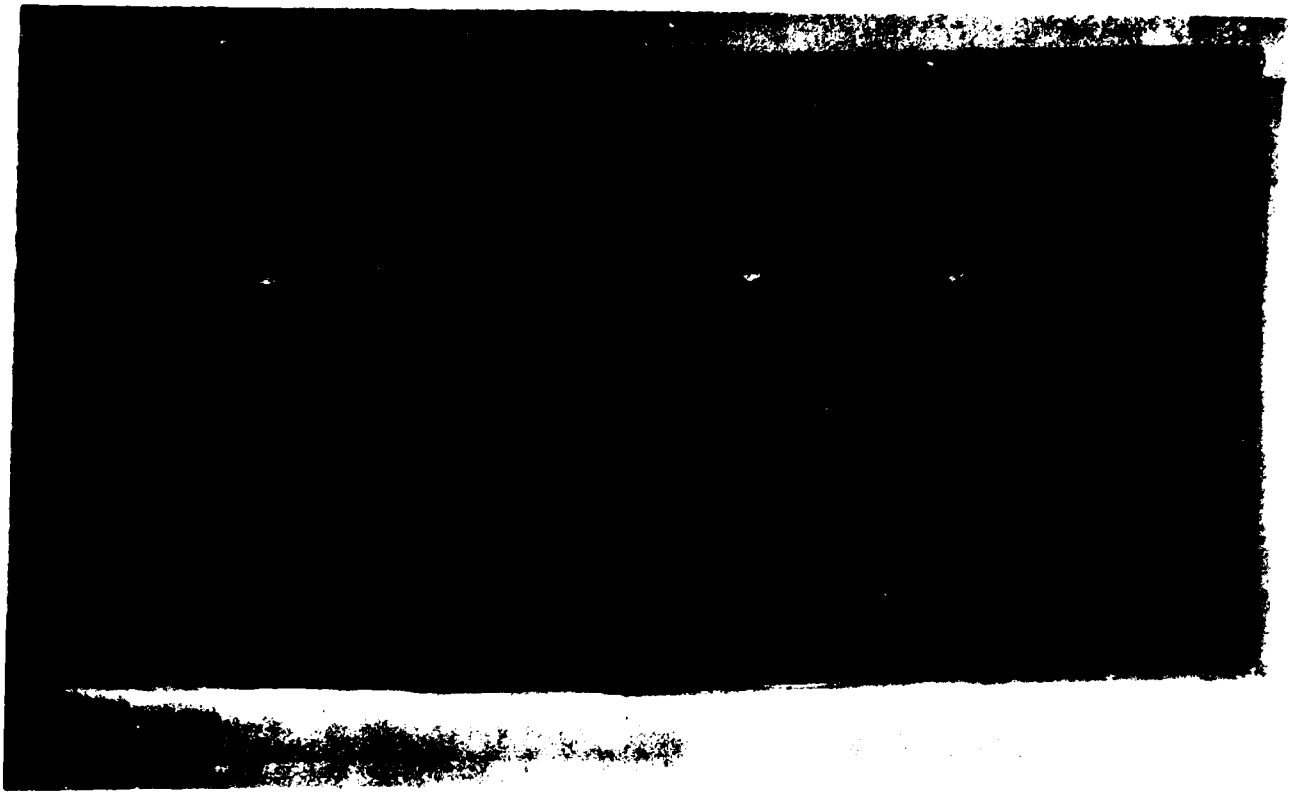

FIGURE 2. NEUTRON RADIOGRAPH OF GRAPHITE/EPOXY COMPOSITE CONTAINING A SERIES OF REFERENCE VOIDS (SIMULATED).

FIGURE 2. In order to determine the sensitivity of neutron radiography for detection of matrix voids or fiber/resin deficiencies in graphite/epoxy panels, a specimen was prepared containing simulated laminar voids, stepped in thickness by 0.127 mm (0.005 in.) increments, from 0.127 to 2.67 mm (0.005 to 0.105 in.), by cutting disks out of the prepreg tape and replacing the portions cut out with aluminum filler disks. The two plies of tape on each of the outer surfaces contained no holes. This specimen was prepared from 25 plies of Narmco 5208/T-300 prepreg material in a hand-layup, vacuum bag/hydraulic press operation using 76.2 mm wide (3 in.) prepreg tape and the manufacturer's recommended cure cycle. The tape was laid up to give a symmetrical ± 45-deg ply orientation. The radiograph is shown in the figure. With each successive hole, beginning with the hole designated by an arrow in the upper right of the figure [hole thickness 2.67 mm (0.105)], the thickness of the void or deficiency decreases by one ply thickness, or 0.127 mm (0.005 in.). As seen in the figure, the single-layer hole 0.127 mm (0.005 in.) thick was barely imaged, providing a sensitivity value of 4 percent of the total specimen thickness.

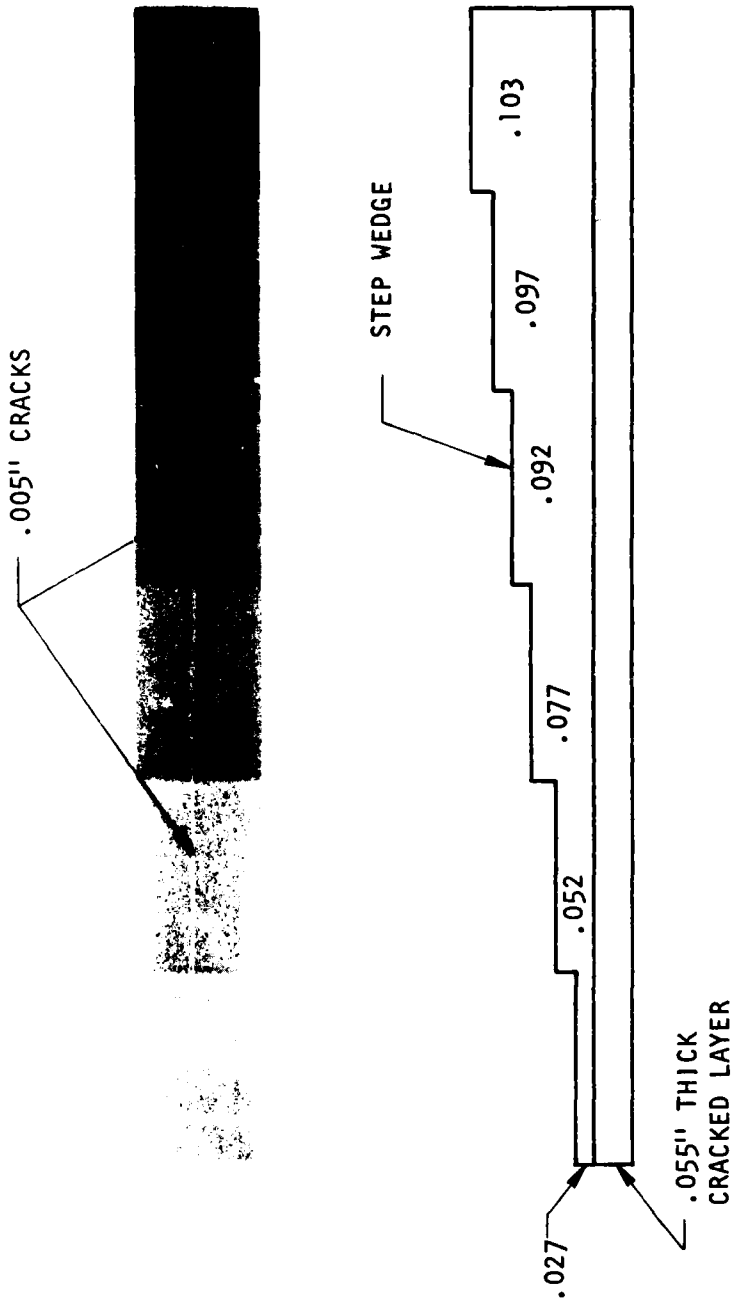

NEUTRON RADIOGRAPH (POSITIVE PRINT) OF GRAPHITE EPOXY COMPOSITE SHEETS SIMULATING INTERNAL CRACK DAMAGE. .005" CRACKS (ARROWS) ARE IMAGED IN A .055" THICK SHEET THROUGH A GRAPHITE EPOXY STEP WEDGE HAVING THICKNESSES RANGING FROM .027" TO 0.103".

FIGURE 3. NEUTRON RADIOGRAPHIC INSPECTION OF GRAPHITE EPOXY COMPOSITES

FIGURE 3. Foreign-object damage in a composite panel characterized by sublayer through-cracking in the plane perpendicular to the panel was simulated by overlaying a 1.40 mm (0.055 in.) graphite/epoxy specimen containing 0.127 mm (0.005 in.) cracks with an unflawed graphite step wedge, as shown in the figure. The step wedge thicknesses ranged from 0.686 to 2.62 mm (0.027 to 0.103 in.) to indicate the sensitivity for detection of the cracks hidden by outer layers. As seen in the neutron radiograph, the 0.127 mm (0.005 in.) cracks were clearly imaged through the maximum step of 2.62 mm (0.103 in.).

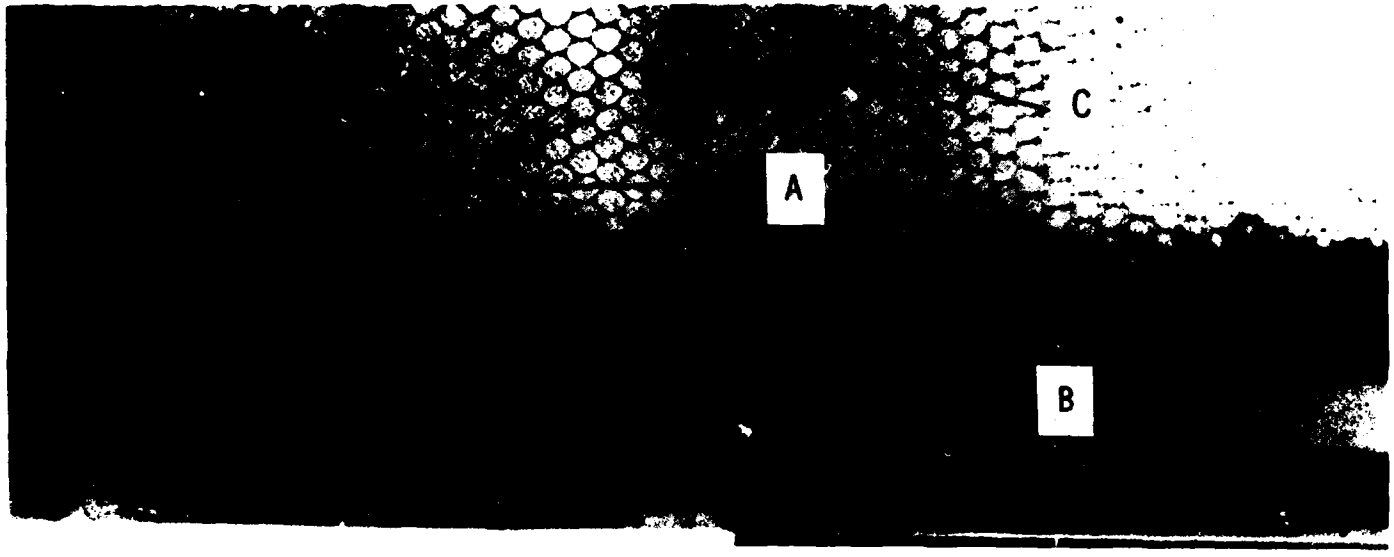

FIGURE 4. NEUTRON RADIOGRAPH SHOWING ADHESIVE STRUCTURE AT TRAILING EDGE CLOSURE IN 737 WING SPOILER

FIGURE 4. This figure is the result of N-ray inspection of an aircraft composite wing spoiler at the trailing-edge closure. This structure involved graphite/epoxy skins bonded to aluminum honeycomb. In addition to the high-contrast imaging of the adhesive pattern at the composite skin-to-core interface [such as at (C) in the figure], the technique also provides an accurate image of the adhesive distribution at the critical core-to-frame interface (A). Voids within a tab-to-frame bondline are indicated at (B).

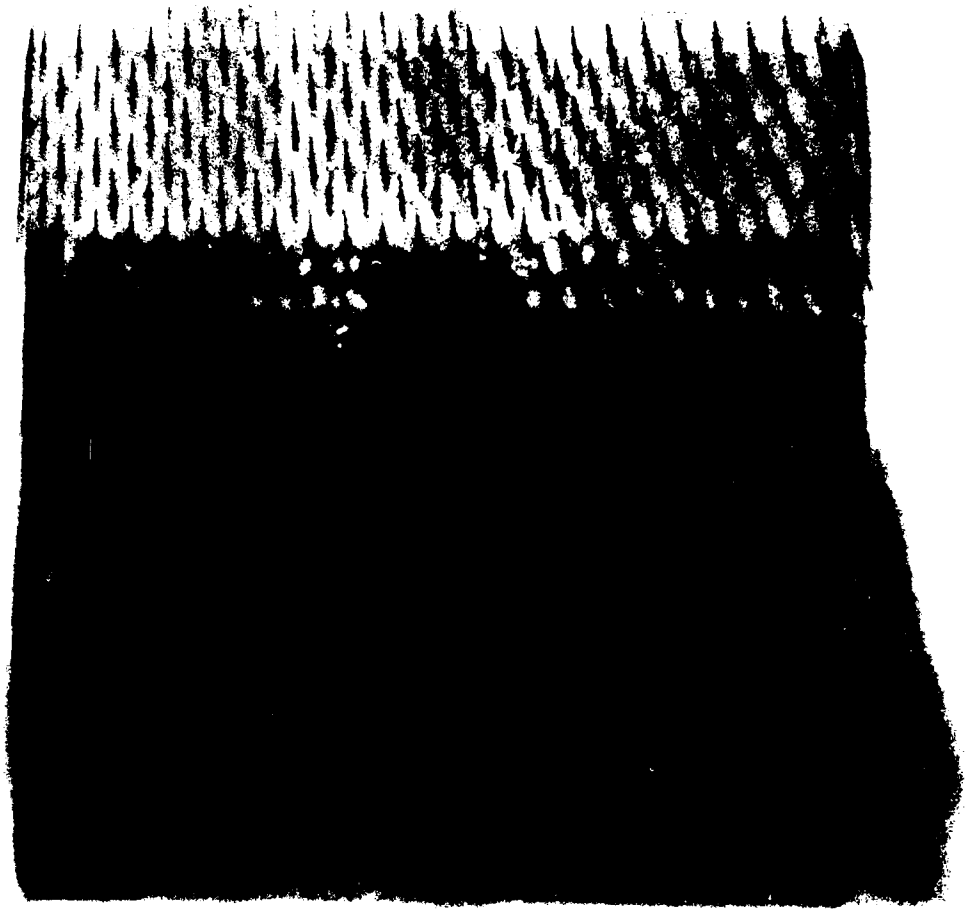

FIGURE 5. NEUTRON RADIOGRAPH OF GRAPHITE/POLYIMIDE BONDED JOINT SPECIMEN

FIGURE 5. An example of N-ray inspection of an all-composite component is given by this figure, which is a radiograph of a T-joint structural member composed of graphite/epoxy face sheets over polyimide honeycomb core. This structure simulates configurations based on honeycomb core panels bonded at right angles to honeycomb rib faces. The N-ray radiograph shows the distributions of the adhesive foam which was injected during manufacture for joint reinforcement. In this case, localized "pooling" of the adhesive in a few core cells is apparent.

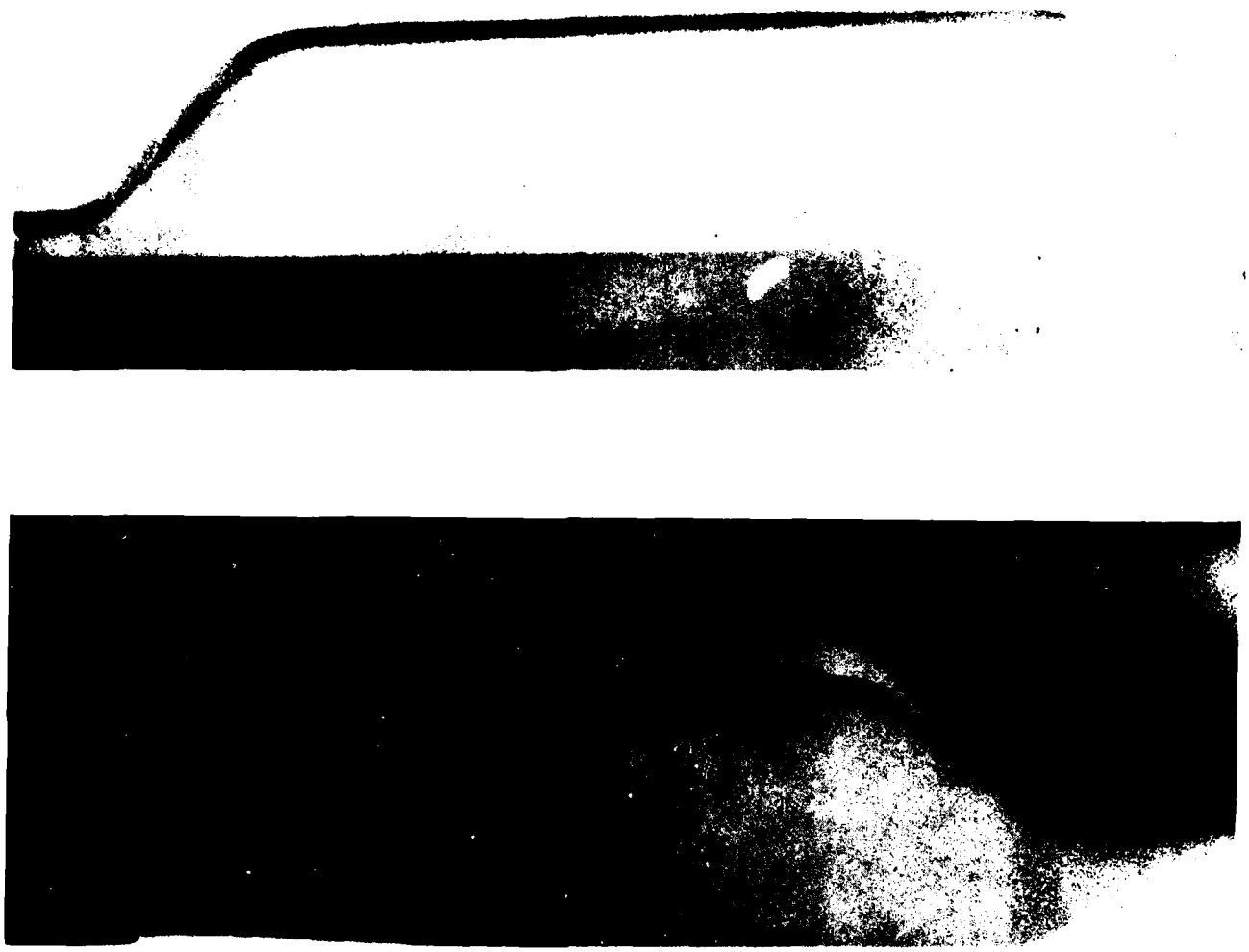

FIGURE 6. N-RAY INSPECTION OF BONDED FIBERGLASS/EPOXY COMPOSITE STRUCTURE

FIGURE 6. In the inspection of the bondlines joining composites in the absence of metal components, the richer hydrogen content of the epoxy adhesive is readily imaged against the lower hydrogen content of the composite matrix. This can be seen in the bonding of different parts of the same composite structure in the figure. These two radiographs image two different bondlines within the same general area of this structure, a square box-beam member with internally bonded reinforcement. In the top radiograph it is seen that edge-flow of the adhesive is deficient along the narrow portion and completely disappears, leaving gaps as the curvature of the reinforcement sleeve increases. The bottom radiograph in the figure shows an adhesive bondline defect in this structure at a structurally critical point. Precise defect location and defect size determination can be made from these radiographs.

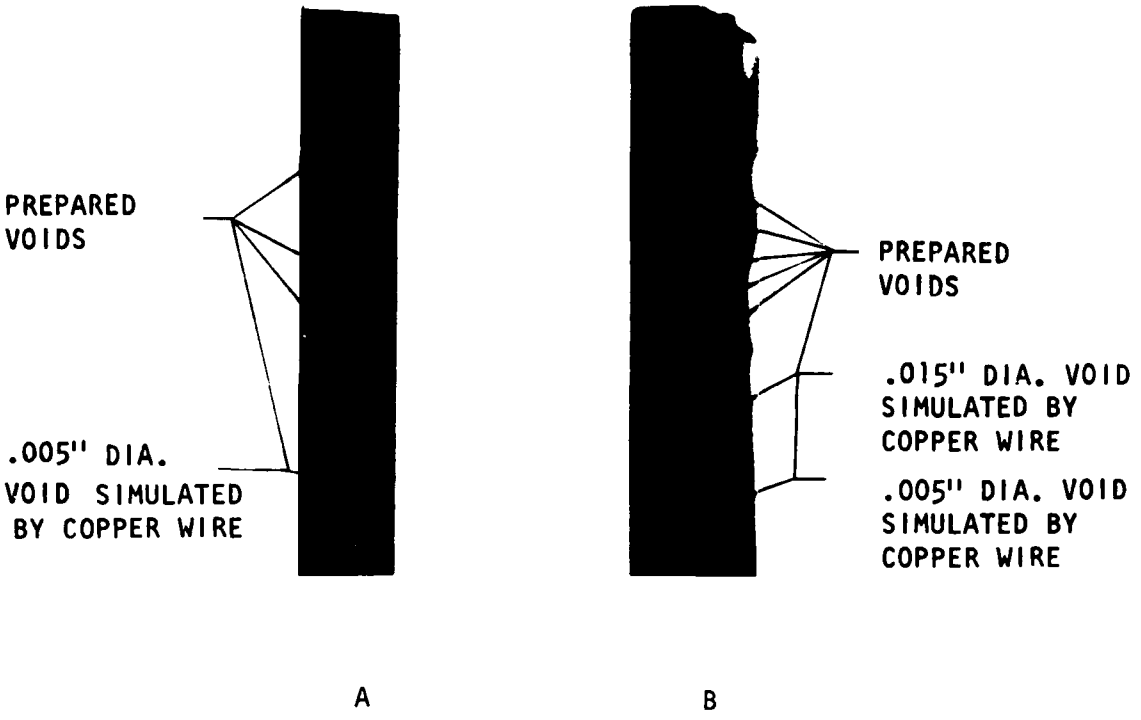

FIGURE 7. These are neutron radiographs of adhesively bonded graphite/epoxy specimens containing prepared bondline voids. Specimen A consists of two 2.54 mm (0.1 in.) adherends with a 0.127 mm (0.005 in.) modified-adhesive bondline. Specimen B includes a 1.68 mm (0.066 in.) titanium sheet bonded between 2.54 mm graphite/epoxy adherends. The prepared voids, with diameters as indicated in the figure, were imaged with good resolution. As seen in the radiograph of Specimen B, the insertion of the 1.68 mm titanium plate, with its extra bondline, did not degrade the image of the bondline voids, even down to the smallest, 0.127 mm diameter (0.005 in.) void.

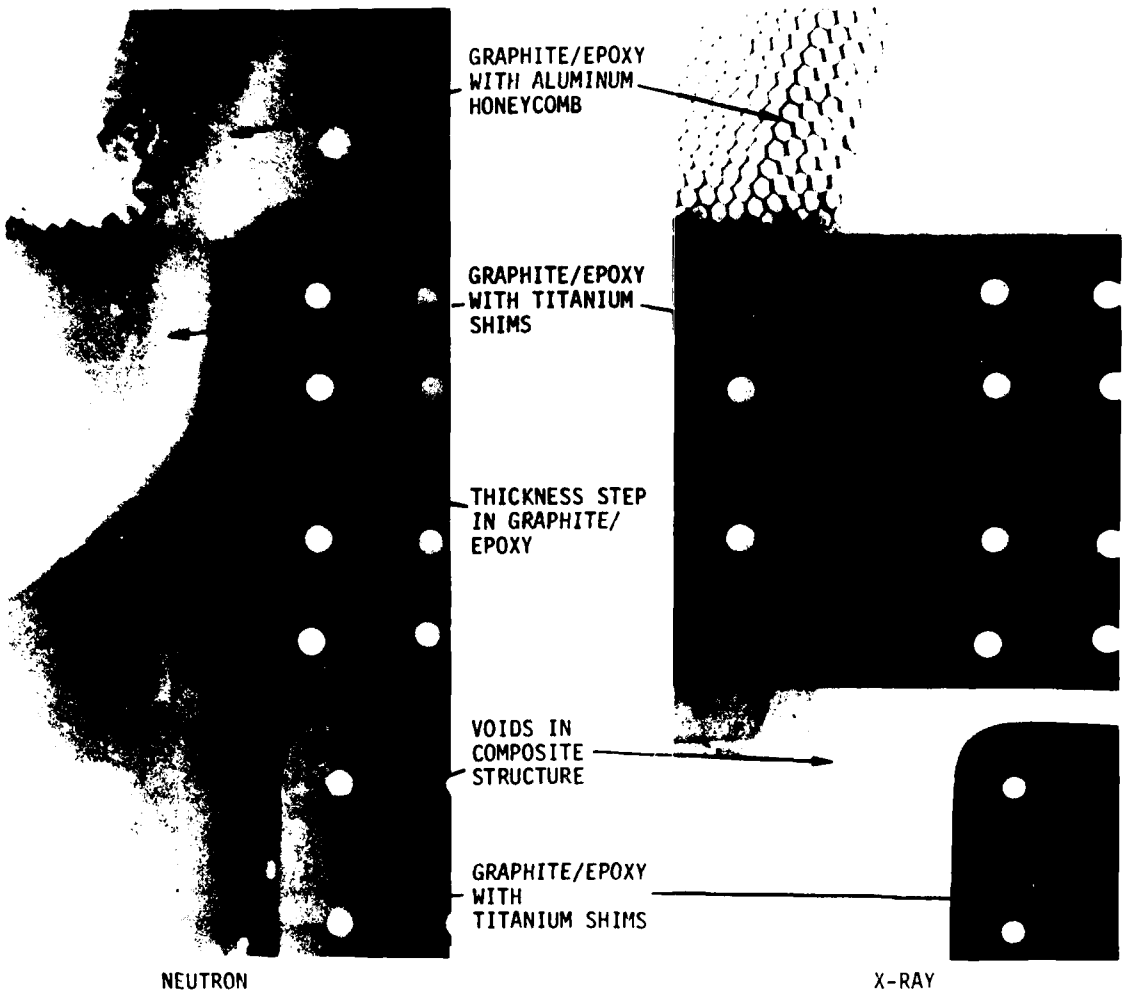

FIGURE 8. NEUTRON AND X-RAY INSPECTION OF A GRAPHITE/EPOXY COMPOSITE STRUCTURE CONTAINING METAL COMPONENTS

FIGURE 8. An example of nondestructive inspection of a more complex hybrid composite/metal structure by means of neutron radiography is shown in this figure. A comparison of neutron and X-ray inspection is made. The specimen was a graphite/epoxy/metal wing skin structure incorporating aluminum honeycomb core, graphite/epoxy face sheets, and titanium shims. The advantage of neutron inspection is illustrated for imaging bondline flaws which are undetected by X-ray and other techniques, due to the thick titanium shims. Voids in the titanium bondlines are clearly imaged in the neutron radiograph at the left. The X-ray on the right, on the other hand, shows the boundaries of the shims, which are essentially opaque to the X-ray beam in this exposure, and provides no information about the bondline.

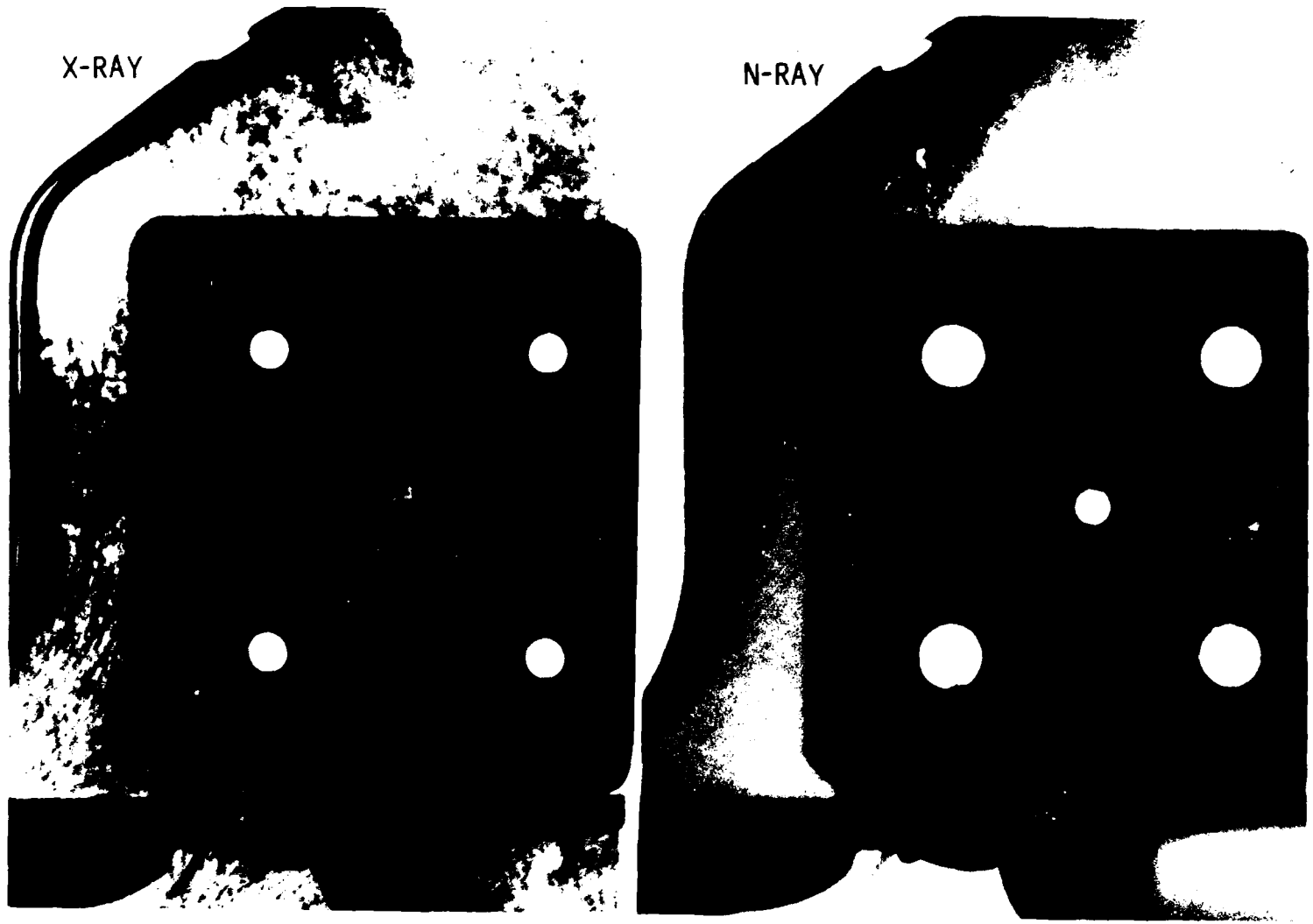

FIGURE 9. INSPECTION OF BONDED METAL-TO-FIBERGLASS/EPOXY COMPOSITE STRUCTURE

FIGURE 9. The results of radiographic inspection of a bonded metal to fiberglass/epoxy composite structure are shown here. As in Figure 8, this figure compares an N-ray radiograph with an X-ray radiograph of the same composite structure. The metal attachment plate containing several bolt holes is bonded with an epoxy adhesive to the shoulder of the fiberglass/epoxy structure. As seen in the X-ray image at the left, the metal attachment plate completely absorbs that type of radiation, thus preventing the imaging of the epoxy bondline. On the other hand, the neutron beam, which is partially transmitted through the metal plate, images a number of voids within the bondline joining the metal plate to the fiberglass composite, as seen in the neutron radiograph on the right. Voids appear as light areas in the neutron radiograph (positive print). Note also in this radiograph two sharp lines denoting inclusions in the bondline. Voids and inclusions are all too common on a localized basis in metal-to-composite or composite-to-composite bonding.

Mobile "On-Off" Neutron Radiography System Engineering Model

Vought - Developed Concept and Technology for Implementing the Transition of Neutron Radiography as a Laboratory Inspection Technique to a Viable Field Unit for Inspection of Aircraft and Missile Structures.

Design, Fabrication, and Validation Testing Supported by Army Materials and Mechanics Research Center

FIGURE 10.

ION ACCELERATOR NEUTRON RADIOGRAPHY

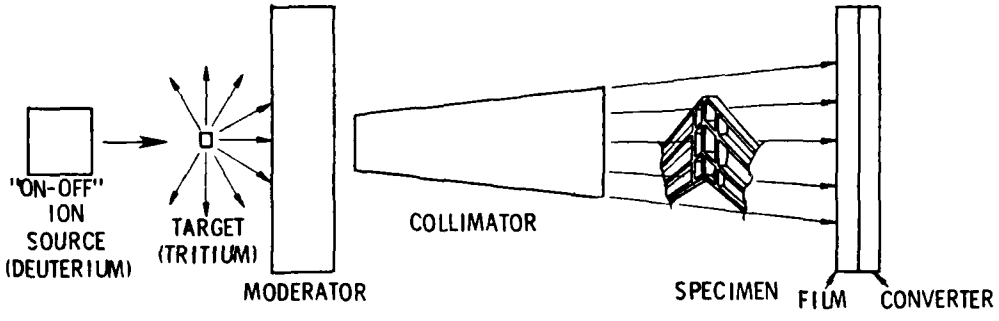

FIGURE 11.

AMMRC MOBILE N-RAY SYSTEM
ENGINEERING MODEL

- PHASE I - DESIGN
  DETAILED DESIGN OF AN ACCELERATOR - BASED SYSTEM CAPABLE OF LABORATORY & LIMITED FIELD OPERATION
- PHASE II - FABRICATION
  MANUFACTURE OF SYSTEM TO APPROVED DESIGN AND INITIAL CHECK-OUT
- PHASE III - EVALUATION
  DEMONSTRATION, VALIDATION TESTING AND DELIVERY/INSTALLATION

FIGURE 12.

RELATION BETWEEN INTERFACIAL PHENOMENA AND ADHESIVE BOND STRENGTH

Arthur D. Jonath and Joe L. Crowley

Lockheed Palo Alto Research Laboratory
Palo Alto, California

ABSTRACT

It is known that structure and electronic properties of thin films are influenced by nucleation and and growth kinetics dependent in part upon the nature and condition of the substrates upon which they are deposited. In both crystalline and amorphous semiconductor films, these effects are seen to propagate several microns from the substrate-film interface into the "bulk" of the film.

Similar effects are being observed in structural adhesive systems whose cure/crosslink mechanisims appear to be influenced by the adjacent bonding surfaces (adherends). Detailed mechanical (ultrasonic probe and locus-of-fracture) and electronic (thermally stimulated dipole relaxation) properties measurements have been made in the adhesive throughout the interfacial region. The results indicate that microstructural gradients persist a considerable distance (>100μm) into the bulk of the adhesive.

The difficulty with accepting these results lies in the current lack of detailed understanding surrounding the process of bond formation and the inability to visualize "forces" acting over macroscopic spatial ranges. Our approach to explain these results sets aside the force/energy considerations in favor of entropic arguments connected with nucleation and growth processes. These are seen more clearly in a model of describing the deposition of simple inorganic amorphous polymer structures such as occur in types of hydrogenated amorphous silicon. An extention of this model to organic polymer adhesives is suggested.

INTRODUCTION

An adhesive interphase region of macroscopic dimension is described. We have labelled this region the Interfacial Accommodation Zone (IAZ) to distinguish it from the usual thin layer interphase of atomic dimensions. The size of the IAZ is determined by the extent of both mechanical and dipolar properties' gradients measured as a function of distance from an adhesive-adherend interface. The locus-of-fracture, for failure modes which contain a shear component, occurs within this zone.

This paper is presented in four sections as follows:

1. Locus of Fracture Observations
2. Mechanical Properties: Shear Modulus
3. Electrical and Optical Measurements:
   Thermally Stimulated Dipole Relaxation
   Electroabsorption Experiment
4. Model for Formation of IAZ: Inorganic
   Polymer Analog

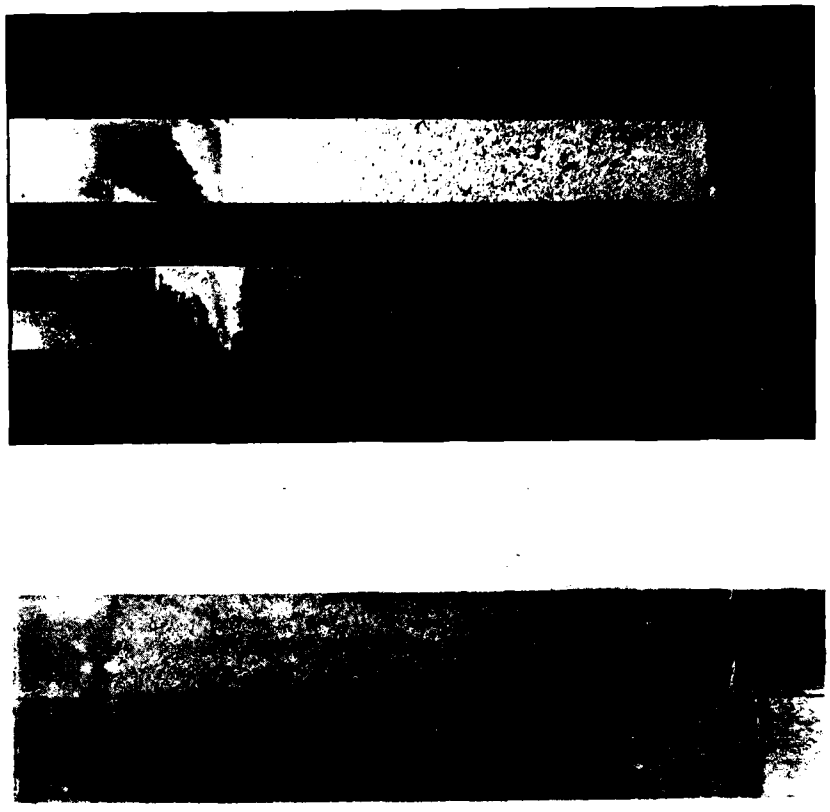

Figure 1.1. Scarf-Joint Fracture Surfaces - Epolyite 810 - Showing Adhesive Failure.

Top: Failure propagates within 40 μm of Al adherend. Bottom: In this sample, the failure locus actually skips from one adhered interfacial accommodation zone (IAZ) to the other.

Note: the scarf-joint is a mixed-mode adhesive test specimen commonly used to introduce shear into the adhesive joint failure mechanism.

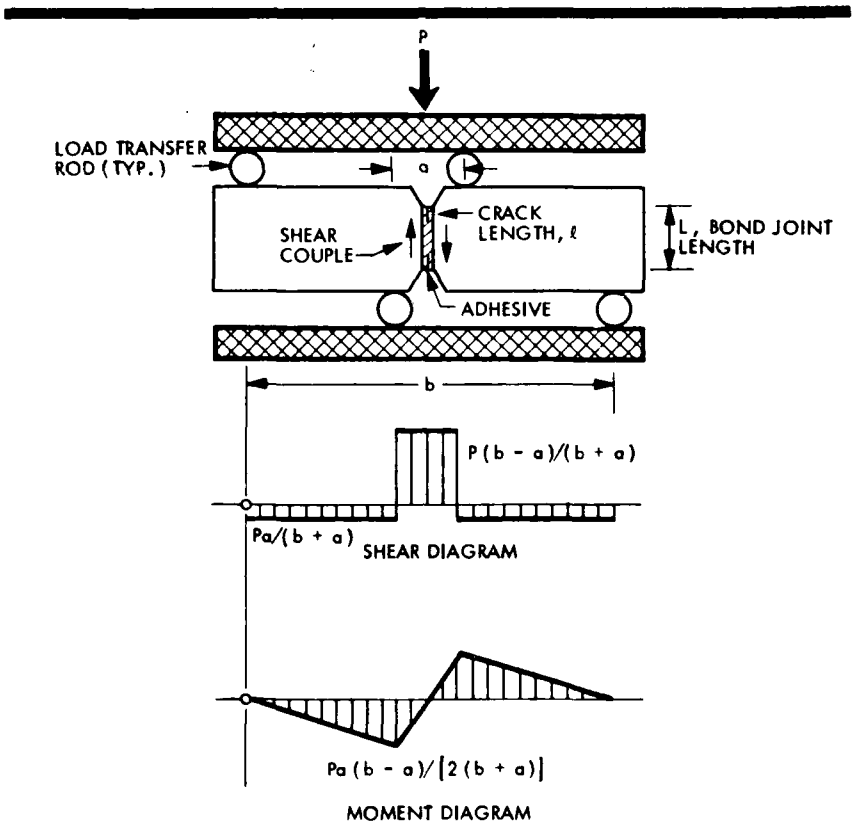

Figure 1.2. Adhesive Shear Test Specimen with Simplified Shear and Moment Diagrams.

To test "geometry" effects observed in scarf-joint test specimens, this symmetric shear test specimen design[1] was adapted for use with adhesives. Symetric pre-cracks of length, ℓ, can be introduced into the adhesive bondline, either in the center-of-bond or at the interface.

[1] N. Iosipescu, Journal of Materials, 6, 371 (1972).

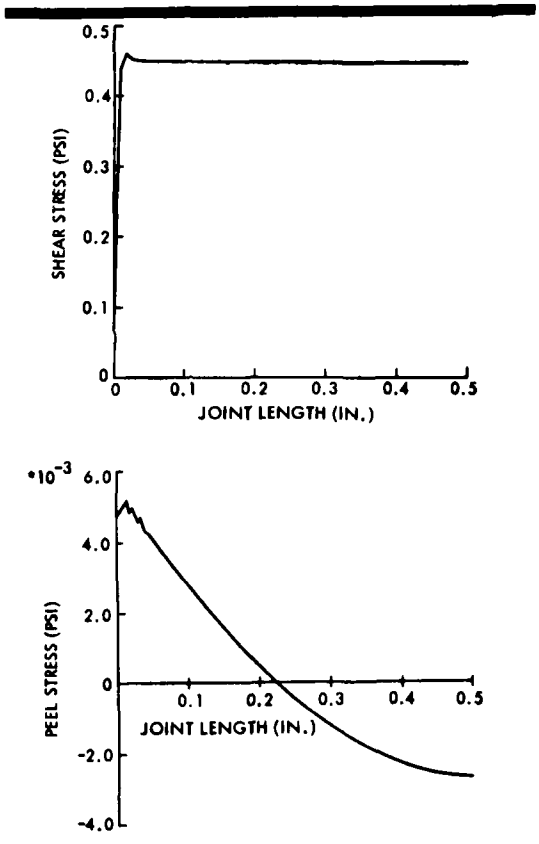

Figure 1.3. Stress Distribution from Half-Length Finite Element Analysis for Shear Test Specimen.

The shear stress is computed to be virtually constant over the joint length and is lower than the average value within the failure locus zone. The maximum peel stress is two orders of magnitude less than the average shear stress.

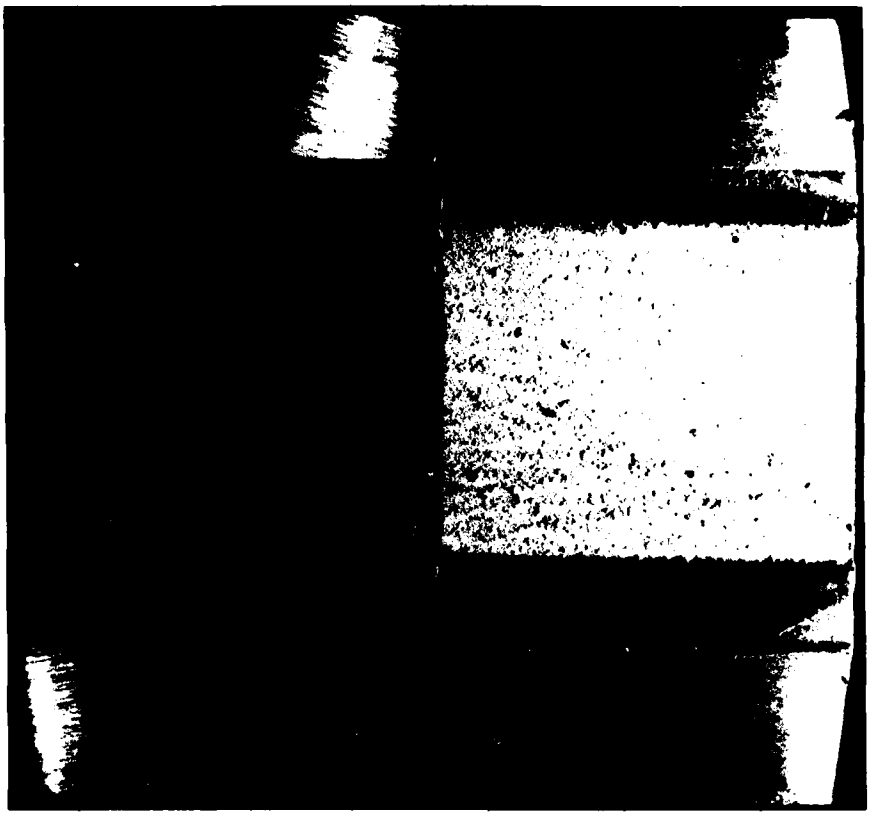

Figure 1.4. Photo of Symmetric Shear Test Specimen Surfaces After Fracture of Epoxylite 810 Adhesive.

As in the non-symmetric (scarf-joint) case, the failure is adhesive in nature with the locus contained in the 20-50 μm region adjacent the interface. Thus geometry arguments for the failure locus must be deleted.

Even with center-of-bond cracks in the adhesive, the failure locus lies within the IAZ. It is seen to propagate either from the crack-tip directly to this region, or wholly within the IAZ after initiating therein. This somewhat surprising result indicates that shear stress concentration does not occur at the crack-tip. And, in fact, subsequent measurements[2] have confirmed the absence of a Mode II failure mechanism.

We conclude that the failure locus is governed neither by the effects of geometry nor stress concentration, but simply by the shear stress being in excess of shear strength in the weakest zone of the material.

In the next section, an ultrasonic method used for probing this zone is presented.

[2] Arthur D. Jonath, Adhesion and Adsorption of Polymers, Pt. A, ed. by L. H. Lee, Plenum Press, New York, N.Y. (1980), p. 175.

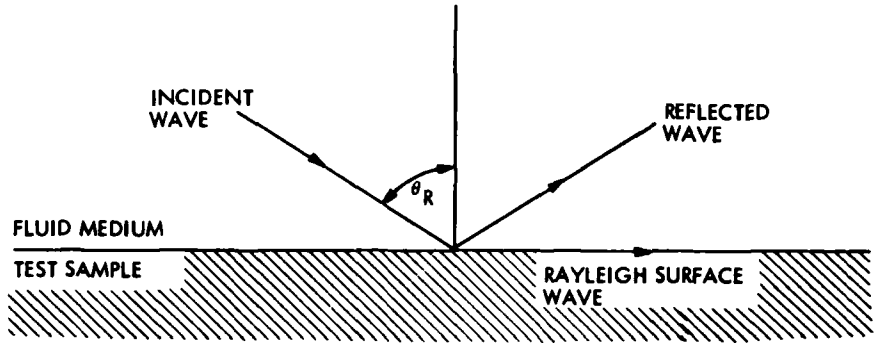

$$V_R = \frac{V_I}{\sin \theta_R} \qquad V_S = \frac{V_R}{K(\mu)}$$

$$G_s = \rho V_s^2$$

MECHANICAL PROPERTIES (SHEAR MODULUS)

The shear modulus is measured in thin layers throughout a bond thickness using ultrasonic Rayleigh (surface) waves.

Figure 2.1. Geometry of Response Waves from a Longitudinal Sound Wave Incident at the Rayleigh Critical Angle.

At the critical angle, Θ_R, a portion of the incident longitudinal wave (25 mHz) is converted to a surface wave at the expense of the reflected wave intensity. The velocity, V_R, of this Rayleigh Surface wave is related to Θ_R and the incident wave velocity, V_I, by Snell's law. The shear wave speed, V_S, is determined from V_R and $K(\mu)$, a material constant dependent upon its Poisson's ratio. The shear modulus is determined from V_S and the density. The shear wave penetrates approximately 30 μm and is thus used as a probe to measure shear modulus in thin layers throughout the bondwidth.

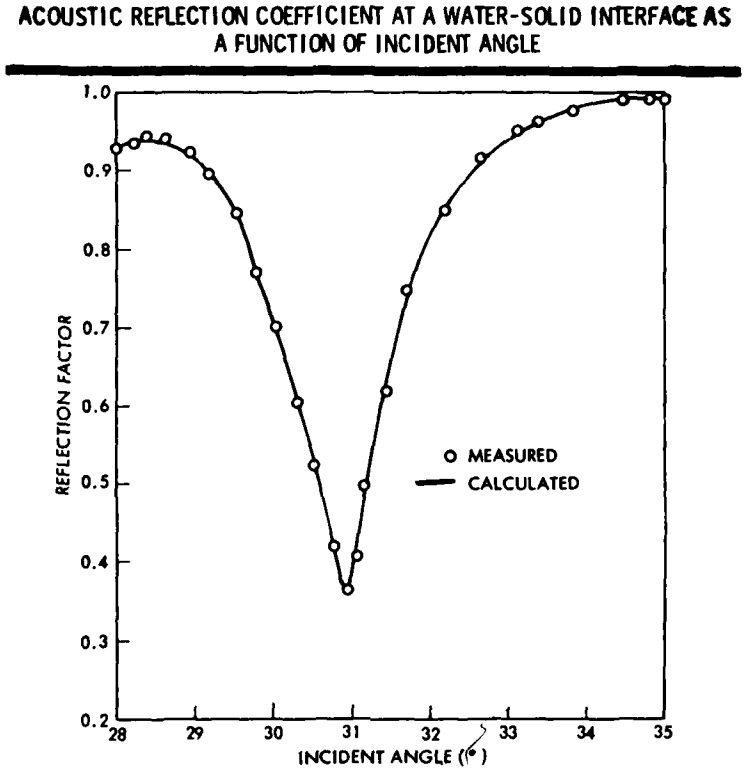

Figure 2.2. Acoustic Reflection Coefficient at a Water-Solid Interface as a Function of Incident Angle.

This is an example of the magnitude of the reflection loss at the surface mode conversion critical angle ($\sim 31^{o}$) in an "ideal," water-metal, interface system. Dow Corning 200 is the fluid medium used with the epoxy-type adhesives.

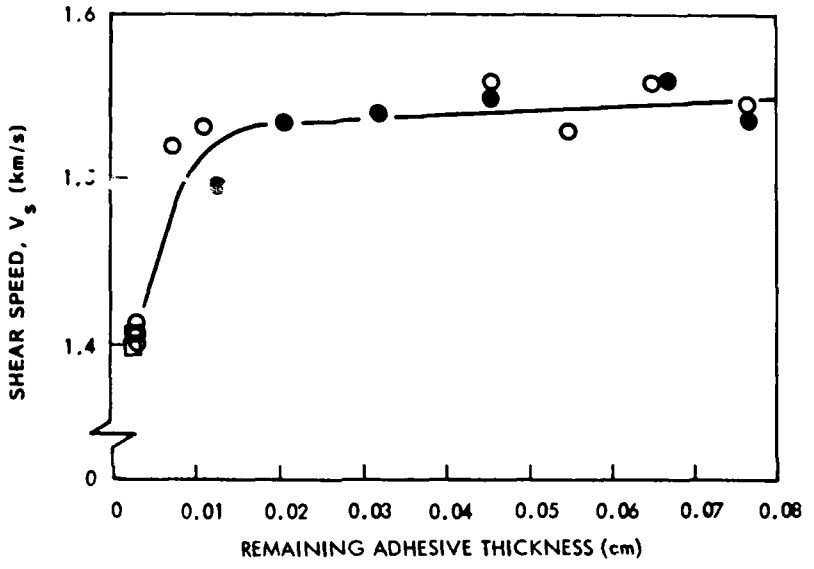

Figure 2.3. Shear Wave Speed Variation Within An Adhesive Bond Thickness.

Metallographically thinned adhesive layers are subjected to ultrasonic Rayleigh Wave probe. The shear speed variation is observed through the bond thickness. The square symbols represent measurements made on boch of the newly exposed fracture surfaces shown in Figure 1.1, and are in excellent agreement with the results of the thinned layer samples. Since there appears to be no gradient in density (Figure 2.4), this is additional evidence that the locus-of-failure occurs in a region of weaker material.

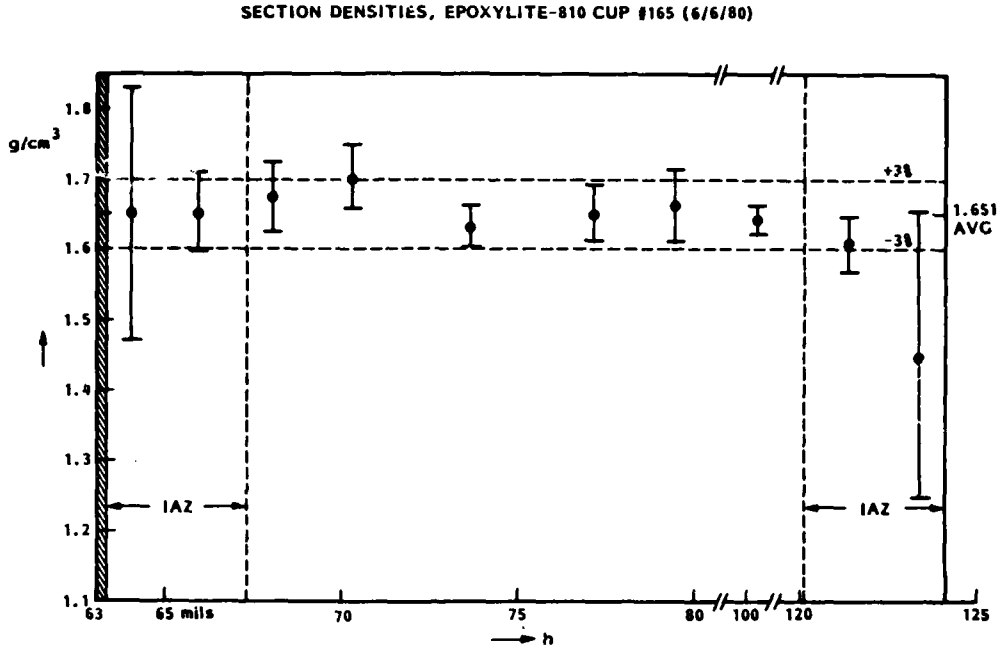

Figure 2.4. Density Variation of Epoxylite 810 Across a Thick Bond.

Within measurement accuracies (error bars), there is no density gradient observed across the bond. Errors increase within the IAZ (see Figure), and perhaps there can be a <u>decrease</u> in density very close to the interface. But to explain the shear speed results of Figure 2.3 solely by density arguments, an <u>increase</u> in density is necessary (see equations in Figure 2.1).

Thus the conclusion from the shear speed and density results is the shear modulus variation of Figure 2.5.

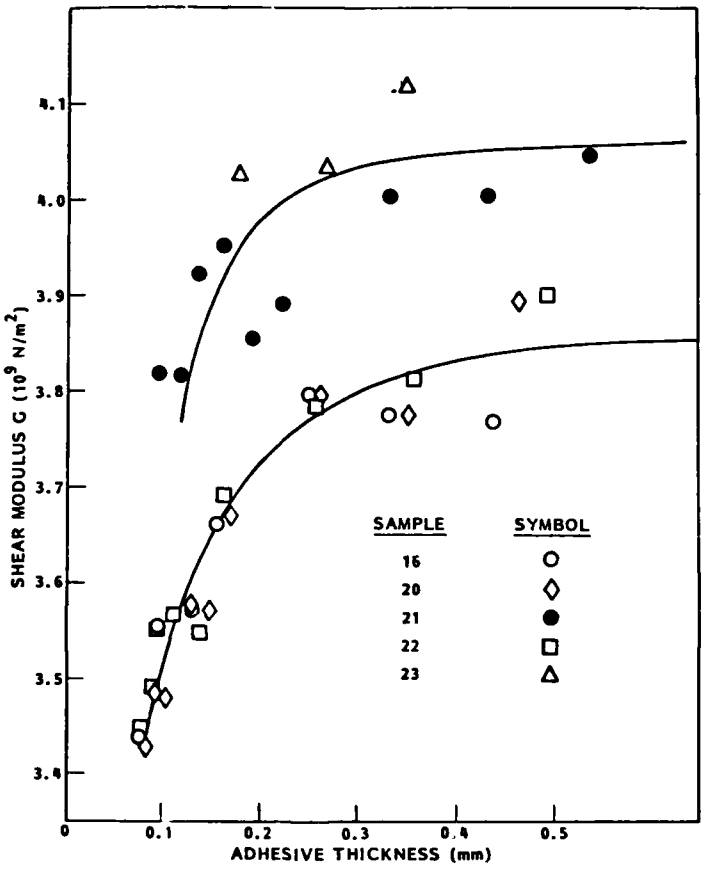

Figure 2.5. Variation of Shear Modulus with Adhesive Bond Thickness Remaining on Dichromate-Etched Aluminum Substrate for Five Samples of Expoxylite 810.

The shear modulus of each metallographically exposed surface is computed from measured values of the shear speed (Rayleigh Wave method) and density. A reduction in shear modulus of 10-20% is observed within 100 to 200 μm of the adherend, the IAZ region. The two data curves correspond to resin age differences.

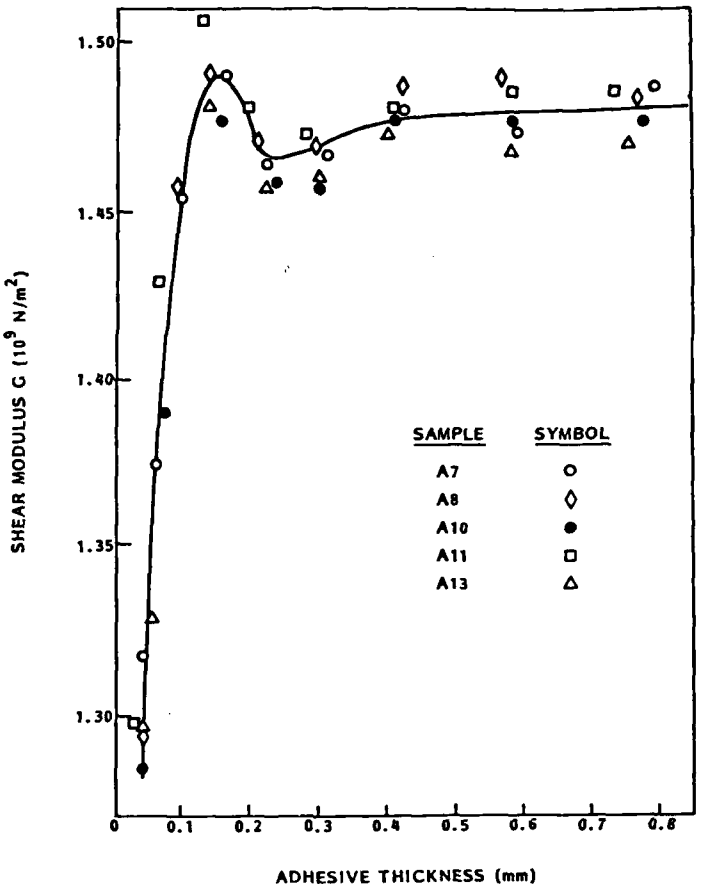

Figure 2.6. Variation of Shear Modulus with Adhesive Bond Thickness Remaining on Aluminum Substrate for Five Samples of American Cyanamide FM-73 Epoxy.

It appears that the shear modulus variation is actually double-valued.

This is a film adhesive without the glass scrim layer. No doubt, part of the film is pre-cured to allow for handling. From the double-valued modulus variation, two interfaces are inferred: (1) aluminum to adhesive and (2) film-surface adhesive layer to pre-cured interior region.

ELECTRICAL AND OPTICAL MEASUREMENTS

Thermally Stimulated Dipole Relaxation (TSDR) measurements are used to probe dipolar microstructure throughout a bond thickness. Both metallographically thinned and fracture exposed samples are interrogated as in the ultrasonic experiments (Section 2).

An electro-optical method, infrared electroabsorption, is used to identify the dipoles.

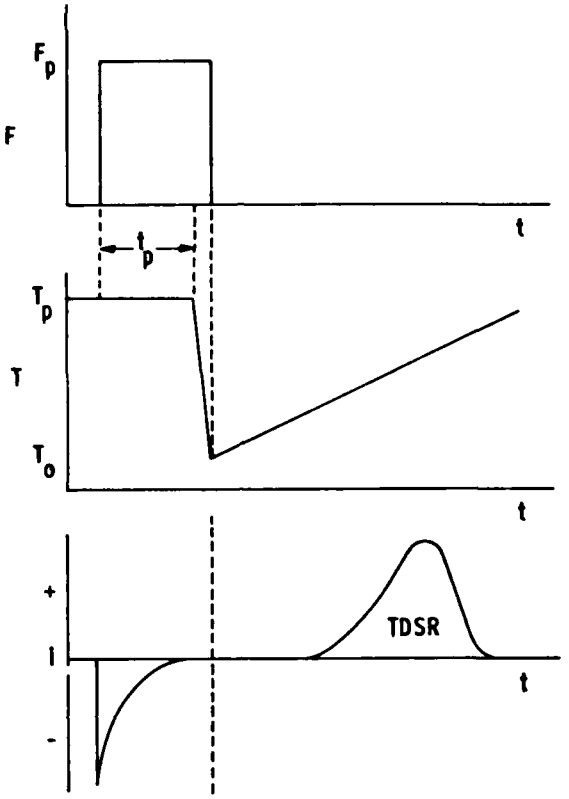

Figure 3.1. TSDR Technique

Polarization field F_p is applied at polarization temperature T_p for duration t_p. A polarization current (left part of bottom curve) reaches zero when polarization is saturated. While the sample is held at F_p it is quickly cooled to T_o. It is then heated at constant rate b subsequent to removal of polarization field. A sensitive electrometer is connected to the sample. As the frozen-in, field-oriented dipoles begin to regain random orientation at a temperature related to their activation energy E and relaxation rate τ_o, a depolarization (TSDR) current is observed in the external circuit:

$$i(T) = \frac{N_d F_p P^2}{kT_p} \left[\tau_o \exp(E/kT)\right]^{-1} \exp\left\{-\int_{T_o}^{T} \left[b\tau_o \exp(E/kT')\right]^{-1} dT'\right\}$$

where P is the dipole moment.

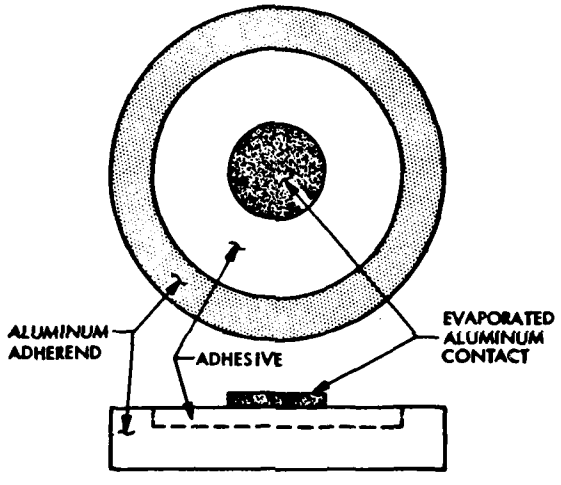

Figure 3.2. Sample Geometry for Thermally Stimulated Dielectric Relaxation (TSDR) Experiment.

TSDR spectra are recorded at intervals throughout the adhesive layer thickness. The adhesive layer is thinned by metallographic methods subsequent to each measurement.

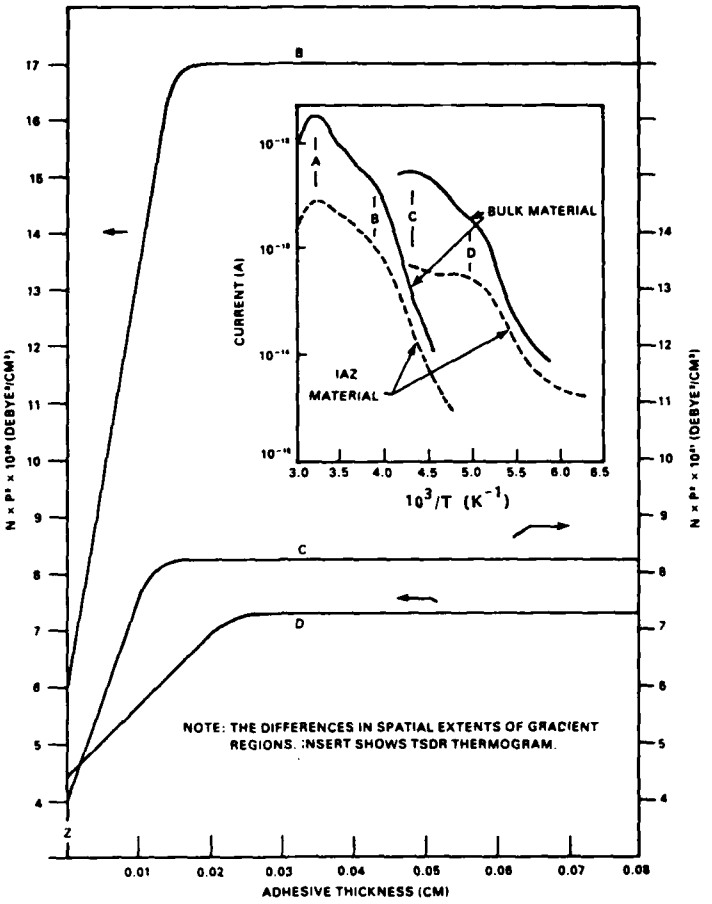

Figure 3.3. Density of Dipoles Represented by Peaks B, C, and D in TSDR Thermogram (Insert) as a Function of Thickness of Adhesive Remaining on Adhren-Epoxylite 810 on Aluminum.

Peak A is non-linear with field and is attributed to depolarization of charged interfaces. Note that the spatial extent of the dipole density gradient is large (>100 μm) and varies among the dipoles. This spatial extent is comparable to the shear modulus gradient extent (Figure 2.5).

PEAK	ACTIVATION EMERGY (eV)	RELAXATION TIME (s) (AS 1/T→0)
B	0.60	$5x10^{-11}$
C	0.40	$5x10^{-8}$
D	0.50	$5x10^{-12}$

Table 3-3

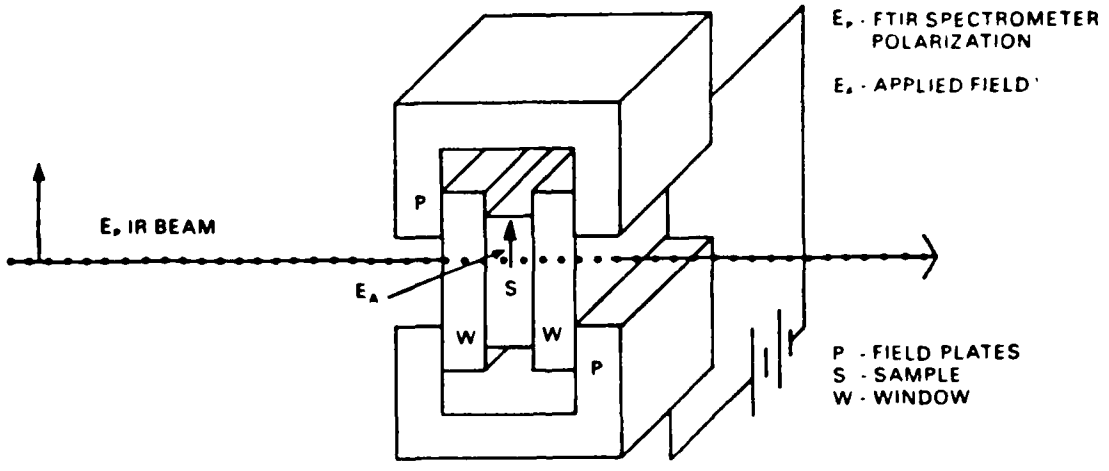

Figure 3.4. Electroabsorption (EAB) Sample Configuration with Electric Field Perpendicular to I.R. Beam.

Spectra are recorded in a Fourier Transform Infrared (FTIR) instrument so that absorption changes sensitive to polarization fields can be observed. Spectral lines in EAB may be used to identify dipoles in TSDR. Complete experiment, wherein dipole relaxation is measured simultaneously with IR absorption, is not complete.

Table 3-5

FTIR FIELD/NO FIELD SPECTRA
IDENTIFY CANDIDATE POLAR GROUPS
FOR EXPLANATION OF TSC DATA

- 850-900 EPOXIDE RINGS
- 1170-1200 ETHER BOND GROUPS
- 1250 ETHER BOND GROUPS
- 1500 AROMATIC RINGS

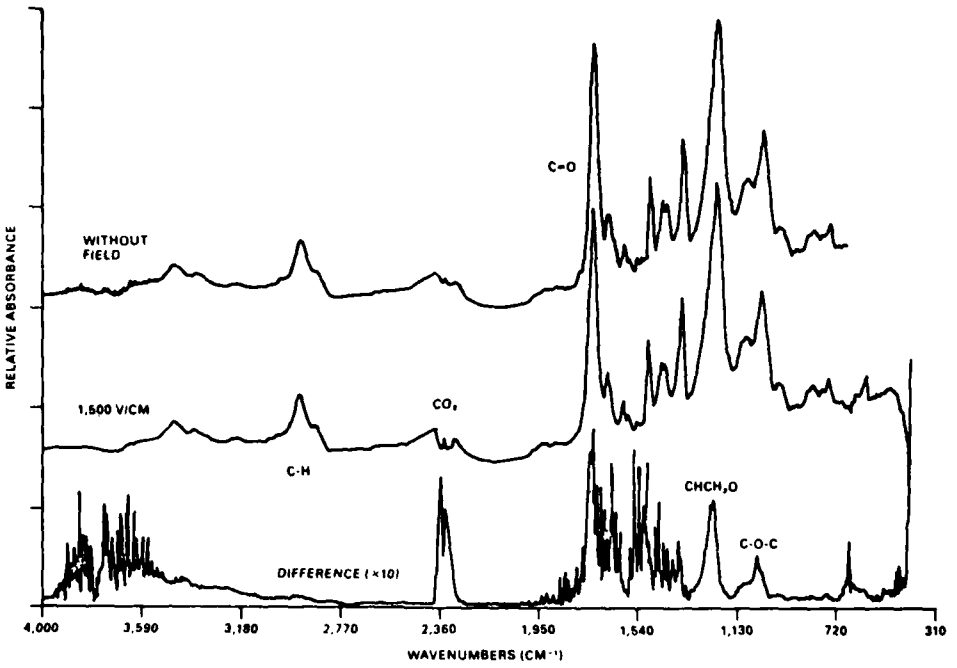

Figure 3.5. IR Electroabsorption for Uncrosslinked Cured Viscous Epoxy.

The electroabsorption spectrum (bottom) is the difference between field-on (middle) and field-off (top) spectra. The resin of Epoxylite 810 adhesive was reacted with acetic anhydride and a small amount of acid catalyst to induce the epoxide ring opening reaction without crosslinking the material. The resultant product was a viscous gel.

Dipoles which respond to the applied field in the EAB experiment, and are thus candidates for explanation of the TSDR data, are listed on Figure 3.5 (Table). Note that the C-H absorption does not respond to the applied field. The CO_2 peak is an instrumental artifact and not an EAB signal.

NOTE: The next two figures represent a digression from the main topic of this paper (interfaces), but do indicate how TSDR can be used in non-destructive evaluation (NDE) applications.

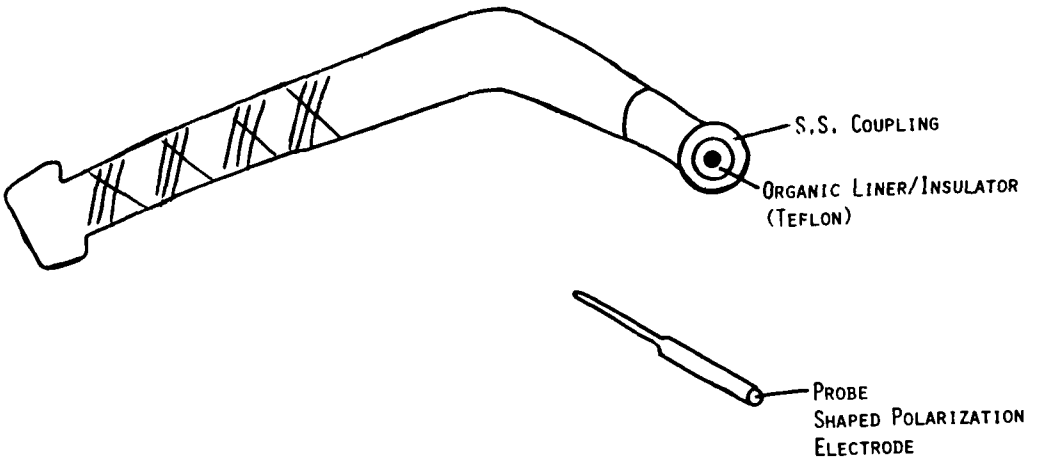

Figure 3.6. Schematic Illustration Showing Application of Thermally Stimulated Dipole Relaxation Method (TSDR) to NDT Inspection of Teflon Hydraulic Tubes.

It was necessary to distinguish between two types of Teflon liners in a series of stainless steel wound hydraulic hoses. The distinguishing characteristic was found by chemical means to be an OCF_3 side-group. Using the stainless-steel winding as one electrode, and copper probe sized to the hose I.D. as the other, TSDR thermograms of the liner material can be recorded.

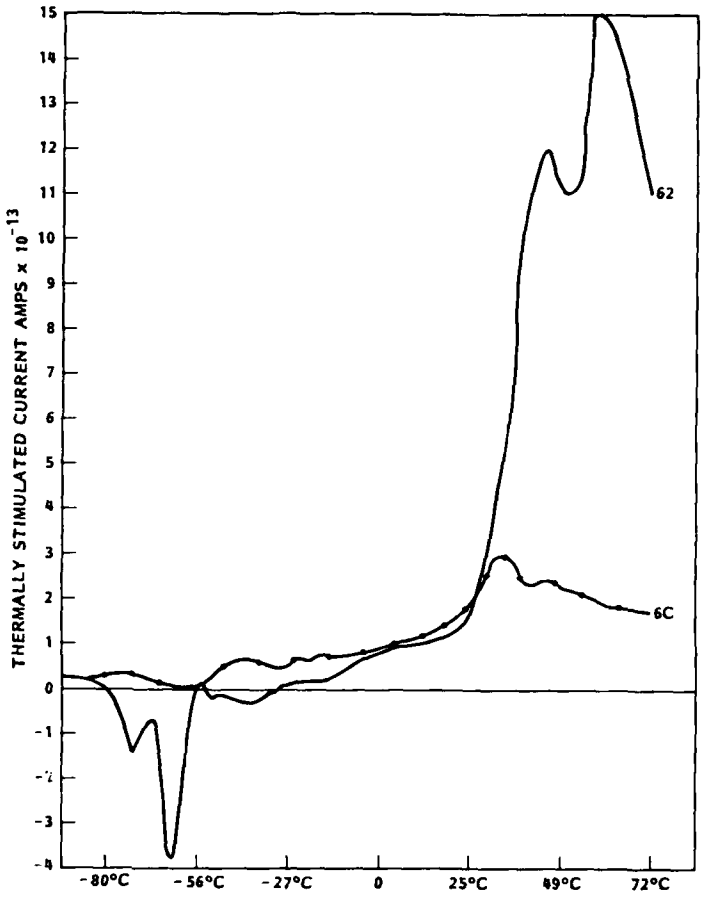

Figure 3.7. TSDR Thermograms Used to Distinguish Between Two Resins in the NDE Inspection of Teflon Hydraulic Tubes.

The 62 resin contains an OCF_3 side-group (absent in the 6C resin) every 40 repeat units along the polymer chain. This side-group, which possesses a large dipole moment, causes the high temperature dipolarization peak used to categorize each tube.

MODEL FOR FORMATION OF IAZ: INORGANIC POLYMER ANALOGUE

The mechanical and dipolar results presented in the previous Sections indicate that structural gradients project a considerable distance (>100 μm) into the adhesive from the interface. These results alone indicate possible shortcomings to the design of structural joints and composite materials based upon bulk strength properties of the adhesive.

How do these structural gradients arise? Current efforts to identify the detailed chemical nature of the IAZ are inconclusive. Since the physical forces associated with bonding are indeed short range, it is difficult to imagine structural inhomogeneities propagating many molecular layers from a bonding surface.

However, bond formation is not simply a statics problem. Nucleation and growth kinetics must be acknowledged, for most structural adhesives undergo a phase change during the curing process. The effects of such dynamics are most easily seen in the gas phase deposition of thin films onto a substrate. The resultant film structure, often macroscopic in nature, depends upon gas phase pressure, substrate temperature and substrate surface condition. In this Section we present recent results, for both polycrystalline and amorphous thin films, showing structural effects extending many molecular dimensions from the substrate surface. The amorphous film case is especially interesting and we wish to propose it as the analogue model for macrostructure in adhesives.

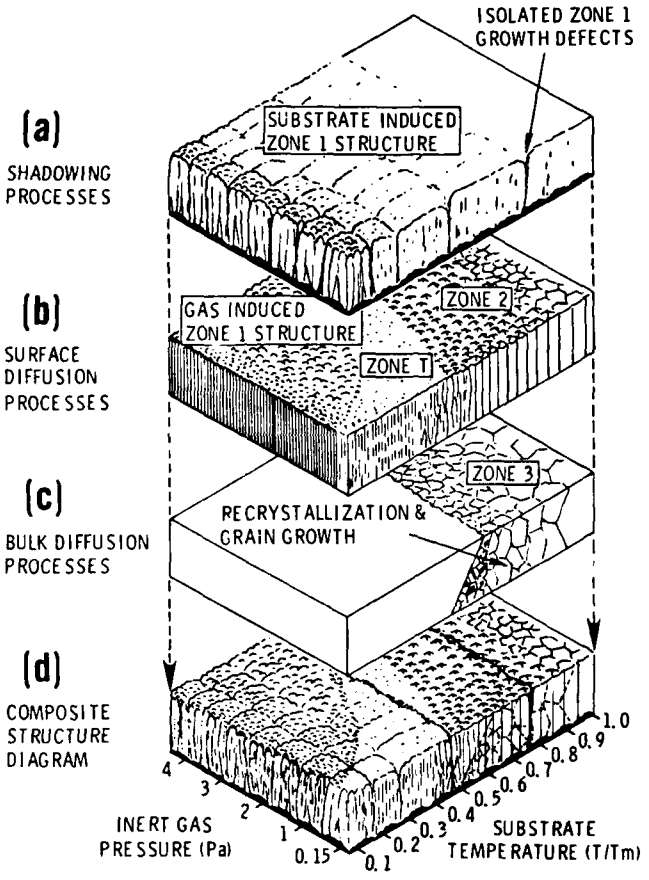

Figure 4.1. Effects of Nucleation and Growth Processes on Microstructure of Thin Films[3].

In the case of polycrystalline films sputter-deposited onto a substrate, the microstructure is seen to depend upon (a) substrate surface (nucleation and subsequent shadowing), (b) substrate temperature and sputter-gas pressure (surface diffusion) and (c) bulk diffusion.

[3] Diagram courtesy of Dr. J. A. Thornton, Telic Corporation.

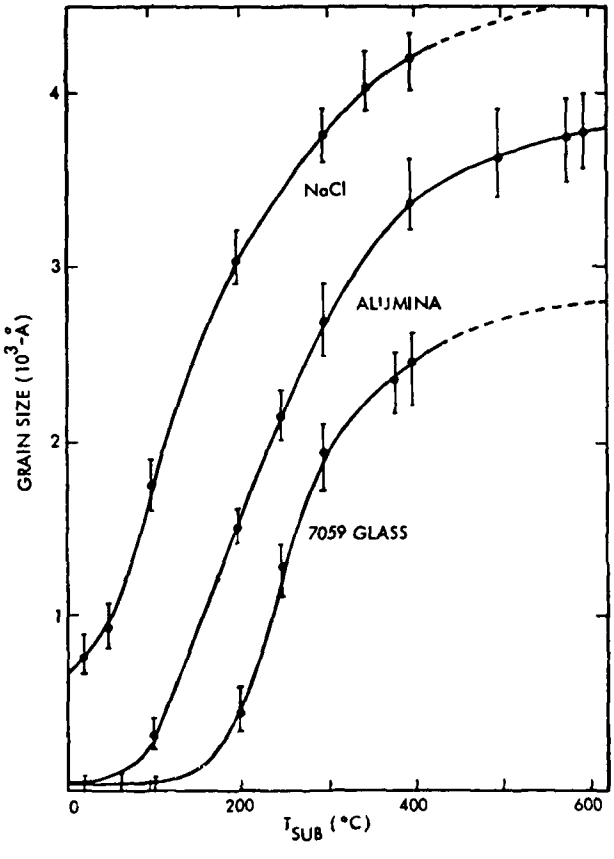

Figure 4.2. Effect of Substrate Material and Temperature on Vacuum-Deposited Polycrystalline Thin-Film Grain Size (Example of $CuInS_2$ From Kazmerski[4]).

A factor of 50 increase in grain size is accomplished when the substrate is changed from glass to single crystal NaCl at a substrate temperature just below 200°C.

[4] L. L. Kazmerski, "Ternary Compound Thin Film Solar Cells," Dept. of E.E., U of Maine, 1st Quarter Report to NSF on Grant No. AEF75-19576 (Nov. 1975).

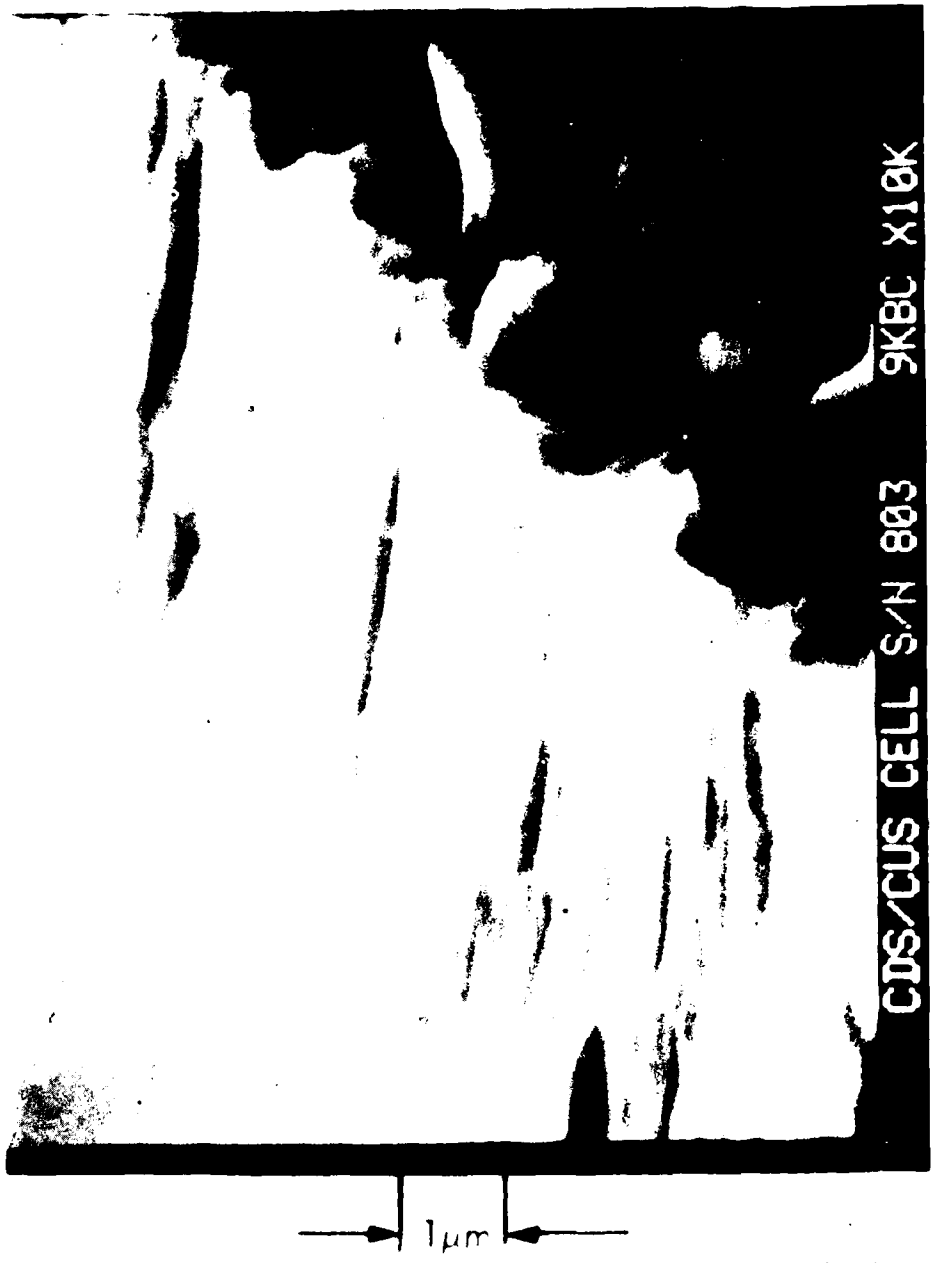

Figure 4.3. Edge SEM Photo of Sputter-Deposited CdS Film Showing Columnar Grains[5].

The densely-packed Zone T (see Figure 4.1) grains measure about 1200-1500Å in width for this film deposited onto metallized glass at $T_{substrate} \approx 270^{\circ}C$.

[5] W. W. Anderson and A. D. Jonath, "Cadmium Sulfide/Copper Sulfide Heterojunction Cell Research," Technical Progress Report, SER/8033-1/3 (LMSC-D682102), Lockheed Missiles and Space Company, February 1980.

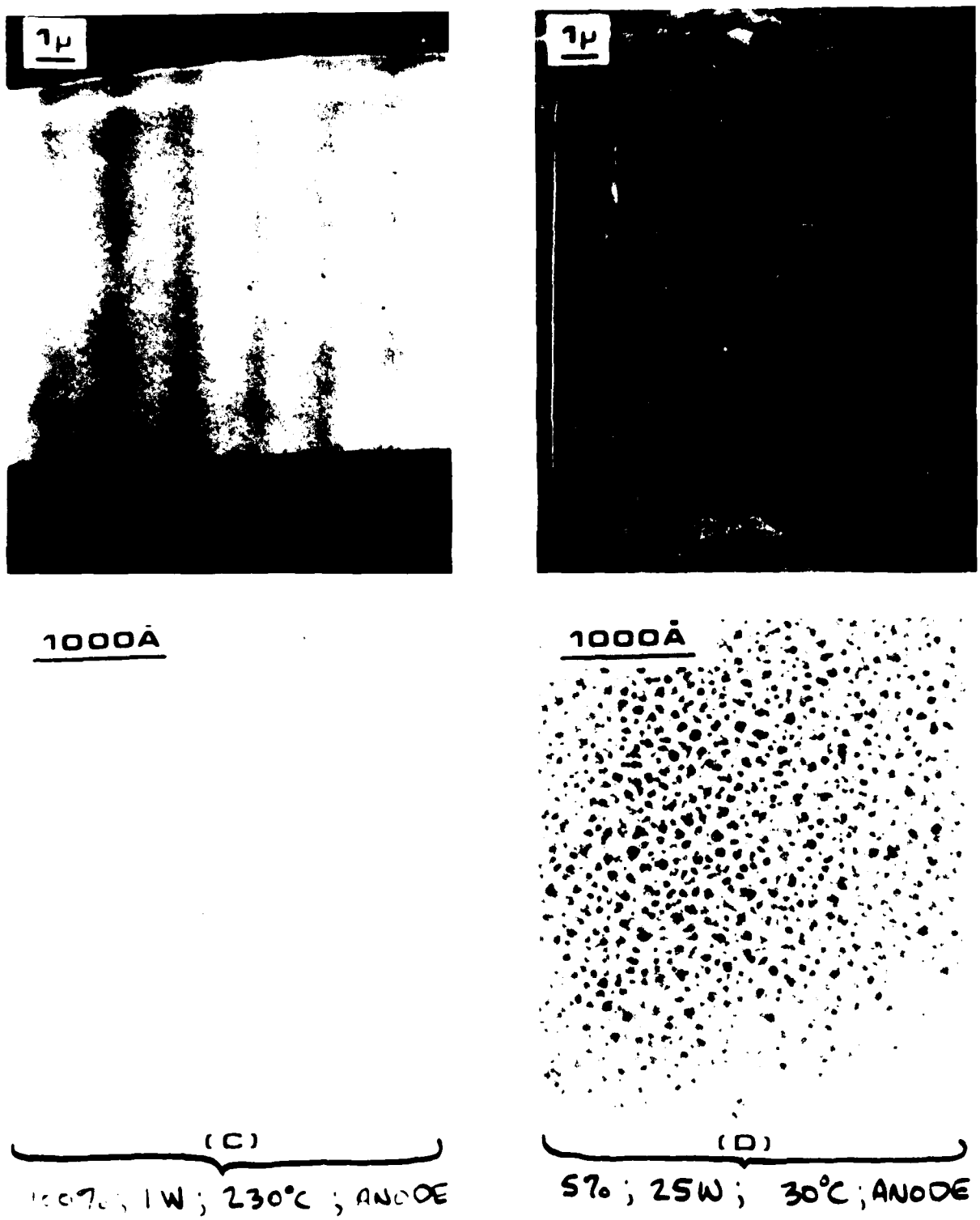

Figure 1.4. Edge (A and C) and Top (B and D) SEM Photos of Hydrogenated Amorphous Silicon Thin Films Deposited from a Silane Plasma Discharge[6].

[6] Photo courtesy of Dr. John Knights, Xerox Palo Alto Research Center.

The film on the left-hand-side was deposited under conditions of high substrate temperature, high SiH_4/Ar pressure ratio and low power level supplied to the discharge. Ignoring the broad periodic pattern which is an instrumental artifact, the film appears to be structureless. This result might be expected from its amorphous state. However, on the right-hand-side, a film deposited at opposite conditions, although still amorphous, comprises columnar grain-like structure. The deposition conditions for this film apparently encourages multiple nucleation sites and restricts surface diffusion. As in the polycrystalline case, the columns propagate many (10^3 - 10^4) atomic diameters from the interface.

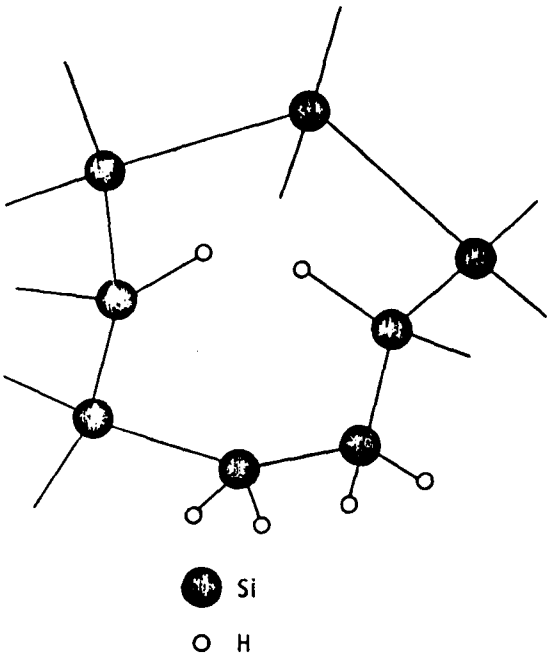

Figure 4.5. Schematic Diagram of Part of An Hydrogenated Amorphous Silicon (a-Si) Film.

The silicon atoms retain their four-fold coordination as in the crystalline state. Bond angle distortion is most likely responsible for their organization into the amorphous form. Somewhere between 0.01 and 1% of the bonds cannot be completed, giving rise to the lack of long range order. These dangling bonds represent unpaired elections which introduce electronic states into the material. Hydrogenation passivates the dangling bonds by forming Si-H bonds with the unpaired electrons.

Two distinct types of Si-H bonding are observed: (a) $Si-H_1$ shown in the center of the diagram and (b) $Si-H_2$ depicted at its lower edge.

Columnar structured material of Figure 4.4 (r.h.s.) generally contains more $Si-H_2$ hydrogenation and has smaller compressive stress than does the "grain-free" material. Furthermore, the $Si-H_2$ species is concentrated between the columns[7]. The column interior contains mostly $Si-H_1$ bonded hydrogen. The hydrogenated a-Si films are mechanically continuous and thus the observed columnar structure is interpreted as phase separation. Evidently the phase between columns provides a mechanism for stress-relief, especially effective when one imagines several $Si-H_2$ species joining to form low-coordinated polymeric material. The evidence[7,8] (I.R., Raman, Luminescence, Low Angle X-ray, and Neutron Diffraction) suggests that the regions between the islands during nucleation, and between the columns during growth contain excess defect sites available for increased hydrogen bonding. These regions become enriched in the $Si-H_2$ monomer, eventually leading to formation of the $(Si-H_2)_n$ polymer.

Thus in the deposition of a simple inorganic amorphous solid containing polymeric material, the kinetics of nucleation and growth play a role in developing phase changes, which in turn cause macroscopic structural organization of the material. Of course, configurational entropy must be acknowledged. The polymer forms at the column boundry because that is the region of increased disorder. That is, there is room for polymer development at the boundaries of (compared to within) the growing columns.

The detailed mechanism of this dynamic process is not understood. For example, one must explain the diffusion processes which bring the excess hydrogen to the surface bonding sites. To apply these ideas to even more complicated organic polymer systems might seem premature. Some might not wish to use gas phase deposition model for a crosslinking solidification process. Also, we do not yet have evidence to corroborate the TSDR data implications of macroscopic structural ordering. But, other indications of

---

[7] J. C. Knights, J. Non-Crystalline Solids, 35&37 (1980) 159.

[8] A. D. Jonath, J. A. Thornton, W. W. Anderson, J. L Crowley, H. F. Mac Millan and G. B. McCauley, "Infrared Absorption in Magnetron Sputtered a-Si:H Films, Proc. 3rd European Communities Photovoltaic Solar Energy Conference, Cannes, 27-31 Oct. 1980, Reidel, Holland/Boston (1981) 840.

macrostructure, ordering and multiple phase phenomena in amorphous organic polymer systems do exist: ordering of floccules in two-phase epoxy polymers has been observed[9]; transcrystalline regions have been formed in high-density polyethylene which were melted and solidified in contact with various substrates[10].

So we propose this sketetal model as an analogue to explore nucleation and growth processes which lead to the observed macroscopic gradients in epoxy adhesive physical properties.

ACKNOWLEDGEMENTS

The authors wish to thank their colleagues at Lockheed for significant contributions in the following areas:

Ultrasonics - G.C. Knollman, J.L. Bellin and J.J. Hartog
Chemistry - R.C. McCalley, E.R. Byrd and R.A. Arcus
Fracture Mechanics - J.G. Bjeletich and D.L. Flaggs

[9] R. E. Cuthrell, J. App. Poly. Sci., 12, 1263 (1968).
[10] L. H. Sharpe, J. Adhesion, 4, 51 (1972).

STUDIES OF THE CHARACTERIZATION OF ORGANIC MATERIALS BY NON-STATIONARY CHEMILUMINESCENCE TECHNIQUES

G. A. George and D. M. Pinkerton

Materials Research Laboratories
Melbourne, Australia

ABSTRACT

The technique of non-stationary chemiluminescence involves measuring the weak light emitted from an organic material when its environment is perturbed. This perturbation may involve either stressing the material, briefly UV irradiating it or changing the gas above the heated polymer from an inert to an oxidizing atmosphere. In all cases the effect of the perturbation is to create a transiently high concentration of free radicals in the material. The rate at which the material reaches the steady state in the new environment, as given by the change in the chemiluminescence intensity, is a measure of the rate of specific free radical reactions in the material. The rates of these reactions are very sensitive to the presence of trace impurities, initiators, stabilizers and the micro-environment of the material. The non-stationary technique is thus useful as a tool for chaaracterizing organic materials when used in conjunction with other methods of physical and chemical characterization.

One particular advantage of the non-stationary method over stationary chemiluminescence studies as well as other methods of measuring oxidation of organic materials is the ability to obtain rate parameters at very low extents of oxidation. Assessment is thus rapid and potentially non-destructive.

Examples of studies at MRL by both stationary and non-stationary chemiluminescence include:

(i) the oxidation, at normal cure temperatures, of liquid epoxy resins of different extents of chemical purity. Resins examined include bisphenol-A epoxies (Epon 828) epoxy novolacs (DEN 438) and diamino diphenyl methane epoxies (MY 720);

(ii) the thermal and stress chemiluminescence of composite materials, in particular, transverse ply matrix cracking in cross-plied RAC 7250 and 3M-1009-26 laminates;

(iii) the thermal and stress-induced chemiluminescence from fibres of nylon 6, nylon 66 and poly(ethylene terephthalate).

From these examples it is concluded that the technique shows promise as a characterization tool for complex composite materials.

1. INTRODUCTION

The oxidation reactions of organic materials are frequently accompanied by the emission of light. The quantum efficiency of this light emission reaction can be as low as 10^{-9}, but by using sensitive light detection apparatus, much information can be gained about the properties of the material from the nature of the emitted chemiluminescence [1]. Our interest at MRL in the use of chemiluminescence has arisen from the need for accurate service life prediction of polymers when used in critical applications. The ability of chemiluminescence to provide kinetic information at low extents of oxidation provides an alternative to the often unreliable method of accelerated ageing, and is an adjunct to methods such as FTS-IR that can be used for studying small changes in the chemical composition of polymers during ageing [2].

The chemiluminescence method is particularly attractive because of the passive nature of the experiment. In principle all we do is look at the sample and it provides us, by way of the intensity of the weak emitted visible light, with the kinetic parameters that determine its rate of oxidation. There are two different types of experiment that can be performed. In the first case the change in light intensity as a function of time of oxidation is measured. At low rates of oxidation there are only small changes in light intensity and this 'steady state' experiment will be of long duration and severely test the stability of the instrumentation as well as the patience of the experimenter. An alternative approach is to perturb the environment of the material and measure the change in the chemiluminescence intensity as the material responds to the perturbation and then returns to the steady state. This perturbation may involving UV radiation, stress or changing the atmosphere above the polymer from inert to oxidizing. We have studied in detail this 'non-stationary' chemiluminescence from one well characterized material - oriented fibres of nylon 66 - to determine the factors affecting chemiluminescence and the kinetic information that can be extracted [3]. We have found that non-stationary chemiluminescence is very sensitive to the presence of trace impurities, stabilizers and the microenvironment of the material. It is thus possible that non-stationary chemiluminescence could be a non-destructive technique for characterizing epoxy resins and their composites when used in conjunction with other analytical techniques. In addition, the overall thermo-oxidative stability of the composite can be assessed.

In this paper we wish to explain the technique with reference to nylon 66 and then indicate our preliminary experiments on liquid epoxy resins and composite materials under non-stationary conditions.

2. APPARATUS

The instrumentation required for the observation of chemiluminescence is simple - an environmentally controlled sample chamber, a light detector and ancillary amplification and recording equipment. Figure 1 shows the basic apparatus used for steady state studies and in non-stationary experiments in which the perturbation is achieved by UV irradiation or gas exchange. The light, emitted by the sample on oxidation, is gathered by the lens and focussed on the photomultiplier, the signal from which is analysed by the photon counting

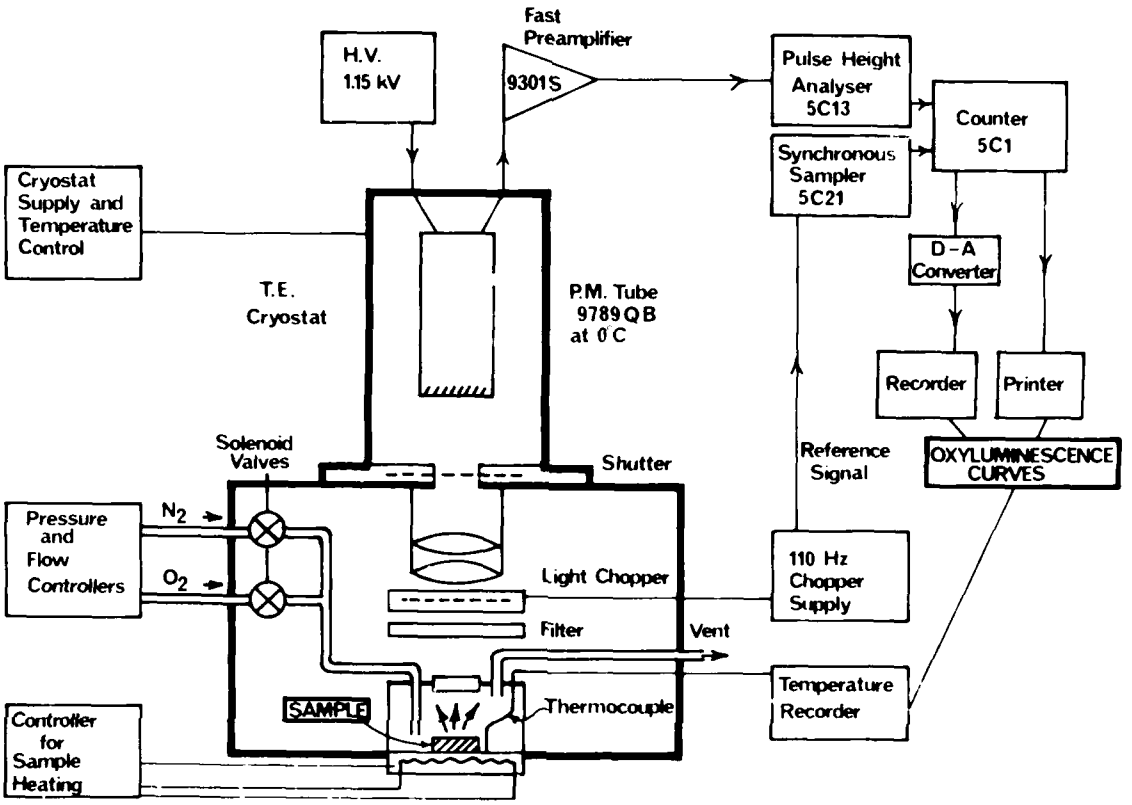

Figure 1 Schematic diagram of photon counting chemiluminescence apparatus used for non-stationary kinetic studies.

system to give a measure of the light intensity. Solenoid valves and a small dead volume provide rapid and reproducible gas exchange at the sample. The sample can be UV irradiated from a lamp outside the apparatus by a small mirror in the filter position. By mounting the mirror on the inside of the access door it is removed from the optical path to the photomultiplier when the door is closed for the observation of chemiluminescence. The delay time between ceasing irradiation and recording chemiluminescence is about two seconds.

For studies of stressed materials we have used a different apparatus as shown in Figure 2. Instead of attaching a stress rig to our chemiluminescence apparatus we have attached a light detection system to a tensile testing machine. The environmental chamber of an Instron Model 1026 bench top machine has been modified by attaching a lens system and cooled photomultiplier to the door. The only other modifications required are the addition of a thermocouple and the blocking-off of all light paths into the chamber. The load-time trace at the chosen rate of elongation and the light intensity-time trace from the photon counter (or electrometer) are simultaneously recorded.

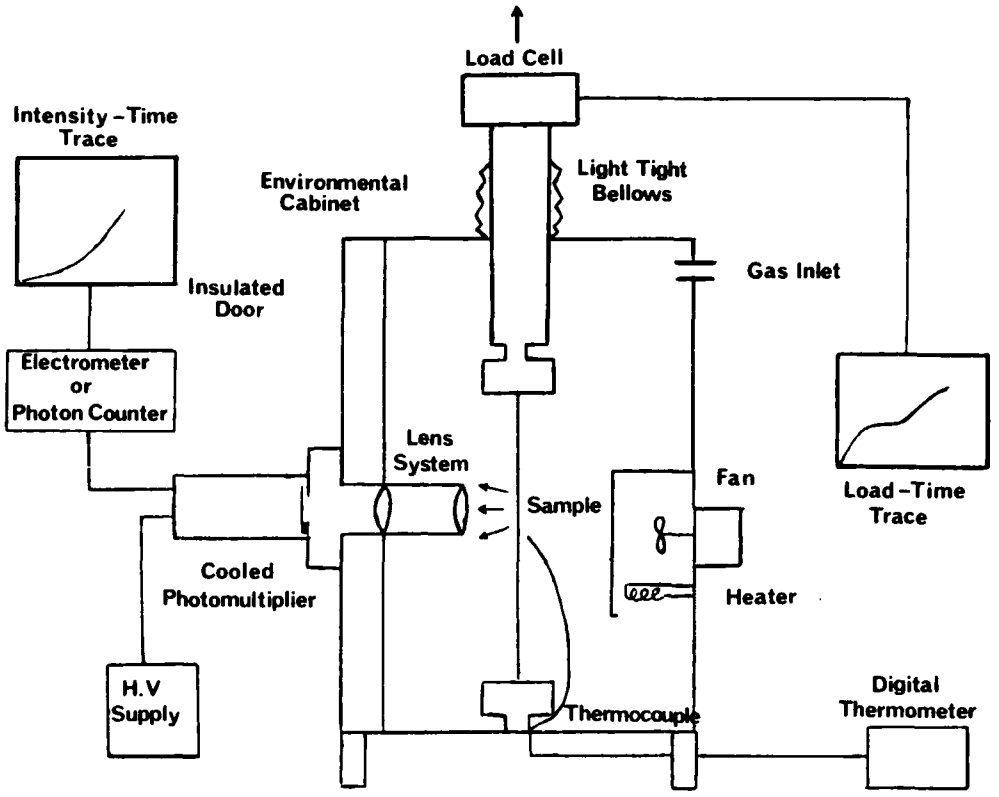

Figure 2 Schematic diagram of apparatus used for studies of stress induced chemiluminescence from fibres and composites. The system is built around the environmental chamber of an Instron Model 1026 tensile testing machine.

3. CHEMICAL ORIGIN OF CHEMILUMINESCENCE

The chemiluminescence reaction during the auto-oxidation of liquid hydrocarbons and solid polymers is considered to be the termination reaction of alkyl peroxy radicals, shown as reaction 5 in Figure 3. This reaction is exothermic by over 100 kcal/mol and this energy is partitioned over the reaction products. About 60 to 70 kcal/mol are required to excite the carbonyl oxidation product to its triplet state and weak phosphorescence from this group is the observed chemiluminescence. Quenching of this excited state by molecular oxygen is partly responsible for the low quantum yield of 10^{-9}. Before this reaction can take place, a six-membered intermediate must be formed (Russell Mechanism) so that at least one of the terminating radicals must be primary or secondary. It is generally found that in those polymers where this requirement is not met (eg. polypropylene, Kevlar) then chemiluminescence is not observed until the material is highly oxidized and secondary oxidation products are formed. Fortunately, in many epoxy resins and composite materials, oxidation of activated methylene groups results in the formation of suitable radicals to observe chemiluminescence.

SIMPLIFIED NYLON 66 AUTO-OXIDATION SCHEME

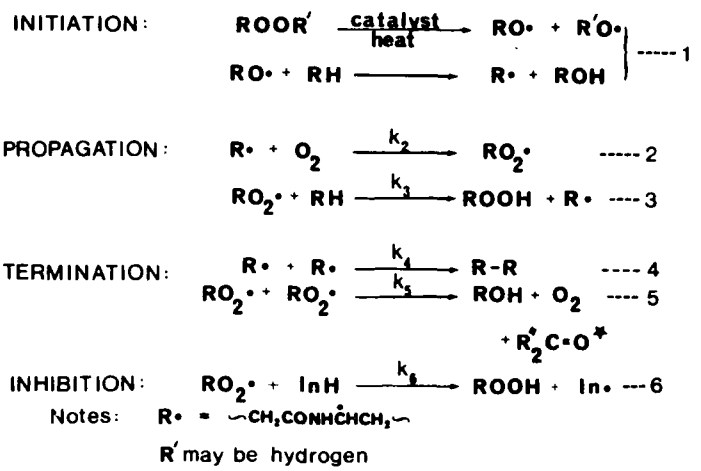

Figure 3 Free radical reaction scheme for the auto-oxidation of a hydrocarbon or polymer.

The intensity of chemiluminescence, I, will be proportional to the rate of termination and will therefore reflect the concentration of alkyl peroxy radicals in the material.

$$I = \emptyset\, k_5\, [RO_2^{\cdot}]^2 \qquad (1)$$

where $\emptyset$ is the chemiluminescence quantum yield. Thus those reactions which change the alkyl peroxy radical concentration will change the intensity of chemiluminescence. This could result from changes in the rate of initiation, since in the steady state the rates of initiation r_i and termination must be equal so that $I = \emptyset r_i$. Other factors affecting the alkyl peroxy radical concentration will be the rate of scavenging by antioxidants (InH) and the competition between the termination reaction of alkyl radicals (Reaction 4) and their reaction with oxygen (Reaction 2). Physical effects such as the morphology and microviscosity of the material will affect the termination rates as these will be diffusion controlled. It should also be noted that in all chemiluminescence experiments it is assumed that the quantum yield $\emptyset$ does not change throughout the experiment. After prolonged oxidation this will not be so as energy transfer to oxidation products as well as secondary oxidation routes will change $\emptyset$. In the shorter term non-stationary experiments this is not a problem.

When the steady state condition is disturbed, by for example, a change in the rate of initiation, then the rate of approach to the equilibrium condition will be determined by the rate constants for the reaction scheme of Figure 3

AD-A116 733 ARMY MATERIALS AND MECHANICS RESEARCH CENTER WATERTOWN MA F/G 11/4
PROCEEDINGS OF THE CRITICAL REVIEW: TECHNIQUES FOR THE CHARACTE--ETC(U)
MAY 82

UNCLASSIFIED AMMRC-MS-82-3 NL

4 OF 6
AD
A116733

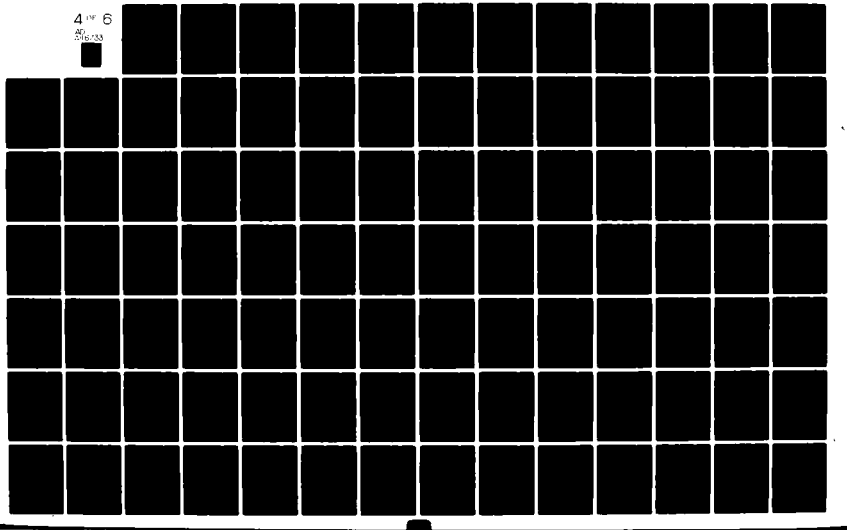

$$\text{ie} \quad \frac{d[RO_2^{\cdot}]}{dt} = r_i - k_5[RO_2^{\cdot}]^2 - k_6[\text{In H}] \neq 0 \qquad (2)$$

This equation can be solved for certain boundary conditions and the instantaneous alkyl peroxy radical concentration expressed as the corresponding chemiluminescence intensity through Equation (1). For example if an unstabilized polymer is briefly UV irradiated and irradiation ceases at time, t = 0, then Equation (2) becomes

$$\frac{d[RO_2^{\cdot}]}{dt} = - k_5[RO_2^{\cdot}]^2$$

and the alkyl peroxy radical concentration should decay by second order kinetics on ceasing irradiation. Converting to chemiluminescence intensities, the solution is

$$\left(\frac{I_0}{I}\right)^{\frac{1}{2}} - 1 = (k_5\, r_i)^{\frac{1}{2}}\, t \qquad (3)$$

The form of the solution thus depends on the experimental conditions of the non-stationary experiment, and experiments are designed to yield the simplest intensity-time relationship.

This will be illustrated in the following section using three perturbation methods to generate non-stationary conditions in *nylon 66 fibres*. *The application of these to epoxy resins and* composite materials and the possible use of the results in characterizing the material will then be described.

4. UV IRRADIATION

4.1 Nylon 66

Figure 4 shows the change in chemiluminescence intensity after irradiating nylon 66 fibres for two minutes before stopping the irradiation and observing the chemiluminescence. The background emission from a sample irradiated in a non-oxidizing atmosphere is shown and it can be seen that the photoluminescence (probably phosphorescence) contributes to the emission intensity for only the first few seconds. Analysis of this curve shows that second order kinetics described by Equation (3) are obeyed and the radical lifetime τ can be measured.

$$\tau = \frac{1}{k_5[RO_2^{\cdot}]_0} = \frac{1}{(k_5\, r_i)^{\frac{1}{2}}}$$

The factors affecting the rate of initiation and termination can now be studied. If k_5 is known, the changes in r_i due to the presence of trace amounts of photosensitive impurities can be determined from the

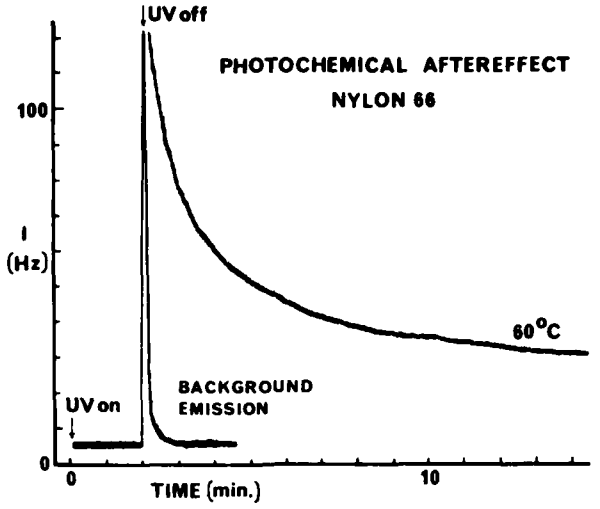

Figure 4 Decay of chemiluminescence from nylon 66 fibres at 60°C after UV irradiation in air at 313 nm for 2 minutes. The background emission in an inert atmosphere is also shown.

value of the radical lifetime. The type and concentration of these impurities depend on the conditions of manufacture and processing of the fibre, so the technique is a sensitive probe of the thermal history of the material.

4.2 Glass-epoxy Composite (3M-1009-26)

The composition of the 3M-1009-26 glass-epoxy composite is shown in Figure 5. It was found that when a small section of 3 ply ($0^o/90^o/0^o$) composite was introduced into the chemiluminescence apparatus there was a high count rate followed by a slow decay over an hour. This was found due to the formation of free radicals in the epoxy resin by photochemical initiation by fluorescent room lights. A typical decay curve after low intensity UV irradiation is shown in Figure 5 and it can be seen that the decay follows second order kinetics. The UV sensitivity of this composite arises from the formation of photosensitive impurities in the surface of the resin from thermal oxidation of the epoxy novolac resin (DEN438) during cure and post-cure [4]. The extent of the oxidation of the composite during cure can be determined from the radical lifetime as in the previous section for nylon 66. Since the radical lifetime is dependent on the diffusion controlled termination rate constant, k_5, it should be a sensitive index of the cross-link density of the composite. This aspect is currently being studied for this and other epoxy resins.

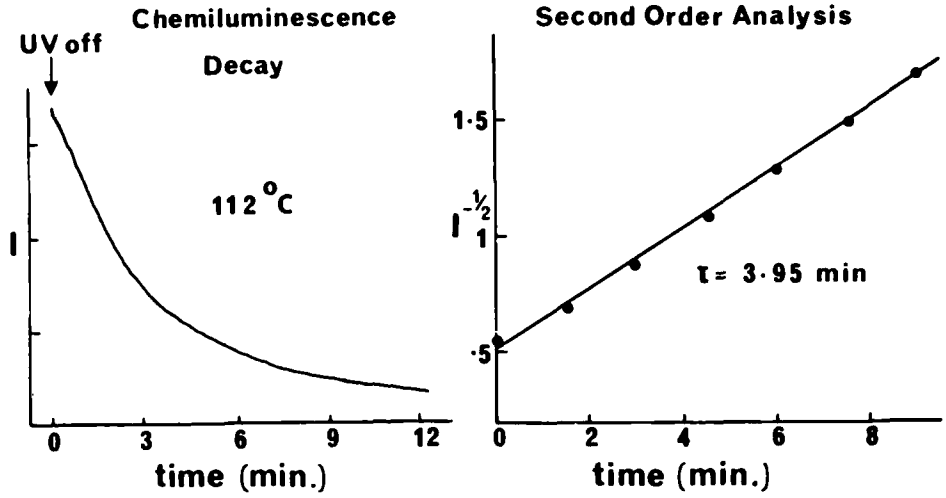

Figure 5 Decay of chemiluminescence from a 3 ply sample of 1009-26 glass epoxy composite after weak UV irradiation in air. The analysis of the decay according to Equation (3) is shown.

5. GAS SWITCHING

The second non-stationary method we have studied is the effect of rapid gas exchange on the chemiluminescence from a heated sample. In the course of our early studies on steady state chemiluminescence we had observed that if a nylon sample was heated in nitrogen for a period from several minutes to hours there was a burst of chemiluminescence when oxygen was then introduced to the sample. The emission then decayed back to the steady state intensity for the particular temperature. We have studied this phenomenon in detail for nylon 66 and we are now applying it to the characterization of uncured epoxy resins.

5.1 Nylon 66

Figure 6 shows the burst of chemiluminescence observed from nylon 66 fibres when heated for different times in nitrogen before admitting oxygen. It can be seen that the peak intensity increases with time of heating but the steady state intensity after the emission decays is the same in each case. The peak intensity approaches a maximum value with heating time as shown in Figure 7.

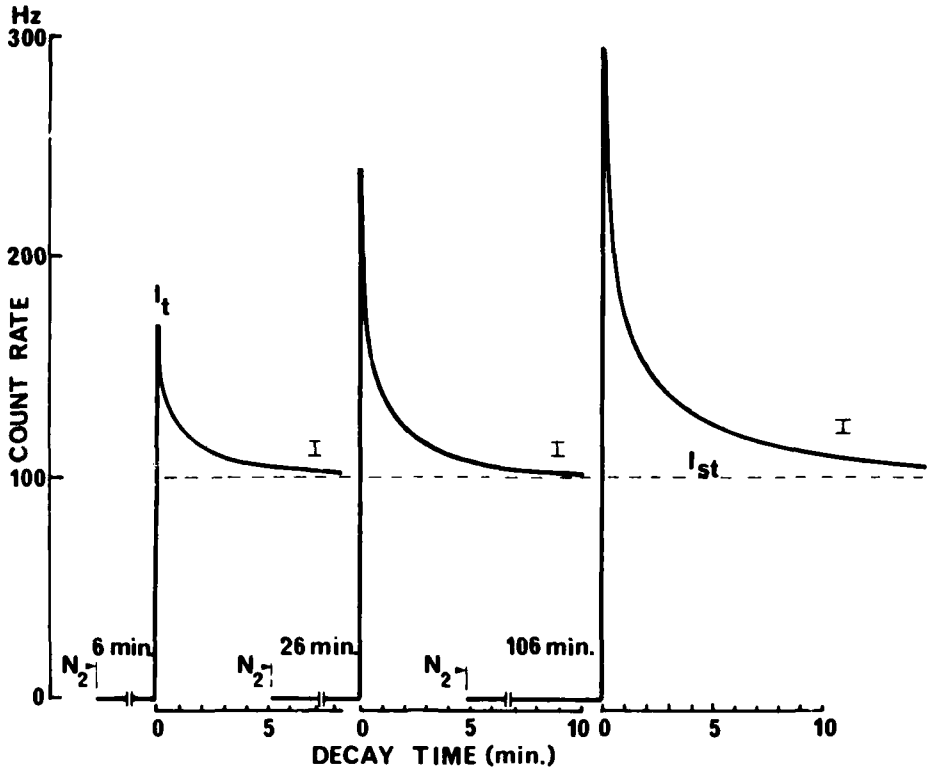

Figure 6 The burst of chemiluminescence observed from nylon 66 when heated for different times in nitrogen before admitting oxygen at zero time. I_t is the emission intensity after a heating time t and I_{st} is the stationary state intensity after decay. The standard deviation of I_{st} is indicated.

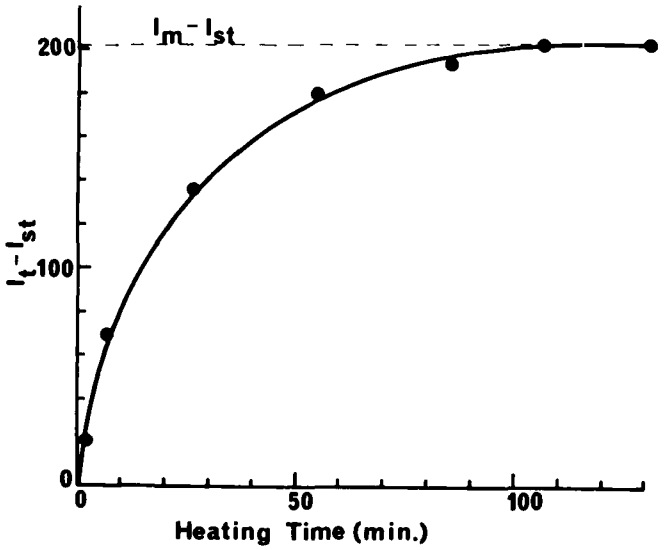

Figure 7 The dependence of the peak chemiluminescence intensity shown in Figure 6 on time of heating in nitrogen. I_m is the maximum observed value.

To understand this process and analyze the growth and decay curves we have to consider the free radical auto-oxidation scheme of Figure 3. If an organic material is heated in the absence of oxygen alkyl radicals will be formed through thermal decomposition of trace impurities at a rate r_i'. These will terminate at a rate $k_4[R^\cdot]^2$ (Reaction 4) so that the steady state concentration will be

$$[R^\cdot]_{st} = \left(\frac{r_i'}{k_4}\right)^{\frac{1}{2}}$$

If oxygen is now admitted, then all of these alkyl radicals should become alkyl peroxy radicals by Reaction 2 at the very fast rate $k_2[R^\cdot]\,[O_2]$. Thus the instantaneous alkyl peroxy radical concentration will equal the steady state alkyl radical concentration $[R^\cdot]_{st}$. However the steady state alkyl peroxy radical concentration is given by

$$[RO_2^\cdot]_{st} = \left(\frac{r_i}{k_5}\right)^{\frac{1}{2}}$$

Thus if $k_4 \neq k_5$ there will be a difference between the instantaneous and steady state chemiluminescence intensities. If $k_4 > k_5$ there will be a growth and if $k_5 > k_4$ (the case for nylon 66) there will be a chemiluminescence burst followed by a decay to the steady state. Examples of these limiting cases are shown in Figure 8.

In the case of nylon 66, the decay curve Figure 5 will be described by the solution to Equation 2 for the chosen boundary conditions. Similarly the growth curve with heating time in nitrogen Figure 6 can be analysed by solving the differential equation for the alkyl radical concentration *[3]*. From these the lifetimes of the alkyl and alkyl peroxy radicals can be calculated. The factors affecting both of these can now be explored. The rate of thermal initiation and thus the radical lifetime depends on the concentration of free radical forming impurities. From the analysis of the non-stationary kinetics it has been found that the alkyl radical termination (Reaction 4) can compete with the oxygen scavenging (Reaction 2) in nylon 66. The chemiluminescence is thus a probe of the solubility and mobility of oxygen in the solid polymer. This is sensitive to the crystallinity and structure of the amorphous region of the polymer and could be a useful characterization tool.

The presence of stabilizers has a pronounced effect on the decay kinetics and the loss of stabilizers on ageing can be followed by chemiluminescence. This is shown in Figure 9 which is a plot of the intensity function against decay time for a fully stabilized sample of nylon 66 and one in which most of the stabilizer has been extracted. The kinetics are complex but the presence of stabilizer clearly lowers the alkyl peroxy radical lifetime (as given by the change in slope).

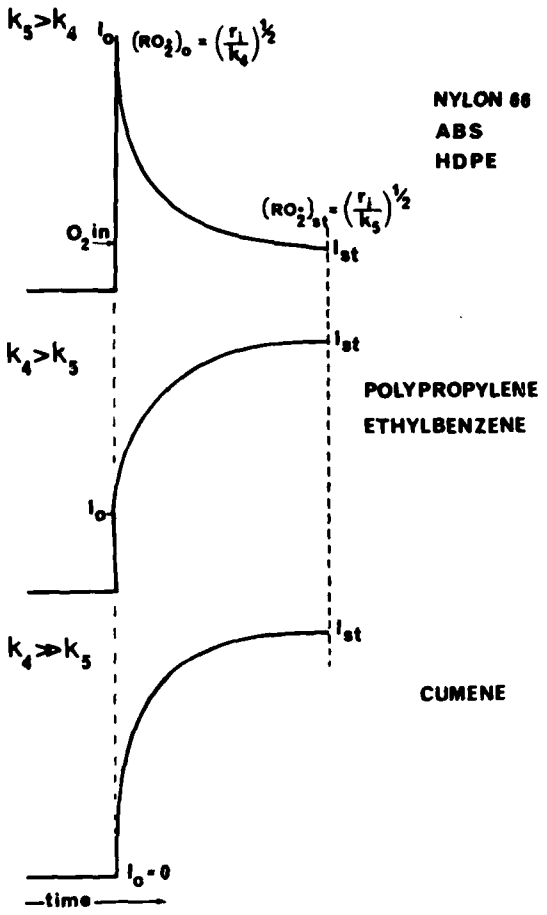

Figure 8. Typical changes in the chemiluminescence intensity from an organic material on admitting oxygen after heating in an inert gas. The resulting curve depends on the relative magnitude of k_4 and k_5.

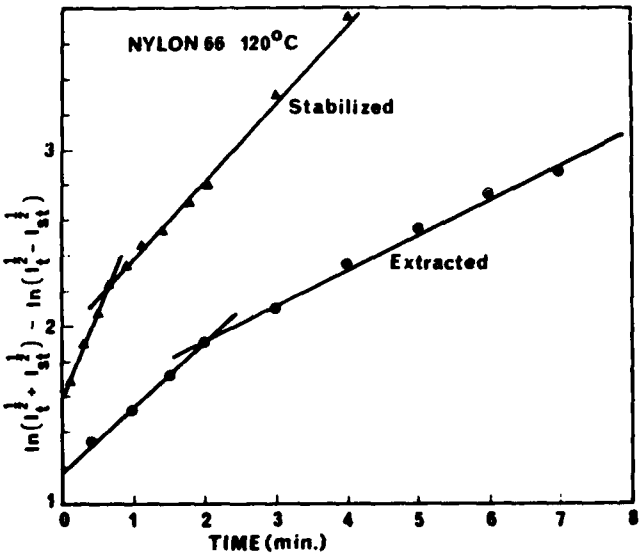

Figure 9. Analysis of the chemiluminescence decay from nylon 66 at 120°C after gas switching. The extracted material shows a slower rate of decay as would be expected from Equation (2) as [In H] is reduced.

5.2 Epoxy Resins

The application of the gas switching technique to several common epoxy resins heated, without hardener, to their cure temperature in air has been explored. Figure 10 gives the structure of the epoxy resins studied. Also shown are those activated methylene groups which are the most likely to oxidize and produce a secondary alkyl peroxy radical - a necessary prerequisite for observing chemiluminescence. In Epon 828 there is probably just one group while in the other resins there may be more than one point of oxidation. If there are substantial differences in reactivity one species will dominate the chemiluminescence reaction. The spectral distributions of the chemiluminescence from these resins at 112°C in air are shown in Figure 11. The resins DEN438 and MY720 are the most intense emitters suggesting a high rate of oxidation. The spectral distribution of Epon 828, believed due to oxidation of the ϕ-OCH_2 - group, also appears in DEN438 and ERL0510 which also contain this group. Similarly, if the spectral distribution of MY720 is attributed principally to the ϕ-N-CH_2 - grouping it can be clearly discerned also in ERL0510. A higher resolution study of chemiluminescence spectra may yield further information, along with I.R. studies of the specific oxidation sites at low extents of oxidation.

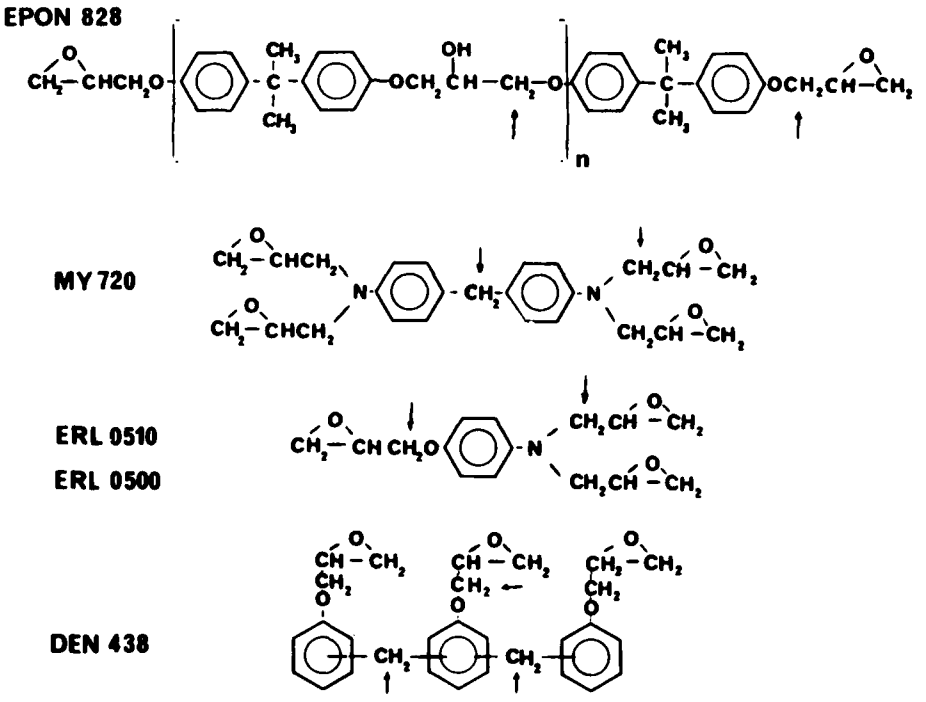

Figure 10 Chemical structure of commercial epoxy resins studied. The arrows indicate the activated methylene groups that would produce chemiluminescent centres on oxidation.

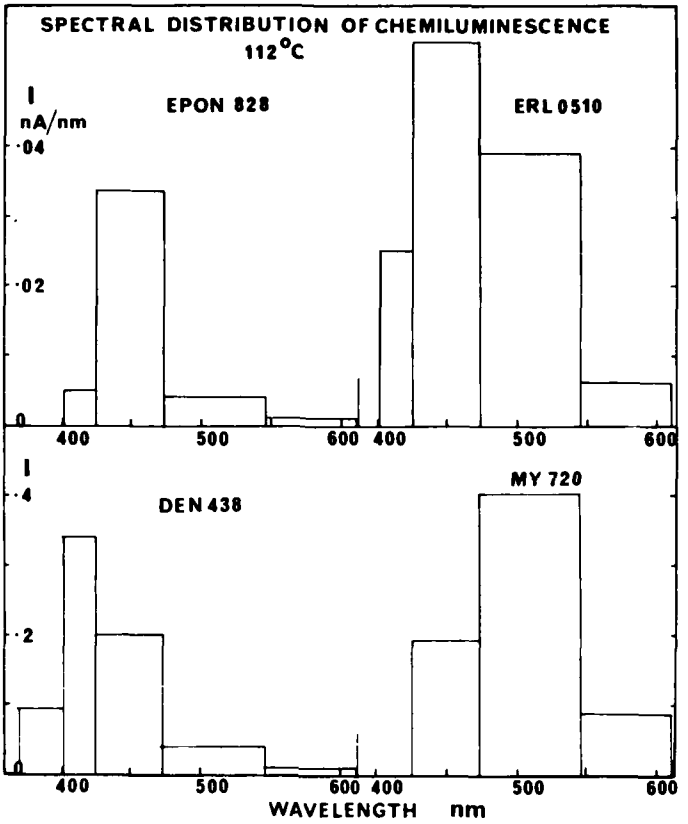

Figure 11 Spectral distribution of chemiluminescence from epoxy resins at 112°C in air.

The non-stationary behaviour on gas switching shows the most interesting differences and typical results for these resins are shown in Figure 12. Epon 828 initially shows kinetics indicating $k_4 > k_5$, but after a short period of oxidation there appears to be a chemiluminescent reaction in which $k_5 > k_4$. This is clearly of value in assessing the thermal history and extent of oxidation of the resin where there is a clear transition in the transient response. The resin ERL0510 shows kinetic behaviour very similar to that studied in nylon 66. There is a strong burst of chemiluminescence on exchanging gases and the intensity of the peak increases with time of heating in nitrogen. In contrast, the less pure form of the same resin ERL0500 (purity 78% compared to 97% for ERL0510 based on epoxy equivalent weight [5]) shows more complex transient behaviour. The behaviour is similar to that observed for MY720 resin and the curve could be resolved as the sum of two separate processes.

Our observations on the non-stationary behaviour of these resins have been necessarily qualitative, and a detailed quantitative study of these curves in conjunction with HPLC and IR analysis of the materials as a function of extent of oxidation is required.

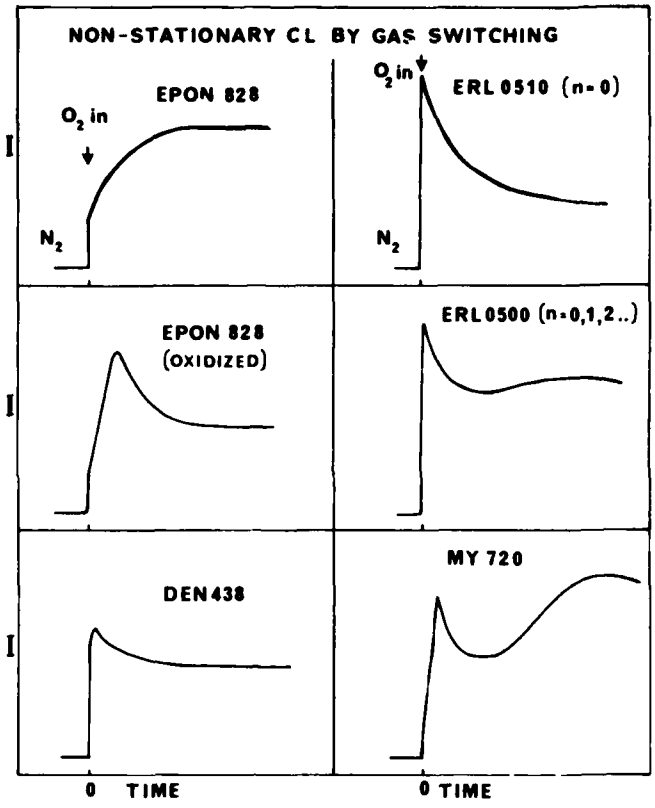

Figure 12 Typical non-stationary chemiluminescence curves generated by heating the epoxy resins in nitrogen for 15 minutes before admitting oxygen. The form of the curve is sensitive to the chemical purity of the resin.

6. STRESS INDUCED CHEMILUMINESCENCE

The final non-stationary technique we have investigated is stress induced chemiluminescence. Several recent reports of chemiluminescence from stressed epoxy resins suggest it may be of value in characterizing complex materials [6,7]. We have sought to understand the phenomenon by a detailed study of oriented nylon 66 and other fibres and we have then applied it to a glass-fibre epoxy composite (RAC 7250).

6.1 Nylon 66

Figure 13 shows the change in chemiluminescence intensity from a sample of nylon 66 yarn at 40°C in air that is elongated at a constant rate of 0.8 cm/min. The following points are noted:

(i) there is a small, almost linear increase in chemiluminescence with sample elongation until about 60% of the ultimate tensile strength

(ii) upon further elongation (after which free radicals can generally be detected in the polymer by electron spin resonance) there is an exponential increase in emission intensity up to the failure of the yarns

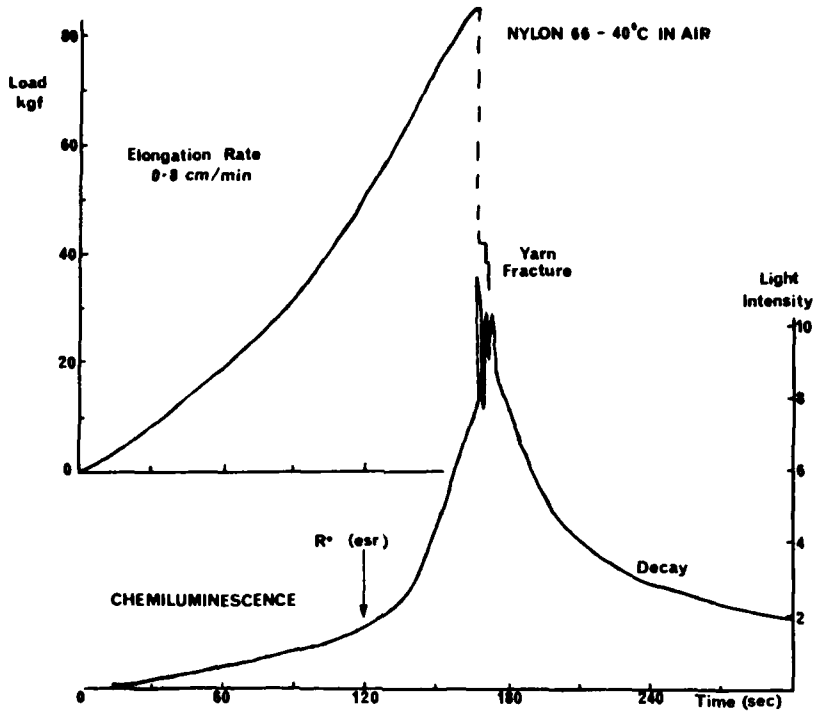

Figure 13 *Chemiluminescence from nylon 66 fibres when elongated at* 0.8 cm/min at 40°C in air. The simultaneous load-time curve is also shown. The load at which free radicals can be detected by esr is indicated.

(iii) fibre failure is accompanied by intense bursts of light (the peak intensities have been reduced by a factor of 3 in Figure 13)

(iv) removal of the applied stress at any point throughout the stress cycle results in a slow decay of the chemiluminescence.

From our studies, the following interpretation of stress chemiluminescence of nylon 66 is presented:

(i) the linear region of low chemiluminescence intensity at stresses less than 60% of ultimate may arise from localized heating of the stressed amorphous region. The increase in chemiluminescence intensity can be transferred to an equivalent temperature rise which is consistent with the hysteresis loss in the polymer. Thus quite low stresses produce free radicals in the polymer (at much lower stresses than esr can detect radicals)

(ii) as the stress increases, those taut tie molecules in the amorphous region that connect crystalline lamellae will fracture due to strain concentration and free radicals will be generated by scission of macromolecules. This culminates in fibre fracture

(iii) the removal of the stress at any point in the cycle should immediately set the rate of initiation of free radicals by the above processes to zero and the chemiluminescence should decay by second order kinetics described by Equation (3). Figure 14 is a plot of the decay at 80°C and it can be seen that the simple relation is obeyed only at short time. The deviation from second order behaviour has been related to the non uniform distribution of radical in the solid state with a resulting distribution of radical lifetimes. The measured lifetime τ, at short times can be used to calculate a radical concentration prior to failure which can be compared with other studies by esr and molecular weight changes *[8]* at the same temperature. These values are shown in Figure 14. While there is good agreement between the chemiluminescence and molecular weight methods, the esr value is lower by a factor of at least 20. This reflects a severe limitation of esr in studies of fracture as it can detect only stable free radicals while the chemiluminescence technique detects those radicals that are reactive.

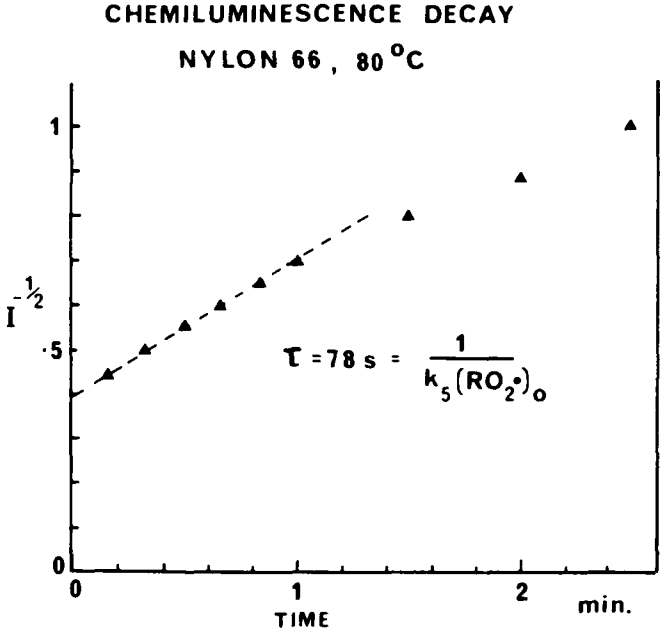

Using $k_5 = 800\ l\ mol^{-1} min^{-1}$

$(RO_2\cdot)_o = 6 \times 10^{17}\ cm^{-3}$

$\bar{M}_v$: (ends) $= 4 \times 10^{17}\ cm^{-3}$

ESR : $(R\cdot) = 2 \times 10^{16}\ cm^{-3}$

Figure 14 Analysis of the decay of chemiluminescence at yarn failure in Figure 13 according to Equation (3). The calculated alkyl peroxy radical concentration is compared with that reported from nylon 66 at the same temperature *[8]*.

It should be noted that the chemiluminescence generated by stressing nylon 66 is identical to that resulting from heating or UV irradiating the polymer. This can be seen from a comparison of the spectral distribution of the stress chemiluminescence and thermal chemiluminescence ('oxyluminescence') in Figure 15. The presence of oxygen is also required to observe stress chemiluminescence.

We have found that stress chemiluminescence from nylon 66 is sensitive to the morphology of the material (its perfection of orientation) the type and concentration of stabilizers and its service history. Stress relaxation can also be studied by observing the decay of intensity while the sample is held at constant elongation.

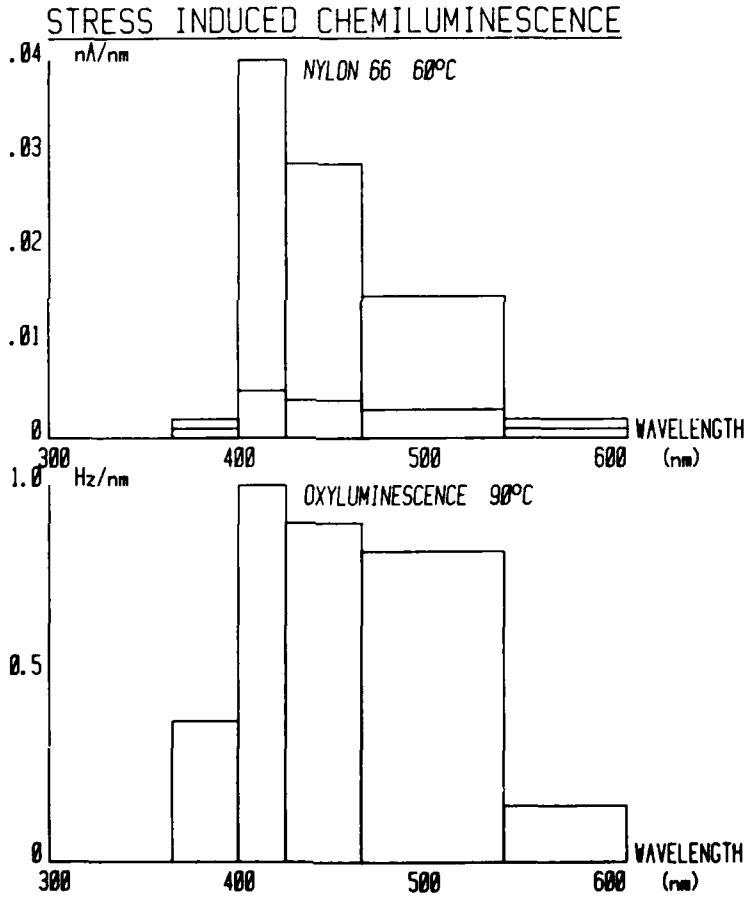

Figure 15 Comparison of the spectral distribution of the stress chemiluminescence from nylon 66 and its thermal chemiluminescence ('oxyluminescence').

6.2 Glass-epoxy Composite (RAC 7250-S2)

The reported stress chemiluminescence from cured MY720 epoxy resin [6,7] seems to show non-stationary behaviour after stressing, with the rate of decay of chemiluminescence being affected by the extent of cure of the resin and the presence of moisture. It was therefore of interest to investigate the stress chemiluminescence of an MY720 based composite - RAC 7250.

Figure 16 shows two experiments performed on single and multiple plies of RAC 7250 composite prepared at AMMRC and provided to MRL for characterization. In the first example, a single ply is strained in the direction of the fibres. No stress chemiluminescence is observed until failure of the specimen when several bright flashes occur. Free radical formation in the matrix cannot occur under these conditions at stresses below failure because of the low stress carried by the matrix ($\sim$ 4% of that applied). However in cross-plied composites, matrix cracking in transverse plies is observed at low applied strains ($\lesssim$ 0.6%) [9]. It was therefore of interest to see if stress induced chemiluminescence from the epoxy matrix could be observed when a $0^{o}/90^{o}$ two-ply section of the composite was stressed. The results obtained are shown in Figure 16. Above a critical strain corresponding to the 'knee' in the stress-strain curve, strong bursts of chemiluminescence are observed. If the stress is immediately removed there is a slow decay of weak chemiluminescence, the intensity of which depends on sample temperature. Free radical formation in the matrix is thus occurring above the critical strain. Successive stress cycles up to failure are shown in Figure 16 and at each increment of stress there are intense bursts of light followed by a slow decay. The bursts of light are accompanied by acoustic emission and each event corresponds to the formation of a crack in the transverse ply. At this stage it is uncertain if matrix radical formation arises from debonding between the fibre and resin or from matrix cracking due to strain magnification. Analysis of the decay curve in Figure 16 yields a radical lifetime of 2.05 min at $60^{o}C$. Factors affecting the radical lifetime should include the extent of cure, the presence of plasticizing impurities, including water, as well as free radical scavenging stabilizers.

7. CONCLUSIONS

Non-stationary chemiluminescence is a very sensitive probe of free radical reactions occurring in organic materials throughout their useful service life. The methods for generating non-stationary conditions discussed here - UV irradiation, gas switching and stressing - may provide similar information about the lifetime of the free radicals formed during oxidation but each can provide different information about the material's microstructure and chemical purity. Much more research is required into the chemiluminescence of epoxy resins and composite materials before the technique can be used as a reliable characterization tool.

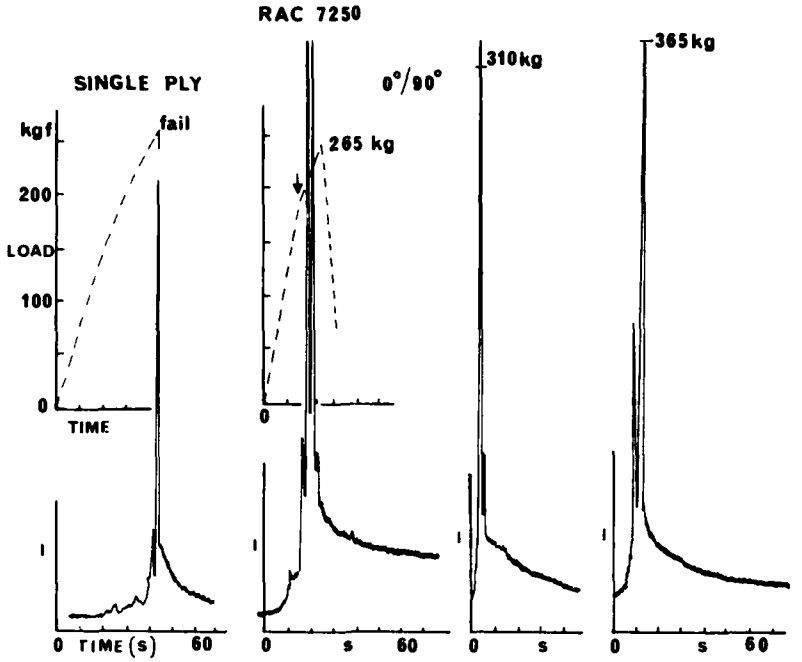

Figure 16 Stress chemiluminescence (SCL) from RAC7250-S2 glass-epoxy composite at 60°C

(i) a single ply strained to failure in the fibre direction. SCL is not observed until just before failure.

(ii) successive stress cycles of a $0^{\circ}/90^{\circ}$ two ply section. SCL is observed after the 'knee' of the load elongation curve as shown. The sample was cycled to 265 kg; 310 kg and 365 kg with production of SCL as shown followed by decay of weak chemiluminescence.

REFERENCES

1. Mendenhall, G.D. : Angew. Chem. Intl. Ed. 16, 225, 1977.

2. George, G.A. : 'Use of Chemiluminescence to Study the Kinetics of Oxidation of Solid Polymers' Chapter 6 in Developments in Polymer Degradation -3, Ed. N. Grassie, Applied Science, London, 1981.

3. George, G.A. : Polymer. Deg. Stabil. 1, 217, 1979.

George, G.A. and Riddell, S.Z. : J. Macromol. Sci. Chem. A14, 161, 1980.

4. George, G.A., Sacher, R.E. and Sprouse, J.F. : J. Appl. Polym. Sci. 21, 2241, 1977.

5. Pearce, P.J., Davidson, R.G. and Morris, C.E.M. : J. Appl. Polym. Sci., in press.

6. Fanter, D.L. and Levy, R.L. : in Durability of Macromolecular Materials (R.K. Eby, Ed.) ACS Symp. Series No. 95, 1979, p. 211.

7. Levy, R.L. and Fanter, D.L. : 'Stress Chemiluminescence (SCL) of Epoxy Resins' McDonnell Douglas Research Laboratories Report, MDRL 79-27.

8. Stoeckel, T.M., Blasius, J. and Crist, B. : J. Polym. Sci. (Phys.) 16, 485, 1978.

9. Parvizi, A. and Bailey, J.E. : J. Mater. Sci. 13, 2131, 1978.

THE USE OF CHEMILUMINESCENCE TO MONITOR THE AGING PROCESSES IN POLYMERS AND COMPOSITES*

Clarence J. Wolf and Dale L. Fanter
McDonnell Douglas Research Laboratories
St. Louis, MO 63166

ABSTRACT

Aging studies can be categorized into one of two areas: 1) those concerned with the determination of a specific environmental effect on a useful property of the material, i.e., an aging mechanism or 2) those concerned with the development of methods and/or techniques to simulate and ultimately predict effects of aging. Of particular interest in the second area is the development of a rapid or real-time aging test so that a short (week to months) test can be used to predict the long-term properties of a material. New testing methods are needed that do not require the large extrapolation from the high-temperature region normally used in accelerated aging studies to the actual service environment. Chemiluminescence (CL), a relatively common phenomenon in which part of the energy of a exoergic chemical reaction is released in the form of electromagnetic radiation, is a potentially powerful technique to monitor the degradation processes occurring during the aging of polymeric materials. The separate and combined environmental effects of temperature, humidity, and mechanical stress on the CL from epoxy resin systems will be presented and discussed.

*This research was conducted in part under Naval Air Systems Command Contract N00019-80-C-0102 and in part under the McDonnell Douglas Independent Research and Development program.

1.0 Aging of Polymeric Materials: Polymers and composites are finding ever-increasing use as structural components on aerospace vehicles because of their attractive strength/weight characteristics. Consequently, the aerospace industry has developed fabrication and testing procedures that are radically different from those traditionally used with metals. Because little is known about the long-term durability of these relatively new nonmetallic composites, there full potential has not been realized. Realistic test procedures and methods are required that can reliably predict the long-term properties of these materials from short-duration (weeks to months) tests. Normally, so-called accelerated aging tests are conducted by exposing the sample to a specific environment while maintaining the sample at high temperature for short periods, possibly as long as several months. The short-time, high-temperature, high-intensity data are then extrapolated to the environmental-use envelope and to the long time periods required. Since the aging mechanism at high temperature may not be identical to the mechanism operative at service conditions, such extrapolations are suspect; therefore the results of accelerated aging experiments are of questionable validity.

Aging of Polymeric Materials

- Aging is a poorly defined term
- Normally accelerated tests are conducted at extreme conditions
- Need realistic tests conducted within the actual service environment

2.0 Aging Prediction: By most standards this new class of materials, the resin matrix composites are considered stable. The deleterious reactions producing changes in their desirable properties are slow, requiring 15-30 years to produce failure. New techniques that are sufficiently sensitive to measure the slow changes in polymeric materials on a real-time basis are needed. The slow chemical changes observed during the aging processes must then be related to the overall macroscopic changes in the mechanical properties of these materials.

Aging Prediction

- Develop ultrasensitve techniques to monitor the microscopic changes in the polymeric materials
- Relate the microscopic changes to the macroscopic properties of the material

3.0 Chemiluminescence: Chemiluminescence (CL) is a relatively common phenomenon in which part of the energy of an exoergic chemical reaction is released in the form of electromagnetic radiation, i.e., light. Many reactions, such as oxidation, hydration, and acid-base, exhibit CL. In general, there are only two requirements for a reaction to be chemiluminescent: 1) the reaction must be sufficiently energetic to raise one of the reaction products to an excited state, and 2) the excited state must be sufficiently long-lived to de-excite by a radiative process. Both of these requirements can be satisfied in reactions in which macroradicals, such as produced by rupture of the main-chain in a polymer molecule, combine to form an excited molecule.

Chemiluminescence

- The reaction must be sufficiently energetic so that products are formed in excited states
- The excited products must either fluoresce or transfer excitation energy to a fluorescent compound
- CL reactions are relatively commonplace

4.0 Proposed Mechanism for Oxyluminescence: The luminescence accompanying the oxidation of hydrocarbons is well known and has been studied in depth. A mechanism which accounts for the chemiluminescence observed during the oxidation of hydrocarbons assumes a chain reaction propagated by alkyl and peroxy radicals and terminated by bimolecular reactions involving these same radicals. Presumably, the peroxy radicals combine and disproportionate into an alcohol and an excited ketone; the latter is responsible for the luminescence. The mechanism responsible for the chemiluminescence observed in solid polymers is not well known, although it has been suggested that reactions involving peroxides or hydroperoxides are important in thermoplastic polymers.

Proposed Mechanism for Oxyluminescence in Hydrocarbons

$$RR \longrightarrow \text{free radicals (R)}$$

$$R + O_2 \longrightarrow RO_2$$

$$RO_2 + RH \longrightarrow ROOH + R$$

$$R + R \longrightarrow R_2$$

$$RO_2 + RO_2 \longrightarrow R_2O_4^*$$

$$R_2O_4^* \longrightarrow \alpha\ RC(=O)R^* + (1-\alpha)\ RC(=O)R + R'(H(OH)R + O_2$$

$$RC(=O) - R^* \longrightarrow RC(=O) - R + h\nu$$

$$RC(=O) - R^* + F \longrightarrow F^* + RC(=O) - R$$

$$R^* \longrightarrow F + h\nu$$

$$F^* \longrightarrow F + \text{heat}$$

5.0 Sensitivity of CL: Sensitive photon counting systems are available which can readily measure counting rates as low 100 photons/s in the visible region of the spectrum. With quantum yields on the order of 10^{-7} and counting efficiencies of only a few percent, luminescence rates as low as 10^{10} molecules/s can be measured. If this radiation can be related to changes in the chemistry of the system which in turn can be correlated with macromechanical properties of the material, short-duration measurements may be useful to predict long-term properties.

Sensitivity of CL

- Photon counting rates as low as 100 counts/s are readily measurable
- Counting efficiencies are typically 10^{-8}
- Detection capability 10^{10} molecules/s which corresponds to 5×10^{-7} moles/year

6.0 Stress CL System: The chemiluminescence system is the third luminescence detection system designed and fabricated at MDRL. Samples can be exposed to selected combinations of atmosphere, temperature, and tensile stress while measuring the luminescence. Generally, air, oxygen, or nitrogen is used to purge the sample chamber; however, other gases can be used. The sample stage incorporates two matched heaters and thermocouples to control temperatures up to 200°C. A gearmotor, belt, and worm-drive mechanism applies tensile stress to the sample through two grips attached to cylinders cast into the tensile coupons. Tensile loads up to 500 N can be applied to coupons and are recorded by the load transducer attached to the fixed grip. The photomultiplier tube (PMT) is coupled to the sample through a quartz dewar which thermally isolates the sample chamber from the cooled PMT.

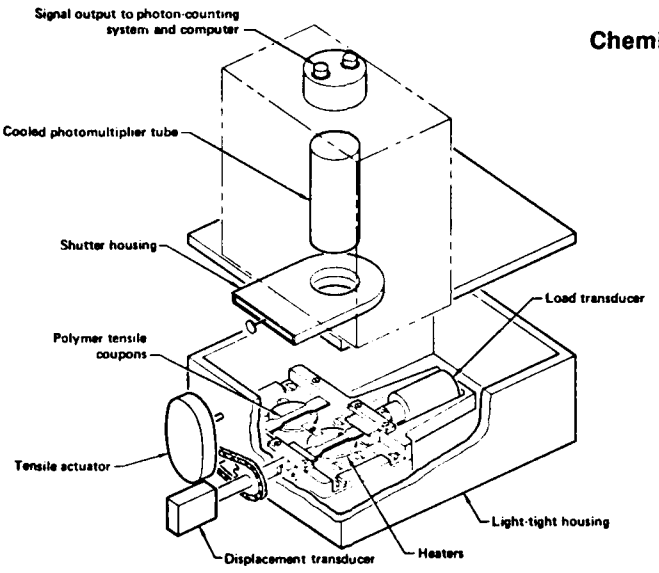

Stress Chemiluminescence System

7.0 Diagram of CL System: The CL experimental variables, photon counts per second, sample temperature, stress, and strain, are monitored continuously by the microcomputer (Digital Equipment Co. MINC 11 with VT105 CRT terminal) and recorded at selected intervals for closed-loop control of the CL experiment and subsequent off-line data storage on flexible disk. The computer is programmed to operate unattended; thus experiments can be performed overnight. Sample temperatures are controlled by the computer based on either a given time interval or a plateau-detection algorithm.

Diagram of Chemiluminescence System

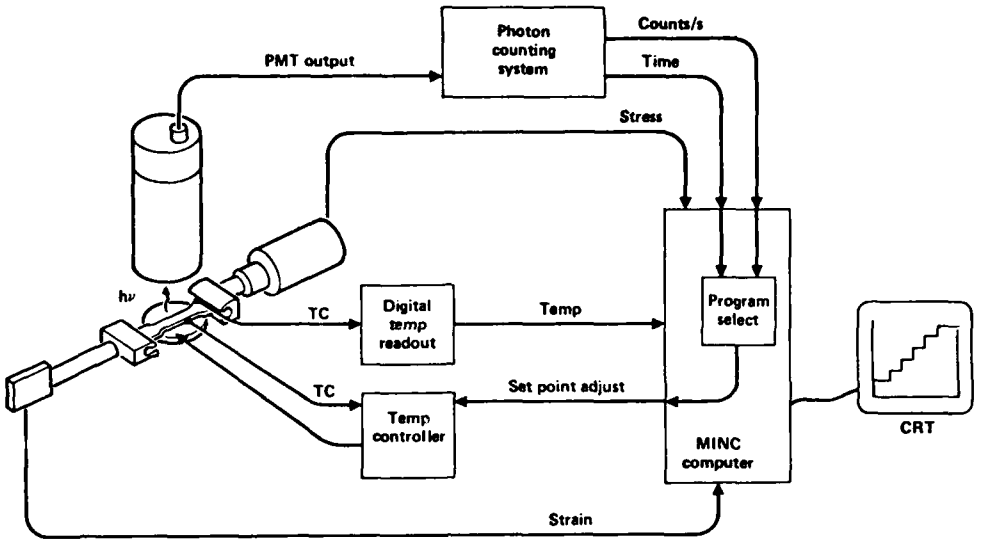

8.0 Sample Preparation: Samples of MY720 (Ciba-Geigy) and Eporal (Ciba-Geigy) resin were cast in silicone rubber molds prepared from a master metal template. The samples, cast in the shape of dogbone coupons with gauge dimensions of 4 x 12 x 25 mm, were cured at 150°C for 1 h followed by a postcure at 177°C for 5 h. The grip portion of the sample was terminated in a cylindrical shape to facilitate mounting in the tensile grips of the CL system.

9.0 Sample Characterization: Several representative samples of the cured resin were chemically characterized immediately upon removal from the curing oven. Prior to cure, the constituents of the MY720 were determined by a combination of liquid chromatography (LC) and in some instances LC followed by mass spectrometry. The attenuated total reflectance (ATR) infrared spectrum of each sample before and after environmental exposure was measured by Fourier transforms infrared spectroscopy (FTIR). The volatile compounds indigenous to or trapped within the cured resin were qualitatively and quantitatively determined by vaporization gas chromatography (Vap GC) and/or Vap GC/MS. The concentration and distribution of water and oxygen in the resin was determined by precision abrasion mass spectrometry (PAMS).

10.0 CL After 1 Year Ambient Exposure: When heated, epoxy resins produce a complex CL intensity-time profile. A typical intensity-temperature-time plot from a resin which was aged at 23°C at a RH of 30-40% for 1 year is shown; the left ordinate is the temperature scale (shown by the solid line on the graph), the right ordinate is the CL intensity (shown as the shaded curve), and the abscissa is time. A sharp spike (referred to as the peak) occurs each time the temperature is increased. The CL intensity slowly decreases to a nearly constant level referred to as the plateau value. The general phenomenon of a sharp peak followed by a plateau region is preserved throughout the thermal cycle, although the CL intensity of both the peak and the plateau decreases markedly with each successive cycle.

CL After One-Year Ambient Exposure

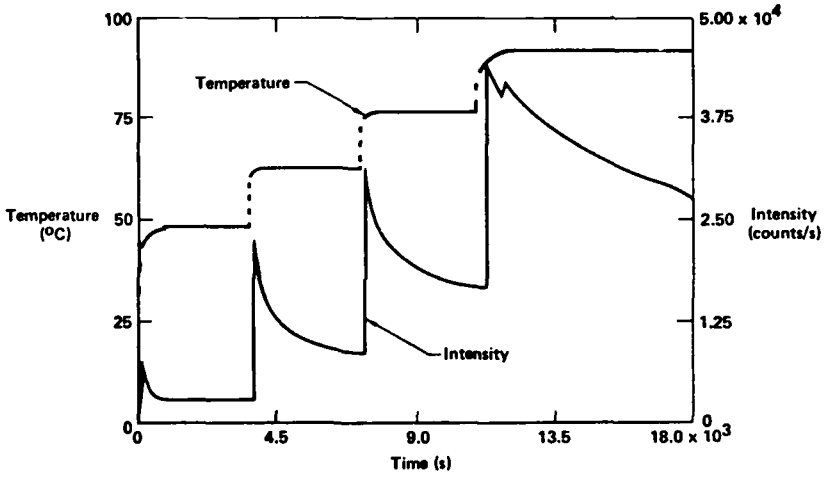

11.0 CL in Nitrogen: The CL intensity-temperature-time measurements also were conducted in a nitrogen atmosphere. The CL intensity rapidly peaked, slowly decreased, and reached a plateau. However, two important differences were observed: 1) the CL intensity at any temperature is 10-20 times less than that observed in oxygen and 2) the plateau value is essentially independent of temperature, reaching a value of approximately 100 photons/s at all temperatures. When the sample was heated through successive cycles, the intensity immediately reached a plateau value of approximately 70-80 photons/s, and no peak was observed.

CL in Nitrogen: Ambient Exposure

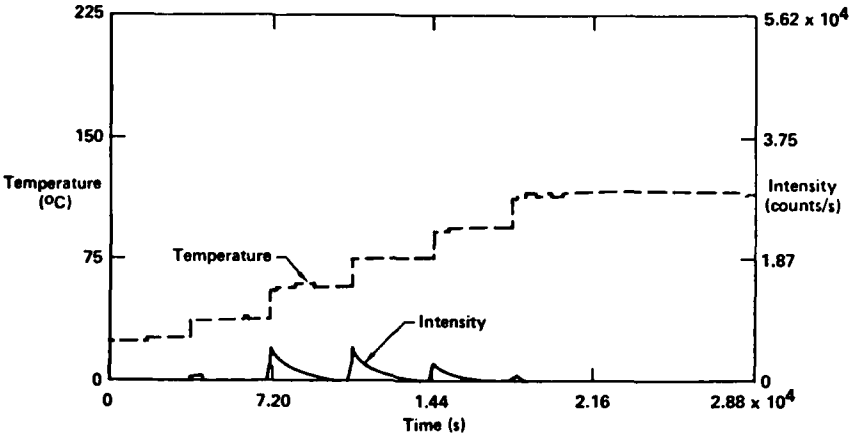

12.0 CL from Epoxy Resin as a Function of Stress: The effect of a cyclic mechanical load on the CL emission from the MY720/Eporal resin was measured. An epoxy tensile coupon was held isothermally at 72°C in an oxygen atmosphere while the tensile loading on the sample was cycled. The sample strain, detected by a linear displacement transducer, is shown by the dashed line, while CL is shown by the solid curve. The initial strain produces a CL peak which decays slightly while the load is maintained. When the load is released, the CL rapidly decays. When the tensile load is reapplied, the CL intensity increases to approximately 80% of the intensity observed in the first cycle.

Chemiluminescence from Epoxy Resin as a Function of Stress

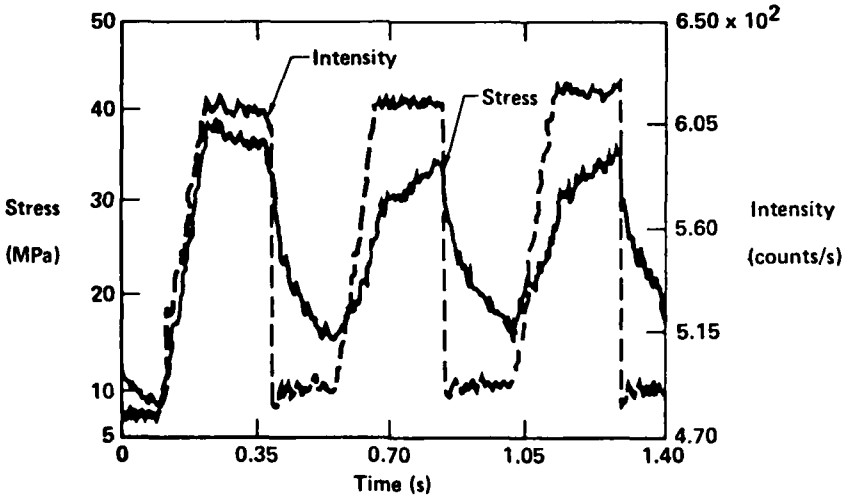

13.0 CL as a Function of Strain (and Fracture): The CL increases in direct proportion to the applied strain. A sharp spike in CL intensity occurs at the instant of fracture.

Chemiluminescence as a Function of Strain (and Fracture)

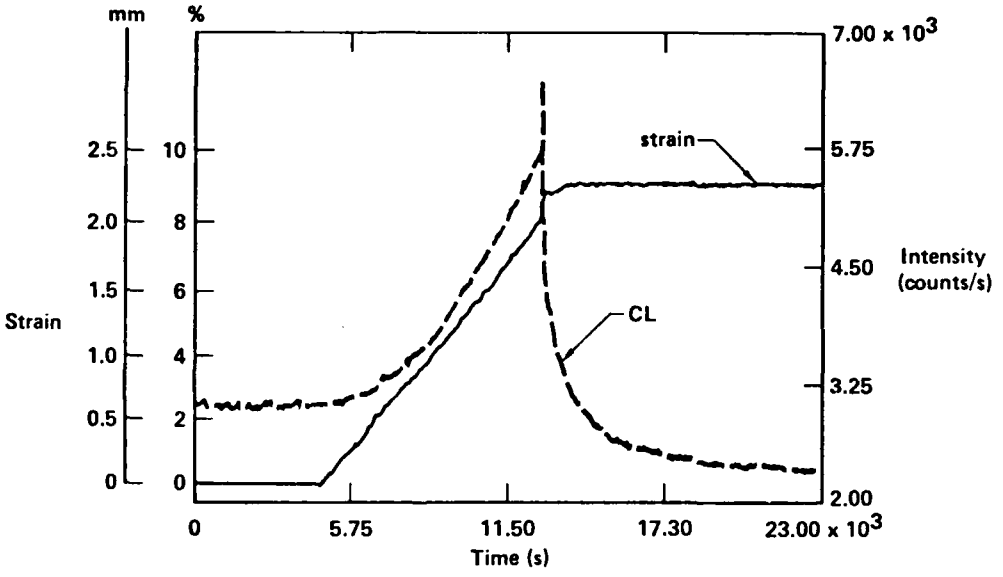

14.0 Exposure: 85°C, 2% RH, 0 Stress: The CL intensity-temperature-time curves were measured for the resin following aging at 85°C with 2% RH for time intervals up to 29 days. Although the CL intensity decreases during the aging period, the rate of decrease is less than that observed in samples aged at higher humidities.

Exposure:
85°C, 2% RH, 0 Stress

— — — Temperature
——— Intensity

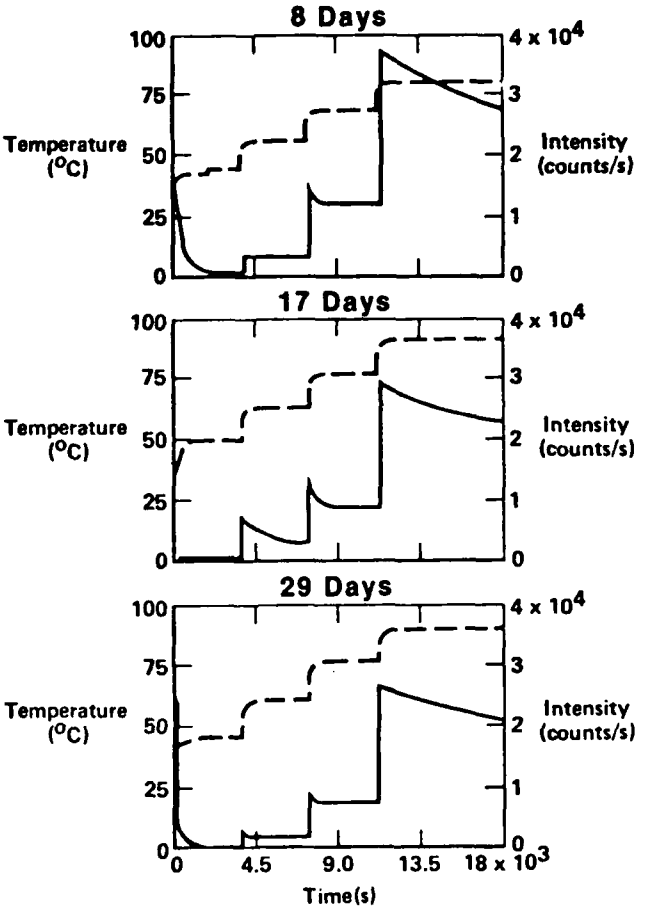

15.0 Exposure: 85°C, 2% RH, 50% UTS: The CL intensity-temperature-time curves were measured for the resin following aging at 85°C with 2% RH while stressed to 50% UTS. The CL intensity decreases during aging; however, at the low humidities used in these experiments, stress has a smaller effect than noted previously.

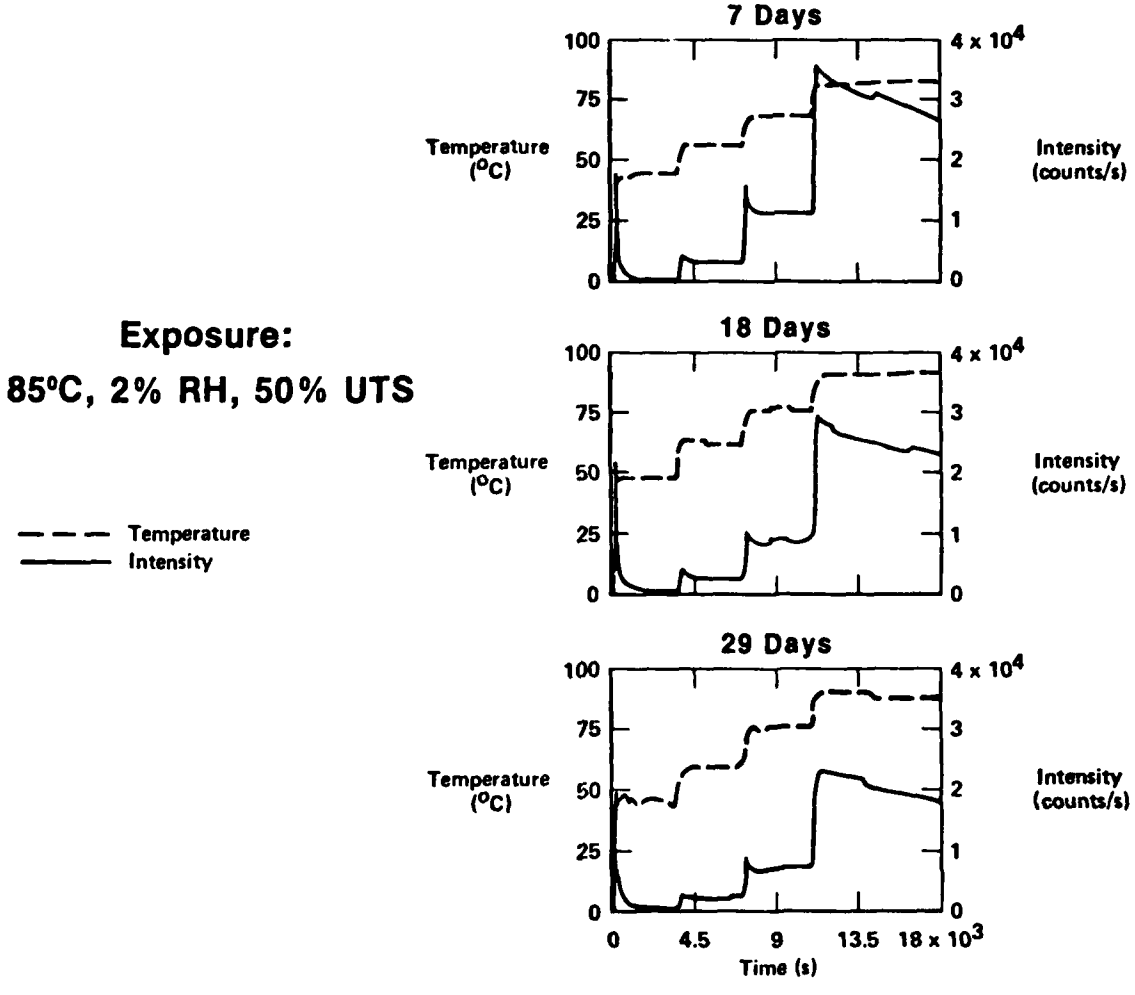

16.0 Exposure: 85°C, 45% RH, 0 Stress: The CL intensity-temperature-time profiles of the resin following environmental aging at 85°C and 45% RH were measured after exposure intervals ranging 1 to 195 days. The CL curves from exposures of 38, 63, 100, 133 and 195 days are shown. The CL curve exhibits the same characteristics of a peak and a plateau region noted in the ambient aging experiments. The CL intensity decreases with exposure time, and the decreases in the first few days are the most pronounced.

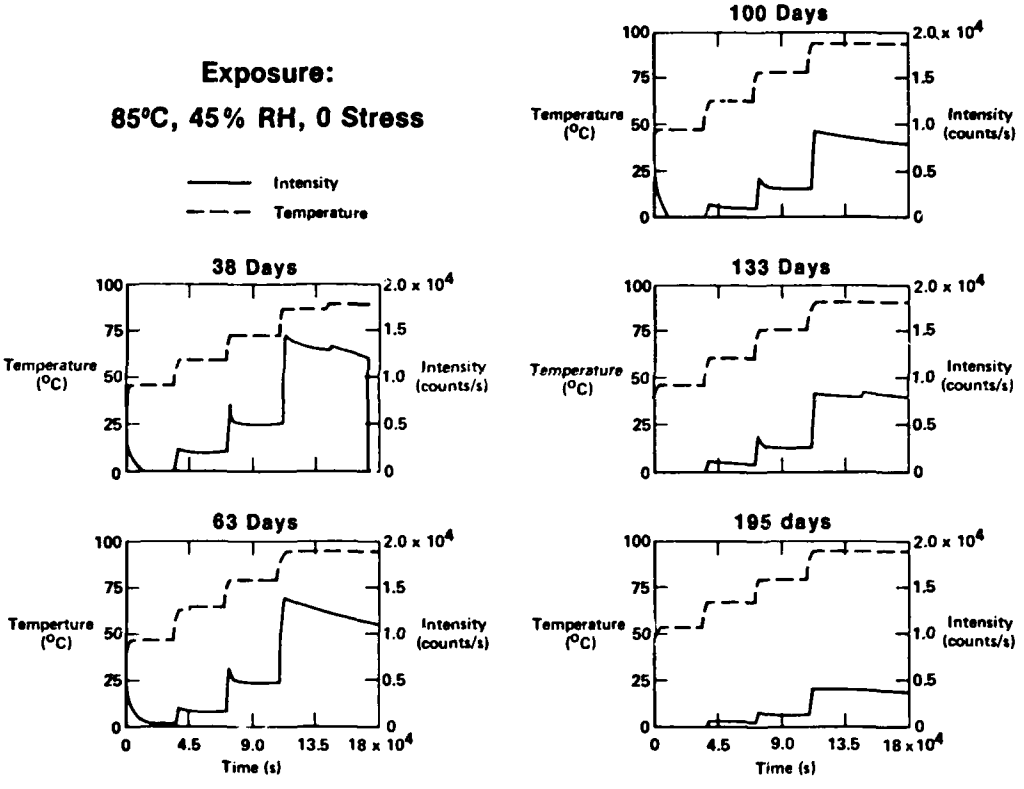

17.0 Exposure: 85°C, 45% RH and 50% UTS: The CL intensity-time-profiles of the resin following environmental aging at 85°C and 45% RH while stressed to 50% UTS were measured. Exposure times varied from 1 to 196 days. The UTS was determined independently to be 78.7± 5.8 kg/mm^2. The curves are similar to that noted with the unstressed samples except that the overall CL intensity for a given set of conditions is slightly lower.

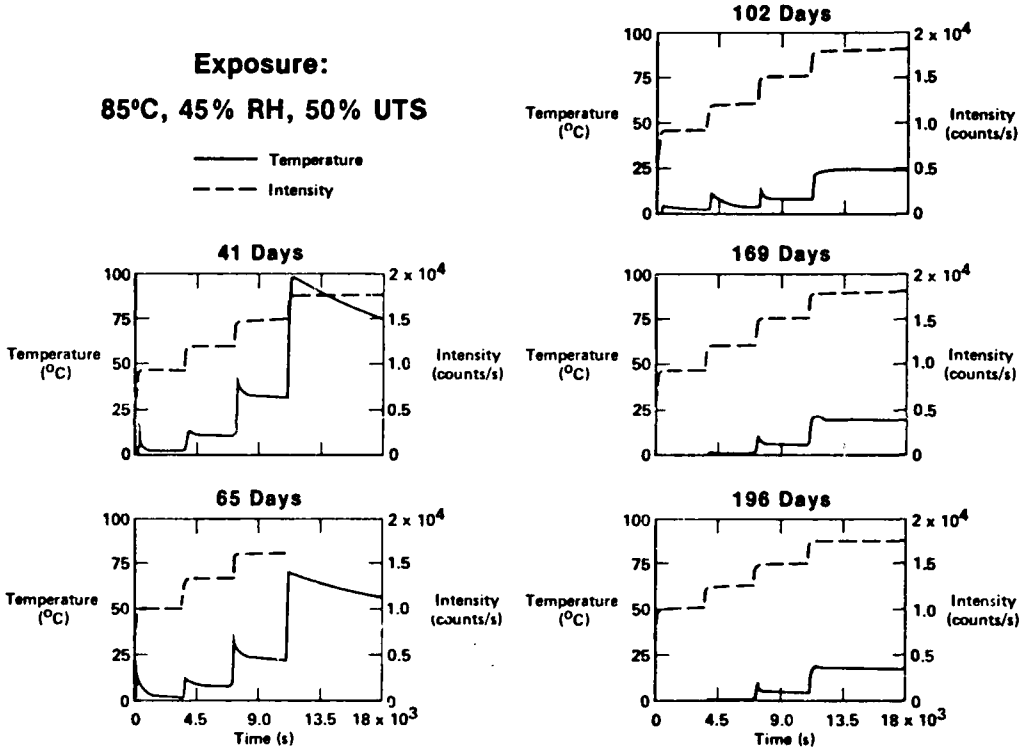

18.0 Exposure: 150°C, 0% RH, 50% UTS: The CL intensity-temperature-time plots for stressed (50% UTS) samples exposed at 150°C and 0% RH for time intervals varying from 6 to 31 days are shown. Short exposures for only 6 days reduce the baseline CL intensity two orders-of-magnitude, and prolonged exposure reduces the CL to near background levels. The CL intensity curves are similar for the unstressed and stressed (50% UTS) samples.

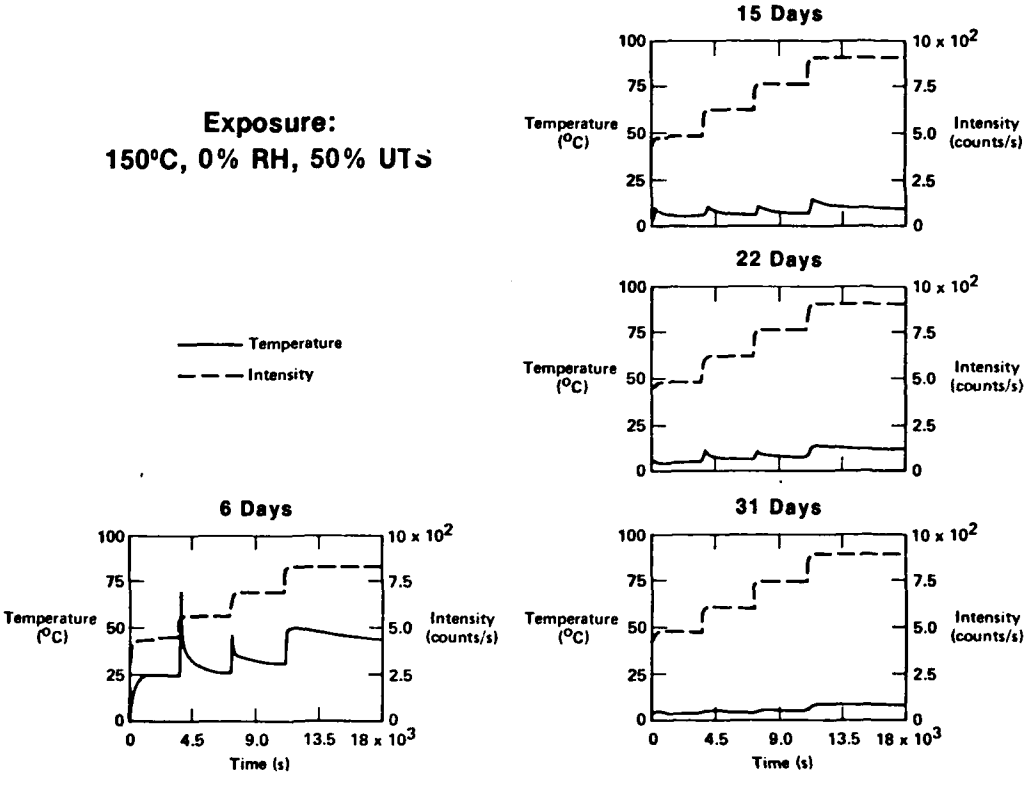

19.0 Activation Energies for CL: The activation energies or temperature coefficients for the CL emission occurring at the 50° to 63°C, 63° to 75°C and the 75° to 90°C transitions were determined. The activation energies for the low-temperature luminescence vary from 5.6 to 6.9 kJ/mole. The latter value occurred in the unstressed sample aged in the ambient environment. The activation energies at the high-temperature transition (i.e., 75°-90°C) vary from 3.9 to 4.7 kJ/mole. The activation energies do not vary appreciably during the aging interval, suggesting that the mechanism responsible for CL emission does not change. In addition, the magnitude of these values (i.e., 4 to 7 kJ/mole) suggest that chemical reactions, rather than diffusion-limited processes, are responsible for the observed luminescence.

Activation Energies for CL after Different Environmental Exposures

Temperature (°C)	RH (%)	UTS (%)	ΔE 50° - 60°C kJ/mole	ΔE 63°C - 75°C kJ/mole	ΔE 75°C - 90°C kJ/mole
23	10-20	0	6.9 ± 0.2	5.4 ± 0.2	3.9 ± 0
85	0	0	6.2 ± 0.2	5.9 ± 0.2	4.8 ± 0.4
85	0	50%	6.5 ± 0.4	5.6 ± 0.7	4.7 ± 0.2
85	50	0	5.7 ± 0.6	5.4 ± 0.5	4.4 ± 0.3
85	50	50%	5.6 ± 0.6	5.2 ± 0.6	4.4 ± 0.2

Session IV: ADVANCES OF SIGNIFICANCE TO COMPOSITES

Chairpersons:

L. H. KRICHEW, N. D., Canada

R. L. VAN DEUSEN, AFWAL, U.S. Air Force

THERMALLY STIMULATED DISCHARGE MEASUREMENT AND PROPERTY CHARACTERIZATION OF EPOXY RESIN SYSTEMS

J. O. Brittain, S. H. Carr, and T. D. Chang

Department of Materials Science and Engineering
and Materials Research Center
Northwestern University
Evanston, IL 60201

ABSTRACT

Thermally Stimulated Depolarization, TSD, measurements have been made on a series of epoxy resins in order to determine the effect of chemical composition and post-curing upon the TSD relaxation spectra from about 100°K to above T_g. Resin systems investigated were DER 332 DGEBA, diglycidyl ether of bisphenyl A, monomer with an epoxy equivalent weight of 172-176; DER 667 self-polymerized solid DGEBA with an epoxy equivalent weight of 1600-2000; DGEB, diglycidyl ether of butanediol; and curing agents EDA, ethylene diamine; DDM, diaminodiphenylmethane; and DDS, 1,4'-sulfonyldianiline. The extent of curing was determined via infrared spectroscopy measurements of absorbance of the epoxy group at 910 cm^{-1}; the absorbance of the phenyl ring 1610 cm^{-1} or, in the case of the DGEBEDA system, the C-O stretch at 1100 cm^{-1} was used as an internal standard. DSC was used to determine T_g at a heating rate of 10°C/min. The results showed that the epoxy resins cured with diamine generally had two secondary relations of localized origins. The β-relaxation at about 185°K increased in strength and occurred at a higher temperature with an increase in the extent of curing. The TSD γ-relaxation at 115°K did not change with the extent of curing. The β-relaxations are attributed to the

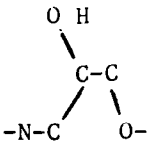

segment, and the γ-relaxations are most likely associated with the ether linkage and the adjacent molecular segments. Both the β and γ relaxations are distributed processes. The addition of the phenyl groups resulted in an increase in the TSD α-relaxation (as well as, T_g), but the β and γ relaxations were not substantially affected by the presence of the phenyl groups.

A more extensive series of observations were made on the DGEB-DDS epoxy system, cured for 12 hours at 112°C, in order to ascertain the effect of post-curing and sub-T_g aging treatments upon the TSD-relaxation spectra, T_g, the compressive yield strength, the density and the retraction of the specimens deformed in compression. Post-curing at 146°C resulted in an increase in the TSD α-relaxation from 58°C to 70°C and an increase in T_g from 45° to 77°C. While the temperature of the TSD α-relaxation increased with post-curing time, the strength of the relaxation decreased very markedly. The β-local mode relaxation increased in temperature paralleling the increase in the temperature of the α-relaxation, however, the strength of the β-relaxation increased with the degree of post-curing. The γ-relaxation remained essentially unaffected by post-curing. Both the static modulus and yield strength had significant increases with post-curing for 27 hours at 146°C.

Sub-T_g aging at 62°C of the DGEB-DDS epoxy system that had been cured for 12 hours at 112°C and post-cured for 27 hours at 146°C resulted in a substantial decrease in the strength of the TSD α-relaxation, while neither the β nor γ relaxations were altered. The DSC measurements of the sub-T_g aged resins revealed essentially no change in T_g, but did show an endothermic peak above T_g that increased in magnitude as the time of aging increased. It was also noted that the endothermic process was eliminated in the aged specimen by deformation. While the density increased slightly upon aging, the yield stress increased approximately 20% from about 745 KN/m^2 to 911 KN/m^2. The effects associated with sub-T_g aging are transitory in that annealing sub-T_g aged material above T_g eliminated the property changes associated with the aging process. Finally, retraction of the specimens deformed in compression was dependent upon the extent of curing and a function of both time and temperature.

ACKNOWLEDGEMENT

This work was supported by the Chemistry Branch of the Office of Naval Research. Facilities for some of this research were made available by the Materials Research Center of Northwestern University (NSF-MRL Program Grant DMR 76-80847).

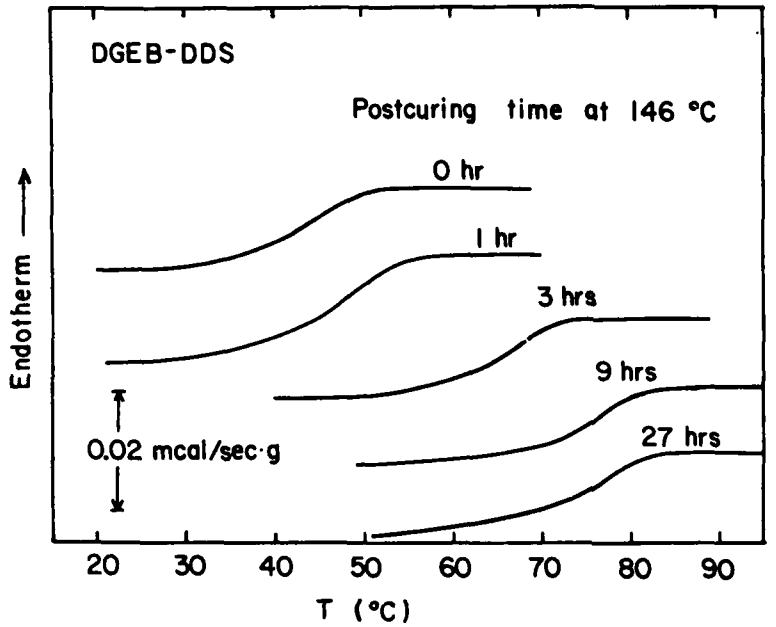

DSC FOR DGEB-DDS EPOXY RESIN

(Figure 1)

Differential scanning calorimetry data for the DGEB-DDS epoxy resin as a function of the post curing time at 146°C is shown. Scans were run at 10°C/min. The glass transition, T_g, increased in temperature but the magnitude of the glass transition decreased as the extent of curing increased.

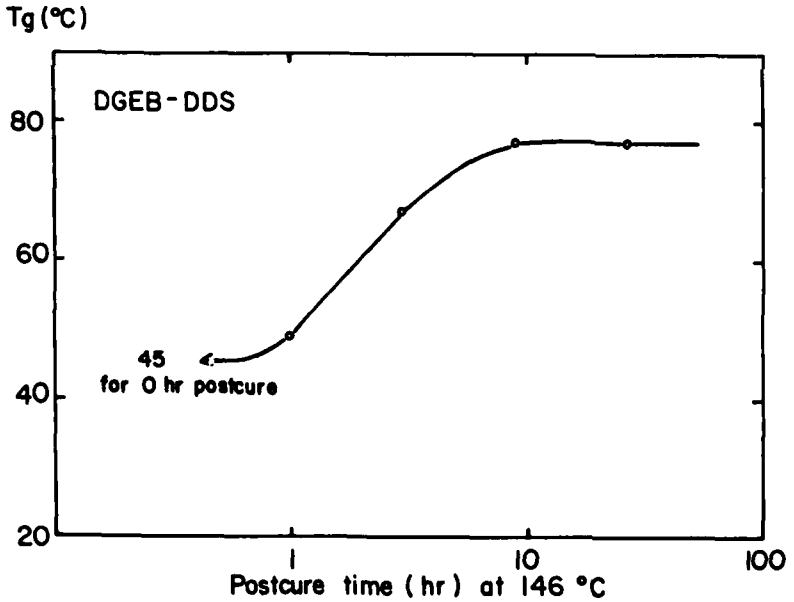

GLASS TRANSITION TEMPERATURE OF THE DGEB-DDS EPOXY RESIN

(Figure 2)

The glass transition temperature increased from 45°C for the DGEB-DDS epoxy resin that was cured for 12 hours at 112°C to 77°C after post curing for 9 hours at 146°C. Additional post curing at 146°C did not affect T_g. This data was used to estimate the molecular weight of the cross-link segments, M_c, and the cross-linking density was, in turn, estimated from M_c. As might be expected, the cross-linking density and the extent of curing were in close parallel, i.e., the change in cross-link density resulting from 9 hours of post curing at 146°C was about 24%, while the extent of curing as measured via FTIR was about 20% for the same degree of post curing.

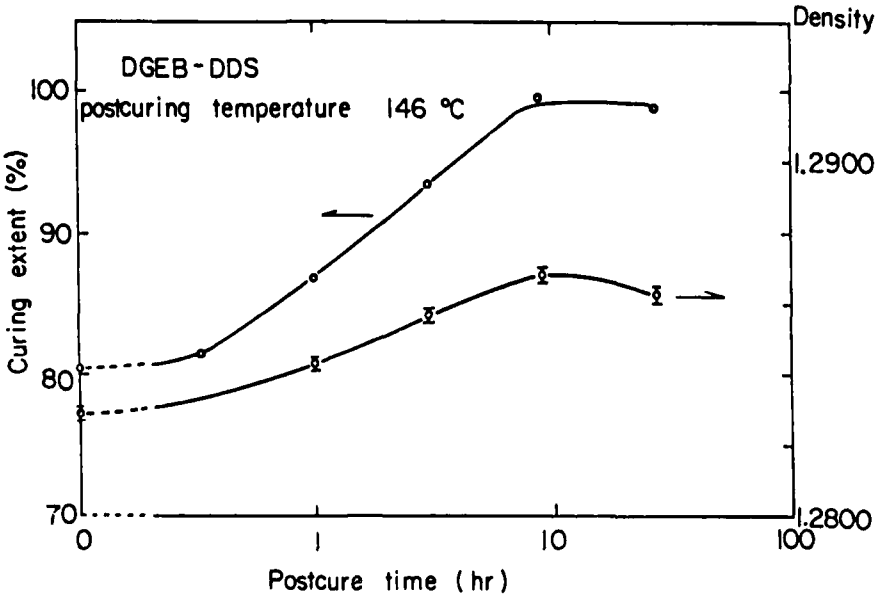

EXTENT OF CURING OF DGEB-DDS EPOXY RESIN

(Figure 3)

The extent of curing of DGEB-DDS epoxy resin, as measured by FTIR for specimens that had been cured for 12 hours at 112°C and then post cured as a function of time at 146°C is shown. The extent of curing was monitored by following the absorption of the epoxy peak at 910 cm^{-1}, the absorbance of the phenyl ring at 1610 cm^{-1} was used as an internal standard. After nine hours at 146°C, the extent of curing reached a level of 99% and stayed at this level for longer post curing times. Note that the resin system was 80% cured by the 12 hours at 112°C treatment and the residual 20% cure is about the maximum extent of curing that can be studied with this system for the measurement of properties on solid specimens. The 20% range is exceptionally large when compared with work reported in literature on the effect of the degree of curing on properties.

Density increased from 1.2830 to 1.2868 after post curing for 9 hours at 146°C, a change of 0.3%. The slight decrease in density after 9 hours at 146°C may be due to thermo-degradation or the vaporization of small molecules. The increase in density with the extent of curing suggests that the free volume of the epoxy resin was reduced by cross-linking.

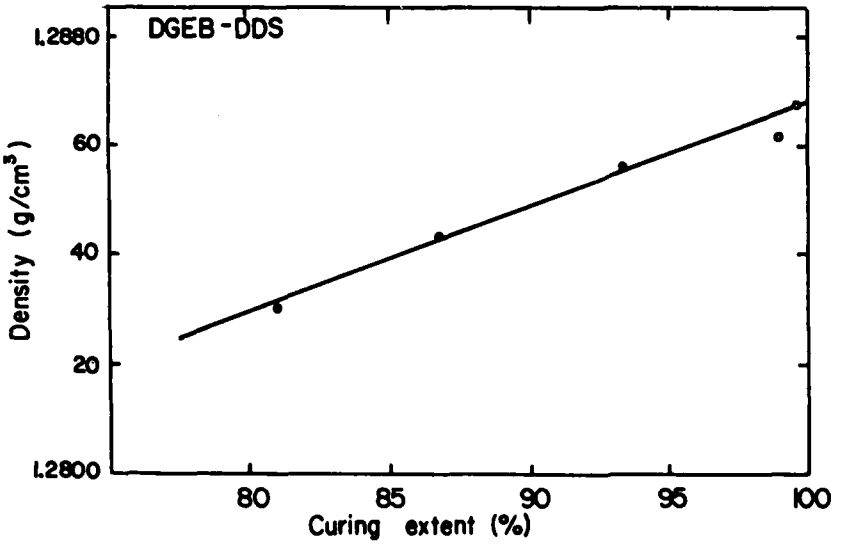

DENSITY VS EXTENT OF CURING
DGEB-DDS EPOXY RESIN

(Figure 4)

Linear relation exists between the density and the extent of curing for DGEB-DDS epoxy resin cured 12 hours at 112°C and post cured at 146°C for time of up to 27 hours. The linear relation between density and the extent of curing suggests that the incremental in cross-linking density corresponds to the decrement in free volume for a given degree of post curing.

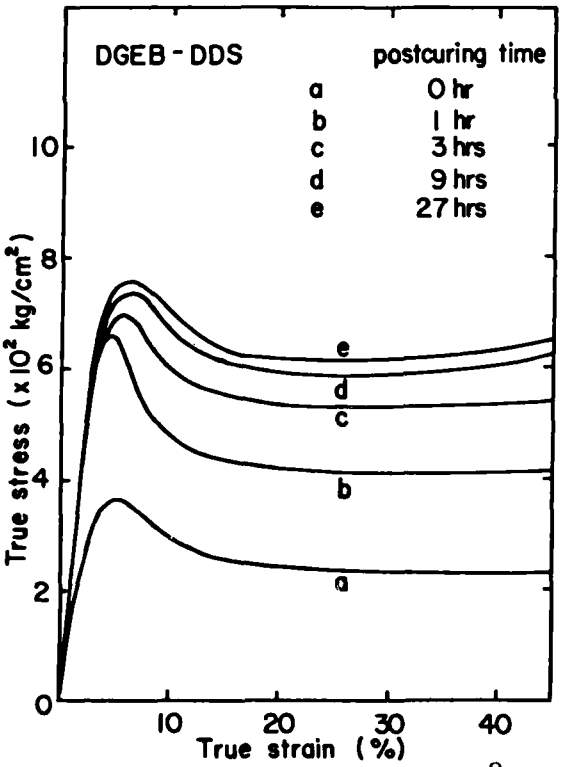

FLOW CURVES IN COMPRESSION OF
THE DGEB-DDS EPOXY RESIN

(Figure 5)

The effect of post curing time at 146°C upon the flow curves in uniaxial compression of the DGEB-DDS epoxy resin, is shown. Without post curing, the compression specimen, cured 12 hours at 112°C, had a yield point at a strain of about 5% and the stress decreased by about 38% after yielding. After post curing at 146°C, the yield point increased but the magnitude of the yield drop remained approximately constant. The stress at the lower yield point increased with the degree of post curing at 146°C.

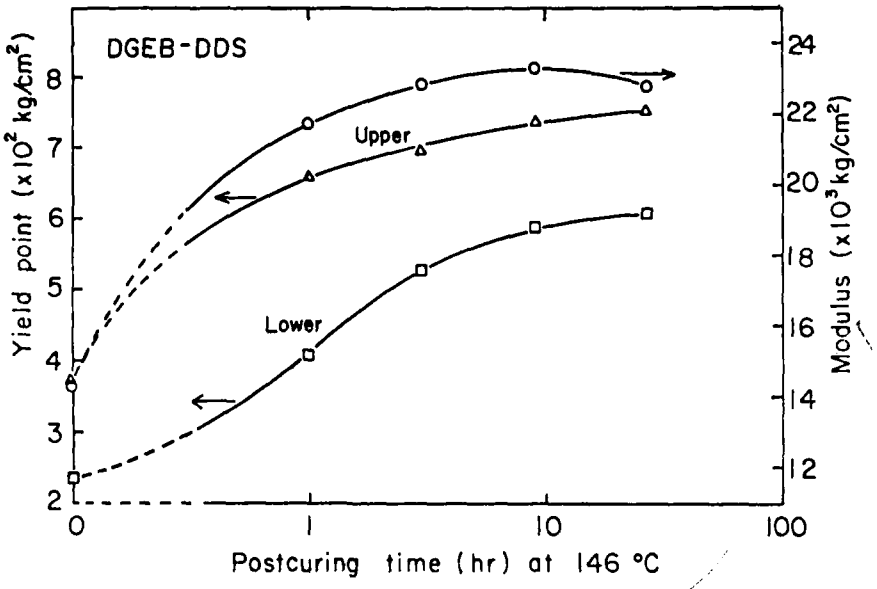

RIGIDITY AND STRENGTH OF DGEB-DDS EPOXY RESIN

(Figure 6)

Post curing at 146°C resulted in an increase of about 60% in the modulus, a doubling of the stress at the upper yield point and almost a tripling of the stress at the lower yield point.

The increase of the modulus with the extent of curing is rationalized on the basis of the increase in density due to the increase in cross-linking. Cross-linking, per se, would also be expected to contribute to an increase in the modulus because of addition of stronger chemical bonds. The increase in the stress at the upper and lower yield point is also associated with the effect of cross-linking upon the density and the ability of the structure to relax under an externally imposed force. The greater the tendency for relaxation to occur or the ease with which a relaxation can occur will inversely affect strength properties. As will be shown, relaxation phenomena are strongly affected by the extent of curing.

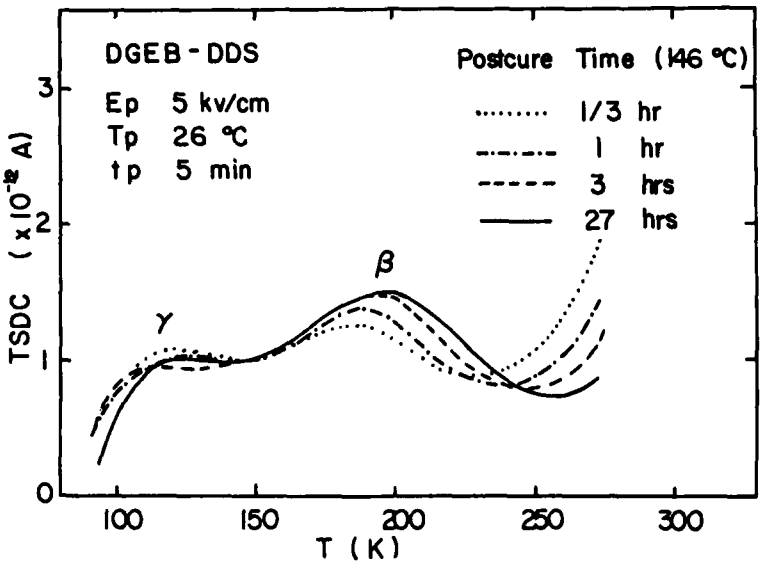

LOW TEMPERATURE RELAXATIONS IN THE DGEB-DDS EPOXY RESIN

(Figure 7)

Since the mechanical properties are so profoundly affected by the last 20% change in the extent of curing, it is precisely this stage of the curing process that requires accurate monitoring. FTIR is relatively insensitive to the last few percent. In the DGEB-DDS epoxy resin system, thermally stimulated depolarization current, TSDC, measurements have been found to be a very sensitive technique for monitoring the curing process.

The low temperature TSDC measurements of this epoxy resin, as a function of the degree of post curing at 146°C, indicate that no systematic variation of the γ-relaxation occurred with extent of curing. The β-relaxation was enhanced by the post curing, both the strength of the relaxation and the peak temperature increased with the time of post curing. The origin of the low temperature relaxations is localized molecular motion. If the γ and β relaxations were due to a large scale cooperative motion, the systematic increase in the strength of the β-relaxation cannot be explained. Large scale cooperative motion should be restricted by cross-linking and thus increased cross-linking should lead to a decrease in the peak height. The β-relaxation is associated with newly created molecular segments during the curing reaction and the 18% increase in the height of the β peak parallels the increase in the extent of curing.

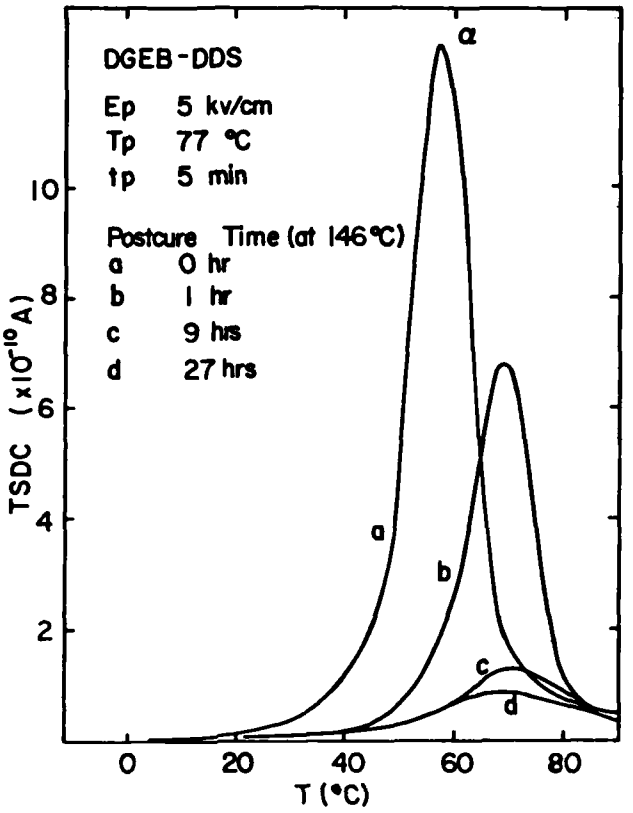

HIGH TEMPERATURE RELAXATION IN THE DGEB-DDS EPOXY RESIN

(Figure 8)

High temperature thermally stimulated depolarization, TSD, current measurements of the epoxy resin is shown. The α-transition corresponds to the glass transition as measured via DSC. The α-transition temperature increased from 57°C for a specimen without post curing to 70°C after post curing for 9 hours at 146°C. Further post curing did not increase the temperature of the α-transition. Post curing reduced the strength of the α-transition by a factor of 14. This result indicates that the TSD technique holds promise for monitoring the extent of curing.

The dramatic decrease in the strength of the α-transition, as compared to the small change in the β-relaxation, implied that numbers of molecular segments which were able to move were reduced and the increase in peak temperature indicated that the activation energy for motion of the molecular segments had increased. This suggests that the origin of the observed changes in the α-transition is the cross-linking density.

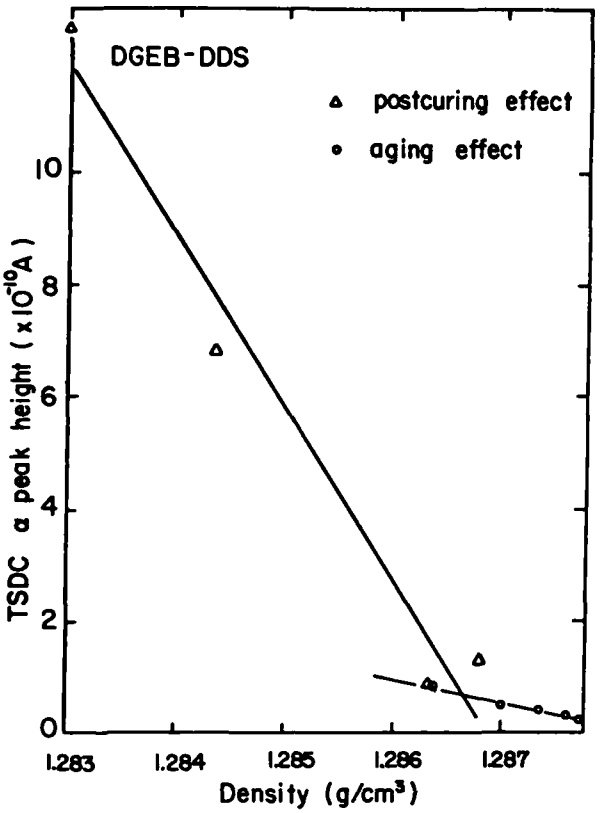

MONITORING OF THE EXTENT OF CURING IN THE DGEB-DDS EPOXY RESIN

(Figure 9)

The variation of height of the α-transition as measured via TSDC is plotted against the extent of curing as determined by density measurements. The relation is fairly linear. The magnitude of the change of the strength of the α-transition with density is much larger than the free volume effect due to sub-T_g aging. The decrease in the magnitude of the α-relaxation must be due to restricted movement of molecular segments, as a consequence of the increased density of cross-linking during the post curing process.

The correlation of the TSDC measurements of the α-transition with cross-linking density demonstrates that the TSD technique has promise for monitoring the cross-linked density, especially in the region close to completion of the curing process where infrared spectroscopy is insensitive. Note the small changes in density, T_g, modulus, and stress at the yield point compared with the 14-fold change in the TSDC α-peak height. Also, recall that specimens post cured for 9 and 27 hours respectively at 146°C had the same T_g, elastic modulus, extent of curing, and only a small difference in mechanical strength, but had a 30% difference in the TSDC peak height.

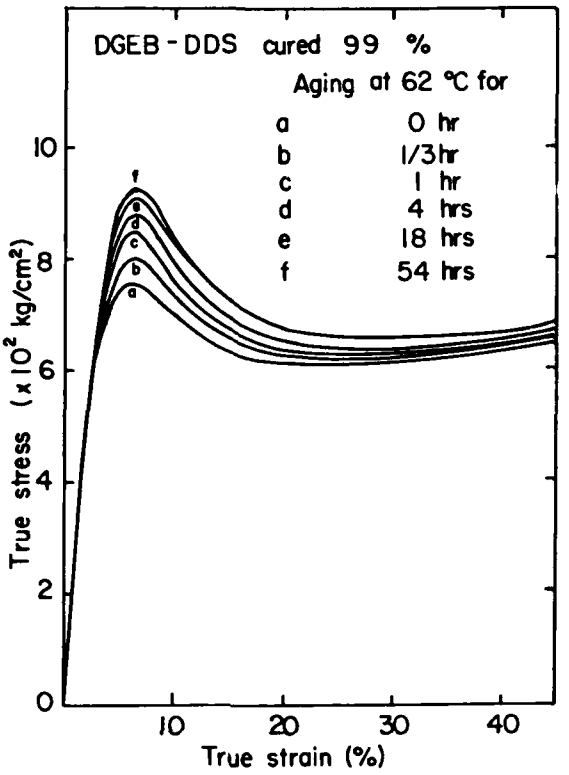

STRESS-STRAIN RELATIONS FOR AGED DGEB-DDS EPOXY RESIN

(Figure 10)

The effect of sub-T_g aging on the stress-strain behavior of the DGEB-DDS epoxy resin previously cured for 12 hours at 112°C and post cured for 27 hours at 146°C, cured 99% as measured by FTIR spectroscopy is shown. The yield point was enhanced by the sub-T_g (15°C below T_g) aging treatment. A 23% increase of the stress at the yield point was obtained by aging for 54 hours at 62°C but the increase in stress at the lower yield point was much less. Neither the elastic modulus nor the strain to yielding was affected by the sub-T_g aging.

The systematic increase in yield strength with sub-T_g aging is similar to the results observed for many thermoplastics. Note also that aging has influenced the yielding process and there was a much smaller effect on the flow curve after yielding.

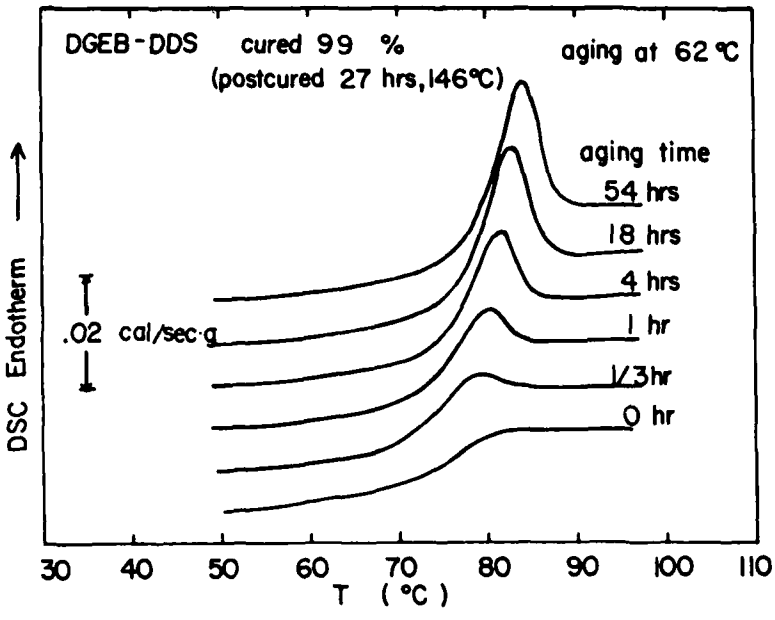

DSC FOR SUB-T_g AGED DGEB-DDS EPOXY RESIN

(Figure 11)

Thermogram of DGEB-DDS epoxy resin as a function of sub-T_g aging indicates the presence of an endotherm peak on the high temperature side of the glass transition. The size of the endothermic peak is dependent upon the aging time at 62°C.

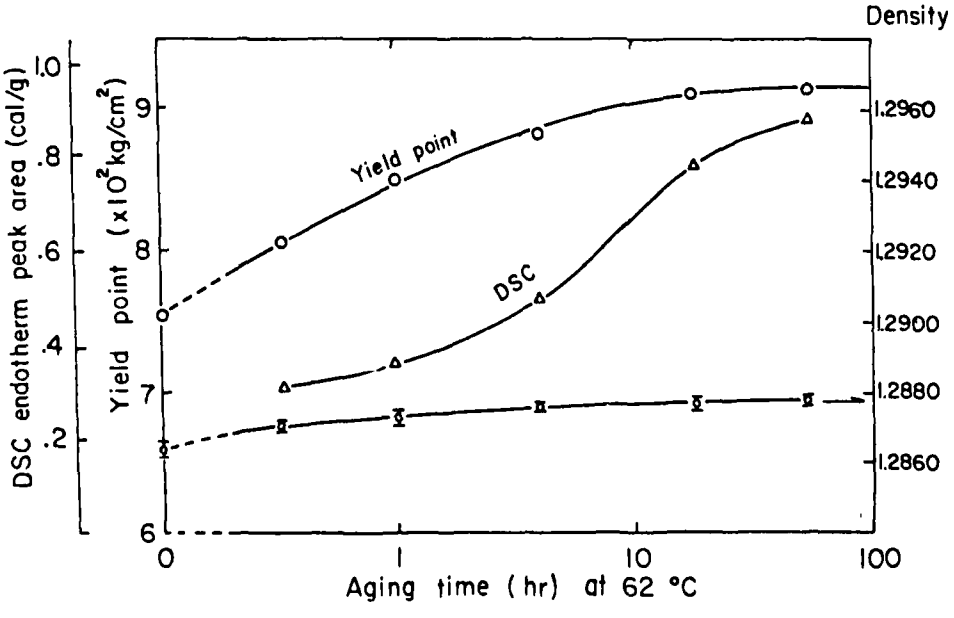

EFFECT OF SUB-T_g AGING ON PROPERTIES OF DGEB-DDS EPOXY RESIN

(Figure 12)

Sub-T_g aging of DGEB-DDS epoxy resin at 62°C resulted in an increase in the stress at the yield point for times up to about 18 hours, the stress level saturated for times greater than 18 hours. The area under the endothermic peak increased rapidly with the time of aging, but unlike the yield point, the endotherm increased for 54 hours at 62°C. The density also increased monotomically with aging time, the increase in density was 0.12% after 54 hours at 62°C.

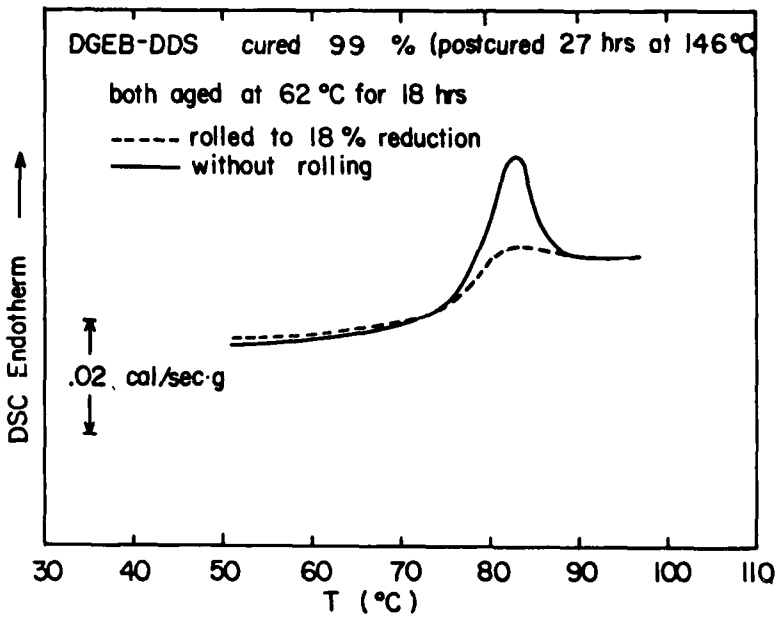

INTERACTION OF AGING AND DEFORMATION OF DGEB-DDS EPOXY RESIN

(Figure 13)

In order to ascertain whether deformation could erase the sub-T_g aging effect in DGEB-DDS epoxy resin, DSC measurements were made on an as-aged specimen, 18 hours at 62°C, and on a specimen aged to the same degree but cold rolled 18% reduction in thickness after aging. The results show that cold rolling has completely eliminated the endothermic peak. Since the aging effect can be eliminated by both deformation and by thermal treatment above T_g, the source of the sub-T_g aging effect cannot be a cross-linking process, but is associated with a free-volume effect, recall the density change observed in the aging experiments.

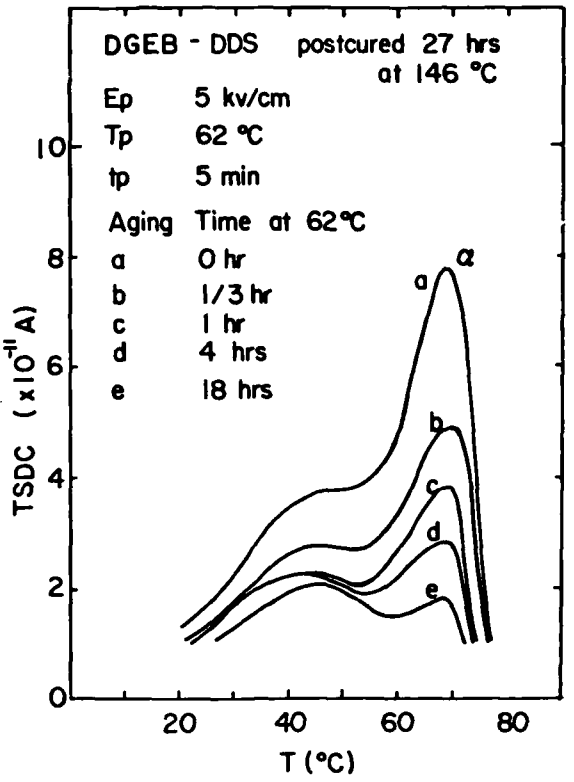

TSD THERMOGRAM OF SUB-T_g AGED DGEB-DDS EPOXY RESIN

(Figure 14)

High temperature thermogram of DGEB-DDS epoxy resin as a function of the aging time at 62°C is shown, the specimens were poled at the aging temperature in order to prevent the loss of the aging contribution by poling at a higher temperature. Two peaks appeared in the thermogram for all specimens. While the strength of the 45°C peak appeared to decrease somewhat with aging, the height of the higher temperature relaxation after aging for 18 hours at 62°C decreased to less than 25% of that of the unaged specimen. It should be noted that the aging effect is reversible in that a specimen aged and subsequently heated above T_g returns to its original as-quenched state in terms of the TSD thermogram, stress-strain relation, density and DSC.

The 4-fold change in the α-peak height in the TSDC measurements for a specimen aged for 18 hours at 62°C, in contrast to the 0.12% change in density and 23% change in the stress at the upper yield point for the same aging treatments, again suggests the sensitivity of TSDC measurements to structural changes in polymers. Note again the correlation between a decrease in the relaxation strength and the increase in mechanical strength. The decrease in the relaxation strength implies a decrease in mobility of molecular segments and a decrease in the mobility of molecular segments is reflected in an increase in the resistance to deformation.

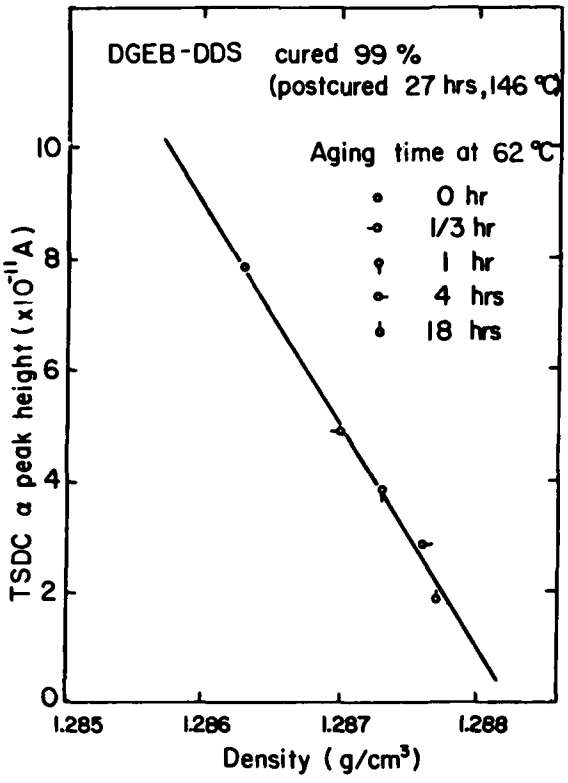

CORRELATION OF THE TSD MEASUREMENTS AND DENSITY

FOR SUB-T_g AGED DGEB-DDS EPOXY RESIN

(Figure 15)

The correlation of the height of the α-transition and the density of the DGEB-DDS epoxy resin aged at 62°C revealed a very good linear relation with a factor of 4 change in peak height vs the quite small change in density of 0.12%. This correlation suggests that the number of molecular segments capable of motion at the aging temperature, as implied from the strength of the α-relaxation, is associated with the density and, consequently, the free volume of the epoxy resin.

PHYSICAL AGING STUDIES OF EPOXY RESINS WITH EMPHASIS ON GRAPHITE FIBER-EPOXY COMPOSITES

Yousef Mohajer, Elaine Yorkgitis,
Garth Wilkes and James McGrath

Departments of Chemical Engineering and Chemistry
and
Polymer Materials and Interfaces Laboratory
Virginia Polytechnic Institute and State University
Blacksburg, VA 24061

Abstract

A brief review of the effects of physical aging on the material properties of some linear and network macromolecular glasses is presented. The free volume concept is used to describe this behavior. The effect of physical aging on properties of some uniaxial graphite/fiber epoxy resin composites is investigated using stress-relaxation in both tensile and flexural modes. The matrix polymers used for this study were Hercules 3501 and NARMCO 5208 resins both of which are based on a 4,4'-methylenedianiline derivative of epichlorohydrin with diamino-diphenylsulfone (DDS) as the curing agent. The matrix resin, as used in the practical application in composites, was found to be not fully cured and the glass transition of the network was found to be dependent on the curing schedule. The physical aging of the bulk crosslinked epoxy was found to depend on the sub-T_g annealing temperature, T_a, and the T_g of the resin. The physical aging of the composite, monitored by the stress relaxation method, was found to be dependent on the testing direction. When the test direction was perpendicular to the fiber direction (series model), the composite showed a considerable amount of stress relaxation in that it displayed a significant change in the percent stress relaxation with time. However, the value of the

percent stress relaxation was found to be lower than that of the bulk resin. No aging effect was observed when the test direction was parallel (parallel model) to the fiber. Thus although the matrix does display changes in properties with time, the composite, depending on the test direction, may or may not provide evidence of physical aging.

INTRODUCTION

In principle any material that can undergo vitrification is susceptible to the later process known as physical aging. This phenomenon arises due to the simple fact that when a system is cooled from the liquid or rubbery state into the glassy state, it is difficult for the molecular system to maintain equilibrium as vitrification proceeds (1). This occurs because of the increase in viscosity as the glass temperature is approached which in turn limits the mobility of the molecules and their ability to acquire equilibrium packing and their lowest energy conformational states.

In essence it is possible that both an excess free volume (volume over and above that of the Van der waal's radii) as well as an excess enthalpy (due to nonequilibrium conformational states and excess volume) exist immediately following the vitrification process. The presence of this nonequilibrium state leads to the process of what is often called physical aging. While we will be addressing this process with regard to polymeric substances, it should be stated that it is not unique to only macromolecular systems. Indeed it is widely accepted that inorganic glasses physically age as do many of the low molecular weight organic systems which can also show vitrification. We will,

however, focus our remarks on macromolecular systems where it has been within the last decade or so that considerable attention has been given to the physical aging process. More specifically, following this introduction, we will address the prominence of physical aging in high strength fiber-reinforced composites utilizing two epoxy matrix resins.

Early on, linear amorphous polymers such as those of polystyrene (1, 2), polymethylmethacrylate (3), polyvinylacetate (4), amorphous polyethylene terephthalate (PET) (1,5), and polycarbonate (6) have been demonstrated to display physical aging. More specifically physical aging can often be recognized as occurring by following the time-dependent changes within mechanical, sorption or dielectric properties. For example, Figure 1 presents

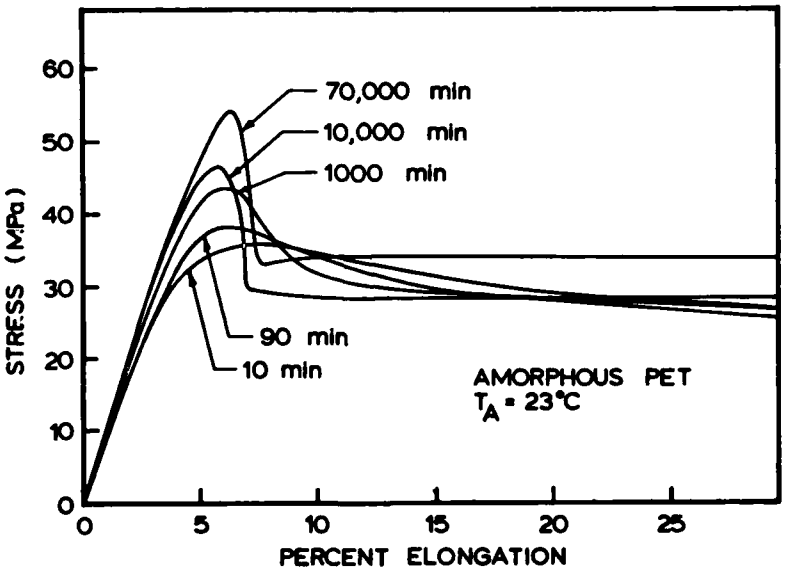

Figure 1. Stress-strain curves of amorphous PET aged at room temperature for 10, 90, 1,000, 10,000 and 70,000 min. Note changes in yield stress, modulus, and characteristic draw ratio. References 7 and 8.

the stress-strain curves for several amorphous PET samples that have undergone sub-T_g annealing at 23°C following rapid quenching. The sub-T_g annealing times range from 10 to 70,000 minutes (7, 8). From this figure it is clear that as aging progresses, the modulus, yield stress and characteristic draw behavior change considerably, thereby imparting an entirely new set of properties to the material.

Similar though not as dramatic changes have been observed in semicrystalline PET as well (9). The smaller change in behavior with sub-T_g annealing, however, arises from the fact that there is less amorphous material present to undergo physical aging as that particular component restores its equilibrium state.

The stress-strain behavior of linear high molecular weight epoxies also parallels those of the more common linear systems already denoted. Trends discussed earlier can be seen in Figure 2

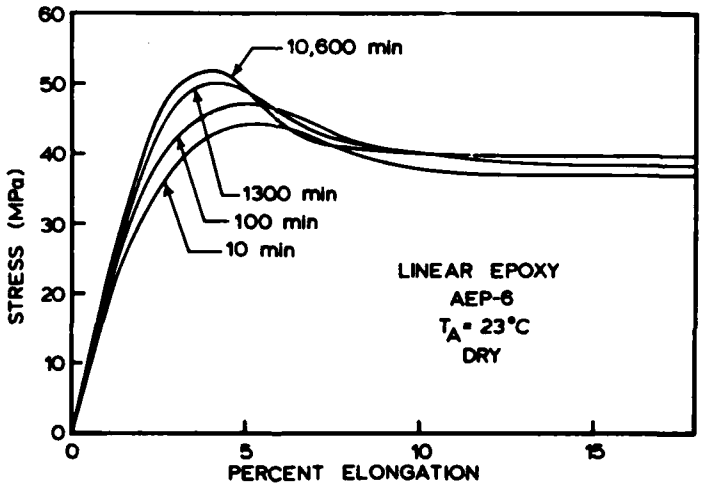

Figure 2. Stress-strain curves for a linear high molecular weight epoxy (AEP-6) aged at room temperature for 10, 100, 1,300 and 10,000 min. Note changes as per Figure 1. Reference 10.

which displays the stress-strain curves for one linear epoxy resin (AEP-6) that has been investigated by the authors (10).

Epoxy resins are more commonly crosslinked and these network glasses also undergo physical aging as has been first systematically demonstrated by work from the authors' laboratory (11). Epon 828 resin cured with nadic methylanhydride (NMA) is one such system. The two stress-strain curves for this material shown in Figure 3

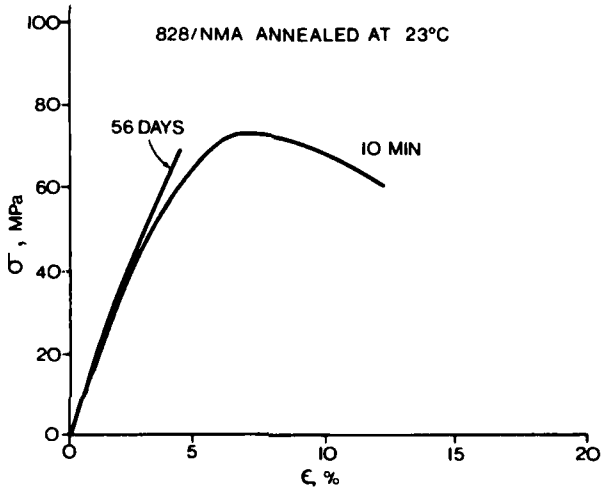

Figure 3. Stress-strain curves for Epon 828 resin crosslinked with nadic methyl anhydride and aged at room temperature for 10 min. and 56 days. Reference 11.

indicate the very pronounced effect of a 56 day sub-T_g annealing carried out at room temperature (11). The data clearly indicate a significant difference in the deformation behavior. With specific regard to this paper, it should be recognized here that it is similar epoxy-based resins that serve as the matrix for many of the high strength resin composites of industrial interest.

Increases in moduli are rather consistently noted in materials undergoing the physical aging process. Consequently, aside from

comparing entire stress-strain curves, one can generally demonstrate the physical aging process by plotting the modulus versus sub-T_g annealing time. Figure 4 displays an example of such a plot for

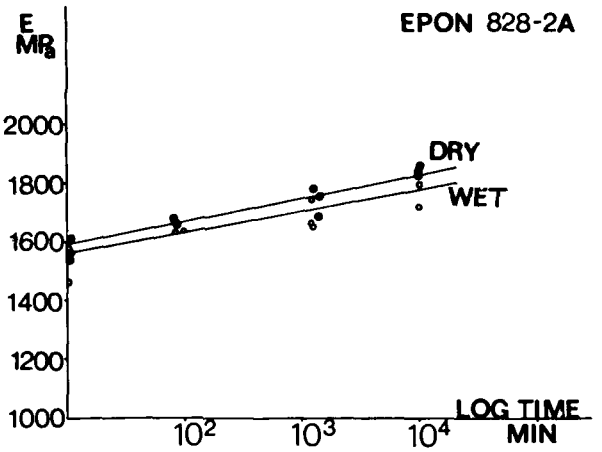

Figure 4. Modulus vs. log time plots for Epon 828 crosslinked with PACM-20 by a two-stage curve. No significant differences are noted between "dry" samples and those subjected to moisture. Reference 10.

a crosslinked epoxy resin (10). In addition, it shows that the effect of moisture on aging is rather insignificant for this particular system since the sub-T_g annealing was carried out both in the dry and wet states.

Returning to the origin of this nonequilibrium phenomenon, it should be realized that the excess volume and enthalpy addressed earlier will influence the given properties of the system at any given time. As indicated in Figure 5, as the system is cooled into the glassy state, the rate of cooling will influence the degree of nonequilibrium character and therefore the driving force for the system's approach to equilibrium (1). However, other factors, such as the sub-T_g annealing temperature, are important variables in

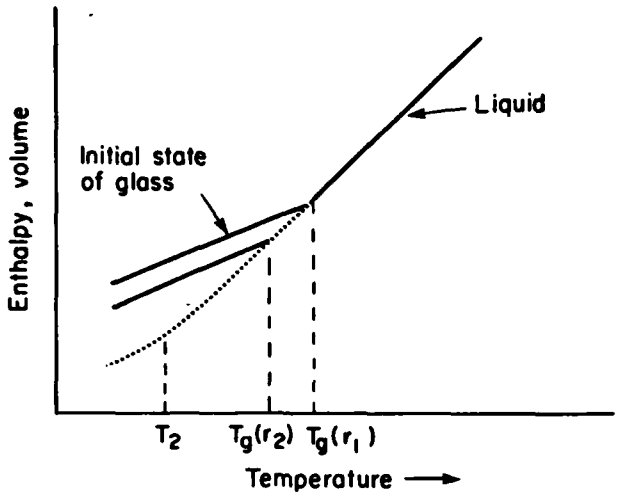

Figure 5. Schematic plots showing changes in enthalpy and volume with changes in temperature. Dotted line indicates the equilibrium state, which is achieved only if the material is cooled infinitey slowly. T_2 is the temperature. Reference 1.

regard to the rate at which a system may approach equilibrium. It is this time dependent shift toward equilibrium that produces changes in properties of the system due to the fact that both the enthalpy and the excess volume (free volume) is decreasing with time.

Selecting the variable of free volume as being indicative of physical aging one can demonstrate changes in free volume through absorption experiments. For example, Figure 6 shows a plot of the percent weight gain of methyl ethyl ketone (MEK) versus sub-T_g annealing time for samples of Epon 828 cured with NMA (11). It is noted from these weight gain data that the rate of MEK absorption is greatest for the samples with the smallest degree of sub-T_g annealing time thereby indicating a higher available free volume.

Stress relaxation tests can also be used as a means of monitoring the physical aging process. This concept can be understood simply from the fact that at a given temperature, a system will relax under an

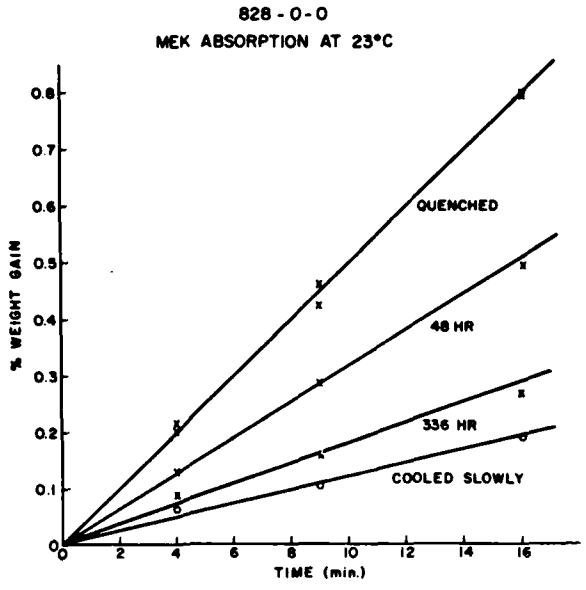

Figure 6. Plots of percent weight gain of methyl ethyl ketone vs. time immersed in MEK for an Epon 828 resin cured with PACM-20. The rate of MEK uptake is reduced with aging time as a result of decreases in free volume. Reference 11.

applied load at a rate that will be coupled to the available free volume (8, 12). The type of data that can be obtained from such an experiment is shown in Figure 7 along with the means of calculating the percent stress relaxation. Within our own laboratory, we have employed the method of stress relaxation to monitor physical aging (9-11). The stress relaxation duration that has been utilized is that of 10 minutes in contrast to the total stress relaxation curve. This time window is, of course, convenient but it does not provide the total picture of the time dependent changes in properties that may occur as has been discussed in previous papers (9-11). Such an approach, however, does yield a self-consistent body of data. For example, Figure 8 displays the percent stress relaxation occurring in 10 minutes versus the logarithm of sub-T_g annealing time for a particular crosslinked resin. These data were obtained on materials similar to those utilized in Figure 4 and

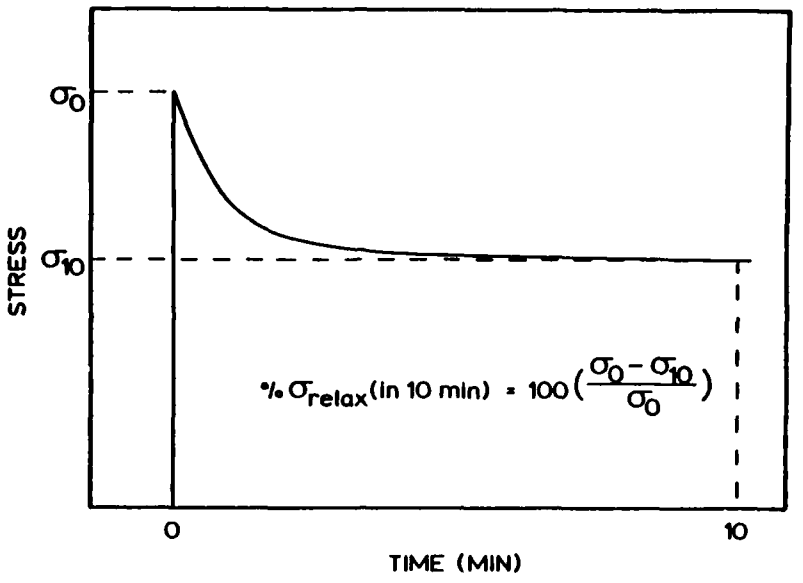

Figure 7. Schematic of a stress relaxation curve in which the stress needed to sustain a particular deformation decays with time. The calculation for percent stress relaxation is described in the figure.

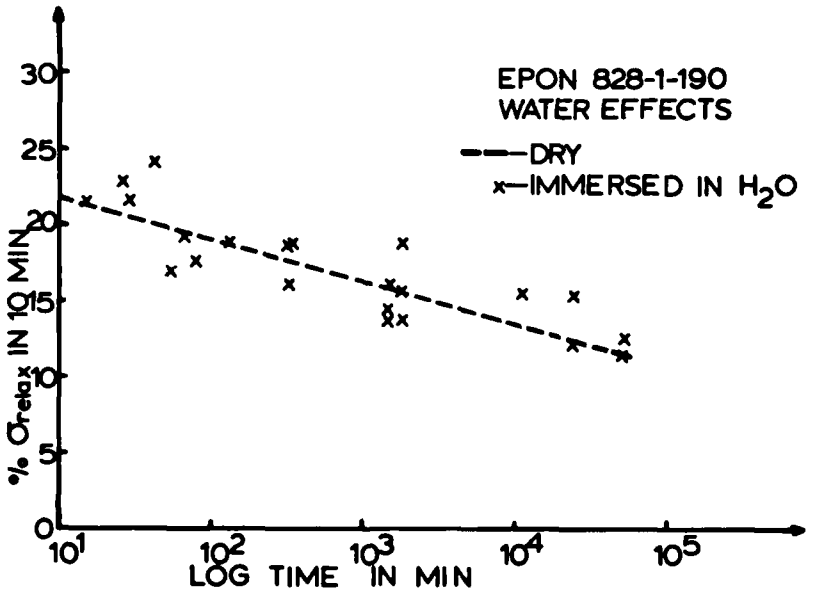

Figure 8. Plot showing the linear decrease in percent stress relaxation with log aging time for Epon 828 cured with PACM-20 in a one-stage reaction. It is seen that the physical aging behavior of this material in the presence of moisture does not differ markedly from that in a dry environment.

again it clearly indicates that the effect of moisture plays a small role at best in terms of the physical aging process when contrasted to dry samples.

Finally Figure 9 presents some additional stress relaxation data for the same system but in this case the variable of sample thickness was investigated (10). It is noted that the data are independent of sample thickness and that again there is a linear behavior when this data is plotted as a function of the log of the sub-T_g annealing time. Had internal stresses been the cause of the change in the properties with time one would have expected to see differences for these samples. This is not to say, however, that internal stresses never contribute to time dependent behavior (13, 14) but rather that the data given in Figure 9 do not suggest this parameter to be of importance.

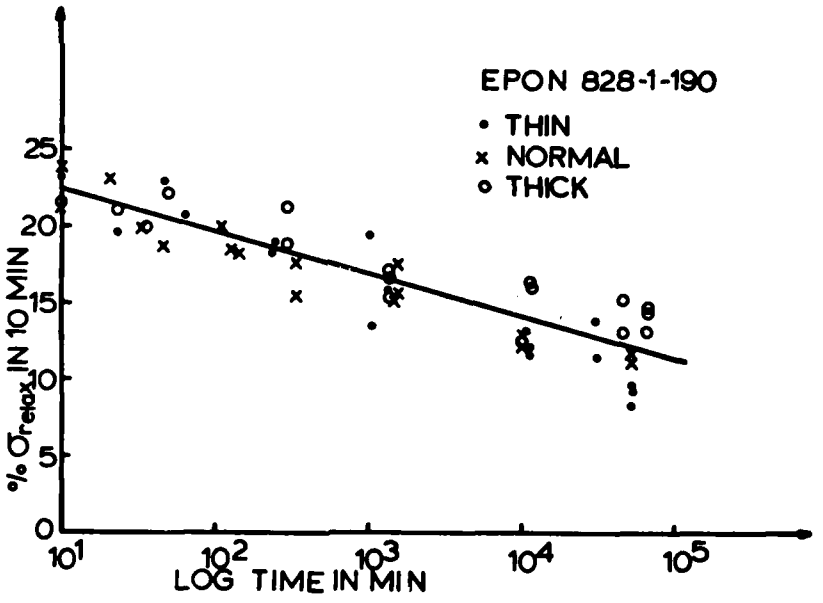

Figure 9. Plot of percent stress relaxation vs. log aging time for Epon 828 cured in one stage with PACM-20 and prepared in samples of different thicknesses. All data points fall on essentially the same line, suggesting that internal stresses did not significantly influence the natural physical aging in this case. Reference 10.

Now that the basis of physical aging behavior has been introduced and demonstrated for some rather common epoxy bulk resins, we will now direct our attention to epoxy based composites to note if the same or similar behavior occurs.

EXPERIMENTAL

Materials

Two uniaxial graphite fiber-reinforced epoxy composites were utilized in this study. Both of these systems were received from NASA/Langley. One of these was based on 8-ply specimens of a uniaxial graphite fiber composite utilizing Hercules 3501 resin -- one of the more common high strength composite resins. The two main constituents of the resin are the epichlorohydrin derivative of 4,4'-diaminodiphenyl methane (a tetrafunctional epoxy) and diaminodiphenylsulfone, DPS (also a tetrafunctional aromatic curing agent). The chemical structure of the epoxy and the curing agent are given in Figure 10. The epoxy apparently was not completely cured because the T_g of the resin was found to be around 84°C. The other graphite fiber composite used in this study was prepared using fiber/NARMCO 5208 resin, another well known composite resin. The curing of the latter system was carried out in our laboratory (after constructing specimens as described later) according to a schedule prescribed by NASA/Langley. The impregnated plys of graphite/NARMCO 5208 which were received in dry ice were warmed to room temperature and were then stacked in a uniaxial fashion (4 or 6 plys). They were then placed between Teflon sheets of 5 ml thickness, cut in the desired dimensions and

NARMCO 5208

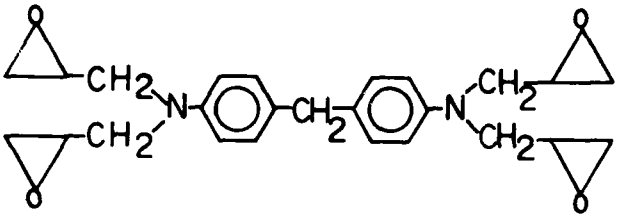

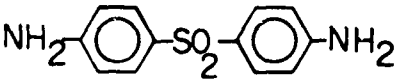

DDS

Figure 10. Chemical structures of major constituents of NARMCO 5208 and Hercules 3501 resins.

directions and sandwiched between two flat metal sheets. The thickness of the top metal sheet was chosen so that the force exerted by the top sheet was around $10g/cm^2$. The samples were heated for 4.5 hours at 149°C (300°F) after which the temperature of the oven was raised to 177°C (350°F) and kept there for an additional 1.5 hours. The samples were then taken out of the oven and quenched to room temperature in air. The bulk (pure) 5208 resin samples were prepared by the following procedure. Uncured resin which was received in dry ice and stored in a freezer was allowed to warm up to room temperature. A desired amount of the resin was weighed into a beaker then heated in a vacuum oven at 120°C and degassed for a period of 10-20 minutes until no gas evolved. The resin was then poured into a Dow Corning RTV 3110 silicone rubber mold which was preheated to 149°C. The curing was carried out at 149°C for 4.5 hours after which the temperature was raised to 177°C and kept there for an additional 1.5 hours. Quenching was done by

placing the hot mold between two large metal pieces at room temperature. The samples were removed from the mold after they had cooled (approximately 1/2 hour). All the samples were stored in a desiccator prior to use.

The Hercules 3501 composite samples had to be cut after they were cured. To cut the samples, the sheet of the composite was sandwiched between two stainless steel dog-bone templates. The composite sheet was then sawed off around the templates using an ordinary electric saw. This was done to minimize formation of cracks in the samples. The samples were cut with the dog-bone axis in both the direction of the fibers (parallel, $\parallel$) and perpendicular to the direction of the fibers (perpendicular, $\perp$). The size of the template was such that the final sample had a width of 0.65 cm and effective length of 4.0 cm.

The NARMCO 5208 composites were cut into appropriate dimensions prior to curing. To prepare samples for tensile studies, the sandwich of Teflon-composite-Teflon was placed between the dog-bone templates. The sample was then cut by sliding a sharp razor blade around the templates. Samples were prepared again in the parallel and perpendicular directions. The effective size of these samples was the same as those prepared from Hercules 3501. The number of plys used in the parallel and perpendicular samples was 4 and 6, respectively, which resulted in respective thicknesses of 0.7 mm and 1.1 mm in the final samples following curing.

The size of the samples used for flexural tests was 7.5 cm x 2.5 cm. These samples were constructed from 4 plys which resulted in a sample thickness of ca 0.8 mm after curing. Samples for both parallel and perpendicular directions were cut prior to curing. Samples of pure resin were cured in rubber molds and had the dimensions 7.5 x

2.5 x 0.1 cm. All NARMCO and Hercules samples were annealed for 10 minutes at 200 and 100°C, respectively, quenched in cool water, quickly dried and aged within a vacuum desiccator.

Measurements

The thermograms of the samples were obtained using a Perkin Elmer DSC-2. The rate of scanning was 10°/min.

The stress relaxation measurements were made on an Instron Model 1122. The stress relaxation tests were done in the tensile mode, but for some samples the test was also performed in the flexural mode. For the stress or relaxation in the tensile mode, the sample was clamped between the jaws of the instrument so that effective initial length of the sample was 4.0 cm. A fixed strain (0.25 or 0.50) was applied rapidly (cross-head speed 10 mm/min) and the "initial" and the time dependent stress were monitored for a period of 10 minutes. The percent relaxation in 10 minutes was then calculated according to Figure 7. While the time scale of 10 minutes is short relative to the complete relaxation curve, it has provided a good index of physical aging behavior as discussed in past studies. Most of the stress relaxation tests were carried out at ambient conditions. The stress relaxation studies via the flexural tests were performed in the manner described below.

Flexural testing was performed using an Instron machine operated with a tensile load cell and fitted with two aluminum/stainless steel pieces. The lower and stationary piece formed a base and held two stainless steel rods 0.6 cm in diameter and 6.35 cm apart, center to center. The upper and mobile piece held a third stainless rod, also

0.6 cm in diameter and parallel to the two base rods. To run the flexural test, the mobile rod was lowered to a position below that of the two stationary rods in the base piece. As illustrated in Figure 11A,

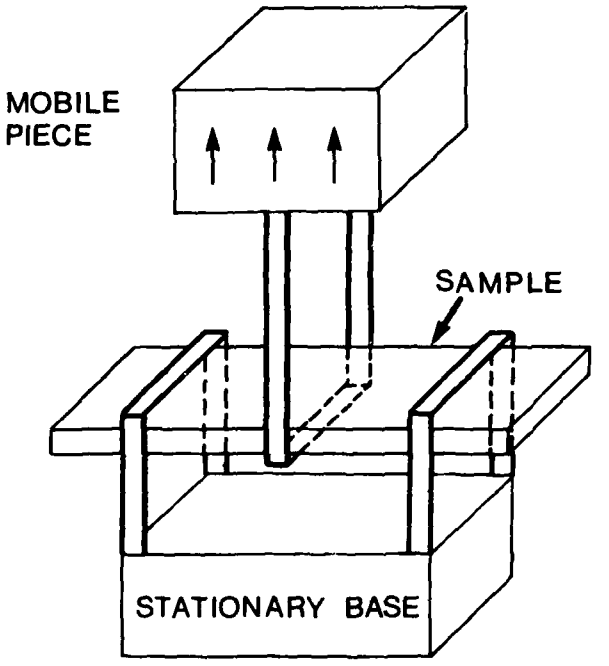

Figure 11A. Schematic drawing of the flexural test device including sample shape, sample and rod positions, and motion of the rods.

a sample was then placed above the single rod and below the pair of base rods. The geometry is then very similar to the common three-point bend test (15), the differences being the relative positions of the three "points" and the sample as well as the motion of the central point.

In the case of a composite material, it is important to note the orientation of fibers with respect to the direction of the flexural rods. Figure 11B illustrates the authors' notation for the two possible situations.

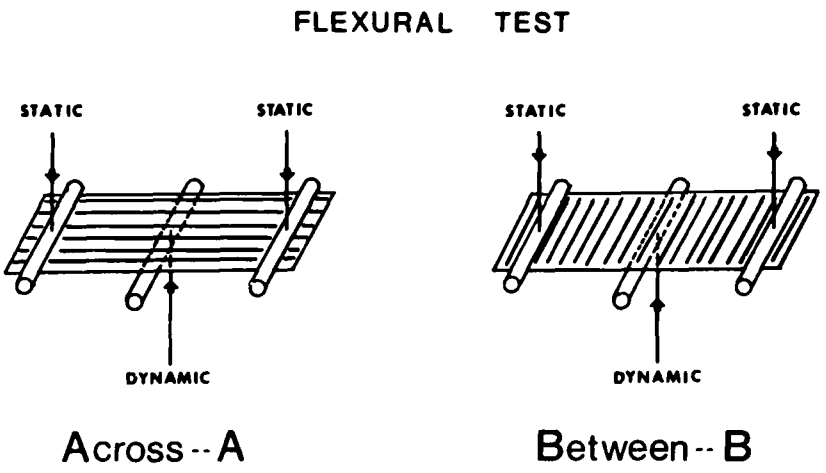

Figure 11B. Schematic drawing showing the authors' notation for the orientation of test device rods and fiber direction in flexural test samples.

This test allows an accurate zeroing of samples in mechanical testing. With a sample in place between the rods, the mobile piece was raised at a crosshead speed of 10 mm/min. until a stress response was observed on the Instron's recording chart. The upper piece was then generally lowered 0.1 mm to ensure that no stresses were imposed on the sample prior to the beginning of testing.

Flexural stress-strain curves on samples aged 10 minutes (crosshead speed, 10 mm/min) showed that the behavior was linear to at least 6 or 7 mm central deflection for both the pure resin and the composites. Accordingly, 5 mm was chosen as a standard deflection to be sure that all testing was done in the linear region.

The flexural device was used to measure the ten-minute stress relaxation of NARMCO samples aged for various times. At a crosshead speed of 100 mm/min, samples were deflected to 5 mm in a deformation time of 3 seconds. This deformation was held for 10 minutes and the percent stress relaxation calculated.

The volume fraction of the resin in the graphite/NARMCO 5208 system was determined by removal of resin from an uncured composite using acetone as a solvent. Taking the density of the cured resin as 1.3 g/cc and that of graphite as 1.8 g/cc (both determined using a volume displacement method), the volume fraction of the resin was determined to be around 0.47.

The value of strain placed on bulk samples in the tensile relaxation experiment was 0.5 percent. The strain imposed on the composites in the perpendicular direction was chosen at 0.25 percent value. This was done taking into account a series model in which the deformation was assumed to be concentrated in the resin matrix. A strain of 0.25 percent was also applied to the composite in the parallel direction because at higher extensions considerable slippage of the samples occurred.

Results and Discussion

The mechanical properties and the aging behavior of the composites are dependent on the sub-T_g annealing temperature, T_a, relative to the transition temperature T_g of the resin. Since the rate of attainment of equilibrium is initially dependent on the temperature increment $\Delta T = T_g - T_a$, either a decrease in T_g and/or an increase in T_a would potentially result in a variation of aging behavior.

The glass transiton temperature of a fully cured bulk NARMCO 5208 resin (chemical structure of major constituent is given in Figure 10) is found to be around 240°C. The transition temperature of the resin in the composites is, however, far away from that of the fully cured state and is dependent on the curing condition employed in the preparation

of the new composites. A comparison of the transition temperature of a composite prepared according to the NASA/Langley procedure to that of a resin which is essentially fully cured is made in Figure 12. The

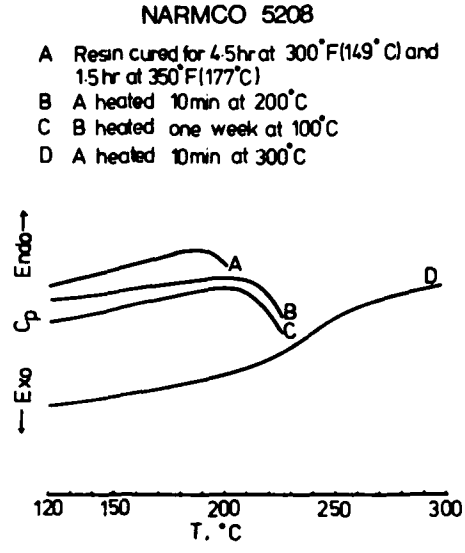

Figure 12. DSC thermograms of NARMCO 5208 resin. The curing schedule and the thermal history of samples are described in the figure. The heating rate is 10°C/minute.

bulk resin, for example, which has been cured for 4.5 hours at 149°C and 1.5 hours at 177°C, displays an exothermic behavior above 180°C (just a few degrees above the highest curing temperature). This indicates that the sample is not yet fully cured and when enough thermal energy is supplied to the chains, the unreacted portions gain enough mobility to continue the reaction of the as yet unreacted species. The energy released from the subsequent chemical reaction is displayed as exothermic behavior. Thus the practical glass transition of such partially cured samples lies close to the highest curing temperature as described by Gillham (16). In order to study the effect of sub-T_g annealing on the physical aging behavior, the resin is generally heated for 5-10 minutes

at 10-15°C above its T_g to erase past history and it is then quenched to the selected annealing temperature T_a. The time the sample is quenched is taken as time zero and thereafter the properties are measured against the sub-T_g annealing time (11). Since neither of our composites were fully cured, it was necessary to differentiate the effect of possible chemical aging from physical aging in our systems. One possible way of reducing chemical aging would be to fully cure the epoxy as done by Kong (17). Such a sample will not undergo further curing when it is heated to erase past histroy or when it is being aged. Unfortunately there are two problems associated with this manner of procedure. First, the curing procedure employed for preparation of a composite has been selected with optimization of the material properties. That is, under that specific curing procedure, and therefore a given apparent T_g of the resin, the material properties of the system may be most desirable when the fully cured condition is not achieved. For example, possibly further curing may result in a more brittle system and therefore the aging study of such a system may not be relevant to practical applications. Secondly, when a system is fully cured its T_g becomes higher and therefore for a given ΔT one has to choose a higher annealing temperature. Moreover, if the system is fully cured, it does not guarantee that no other chemical reactions can occur. Indeed we have observed that annealing at above 120°C for a period of one week, even in vacuum ($P_{air} \leq .5$mmHg), resulted in a noticeable discoloration of bulk NARMCO 5208 in the first 0.2 - 0.5 mm of the sample thickness. Because of these complications, it was decided to study the aging behavior of these composites prepared according to the "standard" prescribed procedure. To investigate the effect of possible chemical aging, a sample of NARMCO 5208 resin which

was cured according to the prescribed schedule, T_g ~185°C, (Figure 12, curve A) was heated for 10 minutes at 200°C (about 15°C above T_g). In this way we introduced a heating cycle which was needed to erase the past history of the sample. A DSC rerun of this sample shows that the apparent T_g of the sample had been raised to 200°C (as expected due to further curing). However, when such a treated sample was aged for 1 week at ambient or even when it was aged for that period at 100°C no noticeable changes in the thermogram of the sample were apparent (Figure 12, curve C). Therefore chemical aging of the sample under those conditions was considered negligible. Therefore aging of the NARMCO samples followed a 10 minute pre-treatment of the composite at 200°C.

The effects of sub-T_g annealing temperature on physical aging are illustrated in Figure 13. Bulk samples of NARMCO 5208 which had been treated identically and, therefore, had the same T_g, 195-200°C, were aged

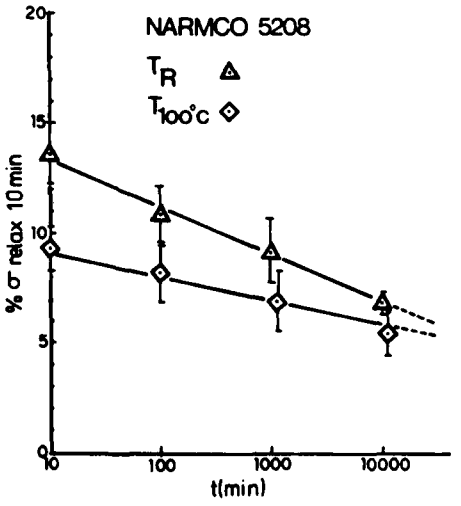

Figure 13. Effect of annealing temperature on the aging behavior of bulk NARMCO 5208 resin. The tests are in the tensile mode and ε = 0.5%.

at ~25°C (T_R) and 100°C (T_{100}). It should be recalled that, as indicated before, this 100°C sub-T_g annealing does not cause any significant change in the chemical structure of the polymer and therefore a difference in mechanical behavior is related to physical aging of the resin. At early aging times (for example, 10 or 100 minutes), the samples at higher sub-T_g annealing temperature (100°C) display lower percentages of stress relaxation than samples stored at T_R. This indicates that a sample aged at a higher annealing temperature has densified (or has lost free volume) more than a sample aged at a lower temperature during the short aging periods used here. At longer aging times (for example, 10,000 minutes), the percentages of stress relaxation in samples aged at T_R and T_{100} have apparently become closer in value to each other. Therefore the data in Figure 13 indicated that at an early aging time, the sample at the higher sub-T_g annealing temperature has come closer to its true equilibrium state than the sample at the lower annealing temperature. However, the rate of aging (that is the slope of lines in Figure 13) is higher for the sample at the lower annealing temperature. Thus it is conceivable that at very long aging times, for example 10^6 minutes, samples aged at T_R may show more embrittlement than samples aged at T_{100}. To explain this phenomenon we will utilize the volume-temperature plots given in Figure 14. Let us assume that the resin sample is cooled down from somewhere above T_g. Once the temperature of the sample is lowered below T_g, the volume of the resin will follow the solid line (nonequilibrium) and, at any given temperature, will deviate from the equilibrium volume (broken line in Figure 14A & B). Initially the sample would be either at point 1

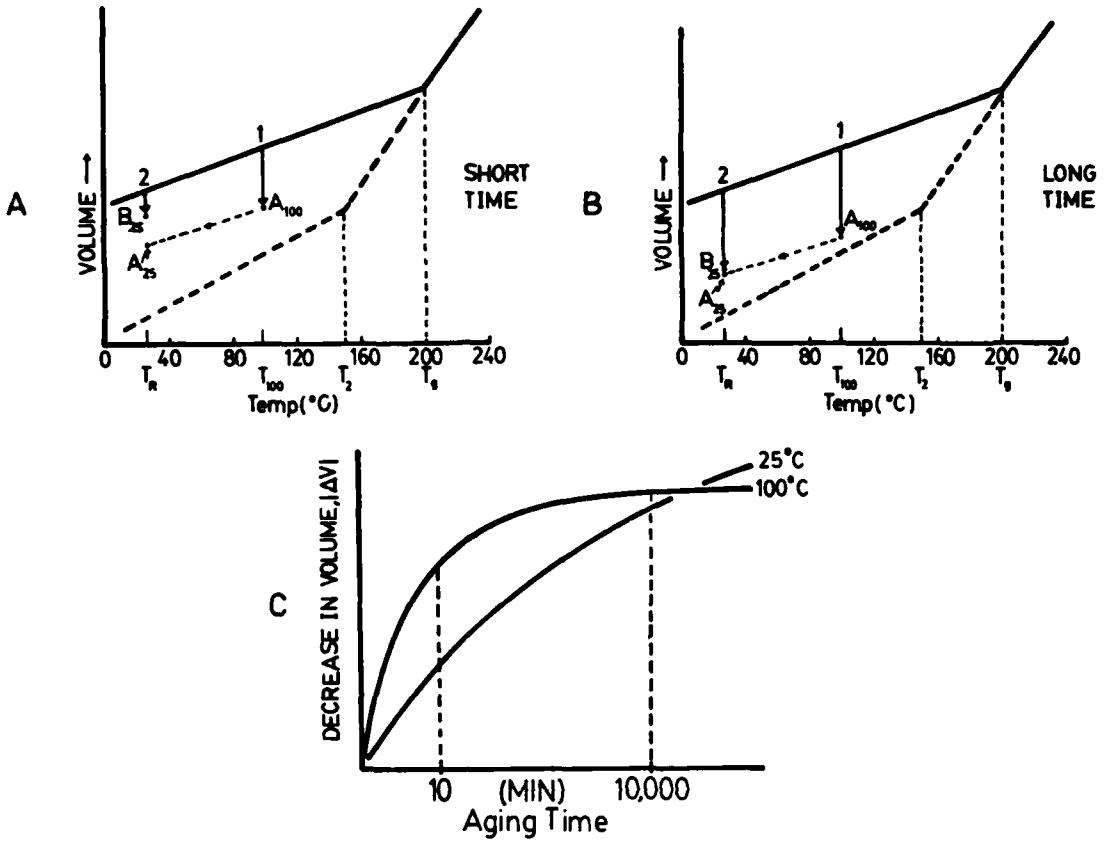

Figure 14A. A schematic representation of volume-temperature behavior of a resin after a short annealing time. Points 1 and 2 refer to volumes of the glass at 100°C and T_R (25°C), respectively, immediately after it is quenched from T_g.

Points A_{100} and B_{25} refer to volumes of the glass after a short period of time at 100 and 25°C. Point A_{25} is the volume of the polymer which was aged at 100°C immediately after it was quenched to T_R. T_2 is the equilibrium second order transition temperature of the resin. (The length of the arrows is proportional to the changes in volume).

Figure 14B. The same as 14A except after a longer annealing time. Prime is used in A'_{100}, A'_{25} and B'_{25} to indicate longer annealing times.

Figure 14C. The dependence of the absolute value of the change in volume of the resin, $|\Delta V|$, with time at 100°C and room temperature, $|\Delta V| = |V_i - V_t|$; V_i is the volume of the polymer immediately after it is quenched and V_t is the volume at time t.

or 2 depending on whether the annealing is done at 100°C or at T_R = 25°C. Figure 14A represents the volume state of the sample at *an early time*. That is after a short aging period the sample annealed at the higher temperature will be at the point A_{100} and the sample at T_R will be at point B_{25}. The larger decrease in volume for the sample at the higher annealing temperature is due to the fact that at higher temperatures more thermal energy is available for the molecules to undergo Brownian motion and thus more readily approach equilibrium.

The lower the temperature (i.e. at 25°C) the less thermal energy is available to overcome viscous forces even though at this temperature the volume of the sample is farther away from its equilibrium state. Thus when the sample at 100°C is quenched in cold water after a short period of aging (for example, 10 min) in order to determine its stress relaxation, the volume decreases following a path that we will presently assume is parallel to the line between points 1 and 2. After this short annealing time, the sample aged at 100°C has densified to a greater extent and consequently has lost more volume (or free volume) than the sample aged at T_R for the same period of time (points A_{25} and B_{25} in Figure 14A.) The sample aged at 100°C will therefore show a lower percentage of stress relaxation than one aged at T_R because the lowering of free volume restricts the mobility of macromolecular segments. At a longer aging time (see Figure 14B) the sample at the elevated temperature T_{100} has come very close to its equilibrium volume, whereas the sample at T_R is still very far away from its equilibrium volume state and therefore continues its densification process. That is, at a longer sub-T_g annealing time, the volume (or free volume) occupied by a sample

aged at T_R (B'_{25} in Figure 14B) and the volume taken up by the sample aged at T_{100} and quenched to 25°C (A'_{25}) are close to each other.† This means that at longer aging times both samples may show similar behavior as suggested by the data in Figure 13.

To elaborate on the above discussion, a schematic representation of the dependence of the volume change, $|\Delta V| = |V_i - V_t|$, is shown in Figure 14C where V_i is the initial volume of the glass after quenching to a given temperature and V_t is the volume at any given time at that temperature. Figure 14C presents changes in ΔV from time zero to infinity. This time-line can be broken into three regions, two of which are, at present, experimentally inaccessible to us. Data given in Figure 13 indicates that in the first ten minutes of aging those samples aged at T_{100} lose free volume much more quickly than those aged at T_R, presumably because of the higher thermal energy available at T_{100}. We begin to measure stress relaxation at 10 minutes, at which time the T_{100} samples have considerably less free volume than the T_R samples and show correspondingly lower values of percent stress relaxation. Within the time frame of the experiment, 10 to 10,000 minutes, those samples aged at T_{100} are already approaching their equilibrium free volume whereas those samples aged at T_R are still losing free volume at an appreciable rate, producing greater decreases in stress relaxation with time, that is, physically aging to a higher degree. As shown by extrapolations beyond 10,000 minutes in Figure 14C, T_{100} samples are nearly at their equilibrium

†The reader realizes that once a sample is quenched to T_R from T_{100} it starts to undergo aging at this lower temperature. However, since the stress relaxation test is done almost immediately after quenching the sample to T_R (aged not more than 1-4 minutes), such aging should be insignificantly small and is therefore not considered here.

volume at very long times. The T_R samples, however, continue to lose free volume at a greater rate, the end result being that their final free volume at infinite time will be significantly smaller than the *equilibrium* free volume of samples aged at T_{100}. In regard to mechanical properties for the case in point, one might anticipate that a sample aged at T_R for infinite time will be much more brittle (at T_R) than one aged at T_{100} for the same amount of time but tested at T_R.

Having discussed the aging properties of the bulk resin, the aging behavior of the composite can now be considered. A comparison of the percentage of stress relaxation in the tensile mode of carbon fiber/NARMCO 5208 composites has been made to that of the bulk resin as shown in Figure 15. The sub-T_g annealing has been done at room temperature ($\sim$25°C). The percentage of stress relaxation for the uniaxial composite is expected to be dependent on the test direction relative to that of the fiber axis. We have performed the test in both the direction per-

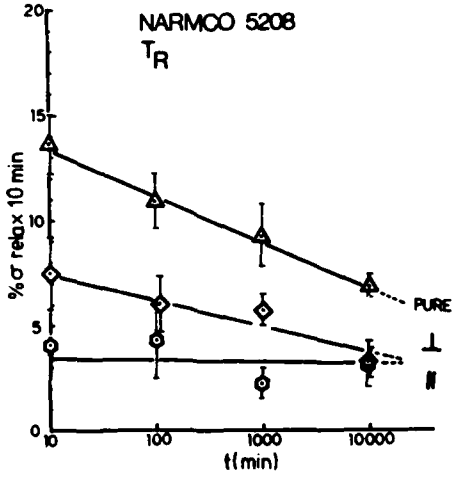

Figure 15. A comparison of aging behavior of bulk NARMCO 5208 resin to that of the graphite fiber composite in the parallel and the perpendicular directions. The aging was done at room temperature; ε = 0.5%, and 0.25%, respectively, for the bulk and the composite. The tests are in the tensile mode.

pendicular to the fiber axis ($\perp$) and parallel to the fiber axis ($\parallel$). Although the pure resin shows a considerable amount of aging with time, the composite may or may not display aging, depending on the test direction. In the test carried out in the direction perpendicular to the fiber axis ($\perp$), the samples show a distinct change in properties with time. This is because in this direction the composite behaves with the matrix and fibers in series. That is, while the graphite matrix may not show any change in properties with time, because the resin does have time dependent characteristics, the system as a whole would show kinetic effects. The absolute value of the relaxation for the perpendicular sample at any given time is approximately half of that for the pure resin. This is probably due to the fact that the volume fraction, ϕ, of the resin in the NARMCO composite is also about one half ($\phi_{resin} = 0.47$).

The stress relaxation of the composite in the fiber direction is noted to be very small. Moreover it is time independent. This is due to the fact that in the parallel direction, mechanical properties are dominated by the stronger graphite fibers. That is, although the resin does undergo physical aging, the composite does not change properties with time in this direction. Even the small percentage of stress relaxation exhibited in the parallel direction is believed to be primarily due to the small slippage of the extremely rigid samples in the grips of the sample holders.

The effects of aging on the tensile stress relaxation of graphite/Hercules 3501 composites are shown in Figure 16. The tests are again run in the parallel and perpendicular direction. The resin used in this composite has basically the same chemical structure as shown in

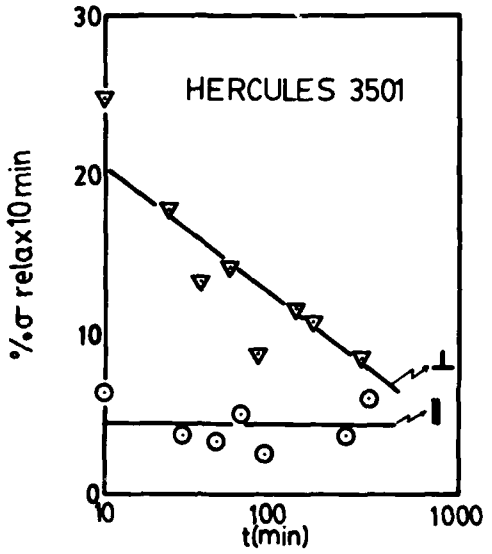

Figure 16. A comparison of aging behavior of graphite fiber/Hercules 3501 composite in the parallel to that in the perpendicular direction. The tests were done at room temperature with $\varepsilon = 0.25\%$.

Figure 10. The glass transition of the resin is, however, much below that of NARMCO 5208 material and is around +85°C. The exact reason for the lower transition of this resin has not been disclosed to us but it could be due to a lower concentration of co-catalyst and/or less severe curing conditions. Whatever the reason, the resin is less fully cured and therefore has a lower transition as discussed earlier. The composite shows basically the same trend as the NARMCO system in that it does not display any change in property with time when measured in the direction of the fiber (i.e. parallel). The stress relaxation behavior of the sample in the perpendicular direction is again time dependent indicating that aging properties of the resin are displayed in this testing direction.

The results of determining physical aging using the flexural test are given in Figure 17. The samples were bent using a three-point

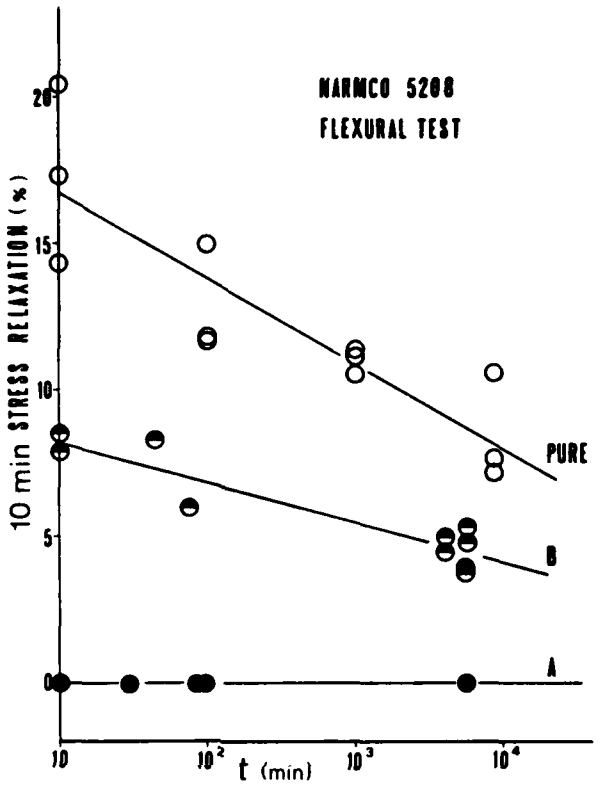

Figure 17. A comparison of the physical aging of bulk NARMCO 5208 resin to that of its graphite fiber composite. The tests were done in the flexural mode in directions against the fiber (A) and along the fiber (B) (See Figure 11 for further description of notation).

set-up and the initial stress and the stress after a lapse of 10 minutes were recorded. The testing was again done in two directions, "Across" and "Between", which correspond respectively to parallel and perpendicular tensile tests (see Figure 11B). The results from this test not only support the earlier tensile results, but in respect to practicality, the ease of measurement as well as the accuracy of the results supersede the earlier tensile tests. The bulk NARMCO 5208 (pure) shows almost identical aging behavior to that of the tensile tests (compare Figures 15 and 17). In the

flexural test in which the composite is bent against the fibers (direction A), which corresponds to the tensile test in the parallel direction, the sample displays zero relaxation which does not change with time. This is expected because in this direction the properties are controlled by the strong time independent graphite fibers which dominate the properties under these conditions. This result indicates that the small relaxations obtained in the tensile mode for samples in the parallel direction at all the aging times were probably due to the slippage of samples from the grips of the clamps. In the opposite direction (i.e. direction B), which corresponds to the perpendicular direction of the tensile test, the sample clearly shows physical aging. This is again due to the fact that in the testing direction the resin (matrix) plays an important role and thus its aging behavior becomes apparent. The results of the tests in this direction are identical to that obtained via the tensile test (compare B in Figure 18 to that perpendicular in Figure 15) and again the absolute value of relaxation at any given time is approximately one-half of that of pure resin. As mentioned earlier, this lower percentage stress relaxation of the composite is principally due to the fact that this composite contains about half as much resin ($\phi_{resin} = .47$). However, the fact that the rate of aging (slope of the line B or slope of perpendicular test direction in Figures 18 or 15, respectively) is different could be related to the difference in the morphology of the resin in the composites. Such a difference could be due to the nature of the gelation front in the pure resin as compared to that in a composite matrix as recently duscussed (18).

SUMMARY

Physical aging of the resin in graphite epoxy based composites affects the material properties of the matrix. This physical aging behavior, which is dependent on the variation of the free volume of the polymer resin with time, can be most noticeable when the testing is done in an appropriate direction. If the directional effect is not noted, a test might indicate no change in a property with time, whereas in actuality the resin has undergone aging and other important properties of the composite such as its toughness or impact resistance may also be affected in an undesirable manner. Stress relaxation in both the tensile and flexural modes provides a means of easily monitorin physical aging provided an appropriate testing direction has been chosen.

REFERENCES

1. S. E. B. Petrie, in Polymeric Materials: Relationship Between Structure and Mechanical Behavior, E. Baer and S. V. Radcliffe, eds. American Soc. for Metals, Metals Park, OH, Chap. 2 (1975).

2. S. Hozumi, Polymer J. 2, 756 (1971).

3. L. C. E. Struik, Physical Aging in Amorphous Polymers and Other Materials, Elsevier, Amsterdam, The Netherlands (1978).

4. A. J. Kovacs, Fortschr. Hochpolym. Forsch., 3, 394 (1963).

5. R. M. Mininni, R. S. Moore, J. R. Flick and S. E. B. Petrie, J. Macromol. Sci., Phys., B8, 343 (1973).

6. A. H. Chan and D. R. Paul, Polym. Eng. Sci., 20, 87 (1980).

7. M. Tant and G. L. Wilkes, Polym. Prep., 20(2), 535 (1979).

8. M. Tant and G. L. Wilkes, Polym. Eng. Sci., in press.

9. M. Tant and G. L. Wilkes, J. Appl. Polym. Sci., in press.

10. E. S. W. Kong, G. L. Wilkes, J. E. McGrath, A. K. Banthia, Y. Mohajer, and M. R. Tant, Polym. Eng. Sci.,in press.

11. Z. H. Ophir, J. A. Emerson and G. L. Wilkes, J. Appl. Phys., 49, 5032 (1978).

12. I. M. Ward, Mechanical Properties of Solid Polymers, Wiley-Interscience, London, Chap. 7 (1971).

13. L. C. E. Struik, Polym. Eng. Sci., 18, 799 (1978).

14. L. J. Broutman and S. M. Krishnakumer, Polymer Eng. Sci., 16, 74 (1976).

15. L. E. Nielsen, Mechanical Properties of Polymers and Composites, Vol. 1, Marcel Dekker, Inc., NY (1974).

16. J. K. Gillham, Org. Coat. Plast. Chem., Prep.,44, 185 (1981).

17. E. S. W. Kong, manuscript submitted,J. Appl. Phys.

18. Hirschbuehler, K. R., Abst. Critical Review, Characterization of Comp., MIT, June 1981.

FRACTO-EMISSION FROM COMPOSITES

J. T. Dickinson
Department of Physics
Washington State University
Pullman, WA 99164

ABSTRACT

The emission of electrons and positive ions from materials undergoing fracture is reported. We present a survey of charged particle emission from a number of materials including crystalline insulators, glass, graphite, polymers, and composites. Particular attention is given to fiber-reinforced epoxy systems which yield unique forms of charge emission. Energy distributions of the emitted particles are given for E-glass/epoxy strands, polybutadiene filled with glass beads, and mica. Surface charging accompanying fracture of these samples has also been measured. Evidence is presented that interfacial failure and charge separation play important roles in the observed emission.

FRACTO-EMISSION is the emission of Particles accompanying fracture. The Particles we have observed include:

Electrons (EE)

$\pm$ Ions (PIE and NIE)

Neutral Species

Photons (Triboluminescence)

PHENOMENA CONTRIBUTING TO EMISSION

1. HIGH TEMPERATURES AT CRACK-TIP
2. ON INSULATORS, SEPARATION OF CHARGES (Electric Field Assisted Processes)
3. DEFECT PRODUCTION (During Fracture)--ANNIHILATION (Releases Energy Locally)
4. ELECTRONIC EXCITATIONS (e.g., hole production, filling or emptying traps, excited atoms or molecules)

   DECAY: Radiatively, Auger de-excitations; PIE may involve ELECTRON STIMULATED DESORPTION MECHANISM.
5. FREE PARTICLES-REACTIVE WITH FRESHLY CREATED CRACK WALL (e.g., neutrals, free radicals produced by Bond Scission. Chemi-Emission)
6. DIFFUSION OF DEFECTS AND REACTIVE SPECIES MAY BE ONE RATE LIMITING STEP

We divide relaxation effects occuring at new fracture surface into three time frames:

FAST 1 us

1 us SLOW .1 s

VERY SLOW .1 s

TABLE I

A wide variety of materials have been fractured to test for electron emission. These include ionic crystals, ceramics, glass, filaments, plastics, elastomers, and composites. Not all decay times have been measured carefully and we simply note that they are less than an upper limit. The Intensities given are calculated on the basis of the samples original cross-sectional area.

All samples fractured were found to emit electrons.

MATERIALS	APPROX. DECAY TIMES OF FRACTO-EMISSION	ELECTRONS DETECTED/ cm^2 OF CRACK WALL
Sapphire	<1 s, minutes	10^3
Alumina	<1 s, minutes	10^4
Al_2O_3 Anodized Layer	.1 - 20 μsec	10^5
BN	<1 s, minutes	10^6
Quartz	<1 s, minutes	10^6
Mica (Muscovite)	1 s, minutes	10^6
Crystalline Sugar	<1 s, minutes	10^6
Fused Silica	Several ms	10^3
Soda Lime Glass	Several ms	10^3
Kelvar 49 Fibers	<<.1 s	10^8
Graphite Fibers	10 μs	10^8
E Glass Fibers	10 μs	10^8
S Glass Fibers	10 μs	10^8
Epoxy (DER 332)	25 μs	10^3
Lucite	<2 ms	10^2
Polystyrene	500 μs, 12.3 μs	10^3
ELASTOMERS		
Neoprene	<1 s	10^2
Viton	<1 s	10^3
Buna N	<1 s	10^2
Natural Rubber	<1 s	10^3
Natural Rubber (abraded)	minutes	10^7
Silicone Rubber	<1 s, minutes	10^5
Solathane	<.2 s	10^4
Vinyl Rubber-filled	<1 s, minutes	10^4
Polybutadiene	0.04 s, minutes	10^3
Polybutadiene-filled	<1 s, minutes	10^7

TABLE II

These are the materials tested for positive ion emission (PIE). All samples tested were found to emit. In many cases we have only determined upper limits on decay times. As in the case of electron emission, the intensities quoted are calculated on the basis of original sample cross-sectional area.

Note for both EE and PIE, the emission from fibers (typically, 10 micron filaments) is both very short lived and very intense. Similarly, epoxy has a fast decay time.

POSITIVE IONS

MATERIAL	APPROX. DECAY TIMES OF FRACTO-EMISSION	IONS DETECTED cm^2 OF CRACK WALL
Mica (Muscovite)	1 s, minutes	10^6
FIBERS		
Kevlar 49	<0.1 s	10^8
Carbon	10 μs	10^8
E-glass	10 μs	10^7
S-glass	11 μs	10^8
PLASTICS		
Epoxy (DER 332)	25 μs	10^3
Lucite	<2 msec	10^2
Polystyrene	35 μs	10^4
ELASTOMERS		
Buna N	<1 s, minutes	10^3
Natural Rubber	<1 s	10^4
Natural Rubber (abraded)	minutes	10^7
Silicone Rubber	<1 s, minutes	10^3
Solathane	<.1 s	10^6
Vinyl Rubber-filled	<1 s, minutes	10^5
Polybutadiene	<.04 s, minutes	10^5
Polybutadiene-filled	<.2 s, minutes	10^6

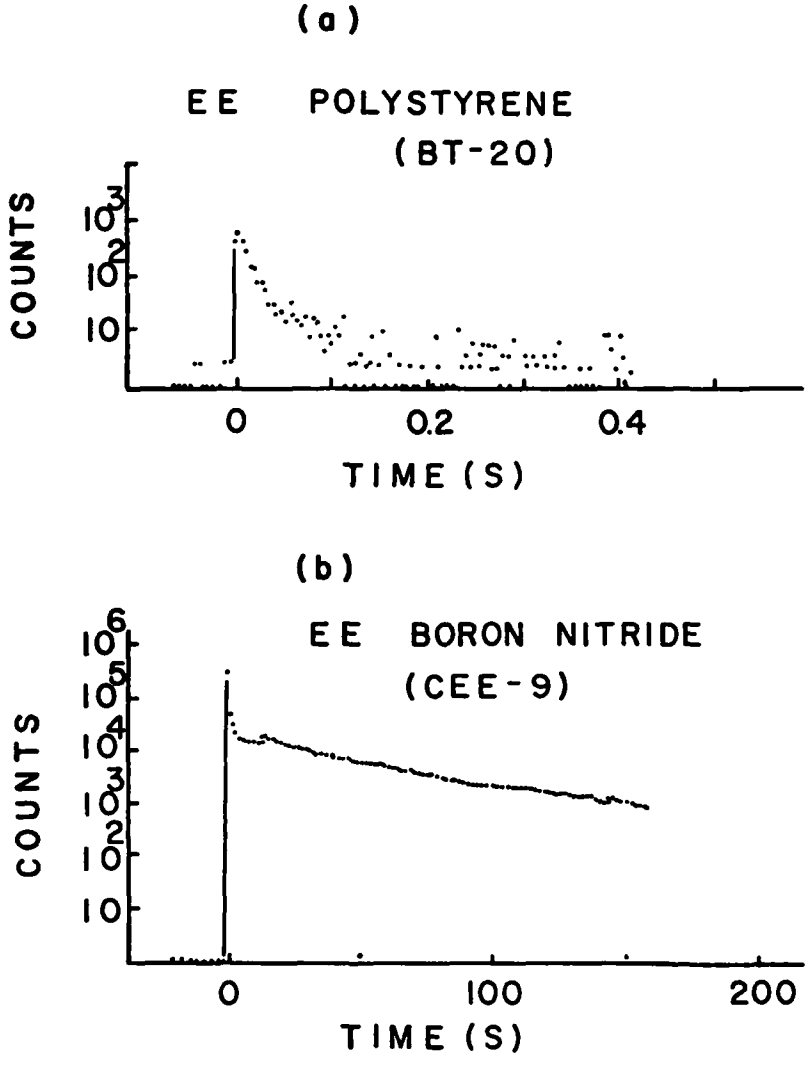

FIGURE 1

THE TIME DISTRIBUTIONS OF ELECTRON EMISSION DUE TO THE FRACTURE OF

a) POLYSTYRENE. b) BORON NITRIDE.

The emission intensity vs time curves for all the materials studied have a common characteristic: highest intensity at or very near fracture, followed by a decay of emission. For polystyrene this decay occurs with time constants on the order of microseconds. Boron Nitride on the other hand shows very intense and long-lasting emission. This decay curve is very similar to those obtained from filament-epoxy strands.

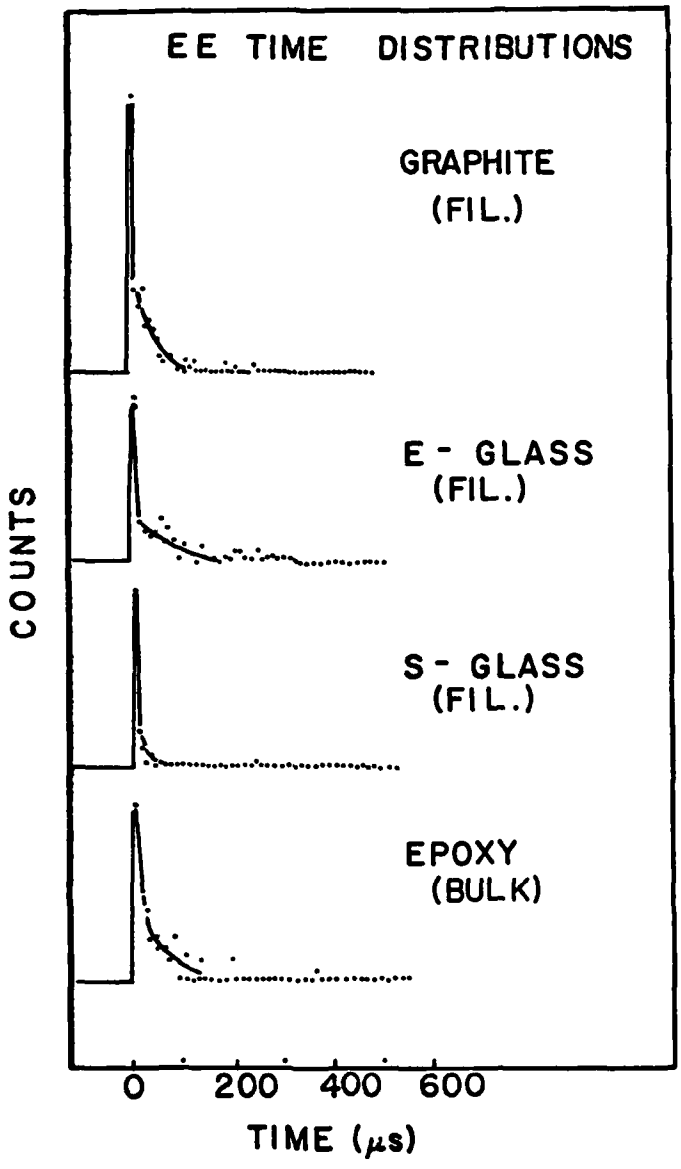

FIGURE 2

EE TIME DISTRIBUTIONS FROM FRACTURE OF GRAPHITE AND GLASS FILAMENTS (10 microns dia.) AND BULK EPOXY (Dow DER 332).

On a linear scale, we see the time distributions from fracture of individual filaments and pure epoxy. The decay constants for the filaments are about 10 us, and 25 us for pure epoxy. The emission appears to occur with a single exponential decay.

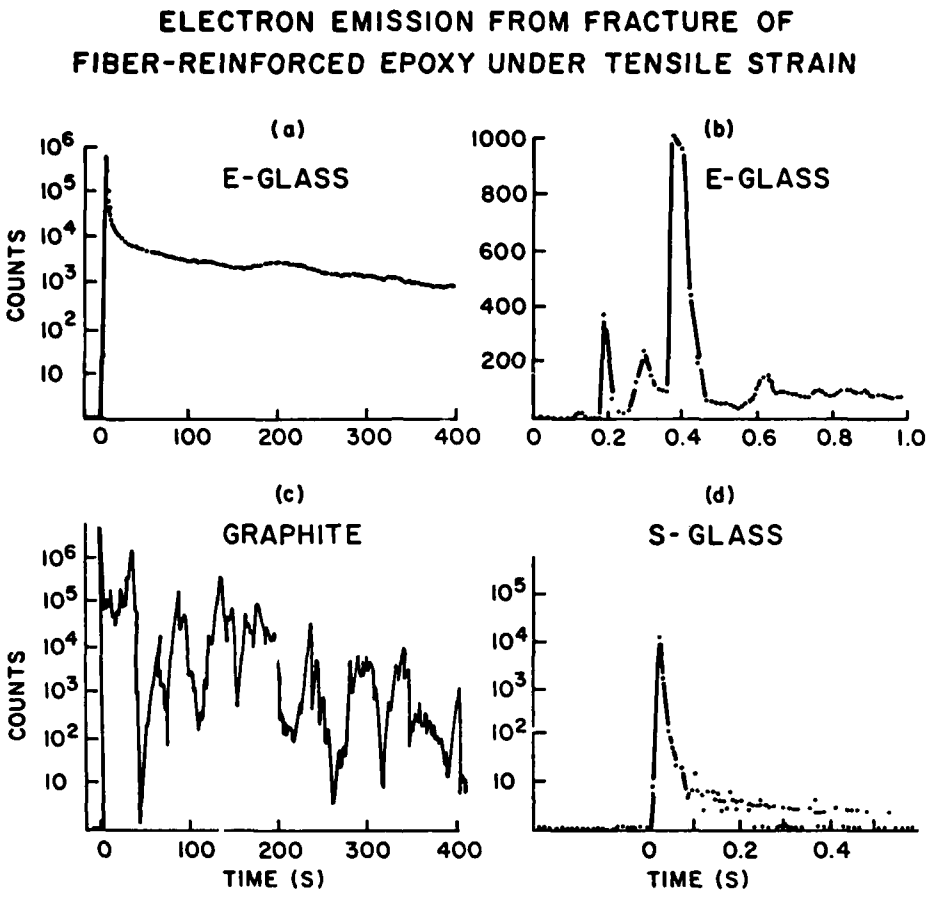

Figure 3

ELECTRON EMISSION FROM FRACTURE OF FIBER-REINFORCED EPOXY UNDER TENSILE STRAIN

We see that the emission curves for the composites differ significantly from the fracture of fiber-reinforced epoxy strands made from the same filaments and epoxy (Fig. 2). Note the very long lasting emission which decays from a rapidly rising peak occuring near the instant of rupture. If we assign time constants to portions of the decay curves, they vary from ms to several minutes. If we examine the initial portion of the curve on a faster time scale (Fig. 3b), we see events prior to rupture, sometimes with decay constants associated with fracture of the pure materials. Different fiber-epoxy systems appear to have different FE curves. The emission from E-glass is more intense and longer lasting than that for S-glass. Microscopy shows that there is considerably more delamination and separation of the filaments in the case of E-glass and graphite than for S-glass, S-glass showing very few clean filaments. The larger diameter E-glass filaments (20 microns) could contribute to the degree of interfacial failure.

Our interpretation: Prior to rupture, the sample under tension suffers minor failures, consisting primarily of fiber breakage and epoxy failure, producing FE similar to that of the pure materials. When the entire strand fails, a large amount of delamination or interfacial failure occurs. It is this latter form of failure that is responsible for the major FE-slow decay component. It is possibly an indicator of the extent of the interfacial failure that has occured.

The erratic behavior of the graphite-epoxy EE is due to surface charging and discharging that tends to push electrons away from the detector. This does not happen in the case of PIE due to a much higher collection voltage.

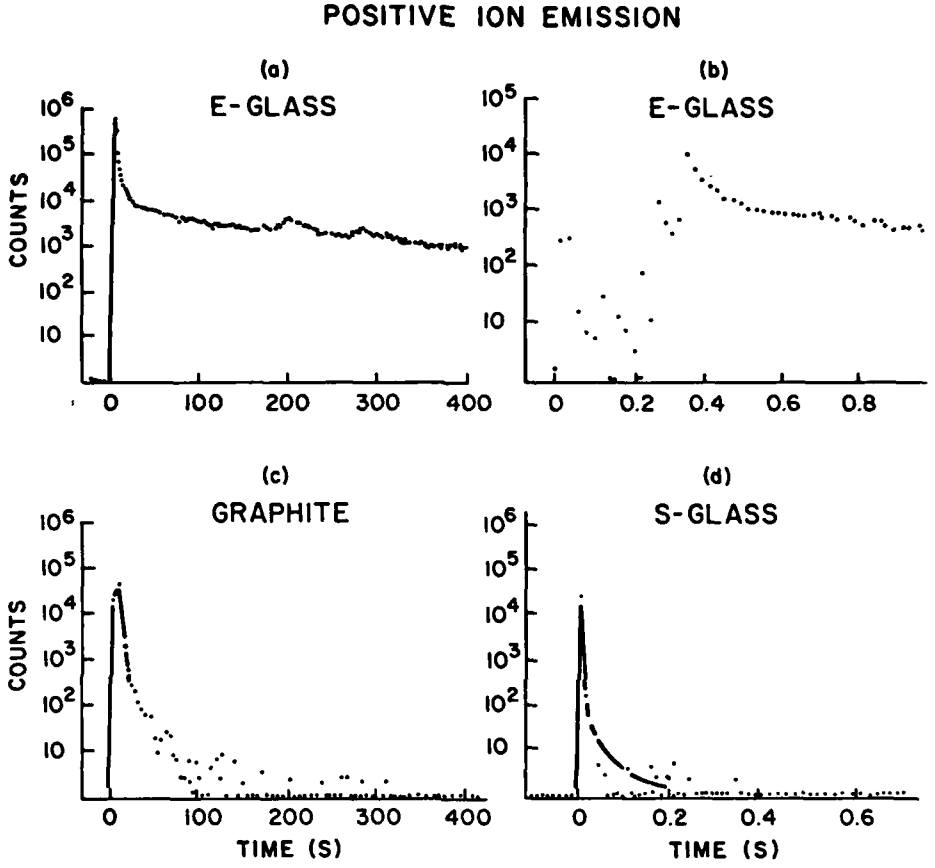

FIGURE 4

POSITIVE ION EMISSION FROM FRACTURE OF FIBER-REINFORCED EPOXY

These are the corresponding PIE curves. With the exception of graphite, they are quite similar to the EE curves.

It should be noted that both EE and PIE curves for E-glass epoxy strands were measured in an ultra-high vacuum system two orders of magnitude lower pressure than most of the reported work. We wished to see if the long lasting emission was due to chemi-emission from reaction of the fracture surfaces with background gases. No influence on either EE or PIE was observed.

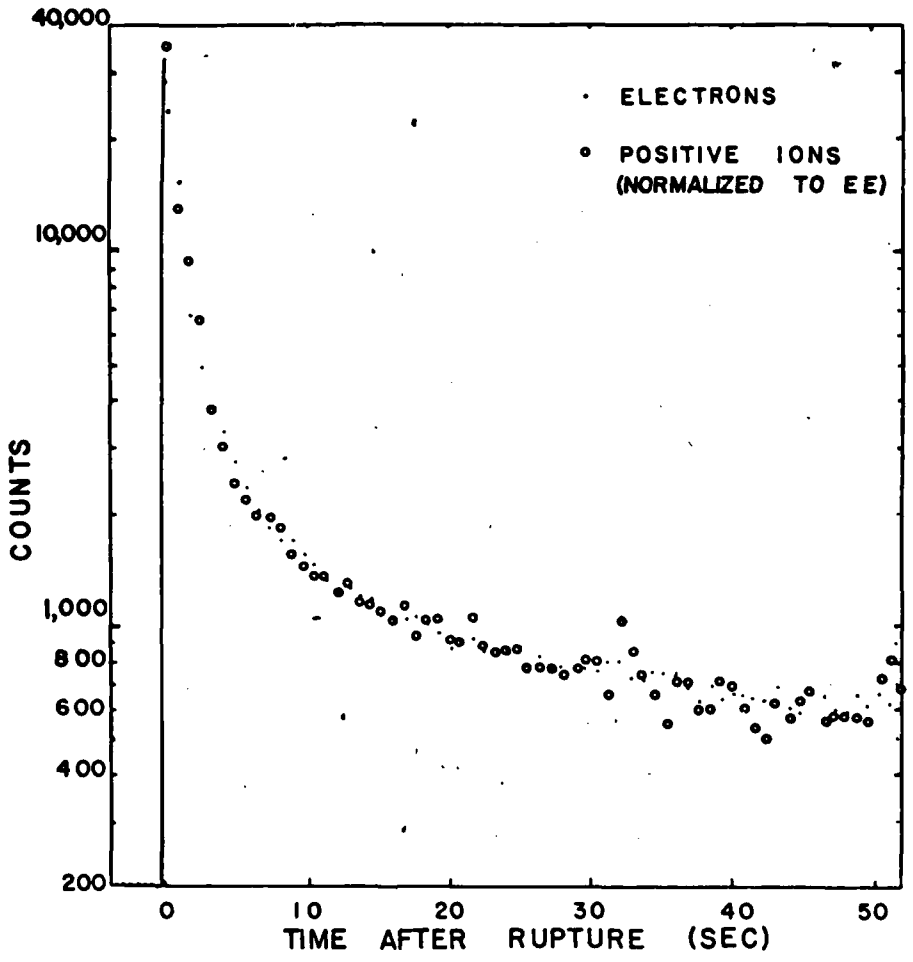

FIGURE 5

COMPARISON OF EE AND PIE FROM E-Glass/EPOXY STRANDS

Here are plotted the emission from two different samples normalized at a single point. The total emission, on the average, is nearly the same. Within the fluctuations of the observed particle counts, the two curves are indistinguishable. This suggests that a common rate-limiting step is involved.

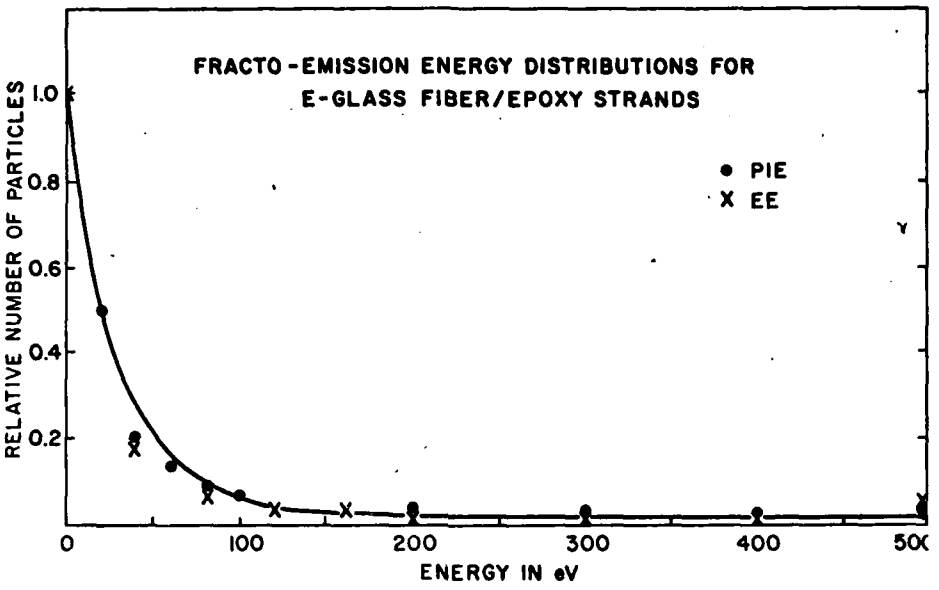

FIGURE 6

EE and PIE Energy Distributions FOR E-GLASS FIBER/EPOXY STRANDS

By using fine mesh grids in the region between the sample and the detector one can perform a retarding potential energy analysis of the EE and PIE accompanying fracture of materials. The derivative of the count rate vs retarding grid potential is the energy distribution of the emitted particles. Both EE and PIE appear to have similar energy distributions peaking near 0 eV with a significant quantity of higher energy particles tailing off in the range of a few hundred eV. Approximately 15% of the particles could not be stopped by potentials in the 500-1000 eV range. This suggests that charging of the fracture surface is playing an important role in the ejection of these particles from the surface. The similarity of the EE and PIE energy distributions provides further support that they share a crucial mechanistic step.

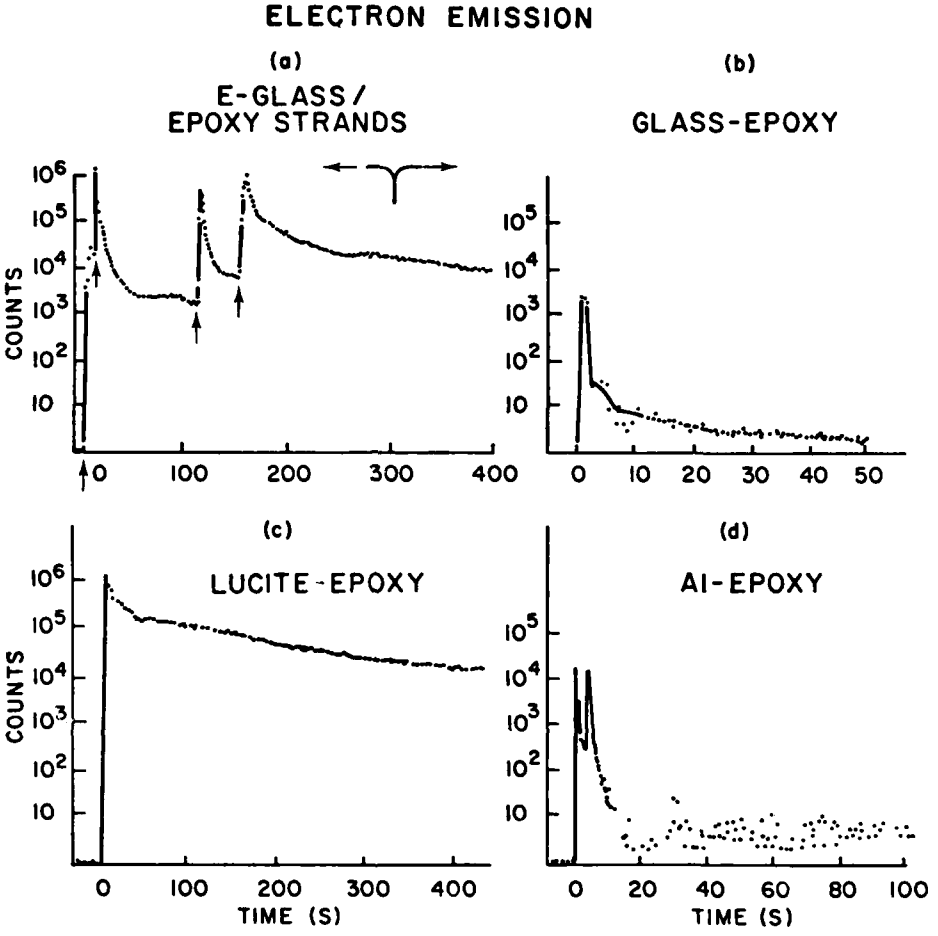

FIGURE 7

ELECTRON EMISSION FROM SYSTEMS INVOLVING INTERFACIAL FAILURE

Systems were chosen that involve failure of an adhesive-like bond.

a) Splitting E-glass/epoxy strands length-wise, causing extensive delamination with only minor fiber and epoxy fracture. This produced the same long time-constant emission seen in rupture of the fiber strands each time the splitting occured (vertical arrows).

b), c), and d) show the EE from failure of the bulk epoxy interface with glass, lucite, and aluminum. Again, long lasting emission was observed.

POLYBUTADIENE

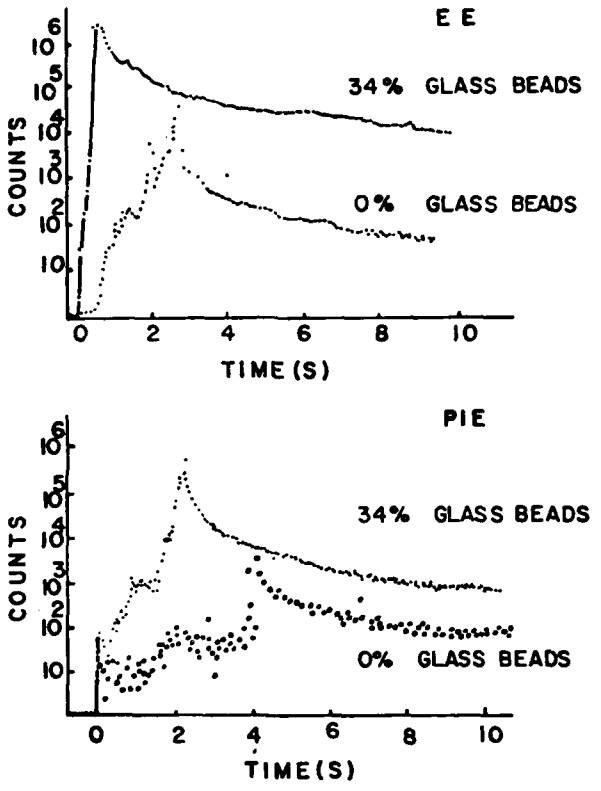

Figure 8

EE and PIE from FRACTURE OF POLYBUTADIENE WITH AND WITHOUT GLASS BEADS

When a filled elastomer fractures, interfacial failure can also occur. In the case of polybutadiene filled with untreated 30-95 micron glass beads, we see considerably stronger emission from such samples. The beads become detached during straining of the material at the crack-tip, and probably causes the enhanced emission. The energy distribution for the FE from filled polybutadiene is very similar to that obtained for E-glass/epoxy.

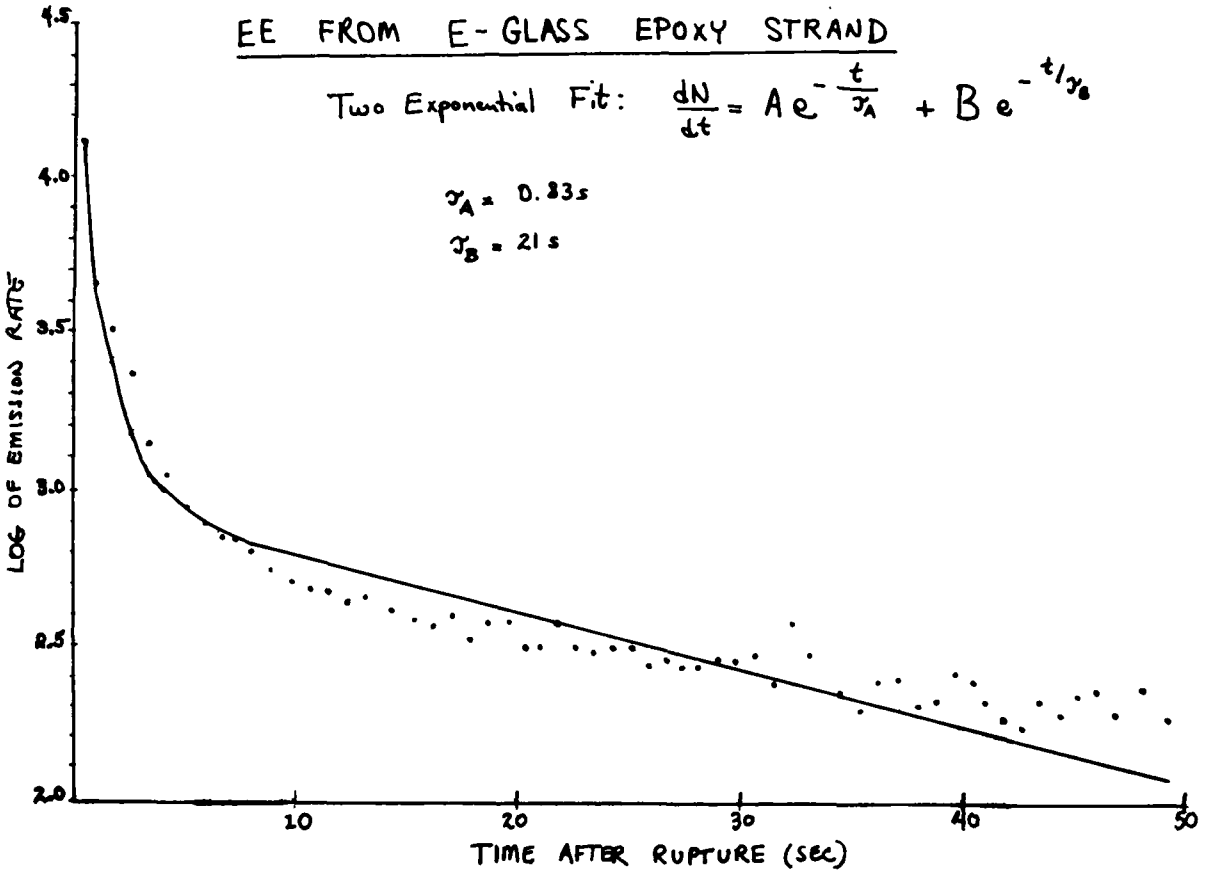

FIGURE 9

COMPUTER FIT OF THE EE FROM E-GLASS/EPOXY STRAND USING THE SUM OF TWO EXPONENTIALS

The solid line is a non-linear least squares fit of the first 50s of the EE emitted from a ruptured strand of E-Glass/Epoxy. The best fit was obtained with the time constants shown (.83s and 21s). Two expontials suggest two independent, first order mechanisms, constant T.

Although the fit looks fairly good, we call attention to the improved fit in Figure 10.

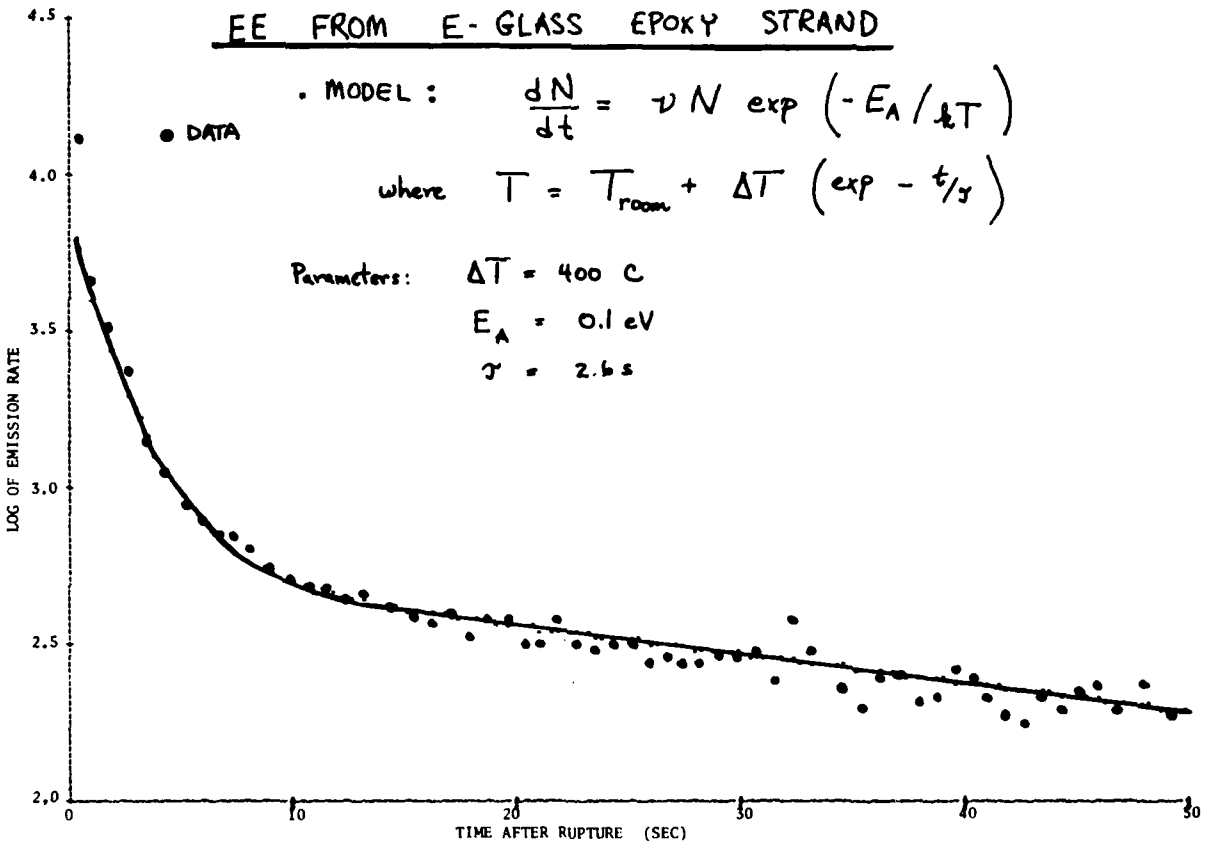

FIGURE 10

COMPUTER FIT OF EE FROM E-GLASS/EPOXY STRAND USING A FIRST ORDER RATE EQUATION AND EXPONENTIALLY DECAYING TEMPERATURE

An improved fit of the data is obtained by assuming that the emission is due to a first order process (i.e., the emission probability is proportional to the number of sites causing the emission) and that fracture causes a sudden rise in temperature which decays back to room temperature with time constant .

The fit is quite sensitive to T, suggesting that such an analysis could provide a good measure of the peak temperature produced by fracture.

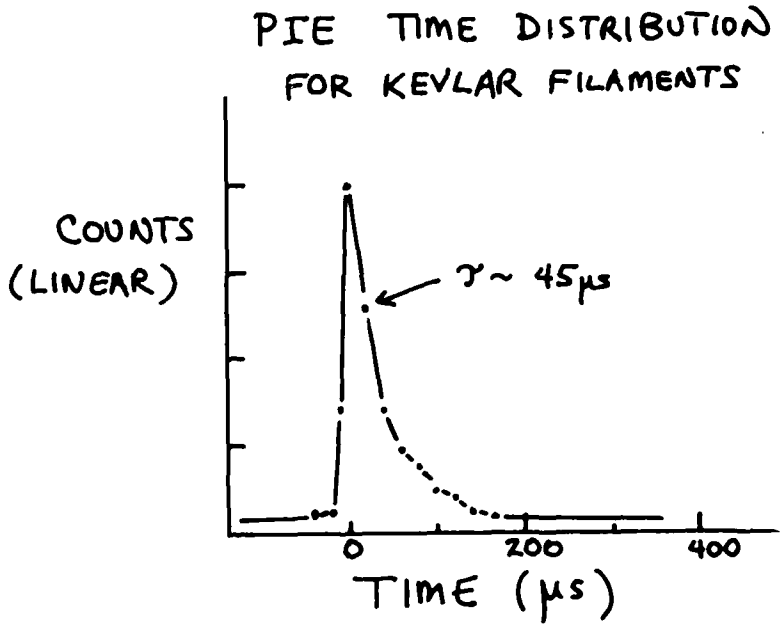

FIGURE 11

PIE TIME DISTRIBUTION for FRACTURE OF 10 micron KEVLAR FILAMENTS

Fracture of Kevlar filaments produces emission that decays with a time constant of 45 us, similar to a number of polymers and certainly longer than the inorganic filaments tested. EE time distributions are quite similar.

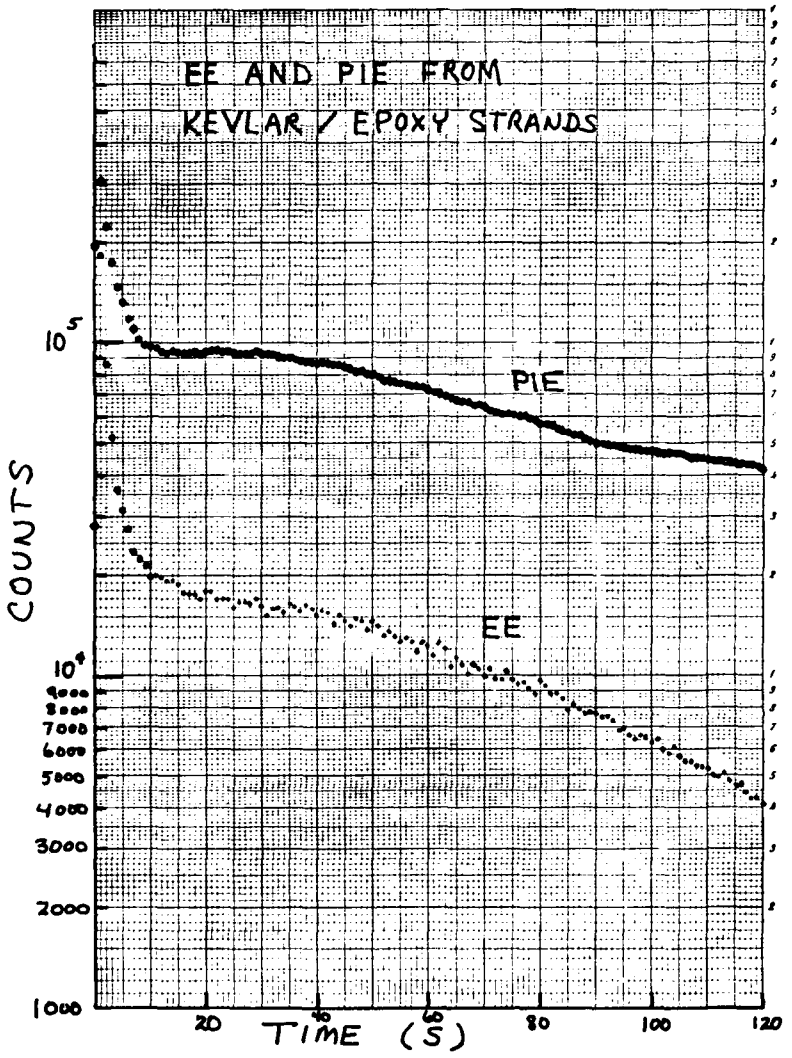

FIGURE 12

EE AND PIE FROM KEVLAR/EPOXY STRANDS ON A LOG PLOT

These strands were made of Kevlar filaments and DER 332, similar to the other strands. As one can see, the emission is very long lasting, has the characteristic initial decay from the peak, but has a departure in slope from simple exponential decay. This has been seen on other systems involving adhesive failure (unpublished) and following the cleavage of mica. This "rise" in emission is as yet unexplained.

SPECULATION

WHAT CAN FRACTO-EMISSION TELL US ABOUT FRACTURE?

1. Often observe FE before rupture. Appears to be sensitive to surface micro-cracking, perhaps sub-critical crack growth.

2. The Emission is most intense during crack growth--may be related to rate of surface formation (e.g., crack velocity).

3. The total intensity and/or peak height may be sensitive to parameters of macro- and micro-scopic fracture mechanics--e.g., Surface Energy, Fracture Toughness, Kinetic Energy.

4. May serve as a monitor of stress-corrosion phenomena.

5. In multi-phase systems, it may be sensitive to <u>where</u> fracture occurred.

6. May be sensitive to mode of fracture.

7. May be able to obtain crack-tip temperatures.

MOLECULAR CHARACTERIZATION OF COMPOSITE INTERFACES

H. Ishida

Case Western Reserve University

ABSTRACT

We have applied Fourier Transform Infrared Spectroscopy in order to elucidate the molecular structures of the glass/matrix interface. Great sensitivity and selectivity of the technique employed allowed us to separately study the various interfaces and interphases.

It was found that the structure of the silane in a treating solution is important in determining the structure of the silane on glass fibers, thus eventually influencing the macroscopic properties of composites. We have studied the amount of silane on glass fibers, the state of hydrogen bonding, orientation, copolymerization of the organicfunctionality with the matrix, curing of the silane, and effect of water on the interface.

Our molecular approach is useful to interpret and predict physicomechanical properties of composites.

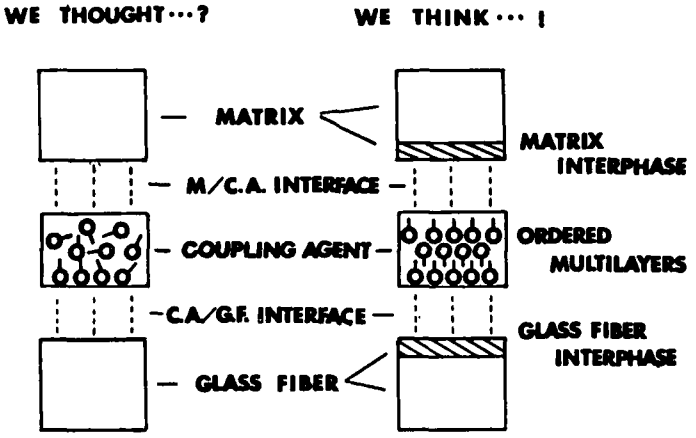

Fig. 1: A traditional view of the glass/matrix interface against our recent view of the more complex interfacial structure: There is no clearly defined thickness for the interphase. It is rather determined by the combination of materials used and the manufacturing conditions of the composite.

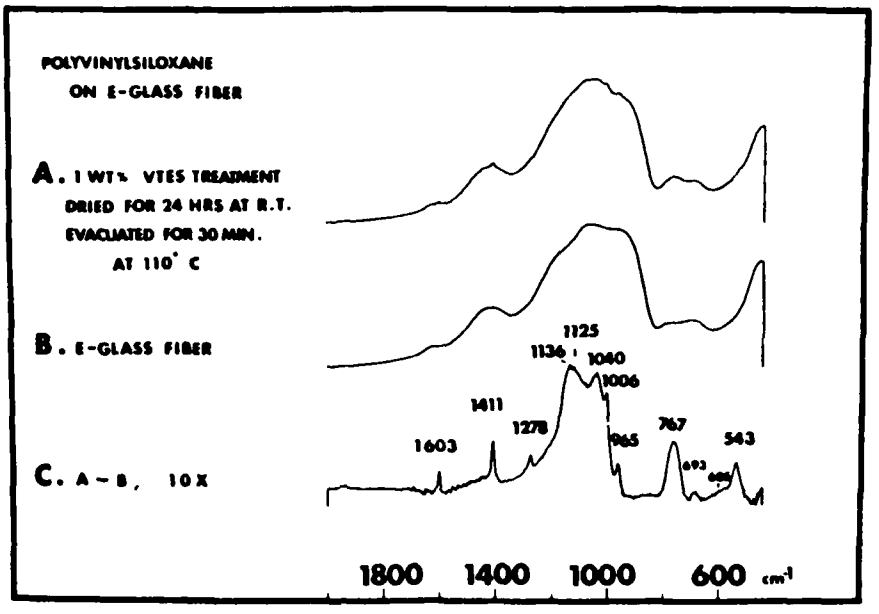

Fig. 2: Fourier transform infrared spectra of E-glass fibers (spectrum B) and the E-glass fibers treated with 1% by weight vinyltrimethoxysilane in water; Spectrum C is an example of the digital subtraction (A - B) of the above spectra showing the spectrum of polyvinylsilsesquioxane on the fiber surface. Note that the spectral contributions of the glass fibers were subtracted and the resultant difference spectrum was scale expanded by ten times.

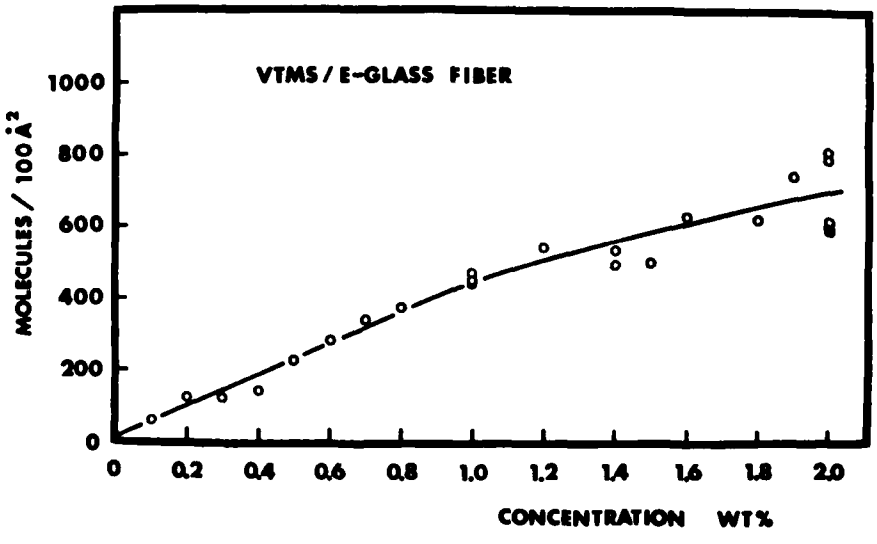

Fig. 3: An infrared evidence of the formation of multilayers of a vinyl-functional silane: The amount of silane up-take on E-glass fibers is a function of the concentration of treating solutions. The multilayer formation is due to the topological factor of the smooth fiber surface. Powders with rough surfaces do not adsorb large quantities of silane molecules as shown in this figure. There is a break point in the curve at around 1% by weight. This point is due to the isolated monomer/associated monomer transition which originates in the treating solution.

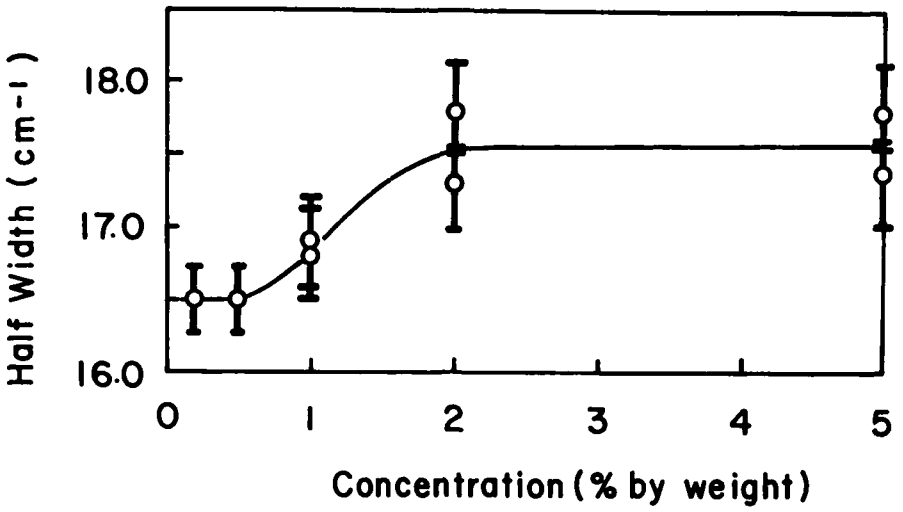

Fig. 4: The half-width at half height of the Raman line, which is due to the symmetric stretching mode of the vinylsilanetriol in water, is plotted as a function of the concentration. At around 1% by weight (which coincides with the break point mentioned in Fig. 3), the half-width suddenly increases. Since the Raman line used for this measurement is characteristic only of the monomeric silane, the transition is likely due to the isolated monomer/associated monomer transition via a hydrogen bonding of the silanol groups.

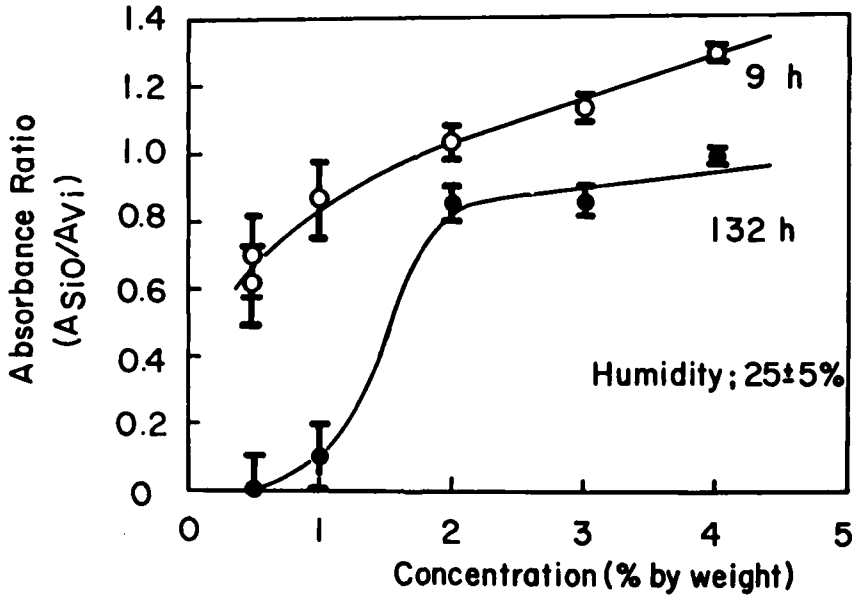

Fig. 5: The mass adjusted residual silanol of polyvinylsiloxanol on E-glass fibers which were treated with aqueous solutions with various concentrations and were dried at room temperature for 9 hrs. and 132 hrs., respectively. No further heat treatments were given in order to better maintain structural information. The glass fibers treated with silane solutions at concentrations below 1% by weight show almost complete siloxane cross-linking indicating molecular organization favorable for higher degree of silanol condensation. The surface catalytic effect does not play a major role at these thicknesses.

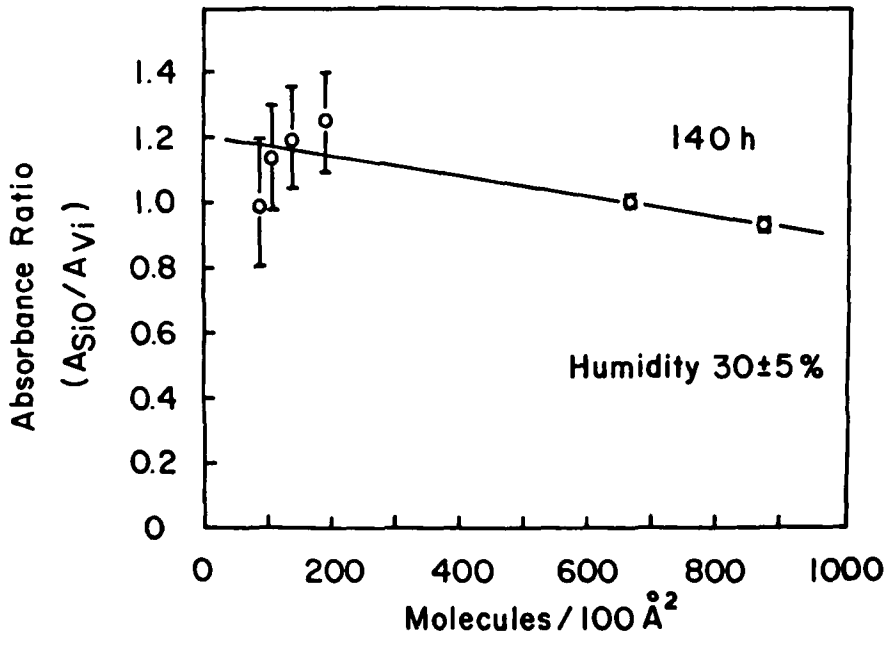

Fig. 6: The mass adjusted residual silanol of the silane on E-glass fibers treated with 4% by weight vinyltrimethoxysilane in water. It should be noted that the treating solution is the same for all the samples, but the thickness of the silane was varied by rinsing briefly with water immediately after the adsorption. Even thin layers below 100 molecules/Å^2, which correspond to the samples at less than 1% by weight in Fig. 5, do not show complete silanol condensation which indicates that the determining factor for the favorable condensation is not the thickness (or surface catalytic effects) but rather the structure of silane in the treating solution.

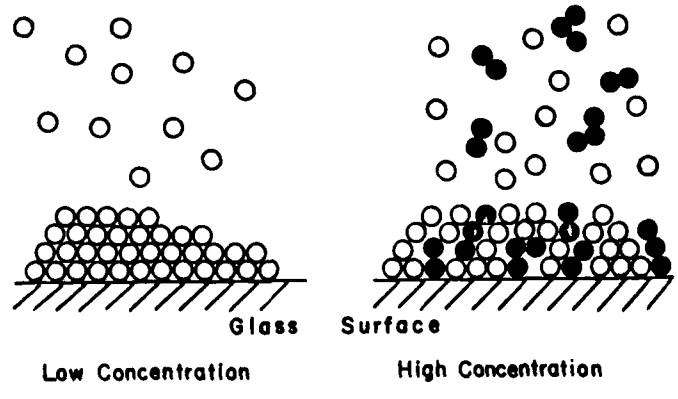

Fig. 7: A schematic diagram of the silane layers deposited on glass fiber surface from the treating solution at concentrations below and above the isolated monomer/associated monomer transition. The associated monomers introduce structural defects and disturb the molecular orientation thus reducing the amount of silane up-take and increasing the residual silanol.

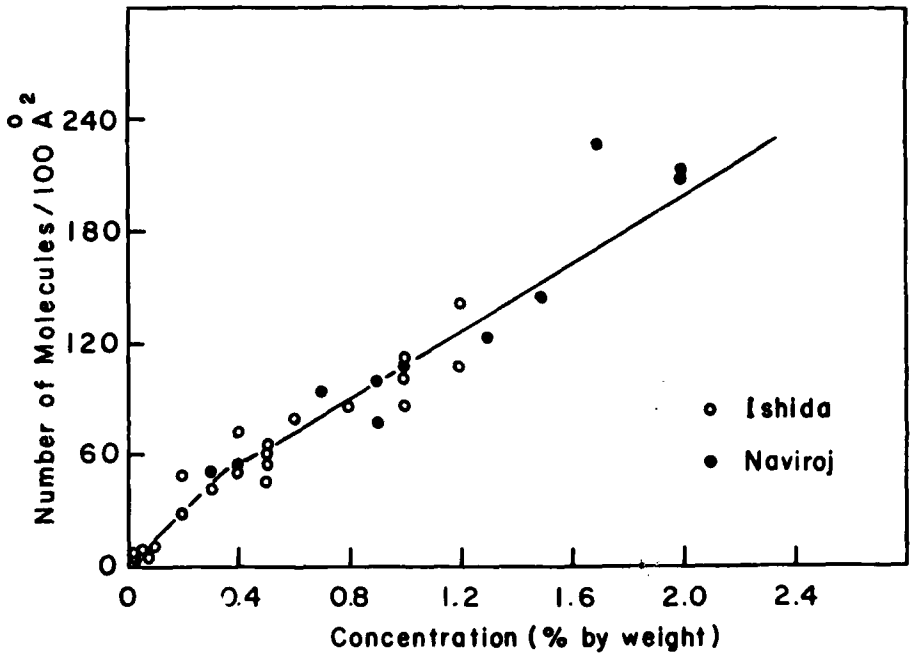

Fig. 8: The amount of silane up-take for γ-methacryloxypropyltrimethoxysilane (γ-MPS) as a function of concentration: Again a break point was observed at about 0.4% by weight above which slightly hazy solution resulted. Data points are a collection of the results by two independent researchers using the same method.

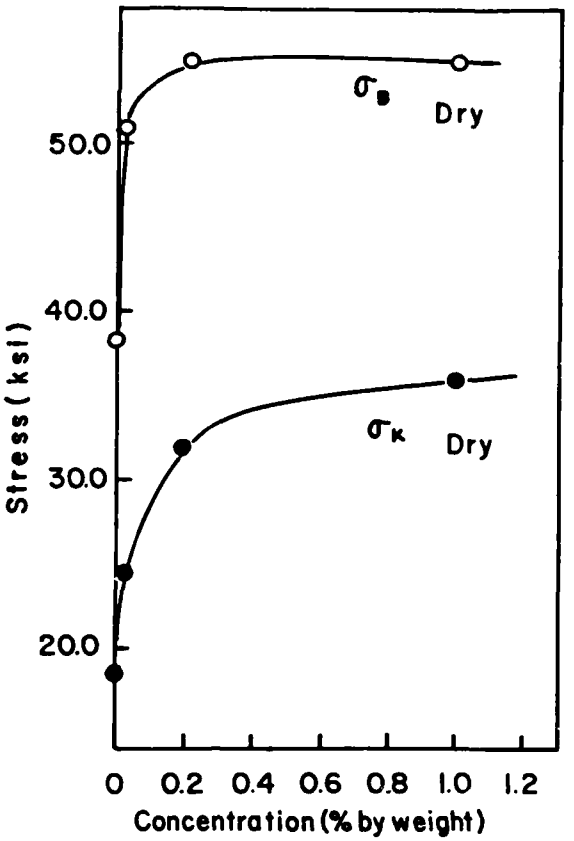

Fig. 9: The flexural strength of E-glass cloth reinforced polyester as a function of the concentration of silane treating solution: The monolayer quantity silane does not yield optimum strength. The strength steadily increases until the concentration mentioned in Fig. 8 (0.4% by weight for γ-MPS).

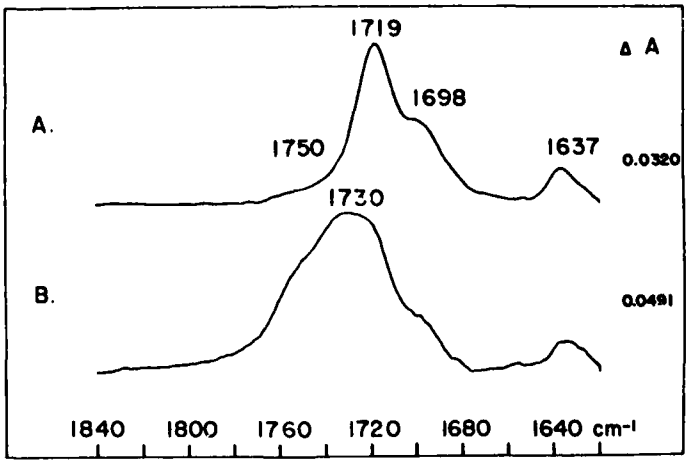

Fig. 10: The FT-IR spectra of γ-MPS 90 hrs. after the treatment on E-glass fibers: THF was used to rinse the glass fibers and the THF solution was placed on a KBr plate in order to cast a film of the physisorbed γ-MPS (spectrum A). After the THF wash, the glass fibers were made into a KBr pellet in order to examine the chemisorbed γ-MPS. Only the chemisorbed γ-MPS shows the surface induced polymerization of the C=C group, which resulted as a frequency shift from 1719 cm^{-1} to 1730 cm^{-1} for the C=O band.

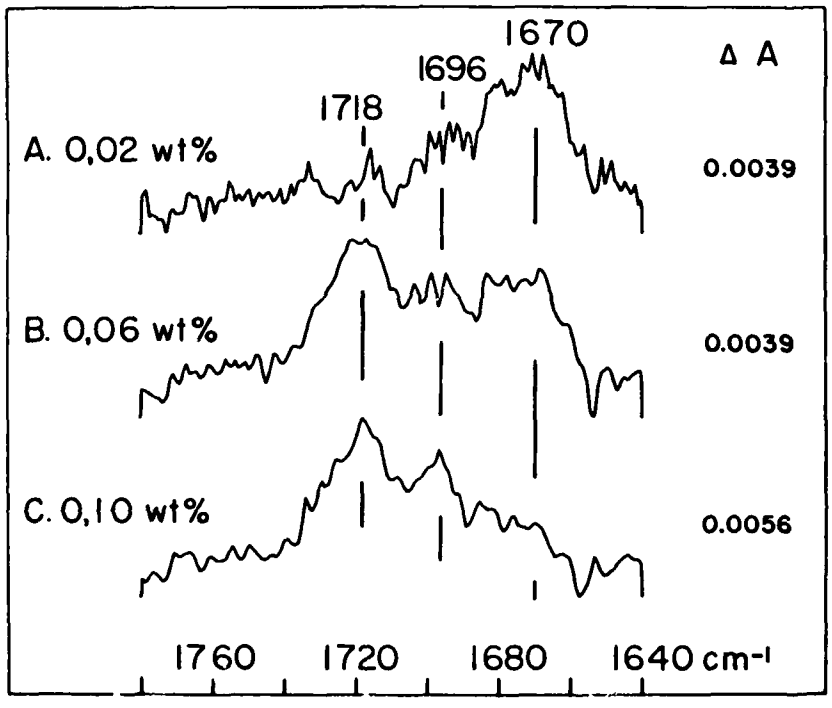

Fig. 11: The FT-IR difference spectra of γ-MPS on E-glass fibers at very low concentrations: The spectrum A was obtained at nearly a monolayer of γ-MPS. Three bands at 1718, 1696, and 1670 cm^{-1} are the free C=O, the hydrogen bonded C=O to silanols, and the strongly interacting C=O with the surface acid centers, respectively. The strongly interacting C=O with the surface is considered to be the cause of the surface induced polymerization.

AD-A116 733 ARMY MATERIALS AND MECHANICS RESEARCH CENTER WATERTOWN MA F/G 11/4
PROCEEDINGS OF THE CRITICAL REVIEW: TECHNIQUES FOR THE CHARACTE--ETC(U)
MAY 82
UNCLASSIFIED AMMRC-MS-82-3 NL

5 OF 6
AD A116733

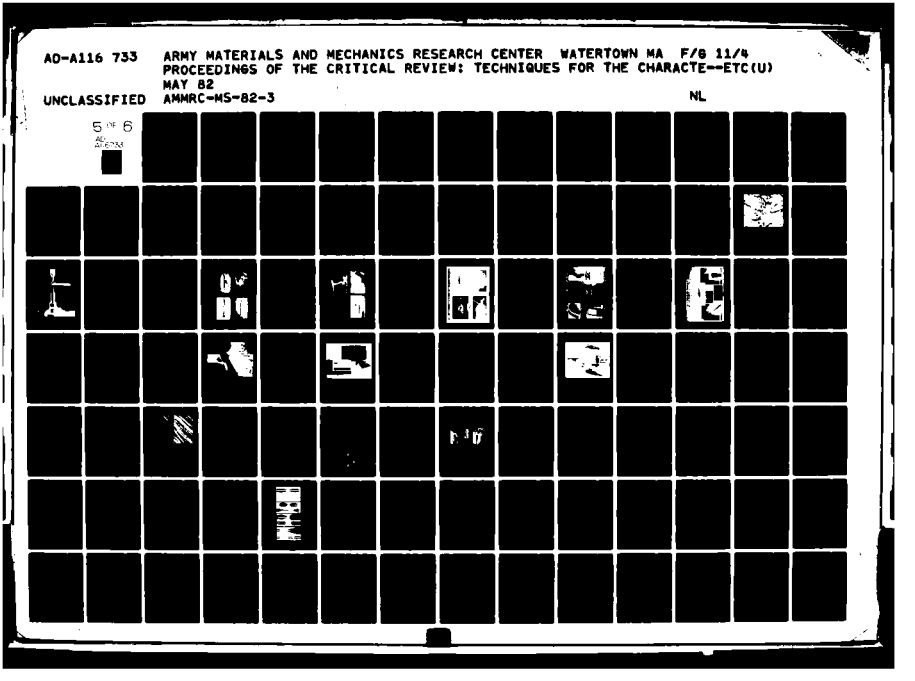

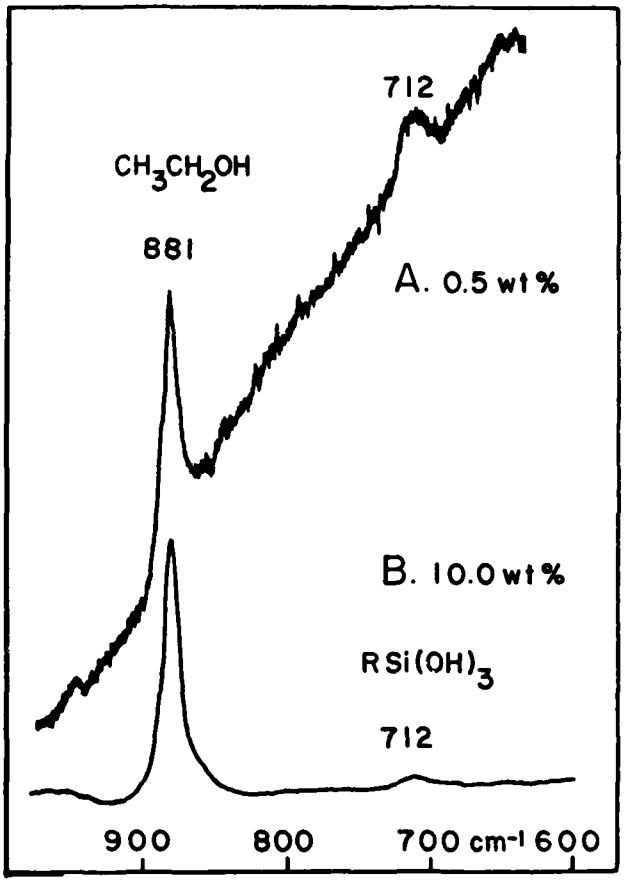

Fig. 12: The Raman spectra of γ-aminopropyltriethoxysilane in water at 0.5% by weight (spectrum A) and 10% by weight (spectrum B): The 712 cm^{-1} can be assigned to the silanetriol providing the evidence of the existence of monomers. The line at 881 cm^{-1} is due to the ethanol produced as a by-product of the hydrolysis of the ethoxy groups.

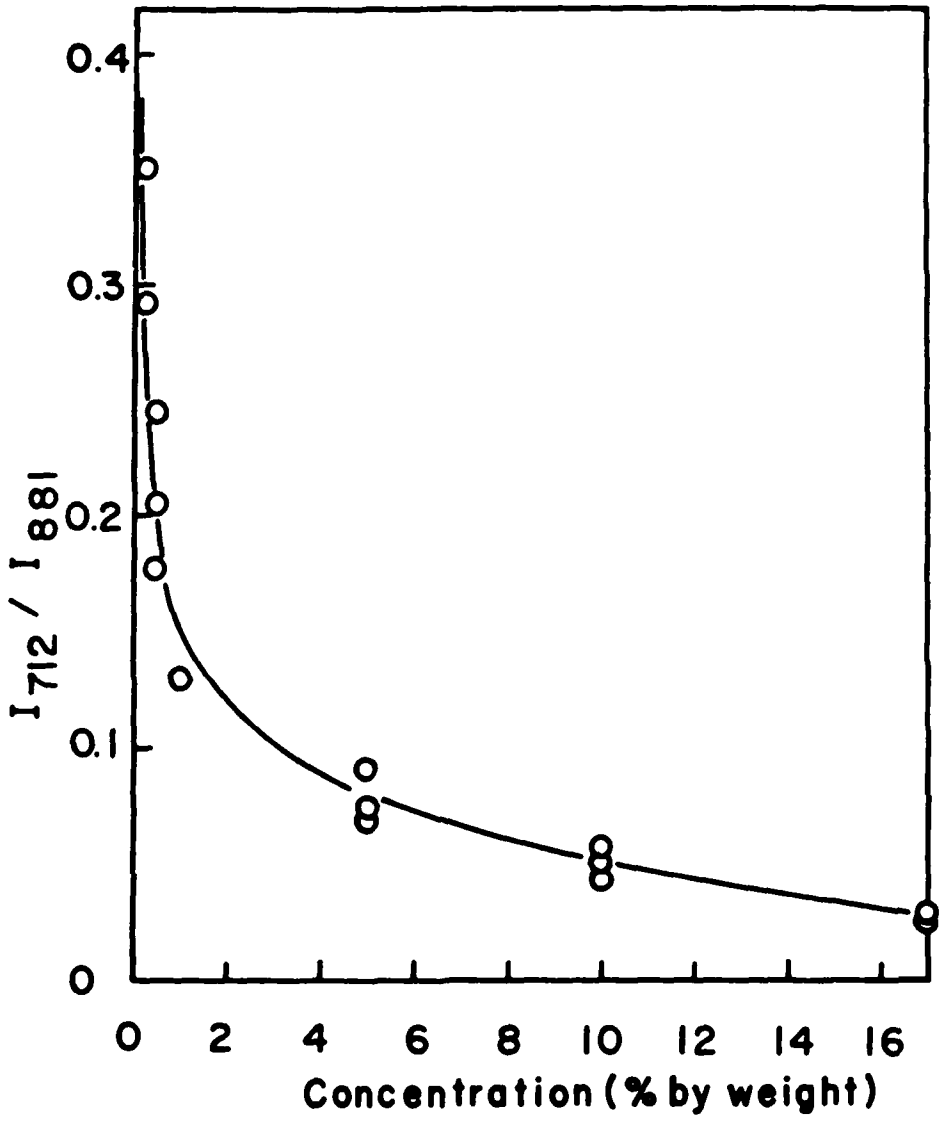

Fig. 13: The relative Raman intensities of the silanetriol peak against the ethanol peak as a function of the concentration of silane treating solutions: The silanetriol content increases dramatically at concentrations below 1% by weight. At around 0.15% by weight, the hydrolyzed silane molecules are predominantly the γ-aminopropylsilanetriol.

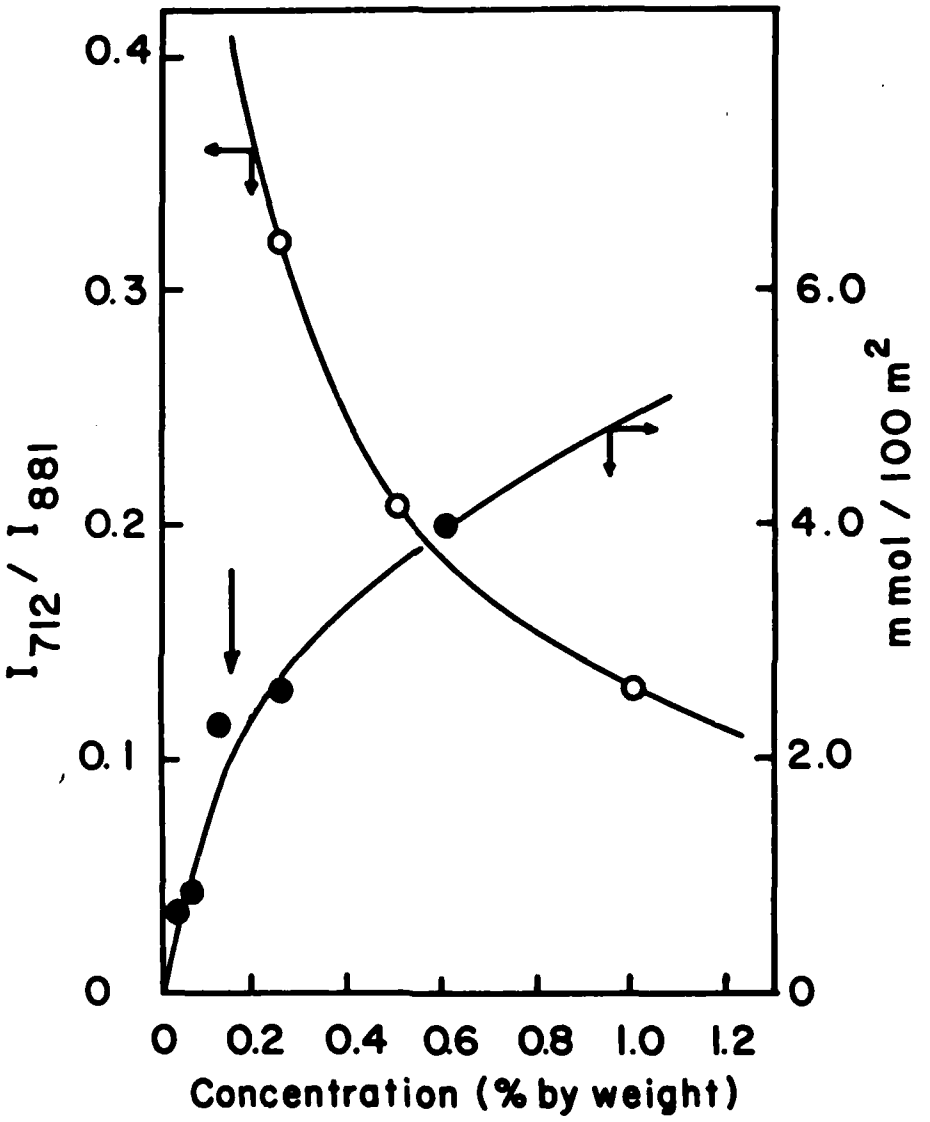

Fig. 14: The open circle represents the relative intensity of the silanetriol read from Fig. 13 and the closed circle shows the silane up-take using ^{14}C-labeled aminosilane reported by Johannson et al. Again a break point is seen on the amount of adsorbed silane at around 0.15% by weight which coincides with the isolated monomer/associated monomer transition. Note that the associated monomers become oligomeric very quickly because of the self-catalytic silanol condensation by the amine group. Hence, the transition is rather the isolated monomer/oligomer transition for this particular silane.

Effect of Moisture on Silanes

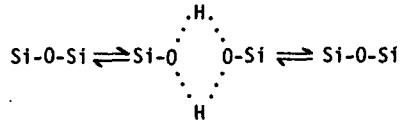

Fig. 15: Possible chemical reactions of silane coupling agents showing the hydrolysis and reformation of the siloxane group.

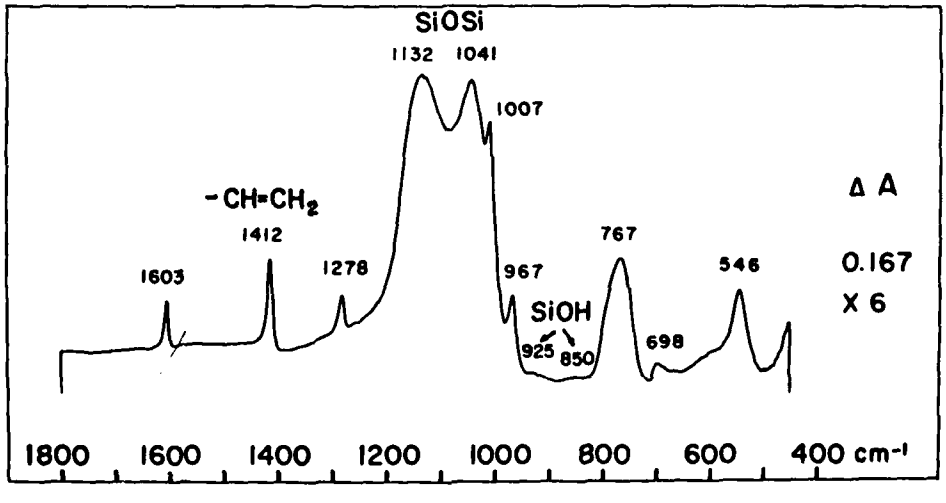

Fig. 16: The FT-IR difference spectra of polyvinylsilsesquioxane on E-glass fibers: The glass fiber/silane system was heat treated at 150°C for 2 hrs. under vacuum showing almost complete condensation of the silanol groups. (Note the lack of bands in the 950-800 cm^{-1} region where the silanol groups of the coupling agent gives rise to strong bands.)

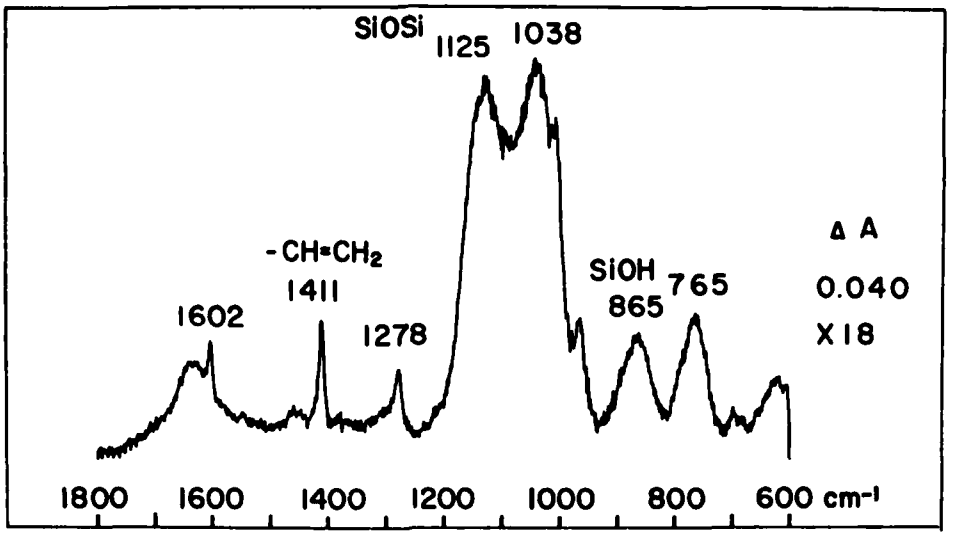

Fig. 17: The FT-IR difference spectra of the same sample as in Fig. 16 except that the silane-treated glass fibers have been immersed in water at 80°C for approximately 1500 hrs: A newly arisen band at 865 cm^{-1} is due to the silanol groups as a result of the hydrolysis of the siloxane groups providing the first direct observation of the effect of water on a coupling agent in the presence of glass fibers.

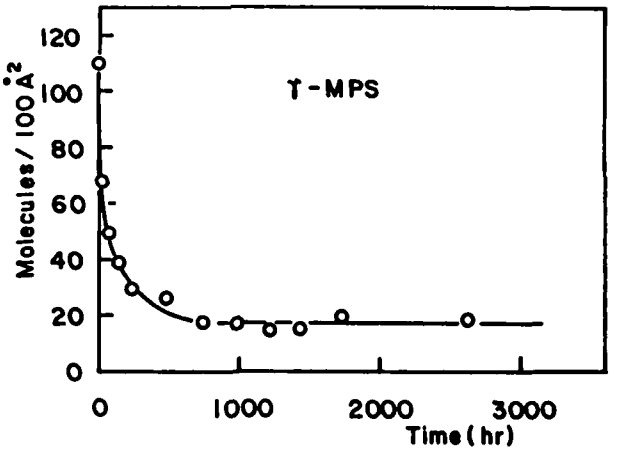

Fig. 18: The desorption curve of E-glass fiber/silane system No. 1: The glass fibers were treated with 1% by weight of γ-methacryloxypropyltrimethoxysilane (γ-MPS) in water. The silane treated glass fibers were immersed in water at 80°C. The silane quickly desorbed as similar to aminosilanes. Beyond 600 hrs., however, the desorption practically halts due to the organic chain formation through -C-C- bonds in addition to the siloxane bonds.

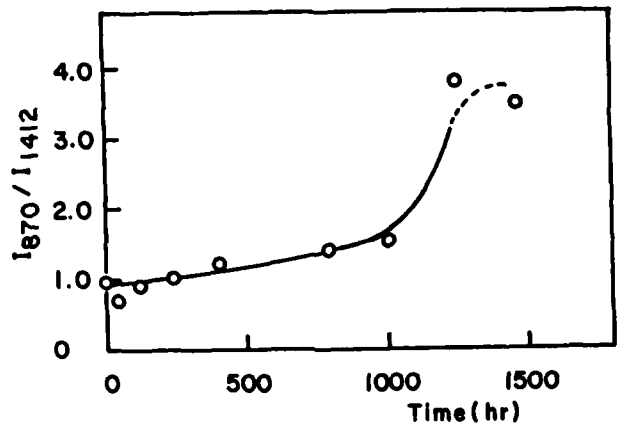

Fig. 19: The desorption curve of E-glass fiber/silane system No. 2: All conditions were the same as in Fig. 18 except the glass fibers were treated with 4% by weight of vinyltrimethoxysilane in water. There is a threshold period for the desorption originating from the extensive siloxane network formation. After 600 hrs., the size of silane oligomers produced by the hydrolysis is small enough to be soluble in water, thus desorbing quickly. This silane forms more organized silane layers than γ-MPS.

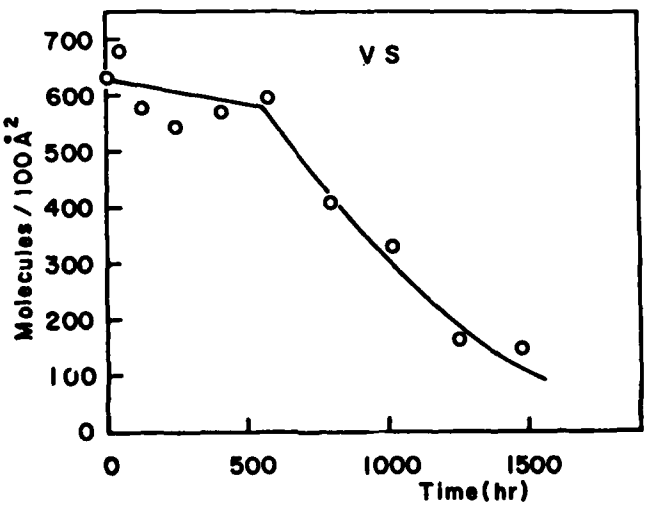

Fig. 20: The mass-adjusted infrared absorbance of the silanol band at 870 cm^{-1} against the immersion time in water at 80°C: The samples are the same used in Fig. 19. The silanol content steadily increases at early part of immersion even though the desorption is negligible during this period.

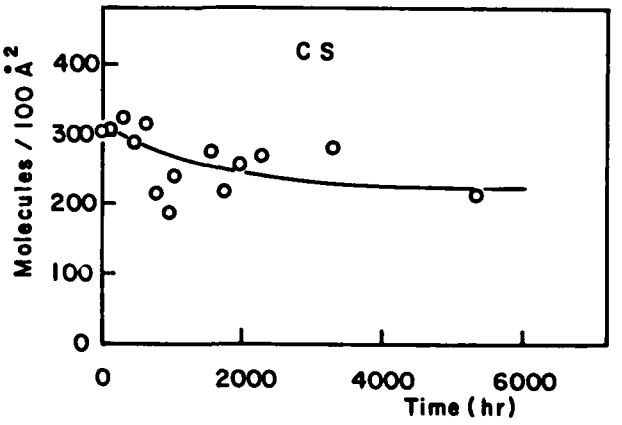

Fig. 21: The desorption curve of E-glass fiber/silane systems No. 3: All conditions are the same as in Figs. 18 and 19 except the glass fibers were treated with 1% by weight cyclohexyltrimethoxysilane in water. Practically no desorption was observed even after 6000 hrs. due to the hydrophobicity of the cyclohexyl group and highly ordered silane layers.

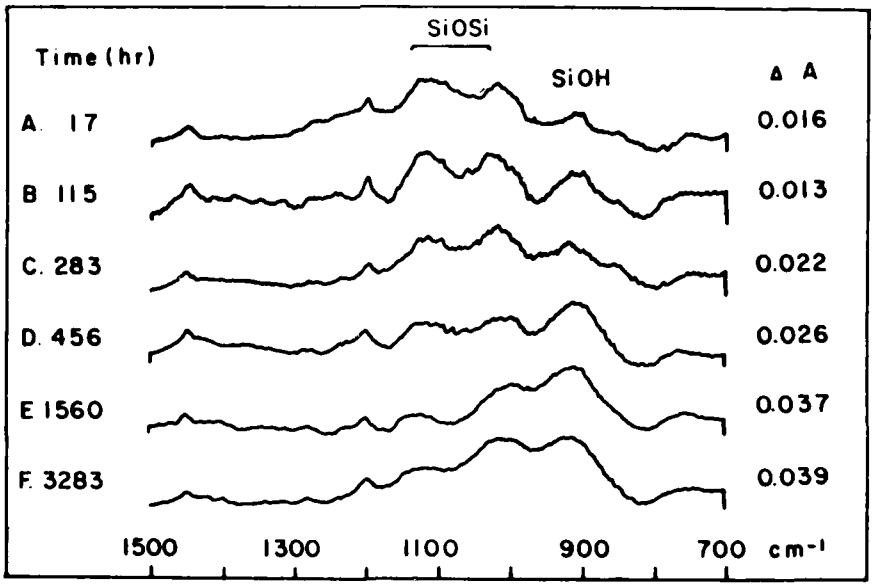

Fig. 22: The FT-IR difference spectra of the samples used for Fig. 21: In spite of the resistance to desorption, the silanes are steadily hydrolyzed as seen by the increase of the silanol band. After approximately 500 hrs., the increase in band intensity levels off indicating that it is now at the $SiOSi \rightleftharpoons SiOH + HOSi$ equilibrium. This silane is known to form a crystalline-like organization on the surface of glass fibers leading to extensively cross-linked networks. Thus, the molecular organization does not prevent from the hydrolytic attack of water.

CALCULATION OF STRUCTURAL PARAMETERS IN MODEL EPOXY SYSTEMS

Bruce Hartmann and Gilbert F. Lee

Naval Surface Weapons Center
Silver Spring, Maryland 20910

ABSTRACT

The assumption of additive properties was applied to a series of eight cross-linked epoxy/amine polymers. Properties of the four independent structural components of these polymers were determined from experimental measurements. This approach has so far been applied to: density, thermal expansion coefficient, heat capacity, bulk modulus, and shear modulus. The moduli and heat capacity results were obtained as a function of temperature while the other properties were only done at room temperature. Using these structural parameters, polymer properties were then calculated with the result that the predictions agree, on the average, with the measurements to within the accuracy of the measurements.

INTRODUCTION

The goal of this work is to relate the thermodynamic properties of crosslinked polymers to their molecular structure using the assumption of additive properties. The assumption of additive properties is best illustrated with a specific property as an example. In the case of molar volume, the assumption is that the total molar volume of a polymer is the sum of the volumes of the individual component groups making up the polymer and that these component volumes are the same in every polymer. In equation form

$$V = \sum_i n_i v_i \qquad (1)$$

where V is the molar volume of a polymer, v_i is the molar volume of component group i, n_i is the number of component groups i in the polymer repeat unit, and the summation extends over all the different components in the polymer. Molar volume plays a pivotal role in additive properties not only because it is intuitively plausible that volumes are additive, but also because all other additive properties can be considered to be derived from volume. If some other physical property is a linear function of volume, then that property will also be additive. Conversely, if a property is additive, then it will be a linear function of volume.

The set of polymers used in this work were a well characterized series of epoxy/diamines that were carefully purified for this study. Two resins were used: diglycidyl ether of bisphenol A (DGEBA) and resorcinol diglycidyl ether (RDGE). Each of these resins was cured with four diamine curing agents: propanediamine (PDA), hexanediamine (HDA), dodecanediamine (DDA), and m-phenylenediamine (MPDA). Thus there were a total of eight crosslinked polymers. Stoichiometric amounts of the curing agents were used in all cases, giving an idealized polymer structure whose repeat unit consists of two resin groups and one curing agent group from Fig. 1.

FIGURE 1

EPOXY POLYMERS USED

Resins:

diglycidyl ether of bisphenol A (DGEBA)

$-CH_2CH(OH)CH_2OC_6H_4C(CH_3)_2C_6H_4OCH_2CH(OH)CH_2-$

resorcinol diglycidyl ether (RDGE)

$-CH_2CH(OH)CH_2OC_6H_4OCH_2CH(OH)CH_2-$

Curing Agents:

propanediamine (PDA)

$-\underset{|}{N}(CH_2)_3\underset{|}{N}-$

hexanediamine (HDA)

$-\underset{|}{N}(CH_2)_6\underset{|}{N}-$

dodecanediamine (DDA)

$-\underset{|}{N}(CH_2)_{12}\underset{|}{N}-$

m-phenylenediamine (MPDA)

$-\underset{|}{N}C_6H_4\underset{|}{N}-$

It has been found to be more convenient to use molecular component groups rather than atomic components (carbon, hydrogen, oxygen, etc) because the atomic contributions vary considerably depending on their neighbors while the molecular components have much less variability (i.e., they obey the assumption of additive properties more closely). For linear polymers, the components are all bivalent while in crosslinked polymers at least one component must be of higher functionality. For the polymer set used here, there are four independent components: $-CH_2-$, $-C(CH_3)_2-$, $-C_6H_4-$, and $-\underset{|}{N}E\underset{|}{N}-$, where E is defined here as the glycol ether group, $E = -OCH_2CH(OH)CH_2-$. In terms of these four components, the repeat units of the eight polymers used in this study can be expressed in component form as shown in Fig. 2.

FIGURE 2

COMPONENT ANALYSIS

Polymer	Component			
	$-CH_2-$	$-C(CH_3)_2-$	$-C_6H_4-$	$-\underset{\|}{E}NE-$
DGEBA/PDA	3	2	4	2
DGEBA/HDA	6	2	4	2
DGEBA/DDA	12	2	4	2
DGEBA/MPDA	0	2	5	2
RDGE/PDA	3	0	2	2
RDGE/HDA	6	0	2	2
RDGE/DDA	12	0	2	2
RDGE/MPDA	0	0	3	2

Our approach has been to measure the physical properties of the eight polymers and then do a mathematical analysis to determine the "best" component values to use. In this case, "best" is defined to be the set that gives the lowest average percent difference between measured and calculated values.

In the sections that follow, the above approach will be applied to (1) room temperature values of density, thermal expansion coefficient, specific heat, and bulk modulus, (2) specific heat as a function of temperature over a range including the glass transition, and (3) bulk modulus and shear modulus as functions of temperature in the glassy state.

ROOM TEMPERATURE VALUES

Room temperature measurements were made of the following physical properties: density, thermal expansion coefficient, specific heat at constant

pressure, and adiabatic bulk modulus. Since the glass transition temperatures of the polymers are above room temperature, these measurements are for the glassy state. The results were analyzed to determine the best values for component properties. The results are given in Fig. 3. (The Rao function is used to

FIGURE 3

COMPONENT VALUES

	$-CH_2-$	$-C(CH_3)_2-$	$-C_6H_4-$	$-ENE-$
Molar volume, $cm^3/mole$	16.08	49.83	65.31	114.1
Thermal expansion, $10^{-4}\ deg^{-1}$	3.58	3.72	1.06	1.71
Rao function*, $cm^3/mole\ (cm/sec)^{1/3}$	854	3779	3099	8728
Heat capacity, cal/mole deg	9.33	23.53	28.47	50.53

$*U = V(K/\rho)^{1/6}$

calculate bulk modulus as will be described fully later.) The first three components are bivalent and occur in linear polymers as well as these crosslinked ones. Van Krevelen[1] has made an extensive study of additive properties for linear polymers. For molar volume (hence density since density = molecular weight/molar volume), he lists values for these three components. Van Krevelen also gives values for heat capacity and bulk modulus. In all cases, our values in Fig. 3 are in fairly good agreement with those of Van Krevelen.

Using the best values for the components, the properties of the starting polymer set can be calculated and compared with the measured values. Density and thermal expansion results are given in Fig. 4 while bulk modulus and heat capactiy are given in Fig. 5. At the bottom of each column of comparisons is the average percent error for the calculations. Density was the most accurately measured property, and it was predicted the most accurately. Thermal expansion coefficient is more difficult to measure than density and there is more error in the measurements and also in the predicted values. In short, the predictions have as much uncertainty as the measurements. Further, in comparison with Van Krevelen's results[1], the accuracy of these predictions for crosslinked polymers is about the same as similar predictions for linear polymers.

FIGURE 4

VOLUMETRIC PROPERTIES

Polymer	Molecular weight, g/mole	Density, g/cm³		Expansion, 10^{-4} deg^{-1}	
		Measured	Calculated	Measured	Calculated
DGEBA/PDA	754	1.1844	1.1844	1.90	1.90
DGEBA/HDA	796	1.1595	1.1620	2.01	2.01
DGEBA/DDA	880	1.1255	1.1255	2.33	2.21
DGEBA/MPDA	788	1.2033	1.2033	1.67	1.69
RDGE/PDA	518	1.2711	1.2736	1.72	1.72
RDGE/HDA	560	1.2299	1.2304	1.65	1.92
RDGE/DDA	644	1.1667	1.1667	2.21	2.21
RDGE/MPDA	552	1.3023	1.2989	1.44	1.41
Average error		0.1%		3%	

1. D. W. Van Krevelen, Properties of Polymers, Correlations With Chemical Structure (Elsevier, Amsterdam, 1972).

FIGURE 5

BULK MODULUS AND HEAT CAPACITY

	bulk modulus, kbar		heat capacity, cal/mole deg	
	Measured	Calculated	Measured	Calculated
DGEBA/PDA	72.6	72.6	294	290
DGEBA/HDA	65.7	65.6	318	318
DGEBA/DDA	53.3	57.7	378	374
DGEBA/MPDA	67.6	67.4	284	291
RDGE/PDA	86.2	90.5	186	186
RDGE/HDA	78.5	78.4	213	214
RDGE/DDA	63.6	62.6	270	270
RDGE/MPDA	82.7	82.3	193	187
Average error	2%		1%	

Based on these room temperature results, we have reached three major conclusions:

(1) Thermodynamic properties can be predicted as accurately as measured

(2) Crosslinked polymers are as additive as linear polymers

(3) Bivalent components have the same properties in linear and crosslinked polymers

The room temperature results have already been published[2] and form the background for the following work in progress.

SPECIFIC HEAT VS TEMPERATURE

Since all of the above work was limited to room temperature, it was natural to extend the procedure to a range of temperatures and specific heat was chosen as the first property to examine. It was our original intention to simply

2. B. Hartmann and G. F. Lee, J. Appl. Phys. 51, 5140 (1980).

repeat the room temperature calculations at a series of temperatures to determine component properties as a function of temperature. Measurements were made in a Dupont 990 Thermal Analyzer with a Differential Scanning Calorimeter attachment. Measurements were carried out over a range of temperatures that, for each polymer, included the glass transition. Results for the eight polymers are shown in Fig. 6.

In attempting to calculate component properties as a function of temperature from Fig. 6, a problem immediately arises. Take 100°C for example. Some of the polymers are in the glassy state, some are in the rubbery state, and some are in the transition region. Since the physical properties of polymers change significantly at the glass transition, we would not expect the assumption of

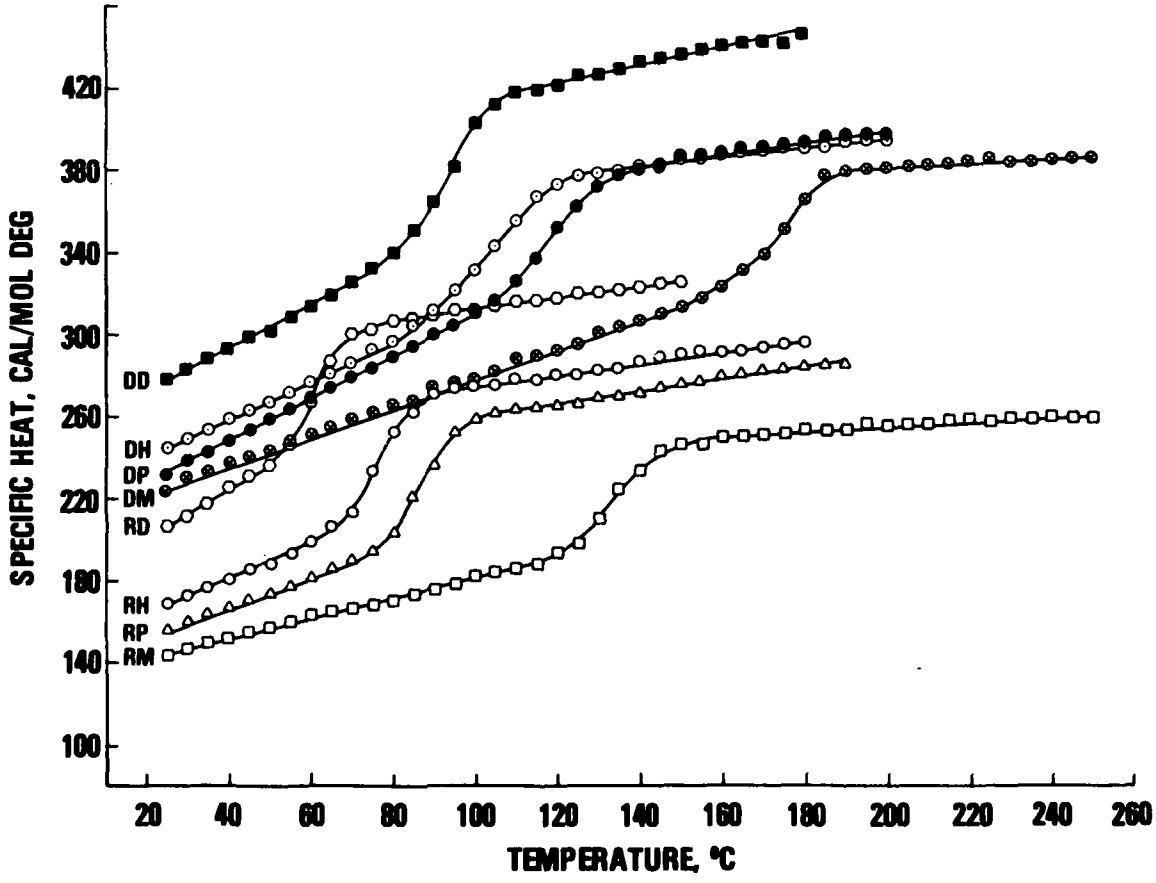

FIGURE 6 SPECIFIC HEAT VS TEMPERATURE

additive properties to hold under these conditions. We then realized that it is not correct to compare polymers to the same absolute temperature but polymers should be compared at the same reduced temperature, T-Tg. In our room temperature calculations, we were careful to note that all the polymers were in the glassy state. We are now led to the conclusion that there are degrees of glassiness and polymers should only be compared at the same degree of glassiness, i.e., at the same value of T-Tg.

Re-plotting the data from Fig. 6 as a function of T-Tg gives the results shown in Fig. 7. The somewhat jumbled mass of data now shows considerably more order. Using the data from Fig. 7, we have calculated component values

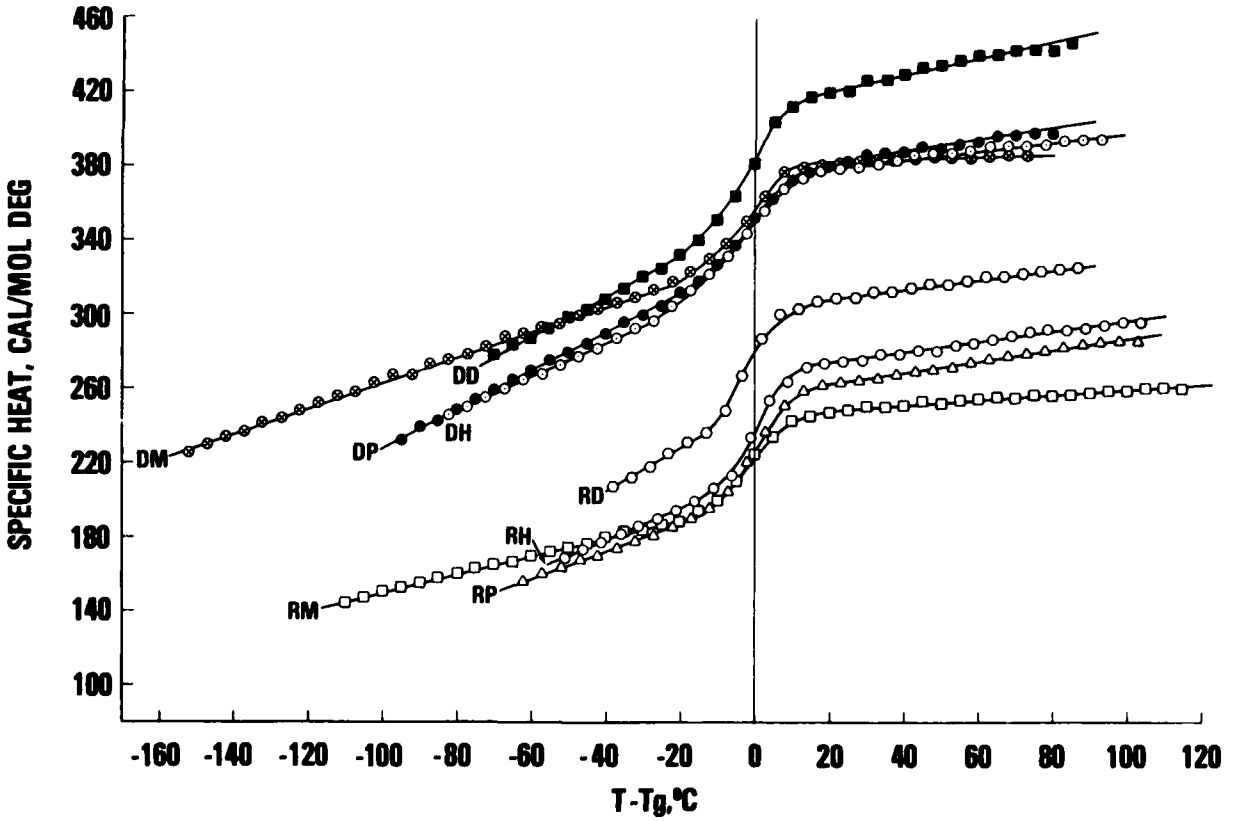

FIGURE 7 SPECIFIC HEAT VS REDUCED TEMPERATURE

as a function of T-Tg. The shape of these curves generally mimics that of the polymer curves in Fig. 7. The exact values are not important here, only the conclusion that polymers should be compared at the same reduced temperature.

MODULI VS TEMPERATURE

Applying the assumption of additive properties to polymer moduli turns out to be somewhat indirect. It is found that the bulk modulus, for example, is not an additive property, but a particular combination of properties including bulk modulus is an additive property.

Our starting point is the additive property for liquids known as the Rao function. It is a well established empirical rule that the Rao function

$$R = Vc^{1/3} = V(K/\rho)^{1/6} \tag{2}$$

is an additive property. Here V is molar volume, c is sound speed, K is adiabatic bulk modulus, and ρ is density. While R is additive, neither c nor K for liquids is additive. R also has the interesting property that it is independent of temperature.

In our room temperature calculations of bulk modulus discussed earlier, we simply applied equation (2) for liquids to our polymer solids. It is expected however that there should be some differences between solids and liquids so we made a more careful study of bulk modulus. We then assumed that the form of equation (2) holds but with a different exponent, to be determined. In other words, we assumed that there is an additive property for solid polymers of the form

$$U = V(K/\rho)^{1/2n} \tag{3}$$

The exponent n is then found by differentiating to be the Gruneisen parameter, γ,

$$n = \gamma = -\frac{1}{2\alpha}\frac{d\ln K}{dT} - \frac{1}{2} \tag{4}$$

where α is thermal expansion coefficient and T is absolute temperature. There is then a property, U, given by

$$U = V(K/\rho)^{1/2\gamma} \tag{5}$$

which is an additive property. We have found, for example, that U is a linear function of volume (though K is not). Further, over the limited temperature range of our measurements (0 to 60°C), U does not vary with temperature.

Shear modulus G was the next property examined. It was assumed that a functional form similar to that for bulk modulus existed, but with a different exponent,

$$W = V(G/\rho)^{1/2g} \tag{6}$$

where the exponent can be shown to be

$$g = -\frac{1}{2\alpha}\frac{d\ln G}{dT} - \frac{1}{2} \tag{7}$$

As before, W is an additive property while G is not. W was found to be a linear function of volume and independent of temperature.

Since U and W are additive properties, component values can be found for the four components of the epoxies. In this way calculations of U and W, hence K and G, can be made. Having both K and G, it is possible to calculate any of the other elastic constants, assuming the epoxies are isotropic. For example, Poisson's ratio σ can be calculated. Results of such calculations of K, G, and σ for one polymer, RDGE/PDA, are shown in Fig. 8 along with the measured values. As can be seen, the agreement is good.

Based on the moduli results, we conclude:

(1) Neither bulk modulus nor shear modulus is additive

(2) Both $U = V(K/\rho)^{1/2\gamma}$ and $W = V(G/\rho)^{1/2g}$ are additive

(3) Both U and W are linear functions of volume

(4) Both U and W are independent of temperature

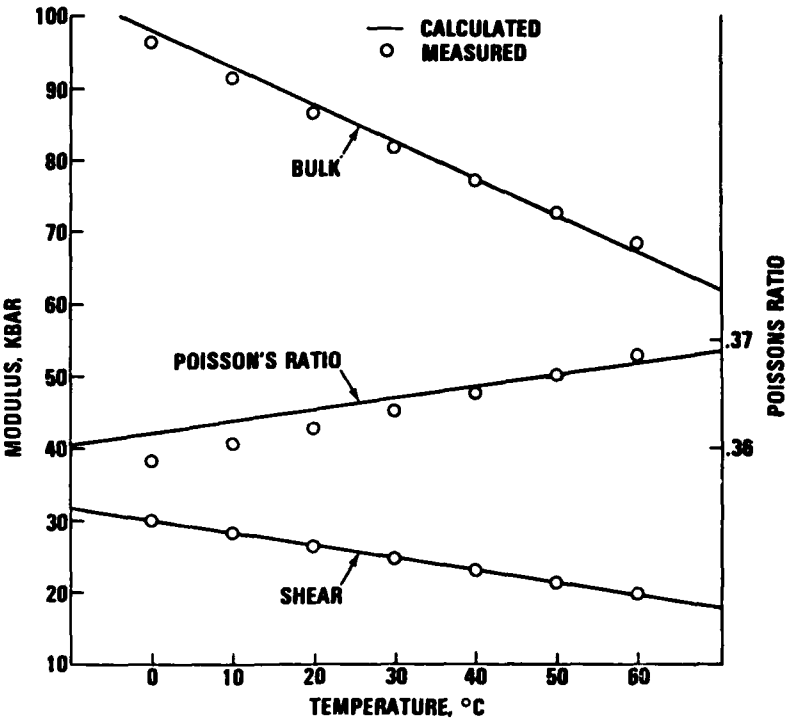

FIGURE 8 Elastic Constants vs Temperature for Polymer RDGE/PDA

ACCURACY OF COMPONENT PROPERTIES

The final topic considered here is the accuracy of the component properties. We have already determined the accuracy of the calculated polymer properties and found that polymer properties were calculated as accurately as they were measured. A separate question is the accuracy of the component properties. Since these properties can be viewed as being determined by the small difference in value between two polymers, it is expected that the percent error in component properties will be much greater than the error in polymer properties.

As an example, consider the specific heat of the -ENE- component as a function of reduced temperature, calculated from the data in Fig. 7. Results for this component are shown in Fig. 9. As mentioned before, the shape of this curve (the solid line) mimics that of the polymer specific heat curves. Also shown in Fig. 8 is the expected uncertainty in the value of component specific heat at each reduced temperature. These "error bars" are calculated by a

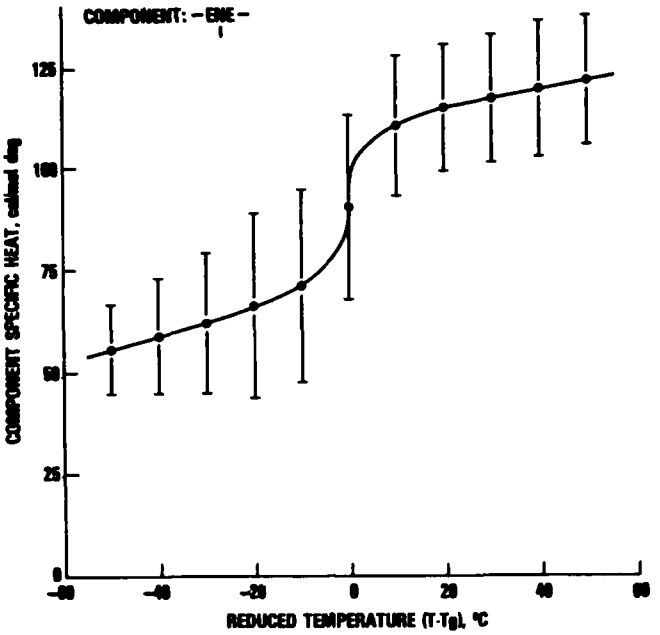

FIGURE 9 COMPONENT SPECIFIC HEAT VS REDUCED TEMPERATURE FOR -ENE-

mathematical procedure for least squares that depends on the coefficients in Fig. 5 and the measured polymer specific heats. From Fig. 8, the -ENE- component can be determined to within ± 30%. Earlier, we found that polymer specific heats can be calculated to within ± 3%. Further calculations were done showing that if the specific heat measurements could be made with ± 0.1% uncertainty, then the -ENE- component could be determined with ± 1% uncertainty. The same result applies to other properties. For density, which is measured to ± 0.1%, component values are known to ± 1%.

The above calculations are specific to the -ENE- component. Uncertainties in other components are different, depending on how that component appears in the set of numbers in Fig. 5. The least accurate component was found to be the phenyl component, $-C_6H_4-$. From Fig. 7 the phenyl component specific heat was calculated with the results shown in Fig. 10. The solid line indicates a temperature dependence opposite that of the other components. However, the

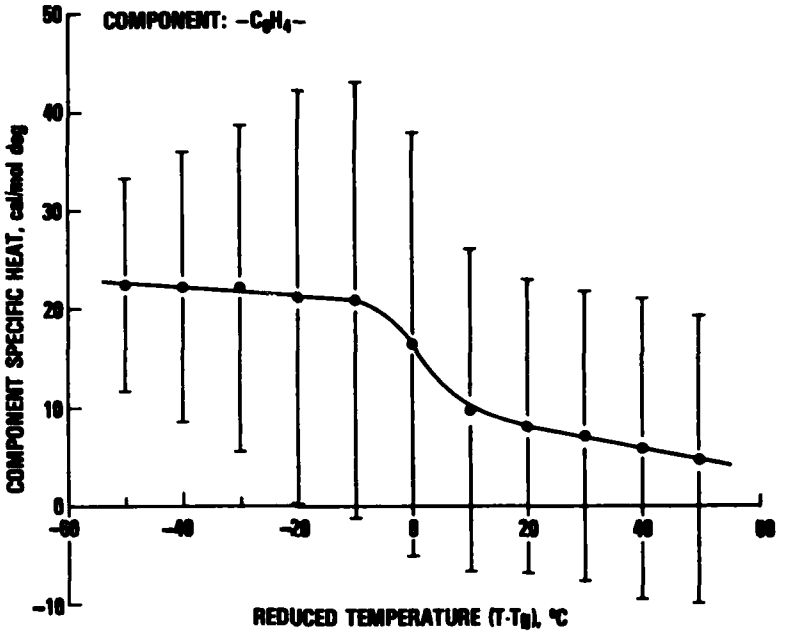

FIGURE 10 COMPONENT SPECIFIC HEAT VS REDUCED TEMPERATURE FOR $-C_6H_4-$

error bars in this case are very large, even extending to physically meaningless negative values. Thus, it is not possible to determine the temperature dependence of the phenyl component. In particular, the temperature dependence could be positive rather than negative and still be within the error bars. Only by making more accurate measurements and/or by using a different polymer set can the temperature dependence of the phenyl group be determined.

From the above calculations, we conclude that the uncertainty in polymer property calculations is the same as the experimental uncertainty while the component uncertainty is at least an order of magnitude higher.

SUMMARY

The assumption of additive properties has been shown to be valid for a series of crosslinked epoxies and predictions were made of the following properties: density, thermal expansion coefficient, specific heat, bulk modulus, and shear modulus all as functions of temperature. The accuracy of these calculations was limited by the accuracy of the input measurements and not by the assumption of additive properties.

THE FRACTURE OF ELASTOMER MODIFIED EPOXIES IN BULK AND AS MATRIX RESINS

W. D. Bascom*
Naval Research Laboratory
Hercules, Inc.

ABSTRACT

A study has been made of the interlaminar fracture of glass and graphite fabric composites. A double cantilever beam specimen was used that was width-tapered for constant change in compliance with crack length so that the fracture energy calculation is independent of crack length. It was found that the interlaminar fracture energy could be significantly increased, either by the addition of elastomeric toughening agents to the epoxy matrix, or by using a thermoplastic matrix resin instead of an epoxy. The largest increase in interlaminar fracture energy (approximately eight-fold) was obtained for an epoxy matrix/graphite fabric composite by the addition of elastomeric modifiers.

A systematic study was made of the fracture behavior of a commercial epoxy resin and of continuous glass and graphite fiber laminates fabricated using this resin. Details of this work are reported elsewhere (1, 2, 3). The composition of the base epoxy resin (designated 205) is given in Table 1. A liquid carboxy-terminated butadiene acrylonitrile (CTBN) elastomer and a solid rubber were added to the base epoxy as indicated in Table 2. Composition F-185 is a commercially available, high toughness resin (Hexcel Corp., Dublin, CA). The fracture energies of these various compositions were determined using compact tension specimens (Figure 1) and the results are listed in Table 3. Note the very considerable increase in toughness attained by addition of the liquid rubber and the solid rubber and that the toughness reached values comparable to thermoplastics in the F-185 composition.

Table 1
Composition of the Epoxy Resin

Component	Approximate Weight %
Epoxides	73
(diglycidyl ether of bispheol A) (epoxidized novolac, epox. eq. wt. 165)	
Diphenols	20
(bisphenol-A) (tetrabromobisphenol-A)	
Catalysts	7
(dicyandiamide) (substituted urea)	

*Present address: Graphite Fibers, Hercules Inc., Magna, Utah 84044.

Table 2
Elastomer Content of Epoxy Resins

Sample	Liquid CTBN[b]	Solid Elastomer
205[a]	0	0
206	8.1 wt. %	0
210	0	8.0
F185	8.1	5.4

[a]Base epoxy of Table 1.

[b]Hycar 1300 X 13, MW $\approx$ 3,500 (B. F. Goodrich)

[c]Hycar 1472, MW $\tilde{\approx}$260,000 (B. F. Goodrich)

TABLE III

Fracture Energy ($\mathcal{G}_{I_c}$) of Epoxy Polymers

Sample No.	$\mathcal{G}_{I_c}$*, kJ/M^2
205	0.20 $\pm$ 0.03
206	1.82 $\pm$ 0.20
207	3.0 $\pm$ 0.13
185	3.8 $\pm$ 0.7

*Average of 4-5 specimens at each composition

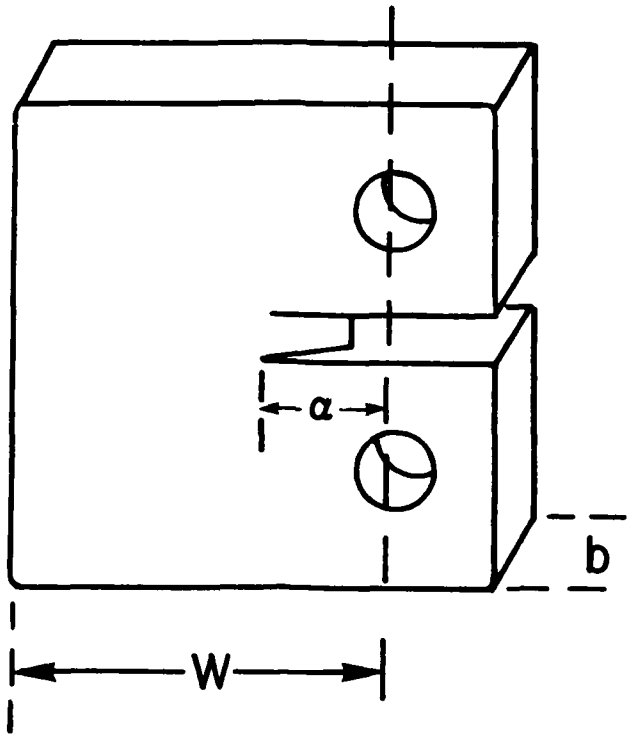

Figure 1 Compact Tension Specimen

It is well established (4, 5) that the addition of a liquid CTBN to an epoxy resin results in a dispersed phase of particles in the cured matrix; in these epoxies the particle size was approximately 0.5 μ. In the triaxial stress field of a crack-tip, the particles undergo dilatational yielding and induce shear yielding deformation of the surrounding matrix. These deformations cannot take place in the unmodified epoxy and so are responsible for the increase in toughness. The purpose of adding the solid rubber was to create particles $\sim$ 5 μ in diameter since it has been shown that a bimodal distribution of particle sizes gives a greater increase in toughness (at constant elastomer content) than a monodisperse formulation (6). SEM examination of the surfaces of the fracture specimens reveals the presence of the smaller particles but the larger particles, presumably formed from the solid rubber, were not unambiguously identified. Nonetheless, there was clear evidence of a localized shear yielding on the specimens containing the solid rubber that was not evident on specimens containing only the liquid rubber (Figure 2).

Composites were fabricated using the unmodified epoxy (205) and the fully toughened epoxy (F-185) and the interlaminar fracture was determined. The specimens were double cantilever beams width taper for constant change in compliance with crack length (2). A schematic of the specimen is shown in Figure 3 and a specimen during test is shown in Figure 4.

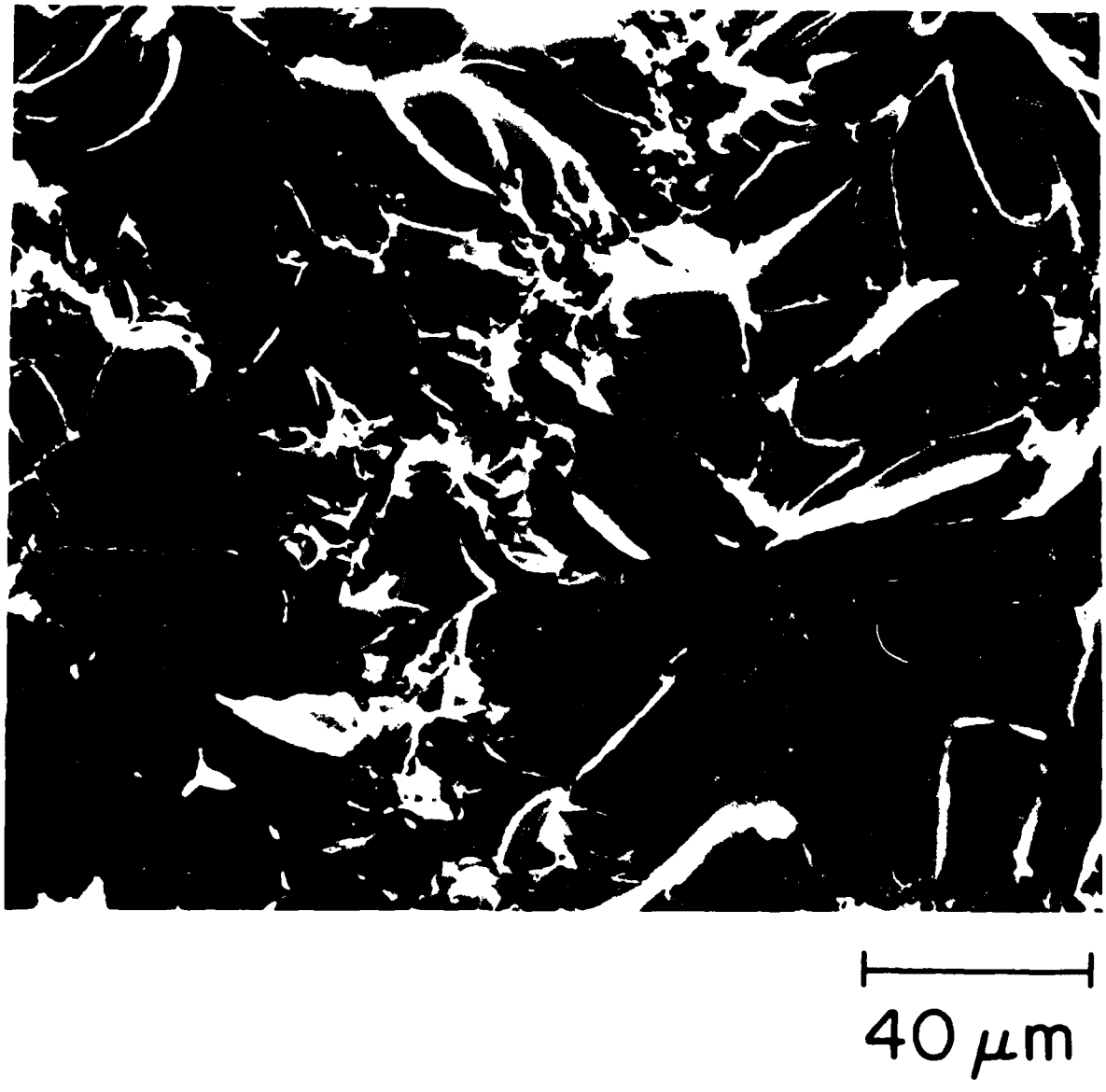

Figure 2 Localized shear yielding around a "large elastomer particle" in the fracture surface of the F185 resin

The results of these tests are given in Table 4. It is clear that the use of a tough matrix improves interlaminar fracture energy by a factor of 4 for glass cloth laminates and almost 8X for graphite cloth laminates. There is some loss in modulus from the addition of the toughening agent and also in the through fiber toughness. However, these are modest tradeoffs compared to the substantial improvement in interlaminar toughness.

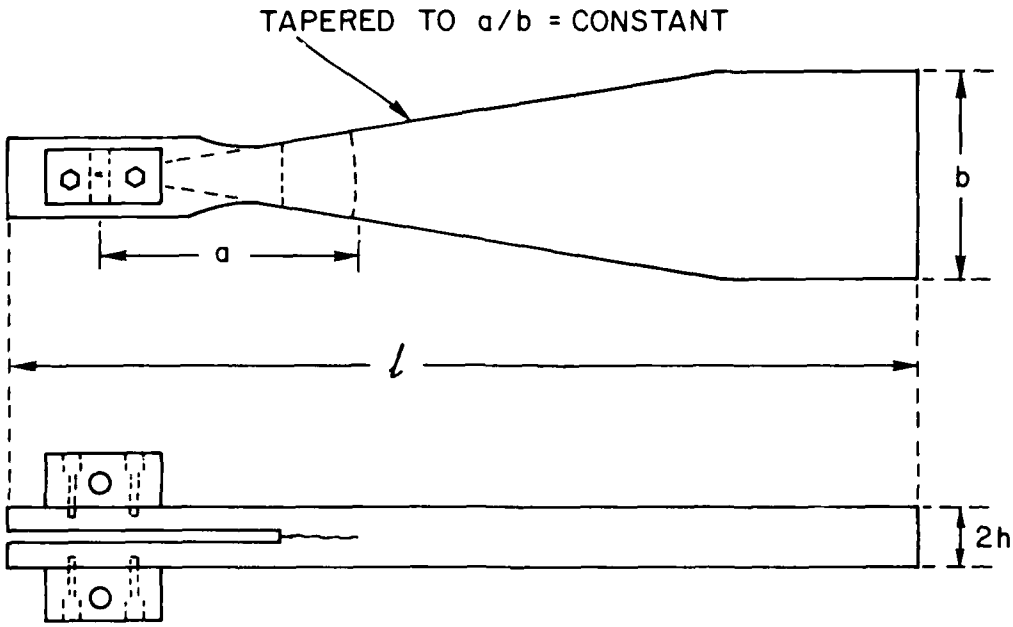

Figure 3 Schematic of a width tapered constant complaince interlaminar fracture specimen. (Cloth layers are in the plane perpendicular to the drawing.)

Table 4. Effect of elastomeric modifiers on resin and composite toughness

Material	Fibre Volume %	Modulus GPa	Fracture energy $\mathcal{G}_{Ic}$ (kJ/m^2)
		Tensile	*Neat resin*
205 resin	0	2.8	0.27
F-185 resin	0	2.2	5.1
		Flexural	*Interlaminar*
205/glass cloth	59.9	31.6	1.0
F-185/glass cloth	59.7	24.0	4.4
205/graphite cloth	61.0	54.1	0.60
F-185/graphite cloth	57.9	42.1	4.6
			Cross fibre
205/glass cloth	59.9	31.6	11.1
F-185/glass cloth	59.7	24.0	8.73

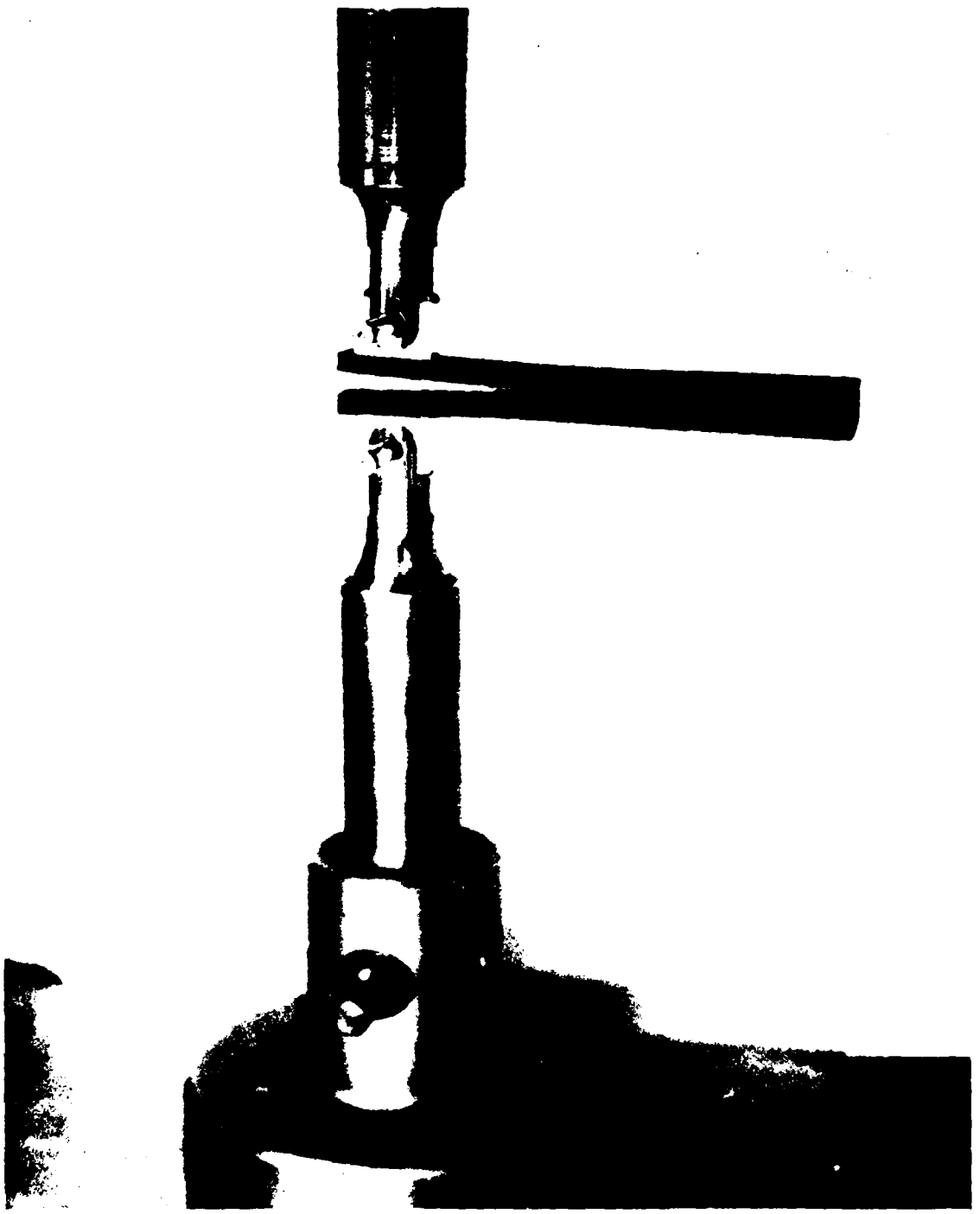

Figure 4 Photo of width tapered constant compliance specimen in test machine.

This work has demonstrated that improving matrix resin toughness does translate into increased interlaminar toughness (damage tolerance). However, many questions remain: What increase in toughness is realized when the reinforcement is non-woven; The fracture energy of these model epoxies are strain-rate dependent (7) and so is the interlaminar toughness also strain-rate sensitive; What are the effects of the elastomer particle-size and size distribution on both resin and interlaminar fracture energy?

WDB:jb

REFERENCES

1. Bascom, W. D., Moulton, R. J., Rowe, E. H., and Siebert, A. R., Organic Coating and Plastics (ACY) 39 164 (1978).

2. Bascom, W. D., Bitner, J. L., Moulton, R. J., and Siebert, A. R., Composites, Jan. 1980, p. 9.

3. Bascom, W. D., Ting, R. V., Moulton, R. J., Riew, C. K., and Siebert, A. R., J. Mat. Sci. 16 __ (1981).

4. Sultan, J. N., Laible, R. C., and McGarry, F. J., J. Appl. Polym. Sci., 6, 127 (1971).

5. Bascom, W. D., Cottington, R. L., Jones, R. L., and Peyses, P., J. Appl. Polym. Sci., 19 2545 (1975).

6. Riew, C. K., Rowe, E. H., and Siebert, A. R., in "Rubber Toughened Thermosets", ACS Symposium 168th ACS Meeting, 1974.

7. Hunston, D. L., in press.

0561b

DURABILITY OF COMMERCIAL AIRCRAFT AND HELICOPTER COMPOSITE STRUCTURES

H. Benson Dexter

NASA Langley Research Center

Hampton, Virginia

ABSTRACT

The NASA Langley Research Center has been instrumental in the development of advanced composite technology during the past decade. In the early 1970's NASA recognized the need to build confidence in the long-term durability of advanced composites and a series of flight service evaluation programs were initiated. Both secondary and primary components fabricated with boron, graphite, and Kevlar composites are being evaluated through worldwide service on both commercial transports and helicopters. Included are spoilers, rudders, and fairings on commercial transports, boron/epoxy reinforced wing structure on C-130 military transports, and doors, fairings, tail rotors, vertical fins, and horizontal stabilizers on commercial helicopters. Over 2 million successful component flight hours have been accumulated during the last eight years on over 150 composite components. The development of composite structures under the NASA Aircraft Energy Efficiency (ACEE) Program has resulted in significant advances in design and manufacturing technology for secondary and primary composite structures for commercial transports. Design concepts and inspection and maintenance results for the components in service are reported.

Concurrent with the flight evaluation of structural composite components, NASA initiated programs to determine the flight, outdoor ground, and controlled laboratory environmental effects on composites. Included are effects of moisture absorption, ultraviolet radiation, aircraft fuels and fluids, and sustained tensile stress. Test results for up to seven years exposure are reported. Results of these tests will be analyzed to identify critical parameters affecting the long-term durability of composite materials.

DURABILITY OF COMMERCIAL AIRCRAFT AND HELICOPTER COMPOSITE STRUCTURES

- FLIGHT SERVICE OF COMPOSITE COMPONENTS
  - TRANSPORT AIRCRAFT
  - HELICOPTERS
- ENVIRONMENTAL EFFECTS ON COMPOSITES
  - WORLDWIDE GROUND-BASED OUTDOOR EXPOSURE
  - FLIGHT EXPOSURE OF MATERIAL COUPONS
  - CONTROLLED LABORATORY EXPOSURE

FLIGHT SERVICE COMPOSITE COMPONENTS ON TRANSPORT AIRCRAFT

L-1011 FAIRING

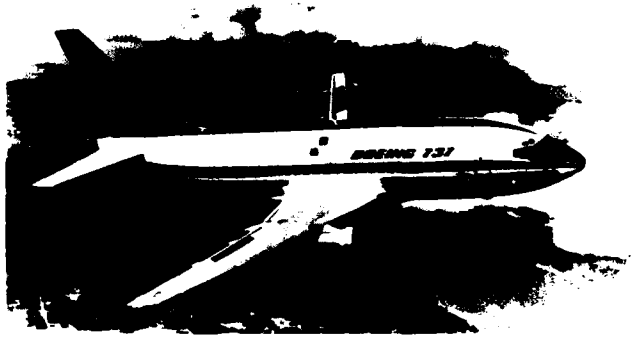

B-737 SPOILER

DC-10 RUDDER AND AFT PYLON

C-130 WING BOX

Figure 1

FLIGHT SERVICE COMPOSITE COMPONENTS ON TRANSPORT AIRCRAFT

(Figure 1)

NASA recognized the need to build confidence in the long-term durability of advanced composites to allow aircraft manufacturers and operators to make production decisions. NASA initiated a systematic program for the design, fabrication, test, and flight service evaluation of numerous composite components that will provide the necessary confidence. Early applications utilized selective reinforcement of military aircraft structures, but major emphasis was subsequently placed on evaluating advanced composites on commercial transport aircraft. Commercial aircraft were chosen because of their high utilization rates, exposure to worldwide environmental conditions, and systematic maintenance procedures. A typical NASA flight service program takes approximately 2 to 3 years for component development, detail design, fabrication, and ground testing and 5 years or more for service evaluation. In some cases, selected components are periodically removed from service for residual strength testing.

The composite components currently being evaluated on transport aircraft are shown in the figure. Eighteen Kevlar/epoxy fairings are being evaluated on three Lockheed L-1011 aircraft. Solid laminate and Nomex honeycomb sandwich panels were installed as a direct replacement for production fiberglass parts. An average mass saving of 26.8 percent compared to the fiberglass panels was achieved. One hundred and eight graphite/epoxy spoilers have been in service on six different commercial airlines for worldwide service. The spoilers are constructed with graphite/epoxy upper and lower skins, corrosion resistant aluminum honeycomb core, aluminum spar and hinge assemblies, and fiberglass closure ribs. The spoilers are 16.9 percent lighter than the standard production aluminum spoilers. Three boron/aluminum aft pylon skin panels are in service on three DC-10 aircraft. These panels are subjected to elevated temperature and high-intensity acoustic loading as a result of their proximity to the center engine. A mass saving of 27.3 percent compared to baseline titanium was achieved. Twelve graphite/epoxy DC-10 upper aft rudders are in service on five commercial airlines. These multi-rib stiffened rudders weigh 32.9 percent less than standard production aluminum rudders. Eight additional graphite/epoxy rudders are scheduled to be installed. Two boron/epoxy reinforced aluminum center-wing boxes are in service with the U.S. Air Force on C-130 transport aircraft. Boron/epoxy bonded to the covers on both wing planks and hat-section stringers resulted in increased fatigue life and a 10 percent mass saving.

ACEE

COMPOSITE SECONDARY STRUCTURES

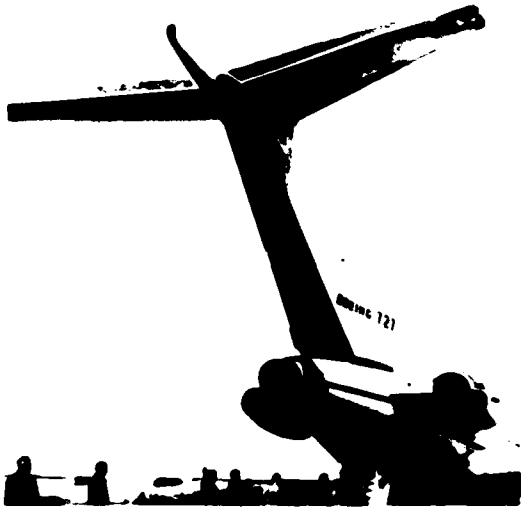

BOEING 727 COMPOSITE ELEVATOR

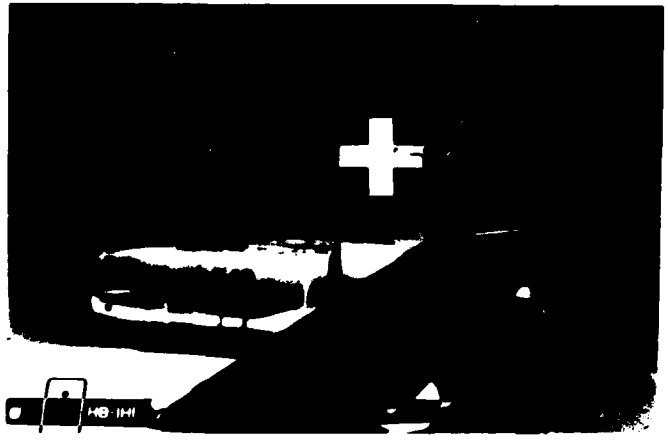

DOUGLAS DC-10 COMPOSITE RUDDER

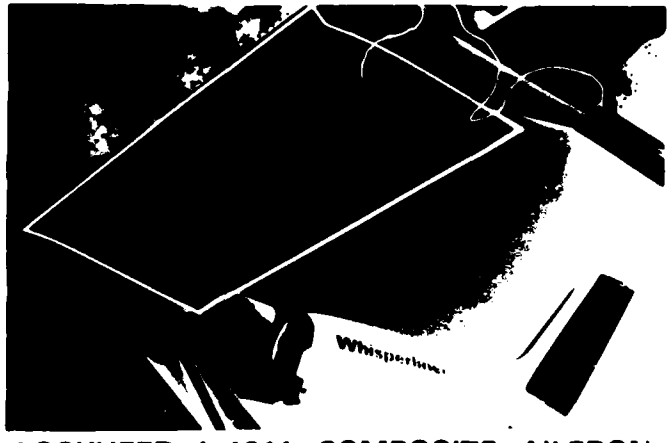

LOCKHEED L-1011 COMPOSITE AILERON

Figure 2

ACEE COMPOSITE SECONDARY STRUCTURES

(Figure 2)

Since 1975, NASA has been sponsoring an extensive program to improve the efficiency of commercial transport aircraft through the development and application of advanced technologies such as composite structures. The broad objective of the composites program is to conduct research to provide technology and confidence so that commercial transport manufacturers can commit to production of composites in their future aircraft. The technology readiness dates are to make such commitments for secondary structures in the 1980-1985 time frame and for primary structures in 1985-1990.

Each of the three major U.S. commercial transport manufacturers are under contract to NASA to design, fabricate, and test major secondary composite components as shown in the figure. Douglas has completed fabrication of 11 additional graphite/epoxy DC-10 upper aft rudders using cost-effective fabrication and tooling methods. Boeing has fabricated 11 graphite/epoxy elevators for the B-727 and Lockheed is in the final stages of fabricating 12 graphite/epoxy ailerons for the L-1011. Several shipsets of these components are being placed into airline service by the manufacturers for evaluation. The elevators for the B-727 are basically a stiffness design and are constructed with graphite/epoxy skins and Nomex honeycomb sandwich to carry normal pressure and in-plane shear loads. The graphite/epoxy elevator has a mass of 44.5 kg and weighs 24.6 percent less than a production aluminum elevator. FAA certification was achieved and flight service evaluation of five shipsets was initiated in March 1980.

Each additional graphite/epoxy rudder fabricated by Douglas in the ACEE program has a mass of 30.4 kg and weighs 26.6 percent less than a production aluminum rudder. FAA certification was achieved and flight service evaluation of 10 additional shipsets was initiated in March 1980. The composite aileron design features a syntactic-core sandwich with graphite/epoxy facesheets. The graphite/epoxy aileron has a mass of 48.5 kg and weighs 23.6 percent less than a production aluminum aileron. FAA certification and initiation of flight service is expected in late 1981.

FLIGHT SERVICE COMPOSITE COMPONENTS ON HELICOPTERS

206L DOORS, FAIRING AND VERTICAL FIN

S-76 TAIL ROTOR AND HORIZONTAL STABILIZER

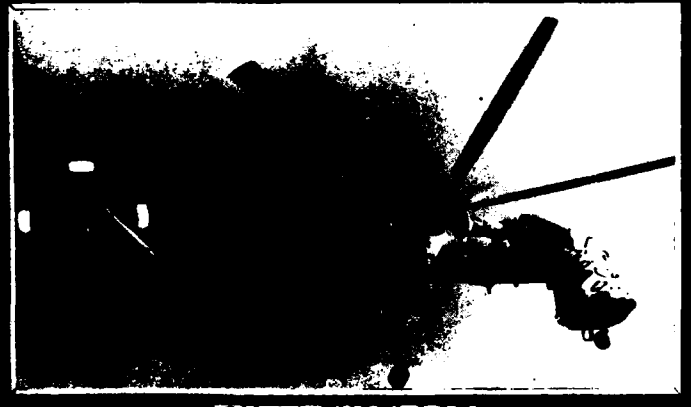

CH-54 FUSELAGE

CH-53 CARGO RAMP SKIN

Figure 3

FLIGHT SERVICE COMPOSITE COMPONENTS ON HELICOPTERS

(Figure 3)

Programs are underway to evaluate composite components on commercial and military helicopters. The components being evaluated are shown in the figure. A development program is underway to design, fabricate and evaluate composite components on Bell 206L commercial helicopters. Forty shipsets of Kevlar/epoxy doors and fairings and graphite/epoxy vertical fins will be installed on 206L helicopters in 1981 for a 5 to 10 year service evaluation period. An overall mass saving of 27.7 percent compared to production components is estimated. The helicopters will operate in diverse environments in Alaska, Canada, and the U.S. Gulf Coast. Selected components will be removed from service and tested to failure to compare residual strength with original strength.

Sikorsky Aircraft has committed to extensive use of secondary and primary Kevlar/epoxy and graphite/epoxy structural composites in their S-76 commercial helicopter. NASA Langley has a contract underway with Sikorsky to determine the effects of realistic operational service environments on typical composite helicopter structures. Ten tail rotors and four horizontal stabilizers will be removed from helicopters after 2 to 10 years of operational service. Static and fatigue tests will be conducted on the components removed from service and the results will be compared with baseline certification test results. In addition, several hundred composite coupons exposed to the outdoor environment will be tested for comparison with the component test results.

A program has been underway for 10 years to evaluate reinforcement of a U.S. Army CH-54B helicopter tail cone with unidirectional boron/epoxy. Boron/epoxy strips bonded to the tail cone stringers increased the tail cone stiffness and permitted the structural mass to be reduced by 14 percent. The CH-54 with the boron/epoxy reinforcement has been out of service since October 1979, at which time structural damage was incurred due to a tornado. The U.S. Army is currently in the process of repairing the helicopter for additional service.

A Kevlar/epoxy cargo ramp skin will be evaluated on a U.S. Marine CH-53 helicopter. The laminated fabric skin may encounter severe handling such as rough runway abrasion and impact. Maintenance characteristics of the Kevlar skin will be compared with a production aluminum skin. The Kevlar/epoxy skin is 9.2 percent lighter than the aluminum skin. Installation and initiation of flight service is expected in 1981.


BELL 206L HELICOPTER COMPOSITE COMPONENTS
FORWARD FAIRING
KEVLAR/EPOXY FABRIC
STIFFENED FOAM SANDWICH
MASS (kg) 2.31
SIZE (m) 0.90 × 0.74
VERTICAL FIN
GRAPHITE/EPOXY TAPE
FIBER TRUSS CORE
MASS (kg) 5.90
SIZE (m) 1.98 × 0.50
LITTER DOOR
KEVLAR/EPOXY FABRIC
TWO SKINS - HOLLOW SECTION
MASS (kg) 3.72
SIZE (m) 1.17 × 0.66
BAGGAGE DOOR
KEVLAR/EPOXY FABRIC
HONEYCOMB SANDWICH
MASS (kg) 1.41
SIZE (m) 0.97 × 0.58

Figure 4

BELL 206L HELICOPTER COMPOSITE COMPONENTS

(Figure 4)

The four composite components which will be evaluated on the Bell 206L are shown in the figure. The forward fairing is a sandwich structure with a single ply of Kevlar/epoxy fabric co-cured on a foam core. The foam is a polyvinylchloride (Klegecell) material that is easily preformed to the double curvature shape using moderate temperature and pressure. Local reinforcements of Kevlar/epoxy fabric are used where increased strength or stiffness are required. The composite forward fairing has a mass of 2.31 kg and weighs 38 percent less than the production aluminum fairing.

The vertical fin is constructed with graphite/epoxy facesheets bonded to a Fibertruss honeycomb core. The graphite/epoxy plies are stepped in thickness to provide adequate bending stiffness and the honeycomb core density is varied to provide the required shear stiffness. A layer of 200 x 200 mesh aluminum wire screen is bonded to the outer surface of each skin to provide for lightning protection. The composite fin has a mass of 5.90 kg and weighs 22 percent less than the production aluminum honeycomb sandwich fin.

The litter door is constructed with Kevlar/epoxy fabric and has local reinforcement at load introduction points (hinges and latch assembly). The litter door is a hollow section with inner and outer skins and unidirectional Kevlar/epoxy tape is used in the post area and in the hat-section stiffeners to add stiffness to the basic Kevlar structure. The composite litter door has a mass of 3.72 kg and weighs 35 percent less than the production bonded and riveted aluminum door.

The baggage door is constructed with Kevlar/epoxy fabric facesheets and Nomex honeycomb core. Additional reinforcements are added in the areas of the latch and along the edges. The composite baggage door has a mass of 1.41 kg; however, a mass saving was not achieved because a bending stiffness requirement equivalent to the metal door added a small mass penalty.

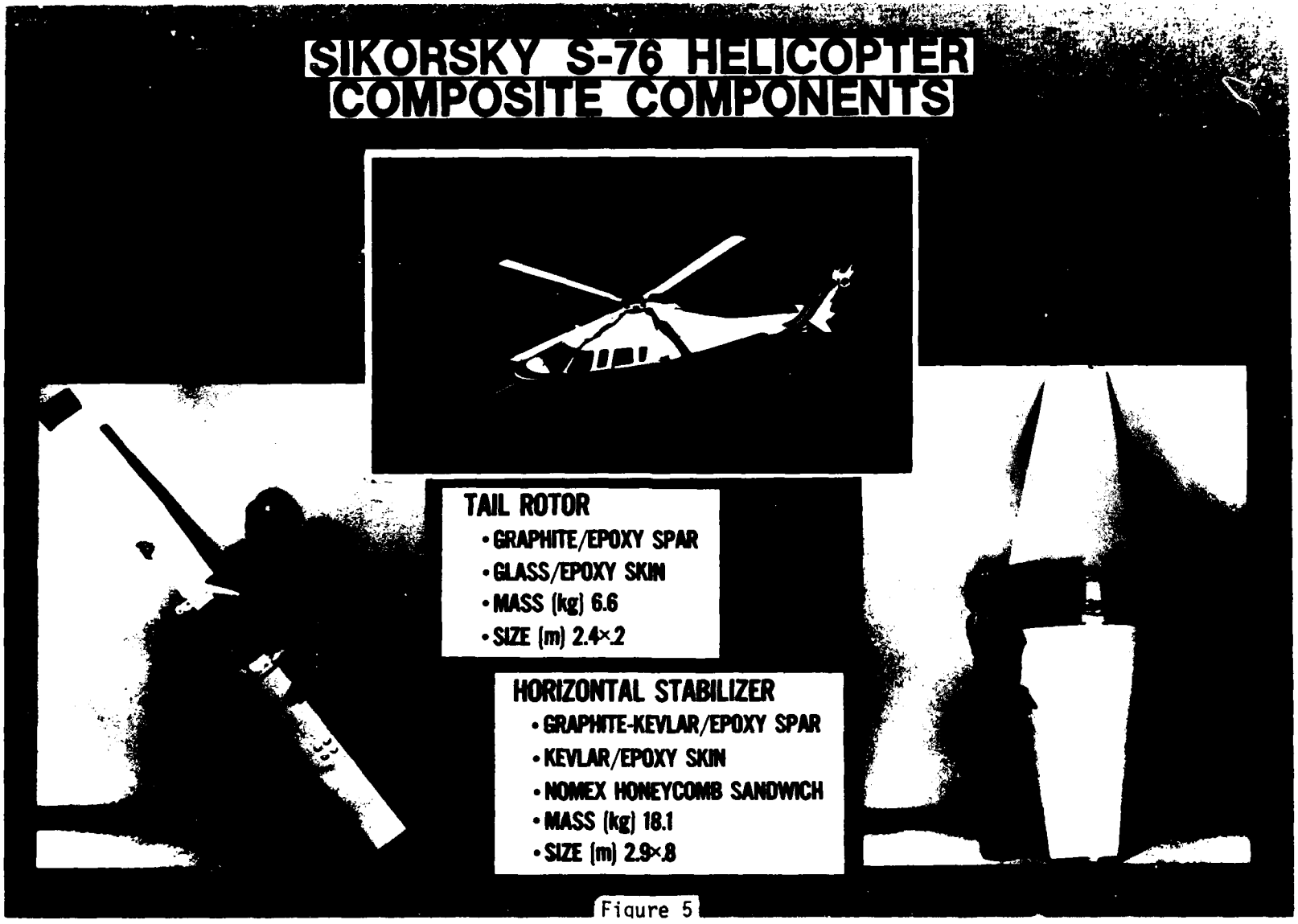
SIKORSKY S-76 HELICOPTER
COMPOSITE COMPONENTS
TAIL ROTOR
• GRAPHITE/EPOXY SPAR
• GLASS/EPOXY SKIN
• MASS (kg) 6.6
• SIZE (m) 2.4×.2
HORIZONTAL STABILIZER
• GRAPHITE-KEVLAR/EPOXY SPAR
• KEVLAR/EPOXY SKIN
• NOMEX HONEYCOMB SANDWICH
• MASS (kg) 18.1
• SIZE (m) 2.9×.8

Figure 5

SIKORSKY S-76 HELICOPTER COMPOSITE COMPONENTS

(Figure 5)

The two composite components that will be evaluated on the Sikorsky S-76 are shown in the figure. The composite components are baseline designs for the S-76 and are currently in commercial production. The tail rotor has a laminated graphite/epoxy spar with a glass/epoxy skin and has a mass of 6.6 kg. The horizontal stabilizer has a Kevlar/epoxy torque tube with graphite/epoxy spar caps, full-depth Nomex honeycomb sandwich core, and Kevlar/epoxy skins. The composite stabilizer has a mass of 18.1 kg.

After the composite components are structurally tested to failure (static and fatigue) small coupons will be cut from the laminated composites to measure moisture absorption and strength retention. Results will be compared with baseline and FAA certification test results and with controlled laboratory environmentally conditioned tests. Test results from the coupons removed from failed components will also be compared with coupons tested after similar exposure times to the outdoor environment.

NASA COMPOSITE STRUCTURES FLIGHT SERVICE SUMMARY

AIRCRAFT COMPONENT	TOTAL COMPONENTS	START OF FLIGHT SERVICE	CUMULATIVE FLIGHT HOURS	
			HIGH TIME AIRCRAFT	TOTAL COMPONENT
CH-54-B TAIL CONE	1	MARCH 1972	1,140	1,140
L-1011 FAIRING PANELS	18	JANUARY 1973	19,343	341,450
737 SPOILER	108	JULY 1973	20,893	1,536,830
C-130 CENTER WING BOX	2	OCTOBER 1974	4,880	9,740
DC-10 AFT PYLON SKIN	3	AUGUST 1975	15,869	47,340
DC-10 UPPER AFT RUDDER	12	APRIL 1976	19,399	142,910
727 ELEVATOR	10	MARCH 1980	3,654	33,250
GRAND TOTAL	154			2,112,660

MARCH, 1981

Figure 6

NASA COMPOSITE STRUCTURES FLIGHT SERVICE SUMMARY

A total of 154 composite components have been in service with 17 different operators, including foreign and domestic airlines, the U.S. Army, and the U.S. Air Force. The NASA flight service program was initiated in 1972 to determine the long-term durability of boron, Kevlar, and graphite composites in realistic flight environments. Over two million component flight hours have been accumulated with the high time aircraft having more than 20,000 hours as shown in the figure. The boron/epoxy reinforced CH-54B helicopter entered service in 1972 but has flown very little compared to the other types of aircraft. Some of the graphite/epoxy DC-10 upper aft rudders have been accumulating flight service time at a rate of over 300 hours per month during the past 5 years. Also, some of the graphite/epoxy elevators have been flying over 300 hours per month during their first year of service. The 108 graphite/epoxy spoilers installed on B-737 aircraft have accumulated the greatest total component flight hours, over 1.5 million, in nearly 8 years of service. Over 50 spoilers have accumulated in excess of 14,000 flight hours. A total of 19 spoilers have been removed from service and structurally tested to failure.

RESIDUAL STRENGTH OF GRAPHITE/EPOXY SPOILERS

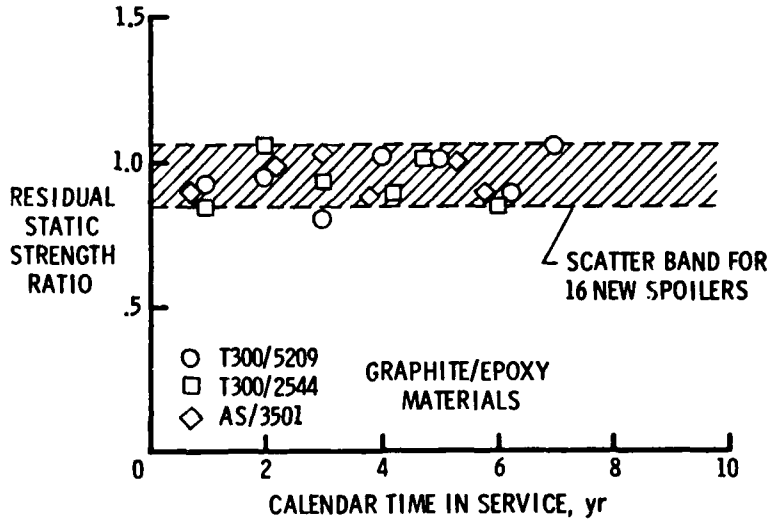

Figure 7

RESIDUAL STRENGTH OF GRAPHITE/EPOXY SPOILERS

The large number of spoilers with graphite/epoxy skins allows planned retrievals from flight service without seriously impairing the total exposure. Six spoilers which include two of each of three material systems used in fabricating the spoilers, are selected at random for removal from service annually. The six spoilers are shipped to Boeing for ultrasonic inspection. Three of the spoilers are returned to service after inspection and three are tested to failure to compare residual strengths with the strength of 16 new spoilers that were tested early in the program. Tests have been completed on all three graphite/epoxy systems after six years service and the seventh year test has been completed on a spoiler constructed with T300/5209. Results of tests conducted to date are shown in the figure.

The strengths for the individual spoilers generally fall within the same scatter band as was defined by strengths of the new spoilers. The results indicate essentially no degradation in strength after the 7 year period of service for the materials indicated. In addition, stiffness measurements for the graphite/epoxy spoilers indicate essentially no reduction in stiffness as a result of 7 years service exposure.

SPOILER MOISTURE LEVELS DETERMINED FROM PLUGS

6 YEARS SERVICE

GRAPHITE/EPOXY	MOISTURE CONTENT, PERCENT
T300/5209	0.67
T300/2544	1.10
AS/3501	0.82

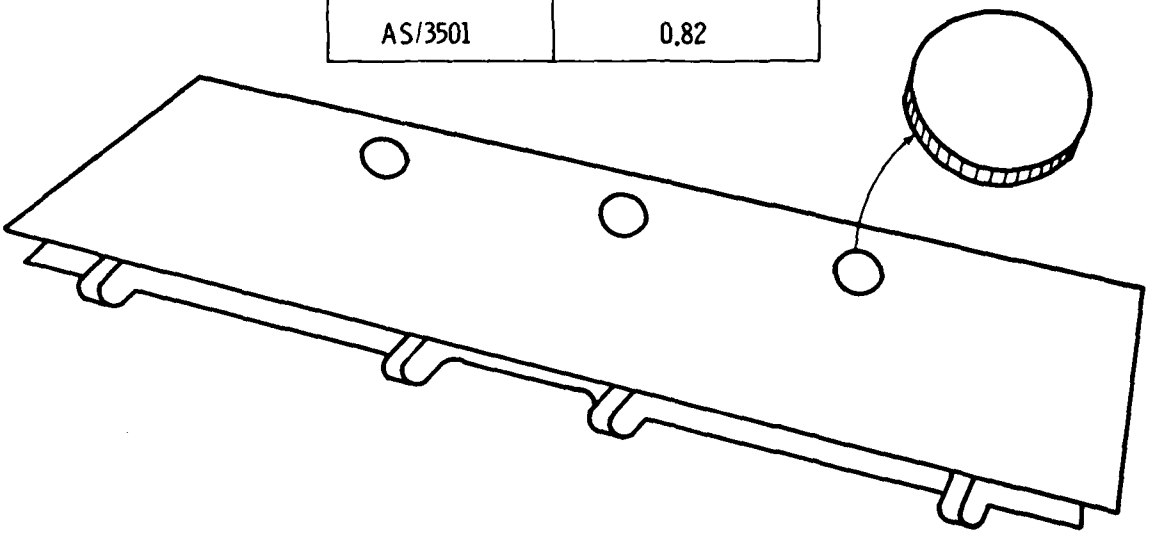

SPOILER MOISTURE LEVELS DETERMINED FROM PLUGS

(Figure 8)

In addition to structural tests of the spoilers, tests are conducted to determine absorbed moisture content of the graphite/epoxy skins. The moisture content in the graphite/epoxy spoilers is determined from 5.7 cm diameter plugs cut near the trailing edge as shown in the figure. The plugs consist of aluminum honeycomb core, two graphite/epoxy facesheets, two layers of epoxy film adhesive, and two exterior coats of polyurethane paint. About 90 percent of the plug mass is in the composite faces, including the paint and adhesive. The moisture content is determined by drying the plugs and recording the mass change. The data shown in the figure for plugs removed from three spoilers after 6 years service indicate moisture levels in the graphite/epoxy skins ranging from 0.67 to 1.10 percent for T300/5209, AS/3501, and T300/2544 material systems. These moisture levels are similar to the levels obtained from coupons exposed outdoors for the same exposure periods. Apparently, these moisture levels have not affected the room temperature strengths of the spoilers as shown in a previous figure.

NASA COMPOSITE COMPONENT INSPECTION AND MAINTENANCE RESULTS

COMPONENT	INSPECTION INTERVAL, months	INSPECTION METHODS	STATUS
CH-54B TAIL CONE	2	VISUAL ULTRASONIC	MINOR DISBONDS NO REPAIR REQUIRED
L-1011 FAIRING PANELS	12	VISUAL	MINOR IMPACT DAMAGE, FIBER FRAYING AND HOLE ELONGATIONS
737 SPOILER	12	VISUAL ULTRASONIC	INFREQUENT MINOR DAMAGE REPAIRED AT BOEING
C-130 CENTER WING BOX	6	VISUAL ULTRASONIC	NO DEFECTS AFTER MORE THAN 6 YEARS SERVICE
DC-10 AFT PYLON SKIN	12	VISUAL	MINOR SURFACE CORROSION ON ONE SKIN
DC-10 UPPER AFT RUDDER	3, 12	VISUAL ULTRASONIC	MINOR RIB-TO-SKIN DISBOND ON TWO RUDDERS MINOR LIGHTNING STRIKE ON ONE RUDDER
727 ELEVATOR	13	VISUAL	MINOR LIGHTNING STRIKE ON ONE ELEVATOR

NASA COMPOSITE COMPONENT INSPECTION AND MAINTENANCE RESULTS

(Figure 9)

The composite components in the NASA flight service evaluation program are being inspected at periodic intervals to check for damage, defects, or repairs that may occur during normal aircraft operation. The maintenance data shown in the figure were reported by the aircraft manufacturers who fabricated the various components. The composite components are being inspected by the aircraft operators and manufacturers and in some cases both visual and ultrasonic inspection methods are being used.

Minor disbonds have been found under small portions of the CH-54B boron/epoxy reinforcement. The disbonds were small and did not require repair. The Kevlar/epoxy fairings on the L-1011 aircraft have incurred minor impact damage from equipment and foreign objects. Fiber fraying and fastener hole elongations have been noted on all the Kevlar/epoxy fairings but no repair has been required. The B-737 graphite/epoxy spoilers are inspected annually by Boeing and defective spoilers are removed from the aircraft for repair. Minor defects are currently being repaired by the airlines but most repairs have been performed by Boeing. Some spar exfoliation-corrosion damage has been found on the spoilers but moisture migration into the aluminum honeycomb core has not been a problem. The boron/epoxy-reinforced C-130 wing boxes have been inspected every 6 months for the past 6 years and no defects have been detected. The boron/aluminum aft pylon skins on the DC-10 aircraft are inspected annually and minor surface corrosion has been reported on one panel. This corrosion is believed to have been caused by improper surface preparation during fabrication of the panels.

Minor rib-to-skin disbonds have been detected on two rudders for the DC-10 aircraft but repairs are not required. These minor disbonds may have been caused by thermal stresses during cooldown after the manufacturing cure cycle. Evidence of a minor lightning strike on one DC-10 graphite/epoxy rudder was discovered during routine repainting of the aircraft. Lightning damage was confined to a small area (4.0 cm long by 1.3 cm wide) and a fiberglass cloth patch was used to repair the damage by airlines personnel. A minor lightning strike was also discovered on one of the B-727 graphite/epoxy elevators. The damage was repaired by airline personnel with a fiberglass patch similar to that used for the graphite/epoxy rudder. Overall, excellent performance has been achieved with the NASA flight service composite components.

DC-10 COMPOSITE RUDDER LIGHTNING DAMAGE

(Figure 10)

One of the graphite/epoxy upper aft rudders flying on DC-10 aircraft sustained a lightning strike as shown in the figure. The damage was localized in an area measuring approximately 1.3 cm by 4.0 cm near the trailing edge of the structural box. The paint layer and four of the outer layers of the graphite/epoxy were removed by the lightning strike. Dry graphite fibers around the edge of the damaged region suggested that the epoxy resin had been vaporized by intense heat generated by the lightning strike. Repair of the rudder was performed in accordance with repair procedures established at the time the graphite/epoxy rudders were certificated by the FAA. The repair consisted of a fiberglass cloth patch and a room temperature curing epoxy adhesive. The repair was performed by United Airlines personnel and the aircraft resumed scheduled airline service.

ENVIRONMENTAL EFFECTS ON LONG TERM DURABILITY OF COMPOSITE MATERIALS FOR COMMERCIAL AIRCRAFT

- GROUND EXPOSURE – 10 YEARS AT AIRPORTS
- FLIGHT EXPOSURE – 10 YEARS ON AIRPLANES
- LABORATORY EXPOSURE – CONTROLLED CONDITIONS
- CORRELATE AND ANALYZE RESULTS
- DEVELOP METHODOLOGIES FOR PREDICTING DURABILITY
  - ACCELERATED TEST METHODS
  - ANALYSIS

ENVIRONMENTAL EFFECTS ON LONG TERM DURABILITY OF

COMPOSITE MATERIALS FOR COMMERCIAL AIRCRAFT

(Figure 11)

Concurrent with the flight evaluation of structural composite components, NASA initiated programs to determine the outdoor ground, flight, and controlled laboratory environmental effects on composite materials. Included are effects of moisture absorption, ultraviolet radiation, aircraft fuels and fluids, and sustained tensile stress. Specimens configured for various mechanical property tests are exposed to real time environmental conditions on aircraft in scheduled airline service and at various ground stations around the world. Composite specimens are also exposed to controlled laboratory environments including temperature, relative humidity, and simulated ultraviolet radiation. The tests, involving more than 17,000 composite specimens, are scheduled to run for up to 10 years. The results of these tests will be correlated to provide a broad data base for environmental effects which will be used to develop methodologies for predicting environmental performance.

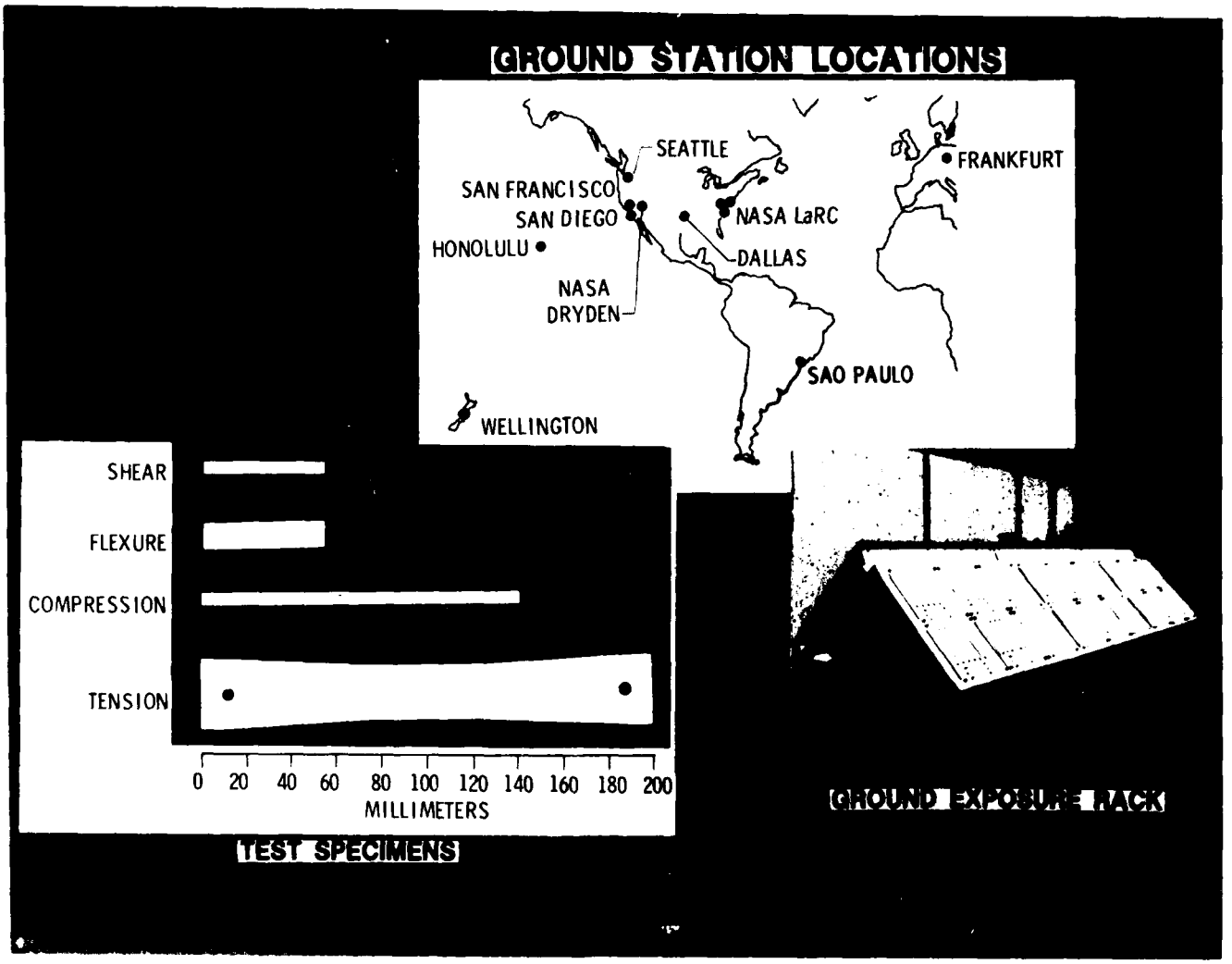

WORLD-WIDE ENVIRONMENTAL EXPOSURE OF COMPOSITE MATERIALS

(Figure 12)

Composite test specimens are being exposed to outdoor environmental conditions at the ground station locations shown in the figure. Specimens are mounted on racks and positioned on building rooftops where they are exposed to ambient environmental conditions. Test specimens are configured for interlaminar shear, flexure, compression and tension tests. Stressed and unstressed tension specimens are being exposed to assess the effects of sustained tensile load. Some specimens are unpainted to evaluate the effects of weathering on unprotected resin matrix materials, while other specimens are painted to evaluate protection afforded by standard aircraft paint. The materials being evaluated include several different graphite/epoxy and Kevlar/epoxy systems. Specimens are removed from the racks at intervals of 1, 2, 3, 5, 7, and 10 years to evaluate mass and mechanical property changes.

MOISTURE ABSORBTION DURING GROUND EXPOSURE

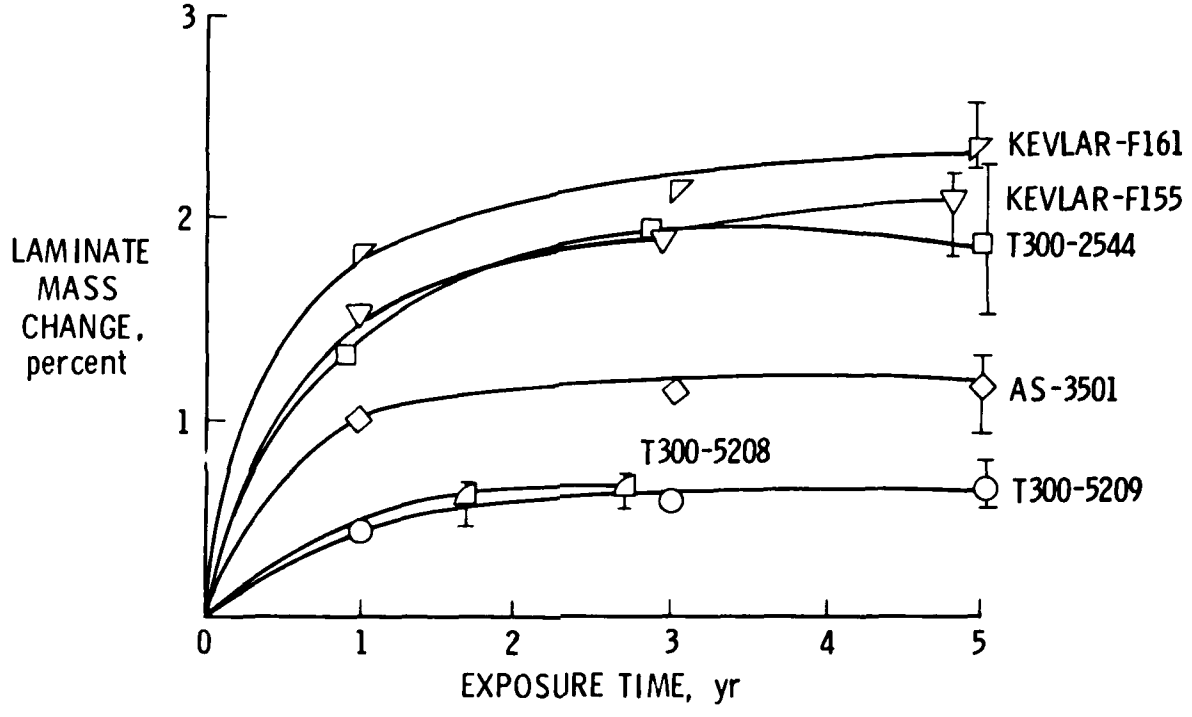

Figure 13

MOISTURE ABSORPTION DURING GROUND EXPOSURE

The moisture contents of four graphite/epoxy and two Kevlar/epoxy material systems after 5 years exposure at six exposure sites are shown in the figure. The data shown were obtained from flexure specimens that were exposed on outdoor racks located at Hampton, Virginia, San Diego, California, Sao Paulo, Brazil, Wellington, New Zealand, Honolulu, Hawaii, and Frankfurt, Germany. Each point plotted represents an average value for eighteen specimens, three at each of the six locations. The graphite/epoxy materials have stabilized after 5 years but the Kevlar/epoxy materials are apparently still gaining a slight amount of moisture. The Kevlar/epoxy materials and T300/2544 have moisture levels of about two percent. AS/3501 graphite/epoxy has a moisture content of about one percent, while T300/5209 and T300/5208 graphite/epoxy have moisture contents of about 0.5 percent. The low value in the 5 year scatter band, in all cases, represents specimens exposed in Frankfurt, Germany; the high value for all material systems except T300/5209 represents specimens exposed in Sao Paulo, Brazil. Additional moisture absorption data will be obtained after 7 and 10 years outdoor exposure.

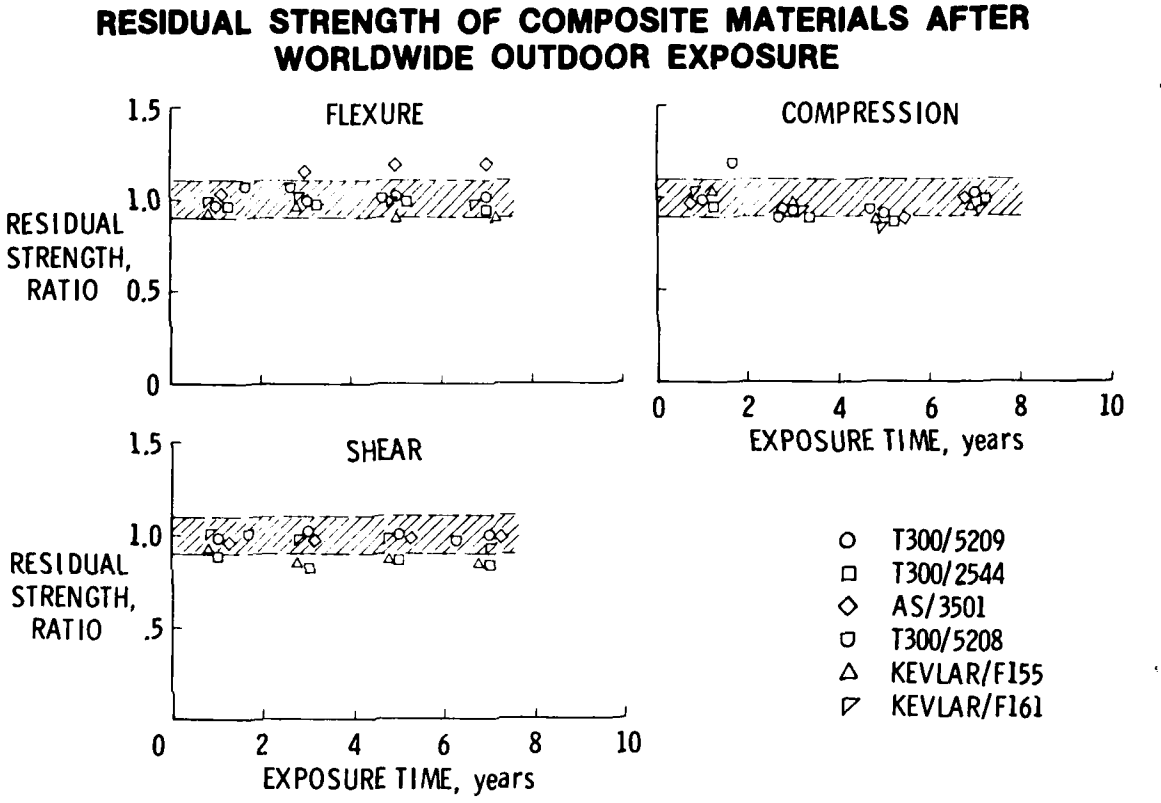

Figure 14

RESIDUAL STRENGTH OF COMPOSITE MATERIALS AFTER WORLDWIDE OUTDOOR EXPOSURE

Data obtained to date on specimens from four graphite/epoxy and two Kevlar/epoxy systems are shown in the figure. The data points represent a comparison of the average strength values at six exposure sites with the average baseline strength value for that material system. The shaded area represents a plus-or-minus ten percent scatter in the baseline strength values. Results of flexure tests indicate little or no degradation in strength over the 7 year exposure period. Compression strengths indicate a slight downward trend, but are still close to the baseline values after 7 years. Short beam shear strength is apparently influenced more by outdoor environmental exposure. The shear strengths for the T300/2544 graphite/epoxy and Kevlar/F-155 systems have dropped below the scatter band of the baseline test results. All the results presented in the figure are for unpainted specimens and several of the materials show evidence of surface deterioration due to solar radiation exposure. It is expected that the flexure strength will start to degrade as more matrix resin is leached away and more surface fibers become free. The data obtained to date confirm that the short beam shear strength tests are more sensitive to variations in matrix properties than the flexure or compression tests. One additional set of test specimens remains to be tested after 10 years outdoor exposure.

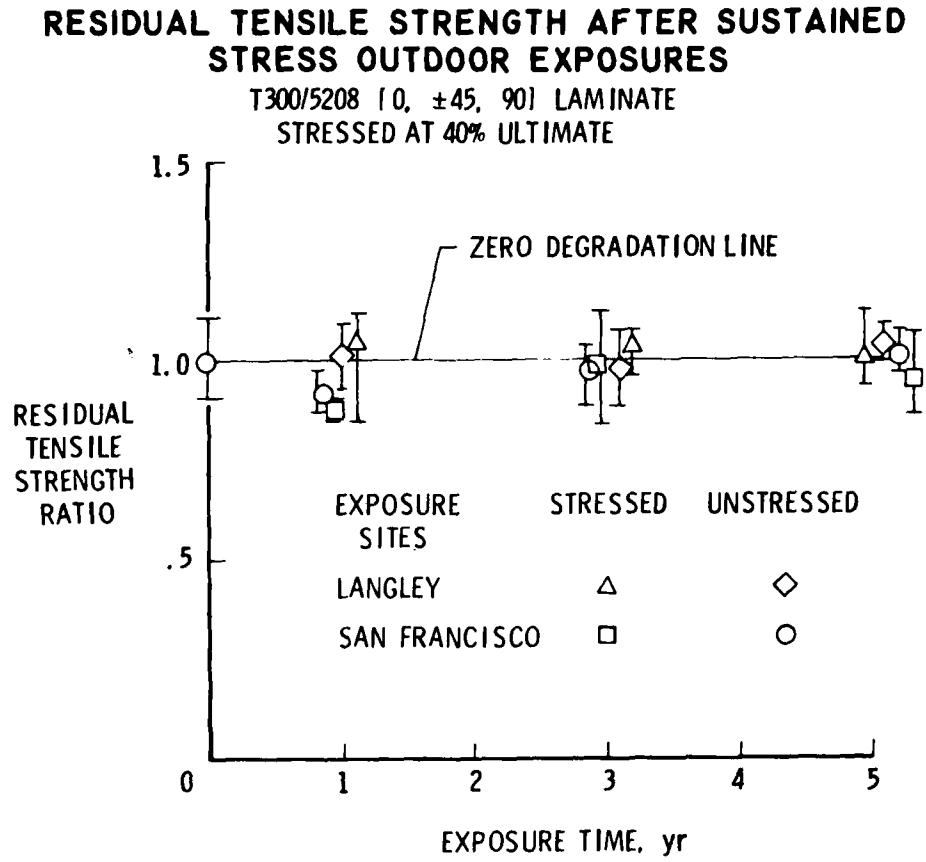

RESIDUAL TENSILE STRENGTH AFTER SUSTAINED STRESS OUTDOOR EXPOSURES

(Figure 15)

Effects of sustained stress during outdoor environmental exposure are evaluated by exposing tension specimens to 40 percent of ultimate baseline strength. Residual tensile strengths of T300/5208 quasi-isotropic laminated specimens, after 5 years outdoor exposure at the Langley Research Center and San Francisco, are shown in the figure. The residual tensile strength is within the scatter band for the strength of unexposed specimens. Results indicate that the T300/5208 quasi-isotropic tensile specimens were unaffected by either outdoor environment or sustained tensile stress at the two exposure sites indicated. Additional data will be obtained after 7 and 10 years outdoor exposure.

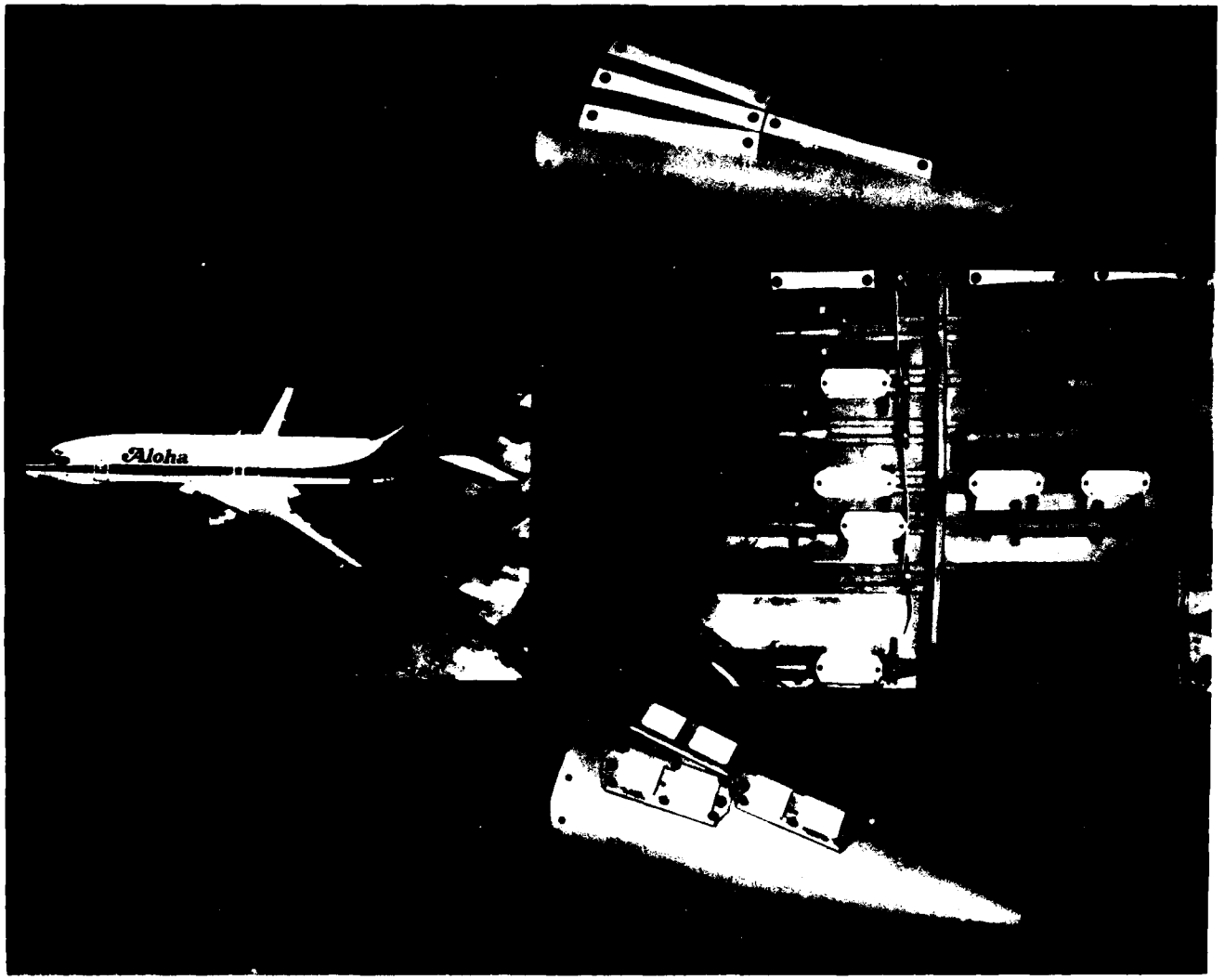

BOEING 737 FLIGHT ENVIRONMENTAL EXPOSURE

(Figure 16)

Composite specimens mounted on B-737 aircraft are exposed to ambient environmental conditions encountered during regional airline operation. Specimens installed on B-737 aircraft are shown in the figure. Specimens mounted externally on the flap track fairing are exposed to all ambient conditions including temperature, humidity, pressure, and solar radiation. Specimens mounted on the fairing upper surface receive somewhat more direct solar radiation then specimens mounted on the lower surface. Specimens mounted internally in an unpressurized aft-fuselage bay are exposed to temperature, moisture, and pressure variations but are shielded from solar radiation. Initially, a 2-year program was initiated to measure moisture absorption only. However, a more comprehensive 10-year program is currently underway to measure both moisture absorption and any strength changes due to exposure to normal airline operating environments. Specimens included in the program are flexure, short beam shear, and stressed and unstressed tension.

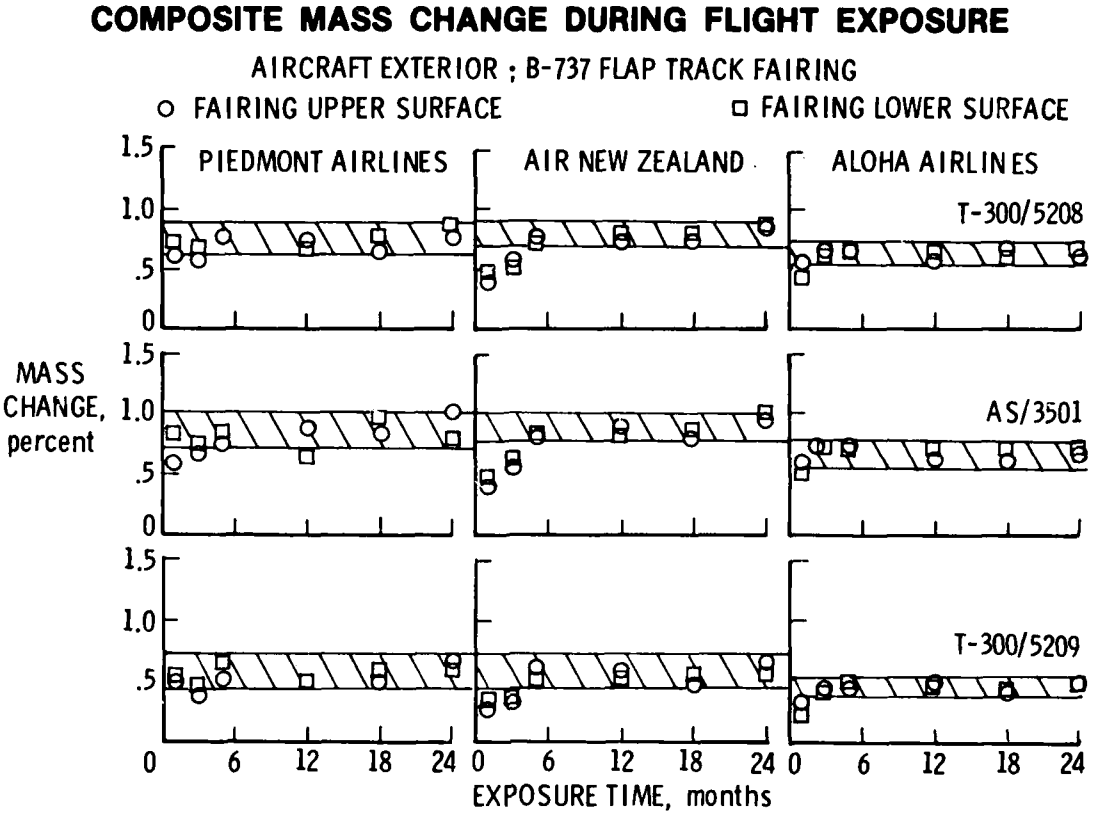

COMPOSITE MASS CHANGE DURING FLIGHT EXPOSURE

(Figure 17)

Mass changes of composite specimens during 2 years exposure on B-737 flap track fairings are shown in the figure. Data for three graphite/epoxy material systems exposed on three different airlines are presented. Piedmont Airlines' region of operation experiences wide seasonal temperature variations and high levels of relative humidity throughout the year. Air New Zealand experiences moderate temperature levels and a wide range of seasonal relative humidity levels. Aloha Airlines operates in high levels of temperature and relative humidity which vary only slightly throughout the year. The data obtained after 2 years exposure indicate that the specimens exposed on Piedmont and Air New Zealand Airlines have absorbed more moisture than the specimens exposed on Aloha Airlines for all three material systems. The bands drawn through the data indicate only slight changes in mass after the initial absorption during the first 6 months of exposure. There is essentially no consistent difference in moisture absorption for specimens exposed on the fairing upper surface or lower surface. In general, the moisture absorption results for flight exposure specimens correlate with moisture absorption data achieved for outdoor ground exposure specimens presented in a previous figure.

FLEXURE STRENGTH - LABORATORY MOISTURE EXPOSURE

EXPOSURE TEMPERATURE 322K

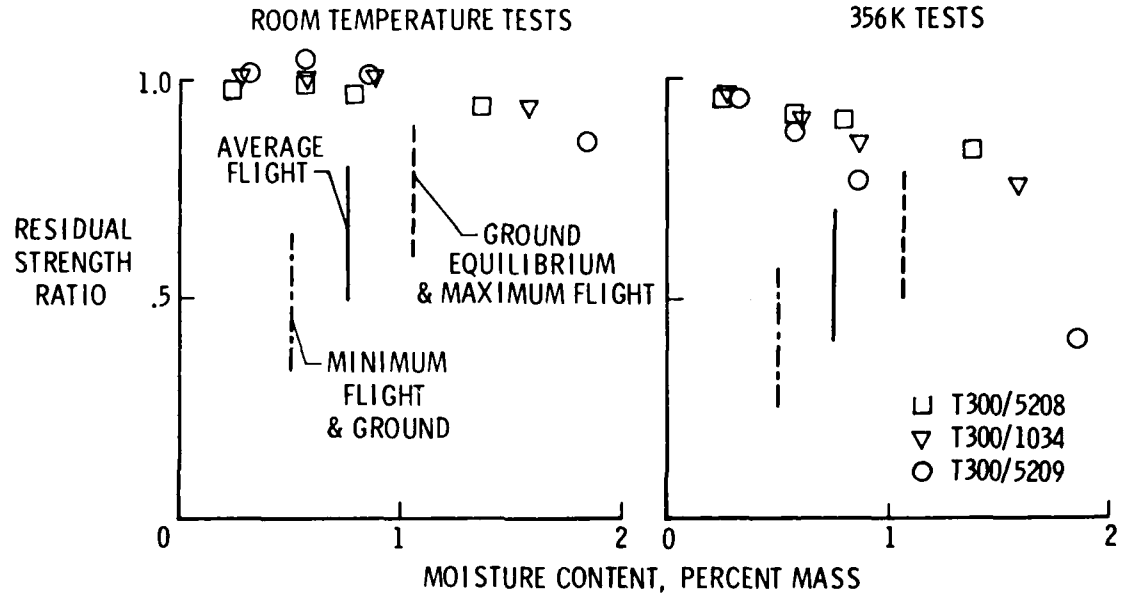

Figure 18

FLEXURE STRENGTH AFTER LABORATORY MOISTURE EXPOSURE

Composite specimens are being exposed to controlled laboratory environmental conditions for comparison with outdoor ground exposure and flight exposure. Results shown in the figure are for flexure specimens exposed at a temperature of 322K and various relative humidity levels to achieve the moisture contents indicated. To achieve moisture levels above one percent for the three material systems indicated, exposures to relative humidities of 75 percent and higher were required. At 95 percent relative humidity T300/5209 absorbed the most moisture, about 1.8 percent. Typical moisture levels for ground and flight exposure as discussed in previous figures are superimposed on the figure. These results show that laminate moisture contents of 0.5 to 1.0 percent experienced during ground and flight exposure did not affect the room temperature residual flexure strength. At moisture levels above 1.0 percent the flexure strength was reduced a modest amount at room temperature, about 15 percent for the T300/5209 material. For moisture absorption up to 1.0 percent the 356K residual flexure strengths were reduced a maximum of 24 percent. At moisture levels above 1.0 percent the 356K residual strengths were reduced from 15 to 60 percent, depending on the material system. As expected the T300/5209 material system, which is cured at 394K was affected the most by the combination of high moisture content and testing at elevated temperature.

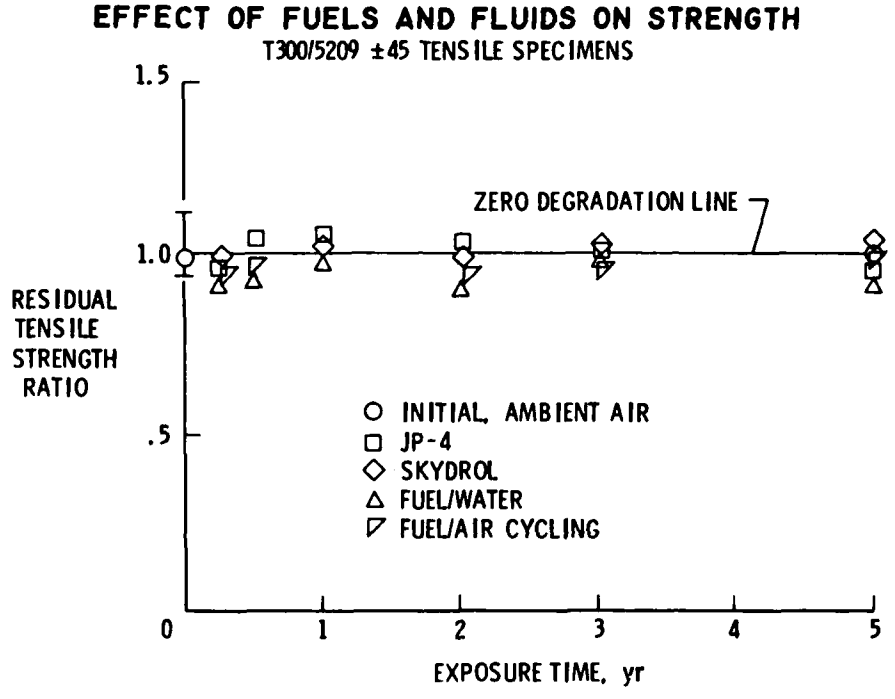

Figure 19

EFFECTS OF FUELS AND FLUIDS ON STRENGTH

Although aircraft composite structures are exposed almost continuously to various levels of moisture in the atmosphere, they are frequently exposed to various other fluids used in aircraft, such as fuel and hydraulic fluid. The effects of various combinations of these fluids on composite materials have been evaluated after 5 years of exposure. Residual tensile strengths of T300/5209 graphite epoxy specimens after exposure to JP-4, Skydrol, fuel/water mixture, and fuel/air cycling are shown in the figure. The greatest strength degradation, about 10 percent, resulted from exposure to a fuel/water mixture. Other materials T300/5208 and Kevlar/5209, were also tested and the fuel/water mixture was again the most degrading.

EFFECT OF FUEL/WATER MIXTURE ON TENSILE STRENGTH

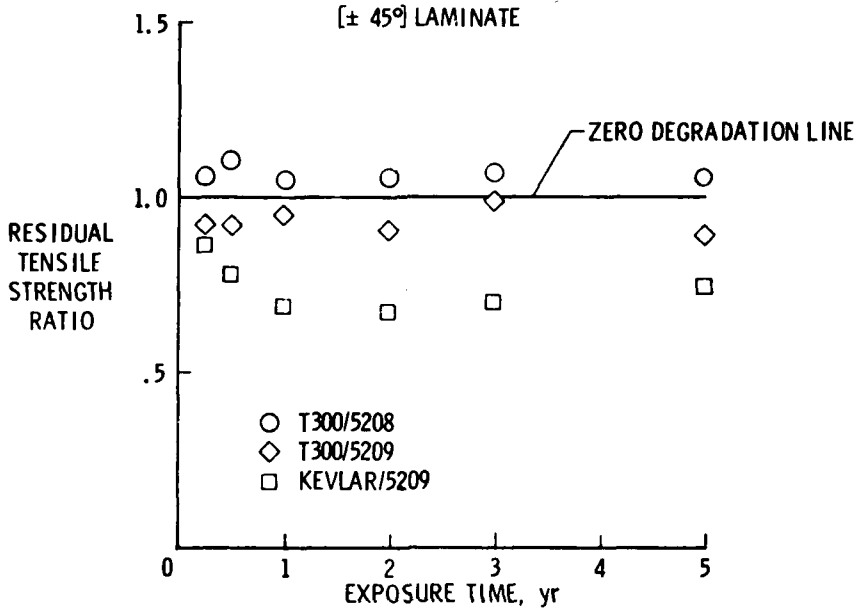

Figure 20

EFFECT OF FUEL/WATER MIXTURE ON TENSILE STRENGTH

As indicated in the discussion of the previous figure, the fuel/water mixture caused the largest reduction in the tensile strength of composite materials exposed to various fuels and fluids. The data shown in the figure are the residual tensile strengths for T300/5208, T300/5209, and Kevlar/5209 composite materials after 5 years of exposure to a fuel/water mixture. Tensile specimens were exposed such that the center of the specimens were at the interface of the fuel/water mixture. Also, bacteria common to fuel tank environments were placed in the test tank. The T300/5208 graphite/epoxy specimens were unaffected by the fuel/water mixture. The T300/5209 specimens lost about 12 percent of their baseline strength after 5 years of exposure and the Kevlar/5209 specimens lost up to 30 percent of their baseline strength during the 5 years of exposure. The strength loss for the Kevlar/5209 specimens occurred during the first year of exposure and remained essentially constant for the remaining 4 years. This result for the Kevlar/5209 is somewhat expected since the Kevlar fibers also absorb moisture. Results for bare Kevlar fibers immersed in water indicated a 15 percent reduction in fiber tensile strength after 5 years of exposure.

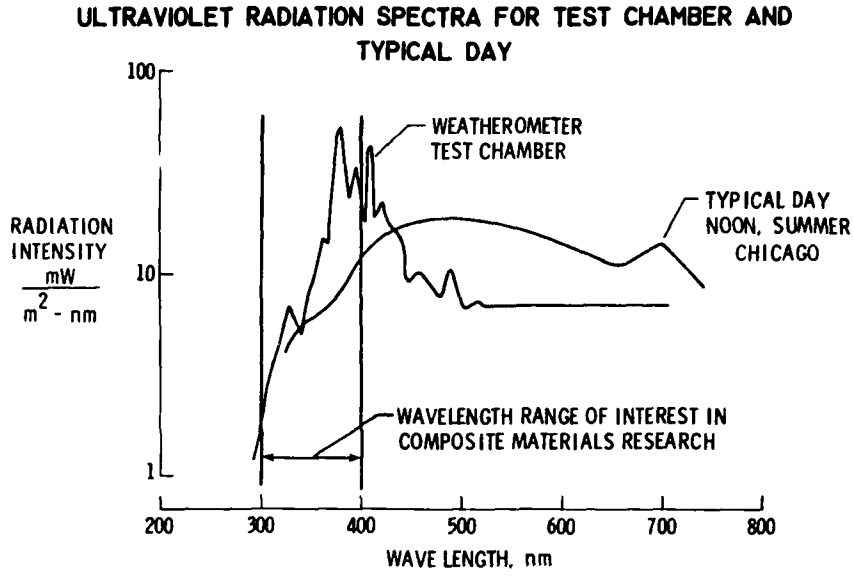

Figure 21

ULTRAVIOLET RADIATION SPECTRA FOR TEST CHAMBER AND TYPICAL DAY

Solar ultraviolet radiation is known to have a degrading effect on organic materials such as the resin matrices used in fiber composites. The effect is being evaluated by exposing composite materials outdoors to actual environmental conditions including sunlight, and to ultraviolet radiation produced in laboratory chambers. The radiation profile at noon for a typical summer day in Chicago and the profile generated by a weatherometer test chamber are shown in the figure. As indicated in the figure, the wavelength range of interest for composite materials research is 300-400 nm. In this range the weatherometer radiation profile is somewhat more intense than the typical Chicago day. Tests are underway to measure composite mass change as a function of exposure time.

EFFECT OF LABORATORY ULTRAVIOLET RADIATION ON GRAPHITE/EPOXY MASS CHANGE

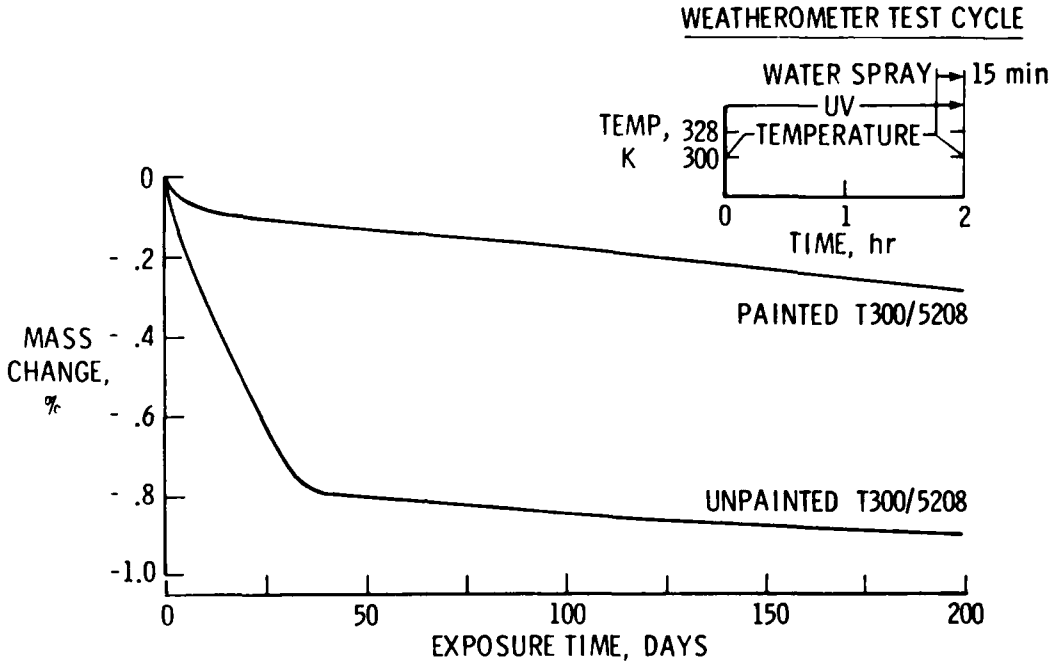

EFFECT OF LABORATORY ULTRAVIOLET RADIATION ON GRAPHITE/EPOXY MASS CHANGE

(Figure 22)

Results from exposing T300/5208 graphite/epoxy laminates to laboratory ultraviolet radiation are shown in the figure. The chamber test cycle is shown in the inset figure. During continuous ultraviolet exposure the temperature was maintained at 328K except for a 15 minute water spray impinging the specimens at the end of each two hour cycle, and a subsequent heatup period at the beginning of the following cycle. An unpainted specimen experienced a mass loss of about 0.8 percent during the initial 40 days of exposure. However, only a slight amount of additional mass loss occurred during the next 160 days of exposure. Apparently the initial mass loss is due to severe attack of the ultraviolet radiation on the outer layer of the matrix material. The leveling off of the mass loss indicates that the surface fibers are shielding the subsurface matrix material from further deterioration.

Specimens coated with a standard polyurethane aircraft paint lost only about 0.3 percent mass during 200 days of exposure. The mass loss is due to chalking and weathering of the paint layer. Obviously the paint provides significant protection to the surface of the graphite/epoxy material, indicating a need to keep graphite/epoxy composite structures painted during normal aircraft operation.

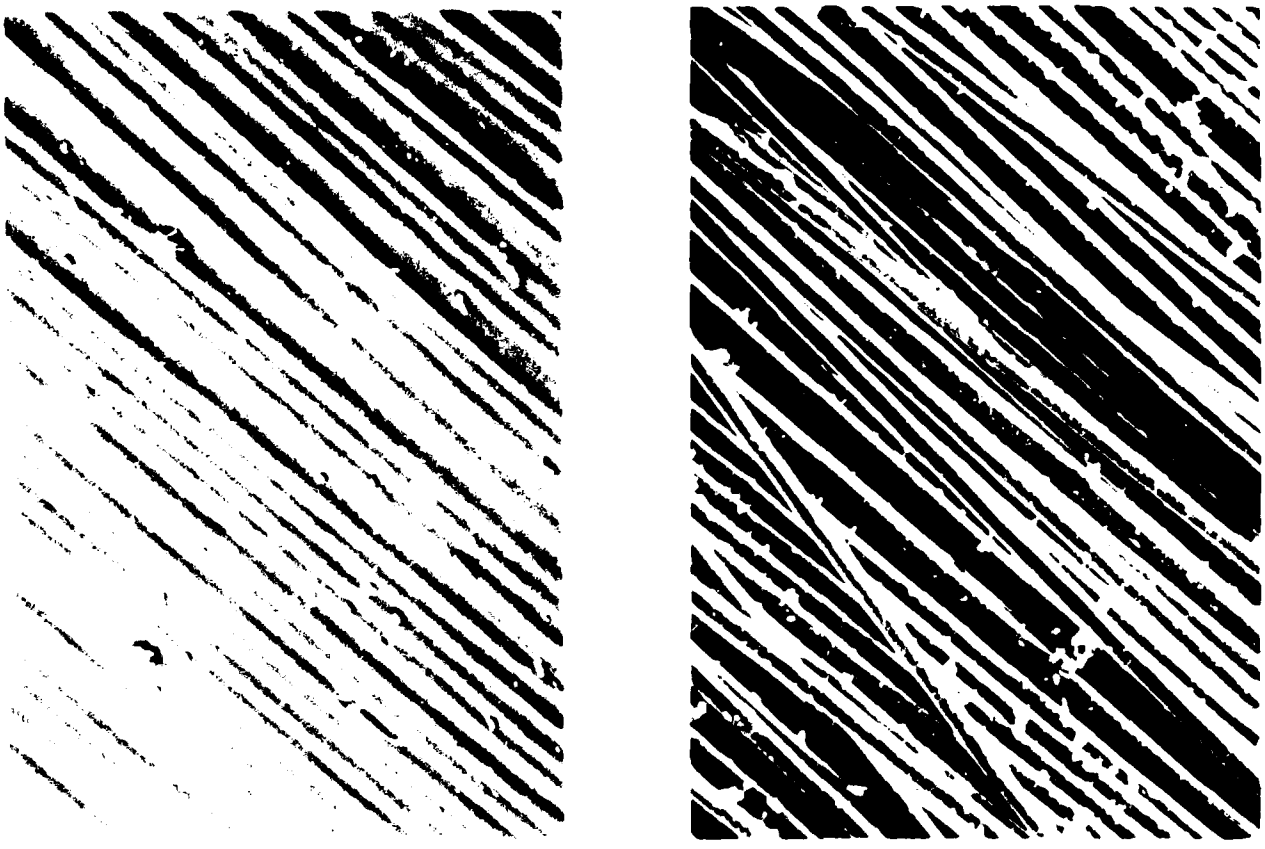

SURFACE DEGRADATION OF AS/3501 GRAPHITE/EPOXY

(Figure 23)

Scanning electron micrographs were taken of AS/3501 graphite/epoxy flexure specimens with no outdoor exposure and after 5 years of outdoor exposure. The micrograph shown on the left of the figure indicates that all the surface fibers are coated with resin for the specimen with no outdoor exposure. The micrograph shown on the right of the figure indicates that the surface fibers are no longer coated with resin after 5 years of outdoor exposure. The 5 years of weathering has removed the outer layer of resin and bare graphite fibers are visible.

As with the controlled laboratory weatherometer results, these micrographs substantiate the need to keep graphite/epoxy composite aircraft structures painted to prevent ultraviolet radiation damage to composite matrix materials.

CONCLUDING REMARKS

- EXCELLENT IN-SERVICE PERFORMANCE AND MAINTENANCE EXPERIENCE HAVE BEEN ACHIEVED WITH OVER 150 COMPOSITE COMPONENTS DURING 8 YEARS AND OVER 2 MILLION HOURS OF FLIGHT SERVICE
- NO SIGNIFICANT DEGRADATION HAS BEEN OBSERVED IN RESIDUAL STRENGTH OF COMPOSITE COMPONENTS OR ENVIRONMENTAL EXPOSURE SPECIMENS AFTER 7 YEARS SERVICE OR EXPOSURE
- CONFIDENCE DEVELOPED THROUGH NASA SERVICE EVALUATION, ENVIRONMENTAL TESTING, AND ADVANCED COMPOSITE COMPONENT DEVELOPMENT PROGRAMS HAS LED COMMERCIAL TRANSPORT AND HELICOPTER MANUFACTURERS TO MAKE PRODUCTION COMMITMENTS TO SELECTED COMPOSITE COMPONENTS

Figure 24

CONCLUDING REMARKS

The NASA Langley Research Center has sponsored design, development, and flight service evaluation of more than 150 composite aircraft components. Excellent in-service performance and maintenance experience have been achieved during 8 years and over 2 million hours of flight service. No significant degradation has been observed in residual strength of composite components or environmental exposure specimens after 7 years service or exposure. Results obtained to date indicate that composite surfaces must be painted with standard aircraft polyurethane paint to protect the matrix from ultraviolet degradation. Test results also indicate that Kevlar/epoxy composites absorb more moisture than most widely used graphite/epoxy composites and a larger reduction in residual strength results for the Kevlar composite systems.

Confidence developed through NASA sponsored service evaluation, environmental testing, and advanced composite component development programs has led commercial transport and helicopter manufacturers to make production commitments to selected composite components.

SURFACE CHARACTERIZATION OF GRAPHITE FIBERS

Lawrence T. Drzal

Mechanics & Surface Interactions Branch
Air Force Wright Aeronautical Laboratories
AFWAL/MLBM
Wright-Patterson Air Force Base
Dayton, Ohio 45433

ABSTRACT

Fiber-matrix adhesion has been shown to be a controlling parameter in composite performance. Various techniques are available for fiber surface characterization, but each by itself is incapable of predicting fiber-matrix adhesion or composite mechanical properties.

Recent work at this laboratory on graphite fibers has shown that application of a number of surface characterization techniques must be applied to provide the required information. These techniques and the information they provide are: Surface Spectroscopics - atomic and molecular information; Thermal Desorption - quantification of material desorbed from the fiber surface during the processing of cycle; Surface Energetics - measurement of the efficacy of surface groups in air; Single Filament Measurements - quantification of interfacial strength, fracture mode and fracture energy; Microtomy and Microscopy - determination of locus of failure and fracture path.

Properly combined, these techniques can provide the methodology to characterize fiber surfaces in the context of composite performance.

BACKGROUND

The use of composite materials in aerospace applications is increasing because of the significant weight, cost and design advantages these materials have over conventional structural materials. To a first approximation, composite properties depend on the properties of the individual components themselves. However, as the degree of sophistication of the aircraft designer increases, composite applications will be extended to a realm where current materials will not operate effectively. This results in a two fold requirement. First, composite properties which do not depend exclusively on the properties of the reinforcement ie.off-axis properties, are becoming important in composite structural design. Second, new generations of composite materials are required where different fibers or matrices are needed to extend the operating environment of existing composites. In order to answer these needs a fundamental understanding of the fiber-matrix interface as well as structure-property relationships for the fiber and matrix are necessary.

The juncture that exists when the matrix and fiber come together in composite materials is a three dimensional interphase rather than a two dimensional boundary. The complexity of this region can best be illustrated with the use of a schematic model which allows the potential important characteristics of this region to be identified as shown in Figure 1. [1]

The interphase exists from some point in the fiber where the local properties begin to change from the fiber bulk properties through the interface into the matrix where the local properties again equal the bulk properties. Components of this region can be identified. The fiber may have morphological variations near the fiber surface which are not present in the bulk of the fiber. The surface area of the fiber can be much greater that its geometrical value because of pores or cracks present on the surface. The atomic and molecular composition of the fiber surface can be quite different from the bulk of the fiber. Surface treatments can add surface chemical groups and remove the original surface giving rise to a chemically and structurally different region. Exposure to air before composite processing can result in the adsorption of chemical species which may alter or eliminate certain beneficial surface reactivity. These adsorbed materials may also desorb at the increased temperatures seen in composite fabrication and be a source of volatiles which disrupt the interface if not removed. Thermodynamic wetting of the fiber surface by the matrix is a necessary condition for fiber-matrix adhesion and is determined by the free energies of the components. Both chemical and physical bonds exist at the interface and the number and type of each strongly influences the interaction between fiber and matrix. The structure of the matrix near

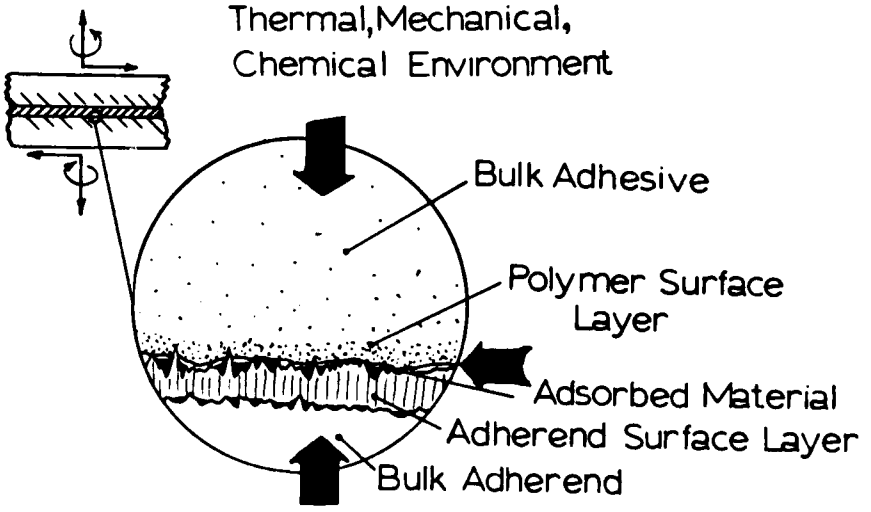

FIGURE 1. Schematic Model of the Fiber-Matrix Interphase

the fiber surface can be influenced. Changes in reactivity due to adsorption of matrix components can alter the local morphology. Unreacted matrix components and impurities can diffuse to the interphase region altering the local structure.

Each of these phenomena can vary in magnitude and can occur simultaneously in the interphase region. Depending on the system the interphase itself can extend from a few to a few thousand Angstroms in depth. The structure of this region can have profound effects on the performance of the composite in terms of its mechanical strength, chemical and thermal durability. Likewise the exact nature of this region must be understood if accurate life prediction models are to be developed. Because of the complexity of this region a need for a multidisciplinary approach must be recognized. Only when the exact nature of this region is understood will the interphase be considered as a material variable to be optimized in composite performance.

This paper presents the results of a program undertaken after recognition of the multidsiciplinary nature of the composite interphase. It is directed at developing the molecular understanding of the graphite fiber-epoxy interphase and the role of graphite fiber surface treatments in promoting fiber-matrix adhesion in composite materials.

EXPERIMENTAL

GRAPHITE FIBERS. Two graphite fibers were chosen as the representative fibers for this study. Both fibers were made from polyacrylonitrile and have mechanical properties which represent the practical extremes for fibers being used in composite materials today. One fiber was graphitized at 1500 C and was designated as a type A fiber. The other was graphitized at 2600 C and was designated a type HM fiber. The mechanical properties of these two fibers are listed in Table 1.

Table 1.

Mechanical Properties of A and HM Fibers

Fiber	Tensile Modulus (psi)	Tensile Strength (psi)
A	35,000,000	425,000
HM	51,000,000	350,000

The main structural elements of the fibers are graphitic ribbons which are oriented roughly parallel to the fiber axis. These ribbons are formed of graphitic crystallites which increase in size with increasing graphitization temperature(ie. 13 graphitic layers and 40 A wide for the 1500 C type A fiber to 20 layers thick and 70 A wide for the ~600 C type HM fiber.) The ribbons twist and undulate along the fiber axis as shown schematically in Figure 2. The A fiber has less alignment and more twisting of the fibrils.

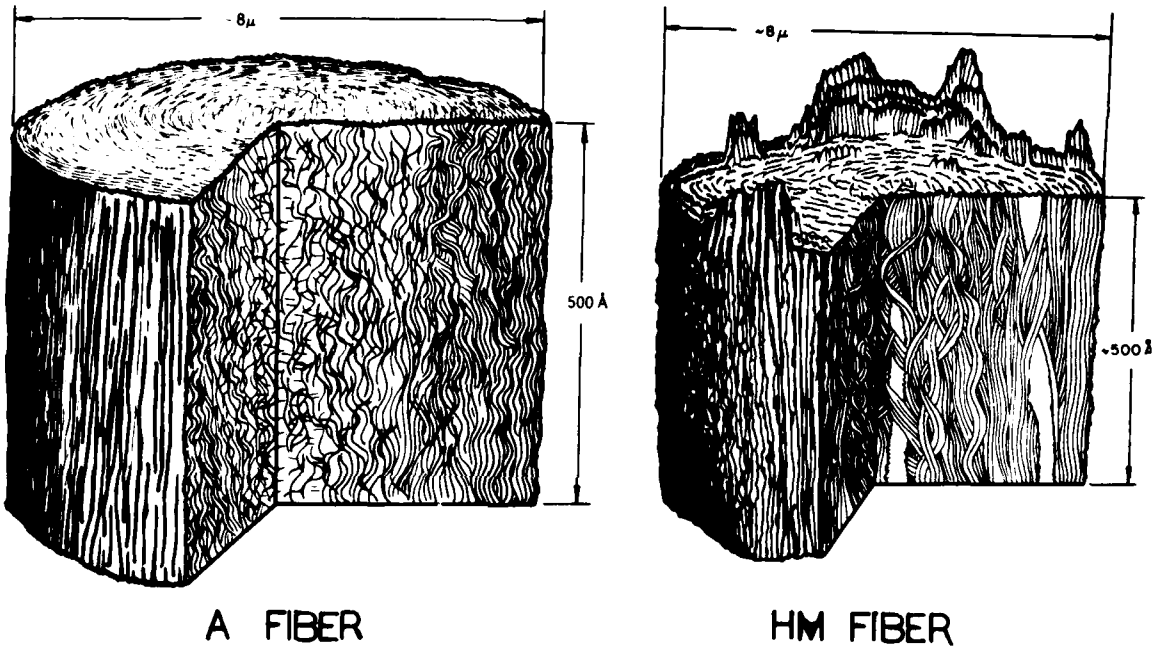

FIGURE 2. Schematic Diagram of the A and HM Fibers

This would produce a surface having not only graphitic basal planes but also corners and edges of the crystallites. The degree of order in the HM fiber is greater because of the higher graphitization temperature. The fibrils are well aligned and the surface of this fiber would be expected to have more basal planes and less corners and edges of the crystallites. Detailed discussions of the structure of the fibers are available in the literature.[2]

These fibers were supplied by the manufacturer without any surface treatment and with the surface treatment designed to improve graphite fiber adhesion to epoxy matrices. [3]. The surface treated fibers are designated AS and HMS and the untreated fibers are designated AU and HMU. Any other fiber treatment was completed by the investigators and is noted by a symbol appearing after the fiber type.

MATRIX RESIN. A model epoxy system was chosen as the matrix for this study. EPON 828 [4] which is a diglycidal ether of bisphenol-A was combined with meta phenylene diamine

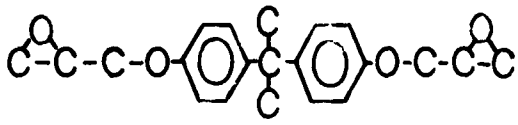

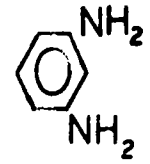

(mPDA) at 14.5 phr. The mixture was vacuum outgassed for two minutes during which time the evolution of bubbles diminished. The mixture was then cured in a closed oven for two hours at 75 C and two hours at 125 C followed by an overnight slow cooldown. The cured system has a tensile modulus of about 400,000 psi and a tensile strength of about 11,000 psi.

SURFACE SPECTROSCOPY. X-ray Photoelectron Spectroscopy (XPS) or ESCA was chosen to provide atomic and molecular information about the graphite fiber surfaces selected for this study. XPS has the potential for providing this information without significantly altering the fiber surface while it is being analyzed because of the small energy flux directed to the surface. In addition a semi-quantitative estimate of the surface concentration can be made.

Samples of graphite fibers were carefully cut and aligned in nickel holders. A mask was placed over the fibers to mechanically hold them in place in the spectrometer. A Physical Electronics [5] model 15-255G double pass cylindrical mirror analyzer was used for the analysis. The vacuum system which housed the unit operated at 1x10exp-9 Pa without bakeout. Both Aluminum and Magnesium anodes were used as the X-ray source. The analyzer was operated in the retarding mode with pass energies of 1,2 or 4 eV. Surface concentrations were calculated by measuring peak areas above background for the element of interest, correcting for elemental sensitivities and normalizing.

SURFACE AREAS. Krypton Adsorption at temperatures between 100 and 120 K was used to determine the graphite fiber surface area and the change in area with surface treatment. The entire adsorption isotherms were measured from less than one percent surface coverage to well beyond the monolayer point. B.E.T. analysis was used to estimate the surface areas.[6] For the graphite fibers used in this study , surface areas of about one-half square meter per gram could be measured accurately to a few percent. Since the krypton molecule has an area per molecule of twenty square Angstroms at these temperatures, surface area estimations by this method are potentially capable of detecting surface features on the order of ten Angstroms.

THERMAL DESORPTION. Every surface adsorbs material from exposure to the environment. Consequently the results of a surface analysis completed in vacuum must be related to the surface after equilibration in air. Furthermore the ease with which the adsorbed material can be removed from the surface must be determined. Adsorbed components which can be desorbed at moderate temperatures could become sources of interfacial bubbles during composite fabrication which in turn could disrupt the interface. Therefore it is important to measure the quantity and composition of the desorbed material and the temperature at which it is removed.

The amount and composition of the thermal desorption products removed from the surfaces of the graphite fibers used in this study were measured at temperatures between 20 and 300 C. The desorbate was trapped in a closed volume held at elevated temperature, the resulting pressure rise was measured, and the material was slowly leaked past a UTI-100C [7] mass spectrometer where its composition was determined. The amount of material desorbed was converted to equivalent monolayers and mole percent for comparison.

SURFACE FREE ENERGY. A necessary condition for fiber and matrix compatability is thermodynamic wetting. This quantity can be measured through determination of the contact angle between fiber and matrix. Further insight into the specific interactions at the interface can be obtained by measuring the contact angle of a variety of liquids on the fiber surface each having different ratios of their polar to dispersive components of their surface free energies. Interaction should be at a maximum for a polar surface interacting with a polar matrix. Likewise since the contact angle measurements to measure surface free energy ratios are completed in air, this technique measures the efficacy of the surface groups in increasing surface free energy even after exposure to air.

Contact angles of eight liquids were measured on the graphite fibers used in this study. Because of the small diameter of the graphite fibers, the contact angles were measured gravimetrically. A single fiber was fixed to the end of the arm or a Cahn [8] RG microbalance. The liquid of interest was raised on a movable platform up to the fiber. At the instant the fiber makes contact with the liquid an increase in force is detected by the microbalance due to the wetting of the fiber by the liquid. The force measured (F) is equal to the surface tension (γ) of the liquid times the perimeter of the fiber (πd) times the cosine of the contact angle ($\cos \theta$).

The cosine of the contact angle could be easily determined from this equation after the fiber diameter was measured.

The eight liquids chosen for this study ranged from very polar to nonpolar. The liquids used and their polar and dispersive components of the surface free energy are listed in Table 2.

Table 2.

Surface Free Energy Components of Contact Angle Liquids

Liquid	γ (mJ/m)	γ^d (mJ/m)	γ^p (mJ/m)
water	72.8	21.8	51.0
glycerol	64.0	34.0	30 0
ethylene glycol	48.3	29.3	19 0
propylene glycol	31.3	24.5	6.8
formamide	58.3	32.3	26.0
n-hexadecane	27.6	27.6	0.0
methylene iodide	50.8	48.4	2.4
bromonaphthalene	44.6	44.6	0.0

The polar and dispersive components of the fiber surfaces are determined with the use of equation 2 where the subscripts L and S refer to the liquid and fiber respectively.

$$\gamma_L(1+\cos\theta)/2\gamma_L^{d^{1/2}} = \gamma_S^{d^{1/2}} + \gamma_S^{p^{1/2}}(\gamma_L^p/\gamma_L^d)^{1/2} \qquad (2)$$

A plot of $\gamma_L(1+\cos\theta)/2\gamma_L^{d^{1/2}}$ versus $(\gamma^p/\gamma^d)_L^{1/2}$ will yield a straight line with the slope and intercept providing a solution for the polar and dispersive components of the surface free energy for the fiber of interest. [9]

INTERFACIAL SHEAR STRENGTH. The desired goal of this research is the relationship between the molecular changes at the fiber-matrix interface and the effect on fiber-epoxy adhesion. It is possible to evaluate this relationship through composite testing. However, the packing density of fibers, testing configuration and change in mode of failure with surface treatment make interpretation of composite test results difficult. Fiber pull-out tests are difficult to conduct with these small brittle fibers. A single filament interfacial shear strength test supercedes these afore mentioned difficulties and provides a mechanical parameter sensitive to interfacial properties alone which can be used for characterizing each fiber-matrix combination. [10].

The method for measuring the fiber-matrix interfacial shear strength involves encapsulating a single graphite fiber in an epoxy tensile coupon, stressing the coupon to near its point of fracture and then measuring the graphite fiber fragment lengths inside of the specimen. Since the graphite fibers have a low strain to failure they will fracture within the coupon because of the stress transferred to them by the shear transfer at the fiber-matrix interface. However the fragments will approach a lower limit in length ℓ_c, which is dependent on the the fiber fracture strength (σ_f), the fiber diameter (d) and the interfacial shear strength (τ). These variables can be related through the expression

$$\tau = \frac{\sigma_f}{2} \frac{d}{\ell_c} \qquad (3)$$

In practice a distribution of lengths is measured and Weibull statistics are used to evaluate the mean value of the critical length.[11]

MODE OF FAILURE. A single parameter like the interfacial shear strength is of limited value when the mode of failure between fiber and matrix is changing. Additional insight can be gained however by observing the interfacial shear strength test with transmitted polarized light with the aid of a microscope. The highly stressed polymer near the ends of the fiber fragments is birefringent and pronounced changes in the micrographs of this region occur with each fiber-matrix combination. The change in this pattern with increasing sample strain gives much insight into the failure process at the interface.

RESULTS

THERMAL DESORPTION. The total amount of material desorbed from the AU and AS fiber surfaces during exposure to increasing temperature is shown in Figure 3. The composition of the desorbate as a function of temperature is shown in Figure 4. It is obvious that a much larger amount of volatiles are produced from the AS fiber than from the AU fiber under the same conditions. This amount of material is driven off at moderate temperatures well within the processing window for many composites. The molecular composition of the desorbate can also be a cause for concern. Water, carbon monoxide and carbon dioxide are volatilized from both fibers and might serve as void generators within the composite if not properly removed.

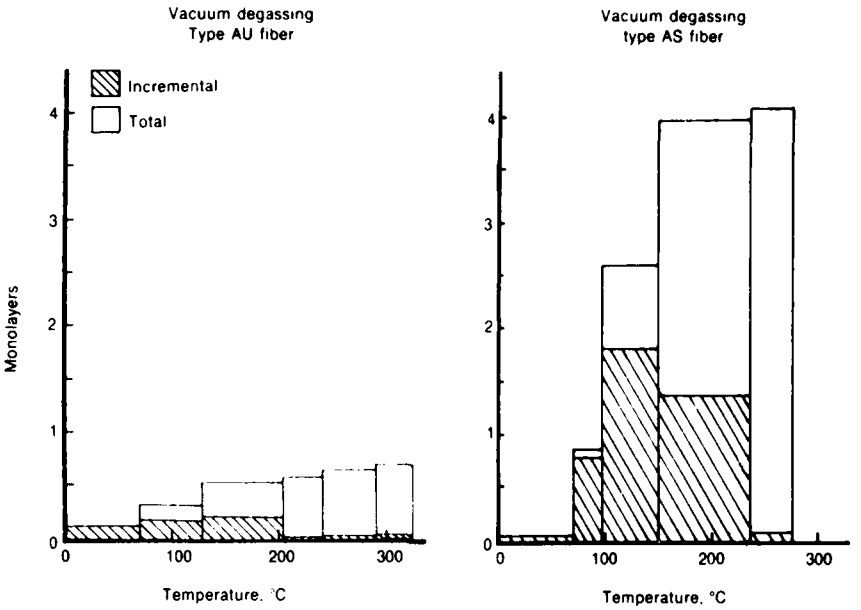

Figure 3. Amount Desorbed as a Function of Temperature

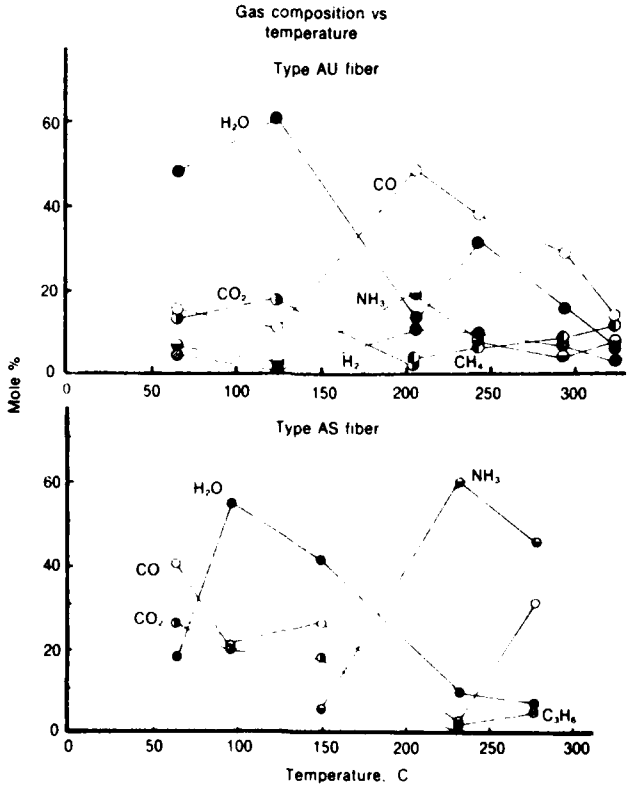

Figure 4. Desorbate Composition as a Function of Temperature

The HM fibers display similar trends. Figure 5 shows the total amount of material desorbed while Figure 6 shows the composition of the desorbate as a function of temperature. For the HM fibers the surface treatment does not cause more volatiles to be desorbed than for the untreated fiber. The major constituents are again water, carbon monoxide and carbon dioxide although the ratio varies with the fiber.

For both types of fiber the material desorbed at temperatures up to 200 C are characteristic of weakly bound physisorbed material. Above this temperature the new species which are desorbed reflect the molecular composition of the fiber surface although the quantity of material is very small.

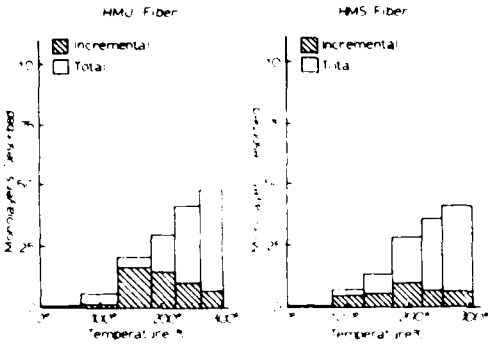

Figure 5. Amount Desorbed as a Function of Temperature

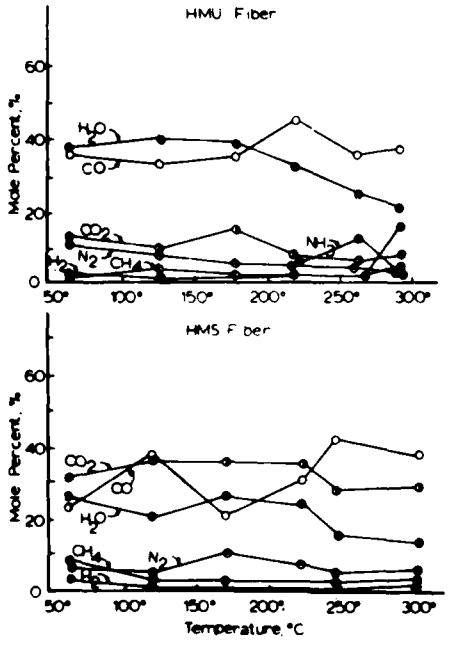

Figure 6. Desorbate Composition as a Function of Temperature

Surface Areas. The surface areas of these graphite fibers determined by krypton adsorption at 104 K and 115 K are tabulated and displayed in Table 3.

Table 3.

Surface Areas of A and HM Graphite Fibers

Fiber	Area(sq m/gm)
AU(VHT)	0.44
AU(AIR)	0.44
AS(VHT)	0.49
AS(AIR)	0.44
HMU(VHT)	0.51
HMS(VHT)	0.51
HMS(AIR)	0.51

These results indicate that no significant increase in surface area has taken place with surface treatment for either the A fiber or the HM fiber.[12,13]

Surface Composition. ESCA analysis of the surfaces of these fibers allows a semi-quantitative estimate to be made of the percent of each surface constituent. The results for the fibers and the subsequent treatments are listed in Table 4.

Table 4.

ESCA Determination of Fiber Surface Composition

Fibers	C	O	Na	N	S
AU	86	9	3	2	-
AS	70	20	4	7	-
AS(300 C VHT)	72	18	6	3	-
AS(600 C VHT)	84	7	5	3	1
AS(750 C/H VHT)	94	3	1	1	1
HMU	95	5	-	-	-
HMS	89	9	-	-	-
HMS(300 C VHT)	97	3	-	-	-

The data indicate the surface chemical changes taking place with surface treatment. The A fiber surface oxygen content more than doubles and the nitrogen content more than triples with surface treatment going from the AU to the AS. Subsequent elevated temperature treatments in vacuum and with hydrogen(H) remove the surface oxygen and nitrogen. The

exposure to higher temperature also causes a small increase in the amount of surface sulphur detected by ESCA. The sodium detected as well as the sulphur are residual from the spinning agents used in the original PAN fiber processing. The increase in surface sodium content with temperature demotes its ability to migrate to the surface with small increases in temperature. The bulk concentration of sodium is only a thousand parts per million so that its concentration on the surface is much higher than expected and should be indicative of its surface activity and perhaps deleterious presence at the interface. The highest temperature treatment with hydrogen successfully removes almost all of the elements except for a small amount of oxygen.

The HM fiber also undergoes an increase in surface oxygen with surface treatment(ie. HMU to HMS) by about a factor of two. No other elements were detected in significant quantities on the HM surfaces. Thermal vacuum treatment at temperaturs of 300 C are effective in removing the oxygen species from this surface also.

Molecular information was experimentally difficult to obtain for these fibers using the ESCA data alone. A series of chemical derivitizations are being conducted to elucidate the exact chemical nature of these surface species and their changes with surface treatment.

Surface Energetic Measurements. The contact angles of the liquids listed in Table 2 were determined for the fibers in this study and the results were analyzed according to equation 2. The polar and dispersive components of the fiber surface free energy as well as the total surface free energy are listed in Table 5.

Table 5.

Graphite Fiber Surface Free Energy Components

Fibers	γ^p(mJ/m)	γ^d(mJ/m)	γ(mJ/m)
AU	24	27	51
AS	30	26	56
AS(300 C VHT)	27	26	53
AS(750 C/H VHT)	12	32	44
HMU	8	33	41
HMS	21	28	49
HMS(300 C VHT)	13	30	43
Matrix			
Epon 828/mPDA	12	29	41

Again a change is noted for the surface treated fibers over the untreated fibers. The total surface free energy increase for both the AS and HMS fibers with surface treatment. This change occurs in the polar component of the surface free energy. The dispersive component remains about the same. ESCA had detected an increase in oxygen and nitrogen for the surface treated fibers. The thermal vacuum treatments have reduced the polar component of the surface free energy and this was coupled with a decrease in the surface species as detected by ESCA.

The total surface free energy for each fiber is greater than or equal to that for the epoxy used in this study so that fiber wetting by the matrix should occur.

The dependence of polar surface free energy component on composition is seen in the graph of Figure 7. Here the polar component of the surface free energy is plotted against the percent surface oxygen as determined by ESCA. (Nitrogen and sodium values were not used in this plot because their operation either separately or associated with the surface oxygen content has not yet been determined. Their inclusion would only shift the curve and would not change the basic relationship.) This graph illustrates not only the dependence between surface polarity as measured by contact angles in air with a vacuum determination of surface composition but also the fact that even after air exposure and equilibration with the environment the surface species are still exerting a strong polar influence.[14].

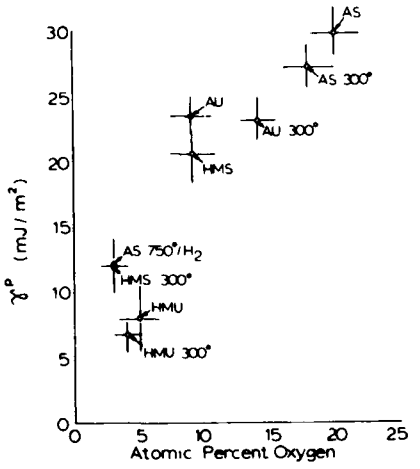

Figure 7. Plot of γ^p versus Percent Surface Oxygen.

Interfacial shear strength. The values for the interfacial shear strength were tabulated according to equation 3 and the results are listed in Table 6.

Table 6.

Interfacial Shear Strength

Fiber	(psi)
AU	3774
AS	10550
AS(300 C VHT)	5614
AS(750 C/H VHT)	8316
HMU	2090
HMS	3740
HMS(300 C VHT)	3032

The interfacial shear strength increases with fiber surface treatment and decreases with removal of surface species . For the A fiber there is a two and one-half fold increase in interfacial shear strength while for the HM fiber there is a two fold increase. The thermal vacuum treatments which change the fiber surface chemistry and surface polarity also reduce the values attainable for the interfacial shear strength for these fibers. It should be noted however that the value measured on the reduced fibers was still greater than expected based on a surface chemical effect alone.

Photoelastic Observation. The single fiber samples used in the interfacial shear strength analysis were observed under increasing strain on a microscope stage with transmitted polarized light. Micrographs were recorded at increasing levels of strain. Qualitative differences could be observed between different fibers in the same matrix. Figure 8 is a compilation of micrographs for the AU, AS, HMU and HMS fibers at 1 and 5 percent strain.

The photoelastics stress pattern shown in the micrograph at 400x for the AU fiber displays some features which change with surface treatment. For example at low strains immediately after the fiber breaks, a highly stressed area appears around the fiber ends at the break. For the AU fiber this stressed region rapidly encompasses the whole fragment as the strain on the specimen is increased. At the same time the separation between the fiber fragments at the break increases indicating that the fiber matrix adhesion in shear is not of sufficient magnitude to prevent the fragments from sliding in the matrix. The alternating light and dark areas in polarized light indicate that some regions on the fiber surface are exhibiting high shear transfer while others are not.

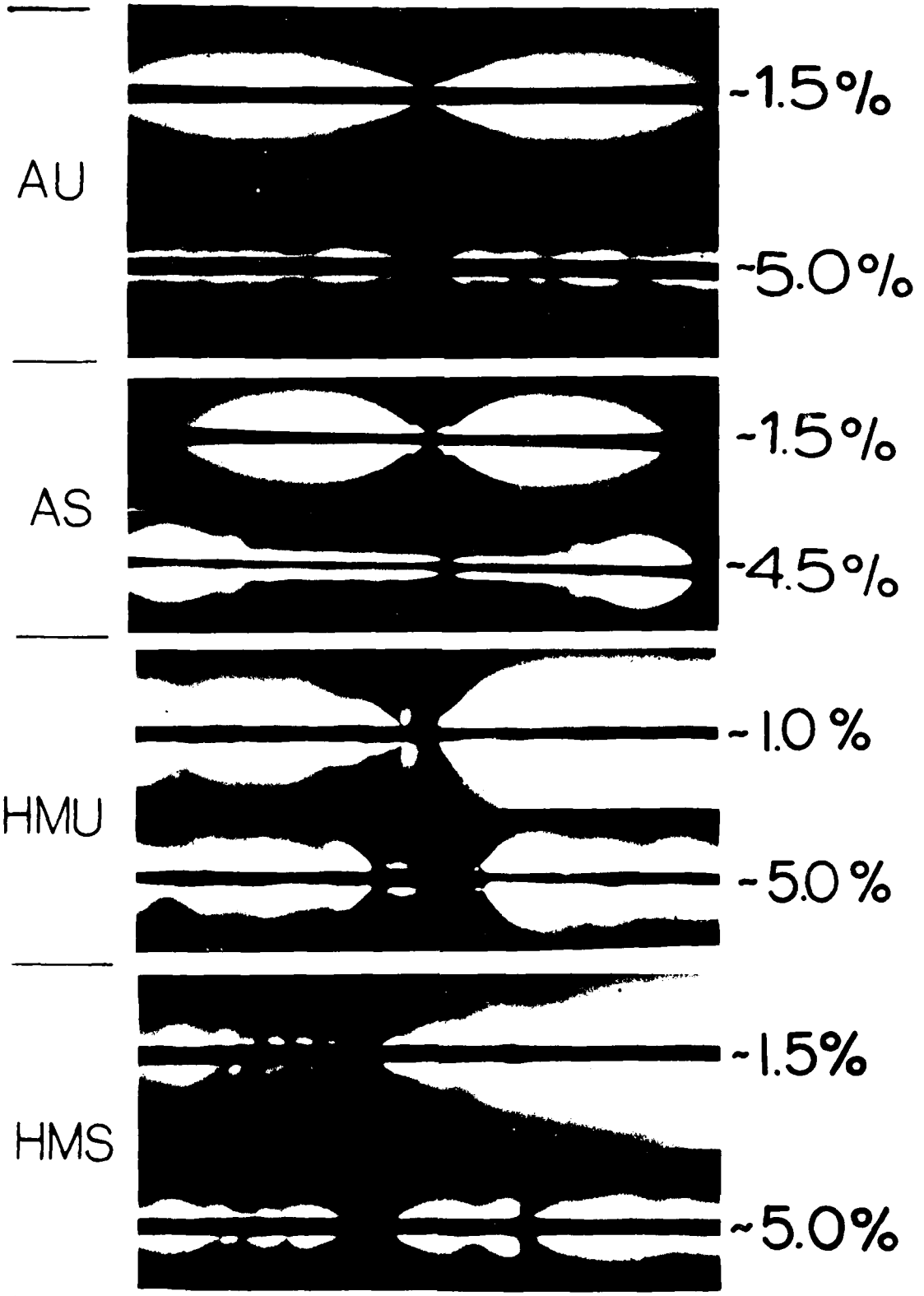

Figure 8. 400x Polarized Light Micrographs of Fibers under Stress

The micrograph for the AS fiber shows differences in these features which reflect the different response to stress at the interface. For the AS fiber in the epoxy matrix, the highly stressed area at the fibe ends immediately after the fibe breaks is more intense and confined to a smaller region. With increasing sample strain this concentrated stressed area moves away from the fiber ends toward the center of the fiber fragment. The region ahead of this area is not photoelastically active indicating that much lower stresses are present there. The region between the advancing front and the fiber end exhibits some residual photoelastic behavior confined to a region within a fiber diameter of the fiber surface in the matrix. The shear adhesion between the fiber and matrix is much higher in this case and there is no observable increase in the separation between fiber fragments with increasing strain as for the AU fiber.

The photoelastic behavior of the AS(750 C/H VHT) fiber which had its chemical groups removed by treatment with temperature and hydrogen is virtually the same as for the AS fiber. The stress patterns are similar and the fiber-matrix shear adhesion is high enough to prevent the fragments from moving apart in the matrix.

The HMU fiber/Epon 828 matrix system displays photoelastic behavior similar to that observed for the AU fiber. As the micrograph shows, the stressed area after the break encompasses the whole fragment at very low values of strain. The separation between fragments is larger and increases with increasing strain. The alteration of light and dark areas suggests a nonuniformity in shear transfer between fiber surface and matrix along the interface.

After surface treatment the HMS fiber exhibits slightly different behavior than the HMU fiber. The stressed area is more intense. there is less alteration in intensity along the fiber surface. The increase in the separation between fragments is reduced over that observed for the HMU fiber.

The HMS(300 C VHT) fiber behavior is very similar to that of the HMS fiber even though the surface groups have been removed to a level below that of the HMU fiber.

The relationships between the parameters which have been investigated in this study which explain the interaction between fiber surface chemistry, the effect of surface treatment on fiber surface chemistry and the relationship to fiber-matrix interfacial shear strength can be illustrated most effectively by plotting the interafacial shear strength against the fiber surface oxygen content. (Total surface gorups other than carbon or the polar component of the fiber surface free energy could be used also without affecting the sense of the graph or the conclusions to be drawn.) These parameters are plotted in Figure 9.

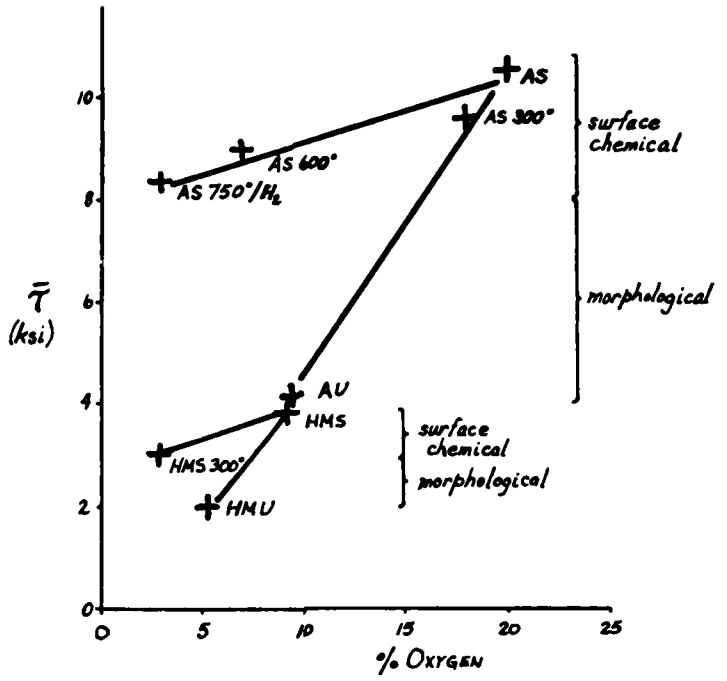

Figure 9. Interfacial Shear Strength as a Function of Percent Surface Oxygen

The data for the A fibers with their various treatments are plotted in the upper portion of the graph. Each point is labelled with the fiber designation. The data for the HM fibers are plotted in the left lower quadrant of the graph.

Concentrating on the A fiber data leads to the conclusion that the surface chemical effect of surface treatment is not the only mechanism responsible for increasing the interfacial shear strength. The fiber treatments applied to the AS fiber after surface treatment which remove the surface chemical groups result in a reduction in interfacial shear strength represented by the upper line on the graph. If the surface chemistry alone was responsible for the improved interfacial shear strength this data would have been expected to fall on the line between the AU and AS fiber points. The measured value are much higher than this however.

Likewise, the data for the HM fibers display similar trends. That is the interfacial shear strength for the surface treated HMS fiber which has had its surface groups removed is much greater than would have been predicted based on the surface chemical changes alone.

The two upper lines for the A and HM fibers represent the change in interfacial shear strength due to the change in surface oxygen groups alone. The parallelism of these two

lines indicates that the specific fiber surface group-epoxy matrix interaction is the same for both fibers. The difference in absolute values for interfacial shear strength between the A and HM fibers reflects the difference in fiber structure. The A fibers have small intertwined fibrils axially aligned along the fiber. These fibrils should be better able to withstand a surface shear loading. The HM fiber has larger fibrils which are aligned very well axially. The interfibril or intrafibril strength would be much lower for this fiber because of the alignment and the weak interbasal plane bonding in graphite. The other mechanism involved in fiber surface treatment which is responsible for improving the interfacial shear strength is the alteration of the fiber surface morpholgy. The original fiber surface on the AU or the HMU fiber has evolved through the entire graphitization process. It might be expected to contain defects reflecting the violent events which were involved in its formation. Oxidative fiber surface treatments remove this outer original layer and leave behind a surface which is structurally more integrated with the fiber core. This fiber surface would then be expected to be able to withstand the shear loadings at the interface much better that the original surface. Therefore the surface treated fibers which have had the surface chemical groups removed are able to exhibit a higher degreee of interfacial shear strength because their outer surface is able to sustain higher shear loadings.

The photoelastic patterns of the behavior of each of these fibers under stress also support the conclusion that a two part mechanism is operating when fibers are surface treated. All of the surface treated A fibers with their surface oxygen groups removed interact with the epoxy matrix in the same way. Their stress patterns are intense and move away from the break with increasing strain leaving behind a narrow stressed region less than a fiber diameter in thickness. The untreated AU fiber shows evidence of disruption of the interface and inability to prevent the fiber from moving in the matrix.

The HM photomicrographs display the same trends although to a much lesser degree. The disruption of the interface for the AU fiber could be due to failure within the outer few fiber layers. For the HM fibers failure is entirely within the fiber outer layers for all cases because of their structure. Small changes observed for the HMS and HMS(300 C VHT) fiber may be due to removal of only a portion of the outer weak original surface or the fibers intrinsic shear strength.

CONCLUSIONS

As a result of this work the following conclusions about the role of the graphite fiber surface and its change with surface treatment can be made:

First, the original as formed graphite fiber surface appears to be weak under shear loading. Interfacial failure within the outer fiber surface layers occurs.

Second, surface treatments are effective in increasing the shear loading capability of the fiber through a two part mechanism. The surface treatments remove the existing surface and leave behind a layer more structurally sound and capable of sustaining higher shear loading as well as adding surface groups, primarily oxygen which interact strongly with the polar epoxy matrix.

Third, increases in surface area do not occur with surface treatments

Fourth, for the A fiber surface treatments change the mode of interfacial failure from weak frictional sliding to matrix interfacial failure. This change does not occur on the HM fiber because of its lower intrinsic shear strength.

Fifth, progress in surface characterization of fibers must incorporate an interdisciplinary approach which takes into account the final fiber application.

REFERENCES

[1] L. T. Drzal, The Role of the Polymer Substrate Interphase in Structural Adhesion, AFML-TR-77-129 (1977)

[2] R. J. Diefendorf and E W. Tokarsky, The Relationship of Structure to Properties in Graphite Fibers, AFML-TR-72-133(1977)

[3] Hercules Inc., Wilmington, DE

[4] Hysol Division, Dexter Corporation, Pitsburg, CA 94565

[5] Physical Electronics Division, Perkin Elmer Corporation, Eden Prarie, MN 55344

[6] S. Brunauer, P. H. Emmett and E. Teller, J Am. Chem., 60 (1938)309

[7] Uthe Technology International, Sunnyvale, CA 94086

[8] Cahn Division, Ventron Instruments Corporation, Paramount, CA 90723

[9] D.H. Kaelble, P. J. Dynes and E. H. Cirlin, J. Adhesion, 6(1974)23

[10] L. T. Drzal, M. J. Rich, J. P Camping and W. J. Park, paper 20-c, Proceedings of the 35th Reinforced Plastic/Composites Institute, SPI Meeting, New Orleans (1980)

[11] S. W. Tsai and H. T Hahn, Introduction to Composite Materials, Technomic Publishing Company, Westport, CN 06880 410

[12] L. T. Drzal, Carbon 15(1977)129

[13] L. T. Drzal, J A Mescher and D. L. Hall, Carbon 17(1979)375

[14] L. T. Drzal and G. E. Hammer, Appl. Surf. Sci., 4(1980)340

OVERVIEW OF CHARACTERIZATION TECHNIQUES

D.H. Kaelble

Rockwell International Science Center
Thousand Oaks, California 91360

ABSTRACT

Advanced composite materials technology has undergone a fundamental transition in the last decade and is now implemented in a wide range of larger scale primary structures ranging from composite helicopter rotor blades to composite cargo bay doors for Space Shuttle orbitor. Part of this technology development for composite reliability is a highly organized advancement in the methods and management of characterization methodologies. These characterization methodologies can be listed in the approximate order of their implementation as follows:

1. Chemical Quality Assurance Testing
2. Processability Testing
3. Cure Monitoring and Management
4. Nondestructive Evaluation (NED)
5. Performance and Proof Testing
6. Durability Analysis and Service Life Prediction

This overview will discuss the detailed characterization methods in the context of the management concept for implementing the specific tests.

Chemical analysis, nondestructive evaluation (NDE) and environmental fatigue testing of composites generates three classes of information on composite reliability which needs to be integrated in a reliability analysis. Several new management methodologies for accomplishing this result are reviewed and discussed. The rapid evolution of computer aided design and manufacturing (CAD/CAM) places new emphasis on automated monitoring and feed-back control during both the manufacture and service usage of composite materials. The idealized feed-back control signal from an NDE monitoring system is a structural margin of safety indicator. Computer models for composite durability and environmental fatigue presently contain margin of safety predictions. A major challenge for characterization methodologies is the development of practical structural margin of safety monitoring systems which operate in the structure during manufacture and service.

The results of a recent overview survey containing "Chemical Characterization for Composite Reliability" will be presented for discussion and comment. This survey interrogates the available reference literature, and evaluates the most important current and future characterization methods.

Report on Questionnaire for Chemical Characterization of Composite Reliability

By:

D. H. Kaelble
Rockwell International Science Center
Thousand Oaks, CA 91360

On March 20, 1981 a questionnaire was sent to about 100 researchers active in the area of chemical characterization of polymer composites. The format of this questionnaire is shown in Table 1. The characterization methods covered by the questionnaire's field of interest were stated to include but not be restricted to:

1. elemental analysis
2. spectroscopy (IR, MS, NMR, atomic, all types)
3. chromatography (HPLC, GPC, GC, all types)
4. calorimetry
5. rheology (all types)
6. dielectrometry (all types)
7. relevant ASTM methods

The purpose of the survey is to present an overview of the subject: "Chemical Characterization of Composite Reliability" at:

1. The SAMPE National Symposium, Los Angeles, Calif., April 28, 1981.
2. The Critical Review: Techniques for Characterization of Composite Materials, Mass. Inst. of Technology, Cambridge, Mass., June 10, 1981.

On April 15, 1981 a compilation of 40 responses to the questionnaire was carried out and the results are summarized in Tables 2-6.

Before reviewing the survey results a note of explanation will clarify the meaning of the score system used to arrange the data in Tables 2-6. As noted in the questionnaire (Table 1) each question asks for a ranked list of five items in order of decreasing importance. For each question the following score rating was assigned:

1st choice score = 5
2nd choice score = 4
3rd choice score = 3
4th choice score = 2
5th choice score = 1
higher choice score = 0

These scores were summed over all questionnaires to produce the scores which appear in Tables 2-6. As an example, two first choices and a third choice from three questionnaires produce a summed score of 13.

As shown in Table 2 the survey shows a high score and current utilization of HPLC (high performance liquid chromatography) in chemical characterization of composites. Thermal analysis by calorimetry, gravimetric, and mechanical analysis is now closely complemented by rheological analysis of dynamic mechanical response. Infrared spectroscopy and other spectroscopic methods follow in importance as chemical characterization tools. Table 2 fairly clearly shows the present emphasis is on molecular separation and identification of polymeric constitutents of composites followed closely by measurements relating to processability and process control.

The survey of presently most wanted chemical characterization methods shown in Table 3 shows the new emphasis on processability and process control. The high scores for rheological analysis reflects the importance of dynamic mechanical measurements in aiding process design. The second high score for dielectrometry evidently reflects the importance of this measurement as an in-process monitor of cure state. Interest in NMR (nuclear magnetic resonance) which include C-13 and magic angle spin methods is indicated by a score comparable to thermal analysis and HPLC. The addition of mass spectroscopy analysis capability to both LC and GC follows and elemental analysis is evidently of increased interest in planned characterization. The relatively high scores given fracture mechanics and acoustic emission/ultrasonic methods shows the evident interest in connecting chemical characterization directly to mechanical reliability of composite response.

The survey of presently most used reference journals summarized in Table 4 shows that the more general publications of polymer engineering receive higher scores than the more specialized reference journals.

In contrast the survey of presently most used reference books shown in Table 5 shows that the more specialized textbooks appear to display greater usage and higher scores. The lists of Table 4 and Table 5 are quite informative and useful in providing a focus for general information availability on both chemical characterization and mechanical reliability of composites. These lists were developed from the first question of the questionnaire (Table 1).

The third category of response to the first question of the questionnaire provides the survey of presently most used specific reports and articles shown in Table 6. It is interesting to note the highest scores given personal communications and nonspecific contractor reports. This response, evidently indicates the importance of meetings, and current information exchange between research laboratories. Next in importance in specific research reports is a periodically revised and updated report edited by Lockheed Missiles & Space Co. Almost all the reports listed in Table 6 are less than five years old and this fact again reflects the evident importance of personal communication in keeping abreast of a rapidly expanding field of knowledge.

The results of this survey provide a sharply focussed overview of 40 expert opinions concerning the important field of chemical characterization of composite reliability. The survey summaries of Tables 2-6 represents the unedited compilation of the questionnaire responses.

Table 1: OVERVIEW QUESTIONNAIRE ON CHEMICAL CHARACTERIZATION OF COMPOSITE RELIABILITY

A. Please list five (or more) references (books, journals, specific reports, or articles) which you personally use in planning your characterization strategy (by all means reference your own research where applicable). List from 1 to 5 in order of decreasing importance.

1.
2.
3.
4.
5.

B. Please list five instruments or characterization methods which you currently utilize and would want to retain over all others. List from 1 to 5 in order of decreasing importance.

1.
2.
3.
4.
5.

C. Please list five instruments of characterization methods which you do not currently utilize and would want to obtain over all others. List from 1 to 5 in order of decreasing importance.

1.
2.
3.
4.
5.

Please return to: David H. Kaelble
Rockwell International Science Center
1049 Camino Dos Rios
Thousand Oaks, CA 91360

Table 2: SURVEY OF PRESENTLY UTILIZED CHEMICAL CHARACTERIZATION METHODS FOR 1981

SCORE	Currently Utilized Methods
142	HPLC (High Performance Liquid Chromatography)
87	Thermal Analysis
81	Rheological Analysis
55	Infrared Spectroscopy
42	Spectroscopy (General)
21	NMR (Nuclear Magnetic Resonance)
21	Mechanical Property
16	GC (Gas Chromatography)
13	Dielectrometry
11	TEM-SEM (Transmission-Scanning Electron Microscope)
10	ASTM Test
10	Mass Spectroscopy
9	Water Vapor Absorption
8	Elemental Analysis
7	Titration
4	Atomic Absorption
4	Specific Volume
3	Photoelasticity
2	Fracture Mechanics
1	X-ray Scattering

Table 3: SURVEY OF PRESENTLY MOST WANTED CHEMICAL CHARACTERIZATION METHODS FOR 1981

SCORE	CURRENTLY MOST WANTED METHODS
105	Rheology Analysis
46	Dielectrometry
36	NMR (Nuclear Magnetic Resonance)
32	Thermal Analysis
28	HPLC (High Performance LC)
21	GC/MS (Gas Chromatography/Mass Spect.)
15	LC/MS (Liquid Chromatography/Mass Spect.)
13	Elemental Analysis
12	Fracture Mechanics
12	Acoustic Emission/Ultrasonics
12	TEM-SEM (Transmission-Scanning Electron Microscope)
9	Mechanical Testing
7	Computer Analysis
6	Raman Spectroscopy
5	Photoacoustic Spectroscopy
5	ESCA (Electron Spect. for Chemical Analysis)
5	TLC/FID (Thin Layer Chrom./Flame Ion Detection)
5	Surface Tension Analysis
5	X-ray Analysis
5	Spectroscopy (General)
5	ESR (Electron Spin Resonance Spect.)
5	Gas Chromatography
4	Titration
4	Polarized Fluorescence Spectroscopy
3	UV Spectroscopy
3	Atomic Absorption
2	Thin Layer Chromatography
1	Mass Spectroscopy
1	Chemiluminescence

Table 4: SURVEY OF PRESENTLY MOST USED REFERENCE JOURNALS FOR COMPOSITE CHEMICAL CHARACTERIZATION FOR 1981

SCORE	REFERENCE JOURNALS
18	J. of Applied Polymer Science
10	Polymer Engineering and Science
10	SAMPE Proceedings
8	J. Polymer Science
7	Applied Spectroscopy
6	Analytical Chemistry
6	J. of Analytical Chemistry
4	J. of Chromatographic Science
4	Chemical Abstracts
4	Polymer Composites
4	J. of High Resolution Chromatography
3	J. of Liquid Chromatography
3	Thermal Analysis
2	J. of Polymer Technology
2	Plastics World
1	J. of Applied Polymer Technology
1	J. of Colloid and Interface Science
1	J. of Chromatography

Table 5: SURVEY OF PRESENTLY MOST USED REFERENCE BOOKS FOR COMPOSITE CHEMICAL CHARACTERIZATION FOR 1981

SCORE	REFERENCE BOOKS
28	H. Lee and K. Neville, "Handbook of Epoxy Resins, McGraw-Hill, New York (1967)
22	ASTM Test Methods
10	P. Hedwig, "Dielectric Spectroscopy of Polymers," Halstead-Wiley, New York
10	D. H. Kaelble, Physical Chemistry of Adhesion, Wiley-Interscience, New York (1971)
6	L. J. Bellamy, "Infrared Spectra of Complex Molecules,"
6	C. A. May and T. Tanaka, "Epoxy Resins," Marcel Dekker, New York, (1973)
5	Enc. of Polymer Sci. & Tech.
5	Scott's Standard Methods of Chemical Analysis
5	Billmeyer, "Textbook of Polymer Science"
5	F. Wehrli and T. Wirthlin, "Interpretation of Carbon 13 NMR Spectra"
5	L. E. Nielsen, "Mechanical Properties of Polymers," Vol. 1, 2, Marcel Dekker, New York (1974)
4	MIL SPECS
4	Whorlow, "Rheological Techniques," John Wiley New York
4	L. R. Snyder and J. J. Kirkland, "Introduction to Modern Liquid Chromatography," Wiley, New York (1974)
4	McCrum, Read and Williams, "Anelastic and Dielectric Effects in Polymer Solids, Wiley, (1967)
4	C. A. May (Ed), "Resins for Aerospace," ACS Symposium Series 132 (1980)
4	Sadtler Spectral Calologs

Table 5: (Continued)

SCORE	REFERENCE BOOKS
4	E. G. Brame, Jr., "Applications of Polymer Spectroscopy," (1978)
4	W. W. Yau, J. J. Kirkland, and D. D. Bly, "Modern Size Exclusion Liquid Chromatography, Wiley, New York (1979)
4	S. L. Rosen, Fundamental Principles of Polymeric Materials, Barnes and Nobel (1971)
3	NIOSH Manual of Analytical Methods
3	Test Manual-Institute of Interconnecting Packaging, Electronic Circuits
3	C. P. Smyth, "Dielectric Behavior of Structure," University Reprints
3	Polymer Handbook
3	SAE Specs.
3	I. M. Ward, "Mechanical Properties of Solid Polymers," Wiley-Interscience, New York (1971)
2	J. Urbanski, et al, "Handbook of Analysis of Synthetic Polymers and Plastics
2	Handbook of Fiberglass
2	G. P. Anderson, S. J. Bennett, and K. L. DeVries, "Analysis and Testing of Adhesive Bonds," Academic Press, New York (1977)
2	Van Krevelen, "Properties of Polymers"
1	J. V. Schmitz, et al (Eds.), "Testing of Polymers," Vol. 1-4, Wiley, New York
1	L. R. Synder, "Principles of Adsorption Chromatography"
1	Deanin, "Polymer Structure Properties and Applications"

Table 6: SURVEY OF PRESENTLY MOST USED SPECIFIC REPORTS AND ARTICLES FOR COMPOSITE CHEMICAL CHARACTERIZATION FOR 1981

SCORE	SPECIFIC REPORTS AND ARTICLES
20	Personal Communications
20	Contractor Reports, Nonspecific
16	D. K. Hadad (Ed.), "Chemical Quality Assurance Test Procedures for Advanced Composite Resin Matrices," Lockheed Missiles and Space Co., Inc., May 1980
15	AFML-TR-76-112
12	Instrument Manufacturer's Literature
8	J. F. Carpenter, "Quality Control of Structural Non-Metallics," U.S. Navy Contract No. N00019-76-C-0138, Final Report for Period Oct. 15, 1975 to Oct. 16, 1976
8	AFML-TR-77-217
5	J. F. Carpenter and T. T. Bartels, "Characterization and Control of Composit Prepregs and Adhesives," SAMPE Quarterly Jan. 1976
5	AFML-TR-79-4180
5	R. Hinrichs and J. M. Thuen, "Advanced Chemical Characterization Techniques Applied to Manufacturing Process Control." SAMPE Vol. 24, (May, 1979) p. 404
5	W. D. Bascom, J. L. Bitner, R. J. Moulton and A.R. Siebert, Composites, Jan. 1980, p. 9.
5	R. J. Morgan, Polym. Plastics Tech. and Eng., 10, 49 (1978)
5	A. A. Wickham, D. D. Rice and R. J. DuBois, "Chemical Analysis of Composite Prepregs and Resins," 24th SAMPE Symposium (May 1979)
5	K. Kawata, S. Hashimoto, K. Kurokawa and N. Kanayama, "A New Testing Method for the Characterization of Materials in High Velocity Tension," in J. Harding Ed., Mechanical Properties at High Rates of Strain, Inst. of Physics, Bristol and London, 1979, p. 71-80
4	C. A. May, et al, SAMPE Symposium (1976), p. 274

Table 6 (continued)

SCORE	SPECIFIC REPORTS AND ARTICLES
4	K. Kawata, "Micromechanical Study of High Velocity Deformationof Solids," in 15th Int. Cong. of Theor. and Appl. Mech. (Editors: F.P.J. Rimrott and B. Tabarrock) North Holland Pub., (1980), p.307-317
4	Customer Specifications
4	H. Stenzenberg and M. Herzog, "Thermal Analytical Methods for Characterization of Resins, Pregregs and Composites, ESA Symp. on Spacecraft Materials (Oct. 1979).
4	Koutsky and Mijouie, Polymer, 20 (1979) p. 1095
4	G. L. Hagnauer, Waters Associates, Inc. Publ. J09/Oct. 1978
4	C. A. May, et al, SAMPE Symposium (1976) p. 274
4	R. Hinrichs, "Environmental Effects on the Control of Advanced Composites Material Processes," SAMPE Journal (Nov.-Dec. 1979), p. 12-20
4	A. G. Miller, P. E. Hertzberg and V. W. Rantala, "Thoughness Testing of Composite Materials," SAMPE Preprints, 12, 269 (1980)
4	AFML-TR-79-4166
3	E. L. McKagaue, J. Reynolds, and J. Halkias, "Swelling and Glass Transition of Epoxy Matrix Material in Humid Environments," J. App. Poly. Sci., 22, (1978), p. 1643-1654
3	Progress Reports, Contract NASI-15371, Rockwell Int. Corp.
3	K. Kawata, A. Hondo, S. Hashimoto, N. Takeda, and H. L. Chung, "Dynamic Behavior Analysis of Composite Materials; Mechanics, Mechanical Properties and Fabrication, (Editors: K. Kawata and T. Akasaka), Japan Soc. of Composite Materials, Tokyo 1981 (in press)
3	J. S. Fritz, "Titration of Bases in Nonaqueous Solvents," Anal. Chem., 22, 1028-1029 (1950)

Table 6 (continued)

SCORE	SPECIFIC REPORTS AND ARTICLES
3	D. H. Kaelble and P. J. Dynes, "Preventative Nondestructive Evaluation (PNDE) of Graphite Epoxy Composites," Ceramic Eng. and Sci. Proc., 1, (1980), p. 458-472
3	"Thermal Analysis Review: Dynamic Mechanical Analysis (DuPont Instruments)
3	J. K. Gillham, "Formation and Properties of Network Polymeric Materials," Poly. Eng. and Sci., 19 (1979) p. 676
3	E. H. Andrews, "Developments in Polymer Fracture," Applied Science Publishers, London (1979)
3	C. A. May, T. D. Helminiak, and H. A. Newey, "Chemical Characterization Plan for Advanced Composite Prepregs," 8th Nat. SAMPE Tech. Conf. (Oct. 1976)
3	R. E. Trujillo and B. P. Engler, Sandia Nat'l. Lab Report No. SAND78-1504
2	J. F. Carpenter, "Test Program Evaluation of 3501-6 Resin," Naval Air Systems Command Contract # N0019-77-C0155, Final Report, May 1978
2	E. L. McKagaue, J. Reynolds, and J. Halkias, "Moisture Diffusion in Fiber Reinforced Plastics," ASME J. of Eng. Material and Tech., 98 H 1, (Jan. 1976) p. 92
2	W. Wendlandt, "Thermal Methods of Analysis," in Chemical Analysis, Vol. 19, Wiley, New York, 1974
2	12th National SAMPE Tech. Conf. Vol. 12 (1980)
1	Manson, Sperling, and Kim, AFML-TR-77-124
1	"Chemical Fingerprinting of Composite Materials," SME Tech. Paper EM-78-403
1	TTCP Proceedings and Conference Reports

EFFECT OF LIMITING STRAIN ON STRUCTURAL EFFICIENCY

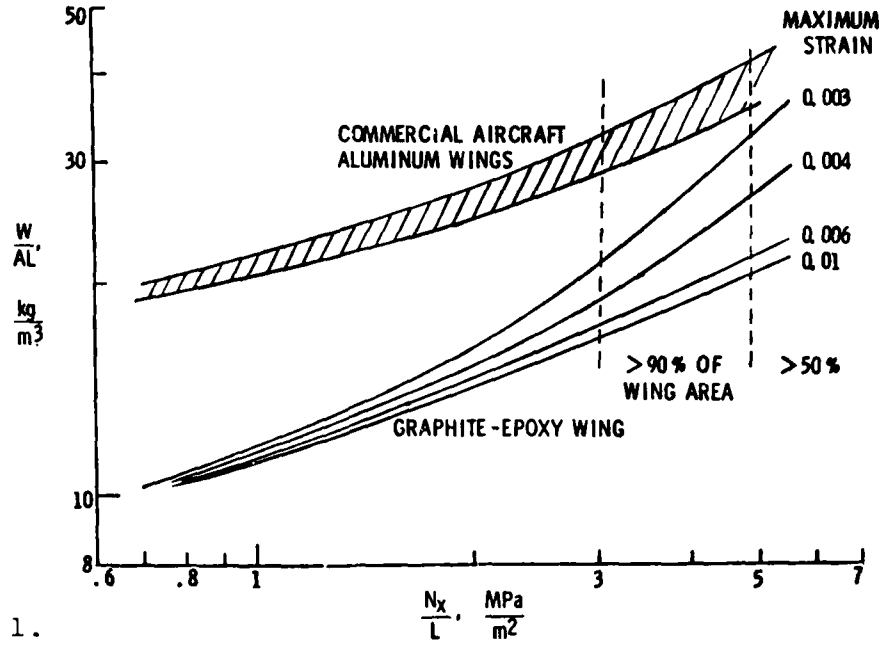

Figure 1.

that the maximum allowable design strain has little influence. However, 90 percent of the wing area on a commercial aircraft falls in the load range above 3 and 50 percent falls beyond 5. The weight saving benefits of an increase in allowable strain to 0.006 (6000 microinches/inch) are obvious.

Figures 2 and 3 illustrate why the current allowable strain is limited to 3500 to 4000 microinches/inch. Figure 2 illustrates the behavior of a 48-ply level loaded in compression while simultaneously being impacted by a one-inch steel ball at various velocities. Under compression only, without impact, the strain to failure is 0.009 or higher, but as impact velocities increase the strain at failure decreases and approaches an asymptote at around 0.003. Figure 3 illustrates a similar effect for holes, with the asymptote at around 0.004.

NASA's Langley Research Center has expended considerable effort to find laminating resins that will allow higher design strains. They found 24 resins that in neat resin form provide a higher strain to failure than the current epoxy resins. However, only 5 of those resins provided a higher strain to failure in composite form in the compression-impact test, and none of them are acceptable for use as laminating resins because of deficiencies in other properties, especially modulus. This raises two questions. How do properties of the neat resin translate to composite properties, and can a laminating resin be developed that has a high strain to failure and a high modulus, and thus a higher strength than current resins?

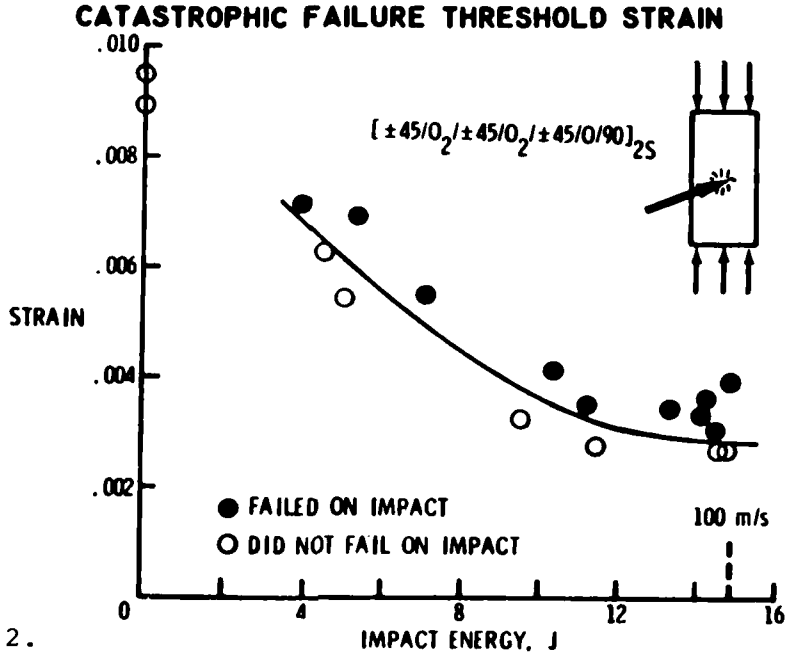

Figure 2.

COMPOSITES PROGRAM

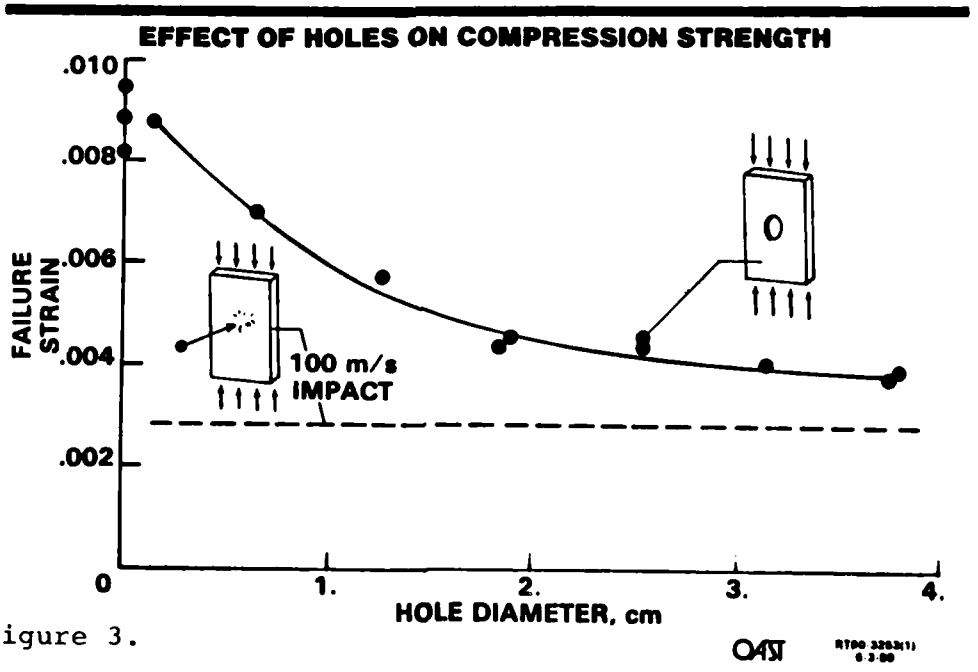

Figure 3.

Question - How expensive can resin materials be and still provide composites that are economical?

Answer - I can't answer that very well. People have done extensive computations based on fuel costs of $1.00 per gallon, $1.50 per gallon, $2.00 per gallon, etc., and, knowing the fuel consumption during one year's flights and the projected lifetime of an aircraft, have estimated the life cycle benefits of utilizing various amounts of composites in aircraft. But I don't know how much increase in first costs would be acceptable in order to achieve downstream improvement. I am working for NASA now but I worked for the Navy till a year ago and I know that despite a lot of lip service to life cycle costs, first costs seemed to carry the day.

Question - Do you see resin improvements coming down the pike anywhere?

Answer - I have to give you a waffling kind of answer. There is lots of work going on. The prepreg suppliers are working hard to meet some recent, demanding specifications from Boeing. And NASA is supporting work in one and two phase rubber toughened epoxies, thermoplastics and other resin systems. We hope some of those efforts are successful.

WHAT WE SHOULD BE DOING

S. H. Carr

Department of Materials Science and Engineering
Northwestern University
Evanston, IL 60201

I certainly do not have the audacity to be the guru that says what we should be doing; we all have, in our minds, ideas of what we should be doing. What I am really going to do over the next 20 minutes is make kind of review of the field and, perhaps, some prognostications based on ideas that I have in my own mind. If you will allow me the liberty of doing that, I think we will do okay. The first point to make is that we have been doing a good job in characterizing composite materials! When you think about where the field has come since the 50's, or even since the mid-70's, I think that you realize that we have been identifying important questions and attacking them in a fairly orderly fashion. Needless-to-say, problems still abound, and we expect to see them press us for another 5, or more, years. I am a materials scientist, so I shall be emphasizing in my presentation the materials in a composite.

This conference is a critical review of composites with special emphasis on the organic matrix, so I bring to your attention just the very simple and obvious view of a cross-section through a composite. What are the materials there? There is a fiber phase. There is a resin phase around it - it is a separate phase. There is an interface, and there is also something very special there: the interphase. It's almost as if it were a 2-dimensional phase itself. Even the region outside the interphase extending into the matrix phase, especially, and for all I know, into the fiber phase as well, are regions where the properties and other characteristics aren't necessarily typical of their respective bulks. Of course, the composite structure itself is important in the processing of these materials and will be recognized as important for many years to come. These points certainly represent the building blocks of the way we will all be dissecting the problem of composite materials.

The way I dissect scientific problems, as a materials scientist, is by a concept that I call the paradigm of materials science and engineering. It is the following very useful way of seeing things. You say that some substance has a composition, chiefly the chemical composition. This composition will determine what structures are possible. Many structures are possible given a particular composition, but it gives you a ball park in which to find your structures. The structures start at the atomic and molecular level and build up to the micron or even millimeter size scale. For example, it depends on whether you are looking at concrete or whether you are looking at a molecular glass. But, given whatever your structures are, then the properties that are possible will be determined. It is not a unique determination, but it establishes bounds on the question: How does the structure determine the kind of properties that you are going to get? In turn, whatever properties you have - optical, mechanical, and electrical - will determine the kind of performance you may have to exploit. Example characteristics are having high strain-to-failure or not having high strain-to-failure, or on the other hand, perhaps, having the ability to dissipate a lot of mechanical energy in getting to a certain strain-to-failure. In other words, performance itself is a combination of properties; it is important to keep that in mind.

You can use this scheme of materials science just to get an idea about how the field has gone about understanding composites to date. I'll start out with chemistry of the matrix as one of the points to survey. First of all, we have been dealing with the epoxide-based systems, and a very ambitious and successful project has been undertaken over the last 5 years or so determining what is in them in the first place. I can recall a day 15 years ago when I was working with Epon 828 and was assuming that was a pure substance! That shows how naive you are when you are an undergraduate, and it is interesting to note that this is still not a completely nailed-down question. What reactions predominate in the various temperature ranges? Well, that's interesting that you should even qualify the temperature ranges, but to say you don't know the chemistry sounds embarrassing. If I were going into an academic chemistry department admitting that I didn't know all of the 4 possible chemical reactions, I would be drummed out of the room, but, of course, there are more than 4 possible ones, as we all know now. What are the degradation reactions that are important? You can think about what makes these materials come apart: there is oxygen and its role, sunlight is a possibility, and ionic impurities may also play a catalytic role.

As we just heard in Bersch's fine summation, new resin systems are being identified and being studied. We are looking forward to some options in the organic phase area, perhaps in seeing improvements in high temperature stability and moisture resistance. As consequences, the mechanical behavior is being improved into ranges where we can really compete with existing metallic materials. I would put availability and economics on here because they are real considerations which will determine many of the factors as to which materials come into being and which materials just simply remain possibilities. Well, that's what we should shoot for, isn't it? Processability and performance of each of the new resins that are identified, of course, will have to be evaluated and mastered before we can really see them being seriously considered.

What about the structure of the matrix? Well, that's being brought under control, as well. First of all, almost all of us here are dealing with thermosetting resins. The reasons are many, but I think some of the more key ones are, as you know, we could get a lot of these properties with other materials, but the crosslinked network is very convenient for taking an arrangement of fibers, preserving that fiber arrangement, and getting an organic matrix to surround and interpenetrate the entire filler arrangement. It is right that these are the kinds of materials of present-day concern. But, what can we say about the molecular structure of the macromolecular network? That is important to bear in mind.

I am going to digress from my scheme here and show you a few things that are coming into a level of understanding at the present time. First of all, a macromolecular network is built up during curing. John Gilham has done a marvelous job of synthesizing and unifying a way of looking at that. I am not going to give a John Gilham talk here because it is certainly his achievement that has brought us his "cure map," but I can, at least, give some brief explanation of it. What this map says is that, if you choose a temperature at which to cure a resin, you will build high polymer which may grow large enough to become a network. You will recall that network the gel and, of course, the lower in temperature of cure, the longer it will take to get that gel. However, as you build high polymer, you also, in many of these systems,

AD-A116 733 ARMY MATERIALS AND MECHANICS RESEARCH CENTER WATERTOWN MA F/G 11/4
PROCEEDINGS OF THE CRITICAL REVIEW: TECHNIQUES FOR THE CHARACTE--ETC(U)
MAY 82

UNCLASSIFIED AMMRC-MS-82-3 NL

6 of 6
AD A
116733

are building polymers that have their vitrification temperature rising. You will reach this temperature ever more quickly at ever higher cure temperatures. Thus, there comes the point in time when the system just vitrifies at the cure temperature before the network has a chance to form. Now you can say the system is cured, even though it lacks a macromolecular network. Prof. Gilham's map also points out which temperatures and times will permit a dissolved rubbery polymer to phase separate and, thereby, create a fine dispersion of the rubber, just like you had wanted all along. I like this diagram because it talks about the building of the molecular structure and even talks a little bit about building physical structure where that is important.

Some other new data, such as that which we have been developing at Northwestern, focus on some idealized model epoxide resin systems. One of the key things to recognize is that these model epoxide resins can be classified as densely crosslinked networks. Does that, you ask yourself, put us out of the range where other statistical theories on networks apply? Highly useful relationships were worked out 35 years ago on lightly crosslinked rubbers: does any of that translate to the case of densely crosslinked networks? Thor Smith, and others, now say yes. So we who have looked at the diglycidyl ether of bisphenol-A/diethylene triamine system and define composition, R, as the ratio of active amine hydrogens to epoxide groups in the formulation. Unity is the stoichiometric mixture. We measure the elastic modulus as a function of temperature. We note that the glass-to-rubber transition varies with composition and that the more amine rich is the system, the less is its stiffness. We can also take the modulous we get in the rubbery range and calculate directly from it the molecular weight between junction points, M_c, in the macromolecular network. It is interesting to note how this simple theory, worked out for lightly crosslinked networks, also turns out to work well for densely or crosslinked networks too. We find, further that M_c is inversely proportional to resin composition, when it is expressed as logarithm of R. Interestingly, you can come with an equally simple relationship that says M_c relates inversely to the resin's glass transition temperature, T_g. Thus, densely crosslinked networks <u>can</u> be handled by straightforward relationships, thereby giving us a handle on their most important structural level.

Other work that we, and others, having done on model epoxy resin systems have yielded some surprises. For example, elastic modulous of the material in its glassy state relates only mildly to composition, but we see a small, but clear, minimum in modulus <u>right at stoichiometric</u>. Well, that's interesting! Materials formulated with R near unity should have common densities and should, therefore, have a moduli corresponding to that density. Yet, there is a minimum, and it occurs right around the stoichiometric value. That same minimum shows up when you plot the yield stress in compression vs. composition. Yield stress data do not show this minimum in a subtle way; there the difference is 35 to 40 percent. Off-stoichiometric networks would seem to have relatively fewer covalent bonds per unit cross-sectional area; yet, we seem to see a better mechanical property develop from them, as opposed to what we get from resins of stoichiometric composition. Now many practitioners know this already, because they always say; here is my resin formulation and I am going to optimize it to get the best performance for some particular property. Take, for example, the property, elastic modulous. One gets guidance on what to expect from points I have heard Garth Wilkes make. He points out that

the most highly crosslinked systems will vitrify at highest temperatures and may, therefore, retain a slightly higher level of free volume than that of less highly crosslinked resin formulations. There are alternative explanations for why the off-stoichiometric materials could give a higher strength material, but I don't need to go through all of them at the present time. I want to come back to one last point. This is the macromolecular network. How important are density fluctuations? That is a question that has been floating around for quite awhile. Do you see structure? Do you see little crystallites? Do you see mixing inhomogeneities, or whatever, in these resins? I do not know the answer, but I think it is an important question that still hasn't been answered satisfactorily.

So much for structure; what about basic mechanical properties? One could come up with a list of many entries, but just the areas of anelasticity/viscoelasticity, elastic modulous, and yield strength pose large intellectual problems in and of themselves. I don't think we know very much about the basis of mechanical properties of epoxy resins, in particular, or densely crosslinked network polymers, in general. We draw on information and facts related to rubber elasticity or anelasticity and try to relate them to these materials in their glassy or rubbery states. I am not sure that a totally complete picture has been built up there and our ability, therefore, to work with behavior that involves anelastic or viscoelastic properties is hampered. As I said, we have optimized many practical formulations for maximum performance but the constituent properties are still incompletely understood. In fact, we still need knowledge on the question of how does the macromolecular network control these properties? I just gave you some data that says we can vary modulous with variations in the network, and we can vary yield stress strongly by adjustments in the network. I went through the details of one and proposed another means of explaining that. In other words, we really don't know.

On a more complicated level, we face the question: How does a complex state of stress affect mechanical behavior? We talk about strength in compression or tension, but we heard only one paper in this symposium that recognized the fact that, if you look at stresses on one axis or simultaneously on two axis, you may expect different mechanical behavior. Standard fracture mechanics text point out that strength in the presence of biaxial or triaxial loading is described by elliptical laws such as those of von Mises. One must realize that, for the case of a special kind of yielding mechanism, normal stress yielding (as opposed to shear stress yielding) can also occur. Normal stress yielding, for example, is craving in the case of thermoplastic glasses, but does crazing occur in the thermosetting resins? I bet that it does. I can point to papers that describe it, but I am not sure that the explanations have been clearly thought out. The point is that the ellipse that would ordinarily delimit the accessible levels of stress gets truncated in the tensile quadrant by this locus all the normal stress yielding events. So polymers in biaxial tensile stressing are not going to deliver the kinds of mechanical properties that you might predict from compressive stress-strain effects, if you overlook the possibility of normal stress yielding.

Another important area of physical properties is sorption and transport. It is important in the eyes of many people, and in some of the people I surveyed when I prepared this talk. They were obsessed with high temperatures and moisture content, but now I am finding that other people have

really opposite opinions of this. So work even needs to address the preliminary point regarding just how important is this issue in the first place.

The last, and most important point is: What can be said about the performance of the matrix? For example, we have the important question what is the origin of toughness of the matrix. We saw an extremely interesting talk this morning, and I think that people are really moving into this area of understanding toughness. But first, we have to identify what are the possible modes of plastic deformation. Is it just simple dilation of a cavity, or is it production of a shear band? Is it a production of a craze? What is it? Is it homogeneous deformation? What about the magnitude of micro-plasticity of defects? Specifically, if you think about the stress where a crack goes critical, you can relate that to the size of a pre-existing crack, the elastic modulus of the material, and the work to advance the crack. What this means, then, is that stability of cracks depends on a combination of material parameters, rather than being an intrinsic, basic property of this material, itself.

Closely related to the role of microplasticity is the aforementioned tendency of sorbed water to form cavities as temperature is changed abruptly. In some cases, this effect occurs upon going up abruptly in temperature, where the water will turn to a gas, and sometimes it occurs upon going abruptly down in temperature, where the water will want to come out as liquid inclusions. In either case, you form defects just by changing the water chemical potential, and possibly permitting it to undergo a phase change in situ. That is all you need to have happen to form holes in a material you had tried desperately to make homogeneous during processing. Physical stability of the epoxy matrix during service involves the various factors of aging, including densification of material, plastization that may have occurred due to extrinsic effects, and deformations. You can think about many kinds of things that will cause polymers, in these kinds of epoxy networks, to come apart, and you can measure the incidence of these things by such tests as acoustical emissions. We, therefore, know they are happening. But, how much damage can you accumulate before the material comes apart?

The next area of interest is the interface. By how much are the concentrations of the reactant species at an interface different from the bulk when you are first making the material. When, if you get a partitioning of different species between the surface and the bulk, then the resin, which polymerizes in the immediate vicinity of a reinforcing fiber might be unexexpectedly different. In addition, it is known that chains are in a perturbed state once you form them at an interface - just because the interface is there. The entropy of a chain that is attached and tethered at a surface is not the same as entropy of chains that aren't attached to such surfaces. Therefore, there is a gradient in thermodynamic potential extending radially from the fiber. We have evidence that the filler fibers themselves, cause an eacceleration of curing, and who knows but that it may be for reasons related to these points. By how much will the local complex state of stress in the region of a fiber or pair of fibers be different from that of the bulk. If the properties of the material are graded right where the load is very different from what it is out in the bulk, then one might conjecture that the material should come apart at the interface. We have evidence for that. But, how much energy does that require if it is an an adhesive failure versus a cohesive failure? People have studied these areas, but I think that the picture has a lot of answers and data left to be put into it.

And now for the composite, itself. The constituents are the fiber and the matrix that I was just talking about. I think there are important areas that we need to continue considering, and one is to monitor the exact state of cure in the mold, so that the optimum cure in molding cycle can be assured. What kind of defects do you get in as-molded parts? Hopefully, there are always none, but you know that they are there. Maybe someday you will understand which ones are important and which ones are not. In a composite, where does water go? For Kevlar-reinforced composites, I bet the water goes inside the Kevlar fibers, although one can not rule out the interphase or the matrix phase, itself.

Of very high importance to advancing our utilization of these kinds of composites is the defining of a "stored energy transfer cascade." It is one of those things you build up as a logic tree of damage to a whole structure. If just one fiber ruptures, then what could happen, and you can come up with a list of several possibilities. Alternatively, your starting point could be, what if a fiber ruptures, as opposed to what if a fiber buckles. That is a different starting point. If the fiber debonds, what then? If a crack starts in the matrix and propagates to the point where it meets a fiber, what then? If a crack propagates down between a lamina, will it transfer into another lamina or not? And you can think about making decisions among the various contingencies, weighing each one on the basis of its energy requirements. Instead of envisioning a set of alternative paths, you can figure out by how much the system may partition energy if several paths of damage are happening simultaneously. From acoustical emission data, you know there is damage going on well in advance of any kind of failure that you can see like macroscopically. If there are multiple damaging events going on, which ones are the critical ones that will determine when the specimen actually gives up and fails?

The attached figure, which I probably could use for a talk on just about anything, I would like to use in conclusion, because it is not to be understated. Here is what we are looking for (and you know it) - superior service. It is service that we do not have right now. We are thinking about getting it by creating new advanced materials. Specifically, in this case, by compositing. To do that, we still need improved understanding of these materials. We are talking about: understanding components in these materials, understanding of the compositing laws, understanding of the principles of their processing, etc. To get the understanding, you need imagination, and new knowledge. The new knowledge is found in the literature, in our own laboratories, and through field experience. They all go together to build from facts to some bigger picture of knowledge to an understanding which will allow us to achieve that final end. I think that is why we are here and that is what we are working toward over the foreseeable future. That is what we are going to do, and that is what we should be doing.

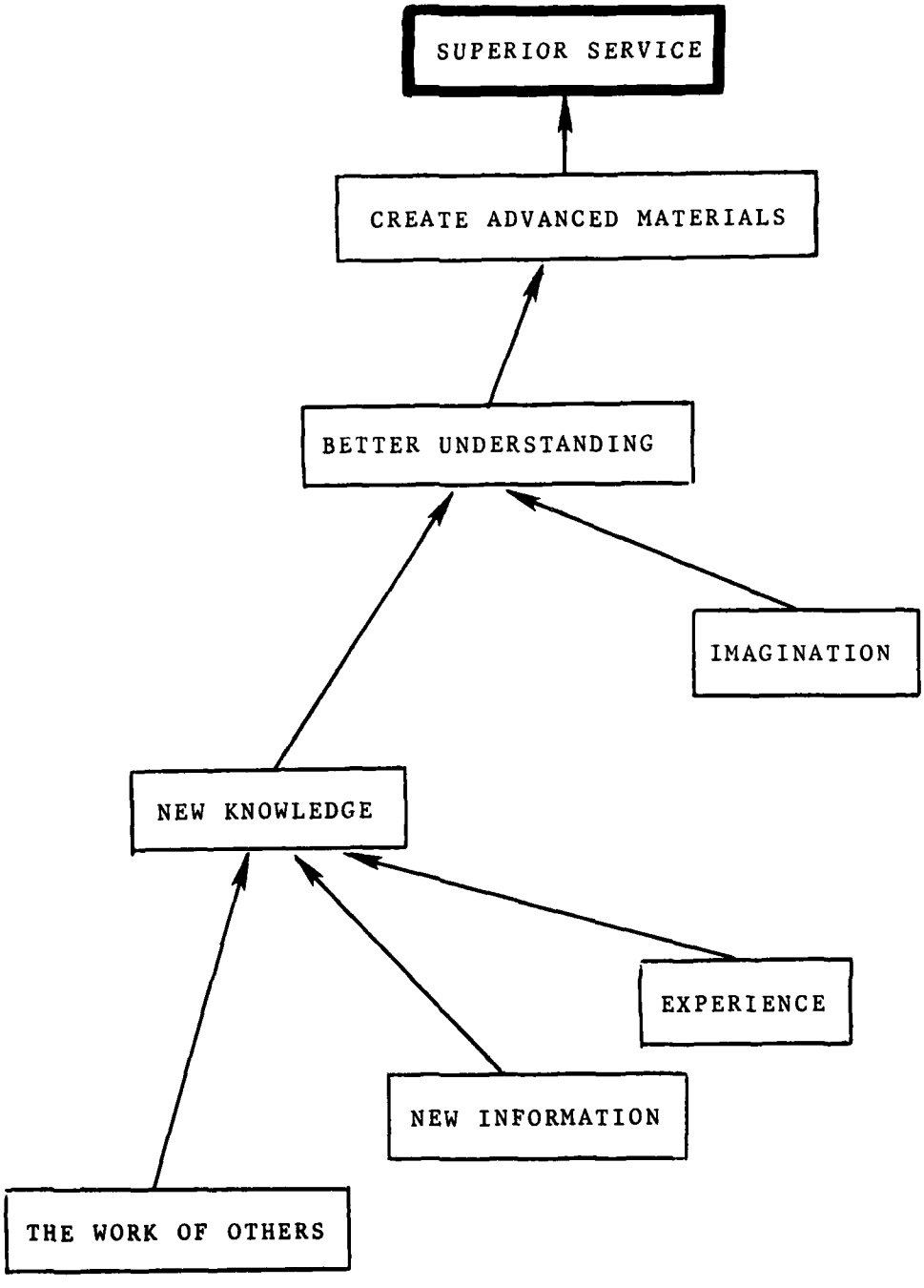
SUPERIOR SERVICE
CREATE ADVANCED MATERIALS
BETTER UNDERSTANDING
IMAGINATION
NEW KNOWLEDGE
EXPERIENCE
NEW INFORMATION
THE WORK OF OTHERS

INDEX TO AUTHORS

☆U.S. GOVERNMENT PRINTING OFFICE: 1982—501-365/62